Vol. 276, No. 1, April 15, 1993 ISSN 0003-2670

ANALYTICA CHIMICA ACTA

An international journal devoted to all branches of analytical chemistry

ELSEVIER

ANALYTICA CHIMICA ACTA
VOL. 276 (1993)

ANALYTICA CHIMICA ACTA

An international journal devoted to all branches of analytical chemistry
Revue internationale consacrée à tous les domaines de la chimie analytique
Internationale Zeitschrift für alle Gebiete der analytischen Chemie

---

Anal. Chim. Acta, Vol. 276 (1993)

ELSEVIER, Amsterdam–London–New York–Tokyo

0003-2670/93/$06.00

ACKNOWLEDGEMENTS TO REFEREES

Scientific reviewers provide an invaluable service to authors and editors alike by offering objective criticisms that help authors to improve their manuscripts and editors to make proper decisions. Accordingly, we thank the following persons for their generous and expert assistance during the past year.

Harry L. Pardue
Alan Townshend
J.T. Clerc
Willem E. van der Linden
Paul J. Worsfold

Achlades, G.E., Thessaloniki, Greece
Adams, F., Wilrijk, Belgium
Adams, M.J., Wolverhampton, UK
Ahel, M., Zagreb, Croatia
Aizawa, M., Yokohama, Japan
Alder, J.F., Manchester, UK
Alexandratos, S.D., Knoxville, TN, USA
Almuaibed, A.M., Hull, UK
Alvarez-Icaza, M., Braunschweig, Germany
Anderson, R.A., Glasgow, UK
André, F., Nantes, France
Anfält, T., Södertälje, Sweden
Appelqvist, R., Lund, Sweden
Ariel, M., Haifa, Israel
Arnold, M., Iowa City, IA, USA

Bachas, L.G., Lexington, KY, USA
Badertscher, M., Zürich, Switzerland
Bador, R., Lyon, France
Baeyens, W.R.G., Ghent, Belgium
Balconi, M.L., Milan, Italy
Baldwin, R.P., Louisville, KY, USA
Ballschmitter, K., Ulm, Germany
Barbosa, J., Barcelona, Spain
Barek, J., Prague, Czechoslovakia
Barnes, R.M., Amherst, MA, USA
Barnett, N.W., Geelong, Australia
Barthel, J., Regensburg, Germany
Bassot, J.-M., Paris, France
Battaglia, R., Zürich, Switzerland
Bax, D., Utrecht, Netherlands
Benson, R., Caulfield East, Australia
Bevers, F.M.J., Oss, Netherlands
Bezegh, A., Budapest, Hungary
Birks, J.W., Boulder, CO, USA
Blaffert, T., Hamburg, Germany
Blundell, N., Plymouth, UK
Bodenhausen, G., Lausanne, Switzerland
Boenke, A., Brussels, Belgium
Bond, A.M., Bundoora, Australia
Bos, M., Enschede, Netherlands
Bowers, G., Hartford, CT, USA
Bradley, J., Braunschweig, Germany
Bratin, K., Groton, CT, USA
Braun, T., Budapest, Hungary
Brereton, R.G., Bristol, UK
Bright, F., Buffalo, NY, USA
Brown, R., Norcross, GA, USA
Brown, S., Newark, DE, USA
Bruins, A.P., Groningen, Netherlands
Brunt, K., Groningen, Netherlands
Buck, R.P., Chapel Hill, NC, USA
Buckner, S., Tucson, AZ, USA
Buffle, J., Genèva, Switzerland
Buldini, P.L., Bologna, Italy
Burguera, J.L., Merida, Venezuela
Burguera, M., Merida, Venezuela
Burns, D.T., Belfast, UK
Buydens, L.M.C., Nijmegen, Netherlands

Calokerinos, A.C., Athens, Greece
Camoes, M.F., Lisbon, Portugal
Campanella, L., Rome, Italy
Campíns-Falcó, P., Burjassot, Spain
Capomacchia, A.C., Athens, GA, USA
Cardwell, T.J., Bundoora, Australia
Caroli, S., Rome, Italy
Carpentier, R., Quebec, Canada
Carr, P.W., Minneapolis, MN, USA
Carter, R.O., Dearborn, MI, USA
Caruso, J., Cincinnati, OH, USA
Casassas, E., Barcelona, Spain
Casey, H., Wareham, UK
Cattrall, R.W., Bundoora, Australia
Cerda, V., Palma de Mallorca, Spain
Christian, G.D., Seattle, WA, USA
Christie, O.H.J., Stavanger, Norway
Cleven, R.F.M.J., Bilthoven, Netherlands
Cline Love, L.J., South Orange, NJ, USA
Coeringer, D., Oak Ridge, TN, USA

Cook, H.E., Menlo Park, CA, USA
Cooks, R.G., Lafayette, IN, USA
Coulet, P.R., Villeurbanne, France
Courselle, P., Brussels, Belgium
Courtheyn, D., Ghent, Belgium
Covington, A.K., Newcastle upon Tyne, UK
Craig, P.J., Leicester, UK
Crews, H.M., Norwich, UK
Crighton, J., Sunbury-on-Thames, UK
Crosby, N.T., Teddington, UK
Crouch, S.R., East Lansing, MI, USA
Cummings, H., Indianapolis, IN, USA

Daeseleire, E., Ghent, Belgium
Dams, R., Ghent, Belgium
Daniele, S., Venice, Italy
Danzer, K., Jena, Germany
Das, H.A., Petten, Netherlands
Dasgupta, P.K., Lubbock, TX, USA
Davison, W., Lancaster, UK
De Boevere, C., Ghent, Belgium
Debruyckere, G., Ghent, Belgium
De Goeij, J.J.M., Delft, Netherlands
DeHaan, J., Sacramento, CA, USA
De Jong, H.G., Wageningen, Netherlands
Del Castilho, P., Haren, Netherlands
De Loos-Vollebregt, M.T.C., Delft, Netherlands
Delves, T., Southampton, UK
De Maine, P.A.D., Auburn, AL, USA
Den Boef, G., Amsterdam, Netherlands
De Noord, O.E., Amsterdam, Netherlands
De Ruig, W.G., Wageningen, Netherlands
De Vitre, R.R., Geneva, Switzerland
De Vos, R.H., Zeist, Netherlands
Diamond, D., Dublin, Ireland
Dietz, M.L., Argonne, IL, USA
Ditzler, M., Worcester, MA, USA
Doerffel, K., Merseburg, Germany
Donini, J.C., Devon, Canada
Dowle, C.J., Wilton, UK
Downard, A.J., Christchurch, New Zealand
Driebergen, R.J., Amsterdam, Netherlands
Dumasia, M.C., Newmarket, UK

Elmann, W.D., Lexington, KY, USA
Emons, H., Leipzig, Germany
Engstrom, R., Vermillion, SD, USA
Esbensen, K., Oslo, Norway
Esteban, M., Barcelona, Spain
Everett, G.L., Royston, UK

Fang, Z., Shenjang, China
Farsang, G., Budapest, Hungary
Fehér, Z., Budapest, Hungary
Fisher, A., Plymouth, UK
Flockhart, B.D., Belfast, UK
Florence, T.M., Oyster Bay, Australia
Fogg, A.E., Loughborough, UK
Fogt, E., Brooklyn, MN, USA
Foley, J., Baton Rouge, LA, USA
Fonong, T., Hampton, VA, USA
Fontain, E., Garching, Germany
Forina, M., Genova, Italy
Freiser, H., Tucson, AZ, USA
Frenzel, W., Berlin, Germany
Fritz, J., Ames, IA, USA
Fujii, Y., Kanazawa, Japan

Gammelgaard, B., Copenhagen, Denmark
Geladi, P., Umeå, Sweden
Gesser, H.D., Winnipeg, Canada
Gevers, E.C.H., Zeist, Netherlands
Ghijsen, R.T., Amsterdam, Netherlands
Gibson, T.D., Leeds, UK
Giger, W., Dübendorf, Switzerland
Girotti, S., Bologna, Italy
Głab, S., Warsaw, Poland
Glennon, J.D., Cork, Ireland
Goewie, C.H., Tiel, Netherlands
Goodall, P., Plymouth, UK
Gooijer, C., Amsterdam, Netherlands
Gordon, G., Oxford, OH, USA
Gorton, L., Lund, Sweden
Gough, D.A., La Jolla, CA, USA
Grasserbauer, M., Vienna, Austria
Gray, N.A.B., Wollongong, Australia
Grayeski, M.L., South Orange, NJ, USA
Green, J.D., Hull, UK
Greenway, G.M., Hull, UK
Gross, M.L., Lincoln, NE, USA
Grossmann, O., Dresden, Germany
Grushka, E., Jerusalem, Israël
Gubitz, G., Graz, Austria
Guilbault, G.G., New Orleans, LA, USA
Guillemin, C.L., Paris, France

Haasnoot, W., Wageningen, Netherlands
Haddad, P., Hobart, Australia
Hahn, G., Kiel, Germany
Hahn-Hägerdal, B., Lund, Sweden
Hall, G.E.M., Ottawa, Canada
Hall, G.F., Cranfield, UK
Hammer, P., Kiel, Germany
Hansen, E.H., Lyngby, Denmark
Hansen, L.C., North Chicago, IL, USA
Harris, J., Salt Lake City, UT, USA
Hart, J.P., Bristol, UK
Haswell, S.J., Hull, UK
Havel, J., Brno, Czechoslovakia
Hayashi, J., Tokyo, Japan
Heineman, W.R., Cincinnati, OH, USA
Heitzman, R.J., Newbury, UK
Helmlin, H.-J., Bern, Switzerland
Henion, J.D., Ithaca, NY, USA

Hennion, M.C., Paris, France
Hernandez Mendez, J., Salamanca, Spain
Heumann, K.G., Regensburg, Germany
Hieftje, G., Bloomington, IN, USA
Higgins, I.J., Cranfield, UK
Higson, S.P.J., Salford, UK
Hinze, W.L., Winston-Salem, NC, U.S.A.
Hippe, Z.-S., Rzeszow, Poland
Hiraide, M., Nagoya, Japan
Holcombe, J., Austin, TX, USA
Hollman, P.C.H., Wageningen, Netherlands
Homma, Y., Tokyo, Japan
Hoogvliet, J.C., Utrecht, Netherlands
Hopke, P.K., Potsdam, NY, USA
Horvai, G., Budapest, Hungary
Horwitz, E.P., Argonne, IL, USA
Houk, R.S., Ames, IA, USA
Howard, A.G., Southampton, UK
Howells, L., Weybridge, UK
Huber, C., Milwaukee, WI, USA
Huber, J.F.K., Vienna, Austria
Hummel, D.D., Köln, Germany
Hurtubise, R.J., Laramie, WY, USA

Imai, K., Tokyo, Japan
Imasaka, T., Fukuoka, Japan
Ingle Jr., J.D., Corvallis, USA
Ingman, F., Stockholm, Sweden
Inczédy, J., Veszprém, Hungary
Isshiki, K., Kochi, Japan
Ivaska, A., Turku, Finland

Jackson, K.W., Albany, NY, USA
Jagner, D., Göteborg, Sweden
Johansson, G., Lund, Sweden
Johnson, D.C., Ames, IA, USA
Johnson, K.S., Moss Landing, CA, USA
Jones, P., Plymouth, UK
Jordan, J., Cincinnati, OH, USA
Jurs, P.C., University Park, PA, USA

Kadish, K., Houston, TX, USA
Kalcher, K., Graz, Austria
Kaljurand, M., Tallinn, Estonia
Kaltenbach, T., Rochester, NY, USA
Kalvoda, R., Prague, Czechoslovakia
Kankare, J., Turku, Finland
Karcher, R., Royal Oak, MI, USA
Karube, I., Tokyo, Japan
Kateman, G., Nijmegen, Netherlands
Kaufmann, J.-M., Brussels, Belgium
Keller, H.R., Basel, Switzerland
Kellner, R., Vienna, Austria
Kettrup, A., Paderborn, Germany
Koh, T., Kanagawa, Japan
Kok, W.Th., Amsterdam, Netherlands
Kokot, S., Brisbane, Australia
Kolev, S.D., Sofia, Bulgaria
Kopanica, M., Prague, Czechoslovakia
Kosmus, W., Graz, Austria
Kotrly, S., Pardubice, Czechoslovakia
Kovar, K.-A., Tübingen, Germany
Kraak, J.M., Amsterdam, Netherlands
Kragten, J.H., Amsterdam, Netherlands
Kricka, L.J., Philadelphia, PA, USA
Krull, U.J., Mississauga, Canada
Küllik, Tallinn, Estland
Kuwana, T., Lawrence, KS, USA
Kvalheim, O.V., Bergen, Norway
Kwakman, P.J.M., Amsterdam, Netherlands

Lagu, A.L., Indianapolis, IN, USA
Lanza, P., Bologna, Italy
Larsen, K., Chicago, IL, USA
Leclercq, P.A., Eindhoven, Netherlands
Lederooy, P.A., Eindhoven, Netherlands
Lewis, R.G., Research Triangle Park, NC, USA
Lewis, S., Plymouth, UK
Leyden, D.E., Richmond, VA, USA
Leyssens, L., Diepenbeek, Belgium
L'Her, M., Brest, France
Lingeman, H., Amsterdam, Netherlands
Lingerak, W., Petten, Netherlands
Littlejohn, D., Glasgow, UK
Liu, C.C., Cleveland, OH, USA
Lohninger, J., Wien, Austria
Lövgren, T., Turku, Finland
Lundin, A., Huddinge, Sweden
Lundström, I., Linköping, Sweden
Lunte, C., Lawrence, KA, USA
Luque de Castro, M.D., Cordoba, Spain
Luten, J.B., IJmuiden, Netherlands
Lyon, W.S., Oak Ridge, TN, USA
Lytle, F.E., West Lafayette, IN, USA

Macdonald, A.M.G., Birmingham, UK
Macini, M., Florence, Italy
MacLaurin, P., Huddersfield, UK
Macrae, R., Hull, UK
Maghuin-Rogister, G., Liège, Belgium
Majiidi, V., Lexington, KY, USA
Malcolm, R.L., Denver, USA
Mallet, A., Paris, France
Mantoura, R.F.C., Plymouth, UK
Marczenko, Z., Warsaw, Poland
Marinsky, J.A., Buffalo, USA
Marko-Varga, G., Lund, Sweden
Marle, I., Södertälje, Sweden
Marsili, M., L'Aquila, Italy
Martinez Calatayud, J., Valencia, Spain
Massart, D.L., Brussels, Belgium
Masuda, A., Tokyo, Japan
Masuda, Y., Kobe, Japan
McCallum, J.J., Teddington, UK

McCreery, R.L., Columbus, OH, USA
McKelvie, I.D., Caulfield East, Australia
McLaurin, P., Plymouth, UK
McLeod, C.W., Sheffield, UK
McLuckey, S., Oak Ridge, TN, USA
Meier, P.C., Schaffhausen, Switzerland
Mellinger, M., Saskatoon, Canada
Meloun, M., Pardubice, Czechoslovakia
Mermet, J., Lyon, France
Meyer, H.H.D., Freising-Weihenstephan, Germany
Meyerhoff, M.E., Ann Arbor, MI, USA
Miller, J.N., Loughborough, U.K.
Minkkinen, P., Lappeenranta, Finland
Miyashita, Y., Toyohashi, Japan
Miyazaki, A., Ibaraki, Japan
Mizutani, F., Ibaraki, Japan
Morgan, S., Columbia, SC, USA
Morisi, G., Rome, Italy
Mota, A.M., Lisbon, Portugal
Mottola, H.A., Stillwater, OK, USA
Mulder, R.J., Deventer, Netherlands
Müller, H., Merseburg, Germany
Munk, M.E., Tempe, AZ, USA

Naes, T., As, Norway
Nagels, L.J., Antwerp, Belgium
Nagy, G., Budapest, Hungary
Nakahara, Y., Tokyo, Japan
Nakamura, M., Tokyo, Japan
Narayanaswamy, R., Manchester, UK
Nielsen, J., Lyngby, Denmark
Nieman, T.A., Urbana, IL, USA
Nomura, T., Matsumato, Japan

Olesik, S., Columbus, OH, USA
Olsson, B., Lund, Sweden
Onishi, H., Ibaraki, Japan
Op de Beeck, J., Ghent, Belgium
Ophaug, R.H., Minneapolis, MN, USA
Opydo, J., Poznan, Poland
Osteryoung, J., Raleigh, NC, USA
Otto, M., Freiberg, Germany

Paanakker, J.E., Oss, Netherlands
Pacakova, V., Prague, Czechoslovakia
Pacey, G., Oxford, OH, USA
Palys, M., Enschede, Netherlands
Park, J.H., Gyongsan, S. Korea
Parry, S.J., Ascot, UK
Patel, B.M., Port Arthur, TX, USA
Patony, G., Atlanta, GA, USA
Pelizzetti, E., Torino, Italy
Pérez-Bendito, D., Córdoba, Spain
Perone, S., San José, CA, USA
Pingarrón Carrazón, J.M., Madrid, Spain
Polo Diez, L., Madrid, Spain
Pons, M.N., Nancy, France
Poole, C.F., Detroit, MI, USA
Porter, S., Weybridge, UK
Powell, H.K.J., Christchurch, New Zealand
Pramauro, E., Torino, Italy
Pretsch, E., Zürich, Switzerland
Pungor, E., Budapest, Hungary

Quevauviller, P., Brussels, Belgium

Rajakovic, L., Belgrade, Yugoslavia
Rapsomanikis, S., Mainz, Germany
Raus, J., Diepenbeek, Belgium
Rechnitz, G.A., Honolulu, HI, USA
Reijn, J.M., Utrecht, Netherlands
Reuvers, Th.B.A., Majadahonda, Madrid, Spain
Robards, K., Wagga Wagga, Australia
Robien, W., Vienna, Austria
Rommers, P., Eindhoven, Netherlands
Rossi, D., Columbus, OH, USA
Rüedi, P., Zürich, Switzerland
Russell, M.A., Poole, UK
Rutan, S.C., Richmond, VA, USA
Rüttimann, G.T., Bern, Switzerland
Ruzicka, J., Seattle, WA, USA

Sanchez-Pedreno, C., Murcia, Spain
Sanz Medel, A., Oviedo, Spain
Savory, J., Charlotteville, VA, USA
Sawada, K., Niigata, Japan
Sawada, T., Tokyo, Japan
Schänzer, W., Cologne, Germany
Schepens, P., Wilrijk, Belgium
Schmid, R.D., Braunschweig, Germany
Schoenmakers, P.J., Amsterdam, Netherlands
Schowen, R.L., Lawrence, KS, USA
Schrader, E.L., Jackson, MS, USA
Schubert, F., Berlin, Germany
Schügerl, K., Hannover, Germany
Schulman, S.G., Gainesville, FL, USA
Schultz, J.S., Ann Arbor, MI, USA
Schulze, G., Berlin, Germany
Seitz, W.R., Durham, NH, USA
Serra, G., Pisa, Italy
Sharma, I., West Lafayette, IN, USA
Sharp, B.L., Loughborough, UK
Shelley, D., Lubbock, TX, USA
Shepherd, M.J., Norwich, UK
Shichiri, M., Kumamoto, Japan
Shoup, R., West Lafayette, IN, USA
Shults, W.D., Oak Ridge, TN, USA
Slangen, J.H., Wageningen, Netherlands
Slater, T., London, UK
Sluyters, J.H., Utrecht, Netherlands
Sluyters-Rehbach, M., Utrecht, Netherlands
Smets, F., Brussels, Belgium
Smit, H.C., Amsterdam, Netherlands
Smith, F., Rochester, NY, USA

Smith, R.M., Loughborough, UK
Smyth, M.R., Dublin, Ireland
Sneddon, J., Lowell, MA, USA
Snook, R.D., Manchester, UK
Snyder, L., Yorktown Hgts, NY, USA
Sommer, L., Brno, Czechoslovakia
Sparks, S., Plymouth, UK
Sperling, M., Überlingen, Germany
Steinwandter, H., Darmstadt, Germany
Stojek, Z., Warsaw, Poland
Stransky, Z., Olomouc, Czechoslovakia
Stulik, K., Prague, Czechoslovakia
Sturgeon, R.E., Ottawa, Canada
Sturrock, P.E., Atlanta, GA, USA
Sturzenegger, E., Basel, Switzerland
Suzuki, K., Yokohama, Japan
Suzuki, N., Sendai, Japan
Suzuki, T., Yamagata, Japan

Tang, P.W., Hong Kong
Taylor, A., Guildford, UK
Taylor, C.G., Liverpool, UK
Taylor, R., Cambridge, MA, USA
Terabe, S., Kyoto, Japan
Terada, K., Kanazawa, Japan
Thomas, J.D.R., Cardiff, UK
Thompson, K.C., Sheffield, UK
Thompson, M., Toronto, Canada
Thornalley, P.J., Colchester, UK
Thornton, J., Berkeley, CA, USA
Thorpe, G.H.G., Birmingham, UK
Thorpe, S.A., Norwich, UK
Tielrooij, J., Delft, Netherlands
Tipping, E., Ambleside, UK
Tranter, R.L., Barnard Castle, UK
Trojanowicz, M., Warsaw, Poland
Tsuji, A., Tokyo, Japan
Tsukioka, T., Nagano, Japan
Turner, A.P.F., Cranfield, UK
Turner, D.R., Plymouth, UK
Tyson, J.F., Amherst, MA, USA

Uchiyama, S., Saitama, Japan
Uden, P.C., Amherst, MA, USA
Uhegbu, C., West Lafayette, IN, USA
Ulrich, M., Dübendorf, Switzerland
Umezawa, Y., Hokkaido, Japan
Ure, A.M., Glasgow, UK

Vadgama, P.M., Salford, UK
Valcarcel, M., Córdoba, Spain
Van Daalen, H., Deventer, Netherlands
Van Damme, F., Terneuzen, Netherlands
Vandeginste, B.G.M., Vlaardingen, Netherlands
Van den Berg, C.M.G., Liverpool, UK
Van den Berg, J.H.M., Weesp, Netherlands
Van der Schoot, B.H., Neuchatel, Switzerland
Van der Wal, S.J., Geleen, Netherlands
Van de Waterbeemd, H., Basel, Switzerland
Van Espen, P., Wilrijk, Belgium
Van Ginkel, L.A., Bilthoven, Netherlands
Van Leeuwen, H.P., Wageningen, Netherlands
Van Opstal, M.A.J., Rijswijk, Netherlands
Van Peteghem, C.H., Ghent, Belgium
Van Staden, J.F., Pretoria, South Africa
Van Veen, E.H., Delft, Netherlands
Van Willigen, J.H.H.G., Enschede, Netherlands
Van Zoonen, P., Bilthoven, Netherlands
Verma, K.K., Jabalpur, India
Viets, J.G., Denver, CO, USA
Vikis, A.C., Manitoba, Canada
Voigtman, E., Amherst, MA, USA
Vytras, K., Pardubice, Czechoslovakia

Waite, M., Burnham-on-Crouch, UK
Waldock, M., Burnham-on-Crouch, UK
Wallace, G.G., Wollongong, Austalia
Walt, D., Medford, MA, USA
Wang, J., Las Cruces, NM, USA
Warner, I., Atlanta, GA, USA
Watson, A.F.R., Manchester, UK
Weber, J., Geneva, Switzerland
Weeks, I., Cardiff, UK
Weers, C.A., Arnhem, Netherlands
Wegscheider, W., Graz, Austria
Wehry, E.L., Knoxville, TN, USA
Wells, D.E., Aberdeen, UK
Welz, B., Überlingen, Germany
Wenzel, T.J., Lewinston, MA, USA
Werner, H.W., Eindhoven, Netherlands
Wesdimoitis, C., Akron, OH, USA
Wightmann, R.M., Chapel Hill, NC, USA
Wilkinson, S.G., Hull, UK
Willie, S., Ottawa, Canada
Wilson, G., Lawrence, KA, USA
Windig, W., Rochester, NY, USA
Winefordner, J.D., Gainesville, FL, USA
Wirth, M., Newark, DE, USA
Wlaters, F., Lafayette, LA, USA
Wolfbeis, O.S., Graz, Austria
Wolff, G., Liverpool, UK
Won Jun, H., Athens, GA, USA
Wylie, P.L., Avondale, PA, USA

Yacynych, A.M., New Brunswick, NJ, USA
Yao, S.Z., Changsha, China
Yonehara, N., Kagoshima, Japan
Yoshikawa, H., Kanagawa, Japan
Yvert, J., Saint Mande, France

Zupan, J., Ljubljana, Slovenia
Zwanziger, H., Merseburg, Germany

Analytica Chimica Acta, 276 (1993) 1–2
Elsevier Science Publishers B.V., Amsterdam

Obituary

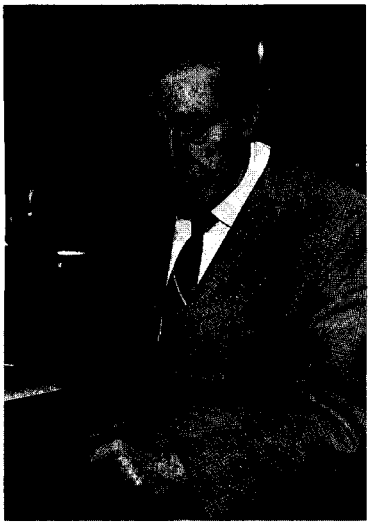

Prof. Sidney Siggia

Sidney Siggia, 72, Emeritus Professor of Analytical Chemistry at the University of Massachusetts, Amherst, died on October 15, 1992 in Amherst after a considerable period of failing health. Born in New York City, he received his bachelor's degree from Queens College in 1942 and his doctorate in analytical chemistry from the Polytechnic Institute of New York in Brooklyn in 1944.

Sid Siggia's life's work in analytical chemistry comprised two distinctive parts. For more than 20 years he pursued a distinguished career in chemical industry which included positions of Director of Analytical Research and Service at the General Aniline and Film (GAF) Corporation and the Olin Corporation. During this time he published actively in the area of organic functional group analysis and with the focus upon the Analytical Chemist as 'problem solver'. His definitive text *Quantitative Analysis Via Functional Groups* went into four editions.

In 1966 he joined the faculty of the University of Massachusetts at Amherst where he was Professor of Chemistry until his retirement in 1986. The transition from industry to academia allowed Sid Siggia to put into action his goal of developing a strong 'Academic–Industrial Interface' in analytical chemistry. He used his industrial experience as a basis for the development of undergraduate and graduate teaching and of analytical chemical research. He directed doctoral dissertations of more than 35 students, many of whom have since assumed leadership positions in the discipline, retaining the active problem-solving philosophy developed under his guidance. Under his guidance also the analytical division at the University of Massachusetts developed one of the leading academic programs in the United States.

Sid Siggia was very active in ACS and in particular in the Analytical Division, for which he served as chairman (1969–1970) and in numerous other capacities. He was a Titular member of the

Commission on Analytical Reactions and Reagents of the International Union of Pure and Applied Chemistry – IUPAC. He received recognition for his work with the ACS Fisher Award in Analytical Chemistry, the Anachem Award, and the Kolthoff Award from the Academy of Pharmaceutical Science of the American Pharmaceutical Association. He was the first recipient of the Theophilus Redwood lectureship of the Analytical Division of the British Royal Society of Chemistry. He twice was named American Chemical Society, Tour Speaker of the Year.

He authored and co-authored 11 books and more than 120 papers and book chapters. He also held 5 patents. He was a member of numerous journal advisory boards including that of *Analytica Chimica Acta*, he chaired the Gordon Conference on Analytical Chemistry and was a member of many learned societies.

Sid Siggia has left a lasting legacy to present and future generations of analytical chemists. He always combined chemical fundamentals with practical applications, never neglecting the 'applied nature' of our field. He was a fine mentor, leader and colleague.

David J. Curran
University of Massachusetts
Amherst, MA (USA)

Analytica Chimica Acta, 276 (1993) 3–13
Elsevier Science Publishers B.V., Amsterdam

Polychlorobiphenyls and persistent organochlorine pesticides in sea water at the pg l^{-1} level. Sampling apparatus and analytical methodology

A.G. Kelly, I. Cruz and D.E. Wells

SOAFD Marine Laboratory, P.O. Box 101, Victoria Road, Aberdeen AB9 8DB (UK)

(Received 9th October 1992; revised manuscript received 20th November 1992)

Abstract

A sampling apparatus has been constructed for the collection and filtration of up to 28 l of water at sea. The apparatus has been designed to minimise possible contamination from both the sampling equipment and the ship's environment. The apparatus has been utilised in the analysis of chlorinated biphenyls (CBs), persistent organochlorine pesticides (OCs), and pentachlorophenol (PCP), in both the aqueous and particulate phases. The apparatus is suitable for collection of estuarine and coastal waters where the levels of dissolved CBs, OCs and PCP are above the limit of determination of 15 pg l^{-1}. The efficiency of the recovery of these compounds and variance of the extraction and analysis have been estimated by analysis of filtered sea water spiked at a range of concentrations from pg l^{-1} ng l^{-1}. Recoveries ranged from 66.5 to 97.3% with coefficients of variation for the complete method from 7.2 to 29.9%. The contribution of the extraction to the variance of the complete method has been estimated utilising on-going laboratory quality control data.

Keywords: Extraction and filtration system; Organochlorine pesticides; Polychlorobiphenyls; Sea water; Waters

The oceans of the world are the main environmental sink [1] of persistent and toxic anthropogenic chemicals such as the chlorobiphenyls (CBs) and organochlorine pesticides. The bulk of these materials are present in the water column it self [1,2]. Analysis of the ultra-trace levels of contaminants present in sea water (ng l^{-1} to pg l^{-1}) requires specialised sampling and extraction techniques. One of the techniques most commonly used is adsorption onto a macroreticular resin such, as XAD 2 or XAD 4 [3–12]. These methods [13] have the disadvantage of requiring extensive clean-up and special storage conditions for the sorbent, but under optimum conditions they can deal with very large sample volumes, i.e., > 100 l.

An alternative approach which overcomes some of the problems of XAD resins is the use of a reversed phase C8 or C18 sorbent [14–16]. The low sample capacity and low breakthrough volume of this technique limit the sample volumes to < 5 l and therefore to waters with relatively high contaminant levels. The continuous flow centrifuge [17,18] is a rapid and efficient method of sampling large volumes, but for particulates only. Solvent extraction of water on a batch basis [3,19–21] has been limited by the practical difficulties of handling large sample volumes and the contamination problems created by use of large amounts of extracting solvent. The counter-current method of solvent extraction [21,22] over-

Correspondence to: A.G. Kelly, SOAFD Marine Laboratory, P.O. Box 101, Victoria Road, Aberdeen AB9 8DB (UK).

comes the problem of sample volume, but is slow in operation.

Elevated levels of trace organic contaminants in sea water caused by sample contaminations continues to be a difficulty in this field. Reported levels of chlorinated biphenyls (CBs) in Atlantic and Pacific waters over the past two decades would indicate a dramatic decline in concentration from 0.3–7.1 ng l^{-1} in the 1970s [1,5,19], to 0.04–0.15 ng l^{-1} in the early 1980s [18]. The most recent report gives values of 0.002 to 0.021 ng l^{-1} for the sum of 18 congeners [4]. Although this may, in part, reflect a true decrease in environmental levels of CBs, it is more likely due to improved sampling and analytical methodologies which have progressively eliminated many sources of contamination. It is now recognised that accurate measurement of organic contaminants in sea water requires all aspects of the sampling and analytical procedure to be specifically designed for the purpose, and rigorously tested.

The organic contaminants in the water column are distributed between water, organic colloids, and the organic component of particulate material. The few studies of marine water which have differentiated between aqueous phase and particulate bound contaminants have found between 2 and 88% of total DDT and PCBs retained on 0.5 m glass fibre filters [17,23]. The octanol–water partition coefficient of these compounds are of the order of 10^5 to 10^7 [24] confirming that a substantial portion of the total water loading is bound to the suspended particles. The percentage actually bound will depend on the particulate load of the particular aqueous environment. As Table 1 illustrates, this varies over several orders of magnitude depending mainly on distance from terrestrial input. Up to 99% of lipophilic contaminants will be bound to particles in river water but $\leq 1\%$ in open ocean water. The PEFS (pressurised extraction and filtration system) apparatus described in this paper is applicable to sampling of estuarine and coastal environments where particle loadings of 1–20 mg l^{-1} may occur. The system can handle sample volumes of 10–150 l of sea water. Colloidal organic matter can enhance the aqueous solubility of poorly soluble compounds. The available methods for separating dissolved and colloid bound compounds such as equilibrium dialysis [25], dynamic headspace analysis [26] and reversed-phase liquid chromatography (LC) [27] are unsuitable for large sample volumes. The PEFS system does not distinguish between dissolved and colloid bound compounds; as the separation is less important in the marine environment where levels of dissolved organic carbon (DOC) are much lower than in terrestrial aqueous systems, e.g., 0.05–0.15 mg l^{-1} in marine waters [28] and 1–100 mg l^{-1} in river water [29]. Concentrations of < 1 mg l^{-1} DOC have been shown to have minimal effect on the apparent aqueous solubility of less soluble compounds such as pp-DDT [25] whilst the solubility of more soluble compounds, such as lindane, are not enhanced at DOC levels up to 100 mg l^{-1} [30,31].

This paper describes the design and operation

TABLE 1

Typical particle loadings in several aquatic environments in relation to aqueous/particulate partitioning of lipophilic organic contaminants

Type of water	Typical aqueous particulate loading (mg l^{-1})	Percentage of lipophilic organics [a] absorbed to particulates for K_{oc} =			Volume of water required to sample particulates [b]	Applicability of PEFS
		10^5	10^6	10^7		
River	100[18]	50	90	99	1.5	
Estuary (salinity < 30)	10[21]	10	50	90	15	yes
Coastal	1	1	10	50	150	yes
Open ocean	0.1[12]	0.1	1	10	1500	

[a] Assuming 10% TOC content. [b] For a detection limit of 1 ng g^{-1} and typical analytical conditions.

of a system suitable for sampling up to 28 l of coastal or estuarine water and also the associated analytical methodology required for analyses at trace contaminant levels. The primary requirements for the system were: (1) To sample and separate particulates of $> 0.7\ \mu m$ and sea water, with minimum contamination of the sample. (2) To enable extraction of the aqueous phase. (3) The system should be mobile, and capable of shipboard use.

The performance of the system has been assessed by recovery experiments from spiked water, field trials involving the sampling of a heterogeneous closed experimental system, and the investigation of the kinetics of the aqueous-particulate partitioning of organic contaminants. The contribution of the sampling technique to the overall variance of the analysis is assessed.

EXPERIMENTAL

Sampling apparatus

The components and the arrangement of the PEFS system in operation is illustrated in Fig. 1, with the principal components (1–5). The 28 l sample containers (1 and 2), were manufactured in the Marine Laboratory workshop.

The containers are detailed in Fig. 2. Full technical drawings are available from the authors. The containers were designed for use with internal working pressures up to 60 p.s.i. and for moderate vacuum. To this end, the walls were constructed of stainless steel and specialised inlet and outlet fittings used. Each container was fitted with inlet/outlet ports for water (Fig. 2, 1–4), for application of pressure or vacuum, (Fig. 2, 5), and for bleeding the container (Fig. 2, 6). A pressure relief safety valve set to the maximum working pressure (Fig. 2,7) was additionally fitted. The Swagelok quick-connect fittings seal when the connection is broken, thereby minimising the risk of contamination to the sample within the system. The vacuum pump (3), (Mono ML), was chosen for its ability to produce the vacuum required to draw water into the sample container, and sustain a high flow rate for flushing of the container.

To filter the sample, the container is connected to a filter holder and a receiving container. The flexible piping used is half inch stainless steel tubing lined with PTFE (Cajon 55 series) and terminated by QC connectors (Swage-

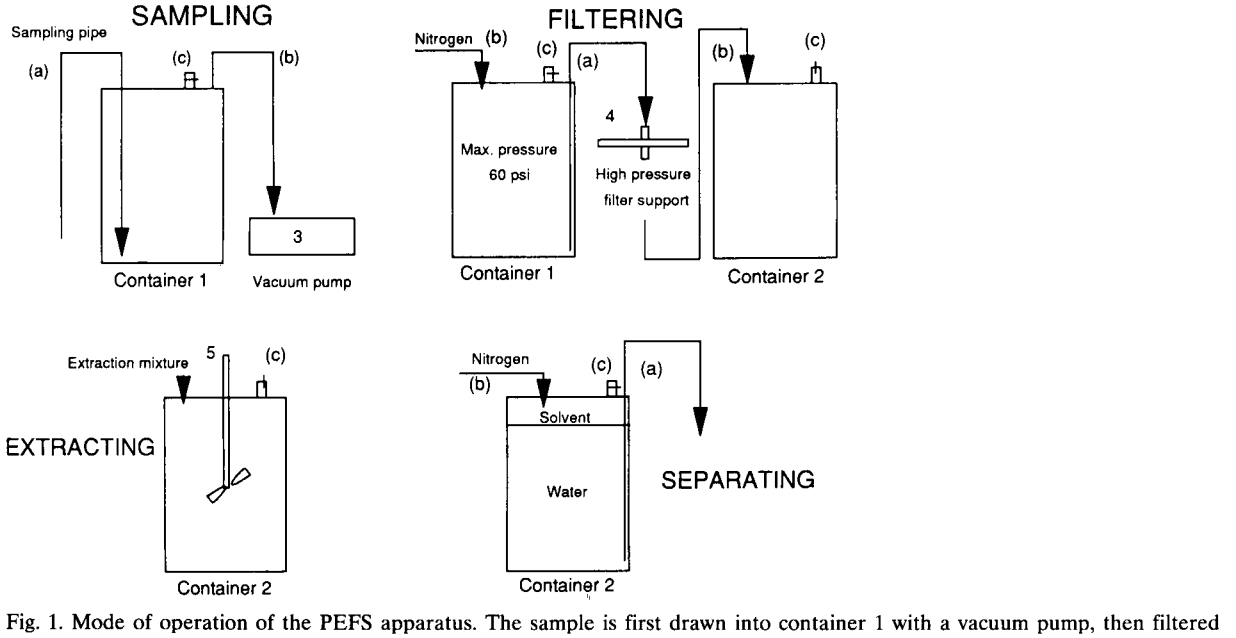

Fig. 1. Mode of operation of the PEFS apparatus. The sample is first drawn into container 1 with a vacuum pump, then filtered under nitrogen pressure. The aqueous phase is then extracted by mixing with pentane, and the extract separated.

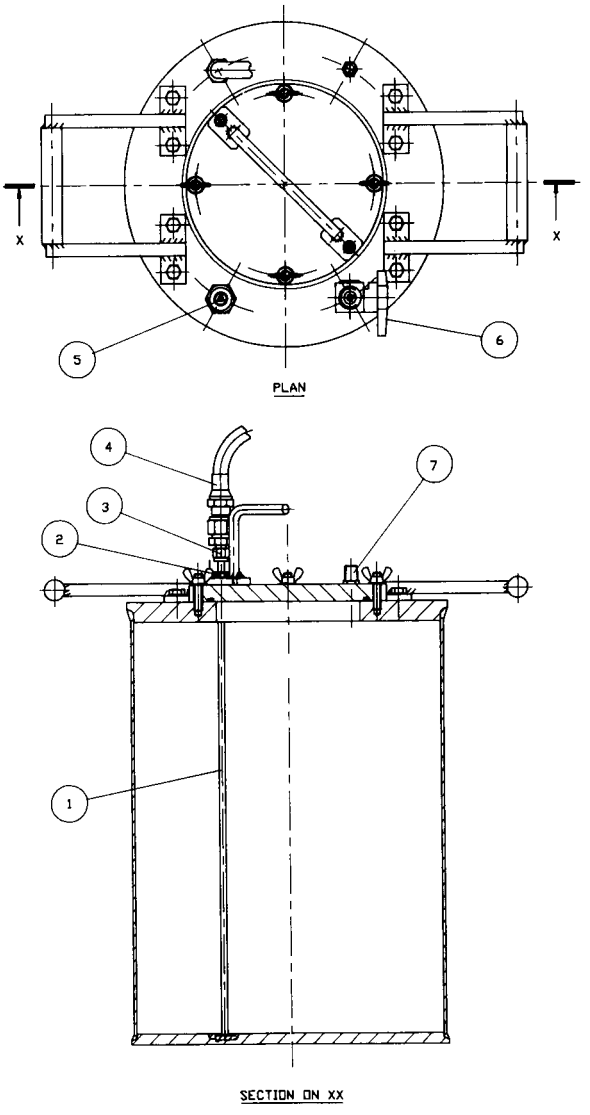

Fig. 2. Plan and vertical section of PEFS containers.

lock QC series). This flexibility enables the configuration of the apparatus to be varied to suit the available laboratory space. The filter holder (4) (Gelman Model 11872) is an all stainless steel design. The unit is equipped with viton O-rings and QC connectors. Glass fibre filters of 142 mm diameter and a nominal 0.7 μm pore size are used. Final solvent extraction of the filtered water uses an ARO air driven stirrer (5). This all-stainless steel unit, (Model 651103) is capable of 0.75 HP output and a maximum 2000 rpm. It permits efficient dispersion of the extracting solvent in the sample.

Operation

The overriding consideration in the design of the PEFS system was to avoid any contamination of the sample from either the ships environment or the PEFS system itself. The design of the system isolates the sample of sea water from the external environment and the system itself is maintained by scrupulous cleaning prior to and during use.

Prior to deployment on ship all in-line components where rinsed with glass distilled grade hexane, acetone and distilled water and the units sealed or covered in aluminium foil for transit. The glass-fibre where cleaned by heating at 450°C for 4 h, weighed and stored in aluminium foil. Pentane was glass-distilled grade suitable for residue analysis. Each batch of solvent was checked by GC-ECD prior to use.

The initial sampling stage of the operation of the PEFS system is illustrated in Fig. 1. The sampling pipe (0.5 inch, stainless steel tubing) was deployed on the lee side of the vessel to the selected depth. This was generally 2–5 m below the surface but may be increased by the addition of further lengths of tubing. The sampling pipe was terminated by a 20 cm diameter (narrow-mesh) steel screen to prevent floating debris or biota being drawn into the system. Pumping was continued until four volumes of water had been flushed through the system (45 min). The sample container (1) was then connected to a compressed nitrogen supply and the filter holder. The system was pressurised to 30–40 p.s.i. until filtration was complete, (10–15 min). The filter was then rinsed with distilled water to remove salt, and stored in aluminium foil at −17°C prior to chemical analysis. The capacity of the filter is approximately 250–300 mg of particulate material. Higher loadings lead to much reduced flow-rates.

Sulphuric acid (20 ml, 5 M) was added to the second container to assist in the extraction of pentachlorophenol followed by pentane (500 ml). The stirrer was inserted through a cover of aluminium foil and the sample stirred at 3000 rpm

for 4 min. The compressed air supply for this unit was vented to the external atmosphere to avoid contamination of the laboratory by lubricants. In operation the pump was earthed through a convenient ground to minimise the risk of a build up of static electricity causing sparking which could ignite the highly flammable pentane vapours.

The sample was left to stand for 15 min to permit the two phases to separate, it was then pressurised and 26 l of water removed. The remaining water, emulsion (if present) and pentane phases were collected and stored at 5°C prior to analysis. The choice of pentane over a more polar solvent such as dichloromethane, limited emul-

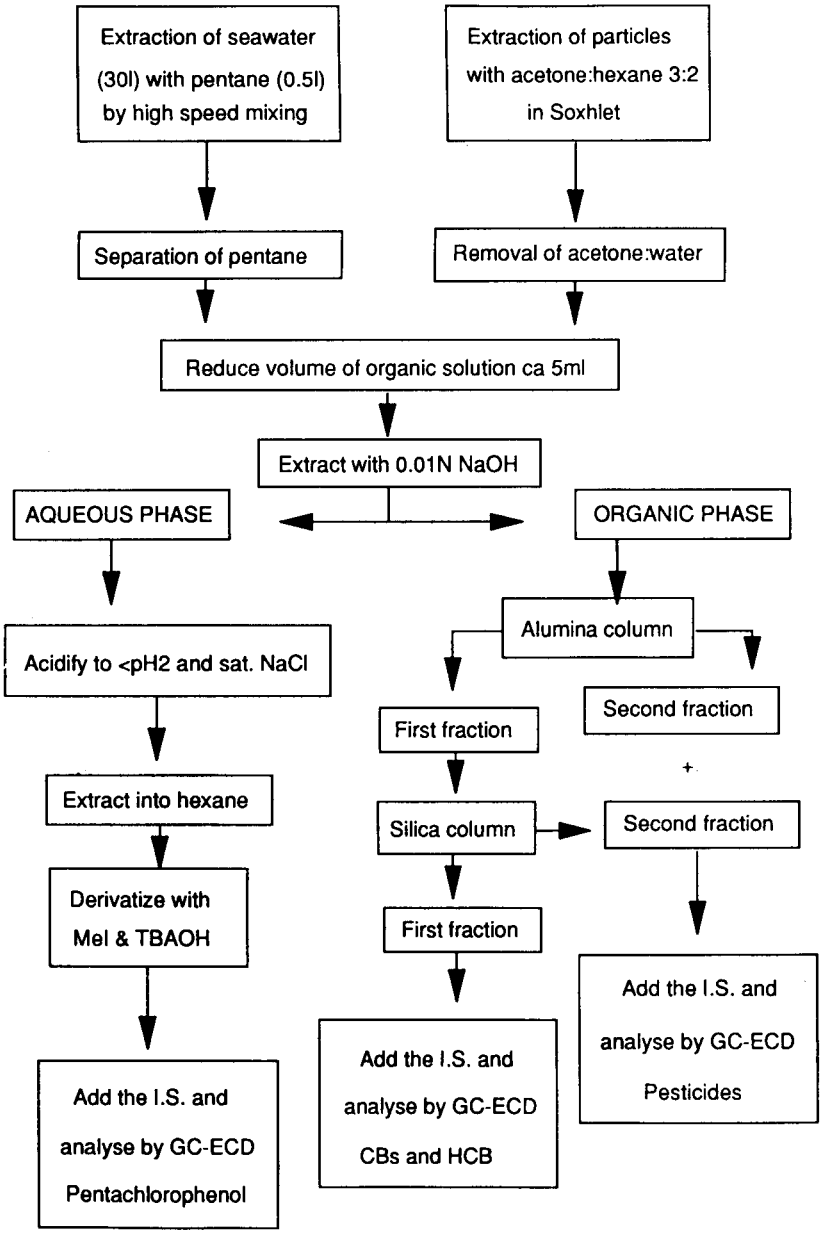

Fig. 3. Analytical procedure for separation and determination of organochlorine contaminants.

sion formation. The extraction container was cleaned before sampling again by rinsing with hexane, acetone and distilled water.

Chemical analysis

The analytical sequence is illustrated in Fig. 3. The sea water extract in pentane was separated from the excess sea water, dried by addition of anhydrous Na_2SO_4, decanted and the volume reduced by rotary evaporation at 30°C, and then finally to 5 ml under a stream of clean nitrogen.

Filters were extracted wet to avoid losses through drying. The wet filters containing the particles were acidified with 0.2 M H_2SO_4 (1.5 ml), placed in a pre-extracted cellulose thimble and extracted in a Soxhlet apparatus with hexane–acetone, (60:40, 100 ml) for 4 h at a syphon rate of 20 cycles per hour. Copper turnings were added to the reflux flask to remove sulphur, which interfered with the electron capture detector determination of these compounds. When the extraction was completed, the acetone and water were removed by liquid–liquid extraction with an aqueous solution of H_2SO_4 (pH 2). The hexane phase was then dried with anhydrous Na_2SO_4, and concentrated to 5 ml. The weight of particulates was determined as the sum of the weight of material on the filter after extraction plus the weight of extracted lipid. The extracts from particles and water were then treated by the same analytical procedure. Each sample was separated into three fractions for the determination of pentachlorophenol, organochlorine pesticides, and CBs and hexachlorobenzene.

Pentachlorophenol (PCP), was separated from the hexane extract with aqueous NaOH solution (0.01 N NaOH, 5 ml) and determined as pentachloroanisole by derivatisation with methyl iodide and tetrabutylammonium hydroxide [32].

The limits of determination of the analysis were between 5 to 105 pg of pentachloroanisole on-column. This limit for each sample depended on the final sample volume prior to injection. This was either 0.2 ng l^{-1} for 400 μl final volume and automated GC injection or 0.025 ng l^{-1} for a 50 μl final volume and manual injection. This corresponds to a determination limit for particulates of ca. 0.25 ng g^{-1} dry weight.

Sample clean-up and group separation of the CBs and pesticides was accomplished by column chromatography with alumina followed by silica [33]. The chlorobiphenyl (CB) fraction which also contained hexachlorobenzene (HCB), and the pesticides fraction containing the cyclodienes, DDT compounds, cyclohexanes and chlordane, were concentrated to 50–500 μl, the internal

TABLE 2

Chromatographic conditions for the analysis of organochlorine contaminants

	CBs and HCB	Pesticides	Pentachlorophenol
Instrument	Varian 3500 with automated on-column injection	Varian 3500 with automated on-column injection	Varian 3500 with automated on-column injection
Column	CP-SIL8 50 m × 0.22 i.d., 0.2 μm phase thickness	CP-SIL19 50 m × 0.22 i.d. 0.2 μm phase thickness	CP-SIL19 50 m × 0.22 i.d., 0.2 μm phase thickness
Carrier gas	Hydrogen, 35 cm s^{-1}	Hydrogen, 40 cm s^{-1}	Hydrogen, 40 cm s^{-1}
Oven programme	80°C, 1 min, 3°C min^{-1} to 270°C, hold 10 min	80°C, 1 min, 3°C min^{-1} to 270°C, hold 10 min	80°C, 1 min, 3°C min^{-1} to 210°C, 1 min, 10°C min^{-1} to 270°C hold 5 min
Injection	0.5 μl on-column	0.5 μl on-column	0.5 μl on-column
Injector programme	120°C, 1 min, 300°C min^{-1} to 280°C, hold 60 min	120°C, 1 min, 300°C min^{-1} to 280°C, hold 60 min	120°C, 1 min, 300°C min^{-1} to 280°C, hold 60 min
Detector	ECD, 320°C	ECD, 320°C	ECD, 320°C

TABLE 3

Recovery of compounds after differing equilibration intervals in filtered sea water

	Spiking level (ng l^{-1})	Recovery (%)	
		3 h	20 h
HCB	19	75	78
CB52	19	94	90
CB101	21	93	89
CB118	17	100	92
CB180	17	97	89

standard added and the fractions analysed by GC-ECD (Table 2). CBs were determined as individual congeners [34] using a five point calibration curve ranging from 3.5 to 490 pg on-column. Pesticides were quantified using two point calibration ranging from 3.5 to 35 pg on-column. The minimum limit of determination for individual pesticides and PCB congeners was 0.015 or 0.115 ng l^{-1} depending on the final volume of the sample for water extract and 0.2 ng g^{-1} dry weight for particulates.

Testing of the system

The performance of the PEFS apparatus for the extraction of hydrophobic organic contaminants from sea water was tested as follows.

An initial study investigated the suitability of direct spiking of filtered sea water as a means of providing aqueous solutions to test extraction efficiency. A methanolic solution of contaminants (1 ml) was added to filtered sea water (28 l) in the second PEFS container to provide an aqueous concentration of contaminants in the range 17–21 ng l^{-1}. The solution was stirred for 15–30 min, left to equilibrate for either 3 h or 20 h then extracted as described above. The results (Table 3) suggest that an equilibration time greater than 3 h has little effect on recoveries, which were generally > 90%. This method was then used to prepare filtered sea water spiked at three levels corresponding to the likely environmental concentrations in coastal waters. The three ranges were 3–4 ng l^{-1}, 0.4–0.6 ng l^{-1} and 0.2–0.3 ng l^{-1} for each of the CBs, HCB, 2,4′-DDE, 4,4′-DDE and PCP (Table 4). The three spiking levels for the remaining pesticides corresponded to 1.5

TABLE 4

Results of the recovery experiment.

(Means, recoveries and standard deviations for each spiking level are listed, together with the overall mean of the 10 experiments. The F value from the one-way anova is below the tabulated critical value of 4.36 ($p = 0.05$), for most compounds)

	High level, $n = 3$		Median level, $n = 4$		Low level, $n = 3$		F	All levels, $n = 10$		
	Mean	S.D.	Mean	S.D.	Mean	S.D.		Mean	S.D.	C.V. (%)
PCP	72	19	75	20	81	20	0	76	20	26
CB52	87	5	106	23	93	14	1	96	16	16
CB101	88	5	92	10	85	9	1	89	9	10
CB118	92	3	94	10	81	10	2	89	9	10
CB153	87	3	93	12	80	9	2	87	10	11
CB138	85	2	93	13	79	7	2	86	9	11
CB180	84	3	89	12	67	3	6	81	8	10
HCB	77	7	95	13	99	18	3	91	13	15
2,4′-DDE	85	7	78	11	74	5	1	79	8	11
4,4′-DDE	85	6	85	12	74	4	2	82	9	11
α-HCH	76	5	90	12	85	18	1	84	13	15
γ-HCH	70	4	81	28	44	14	3	67	20	30
Dieldrin	72	5	82	8	88	5	5	81	6	8
Endrin	91	8	96	9	107	7	3	97	8	8
2,4′-DDT	69	10	96	5	94	23	4	87	14	16
4,4′-DDT	85	8	97	22	94	12	1	93	16	18

ng l^{-1}, 0.2–0.3 ng l^{-1} and 0.1–0.2 ng l^{-1}. The spiking solution was prepared in methanol and weighed aliquots added to 28 l of filtered water in container 2. After 2–3 h the water was extracted as detailed above. Three replicates of the lower and upper levels and four replicates of the median level were completed. Additionally, unspiked sea water was extracted to investigate background concentration of these contaminants.

RESULTS AND DISCUSSION

The recoveries of selected determinands from spiked filtered sea water are listed in Tables 3 and 4. The data has been corrected for background levels of α-HCH 0.22 ng l^{-1} and γ-HCH 0.1 ng l^{-1} found in the blank. Dieldrin was also detected but at a level below the limit of determination, so no correction was applied. The mean

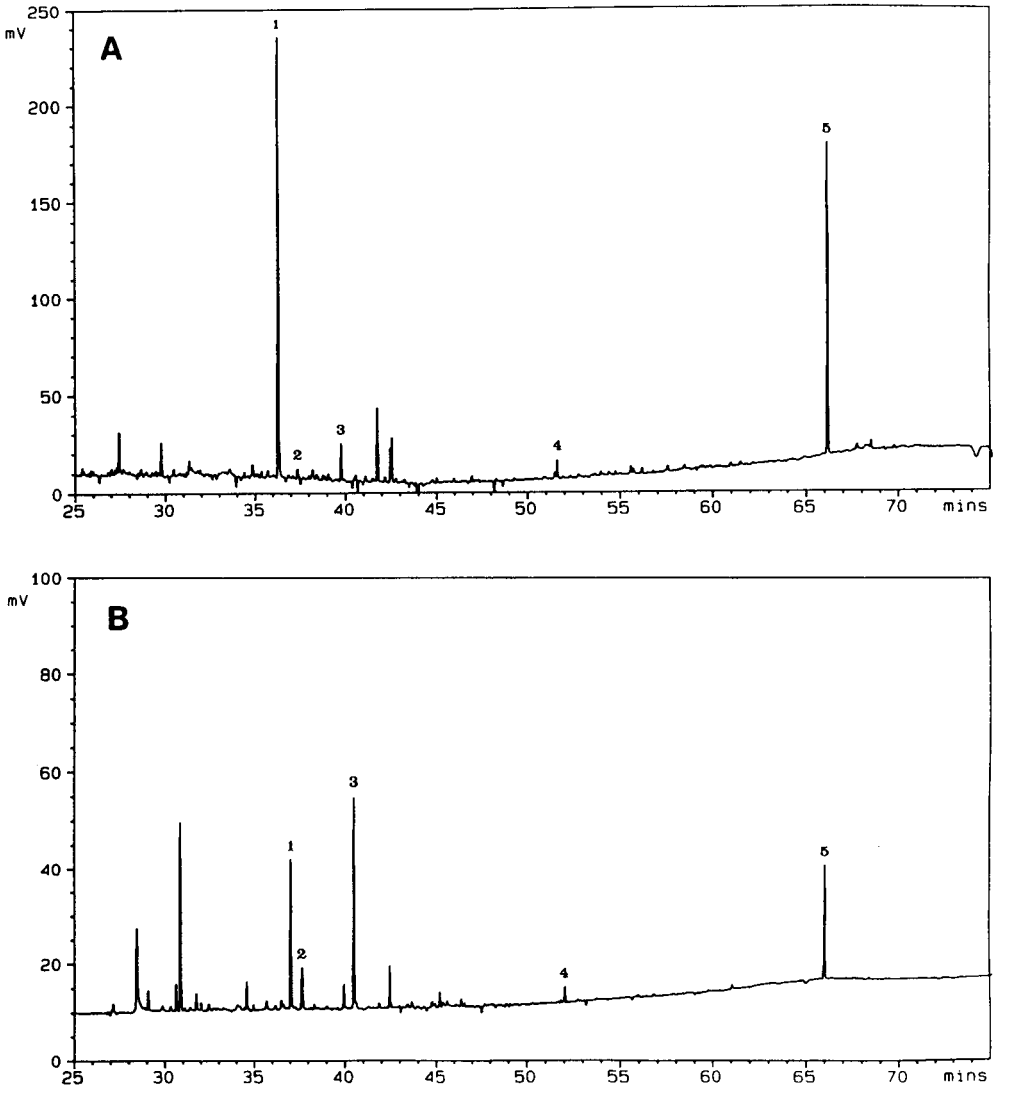

Fig. 4. Chromatograms of the pesticides fraction from particles (A) and water (B) extracts of one sample from the field experiment. Peaks 1–5 correspond to: (1) DCBE6, reference peak; (2) α-HCH; (3) γ-HCH; (4) dieldrin; (5) DCBE 16, reference peak and internal standard.

recovery and coefficient of variance (C.V.), was calculated for each spiking level. A one-way ANOVA method showed that only data for CB180 and dieldrin were significantly different at ($F = 4.26$), $p = 0.05$ (Table 4). For CB180 this reflected an anomalously low recovery from the lowest spike. The remaining CBs showed no significant "between-level" difference, which suggested that efficiency of extraction for these compounds was not dependent on concentration within the limits examined.

The overall mean recoveries of CBs ranged from 81 to 96%. For dieldrin the significant difference in recovery between levels may be due to

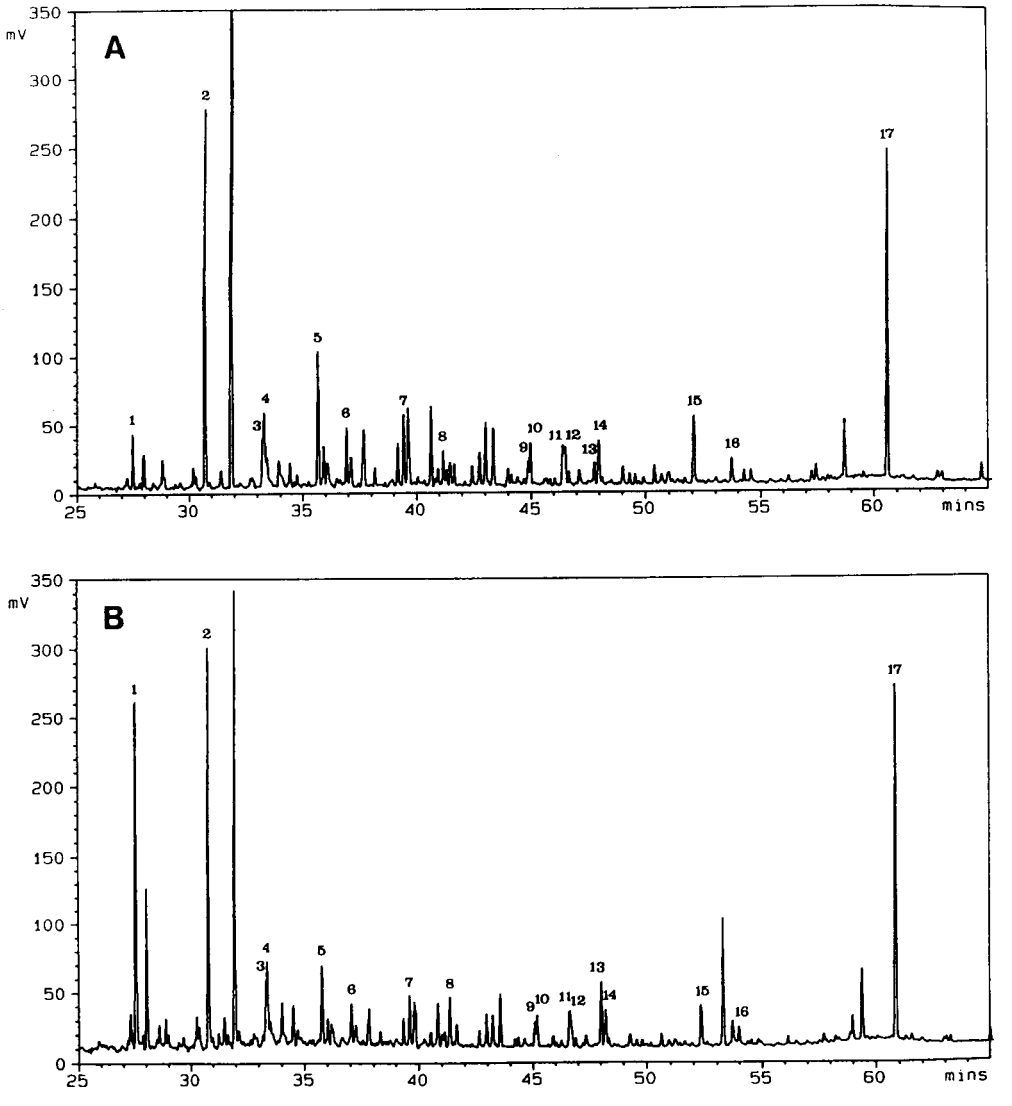

Fig. 5. Chromatograms of the PCBs and HCB fraction from the particulate (A) and water (B) extracts of one sample from the field experiment. The peaks corresponds to: (1) HCB; (2) DCBE 6, reference peak; (3) CB31; (4) CB28; (5) CB52; (6) CB44; (7) CB77; (8) CB101; (9) CB149; (10) CB118; (11) CB153; (12) CB105; (13) CB138; (14) CB158; (15) CB180; (16) CB170; (17) DCBE 16, reference peak and internal standard.

the contribution of the uncorrected background concentration increasing the estimated recovery at the lower spiking levels. The overall mean recoveries for the pesticides, excluding lindane and pentachlorophenol, ranged from 79 to 97%. Both γ-HCH and pentachlorophenol exhibited lower mean recoveries of 67 and 76% respectively. Although this may be related to the relatively higher water solubility of both these compounds of around 8 mg l^{-1} [30,35,36] other factors may also be involved. The recovery of PCP is comparable to that determined in the development of the analytical method for PCP [32]. The reported recovery of PCP from 100 ml spiked water was 79% with a coefficient of variance of 3.5%. This indicated that the present recovery of PCP from aqueous solution was reduced by the efficiency of the clean-up and derivatisation and not the initial solvent extraction step. The low mean recovery of γ-HCH was principally due to a very low recovery of 44% from the lowest spiking level. These recoveries were corrected for a background concentration of γ-HCH of 0.22 ng l^{-1}, which is comparable to that of the lowest spike. It is likely that this correction has biased the recovery figures.

The precision of the extraction and analysis of filtered sea water as expressed by the coefficient of variance (C.V.), ranged from 8 to 30% for all determinands (Table 4). The more water soluble PCP and γ-HCH had the highest variance. The C.V. for PCP of 26% was much higher than the 3.5% reported for the analytical method [32]. This reflects the loss in precision associated with measurement at lower concentrations and the influence of the sample matrix [37]. The mean C.V. for the CBs was 11% and for the pesticides with the exception of γ-HCH and PCP was 13%. These values are comparable to those obtained for short-term analytical variance from in-house quality control procedures. The mean C.V. for CBs and for pesticides for the analysis of a laboratory reference material (LRM) derived from sewage sludge contaminated marine sediment [37] (1 g) was 13 and 14%, respectively. Apart from the initial extraction step, the analytical methodology for this LRM is common to that for the water. Chromatograms of the pesticide and CB fractions of water and particulates obtained in the field by the PEFS system are illustrated in Fig. 4 and 5 respectively.

Conclusions

The efficiency of extraction of filtered sea water by PEFS has been shown to be independent of concentration over the range of 0.1 ng l^{-1} to 3 ng l^{-1} for CBs, pentachlorophenol and certain organochlorine pesticides, and is generally > 80%. Results from field trials have confirmed that the precision of the separation and analysis of the particulate phase is comparable to that of the aqueous phase. The system is successful in drastically reducing sample contamination, with blank levels being below the limit of determination (0.015 ng l^{-1}). The separation and clean-up methodology is suitable for GC-ECD determination with aqueous sample concentration factors up to 520 000.

The system can be readily deployed in the field and requires minimal laboratory support facilities. Sampling, processing and storage of particulate and water fractions are possible within 1.5 h, extensive post sampling treatment is not required.

The PEFS system appears suitable for the measurement of contaminant levels in estuarine and coastal waters. The high precision of the PEFS system and associated analytical methodology enable its use in the study of particle based partitioning processes.

The authors wish to thank the staff of the engineering workshop of the Marine Laboratory for valuable assistance in the construction of the system. The technical specifications of the containers (Fig. 2) were drawn by Brian Ritchie. The Spanish Ministerio de Educacion y Ciencia are thanked for financial support to IC during this study.

REFERENCES

1 S. Tanabe and R. Tatsukawa, in J.S. Waid (Ed.), PCBs and the Environment, Vol. 1, CRC Press, Boca Raton, FL, 1986, p. 143

2 G.C. Harding, Mar. Ecol. Prog. Ser., 33 (1986) 167.

3 G.R. Harvey, W.G. Steinhauer and J.M. Teal, Science, 180 (1973) 643.
4 D. Elder, Mar. Pollut. Bull., 7 (1976) 63.
5 G.R. Harvey and W.G. Stienhauer, J. Mar. Res., 34 (1976) 561.
6 R. Dawson and J.P. Riley, Estuarine Coastal Mar. Sci., 4 (1977) 55.
7 D.L. Elder and J.P. Villeneuve, Mar. Pollut. Bull., 8 (1977) 19.
8 S. Tanabe and R. Tatsukawa, J. Oceanogr. Soc. Jpn., 36 (1980) 217.
9 S. Tanabe, M. Kawano and R. Tatsukawa, Trans. Tokyo Univ. Fish., 5 (1982) 97.
10 S. Tanabe, R. Tatsukawa, M. Kawano and H. Hidaka, J. Oceanogr. Soc. Jpn., 38 (1982) 137.
11 J.J. Richard and G.A. Junk, Anal. Chem., 58 (1986) 723.
12 D.E. Schultz, G. Petrick and J.C. Duinker, Mar. Pollut. Bull., 19 (1988) 526.
13 J.A. Junk, J.J. Richard, M.D. Greiser, J.S. Fritz and G.V. Calder, J. Chromatogr., 99 (1974) 745.
14 W.E. May, S.N. Chesler, S.P. Cram, B.H. Gump, H.S. Hertz, D.P. Enagonia and S.M. Dyszel, J. Chromatogr. Sci., 13 (1975) 535.
15 J.P. Thorne and Y. Vandale, Int. J. Environ. Anal. Chem., 29 (1987) 95.
16 D.A. Hinckley and T.F. Bindleman, Environ. Sci. Technol., 23 (1989) 995.
17 J.L. Cox, Fish. Bull. US, 69 (1971) 443.
18 R. Van Zoest and G.T.M. Van Eck, Neth. J. Sea Res., 26 (1990) 89.
19 T.F. Bidleman and C.E. Olney, Science, 143 (1973) 516.
20 J.C. Duinker and M.T.J. Hillebrand, Neth. J. Sea Res., 13 (1979) 257.
21 H.R. Rodgers, B. Crathorne and T.M. Leatherland, Mar. Pollut. Bull., 20 (1989) 276.
22 M. Ahnoff and B. Josefsson, Anal. Chem., 46 (1974) 658.
23 S. Tanabe and R. Tatsukawa, J. Oceanogr. Soc. Jpn., 39 (1983) 53.
24 B.J. Brownawell and J.W. Farrington, Geochim. Cosmochim. Acta, 50 (1986) 157.
25 C.W. Carter and I.H. Suffet, Environ. Sci Technol., 16 (1982) 735.
26 C.G. Yin and J.P. Hassett, Environ. Sci. Technol., 20 (1986) 1213.
27 P.F. Landrum, S.R. Nikart, B.J. Eadie and W.S. Gardner, Environ, Sci. Technol., 18 (1984) 187.
28 G. Liebezeit, in Biogeochemistry and Distribution of Suspended Matter in the North Sea and Implications to Fisheries Biology. Mitt. Biol.-Palaont. Inst. Hamburg, SCOPE/UNEP. Sonderbd., 65 (1988) 153.
29 J.F. Pankow and S.W. McKenzie, Environ. Sci. Technol., 25 (1991) 2046.
30 C.T. Chiou, H.U. Freed, D.W. Schmedding and R.L. Kohnert, Environ. Sci. Technol., 11 (1977) 475.
31 C.T. Chiou, R.L. Malcolm, T.I. Brintopn and D.E. Kile, Environ. Sci. Techol., 20 (1986) 1231.
32 I. Cruz and D.W. Wells, Int. J. Environ. Anal. Chem., 48 (1992) 101.
33 D.E. Wells, A.E. Cowan and A.E.G. Christie, J. Chromatogr., 328 (1985) 372.
34 J.C. Duinker, D.E. Schultz and G. Petrick, Mar. Pollut. Bull., 19 (1988) 19.
35 L. Weil, G. Dure and K.E. Quentin, Z. Wasser Abwasser Forsch., 7 (1974) 169.
36 R. Haque and A. Schemedding, Bull. Environ. Contam. Toxicol., 14 (1975) 13.
37 D.E. Wells and A.G. Kelly, Microchim. Acta, III (1991) 23.
38 I. Cruz, PhD Thesis, University of Aberdeen, 1992.

Analytica Chimica Acta, 276 (1993) 15–23
Elsevier Science Publishers B.V., Amsterdam

Determination and degradation study of chlorothalonil residues in cucumbers, peppers and cherry tomatoes

A. Valverde-Garcia, E. Gonzalez-Pradas, A. Aguilera-Del Real and M.D. Ureña-Amate

Departamento de Química Inorgánica, Universidad de Granada, Campus de Almería, 04071 Almería (Spain)

F. Camacho-Ferre

Campos de Nijar SA, Almería (Spain)

(Received 28th September 1992; revised manuscript received 19th November 1992)

Abstract

Residue levels and degradation rates of chlorothalonil in cucumbers, peppers and cherry tomatoes grown in commercial greenhouses (Almería, Spain) were studied. Chlorothalonil residues were extracted by the Mills method, analysed by gas chromatography with electron-capture detection and confirmed by gas chromatography–mass spectrometry. The recoveries of chlorothalonil were determined at three different fortification levels, the average values being greater than 80% with standard deviations less than 8% in all instances. The limit of quantification was 0.01 mg kg^{-1} for all vegetables. Statistical interpretation of residue levels in the plantations was done assuming a pseudo-first-order reaction for the degradation behaviour of chlorothalonil residues. The half-life periods were 5.3 days for cucumbers, 7.3 days for peppers and 11.5 days for cherry tomatoes.

Keywords: Gas chromatography; Gas chromatography–mass spectrometry; Chlorothalonil; Fungicides; Pesticides; Vegetables

Chlorothalonil (tetrachloroisophthalonitrile) is a non-systemic fungicide effective against a broad range of plant pathogens attacking many agronomic and vegetable crops. It was introducted by Diamond Alkali with the trade names Bravo, Daconil and Exotherm Termil [1], and its fungicidal properties were first described by Turner [2].

Chlorothalonil is now used extensively worldwide, and its residues have been commonly found in a great variety of vegetables by national administration responsible for food control, such as the US Food and Drug Administration (FDA) [3] and the National Food Administation of Sweden (NFA) in Europe [4].

Although several specific analytical methods have been described for chlorothalonil [5], residues of this pesticide in fruits and vegetables are usually determined by applying multi-residue procedures [5]. According to the review by Ambrus and Thier [6], in which the applicability of seven well established multi-residue procedures is critically assessed, residues of chlorothalonil are well recovered from vegetables with different procedures such as the Luke method [7,8] and its modifications [6]. Nevertheless, there are no data for this pesticide using the Mills extraction procedure [9].

The Luke method, which uses extraction with

Correspondence to: A. Valverde-Garcia, Departamento de Química Inorgánica, Universidad de Granada, Campus de Almería, 04071-Almería (Spain).

acetone and partitioning with light petroleum and dichloromethane, is nowadays the method most often used for chlorothalonil residues in vegetables, this being the AOAC general multi-residue method for organochlorine and organophosphorus pesticides [10]. However, a rapid one-step extraction method, which uses only extraction with ethyl acetate and sodium sulphate [11], has recently been tested for potential use as a multi-residue procedure, and the results obtained were very promising [12,13]; in fact, this method is already used in the Swedish NFA monitoring of pesticide residues, including chlorothalonil [4].

The objectives of this work were to study the use of the Mills multi-residue method for the extraction of chlorothalonil residues from cucumbers, peppers and cherry tomatoes, and to determine the characteristic degradation parameters of chlorothalonil residues on these vegetables grown in commercial greenhouses in Almería (Spain). A knowledge of these parameters is important, because in Almería there are about 38000 Ha of greenhouses where about 400000 metric ton (Tm) of vegetables are produced yearly for exportation (33% peppers, 17% cucumbers, 11% tomatoes).

EXPERIMENTAL

Apparatus

A Perkin-Elmer Model 8700 gas chromatograph equipped with an electron-capture detector and 5% SE-30 on Chromosorb W HP (80–100 mesh packed column (2 m × 1/8 in i.d.) was used for determinations. A Hewlett-Packard HP-5971 gas chromatograph–mass selective detector equipped with an HP-Ultra 2 fused-silica capillary column (25 m × 0.2 mm i.d.; 0.33 μm film thickness) and an HP-7673 Autosampler, was used for confirmation purposes.

Chemicals

Standard Pestanal chlorothalonil (purity > 99%) was obtained from Riedel-de Haën (Seelze, Germany). All solvents (pesticide residue grade) were obtained from Merck (Darmstadt, Germany). Chlorothalonil standard solutions for gas chromatographic analysis with electron-capture detection (GC–EQ) were prepared using light petroleum as solvent, whereas cyclohexane was used in the standard solutions for gas chromatographic–mass spectrometric (GC–MS) confirmation.

Extraction procedure and recovery study

Extraction of chlorothalonil residues from peppers, cucumbers and cherry tomatoes was carried out according to the Mills procedure [9,14] without a Florisil clean-up step. A brief description of the procedure is as follows. Weigh 100 g of chopped sample into a high-speed blender jar, add 200 ml of acetonitrile, blend the mixture for 2 min and filter through a 12-cm Büchner funnel. Transfer the filtrate into a 1000-ml separating funnel, add 100 ml of light petroleum and shake vigorously for 2 min. Add 10 ml of saturated NaCl solution and 600 ml of water and mix thoroughly. Discard the aqueous layer and wash the solvent layer with two successive 100-ml portions of water. Filter the light petroleum layer through 10 g of anhydrous sodium sulphate and rinse the filter with 10 ml of light petroleum. Evaporate the light petroleum sample extract to 1–2 ml using a vacuum rotary evaporator (40°C water-bath) and dilute to exactly 10 ml with light petroleum in a volumetric flask. In all instances it was assumed that this extract contained 10 g sample ml^{-1}.

The chlorothalonil recovery study was carried out by fortifying fresh pepper, cucumber and cherry tomato samples grown in commercial greenhouses (Campos de Níjar, Almería, Spain), which had not been treated with the pesticide studied. As chlorothalonil is a non-systemic and water-insoluble pesticide that is administered by foliar application, the fortification process of plant tissue was carried as follows: 5 ml of a light petroleum standard solution of chlorothalonil were added to 100 g of chopped sample in a high-speed blender jar. After evaporation of the light petroleum by an air stream (see Fig. 1), the sample was homogenized for 2 min. After 30 min, the sample was again homogenized for 1 min and immediately analysed. Recoveries were calculated at three different fortification levels, 0.51,

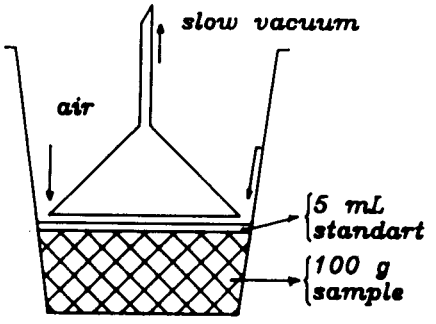

Fig. 1. Fortification process of plant tissue.

0.10 and 0.01 mg kg^{-1}, values corresponding to concentrations of chlorothalonil in the added solution of 10.2, 2.0 and 0.2 mg l^{-1}, respectively. Three replicates at each fortification level and three check samples of each vegetable were analysed.

Analysis by GC–ECD

Chlorothalonil in the light petroleum sample extracts was determined by GC–ECD using the SE-30 packed column and the following operating conditions: oven temperature, 200°C; injector temperature, 250°C; detector temperature, 350°C; carrier gas (nitrogen) flow-rate, 20 ml min^{-1}; make-up gas (nitrogen) flow-rate, 40 ml min^{-1}; and injection volume, 1 μl.

Residue confirmation by GC–MS

Confirmation of chlorothalonil residues was carried out by GC–MS using the Ultra 2 fused-silica capillary column and the following operat-

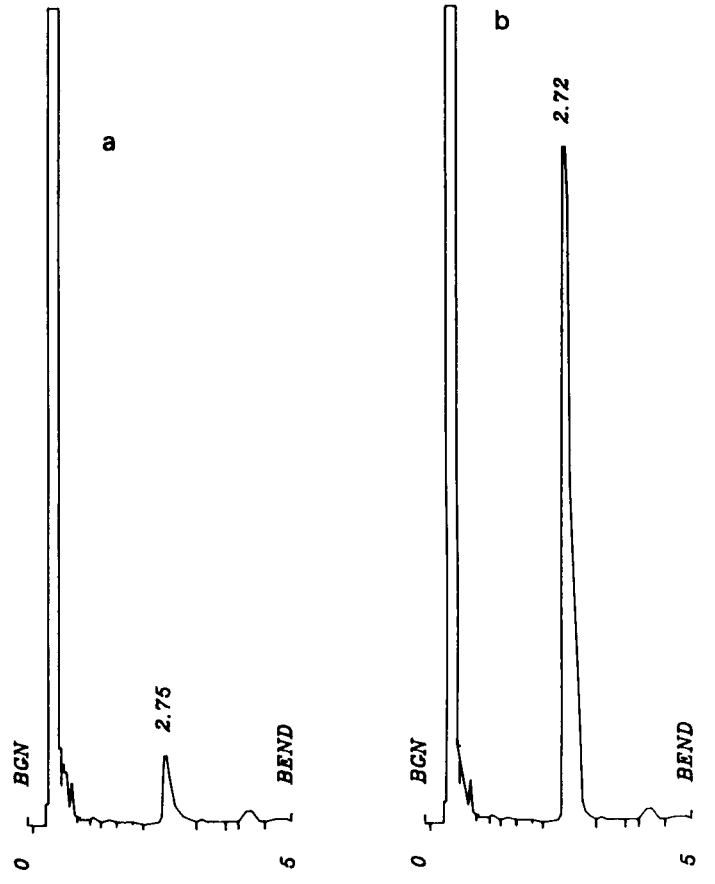

Fig. 2. GC–ECD traces corresponding to two standard solutions of chlorothalonil: (a) 0.05; (b) 0.50 mg l^{-1}.

ing conditions: oven temperature programme, 55°C (1 min), heated at 40°C min^{-1} to 140°C (1 min), then at 5°C min^{-1} to 260°C (6 min); injector temperature, 280°C; detector temperature, 280°C; carrier gas (helium) flow-rate, 1 ml min^{-1}; split flow-rate, 20 ml min^{-1}; splitless time, 0.5 min; injection volume, 5 μl; mass range (total ion current scan), m/z 40–400; and selected ion monitoring, m/z 266.

Sample extracts for confirmation were obtained as follows: 5 ml of the light petroleum sample extract were evaporated to dryness on a vacuum rotary evaporator using a 40°C water-bath and the residue was dissolved in exactly 5 ml of cyclohexane.

Degradation study

Degradation experiments were conducted in three greenhouses (pepper, 0.52 Ha, 17500 plants Ha^{-1}; cucumber, 0.55 Ha, 16000 plants Ha^{-1}; tomato, 0.38 Ha, 20000 plants Ha^{-1}) belonging to Campos de Níjar and located in Níjar, 40 km northeast of Almería (Spain).

Pepper (variety Mazurca), cucumber (variety Brunex) and tomato (variety Cheresita) plants, receiving routine horticultural treatment, were sprayed with Bravo 50 (50% chlorothalonil) at a dose of 3 ml l^{-1} and consumptions of 845 l Ha^{-1} (pepper), 770 l Ha^{-1} (cucumber) and 615 l Ha^{-1} (cherry tomato). The treatment date was 28th October 1991.

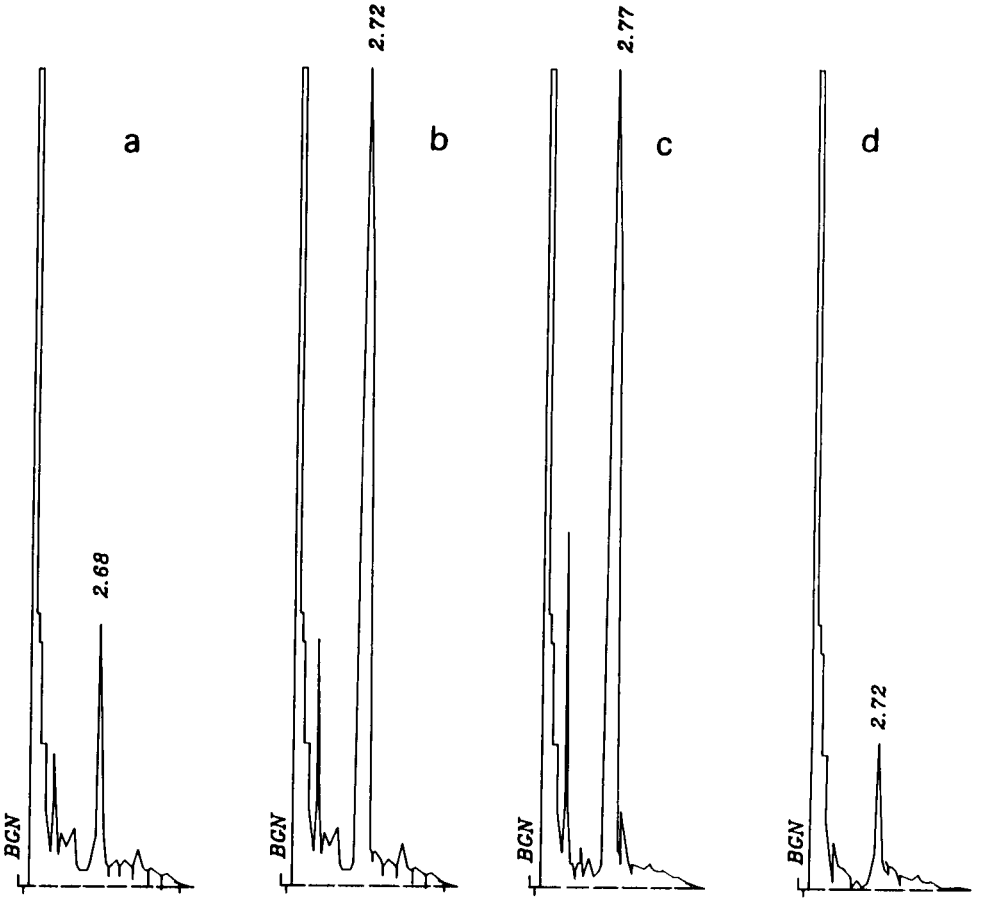

Fig. 3. GC–ECD traces corresponding to three extract samples of the degradation study: (a) pepper sample (t = 38 days, R = 0.02 mg kg^{-1}); (b) tomato sample (t = 22 days, R = 0.10 mg kg^{-1}); (c) cucumber sample (t = 1 days, R = 0.13 mg kg^{-1}); (d) the same extract sample as in (c) but diluted tenfold.

For each vegetable, three samples were collected at random from a sampling plot of 200 m^2 at 1, 3, 7, 14, 22 and 38 days after application. The samples consisted of 15–20 pieces of peppers (160–180 g per piece), 10 pieces of cucumbers (400–500 g per piece) and 60–70 pieces of cherry tomatoes (7–9 g per piece). As soon as the samples had been picked, they were transferred to the laboratory where they were chopped and blended. The blends were thoroughly mixed and three subsamples (100 g of each) were weighed into polyethylene bags and kept deep-frozen until extraction.

RESULTS AND DISCUSSION

Figure 2 shows the chromatograms obtained by GC–ECD corresponding to chlorothalonil standard solutions of 0.05 and 0.5 mg l^{-1}. The retention time of chlorothalonil was 2.72 ± 0.05 min. The detector response was linear for the

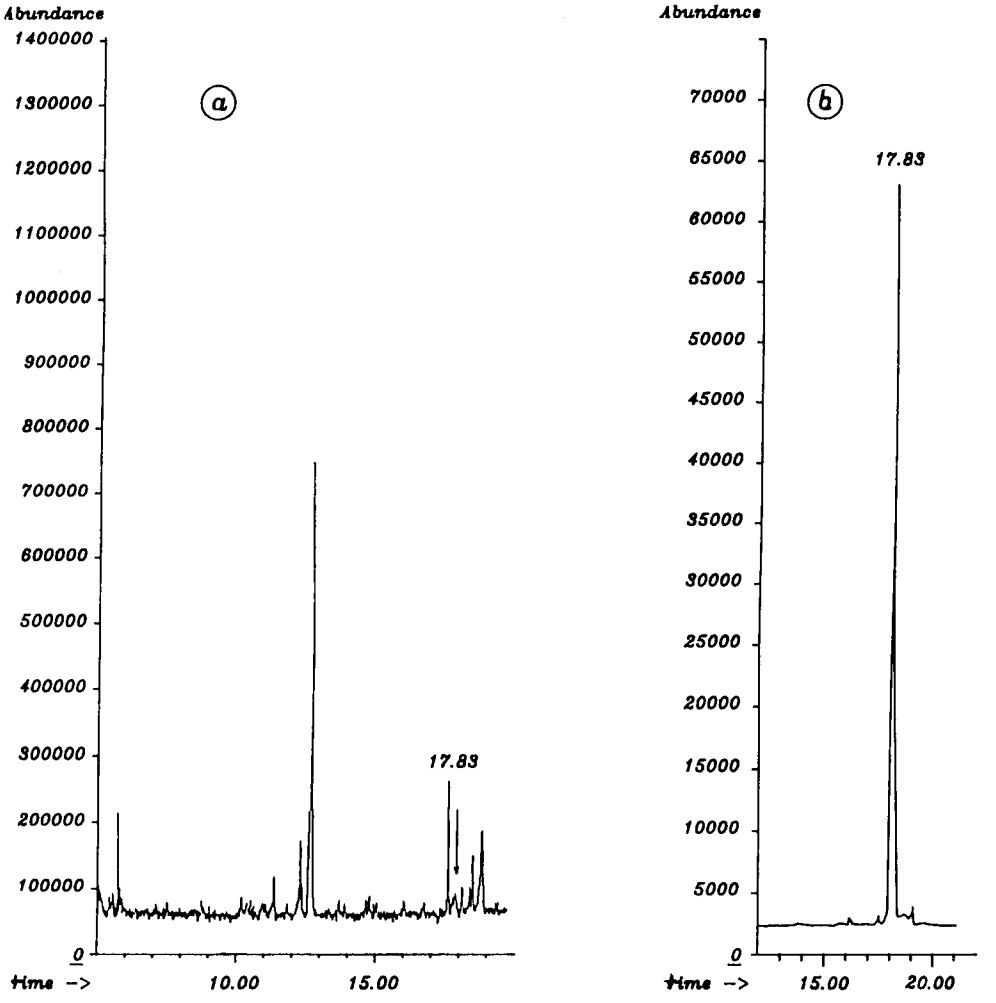

Fig. 4. GC–MS total ion current traces corresponding to the cucumber sample for which the GC–ECD trace is shown in Fig. 3c: (a) scan mode; (b) SIM mode.

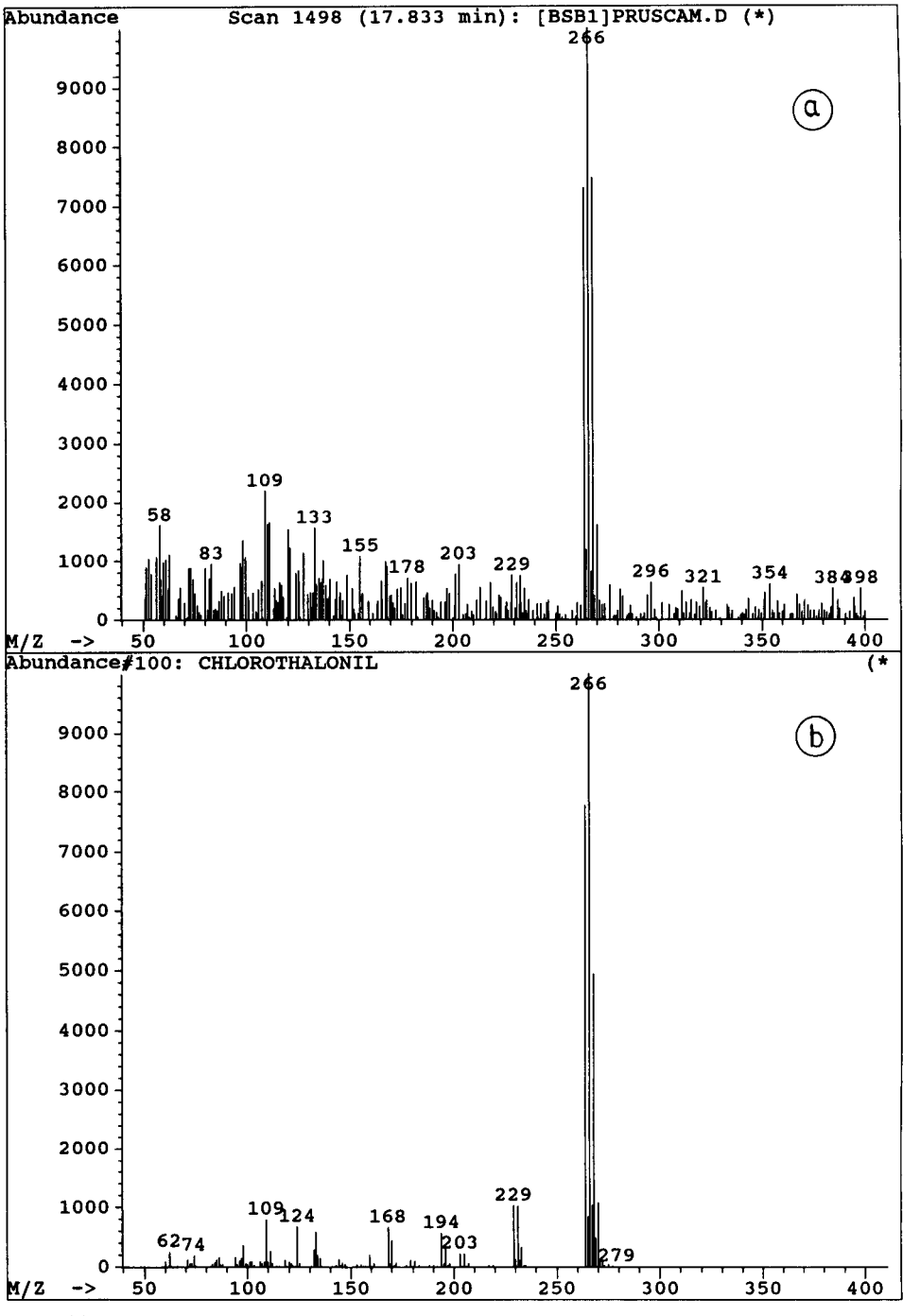

Fig. 5. (a) Mass spectrum obtained at 17.833 min from the total ion current scan chromatogram in Fig. 4a; (b) library match for chlorothalonil.

TABLE 1

Chlorothalonil recoveries in pepper, cucumber and cherry tomato

Fortification level (mg kg^{-1})	Mean recovery ± S.D. (%) [a]		
	Pepper	Cucumber	Tomato
0.51	89.3 ± 2.9	90.4 ± 5.3	82.4 ± 3.6
0.10	92.7 ± 6.4	89.2 ± 2.6	91.2 ± 6.4
0.01	98.5 ± 8.0	90.0 ± 1.4	91.0 ± 2.4

[a] Averages of three replicate determinations.

range 0.05–1.0 ng of chlorothalonil and the ECD sensitivity was about 1.5×10^5 peak height per nanogram. The relative retention time and relative response factor (for 1.0 ng) of chlorothalonil will respect to chlorpyrifos (a pesticide normally used for expressing relative chromatographic parameters) were 0.58 and 0.93, respectively.

Table 1 shows the average recoveries of chlorothalonil from pepper, cucumber and cherry tomato at the three fortification levels studied. In all instances the average recoveries were greater than 80% with standard deviations less than 8%. These values are generally considered satisfactory for residue determinations [6], and they are comparable to chlorothalonil recoveries obtained from different vegetables by using the Luke multi-residue extraction method and its modifications [6,8,15].

The limit of quantification (LOQ) of the method for chlorothalonil was calculated to be 0.01 mg kg^{-1} for all three vegetables (the lowest concentration actually tested and validated [13]).

TABLE 2

Residues of chlorothalonil on pepper, cucumber and tomato at various times after application

Time (days)	Residual concentration ± S.D. (mg kg^{-1}) [a]		
	Pepper	Cucumber	Tomato
1	0.33 ± 0.09	0.15 ± 0.05	0.45 ± 0.11
3	0.24 ± 0.07	0.09 ± 0.02	0.43 ± 0.10
7	0.24 ± 0.04	0.09 ± 0.03	0.26 ± 0.04
14	0.11 ± 0.04	0.02 ± 0.01	0.24 ± 0.06
22	0.05 ± 0.02	0.01 ± 0.00	0.11 ± 0.03
38	0.01 ± 0.01	–	0.05 ± 0.01

[a] The reported values are the means of triplicate analyses from three replicates.

Figure 3 shows the GC–ECD traces corresponding to the degradation study for a sample of pepper, cucumber and cherry tomato. The retention time of chlorothalonil under the GC–MS conditions was 17.83 ± 0.01 min. Fig. 4 shows the GC–MS total ion current traces [scan mode and selected ion monitoring (SIM) modes] for the cucumber sample for which the GC–ECD trace is shown in Fig. 3c. Fig. 5 shows the mass spectrum of the cucumber sample at 17.833 min from the total ion current chromatogram in Fig. 4a, with a library match for chlorothalonil.

The residue data obtained in the degradation study of chlorothalonil on pepper, cucumber and cherry tomato are summarized in Table 2. These data were subjected to statistical analysis by the method of Timme and Frehse [16], who assumed that the degradation behaviour of pesticide

TABLE 3

Statistical parameters corresponding to the degradation study

Parameter	Mean (± C.I.) [a]		
	Cucumber	Pepper	Tomato
K (days^{-1})	0.13 (±0.05)	0.09 (±0.01)	0.06 (±0.02)
R_0 (mg kg^{-1})	0.16 (+0.14/−0.07)	0.38 (+0.11/−0.08)	0.47 (+0.20/−0.14)
r^2	0.9576	0.9903	0.9764
D	0.100	0.184	0.167
$t_{1/2}$ (days)	5.28 (±1.94)	7.34 (±1.00)	11.53 (±3.50)
$t_{1/10}$ (days)	17.54 (±6.44)	24.39 (±3.33)	38.29 (±11.58)
R_{15} (mg kg^{-1})	0.02 (+0.02/−0.01)	0.09 (+0.02/−0.01)	0.19 (+0.05/−0.04)

[a] Confidence intervals at a level of significance of 95% ($p = 0.05$).

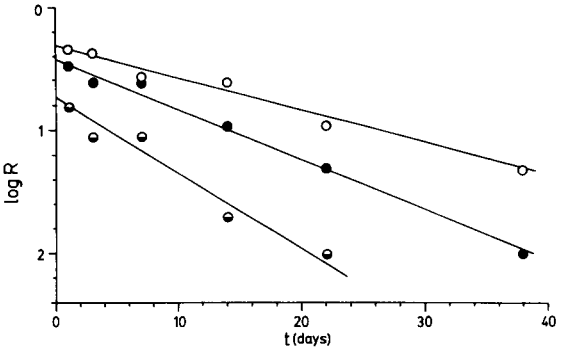

Fig. 6. Degradation of chlorothalonil on (●) pepper, (◒) cucumber and (○) cherry tomato.

TABLE 4

Chlorothalonil maximum residue levels (MRLs) established by the Codex Alimentarius and in different European countries

Country	MRL (mg kg^{-1})		
	Pepper	Cucumber	Tomato
Spain	0.01	0.01	1.00
Italy	3.50	3.50	3.50
Finland	0.50	0.50	0.50
Sweden	1.00	1.00	1.00
Germany	0.02	0.02	0.02
EEC	–	5.00	5.00
Codex Alimentarius	10.00	5.00	5.00

residues can be described mathematically as a pseudo-first-order reaction:

$$dR/dt = KR$$

or, by integration and using common logarithms

$$\log R = \log R_0 - 0.434Kt$$

where R is the residue level at t days after pesticide application, R_0 is the residue level at time $t = 0$ and K is the degradation rate constant.

According to the above, the logarithms of residue values in Table 2 were plotted versus time (Fig. 6). The straight lines that best fit the measured values were computed by regression analysis, and the parameters given in Table 3 were obtained.

The coefficient of determination (r^2) and test quantity for correlation (D) values confirm that the degradation behaviour of chlorothalonil on pepper, cucumber and tomato can be described as a pseudo-first-order reaction under the experimental conditions studied. The half-life periods ($T_{1/2}$) were 5.3 days (cucumber), 7.3 days (pepper) and 11.5 days (cherry tomato), this order being similar to that of the surface/weight ratio of the vegetables (cucumber < pepper < cherry tomato). The tenth-life period ($t_{1/10}$) varied between 17.5 and 38.3 days, indicating that even after the safety interval or preharvest time, which is 15 days for chlorothalonil [17], the presence of residues is to be expected in the three plantations. Finally, according to the maximum residue levels given in Table 4 [18], it is interesting that the chlorothalonil residue levels in peppers and cucumbers at the preharvest time (R_{15}) were higher than the maximum residue levels (MRLs) established by Spanish legislation, although in all instances the residue levels found throughout the degradation study were lower than the Codex Alimentarius MRLs and than those established in many European countries.

The authors thank J. Herrera de Pablo (Ministerio de Agricultura, Delegación de Almería, Spain) and F. Montoya (Campos de Níjar SA) for their collaboration in this work, which was supported by the CICYT, Project ALI89-0020.

REFERENCES

1 US Pat., 3 290 353 and 3 331 735.
2 N.J. Turner, Contrib. Boyce Thompson Inst., 22 (1964) 303.
3 M.A. Luke, H.T. Masumoto, T. Cairms and H.K. Hundley, J. Assoc. Off. Anal. Chem., 71 (1988) 415.
4 A. Andersson and T. Bergh, Fresnius' J. Anal. Chem., 339 (1991) 387.
5 C.R. Worthing (Ed.), The Pesticide Manual, British Crop Protection Council, Croydon, 9th edn., 1991.
6 A. Ambrus and H.P. Thier, Pure Appl. Chem., 58 (1986) 1035.
7 M.A. Luke, J.E. Froberg and H.T. Masumoto, J. Assoc. Off. Anal. Chem., 58 (1975) 1020.
8 M.A. Luke, J.E. Froberg, G.M. Dosse and H.T. Masumoto, J. Assoc. Off. Anal. Chem., 64 (1981) 1187.

9 P.A. Mills, J.H. Onley and R.A. Gaither, J. Assoc. Off. Anal. Chem., 46 (1963) 186.
10 Official Methods of Analysis of the Association of Official Analytical Chemists, AOAC Arlington, VA, 14th edn., 1990.
11 J.B. Leary, J. Assoc. Off. Anal. Chem., 54 (1971) 1396.
12 A. Andersson and H. Palsheden, Fresenius' J. Anal. Chem., 339 (1991) 365.
13 A. Valverde-García, E. González-Pradas, J. Martínez-Vidal and A. Agüera-López, J. Agric. Food Chem., 39 (1991) 2188.
14 A. Valverde-García and E. González-Pradas, Análisis de Residuos de Plaguicidas: Métodos de Extracción, Instituto de Estudios Almerienses, Almería, 1989.
15 A. Andersson and B. Ohlin, Var Föda, 38 (1986) 79.
16 G. Timme and H. Frehse, Pflanzenschutz-Nachr., 33 (1980) 47.
17 C. de Liñan, Vademecum de Productos Fitosanitarios y Nutricionales, Carlos de Liñan y Vicente, Madrid, 1990.
18 M. Contreras and A. Agüera, Plaguicidas Agrícolas: Recopilación de Propiedades y LMRs, Coexphal, Almería, 1991.

Analytica Chimica Acta, 276 (1993) 25–32
Elsevier Science Publishers B.V., Amsterdam

Determination of nitrate in natural waters with the photo-induced conversion of nitrate to nitrite

Kazuhiko Takeda and Kitao Fujiwara

Faculty of Integrated Arts and Sciences, Hiroshima University, Higashisenda-machi, Hiroshima 730 (Japan)

(Received 14th August 1992; revised manuscript received 16th November 1992)

Abstract

A rapid, sensitive and maintenance-free method for the determination of nitrate ion using the photo-induced conversion of nitrate to nitrite is described. A flow-injection system, equipped with a spectrophotometric detector and a UV irradiation coil cell in which nitrate ion was reduced to nitrite ion, was developed and tested for river and sea waters. With this flow system, the signal intensity depended strongly on the pH of the carrier solution. The detection limit for nitrate was ca. 0.05 μM and ten samples could be determined per hour. The method permitted the determination of nitrate without a copperized cadmium column.

Keywords: Flow injection; UV–Visible spectrophotometry; Nitrate; Waters

The determination of nitrate ion in natural waters is important in environmental and marine chemistry, as it is one of the nutrient species limiting the amount of biomass. Many methods have been proposed for the determination of nitrate [1–9]. For example, ion chromatography has sometimes been employed for environmental samples [9]. However, the use of ion chromatography is restricted by its insufficient sensitivity and the requirement to reduce the salinity in the sample, which imposes difficulties in the practical analysis of samples containing abundant electrolytes, such as sea water. A major detection method for nitrate in natural waters including sea water, lake water and rain water is spectrophotometry [1–5]. In most spectrophotometric measurements of nitrate, reduction of nitrate to nitrite is involved, i.e., after producing nitrite by the reduction of nitrate, nitrite is converted into an azo dye coupled with aromatic amines. As this method gives stable colour development with high sensitivity, not only NO_3^- in natural waters but also NO_x in air is measured. A more sensitive fluorimetric method using the formation of a fluorescent azoic acid salt has been reported [6,7], in which reduction of nitrate to nitrite is also necessary.

Production of nitrite from nitrate was generally carried out by passing the sample solution through a copperized cadmium column. Many commercial columns are available. However, this procedure leads to many problems with the measurement. The copperized cadmium column needs washing and preconditioning with buffer and/or EDTA solutions to sustain a high reduction activity for nitrate. Also, incorporation of air in the solution removes the activity from the column. Further, the solutions eluted from the copperized cadmium column contain cadmium and copper, which must be eliminated before discharge. In addition, phosphate ion sometimes suppresses the reduction activity of the column [10].

Correspondence to: K. Fujiwara, Faculty of Integrated Arts and Sciences, Hiroshima University, Higashisenda-machi, Hiroshima 730 (Japan).

Nitrate ion in aqueous solution provides strong ultraviolet (UV) absorption with a maximum at 200 nm and a weak absorption with a maximum at 300 nm. Nitrite ion and oxygen are formed by means of photo-excitation at 200 and/or 300 nm in aqueous nitrate solution [11,12]. Wargner et al. [13] studied the dissociation kinetics of the flash photolysis in aqueous nitrate solution. They reported that overall reaction was the photo-induced decomposition of nitric acid according to $NO_3^- \rightarrow NO_2^- + 1/2O_2$.

In this paper, the determination of nitrate without the use of a copperized cadmium column, by using the photo-induced reduction of nitrate to nitrite, is described. A flow-injection analysis (FIA) system, equipped with a UV irradiation coil cell (UV-coil cell) and a spectrophotometric detector, was developed and applied to the determination of nitrate in sea and river waters.

EXPERIMENTAL

Apparatus

A schematic illustration of the FIA system used is shown in Fig. 1. A plunger pump (Shimadzu LC-3A) was used to propel the carrier solution (CS). The CS was phosphate buffer solution or distilled water. Samples were injected via a port (Rheodyne Model 7125) with a 1-ml sampling loop. The sample injected into the carrier stream flowed into a UV-coil cell made from a quartz glass tube.

Three types of UV-coil cells were tested (Fig. 2a–c). The type A and B UV-coil cells were formed as a single quartz coil. Type C was a triply

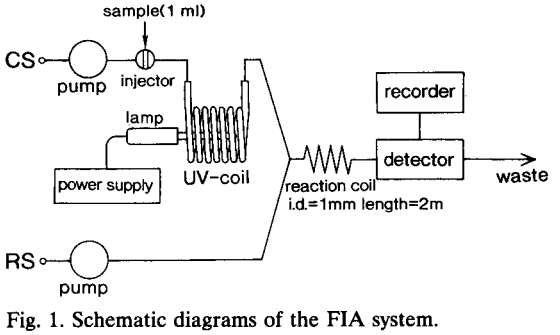

Fig. 1. Schematic diagrams of the FIA system.

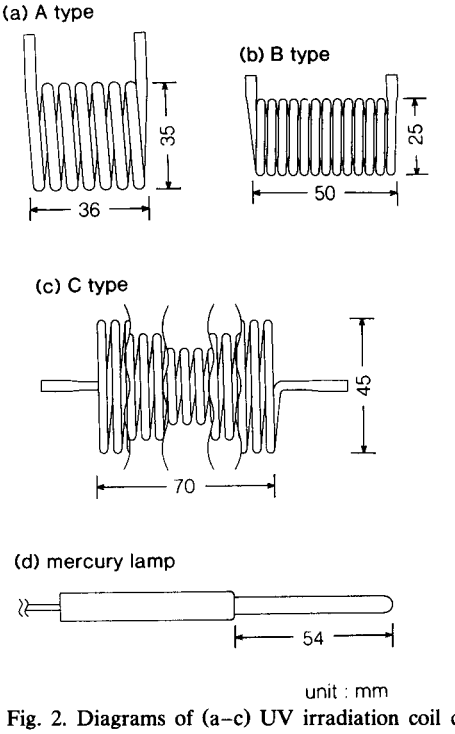

Fig. 2. Diagrams of (a–c) UV irradiation coil cells (UV-coil cells) and (d) low-pressure mercury lamp. The dimensions of the quartz glass tubes are 1.5–2.0 mm i.d. and 3.0 mm o.d. for type B and C cells and are 2.5–3.0 mm i.d. and 4.0 mm o.d. for the type A cell.

coiled quartz coil in order to increase the residence time of the sample solution in the UV-coil cell. The i.d. of the quartz tube was 1.5–2.0 mm for types B and C and 2.5–3.0 mm for type A. The total volumes of the cells were 3.6, 2.5 and 9.9 ml for type A, B and C, respectively. The estimated residence times of solutions were 1.8, 1.25 and 4.95 min for the type A, B and C cells, respectively, at a CS flow-rate of 2.0 ml min^{-1}. A low pressure mercury lamp, illustrated in Fig. 2d, was mounted in the centre of the UV-coil cell. This lamp is commonly called a "pen ray lamp", and is generally used for calibration of spectrophotometers. The power of the lamp was about 5 W.

The reagent solution (RS), containing 1.9 mM *N*-1-naphthylethylenediamine, 29 mM sulphanilamide and 0.6 M HCl, was propelled by a plunger pump (Sanuki Kogyo, DMX-2300) to a reaction coil which was kept at room temperature. The

absorbance of the solution was monitored at 540 nm by a Jasco 870-UV spectrophotometer and the peak height of the absorbance was taken as the signal intensity.

Reagents

N-1-Naphthylethylenediamine dihydrochloride and sulphanilamide were purchased from Nacalai Tesque and used as received.

Nitrate and nitrite stock standard solutions (10 mM) were prepared from analytical-reagent grade sodium nitrate and sodium nitrite, respectively, which were dried at 100–110°C before weighing. To construct calibration graphs, working standard solutions were freshly prepared from the stock standard solutions. Standard solutions diluted with filtered surface sea water (FSW) collected from the Pacific Ocean were also employed for the analysis of sea water. It was confirmed that the concentrations of nitrate and nitrite in the FSW were less than 0.1 μM.

RESULTS AND DISCUSSION

Photo-reduction of nitrate to nitrite

The absorption spectrum for NO_3^- and emission lines for the mercury lamp are shown in Fig. 3. The locations of the emission lines from the mercury lamp overlap with the absorption band of nitrate around 300 nm. Assuming that reduction of NO_3^- to NO_2^- is promoted by the excitation of NO_3^- with 300-nm light, the low-pressure mercury lamp used in the proposed method is advantageous for the photo-induced reduction of nitrate to nitrite.

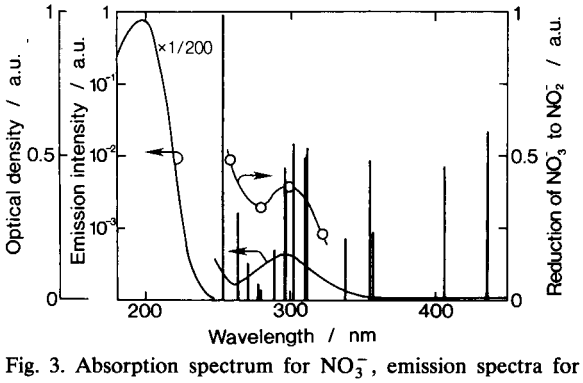

Fig. 3. Absorption spectrum for NO_3^-, emission spectra for the mercury lamp and action spectrum for photo-induced reduction of nitrate to nitrite.

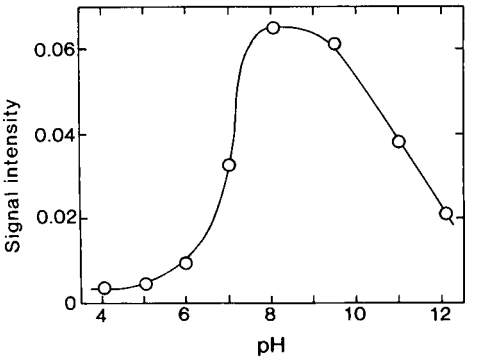

Fig. 4. Dependence of the signal intensity on the pH of the CS solution. The concentration of nitrate was 10 μM and phosphate buffer was used as the CS solution.

An action spectrum for the photo-induced reduction of nitrate to nitrite is partly shown in Fig. 3. This action spectrum was obtained in the following manner: the RS mentioned previously was added to aqueous nitrate solution after the solution had been irradiated with monochromatic light for 10 min, and the absorbance was measured at 540 nm. The action spectrum in the range 260–320 nm was obtained: it is difficult to measure the reduction rate of NO_3^- to NO_2^- at wavelengths shorter than 260 nm owing to the decrease in the irradiation power of the light source. It was confirmed that the rate of production of NO_2^- by irradiation at wavelengths longer than 320 nm light is negligibly small. The action spectrum for photo-induced reduction is similar to the absorption band of aqueous nitrate solution, indicating that the irradiation at 300 nm of NO_3^- solution is effective for generating NO_2^- ions.

Optimization of measurement conditions

When the CS is phosphate buffer, the signal intensity shows a strong dependence on the pH of the CS, as shown in Fig. 4 (the type B UV-coil cell was employed). The maximum signal intensity is given at pH 8, where the conversion efficiency of nitrate to nitrite is about 50%. Shuali et al. [12] investigated the yield of nitrite production by the photolysis of aqueous nitrate solution, and

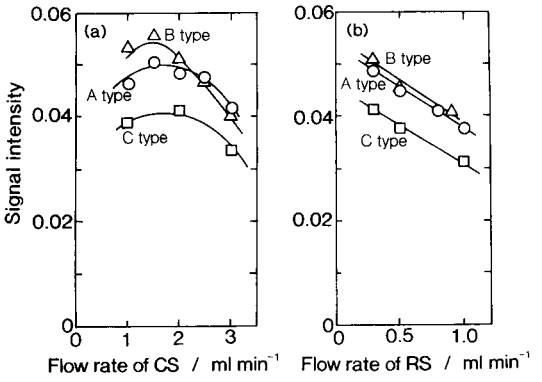

Fig. 5. Plots of the signal intensity vs. flow-rate of (a) CS (RS at 0.3 ml min^{-1}) and (b) RS (CS at 2.0 ml min^{-1}) with various UV-coil cells, where the CS is phosphate buffer adjusted to pH 8.0. The concentration of nitrate measured was 10 μM.

found that the yield of nitrite production is low at low pH and increases with an increase in pH in the range 6–10, reaching a constant value above pH 10. Up to pH 9, the pH dependence of the signal intensity is similar to the yield of nitrite ion reported, while the signal intensity above pH 9 decreases with increasing pH. The decrease in signal intensity at pH > 9 can be explained the suppression of the diazotization/coupling reaction.

Figure 5a shows the dependences of signal intensity on the flow-rate of CS (phosphate buffer adjusted to pH 8.0). With the type C UV-coil cell the signal intensity is lower than those with the type A and B UV-coil cells, in spite of increasing the time of irradiation of the sample solution. Two reasons can be considered: diffusion of sample and recombination of the generated nitrite and dissolved oxygen under UV irradiation in the longer UV-coil cell. In all types of cell, an increase in the flow rate of the CS up to 1.5 ml min^{-1} led to an increase in the signal intensity, although there was a decrease in the residence time of the sample in the cell. Two mechanisms (diffusion and recombination) inside the UV-coil cell can also be considered to decrease the signal intensity. The signal intensity becomes a maximum at CS flow-rates of 1.8, 1.5 and 2.0 ml min^{-1} for the type A, B and C UV-coil cells, respectively. The decline in the signal intensity at CS flow-rates higher than that giving the maximum signal intensity can be understood by the shortness of the irradiation time in the UV-coil cell and the incomplete colour development in the reaction coil. It can be concluded that the type B UV-coil cell is superior to the type A and C cells for obtaining a higher signal intensity.

As shown in Fig. 5b, an increase in the RS flow-rate leads to a decrease in the signal intensity, as the residence time of sample in the reaction coil cell is reduced.

When using the distilled water as the CS, the signal intensity is only about 10–20% of those obtained with phosphate buffer (pH 8). The signal intensity becomes a maximum at a CS flow-rate of 1.5 ml min^{-1} for the type A and B UV-coil cells, as when the CS is phosphate buffer. The signal intensity obtained with the type C UV-coil cell becomes ca. 20–30% smaller than those obtained with the type A and B cells when the CS is distilled water. In addition, the signal intensity for type C UV-coil cell is found to increase with increase in the flow-rate of the CS up to 2.5 ml min^{-1}.

The reverse conversion of nitrite to nitrate with UV irradiation was studied using ion chromatography. When an aqueous solution of nitrite (10 μM) was illuminated with UV radiation in the type B UV-coil cell at a flow-rate of 2.0 ml min^{-1}, about 80% of the nitrite in distilled water is converted into nitrate. In other words, nitrite ions return to nitrate ion under UV irradiation. Table 1 shows the signal intensity for 0.5 μM nitrite with the UV lamp on and off. The ratio I_{on}/I_{off}, which indicates the re-oxidation of nitrite to nitrate by UV irradiation, decreases when the total volume of the cell is increased. When the type C UV-coil cell is used with flowing distilled water as the CS, the dependence of the signal

TABLE 1

Signal intensity for nitrite with the UV lamp on and off [a]

UV-coil cell	I_{off}	I_{on}	I_{on}/I_{off}
Type A	0.0043	0.0009	0.21
Type B	0.0057	0.0014	0.25
Type C	0.0044	0.0004	0.09

[a] Concentration of nitrite = 0.5 μM.

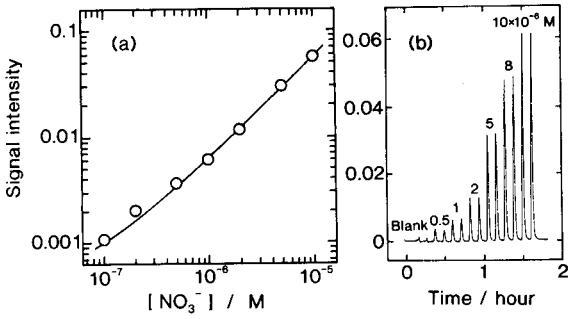

Fig. 6. (a) Calibration graph and (b) typical recorder tracks for nitrate. Phosphate buffer adjusted to pH 8.0 was used as the CS solution. The flow-rates of the CS and RS solutions were 2.0 and 0.3 ml min^{-1}, respectively.

TABLE 2

Effects of co-existing species

Compound	Concentration (M)	Interference (%) [a]
NaCl	0.2	−32
KCl	0.2	−48
KI	1.1×10^{-5}	−67
KBr	1.1×10^{-5}	0
Na_2SO_4	1.2×10^{-5}	0
Na_2CO_3	1.1×10^{-5}	0
NH_4Cl	1.1×10^{-5}	0
$CaCl_2$	0.05	−28
MgCl	0.05	−20

[a] The influence of the interferent was expressed with respect to the signal intensity given by 10 μM nitrate without any concomitants.

intensity on the flow-rate of the CS can be accounted for by the re-oxidation of nitrite to nitrate under UV irradiation.

In phosphate buffer, the recombination reaction is suppressed: only 5–10% of nitrite is re-oxidized to nitrate by UV irradiation in the type B UV-coil cell at a flow-rate of 2.0 ml min^{-1}. The re-oxidation becomes serious for the smaller signals in distilled water compared with those in phosphate buffer. Degassing of the CS seems to be effective in preventing the re-oxidation between oxygen and nitrite. With phosphate buffer, however, a slight increase in the signal intensity is observed on degassing the CS, as the oxygen dissolved in the sample solutions cannot be completely removed.

Heating of the reaction coil slightly affects the signal intensity: the signal intensity at 80°C is 1.2 times larger than that at 20°C.

A typical calibration graph and recorder trace for nitrate in distilled water are shown in Fig. 6a and b, where the type B UV-coil cell was employed (phosphate buffer adjusted to pH 8.0 was used and the flow-rates of the CS and RS were 2.0 and 0.3 ml min^{-1}, respectively). Ten samples can be measured per hour and the detection limit is ca. 0.05 μM, which is a sufficient sensitivity to detect nitrate not only in sea water but also in rain and river water and other environmental samples. The relative standard deviation for ten injections of 10 μM nitrate is 3%.

Interferences

Table 2 shows the effects of various compounds added to an aqueous solution containing 10 μM nitrate, expressed as the ratio of the signal intensities with and without co-existing species. Chloride and iodide ions tend to interfere negatively with the nitrate signal. Therefore, as shown in Fig. 7, the slope of the calibration graph for nitrate in FSW (filtered surface sea water) is smaller than that for nitrate in distilled water when the CS is the phosphate buffer without EDTA. In addition, at concentrations of ni-

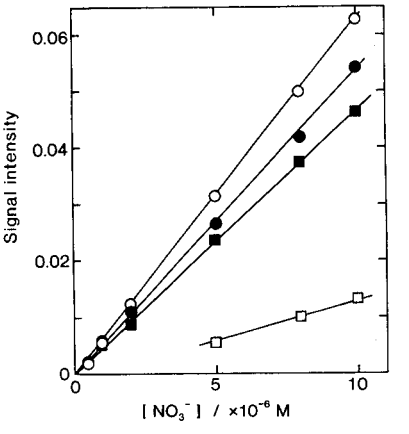

Fig. 7. Effect of EDTA on the calibration graphs for nitrate in distilled water and sea water. ○ = Calibration graph for nitrate in distilled water using the CS without EDTA; ● = in distilled water with 1 mM EDTA; □ = in sea water without EDTA; ■ = in sea water with 1 mM EDTA.

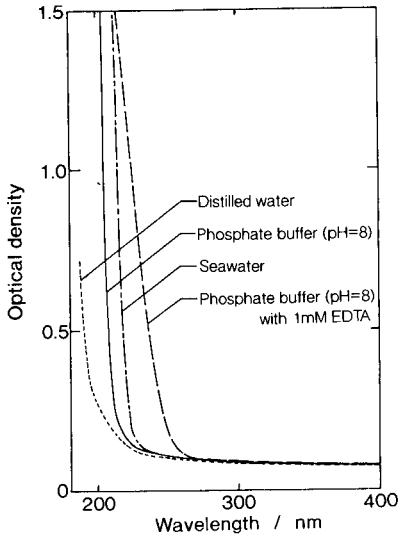

Fig. 8. Absorption spectra for distilled water, sea water and phosphate buffer with and without 1 mM EDTA.

trate in FSW less than 5 μM, the signal peak was distorted and it was impossible to measure the signal intensity. However, after the addition of about 1 mM EDTA to CS, the calibration graph for nitrate in FSW is restored and almost the same as that in distilled water. Hence the interference by chloride and iodide ion can be eliminated.

In Fig. 8, the absorption spectra for distilled water, sea water and phosphate buffer with and without EDTA are shown. The absorption for sea water is attributable to the absorption of halide ions, which is ascribed to the charge transfer to the solvent [14]. In phosphate buffer without EDTA, excitation of halide ions must be promoted by the UV irradiation because the absorption edge of phosphate buffer is at a shorter wavelength than that of sea water, as shown in Fig. 8. The excited halide ion interferes in the reaction to produce nitrite from nitrate and the diazotization/coupling reaction of sulphanilamide and *N*-1-naphthylethylenediamine. However, the absorption edge of phosphate buffer is shifted to longer wavelength on addition of EDTA. The effects of addition of EDTA to the CS can be explained in terms of the spectroscopic masking of halogens in the samples. Thereby, the production of excited halide ions is suppressed by addition of EDTA to the CS. Addition of EDTA is also effective in masking the interference of metal ions which obstruct the diazotization/coupling reaction with sulphanilamide and *N*-1-naphthylethylenediamine.

Armstrong et al. [15] proposed the UV decomposition of dissolved organic nitrogen in sea water. Lowry and Mancy [16] constructed an automated system for the determination of dissolved organic nitrogen using the UV irradiation. In both studies, samples were irradiated with a high-power mercury lamp of more than 1 kW for 10 min–2 h, where pH of the solution having been previously increased above 13 or decreased below 2, in order to achieve a high decomposition rate. In contrast, the power of the mercury lamps used in this study was about 0.5% of that used for the decomposition of organic nitrogen compounds. Therefore, an increase in nitrite concentration due to the decomposition of dissolved organic nitrogen can be considered negligible with the present UV irradiation. For example, addition of 1 mM EDTA to the CS does not cause any change in the signal.

Application to the analysis of natural waters

Figure 9 shows the depth profiles of nitrate in sea water sampled at Sagami Bay (139′24.6″E 34′56.7″N), Japan. Collection was carried out during the research cruise of the R/V Tansei-maru, University of Tokyo, on 17th March, 1992. As can be clearly seen, the results obtained by the proposed method coincide with those obtained with a commercial automated analyser in which a copperized cadmium column is used for reduction of nitrate to nitrite.

In Figure 10 and Table 3, the concentrations of nitrate in river, inland sea and open sea waters measured by the proposed method are compared with those obtained by the conventional spectrophotometric method with a copperized cadmium column. The samples were collected from the river at Eta-jima Island, Seto Inland Sea, Japan. Inland sea waters were collected in the Hiroshima Bay from the R/V Toyoshio-maru, Hiroshima University on 1st February, 1992. The results shown in Fig. 9 are also plotted in Fig. 10

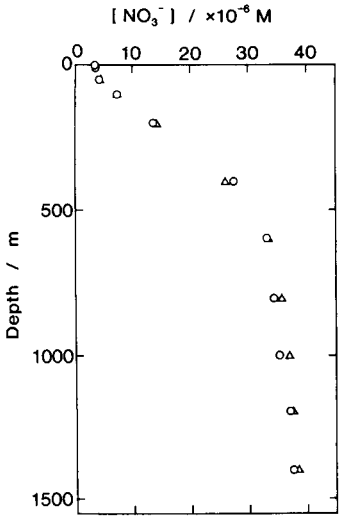

Fig. 9. Depth profiles of nitrate at Sagami Bay (139'24.6"E 34'56.7"N) determined (○) by the present method and (△) with a commercial automated analyser equipped with a copperized cadmium column.

as the samples for open sea water. The results obtained by the proposed method are in good agreement with those obtained by the conventional method. For nitrate in sea water, the limit of detection is ca. 0.05 μM and the calibration curve is linear up to 100 μM. These facts show the photo-reduction method proposed in this paper is practical and can replace the copperized cadmium column method.

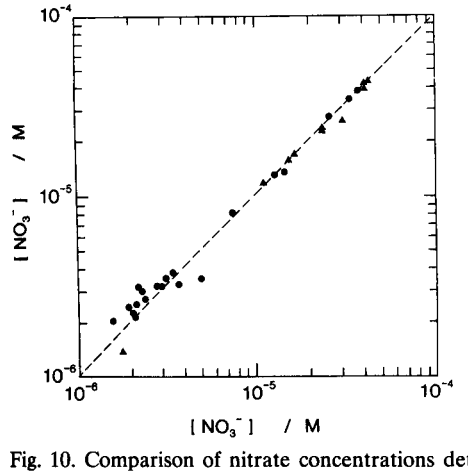

Fig. 10. Comparison of nitrate concentrations determined by the proposed method (ordinate) and the method using a copperized cadmium column (abscissa). Samples are (●) sea waters and (▲) river waters.

TABLE 3

Determination of nitrate in environmental water

Water sample	Nitrate ($\times 10^{-6}$ M)	
	Present method	Conventional method [a]
River		
1	1.4	1.8
2	15.9	16.0
3	42.1	42.0
Open sea		
1	3.7	3.8
2	14.2	13.5
3	33.7	33.8
Inland sea		
1	2.75	2.45
2	2.30	2.03
3	2.28	2.21

[a] Using a copperized cadmium column.

Although the present reduction method is installed in a FIA system, it is preferable to a commercial auto-analyser in which air segmentation is carried out in the stream of the solution. It should be emphasized that the present method is resistant to the introduction of air, which sometimes leads to serious problems with commercial automated systems with a copperized cadmium column. In the air segmentation method, elimination and incorporation of air bubbles are performed before and after the copperized cadmium column, respectively. These tedious processes are not required in the present method, which is a major advantage. Although the reduction of nitrate to nitrite is an essential step in the determination of nitrate in natural waters at present, the photolytic conversion proposed here makes the method simple, convenient and rapid compared with that involving a copperized cadmium column.

The authors thank the captain and crew of the vessels Tansei-maru and Toyoshio-maru for their cooperation, and Hiroshi Minami for making the UV-coil cells. This work was partially supported by a Grant in Aid 023248101 from the Ministry of Education, Science and Culture, Japan.

REFERENCES

1 P.W. West and G.L. Lyles, Anal. Chim. Acta, 23 (1960) 227.
2 B.E. Saltzman, Anal. Chem., 26 (1954) 1949.
3 L. Anderson, Anal. Chim. Acta, 110 (1979) 123.
4 M.F. Gine, H. Bergmin F°., E.A. G. Zagatto and B.F. Reis, Anal. Chim. Acta, 114 (1989) 191.
5 J.F. Staden, Anal. Chim. Acta, 138 (1982) 403.
6 H.D. Axelrod and N.A. Engel, Anal. Chem., 47 (1975) 922.
7 S. Motomizu, H. Mikasa and K. Toei, Talanta, 33 (1986) 729.
8 R.D. Cox, Anal. Chem., 52 (1980) 332.
9 J. Mulik, R. Puckett, D. Williams and E. Sawicki, Anal. Lett., 9 (1976) 653.
10 R. Olson, Limnol. Oceanogr., 25 (1980) 758.
11 M. Daniels, R.V. Meyers and E.V. Belardo, J. Phys. Chem., 72 (1968) 389.
12 U. Shuali, M. Ottolenghi, J. Rabani and Z. Yelin, J. Phys. Chem., 73 (1969) 3445.
13 I. Wargner, H. Strehlow and G. Busse, Z. Phys. Chem. (Munich) 123 (1980) 1.
14 R. Platzman and J. Franck, Z. Phys., 138 (1954) 411.
15 F.A.J. Armstrong, P.M. Williams and J.D.H. Strickland, Nature, 211 (1966) 481.
16 J.H. Lowry and K.H. Mancy, Water Res., 12 (1977) 471.

Analytica Chimica Acta, 276 (1993) 33–37
Elsevier Science Publishers B.V., Amsterdam

Determination of antimony(III,V) in natural waters by coprecipitation and neutron activation analysis

Y.C. Sun, J.Y. Yang, Y.F. Lin and M.H. Yang

Institute of Nuclear Science, National Tsing Hua University, 30043 Hsinchu (Taiwan)

Z.B. Alfassi

Department of Nuclear Engineering, Ben Gurion University, 80142 Beer Sheva (Israel)

(Received 8th September 1992; revised manuscript received 9th November 1992)

Abstract

A simple and quantitative method for separating antimony(III) from antimony(V) by coprecipitation with thionalide is described. The total concentration of antimony is determined through addition of tin(II) chloride followed by thionalide coprecipitation and antimony(V) is determined by subtraction. The coprecipitation system was investigated with the use of ^{122}Sb radiotracer. The precipitate was collected on a membrane filter for neutron activation analysis. The dectection limit of antimony was found to be in the order of ng l^{-1} under the experimental conditions. The reliability was checked with National Research Council of Canada standard reference material.

Keywords: Neutron activation methods; Antimony; Coprecipitation; Speciation; Waters

The determination of various species of antimony at low concentration levels in water is important in environmental studies owing to its toxicity and as the biological activity of antimony depends on its oxidation state. The different toxicities of Sb(III) and Sb(V) are similar to those of the corresponding arsenic species, with Sb(III) being more toxic [1]. In order to differentiate between the two species, chemical separation is essential. This will also help in the determination itself, as the chemical separation can be incorporated into the measurement as a preconcentration process.

There are several reports on the determination of Sb by anodic stripping voltammetry [2,3], inductively coupled plasma atomic emission spectrometry [4], hydride generation atomic absorption spectrometry [5–7], direct graphite furnace atomic absorption spectrometry [8] and neutron activation analysis [9]. As Sb occurs in the environment at very low concentrations (< 1 ng ml^{-1}), the development of a method for the determination of Sb(III) and Sb(V) has received considerable attention. The accurate determination of low levels of Sb in natural waters can be accomplished only by techniques that are very sensitive and selective. Neutron activation analysis (NAA) usually meets these requirements.

Under interference-free conditions, the sensitivity of NAA in a medium-flux reactor for Sb is of the order of several nanograms. In order to eliminate possible interference to NAA, a separation process is essential. Mok and Wai [9] developed a method for the selective extraction of Sb(III) in the presence of Sb(V) with an ammonium pyrrolidinedithiocarbamate (APDC)–chloroform system. Total antimony was determined after reduction of Sb(V) to Sb(III) with potassium

Correspondence to: M.H. Yang, Institute of Nuclear Science, National Tsing Hua University, 30043 Hsinchu (Taiwan).

iodide. The difference between the two determinations gives the concentration of Sb(V). Chung et al. [10] developed APDC–$CHCl_3$ + CCl_4 extraction system to extract Sb(III), Se(IV) and As(III) selectively in the presence of Sb(V), Se(VI) and As(V). The total amounts of these elements are simultaneously determined after reduction of the higher to lower oxidation state species with titanium(III) chloride. The concentrations of the higher oxidation state species are obtained by subtraction. Matsui et al. [11] described the preconcentration of Sb(III) with 2-mercapto-*N*-2-naphthylacetamide (thionalide) loaded on glass beads. Thionalide is insoluble in water and yields water-insoluble white precipitates with most di- or trivalent metals by precipitation with the sulphide group of the reagent. However, they only measured Sb(III), and no information about Sb(V) measurement was given. In addition to thionalide, Brilliant Green [12], APDC–2-methyl-4-pentanone [13] and crown ethers [14] have also been used as reagents for preconcentration of Sb(III) or Sb(V). Elson et al. [15] coprecipitated total antimony by addition of Se(IV) and $SnCl_2$ in acidic solution. $SnCl_2$ reduces Se(IV) to elemental Se, and Sb is coprecipitated with elemental Se. However, this method can measure only total Sb and cannot differentiate between the various valence states. It has been found that Sb(III) can be coprecipitated with lead pyrrolidinedithiocarbamate or with bismuth quinolin-8-olate plus thionalide [16].

This paper describes the determination of the various species of antimony in aqueous solution through thionalide coprecipitation and NAA. Sb(III) can be readily separated from Sb(V) by thionalide coprecipitation over a wide range of pH. Sb(V) can then be reduced to a lower oxidation state with $SnCl_2$. By this method, antimony can be readily determined in its different oxidation states at ng l^{-1} levels.

EXPERIMENTAL

Reagent and instruments

All chemicals were of analytical-reagent grade. Glassware was cleaned with nitric acid (1 + 1). Standard river water (SLRS-1) was obtained from the National Research Council of Canada. ^{124}Sb radiotracer was used for the determination of the yield of coprecipitation. ^{124}Sb ($t_{1/2}$ = 60.3 days, $E_{1/2}$ = 602.7 keV) was produced by irradiation of Sb in the National Tsing Hua University Open-Pool reactor (THOR) at a flux of 1×10^{12} n s^{-1} cm^{-2}, after cooling for more than 2 weeks, for the decay of ^{122}Sb. The use of ^{124}Sb alone, not together with ^{122}Sb, makes decay correction simpler and almost negligible. Sb(III) and Sb(V) solutions were prepared by irradiating about 10 mg of Sb_2O_3 and Sb_2O_5, respectively, in the reactor for 4 h. The irradiated antimony oxides were dissolved in 2.5 M HCl. Hydrazine was added to the ^{124}Sb(III) solution to ensure that all the Sb ions were in the Sb(III) state. Hydrogen peroxide was added to the Sb(V) solution and heated (ca. 80°C) for 30 min to ensure that all the Sb ions were in the Sb(V) state.

Thionalide solution was prepared by dissolving 1 g of reagent in 100 ml of acetone. The reducing agent, tin(II) chloride, was prepared by dissolving 5 g of $SnCl_2 \cdot 2H_2O$ in 25 ml of warm HCl and diluting to 100 ml. Titanium(III) chloride solution was 15% (w/v) in 12 M hydrochloric acid.

The coprecipitation yield was measured from the radioactivity counts [using an NaI(Tl) well detector] of the original radiotracer solution and of the precipitate. The precipitates of actual samples were analysed by NAA, irradiated for 6 h followed by 5 days of cooling. The counting system consists of a 38-cm^3 Ge(Li) detector coupled with a TN-1710 4096-channel pulse-height analyser (Tracor Northern) and the usual electronics. The energy resolution of the system was 2.4 keV for 1332 keV. The irradiated samples were counted for 1800 s.

Method

All water samples were filtered through 0.45-μm Millipore membrane filters if there was any suspended matter or sediment. The coprecipitation of Sb(III) was done by addition of 10 mg of thionalide to 250 ml of sample solutions and 1 ml of ammonium acetate buffer was added to adjust the pH to ca. 5.5. After 5 min of stirring and standing, the precipitate was collected with a

0.45-μm membrane filter. The membrane filter precipitate was placed in a vacuum desiccator and dried. The membrane with the filter was then inserted in polyethylene vial and sealed for irradiation. Total Sb was determined by reducing Sb(V) with 40 mg of $SnCl_2$ at pH 4 for 5–10 min, then the treatment as for Sb(III) was followed. The difference between the two determinations gives the concentration of Sb(V).

RESULTS AND DISCUSSION

Spectral interferences

The most sensitive gamma peak for NAA of antimony is the 564.1-keV peak of ^{122}Sb ($t_{1/2}$ = 67.2 h). The major interferences for the determination of Sb in various samples by NAA are the 559.1-keV peak of ^{76}As ($t_{1/2}$ = 26.4 h) and the 554.3-keV peak from the decay of ^{82}Br ($t_{1/2}$ = 35.3 h). Another major feature of the spectrum of activated water samples is a high background caused primarily by the presence of high levels of ^{24}Na, ^{42}K and ^{32}P in the system. The thionalide coprecipitation procedure effectively removes the alkali metal ions, halides and phosphorus species from the system. As(III) and As(V) are slightly coprecipitated from aqueous solution by the thionalide coprecipitation system and the recovery is only 1% at pH 4.5. The 559.1-keV peak of As will cause spectral interference when the 564.1-keV peak is used for Sb measurement if the As/Sb mass ratio is > 10. The 602.7-keV peak of ^{124}Sb ($t_{1/2}$ = 60.3 days) does not suffer from a similar interference and consequently was chosen for Sb determination. Spiking Sb(III) into distilled water and recovering it under the present experimental conditions indicated that the detection limit of Sb in water samples is at the ng level at a signal-to-noise ratio > 3.

From the point of view of neutron activation, both $TiCl_3$, and $SnCl_2$ are suitable for the reduction of Sb(V). Ti produces only a radionuclide with $t_{1/2}$ = 5 min after neutron activation, and this activity is eliminated by cooling for several hours. Although Sn forms a longer lived radionuclide, it was found that the gamma spectra of the Sn precipitate is very simple and Sb can be determined easily. From the point of view of filtering, the filtration of the Sn precipitate is much easier.

Selective coprecipitation of antimony(III) and antimony(V)

The effects of various factors on the selective coprecipitation of Sb(III) and Sb(V) with thionalide were studied, viz., the pH of the solution,

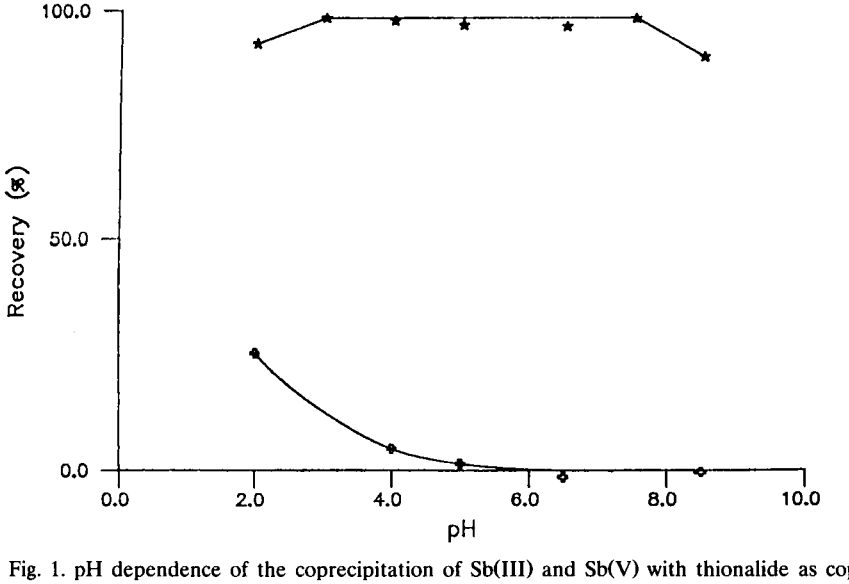

Fig. 1. pH dependence of the coprecipitation of Sb(III) and Sb(V) with thionalide as coprecipitating agent (250 ml of solution, thionalide 10 mg in 1 ml of acetone). * = Sb(III); + = Sb(V).

TABLE 1

Recovery tests on Sb(III) and Sb(V) in various concentration ratios by coprecipitation with thionalide and radiotracer technique

Concentration ratio of Sb(III) to Sb(V)	Initially added activity (cpm)		Activity recovered in the filtrate after coprecipitation (cpm)
	Sb(III)	Sb(V)	
1:1	29711	38919	39023
1:2	30540	76631	76631
1:5	29854	194590	183718
1:10	40137	393752	385277

the amount of thionalide for complete recovery of Sb(III) from solution and the amount of the reducing agent on the recovery of Sb(V).

Figure 1 indicates that Sb(III) can be coprecipitated quantitatively over the pH range 5–8, but there is virtually no coprecipitation of Sb(V) over this pH range. A 5-mg amount of thionalide is sufficient to precipitate all of the Sb(III) present. Below this level the recoveries are < 100%. To be safe, 10 mg of thionalide were used for coprecipitation in all subsequent studies. Sb(V) will be coprecipitated if it is reduced prior to coprecipitation. $TiCl_3$ and $SnCl_2$ can be used as reducing agents. If the pH of the aqueous solution is in the range 0.5–4 (adjusted with HCl), addition of 100 mg of $TiCl_3$ and standing for 5–10 min will give quantitative reduction of Sb(V). The recovery of Sb(V), treated by reduction with $TiCl_3$ followed by coprecipitation with thionalide, is complete at pH < 4. However, the precipitate which also contains titanium is difficult to filter off. When reducing Sb(V) with $SnCl_2$, if the pH is in the range 2–6 (adjusted with HCl), addition of $\geq$ 40 mg of $SnCl_2$ and standing for 5–10 min will give quantitative reduction of Sb(V). Smaller amounts of $SnCl_2$ give incomplete reduction. The recovery of Sb(V) treated by reduction with $SnCl_2$ followed by coprecipitation is complete in the pH range 4–8. The filtration of the precipitate of Sn is much easier than that of Ti, so $SnCl_2$ was chosen as the reducing agent. The optimum reduction conditions are pH 4, 40 mg of $SnCl_2$, reduction time 5–10 min and coprecipitation at pH 4–5.

Table 1 gives the results of the selective coprecipitation of Sb(III) and Sb(V) with thionalide at various concentration ratios of Sb(III) to Sb(V) (1:1, 1:2, 1:5 and 1:10) at ng ml^{-1} levels of total antimony. It can be seen that there is no mutual interference over this range of concentration ratios and the thionalide system could differentiate Sb(III) and Sb(V) precisely.

Analysis of water samples

Complete recoveries of radioactive Sb(III) added to three types of water samples (sea, tap and distilled water) were found, as can be seen in Table 2. The results show a very low recovery of Sb(V); however, the recovery of Sb(V) is complete when prior reduction is applied followed by coprecipitation. The selective coprecipitation and reduction procedures for Sb(III) and Sb(V) + Sb(III), respectively, were therefore considered to be quantitative and free from matrix interferences.

In trace analytical techniques that involve a series of sample pretreatment steps, strict control of a stable and low blank value is very important. In this study a blank determination was made by following the established preconcentration process, using 250 ml of doubly distilled water as blank solution and then NAA of the separated precipitate. The result indicated that the blank

TABLE 2

Recovery tests on Sb(III) and Sb(V) by coprecipitation with thionalide and radiotracer technique

Species	Recovery (%) [a]		
	Distilled water	Tap water	Sea water
Sb(III)	98.9 ±0.4	95.6 ±1.3	99.9 ±0.2
Sb(V)	0.29±0.23	0.39±0.09	0.30±0.17
Sb(V) [b]	–	97.2 ±0.9	94.4 ±0.6

[a] Mean ± standard deviation ($n = 3$). [b] With prior reduction of $SnCl_2$.

TABLE 3

Results of natural water analysis (published values and this work)

Sample	Concentration (ng l^{-1})		
	Sb(III)	Sb(V)	Total Sb
Apalacheo Bay [2]	19	164	–
Gulf of Mexico [2]	44	149	–
Boston Light-Ship [17]	–	–	180
Sea water [18]	ND [c]	300	–
Sea water [a]	33 ± 6	127 ± 15	160 ± 14
Lake water [a]	5 ± 1	275 ± 10	280 ± 10
Ground water [b]	8	12	20

[a] This work: mean ± standard deviation ($n = 3$). [b] This work ($n = 1$). [c] ND = not detected.

concentration of Sb obtained is below the limit of detection.

Next, the potential analytical accuracy of the proposed procedure was tested by using a natural matrix standard reference water sample (SLRS-1) obtained from the National Research Council of Canada. The result for total Sb was 0.59 ± 0.02 $\mu g\ l^{-1}$, in close agreement with the certified value (0.63 ± 0.05 $\mu g\ l^{-1}$). Table 3 gives the results for sea, lake and ground waters and published values for similar cases. The results agree fairly well with the previous results that most of Sb is in the +5 valence state. The result for the sea water sample is in reasonable agreement with published values [2,17,18]. The Sb(III)/Sb(V) ratio in most natural water systems was reported to be of the order of 0.01 [19], but it is variable under different geological and biological (in particular algae activity [18]) conditions. For the reason discussed above, the Sb(III)/Sb(V) ratios in sea, ground and lake waters are different.

Antimony enters the aquatic environmental as a result of the weathering of rocks (which contain an average of 0.16 $\mu g\ ml^{-1}$ Sb), from soil run-off and through effluents discharges. Typical concentrations in unpolluted waters are in the sub-$\mu g\ ml^{-1}$ range [19]. Sensitive and reliable methods for measuring antimony species in natural water systems are needed for speciation studies. The present results indicate that the coprecipitation method described here can be used efficiently for differentiating trace Sb(III) and Sb(V) species in natural water systems.

The authors thank the National Science Council of the Republic of China for support of this work (Grant No. NSC 80-0208-M007-75).

REFERENCES

1 J.E. Fergusson, The Heavy Elements/Chemistry, Environmental Impact and Health Effects, BPCC Wheatons, 1990.
2 T.R. Gilbert and D.N. Hume, Anal. Chim. Acta, 65 (1973) 451.
3 G. Gillain and G. Duychaerts, Anal. Chim. Acta, 106 (1979) 23.
4 D.D. Nygaard and J.H. Lowry, Anal. Chem., 54 (1982) 803.
5 P. Fodor and R.M. Barnes, Spectrochim. Acta, Part B, 38 (1983) 229.
6 D.L. Colett, D.E. Fleming and G.A. Tayler, Analyst, 104 (1987) 1074.
7 H. Narasaki, Anal. Sci., 2 (1986) 371.
8 S. Costantini, R. Giordano, M. Rizzica and F. Benedetli, Analyst, 110 (1985) 1355.
9 W.M. Mok and C.M. Wai, Anal. Chem., 591 (1987) 233.
10 C.H. Chung, E. Iwamoto, M. Yamamoto and Y. Yamamoto, Spectrochim. Acta, Part B, 39 (1984) 459.
11 M. Matsui, K. Matsumoto and K. Terada, Anal. Chim. Acta, 193 (1987) 381.
12 R.W. Burke and O. Menis, Anal. Chem., 38 (1966) 1719.
13 R. Kobayashi and K. Imaizumi, Anal. Sci., 51 (1989) 61.
14 H. Koshima and H. Onishi, Analyst, 111 (1986) 1261.
15 C.M. Elson, J. Milley and A. Chatt, Anal. Chim. Acta, 142 (1982) 269.
16 C.R. Lan, Y.C. Sun, J.H. Chao, C. Chung, M.H. Yang, N. Lavi and Z.B. Alfassi, Radiochim. Acta, 50 (1990) 225.
17 H.-W. Sun, X.-Q. Shan and Z.-M. Ni, Talanta, 29 (1982) 589.
18 E. Nakayama, Y. Sueki, K. Fujiwara and Y. Kitano, Anal. Sci., 5 (1989) 129.
19 M.O. Andread, J.F. Asmode, P. Foster and L. Van 't Dack, Anal. Chem., 531 (1981) 1766.

Analytica Chimica Acta, 276 (1993) 39–45
Elsevier Science Publishers B.V., Amsterdam

Analysis of toxic elements in plastic components for toys. Multi-elemental determination by x-ray fluorescence

J.V. Gimeno Adelantado, V. Peris Martinez, F. Bosch Reig, M.T. Doménech Carbó and F. Bosch Mossi

Department of Analytical Chemistry, Faculty of Chemistry, University of Valencia, C/. Dr. Moliner 50, 46100 Burjasot, Valencia (Spain)

(Received 7th May 1992; revised manuscript received 9th November 1992)

Abstract

An x-ray fluorescence method is proposed for the multi-elemental determination of toxic elements in plastic articles for children, viz., Sb(III), Ba, Cd, Cr(III), Hg, Pb and As(III). Mineralization is achieved by using molten sodium hydroxide to decompose the organic matrix, with sodium nitrate as auxiliary oxidant. Stable solutions containing the chemical species for analysis are obtained. The species are separated from the solution by (co)precipitation, in a medium of NH_4^+–NH_3 buffer (pH 8.5) with sodium diethyldithiocarbamate, sodium rhodizonate and Fe^{3+}, which acts as a carrier. The precipitates deposited on filter-paper are placed in the x-ray spectrometer in fine layer morphology. The method was applied to several plastics of different characteristics, all components of children's toys. The suggested method is statistically comparable to the method that includes a reference destruction of organic matter for each element studied and subsequent determination by atomic absorption spectrometry.

Keywords: X-ray fluorescence spectrometry; Plastic toys; Toxic elements

Products are considered to be toxic if, when ingested, they are capable of altering the vital functions of the human organism. Special consideration should be given to products where children come into direct contact with materials that may contain toxic elements, with the additional risk of accidental ingestion of these materials. Strict controls are therefore needed for objects such as toys and other utensils produced for this sector of the population to avoid the risk of intoxication.

Metals are toxic when they accumulate in the living organism, interfere in the redox and enzymatic systems, are capable of forming organometallic compounds or interact with nucleic acids.

Correspondence to: J.V. Gimeno Adelantado, Department of Analytical Chemistry, Faculty of Chemistry, University of Valencia, C/. Dr. Moliner 50, 46100 Burjasot, Valencia (Spain).

The European Standard EN 71/3 concerning toy safety [1] in European Community countries was prepared by the Technical Committee CEN/TC52. "Safety of Toys" Part III deals with "Toxicity of Toys". This standard sets out the maximum concentrations in the soluble state of the following elements: Sb 250, As 100, Ba 500, Cd 100, Cr 100, Pb 250 and Hg 100 mg kg^{-1}, for plastics which constitute the whole or part of the toy.

For this type of sample, the multi-elemental determination of the toxic species (metallic and non-metallic) is of particular interest, as the whole analytical procedure is carried out in a single stage, which considerably reduces the time required for analysis. One of the most appropriate techniques for this objective is x-ray fluorescence; however, a simultaneous multi-elemental preconcentration is needed to increase the sensitivity of

this technique [2], once the sample has been correctly decomposed. There are several different preconcentration procedures: ion-exchange paper [3], reagents with silica gel [4] or cellulose supports [5], precipitation with inorganic [6] or organic reagents [7–9], with occasional use of the coprecipitant action of metallic hydroxides [10–12].

The decomposition of the plastic material is essential for the determination of heavy elements. This is extremely difficult, however, owing both to the high resistance that this type of material offers to disintegration, characteristic of this type of organic matrix, and to the diversity of procedures recommended in relation to the different elements to be measured [13].

This paper proposes the determination of the total content of Sb, As(III), Ba, Cd, Cr(III), Pb, and Hg in toys made from plastics. The organic matrix is destroyed, in an open system, with sodium hydroxide in a silver crucible, using sodium nitrate as auxiliary oxidant. The molten sodium hydroxide medium ensures the complete retention of elements such as arsenic, antimony, lead and mercury, which tend to form volatile species [13]. The proposed procedure was applied to twelve different plastics from toys already on the market. The results obtained with the proposed method were compared with the values found by applying, separately, the organic material destruction methods recommended for each analyte element and subsequent determination using x-ray fluorescence (proposed method) and atomic absorption spectrometry (AAS) (independent method). Finally, an extraction with hydrochloric acid [1] was performed, specifically in order to study the toxic elements when their total content is higher than the maximum allowed in the legislation (note that the values expressed in the legislation refer to the soluble element liberated in the extraction).

EXPERIMENTAL

Apparatus

A Siemens Kristalloflex 805 SRS 200 x-ray spectrometer with a chromium target x-ray tube, controlled by a Siemens System 300-310 LC 200 computer was used. The instrumental measurement conditions are given in Table 1.

A Perkin-Elmer Model 5000 atomic absorption spectrometer was used with the instrumental parameters recommended in the instrument manual. A flow spoiler was employed as impactor. A Perkin-Elmer MHS-10 mercury/hydride system was employed for mercury determination.

A Barnstead Nanopure II water purifier was used.

Reagents

Analytical-reagent grade chemicals were used.

Stock standard solutions of 100 μg ml^{-1} of each analyte and Fe^{3+} were prepared by dissolv-

TABLE 1

Experimental conditions for measurement of x-ray fluorescence intensity.

Experimental conditions			Common conditions
Element (line)	Analyser crystal	Angular value (2θ)	
Sb(III)(Lα)	LiF(100)	117.314	40 kV, 30 mA x-ray tube
Ba(Lα)	LiF(100)	87.163	Detector: proportional gas flow, Sb, Ba, Cd, Cr, Hg;
Cr(III) [a](Kα)	LiF(110)	69.267	scintillation, Pb, As
Cd(Lα)	PET	53.791	Counting time, 40 s
Hg(Lα)	LiF(100)	35.873	Collimator at 0.15°
Pb(Lβ)	LiF(100)	28.186	Measurements carried out in vacuo
As(III)(Kα)	PET	15.460	

[a] The filter II is used to eliminate the chromium target radiation.

ing the pure salts, oxides or metals with HCl or HNO_3. A 1% (w/v) solution of sodium diethyldithiocarbamate (DDTC) (Merck) and a 0.1% (w/v) solution of sodium rhodizonate (R) (Merck) were prepared. The buffer solution used as NH_4^+–NH_3 (pH 8.5). $SnCl_2 \cdot 2H_2O$ was obtained from Merck.

Samples

The samples used consisted of different plastic materials from the components of several commercially available toys for children. Several toys were chosen and parts with different colours were taken from them. For the analysis, the sample was cut into strips 0.5–1 mm thick. Twelve different samples of various colours (red, orange, yellow, green, blue and pink) were thus obtained.

Proposed procedure

Melt 4 g of sodium hydroxide pellets in a 50-ml silver crucible using a Bunsen burner. Cool by swirling so that the melt solidifies on the bottom and sides of the crucible. Add 0.2–1 g of the plastic material and heat moderately over a direct flame until alkaline fusion occurs. Increase the intensity of the flame. Add 0.1–0.2 g of sodium nitrate in several stages until a transparent melt is obtained. Cool to room temperature, dissolve the melt with small amounts of hot water (each amount no greater than 10 ml) and transfer into a 250-ml vessel. Add 3 M HCl dropwise with vigorous stirring until a transparent acid solution is obtained. Dilute to ca. 100 ml. Add 10 ml of Fe^{3+} solution, 5 ml of each of the DDTC and R solutions 10 ml of the NH_4^+–NH_3 buffer solution. Leave the precipitated mixture on a sand-bath for 25 min. Filter through Whatman No. 42 filter-paper over a glass filter layer. Wash and dry the paper bearing the precipitate at 50°C for 25 min and keep in a desiccator until fluorescence intensity measurements are made.

Reference procedure

The destruction methods used for each element were the following. *Antimony*: dry ashing was 550°C using magnesium nitrate as ashing aid [14]. *Barium*: careful ashing at 450°C [15]. *Cadmium*: wet ashing using sulphuric acid and hydrogen peroxide [16]. *Chromium and lead*: wet oxidation using mixtures of nitric, sulphuric and perchloric acids [14]. *Mercury*: oxidation with mixtures of nitric and sulphuric acids [17]. *Arsenic*: wet oxidation using either sulphuric acid and hydrogen peroxide [16] or mixtures of nitric, perchloric and sulphuric acids [14].

Elemental determinations were performed by x-ray fluorescence spectrometry following the previously described procedure, and also using AAS as an independent technique.

RESULTS AND DISCUSSION

To achieve multi-elemental determination and increase the number of species preconcentrated in a single operation, the precipitating action of an organic reagent, sodium diethyldithiocarbamate, was combined with the coprecipitation action of a carrier, Fe(III). However, for one of the analyte species, barium, the optimum separation conditions differed greatly from those for the other elements, so a second precipitant, sodium rhodizonate, was introduced. Inorganic qualitative analysis [18] was used to identify the oxidation states of the species in the solution obtained by decomposition of the organic matter in the sample.

Optimized preconcentration procedure

The operation for obtaining the precipitate from the solution containing the analytes, using

TABLE 2

Equations for calibration graphs obtained for the elements studied

Element	$I = A + BX$ [a]		r	Linear range (μg)
	A	B		
Sb(III)	−0.3	0.9	0.9994	0– 100
Ba	6.9	0.2	0.9998	0–1000
Cd	−3.6	3.7	0.9995	0– 200
Cr(III)	20.7	0.6	0.998	0– 200
Hg	−0.9	0.4	0.9997	0– 200
Pb	6.7	0.2	0.9998	0– 150
As(III)	0.2	0.3	0.9997	0– 200

[a] I = counts s^{-1}; $X = \mu g$.

TABLE 3

Results of determination of toxic elements in plastics of toys: comparison of the precision between the suggested method (multi-elemental determination) and both procedures that include a reference destruction with XRF and AAS elemental determination

Element	Sample 1 (red)			Sample 2 (red)			Sample 3 (orange)			Sample 4 (orange)			Sample 5 (yellow)			Sample 6 (yellow)		
	$\bar{x}$ [d]	s [d]	$\epsilon_r(\%)$ [e]	$\bar{x}$ [d]	s [d]	$\epsilon_r(\%)$ [e]	$\bar{x}$ [d]	s [d]	$\epsilon_r(\%)$ [e]	$\bar{x}$ [d]	s [d]	$\epsilon_r(\%)$ [e]	$\bar{x}$ [d]	s [d]	$\epsilon_r(\%)$ [e]	$\bar{x}$ [d]	s [d]	$\epsilon_r(\%)$ [e]
Sb(III) [a]	35	2.5	5.1	28	2	5.1	22	1	3.3	26	2	5.5	20	0.8	2.9	24	1	3.0
[14] [b]	38	3	5.6	30	3	7.2	20	2	7.2	25	3	8.6	18	0.7	2.8	25	2	5.7
[14] [c]	36	2	4.0	29	2	4.9	22	1	3.2	26	2	5.5	20	0.6	2.1	24	1	3.0
Ba [a]	109	12	7.9	82	9	7.9	31	5	11.5	52	8	11	375	17	3.2	390	20	3.7
[15] [b]	101	13	9.2	90	10	7.9	30	5	11.9	60	9	10.7	386	20	3.7	380	25	4.7
[15] [c]	106	9	6.1	85	6	5.1	32	3	6.7	58	6	7.3	380	15	2.8	390	19	3.4
Cr(III) [a]	nd [f]			nd			nd			nd			nd			nd		
[14] [b]	nd			nd			nd			nd			nd			nd		
[14] [c]	0.10	0.002	1.4	0.07	0.0009	0.9	0.08	0.001	0.9	0.08	0.0009	0.8	0.11	0.001	0.7	0.15	0.0015	0.7
Cd [a]	15.7	0.3	1.4	19.3	0.4	1.5	12.8	0.2	1.1	16.3	0.3	1.3	10.5	0.2	1.4	13.6	0.3	1.6
[16] [b]	16.5	0.5	2.2	21.2	0.5	1.7	12.5	0.3	1.7	17.5	0.5	2.0	9.2	0.3	2.3	13.9	0.4	2.1
[16] [c]	15.9	0.2	0.9	19.1	0.3	1.1	13.0	0.2	1.1	16.0	0.2	0.9	10.3	0.2	1.4	13.5	0.1	0.5
Hg [a]	1.85	0.03	1.2	1.60	0.15	6.9	1.96	0.08	2.9	1.25	0.03	1.7	1.75	0.08	3.3	1.9	0.2	7.5
[17] [b]	1.72	0.04	1.7	1.5	0.2	9.5	1.7	0.1	4.2	1.10	0.05	3.3	1.56	0.12	5.5	1.6	0.3	13.4
[17] [c]	1.81	0.01	0.8	1.6	0.1	4.5	1.9	0.1	3.8	1.20	0.04	2.4	1.55	0.10	4.6	1.9	0.2	7.5
Pb [a]	18	2	7.9	16	2	8.9	1.36	0.03	1.6	1.15	0.02	1.2	12	1	6	15	2	9.5
[14] [b]	20	2	7.2	16	3	13.4	1.53	0.05	2.3	1.26	0.04	2.3	12	2	12	16	2	8.9
[14] [c]	19	1	3.8	15	2	9.5	1.41	0.02	1.0	1.10	0.02	1.3	11	1	7	15	2	9.5
As(III) [a]	15	4	19.1	19	4	15.1	17	3	12.6	16	4	17.9	20	5	18	18	4	15.9
[16] [b]	13	4	22	15	5	23.8	15	4	19.1	13	4	22.0	19	6	22.6	18	5	19.8
[16] [c]	16	3	13	18	3	11.9	16	4	17.9	15	4	19.1	18	5	19.9	17	3	12.6
[14] [b]	12	4	24	16	5	22.4	17	4	16.8	15	5	23.8	17	5	21.0	16	5	22.4
[14] [c]	15	3	14	18	3	11.9	17	3	12.6	15	3	14.3	18	4	15.9	17	3	12.6

Element	Sample 7 (green)			Sample 8 (green)			Sample 9 (blue)			Sample 10 (blue)			Sample 11 (pink)			Sample 12 (pink)		
	$\bar{x}$ [d]	s [d]	ϵ_r(%) [e]	$\bar{x}$ [d]	s [d]	ϵ_r(%) [e]	$\bar{x}$ [d]	s [d]	ϵ_r(%) [e]	$\bar{x}$ [d]	s [d]	ϵ_r(%) [e]	$\bar{x}$ [d]	s [d]	ϵ_r(%) [e]	$\bar{x}$ [d]	s [d]	ϵ_r(%) [e]
Sb(III) [a]	40	3	5.4	38	4	7.5	30	3	7.2	28	3	7.7	25	3	8.6	22	2	6.5
[14] [b]	42	4	6.8	36	4	7.9	28	4	10.2	25	3	8.6	28	4	10.2	24	3	8.9
[14] [c]	39	2	3.7	37	3	6.6	29	2	4.9	27	2	5.2	25	2	5.8	22	2	6.5
Ba [a]	480	30	4.5	620	40	4.6	4700	600	9.1	5100	600	8.4	3300	400	8.7	2800	250	6.4
[15] [b]	490	40	5.8	610	40	4.7	5000	600	8.6	5000	600	8.6	3100	400	9.2	3000	300	7.2
[15] [c]	470	30	4.6	630	40	4.5	4800	500	7.4	5000	500	7.1	3200	400	8.9	2900	200	5.1
Cr(III) [a]	nd			nd			nd			nd			nd			nd		
[14] [b]	nd			nd			nd			nd			nd			nd		
[14] [c]	0.14	0.0016	0.8	0.22	0.0025	0.8	0.25	0.003	0.9	0.23	0.004	1.2	0.31	0.023	5.3	0.27	0.017	4.5
Cd [a]	7.5	0.8	7.6	9.0	1.1	8.7	15.3	0.3	1.4	10.7	0.4	2.7	21	1	3.4	28	2	5.1
[16] [b]	8.1	0.8	7.1	9.5	1.3	9.8	15.0	0.4	1.9	11.0	0.4	2.6	22	2	6.5	31	3	6.9
[16] [c]	7.8	0.5	4.6	9.0	0.8	6.4	15.0	0.3	1.4	10.5	0.3	2.0	21	1	3.4	29	2	4.9
Hg [a]	1.51	0.04	1.9	1.45	0.03	1.5	1.23	0.07	4.1	1.41	0.11	5.6	1.92	0.04	1.5	1.72	0.05	2.1
[17] [b]	1.60	0.5	2.2	1.25	0.03	1.7	1.15	0.09	5.6	1.32	0.13	7.0	1.85	0.05	1.9	1.70	0.06	2.5
[17] [c]	1.55	0.03	1.4	1.30	0.04	2.2	1.20	0.06	3.7	1.35	0.09	4.8	1.95	0.04	1.5	1.75	0.04	1.6
Pb [a]	1.33	0.03	1.6	1.21	0.04	2.4	1.09	0.06	3.9	1.22	0.08	4.7	190	15	5.6	230	20	6.2
[14] [b]	1.40	0.05	2.6	1.35	0.05	2.6	1.16	0.08	4.9	1.35	0.10	5.3	195	20	7.3	230	20	6.2
[14] [c]	1.35	0.03	1.6	1.30	0.05	2.8	1.10	0.04	2.6	1.20	0.09	5.4	190	12	4.5	240	25	7.5
As(III) [a]	19	6	22.6	15	4	19.1	25	6	17.2	35	8	16.3	148	10	4.8	210	10	3.4
[16] [b]	16	6	26.8	15	5	23.8	24	7	20.9	33	8	17.3	130	10	5.5	200	11	3.9
[16] [c]	20	5	17.9	14	3	15.3	26	4	11.0	34	7	14.7	140	9	4.6	215	10	3.3
[14] [b]	17	6	25.2	13	5	27.5	22	7	22.7	34	9	18.9	140	12	6.1	200	12	4.3
[14] [c]	18	4	15.9	15	3	14.3	26	5	13.7	35	7	14.3	150	9	4.3	210	10	3.4

[a] Suggested method: multi-element determination by XRF. [b] Method including a reference decomposition of organic matter for each element: independent element determination by XRF. [c] Same by AAS. [d] $\bar{x}$ = Mean concentration and s = standard deviation (μg g^{-1}) ($n = 10$). [e] ϵ_r = Relative error. [f] nd = Not detected.

precipitation and coprecipitation, requires a prior study to establish the optimum conditions. For the elements in this study, these conditions proved to be precipitation pH 8.5; precipitate flocculation time, 25 min; Fe^{3+} carrier, 1000 μg (for maximum contents of 250 μg of each element and 1000 μg of barium); DDTC and R, 5 ml of each solution; and salinity, 0.40 M (approximately that of the solution obtained after fusion with NaOH and adding HCl to the dissolved melt).

Calibration

Calibration graphs were obtained for the elements in this study using the procedure developed under the optimum working conditions established previously. Six series of solutions were used (with five replicates of each) with contents of each of the analyte elements of 0, 50, 100, 150, 200 and 250 μg, except barium, for which the contents were 0, 200, 400, 600, 800 and 1000 μg. Table 2 shows the equations for the different calibration graphs obtained and the regression coefficients. It also shows the linear interval for each straight line used in this work.

Determination of toxic elements in plastics used in toys

Twelve plastics from twelve different toys were analysed and characterized by different colours. The multi-elemental determination of the toxic elements was carried out using the proposed method, involving x-ray fluorescence of the precipitate obtained by (co)precipitation in order to study the concentration of the elements. A reference method for the decomposition of organic matter for each element was used. The reference values were determined by two methods: the same x-ray fluorescence technique with (co)precipitation as described for the proposed method, although each element was determined separately, and AAS as an independent method.

The results found for the different elements with the proposed method and both reference methods are summarized in Table 3, which gives, for each element, the average value of the content ($\mu g\ g^{-1}$) from ten replicate analyses, including the taking of the sample and different decomposition, the standard deviation for each series and the relative error, which was calculated with a probability level of 95% [19]. This last parameter allows the evaluation of the precision of the average results obtained by the proposed method.

Antimony was found in the different samples between the confidence intervals 20.0 ± 0.6 (sample 5, yellow) and 40 ± 2 $\mu g\ g^{-1}$ (sample 7, green), with a precision of the relative error of less than 8.6%. Barium was found between the confidence intervals 31 ± 4 (sample 3, orange) and 5100 ± 430 $\mu g\ g^{-1}$ (sample 10, blue), with a relative error of less than 11.5%. Cadmium was found between the confidence intervals 7.5 ± 0.6 (sample 7, green) and 28.0 ± 1.4 $\mu g\ g^{-1}$ (sample 12, pink), with a relative error of less than 8.7%. Mercury was found between the confidence intervals 1.23 ± 0.05 (sample 9, blue) and 1.96 ± 0.06 $\mu g\ g^{-1}$ (sample 3, orange), with a relative error of less than 7.5%. Lead was found between the confidence intervals 1.09 ± 0.04 (sample 9, blue) and 230 ± 14 $\mu g\ g^{-1}$ (sample 12, pink), with a relative error of less than 9.5%. Arsenic was found between the confidence intervals 15 ± 3 (sample 1, red and 8 green) and 210 ± 7 $\mu g\ g^{-1}$ (sample 12, pink) with a relative error of less than 23%. The greater dispersion of the results found for arsenic may be due to the heterogeneity of the distribution of this element in the matrix of the plastic material, as shown by scanning electron microscopy.

In all instances, the average values obtained by the proposed method and both reference methods are statistically comparable (t_{Fischer} test); the precisions calculated are also statistically concordant (F_{Snedecor} test).

The major advantage of the proposed method is its multi-elemental character, which makes it possible to determine all the toxic elements in the same preparation when x-ray fluorescence is used; consequently, the method is rapid. Another advantage is that as the organic matrix of the sample is totally decomposed; it is converted into an aqueous solution of the ions of the species to be determined and so the reference standards required for calibration can be the aqueous solutions of the species to be determined.

Using the proposed method, the total content of the analyte elements can be determined rapidly

and accurately. When this content is lower than the maximum permitted by the standard for the soluble species extracted with hydrochloric acid, the method provides and advantageous alternative, avoiding the laborious procedures recommended by the legislation. Whatever the case, this method makes it possible to ascertain quickly the total toxic elements present in a sample.

Determination of barium and arsenic after extraction with hydrochloric acid

The results found indicate total contents below the limits established by law (for extractable species), except for barium (five samples) and arsenic (two samples); for these elements an extraction is carried out to evaluate the proportion liberated from the plastic under study.

As in five of the plastics analysed, sample 8 (green), sample 9 (blue), sample 10 (blue), sample 11 (pink) and sample 12 (pink), the total barium content was above the maximum permitted by the legislation for soluble species, a determination after the extraction of soluble especies was carried out following the normal procedure established for this type of operation [1]. Similarly, the determination of arsenic in pink samples (Nos. 11 and 12) after leaching was also carried out. The determination of barium and arsenic in the solution obtained was carried out in accordance with the optimized procedure. The results found are given in Table 4, which expresses the average value (five replicates), standard deviation and relative error with reference to the mean, calculated for a probability level of 95% [19]. It can be seen that the two blue samples (Nos. 9 and 10) have a soluble barium content slightly higher than the maximum permitted by the legislation, whereas the remainder are below 500 $\mu g\ g^{-1}$. For arsenic, the concentrations found after leaching are below the statutary limits. For all the samples, the relative error was calculated to be between 5.4% and 9%.

TABLE 4

Results of determination of soluble barium and arsenic in plastics of toys using an extraction process with hydrochloric acid [1]

Sample No.	Colour	Element	$\bar{x}$ [a]	s [a]	$\epsilon_r(\%)$ [b]
8	Green	Ba	124	9	9.0
9	Blue	Ba	520	35	8.3
10	Blue	Ba	550	38	8.5
11	Pink	Ba	480	25	6.5
		As	15	1	8.2
12	Pink	Ba	450	22	6.0
		As	23	1	5.4

[a] $\bar{x}$ = Mean concentration and s = standard deviation ($\mu g\ g^{-1}$) ($n = 10$). [b] ϵ_r = Relative error.

REFERENCES

1 European Standard EN 71/3, Safety of Toys, Part III, Toxicity of Toys, Assoc. Française de Normalisation (AFNOR), Paris, 1982.
2 A. Mizuike, Fresenius' Z, Anal. Chem., 319 (1984) 415.
3 H.F. Haas and V. Krivan, Fresenius' Z. Anal. Chem., 322 (1985) 261.
4 C. Samara and Th.A. Kovimtzis, Fresenius' Z. Anal. Chem., 327 (1987) 509.
5 G. Reggers and R. Van Grieke, Fresenius' Z. Anal. Chem., 317 (1984) 520.
6 Th.W.S. Pang, A.M. D'Onofrio, F.B. Lo, D.K. Arai and M.A. Nazar, X-Ray Spectrom., 16 (1987) 45.
7 A.T. Ellis, D.E. Leyden, W. Wegscheider, B.E. Jablonski and W.B. Bodnar, Anal. Chim. Acta, 142 (1982) 73.
8 Th. Tisue, Ch. Seils and R.Th. Keel, Anal. Chem., 57 (1985) 82.
9 Ch. Jörrens and H. Hoffmann, Fresenius' Z. Anal. Chem., 303 (1980) 257.
10 R. van Grieken, Anal. Chim. Acta, 143 (1982) 34.
11 C.P. Weisel, R.A. Duce and J.L. Fasching, Anal. Chem., 56 (1984) 1050.
12 D.E. Leyden, K. Goldbach and A.T. Ellis, Anal. Chim. Acta, 171 (1985) 369.
13 T.T. Gorsuch, The Destruction of Organic Matter, Pergamon, Oxford, 1970.
14 T.T. Gorsuch, Analyst, 84 (1959) 135.
15 R.E. Thiers, Methods of Biochemical Analysis, Vol. 5, Interscience, New York, 1957, p. 273.
16 J.L. Down and T.T. Gorsuch, Analyst, 92 (1967) 398.
17 Analytical Methods Committee, Analyst, 90 (1965) 515.
18 F. Feigl and V. Anger, Spot Tests in Inorganic Analysis, Elsevier, Amsterdam, 6th edn., 1972.
19 Y. Lacroix, Analyse Chimique. Interprétation des Résults par le Calcul Statistique, Masson, Paris, 1973.

Analytica Chimica Acta, 267 (1993) 47–64
Elsevier Science Publishers B.V., Amsterdam

Studies on metal speciation in the natural environment

C.L. Chakrabarti, Yanjia Lu and Jianguo Cheng

Centre for Analytical and Environmental Chemistry, Department of Chemistry, Carleton University, Ottawa, Ontario K1S 5B6 (Canada)

M.H. Back

Centre for Analytical and Environmental Chemistry, Department of Chemistry, University of Ottawa, Ottawa, Ontario K1N 6N5 (Canada)

W.H. Schroeder

Atmospheric Environment Service, Environment Canada, 4905 Dufferin Street, Downsview, Ontario M3H 5T4 (Canada)

(Received 19th August 1992; revised manuscript received 2nd December 1992)

Abstract

A scheme for metal speciation has been developed and applied to samples of river water, rain and snow. The scheme combines physical speciation by size using ultrafiltration of the soluble metal species with chemical characterization of the metal species by their dissociation kinetics. The kinetics of metal complex dissociation was studied by anodic stripping voltammetry and by ion exchange at Chelex-100 cation-exchange resin, using both the Chelex column and the Chelex batch technique. These kinetic studies cover a time scale of measurement of ca. 2 ms for anodic stripping voltammetry and up to 6 days for Chelex batch technique, a range of about 8 orders of magnitude. The kinetic results suggest that the copper in the snow sample (pH 3.9) is probably bound to different sites having different bonding energies in polyfunctional complexing agents. Four different copper species having dissociation rate constants of 3.1×10^{-2}, 1.6×10^{-3}, 6.2×10^{-5}, and 8.8×10^{-6} s^{-1} have been observed. All of these species fall in the small size fractions of ultrafiltration. The Al in the Rideau River water sample (pH 8) is probably bound to the different sites in humic materials to yield dissociation rate constants 1.6×10^{-4}, 1.0×10^{-6} and $< 10^{-6}$ s^{-1}. In the Rideau River water sample, most of the soluble Al species have a large molecular size and are probably associated with humic materials. On the other hand, most of the soluble Al species in the small size fraction are Chelex-nonlabile and are probably $Al(OH)_4^-$. Use of graphite platform furnace atomic absorption spectrometer allows direct determination of trace metals in freshwaters, to be done routinely, rapidly, and inexpensively.

Keywords: Anodic stripping voltammetry; Ion exchange; Kinetic analysis; Metal speciation; Size fractionation; Waters

Both metal speciation and biological availability or toxicity are functions of the tendency of the metal to react, as quantified by the free metal ion activity under pseudo-equilibrium conditions [1–3]. During the past 20 years, substantial progress has been made in the understanding of the relationship between a metal form and its toxicity to biota [4,5], of metal–organic interactions in natural waters [6–8], of solubilization and transport of common minerals by organic acids in the terrestrial environment [9], and in the development of metal speciation in environmental samples [10–

Correspondence to: C.L. Chakrabarti, Centre for Analytical and Environmental Chemistry, Department of Chemistry, Carleton University, Ottawa, Ontario K1S 5B6 (Canada).

31]. Kinetic studies of metal speciation have emerged as a powerful approach to chemical speciation (i.e., the distribution of metal forms). The theoretical background for kinetic studies has been developed and discussed in several publications [32–42]. Development and applications of various schemes for study of metal speciation in the aquatic environment have been reported and critically evaluated in the literature [10–31]. Essentially, three approaches have been applied to the study of metal speciation: (1) the experimental determination of the interactions of the metal with the different components of a water body in simplified model systems [6–8,10,11,13]; (2) the development of theoretical models based upon experimentally determined stability constants and thermodynamic considerations [43]; (3) the determination of metal forms in actual water samples [44]. All these approaches are complementary in nature as alone none will provide definitive answers. However, it is clear from some recent publications [14,15] that kinetic studies of metal speciation have a great potential, especially if such studies are done in conjunction with studies on physical speciation of the metal species by their size-fractionation and correlation of the size fractions with the dissociation kinetics of the metal-complex, the underlying assumption being that the "free" metal ion, i.e., the aqua ion and the highly labile metal complexes in the sample are the bioavailable fraction of the total metal in the sample [45]. The dissociation rate constants of metal complexes are of particular interest because the dissociation kinetics of metal complexes may be related to the bioavailability and toxicity of the metal. More importantly, kinetics are important in detailed models of natural systems; in some cases they predominate over equilibrium considerations [22,46–48].

In this paper we report the development of a relatively comprehensive scheme (Fig. 1) for physical and chemical speciation of metals in extension of the earlier work on metal speciation done in our laboratory [6–8,10–13], and by other workers [20,21,29], and the application of this scheme to metal speciation in freshwater samples (Rideau River), and in atmospheric precipitation samples (snow and rain water). The wide range of possible metal species in natural waters can be usefully classified according to the size fractions. Guy and Chakrabarti [7,10] have earlier suggested that differentiation by size, in conjunction with studies of

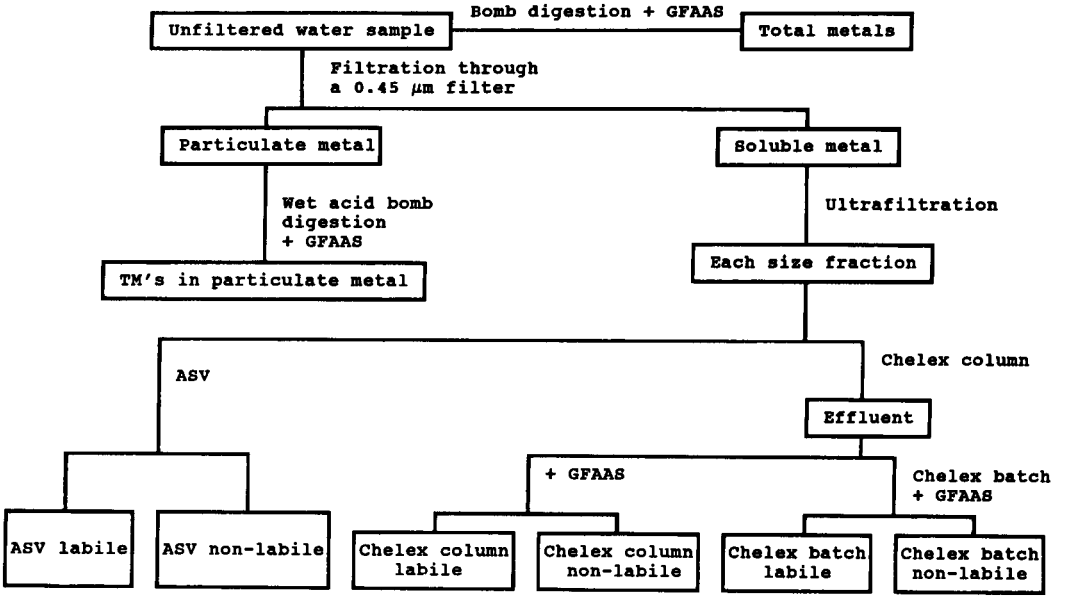

Fig. 1. Scheme for metal speciation. TM = Trace metals; ASV = anodic stripping voltammetry; Chelex = Chelex-100 cation-exchange resin; GFAAS = graphite platform furnace atomic absorption spectrometry.

the chemical behaviour of the size groupings, may serve as a definitive speciation scheme. Such an approach has the advantage that it recognizes the size continuum of metal species [6,7,10]. The scheme of speciation proposed in Fig. 1 has a significant advantage in that it has integrated the physical speciation by size fractionation with the chemical speciation by characterization of metal complexes of each size grouping by dissociation kinetics of metal complexes. We have also studied the applicability of this comprehensive scheme of metal speciation to some selected environmental samples from the aquatic and the atmospheric environment.

Based on the following considerations we have limited the application of our speciation scheme to a few selected elements: Al, Zn, Cu, Cd, Pb, Ni and Fe. As pointed out by Hutchinson [49], there is a long history on the role of aluminium in determining toxicity to aquatic and terrestrial organisms; the great deal of emphasis that has been placed in later years on aluminium in the natural environment only reinforces its great importance. It is now clear that there is strong relationship between aluminium and toxicity [50]. There is considerable evidence to show that cognitive impairment from aluminium is related to aluminium species in drinking water [51]. Speciation of aluminium in acid surface waters has been reported by Courtyn et al. [52]. The other elements: Zn, Cu, Cd and Pb are heavy metals, the toxicity of which are related to their speciation [30]. Nickel and Fe have been added to this list because both are transition elements, having interesting coordination chemistry in aqueous solutions and are therefore of interest to the aquatic environment [53]. Since toxicity of all these metals is related to their speciation [30], total metal determination alone is of limited use for monitoring or assessing environmental effects.

DEVELOPMENT OF THE SPECIATION SCHEME

Filtration

Filtration through a 0.45-μm membrane filter separates the "soluble" metal forms from the particulate metal forms. The soluble metal forms include the colloidal and macromolecular matter (which may have metal species adsorbed, trapped, and/or complexed by the ligand groups on them).

Ion-selective electrodes (ISEs)

ISEs measure the concentration (strictly, activity) of free ions. However, the ISEs do not have sufficiently low detection limits for the determination of most trace metals in natural waters [10,11,54], and hence, ISE has not been included in Fig. 1. ISEs are particularly useful for toxicity studies and for the determination of the complexation capacity of freshwaters [54]. An ISE is also most useful for the determination of the free F^- ion in water samples, which is an important parameter of water quality, and when present in a substantial amount it determines the chemical speciation of aluminium in water by virtue of its forming strong complexes with aluminium at a pH of ca. 5.

Ultrafiltration

The differentiation of metal species by ultrafiltration is by size, shape and charge characteristics rather than by molecular weight [10,11]. Size fractionation of the soluble metal is done by ultrafiltration through a series of Amicon ultrafilters with the following molecular weight (MW) cut-off: 100 000, 50 000, 30 000, 10 000, 5000, 1000 and 500. The purpose of ultrafiltration is to separate the soluble metal species into convenient size groups; the metal species in each size group are then characterized as free metal ions [ISE and anodic stripping voltammetry (ASV)], as metal complexes which are "very labile" (ASV-labile), "moderately labile" (Chelex-column-labile), "slowly labile" (Chelex-batch-labile), and "inert" (the difference between the total soluble metal and the sum of the above three types of labile species). The ultrafiltration technique, when coupled with characterization of the metal species in each size fraction, thus provides a more comprehensive picture and an insight into the physical and the chemical characteristics of the metal species than either the ultrafiltration technique or the three kinetics techniques (ASV, Chelex column and Chelex batch technique) can do alone. However, adsorption loss of metal species on

some ultrafilters is a possibility [10,11], and such loss needs to be guarded against, and if necessary, corrected for.

Anodic stripping voltammetry

An aliquot of each size fraction of ultrafiltration is tested by the ASV technique. The ASV technique mostly uses a hanging mercury drop electrode (HMDE) and measures the concentration of free metal ions as well as easily reducible (labile) metal complexes, whereas inert complexes are not detected [54]. In ASV, the electrodeposition step is characterized by the kinetic parameters of the dissociation of the metal complex, the thickness of the diffusion layer, and the concentration of the ligand [55]. In the ASV method, a metal complex whose dissociation into electroactive species is fast compared to the rate of electrodeposition at a hanging mercury drop electrode in a particular experiment is called "ASV-labile" (i.e., rapidly dissociable) [10,11], or "very labile" [21]. In the ASV method, a water sample is mixed with an appropriate buffer solution and is then tested by the ASV technique using the least negative potential (that gives the maximum electrodeposition efficiency for the uncomplexed metal ion) as the electrodeposition potential [20,21]. The transient measurement time of ASV is of the order of 10^{-3} s [56], which limits ASV to measuring free metal ion plus metal in rapidly dissociable complexes, which may include both strong and week complexes of the metal as the metal ions will be removed at the HMDE during deposition making the dissociation of the complex at the surface of the mercury drop an irreversible process [29]. The metals in natural waters which can be determined by differential pulse anodic stripping voltammetry (DPASV) are copper, lead, cadmium and zinc which form soluble amalgams [10,11]. The application of ASV to metal ion speciation is based on the following two assumptions: (1) the nonlability of metal species is the property of that species only and is not due to an interfering species; (2) each stripping peak corresponds to a single species in solution. It can be shown, however, that both of these assumptions are invalid if surfactants are present in solution [10,11]. Another problem, that of differentiating between a rapidly dissociating and directly-reducible complexes, inherent in the ASV technique, can be avoided by using the Chelex column technique (described below) for a "moderately labile" complex. However, for a "very labile" complex, the present speciation scheme offers no alternative to ASV.

Chelex-100 technique

Chelex-labile (both the column and the batch technique) metal includes free metal, plus metal bound in complexes weaker than the Chelex–metal complex. In addition, metal complexes stronger than the Chelex–metal complex may appear as Chelex-labile if the Chelex resin is present in considerable excess relative to the concentration of the stronger ligand [29]. Another aliquot of the same size fraction as used in the ASV technique is tested sequentially by the Chelex column and the Chelex batch technique as described below.

Chelex column technique

As mentioned above, another aliquot of the same size fraction as used in the ASV technique is tested sequentially by the Chelex column and the Chelex batch technique. In the Chelex column technique, Chelex-100 is used in a column as a cation-exchange resin. This technique can be regarded as a transient technique with a time scale of measurement 6–9 s, which can be changed by varying the flow-rate or the column length. Thus, the Chelex-column labile fraction is defined operationally as the fraction of the metal taken up by the resin in 6–9 s. This time scale is about 3 orders of magnitude longer than the time scale of measurement by ASV. Hence the Chelex-column labile fraction may well include some ASV-nonlabile metal species. Since the ASV and the Chelex-column techniques are performed on separate aliquots of the same size-fraction of the ultrafiltered sample, the Chelex-column-labile fraction includes the ASV-labile fraction also.

Chelex batch technique

The effluent from the Chelex column technique is directly used in the Chelex batch tech-

nique, which consists of adding an appropriate amount of fresh Chelex-100 to the effluent and shaking the mixture up to 144 h and measuring uptake of the metal by the Chelex resin at suitable intervals. The Chelex batch technique will define labile species in a different sense from the ASV technique. Chelex-batch-labile metal will be largely independent of the dissociation kinetics of the metal complexes, given the long equilibration time up to 144 h used in our work.

Graphite platform furnace atomic absorption spectrometry (GFAAS)

In Fig. 1, the metals are determined by graphite platform furnace atomic absorption spectrometry which has detection limits several orders of magnitude better than those of ASV, and which, unlike ASV, can determine all metals. Because of its extremely high sensitivity and relative freedom from interferences, direct (i.e., without any preconcentration) determination of all trace metals found in freshwaters is done routinely, rapidly and inexpensively. This technique provides routinely high accuracy and precision and is excellent for direct determination of trace metals in freshwaters.

A limitation of the speciation scheme presented in this paper is that the results it generates are operationally defined and are therefore difficult to be interpreted in terms of bioavailability. However, correlation of chemical characteristics (dissociation kinetics) of metal species with toxicity gives a valuable indication of the toxic metal species. For example, the toxicities to salmon of cadmium in river water and treated sewage effluents have been reported to correlate with Chelex-batch-labile fraction of cadmium [57]. The Chelex batch technique should therefore provide results which would be biologically significant. With respect to metal transport and for comparing one water body with another, it should be possible to make meaningful observations on the basis of the speciation data concerning differences in trace metal associations. The information provided by this scheme will be of particular value when assessing changes brought about by the introduction of a polluting discharge, i.e., the difference between the metal distribution upstream and downstream of an effluent outfall [29].

KINETIC MODEL

Dissolved organic materials collectively termed humic materials (HM) in natural waters are polyelectrolytes and are poorly characterized, polydisperse macromolecules having binding sites of different chemical affinities, i.e., polyfunctional [7,14,22,23,41]. Determination of the metal dissociation rate constant for each of these binding sites reduces to the problem of analyzing a multicomponent mixture for which the dissociation mechanisms, relative rate constants, and the nature and the number of binding sites are unknown [23].

The kinetic model was developed to study the dissociation kinetics of MHM, where M is a metal ion, say Cu^{2+} [23]. In the CuHM, Cu^{2+} is bound by multiple sites in HM, all of which dissociate independently and simultaneously at a rate that depends on the nature of the functional group, its position on the macromolecule (HM), and the residual charge. Consider an aqueous mixture of n components in which each component, designated $CuHM_i$, exists in equilibrium with its dissociation products:

$$CuHM_i \rightleftharpoons Cu^{2+} + HM_i \quad (1)$$

where HM_i is the ith Cu^{2+} binding site on HM. Equation 1 is a general statement of the reaction in which electrochemical neutrality is neglected since the charge on CuHM varies with the extent of metal binding. The model therefore describes a system of simultaneous, first-order (or pseudo-first-order) reactions in which either reactant or product concentration can be monitored over time. Each complex, $CuHM_i$, undergoes independently and simultaneously, a first-order, or pseudo-first-order dissociation reaction as shown by Eqn. 2:

$$CuHM_i \xrightarrow{k_i} Cu^{2+} + HM_i \quad (2)$$

where k_i is the rate constant for the dissociation of $CuHM_i$ species. Although HM has been used in the above model, any other polyfunctional

complexing agent can be substituted for HM. The model, however, requires that the reaction shown in Eqn. 2 be first-order or pseudo-first-order.

Chelex resin contains an iminodiacetic acid chelating functional group; when fully ionized Chelex may be represented as $Chelex^{2-}$. The reaction between Chelex-100 cation-exchange resin and $CuHM_i$ is:

$$Chelex^{2-} + CuHM_i \rightleftharpoons Chelex - Cu + HM_i^{2-} \quad (3)$$

If the rate-limiting step in reaction 3 is assumed to be the dissociation of $CuHM_i$ (reaction 2), then the measured kinetics will represent the kinetics of the slow step, i.e., the dissociation of the metal complex, $CuHM_i$ (reaction 2). Experiments done at our laboratory have justified this assumption. The concentration of copper left in the water sample after uptake of copper by Chelex resin is monitored by graphite platform furnace atomic absorption spectrometry (GFAAS).

EXPERIMENTAL

Reagents

Stock solutions (1000 μg ml^{-1}) of Cd, Cu, Ni, Pb were prepared by dissolving an appropriate quantity of CdO (Baker, Analyzed reagent), copper metal (99.9% pure), nickel metal powder (SPEX, 99.999%) and $Pb(NO_3)_2$ (Fisher, A.C.S. reagent), in nitric acid with heating and diluting to the appropriate volume with ultrapure water; the final solutions contained 1% (v/v) ultrapure HNO_3. Stock solution (1000 μg ml^{-1}) of aluminium was prepared by dissolving 0.5000 ± 0.004 g aluminium powder (SPEX) in 20 ml $HCl-H_2O$ (1:1) (the HCl was Ultrex brand) with heating and diluting to 500 ml with ultrapure water. A reagent solution (1000 μg ml^{-1}) of Zn was purchased from BDH. Ultrapure water of resistivity of 18.2 MΩ cm was obtained directly from a Milli-Q-plus water purification system (Millipore). Ultrapure HNO_3 (Ultrex) was used for the acidification of all samples.

2.0 M sodium acetate solution was prepared by dissolving an appropriate quantity of sodium acetate (BDH) in ultrapure water. This solution then was purified by electrolyzing at −1.4 V vs. SCE for 48 h and then stored in a covered PTFE container till used.

Cleaning procedure

The following cleaning procedure was used. All containers used in this research project were sequentially soaked in $HCl-H_2O$ (1:1) (HCl was AR grade) and HNO_3-H_2O (1:1) for one week at room temperature (HNO_3 was AR grade), followed by a five-time rinse with ultrapure water. In order to leach out trace analytes, these containers were then soaked in 6 g l^{-1} Na_2EDTA aqueous solution [58–60] for 24 h, followed by a rinse with ultrapure water. Finally, they were soaked in ultrapure water for two or more weeks until they were used. The containers used for the Chelex batch experiment and for the sample storage were pre-equilibrated with the water sample for 24 h before use.

The 0.45-μm filters (Gelman) were soaked in 0.5% HNO_3 for 24 h, followed by a rinse with ultrapure water to leach out trace metals.

In order to remove both heavy metal contaminants and organic wetting agents which might interfere with subsequent analysis, the Amicon disc membrane filters (diameter of 62 mm) for ultrafiltration were preconditioned [29] by successively soaking in dilute NaOH aqueous solution (pH < 11), 0.5% ultrapure HNO_3 (Ultrex), and finally in ultrapure water. The ultrafilters were then stored in a 10% ethanol in water solution till use.

Chelex-100 resin (Bio-Rad, 100–200 mesh, sodium form) was washed with ultrapure water and was then equilibrated with ultrapure water at the pH of the water sample for at least 24 h.

Collection and pretreatment of water samples

A water sample (5–10 l) from Rideau River was collected using a precleaned polyethylene water sampler from a site at Carleton University. Samples of rain water and snow were collected at a site on the roof top of the chemistry building at Carleton University.

The pH and conductivity of the water samples were measured (using Fisher Scientific, Accumet

TABLE 1

Analysis lines and instrumental conditions for graphite platform furnace atomic absorption spectrometry

Element	Analysis line (nm)	Ashing temperature (°C)	Atomization parameters	
			Temp. (°C)	Duration (s)
Al	309.2	1300	2400	7
Cd	228.8	400	1600	4
Cu	324.8	1200	2300	5
Fe	248.3	900	2500	6
Ni	232.0	1000	2400	8
Pb	283.3	500	1900	5
Zn	213.9	500	2000	5

925 pH/ion meter and a Model 31 YSI conductivity bridge, respectively) immediately after the sample collection.

An aliquot of the water sample was acidified to contain 1% HNO_3 (Ultrex) right after the sample collection to preserve metal ions for the determination of total metal [61]. Another aliquot of the water sample was set aside for measurement by DPASV. The remaining water sample was immediately filtered through a 0.45-μm filter. For each filter, the first 200 ml of the filtrate was discarded. The insoluble matter retained on the filter was used for the determination of the metal content in the particulate phase. The filtrate was used for determination of the metal speciation in the soluble phase.

Analysis of water samples

The concentrations of the metals of interest in the water samples were determined by graphite platform furnace atomic absorption spectrometry (GFAAS). The equipment used was a Perkin-Elmer Zeeman Model 5000 atomic absorption spectrophotometer, equipped with a HGA-500 graphite furnace. Pyrolytically-coated graphite tubes (Perkin-Elmer catalog No. 109322) and laboratory-made platforms fabricated from anisotropic graphite were used. Table 1 shows the instrumental parameters used in the graphite platform furnace atomic absorption spectrometric (GFAAS) determination of the metals: Al, Cd, Cu, Fe, Ni, Pb and Zn. Aliquots of the test solutions (1 ml) were acidified with 10 μl of concentrated nitric acid in small plastic vials. For determination of the metal concentrations, 10–20 μl of this acidified solution was injected into the graphite furnace, where it was dried, charred and atomized. The signal was measured in the peak area mode. Each completed determination was followed by a 3-s clean-up step of the graphite tube at 2600°C. During the drying, charring and clean-up cycles, the internal argon gas was passed through the furnace at 300 ml min^{-1}. The internal argon gas flow was interrupted during the atomization cycle.

Determination of total metal in the unfiltered water sample. The total metal in the unfiltered water sample was determined by graphite platform furnace atomic absorption spectrometry using the following two methods (i) and (ii).

(i) The total metal in the unfiltered sample was determined using two procedures for wet acid digestion of the unfiltered water sample: (1) atmospheric-pressure digestion, and (2) high-pressure bomb acid digestion. The atmospheric-pressure digestion was done following the procedures prescribed in the standard methods of analysis [62]. The high-pressure bomb digestion was carried out in 10% HNO_3 solution in a PTFE-lined steel bomb by heating the steel bomb in an air oven for 4 h at a temperature of 150°C. The high pressure bomb digestion procedure yielded higher recoveries (ca. 100%) than the atmospheric-pressure digestion procedure and was therefore adopted for all further work.

(ii) The total metal in the soluble and the particulate phase was determined separately. The sum of these two values gave the total metal concentration in the water sample.

Table 2 shows that both the methods (i) and (ii) are satisfactory for determination of the total

TABLE 2

Total aluminium in the Rideau River water samples

Date of sampling	Aluminium concentration ($\mu g\, l^{-1}$)	
	Method 1	Method 2
January 3, 1992	91.9 ± 6.0	97.7 ± 2.1
January 28, 1992	111.1 ± 8.3	106.4 ± 7.9
February 27, 1992	97.6 ± 2.1	97.3 ± 2.2

aluminium concentrations in natural water samples. Direct determination of the aluminium in water sample was also studied but the results showed unacceptable variations which were due to lack of homogeneity in the water sample, especially in the microlitre volumes of test solution taken for direct determination by graphite platform furnace atomic absorption spectrometry.

Determination of the total metal in the particulate phase. After 500 ml water sample had passed through a 0.45-μm filter, the filter containing the retained particulate matter was transferred into a PTFE-lined bomb and digested with 20 ml of 10% HNO_3 for 4 h in an air oven at 150°C. The solution was then transferred into a 500-ml volumetric flask and diluted to the mark with ultrapure water containing 1% HNO_3. Aliquots of this 500 ml solution were used for determination of their metal content by GFAAS.

Speciation of metal in the soluble phase. The filtrate of the 0.45-μm filter was used for the speciation of metals, employing ultrafiltration, the Chelex-100 column and the Chelex-100 batch technique, and DPASV.

Ultrafiltration was carried out by using Amicon ultrafiltration stirred cell, Model 8200. When filtering a sample, the first 10% and the last 50% of the ultrafiltrate were discarded, collecting only the middle fraction, since the initial volume could contain a reduced concentration of species in the ultrafiltrate because of dilution by water trapped in the filter [30] and the last 50% of the ultrafiltrate often contained higher concentrations of organic carbon because of leakage of high-molecular-weight substances occurring as the concentration of retained species above the membrane increased [63].

Both the Chelex-100 column and the Chelex-100 batch technique were used for metal speciation. In the Chelex column technique, the water sample passed through a Chelex-100 column which contained 5 g of Chelex-100 resin. The effluent was collected for determination of the Chelex-column-nonlabile metal species. Subtraction of the Chelex-column-nonlabile species from the total soluble metal gave the Chelex-column-labile metal species. In the Chelex batch technique, the resin (1%, w/w) was added to the effluent of the Chelex column technique and the mixture was shaken with a wrist-action mechanical shaker. At specific times, the shaking was stopped for a short period of time (< 1 min) to let the Chelex resin settle down, and 1 ml of the clear solution was withdrawn to a small plastic vial. This solution was acidified to contain 1% HNO_3 for the determination of its metal content by graphite platform furnace atomic absorption spectrometry. The initial and the final pH of the Chelex-100 batch test solution were measured.

The DPASV measurements were carried out using a PAR Model 174A polarographic analyzer (Princeton Applied Research, NJ), equipped with an Omnigraphic recorder Model 3000. The 50-ml-Pyrex glass cell was equipped with three electrodes: a Metrohm Microfeed hanging mercury drop electrode (HMDE) E410 as the working electrode, a Pt-coil as the auxiliary electrode and a saturated calomel electrode (SEC) as the reference electrode. The glass cell was also equipped with a magnetic stirrer (Metrohm Model 405). The DPASV measurement of Al in Rideau River water sample was done at pH 6.1 as follows. An aliquot of 50 ml of the soluble phase was transferred into the glass cell. After deaeration (by bubbling 99.999% N_2 for 10 min), electrodeposition of the aluminium was done at the $E_{appl.} = -1.7$ V (vs SCE) for 5 min using continuous stirring of the sample solution. After this operation, the stirring was stopped and the sample solution allowed to rest for 30 s before the metal was stripped by using a linear scan in the anodic direction at a rate of 10 mV s^{-1}. The DPASV measurement of Cu, Pb and Zn in the snow sample (pH 6.1), was done sequentially, at the electrodeposition potential -0.07 V, -0.45 V, and -1.15 V, respectively, vs. SCE, for 60 s with stirring, followed by a 30-s rest period (i.e., without stirring). In the stripping step the applied voltage was increased in the positive (anodic) direction in a linear sweep, the sweep rate was 10 mV s^{-1} with an imposed pulse of 10 mV every 0.5 s, and the scan range was 0.75 V. A 0.040 M sodium acetate aqueous solution was used both as a supporting electrolyte and a buffer. The initial and the final pH of the test solution were measured.

RESULTS AND DISCUSSION

pH and conductivity

Table 3 shows the pH and the conductivity of the samples of Rideau River water, rain water and snow-melt. The pH and the conductivity are important parameters of water quality, the conductivity reflects the ionic concentrations of the soluble solute. The pH of the Rideau River water sample was found to be higher than those of the rain water and the snow-melt. The pH of Rideau River water was relatively constant (8.0 ± 0.1), whereas the pH of the rain water and the snow-melt varied day to day from 3.8 to 6.0. The conductivity averaged between 389.8 and 470.1 $\mu S\ cm^{-1}$ for the Rideau River water samples, between 17.0 and 37.7 $\mu S\ cm^{-1}$ for the rain water samples, and between 8.1 to 28.8 $\mu S\ cm^{-1}$ for the snow-melt samples. There was no significant difference in the pH and the conductivity between the unfiltered and the filtered (through a 0.45-μm filter) samples.

TABLE 3

pH and conductivity of the Rideau River water, the rain water and the snow samples

Sample	Date of sampling	pH	Conductivity ($\mu S\ cm^{-1}$)
River water	December 24, 1991	8.0	400.0
River water	January 3, 1992	7.9	389.8
River water	January 28, 1992	8.0	470.1
River water	February 26, 1992	8.0	389.8
Rain water	September 15, 1991	3.8	23.7
Rain water	September 26, 1991	5.9	37.7
Rain water	November 24, 1991	6.1	26.9
Rain water	April 17, 1992	5.3	17.0
Snow-melt	December 3, 1991	5.7	8.1
Snow-melt	January 10, 1992	3.9	28.8
Snow-melt	April 12, 1992	4.7	11.0

Fluoride

Table 4 shows the fluoride concentrations in the Rideau River water samples. However, at pH 8 of the water sample, the equilibrium distribution of Al-species in the water sample shows that the predominant species were $Al(OH)_4^-$; only at a pH of ca. 5 would there be a significant fraction of the Al present as AlF^{2+} [64].

TABLE 4

Fluoride in the Rideau River water samples

Date of sampling	Fluoride concentration ($\mu g\ l^{-1}$)
March 5, 1992	53
March 10, 1992	140

Metal species in water samples

Rideau River water. Tables 5 and 6 show the aluminium species in the Rideau River water samples. The total aluminium concentration in the river water samples averaged 100.5 $\mu g\ l^{-1}$, of which ca. 78% of the aluminium species was in

TABLE 5

Aluminium species in the Rideau River water samples

	Aluminium concentration ($\mu g\ l^{-1}$)		
	January 3, 1992 (pH 7.9)	January 28, 1992 (pH 8.0)	February 26, 1992 (pH 8.0)
Total aluminium conc.	97.7 ± 2.1 (100.0)	106.4 ± 7.9 (100.0)	97.3 ± 2.2 (100.0)
Aluminium conc.:			
In the particulate phase	71.9 ± 1.7 (73.6)	84.4 ± 6.5 (79.3)	76.6 ± 0.8 (78.7)
In the soluble phase	25.8 ± 0.4 (26.4)	22.0 ± 1.4 (20.7)	20.7 ± 1.4 (21.3)
Lability of the soluble-phase aluminium species:			
ASV-labile	Nil (0.0)	Nil (0.0)	Nil (0.0)
Chelex-column-labile	15.1 ± 1.8 (58.5)	13.4 ± 2.3 (60.9)	11.3 ± 1.8 (54.6)
Chelex-batch-labile	6.7 ± 1.6 (26.0)	5.8 ± 2.7 (26.4)	5.8 ± 0.1 (28.0)
Inert	4.0 ± 0.2 (15.5)	2.8 ± 1.8 (12.7)	3.6 ± 0.5 (17.4)

TABLE 6

Soluble aluminium species in the Rideau River water sample (pH 8.0) (date of sampling, February 26, 1992)

	Total Al conc. ($\mu g\,l^{-1}$) (%)	Chelex-column-labile Al conc. ($\mu g\,l^{-1}$) (%)	Chelex-column-nonlabile Al conc. ($\mu g\,l^{-1}$) (%)
Total aluminium in the soluble phase	20.7 (100.0)	11.3 (100.0)	9.4 (100.0)
Ultrafiltration MW cut-off:			
> 100 000	9.9 (47.8)	3.4 (30.1)	6.5 (69.2)
100 000–5000	2.8 (13.5)	1.7 (15.0)	1.1 (11.7)
5000–500	5.8 (28.0)	5.7 (50.4)	0.1 (1.0)
< 500	2.2 (10.7)	0.5 (4.5)	1.7 (18.1)

the particulate phase and ca. 22% in the soluble phase. At pH 8, no aluminium species in the soluble phase was ASV-labile, which merely reflected the fact that the aluminium species were not reducible at the mercury electrode in ASV under the experimental conditions we used. About 60% of the soluble species of aluminium was Chelex column-labile, > 26% was Chelex-batch labile, and < 20% was inert; the last fraction was probably the aluminium species adsorbed on and/or trapped by colloidal matter. Only 10.7% of the total soluble aluminium species passed through the ultrafilter with a MW cut-off 500; of this fraction about 77% was Chelex-column-nonlabile. Equilibrium calculations indicated that at pH 8 the predominant soluble Al species in water was $Al(OH)_4^-$ [64]. The $Al(OH)_4^-$ species was probably small enough to pass through the ultrafilter with a MW cut-off 500, and was Chelex-column-nonlabile probably because the fully ionized $Chelex^{2-}$ repelled the negatively charged $Al(OH)_4^-$ species.

Humic materials, which have relatively large molecular weights and a wide range of distribution of molecular weights depending upon their sources, are abundant in natural waters. In natural waters, the polyfunctional humic materials bind metal ions to their functional groups. On the other hand, because of its small ionic radius and high charge density, Al^{3+} ion is a very strong Lewis acid and can therefore easily form strong complexes with many ligands. Also, polymeric colloidal materials which abound in natural waters can adsorb and/or trap Al^{3+} ions on or inside these materials. With the aluminium associated with such macromolecules, ca. 90% of the soluble aluminium species was retained by the ultrafilter with a MW cut-off of 500, and 47.8% was retained by the ultrafilter with a MW cut-off 100 000, i.e., the soluble aluminium species were

TABLE 7

Metal species in the rain water and the snow samples

	Al ($\mu g\,l^{-1}$) (%)	Cu ($\mu g\,l^{-1}$) (%)	Ni ($\mu g\,l^{-1}$) (%)	Fe ($\mu g\,l^{-1}$) (%)
April 12, 1992, snow (pH 4.7)				
Total metal conc.	600.9 ± 18.4 (100.0)	24.6 ± 0.4 (100.0)	94.4 ± 25.6 (100.0)	345.2 ± 12.0 (100.0)
Metal conc.:				
In the particulate phase	593.9 ± 18.5 (98.8)	19.8 ± 0.6 (80.5)	89.2 ± 26.9 (94.5)	336.2 ± 13.0 (97.4)
In the soluble phases	7.0 ± 0.8 (1.2)	4.8 ± 0.2 (19.5)	5.2 ± 0.3 (5.5)	9.0 ± 1.0 (2.6)
April 17, 1992, rain water (pH 5.3)				
Total metal conc.	211.6 ± 17.5 (100.0)	30.3 ± 3.4 (100.0)	22.3 ± 0.7 (100.0)	129.9 ± 6.6 (100.0)
Metal conc.:				
In the particulate phase	169.6 ± 18.9 (80.2)	0.5 ± 0.05 (1.7)	17.8 ± 0.5 (79.8)	85.3 ± 4.3 (65.7)
In the soluble phase	42.0 ± 1.4 (19.8)	29.8 ± 0.7 (98.3)	4.5 ± 0.3 (20.2)	44.6 ± 0.7 (34.3)

TABLE 8

Lability of metal species in the rain water and the snow samples

	Al ($\mu g\ l^{-1}$) (%)	Cu ($\mu g\ l^{-1}$) (%)	Ni ($\mu g\ l^{-1}$) (%)	Fe ($\mu g\ l^{-1}$) (%)
April 12, 1992, snow (pH 4.7)				
Total soluble metal species	7.0 ± 0.8 (100.0)	4.8 ± 0.2 (100.0)	5.2 ± 1.3 (100.0)	9.0 ± 1.0 (100.0)
Chelex-column-labile metal species	3.8 ± 1.0 (54.3)	4.0 ± 0.4 (83.3)	2.4 ± 2.0 (46.2)	2.6 ± 2.1 (28.9)
Chelex-column-nonlabile metal species	3.2 ± 0.2 (45.7)	0.8 ± 0.2 (16.7)	2.8 ± 0.7 (53.8)	6.4 ± 1.1 (71.1)
April 17, 1992, rain water (pH 5.3)				
Total soluble metal species	42.1 ± 1.4 (100.0)	29.8 ± 0.7 (100.0)	4.5 ± 0.8 (100.0)	44.6 ± 0.7 (100.0)
Chelex-column-labile metal species	35.6 ± 1.6 (84.8)	24.7 ± 1.0 (82.9)	0.9 ± 0.1 (19.2)	11.2 ± 1.0 (25.1)
Chelex-column-nonlabile metal species	6.41 ± 0.2 (15.2)	5.1 ± 0.3 (17.1)	3.6 ± 0.6 (80.8)	33.4 ± 0.3 (74.9)

predominantly large-sized charged species, likely to be non-labile and not bioavailable [50].

Rain water and snow. Tables 7 and 8 show Al, Cu, Ni and Fe species and their lability in the rain water and the snow samples. The total Al concentrations in the rain and the snow samples were 211.6 $\mu g\ l^{-1}$ and 600.9 $\mu g\ l^{-1}$, respectively, of which > 80% of the aluminium species was in the particulate phase. At pH 5, no aluminium species in the soluble phase were ASV-labile, and > 50% of the soluble species of aluminium in the snow sample was Chelex-column-labile, whereas > 80% in the rain water sample was Chelex-column-labile.

The total Cu, Ni and Fe concentrations were 24.6, 94.4, 345.2 $\mu g\ l^{-1}$, respectively, in the snow sample (pH 4.7), and 30.3, 22.3, 129.9 $\mu g\ l^{-1}$, respectively, in the rain water sample (pH 5.3). Most of these metals (65%–97%) was in the particulate phase except the Cu in the rain water (1.7%). In the soluble phase, > 80% of the copper and < 30% of the iron were Chelex-column-labile in both the snow and the rain water, whereas 46.2% of the Ni in the snow and 19.2% of the Ni in the rain water were Chelex-column-labile. The atmospheric precipitation samples were affected by weather conditions, and hence, species of the same element in these samples could be quite different from sample to sample. Since the pHs of the snow and the rain water were < 6, the metal species in these sample were probably positively charged, and they were, therefore, exchangeable at Chelex-100 resin. Hence, most of these species were found to be Chelex-column-labile.

Table 9 shows the results of size fractionation by ultrafiltration and the lability of the aluminium species in the snow sample (pH 4.7) in

TABLE 9

Soluble aluminium species in the snow sample (pH 4.7) (Date of sampling, April 12, 1992)

	Total Al conc. ($\mu g\ l^{-1}$) (%)	Chelex-column-labile Al conc. ($\mu g\ l^{-1}$) (%)	Chelex-column-nonlabile Al conc. ($\mu g\ l^{-1}$) (%)
Total aluminium in the soluble phase	7.0 ± 0.8 (100.0)	3.8 ± 1.0 (54.3)	3.2 ± 0.2 (45.7)
Ultrafiltration MW cut-off:			
> 5000	0	0	0
5000–500	1.8 ± 1.2 (100.0)	0 (0.0)	1.8 ± 0.2 (100.0)
< 500	5.2 ± 0.4 (100.0)	3.7 ± 0.4 (71.2)	1.5 ± 0.2 (28.8)

TABLE 10

Size fractionation of zinc, copper, lead and cadmium species in the snow sample (pH 3.9) by ultrafiltration (Date of sampling, January 10, 1992)

Description of the metal species	Zn ($\mu g\ l^{-1}$)	Cu ($\mu g\ l^{-1}$)	Pb ($\mu g\ l^{-1}$)	Cd ($\mu g\ l^{-1}$)
Total metal conc.	9.0 ± 0.1	5.7 ± 0.2	5.5 ± 0.3	0.11 ± 0.01
Metal conc.:				
In the particulate phase	0.90 ± 0.09	1.08 ± 0.05	1.00 ± 0.08	0.005 ± 0.001
In the soluble phase	8.13 ± 0.02	4.7 ± 0.2	4.4 ± 0.3	0.11 ± 0.01
Ultrafiltration				
MW cut-off:				
> 100000	0	0	0	0
100000–50000	0	0	0	0
50000–30000	0	0	0	0
30000–10000	0	0	0	0
10000–1000	2.5 ± 0.1	2.0 ± 0.1	2.3 ± 0.1	0.035 ± 0.010
< 1000	5.6 ± 0.1	2.7 ± 0.1	2.1 ± 0.1	0.075 ± 0.002

the soluble phase; > 70% of the aluminium species passed through the ultrafilter with MW cut-off 500, of which 71.2% was Chelex-column-labile. Since the samples of snow and rain water contained relatively low levels of organic matter, the size and molecular weight of aluminium species in these samples were small. The snow and the rain water samples at pH < 6 had more aluminium species that were Chelex-column-labile compared to those in the Rideau River water sample at pH 8. The aluminium species in the snow and the rain water samples at pH < 6 were probably a mixture of $Al(OH)^{2+}$, $Al(OH)_2^+$, $Al(OH)_4^-$ and other small inorganic complexes of aluminium.

Table 10 shows the results of size fractionation of Zn, Cu, Pb and Cd species in the snow sample (pH 3.9). The total Pb, Cd, Cu, and Zn metals in the snow sample were 5.5, 0.11, 5.7, and 9.0 $\mu g\ l^{-1}$, respectively, which represented more than 80% of these metals in the soluble phase.

TABLE 11

ASV-lability of metal species in the snow sample (pH 3.9) (Date of sampling, January 10, 1992)

	Zn ($\mu g\ l^{-1}$)	Cu ($\mu g\ l^{-1}$)	Pb ($\mu g\ l^{-1}$)	Cd ($\mu g\ l^{-1}$)
ASV-labile	7.5 ± 0.1	2.0 ± 0.1	4.7 ± 0.5	N.D. [a]
ASV-nonlabile	0.6 ± 0.1	2.7 ± 0.2	N.D. [a]	N.D. [a]

[a] Not detectable.

Table 11 shows the results of the ASV measurements of Cd, Cu, Pb and Zn species in the snow sample (For the ASV measurement, the added sodium acetate changed the snow solution pH to 6.1). The cadmium was not detectable because of its low concentration; 42.6% of the copper, 100% of the lead and 92.6% of the zinc were ASV-labile.

Table 12 shows the results of determination of the Chelex-batch-lability of Zn, Cu, Pb and Cd species in the snow sample (the addition of Chelex-100 resin to the snow-melt changed the

TABLE 12

Chelex-100-batch lability of the metal species

Metal	$C_{o,i}$ ($\mu g\ l^{-1}$)	Rate constant (s^{-1})	Half-life (s)
January 10, 1992, snow (pH 3.9)			
Cu	2.4 ± 0.1	$(3.1 \pm 0.5) \times 10^{-2}$	22.4
	0.7 ± 0.1	$(1.6 \pm 0.1) \times 10^{-3}$	4.33×10^2
	0.9 ± 0.1	$(6.2 \pm 1.1) \times 10^{-5}$	1.12×10^4
	0.8 ± 0.1	$(8.8 \pm 0.3) \times 10^{-6}$	7.88×10^4
Zn	8.0 ± 0.1	$(4.0 \pm 0.1) \times 10^{-3}$	1.73×10^2
	0.13 ± 0.03	$< 2.8 \times 10^{-6}$	$> 2.5 \times 10^5$
Pb	4.4 ± 0.1	$(1.0 \pm 0.3) \times 10^{-2}$	69.3
CdR	0.11 ± 0.01	$(8.2 \pm 0.7) \times 10^{-3}$	84.5
February 26, 1992, river water (pH 8.0)			
Al	12.2	$(1.6 \pm 0.2) \times 10^{-4}$	4.3×10^3
	3.4	$(1.0 \pm 0.2) \times 10^{-6}$	6.9×10^5
	6.0	$< 10^{-6}$	$> 6.9 \times 10^5$

pH to 6.2), and Al in the Rideau River water sample. The symbol $C_{o,i}$ stands for the initial concentration of the metal species at the ith site of the ligand molecule. The Chelex-100 batch study showed that 100% of the lead, cadmium and copper species, and 98% of the zinc species were labile, with half-lives of the first-order (or the pseudo-first-order) reactions covering a wide range. The results of Table 12 and Figs. 2 and 3 can be interpreted in terms of polyfunctionality of complexing agents having different complexing sites (i.e., of different chemical affinities) on the ligand molecule for binding metal ions [7,14,22, 23,41]. For the copper species, four distinct species were observed, dissociating at different rates, with dissociation rate constants: 3.1×10^{-2} s^{-1}, 1.6×10^{-3} s^{-1}, 6.2×10^{-5} s^{-1}, and 8.8×10^{-6} s^{-1}. For the zinc species, two distinct zinc species were observed, one with a rate constant of 4.0×10^{-3} s^{-1}, and the other with a rate constant $< 2.8 \times 10^{-6}$ s^{-1} (Fig. 4 shows only the former and not the latter because of the short time covered by Fig. 4). The lead and the cadmium species showed only one metal complex each, with a rate constant 1.0×10^{-2} s^{-1} and 8.2×10^{-3} s^{-1}, respectively. Ultrafiltration results (Table 10) show that all of the soluble species passed through the 10000 MW cut-off ultrafilter, and 40% of the lead, 68% of the cadmium, 57% of the copper and 70% of the zinc species passed through the 1000 MW cut-off ultrafilter. All of the species that passed through the 1000 MW cut-off ultrafilter were Chelex-column-labile at a column flow-rate of 2 ml min^{-1}. In the Chelex-column technique, the amount of the Chelex-100 resin was large and the contact time was short, and hence, the uptake of metal species in the snow-melt was kinetically controlled (diffusion-limited), and only the small-size fractions of the metal species were Chelex-column-labile. In the Chelex-batch technique, the ion-exchange reaction was allowed to proceed as long as it was necessary for equilibrium to be attained, and the uptake of the metal species was independent of the kinetics of the processes involved; this meant that the large-size-fractions of the metal species also were Chelex-batch-labile.

Unlike the Rideau River water sample, the

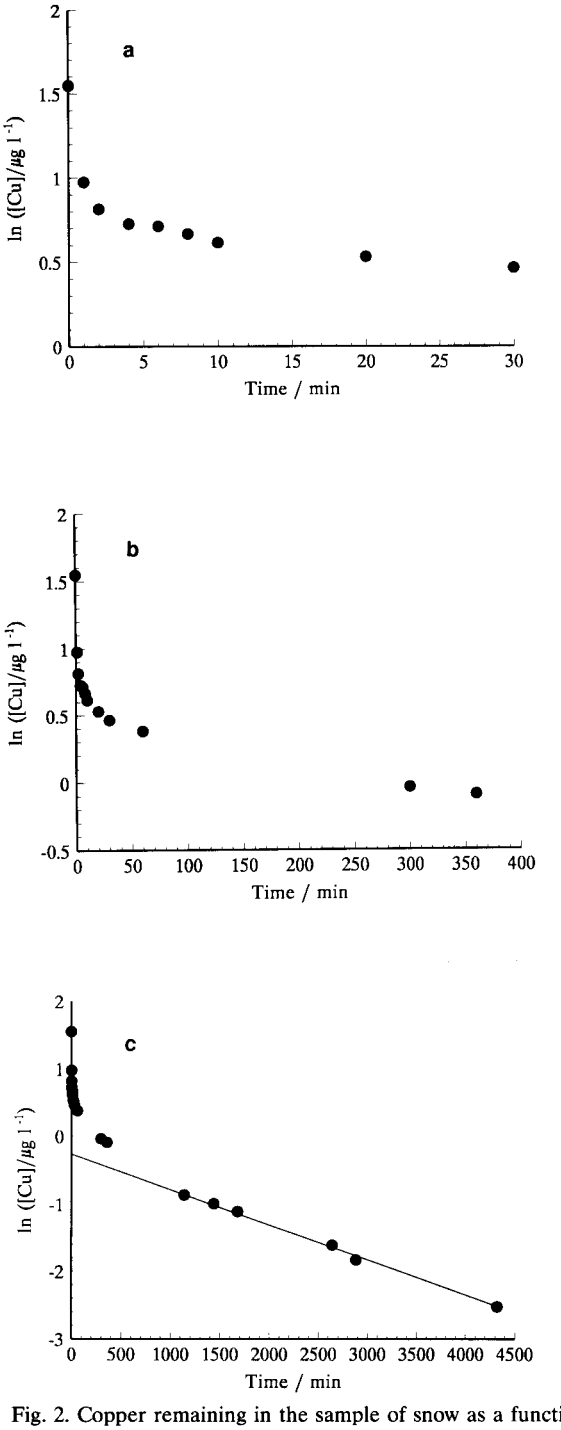

Fig. 2. Copper remaining in the sample of snow as a function of time after uptake of the copper by Chelex-100 in the Chelex batch technique. (a) and (b) are the expansions of (c) in the specific time ranges. The concentration of Chelex-100: 1% (w/w). pH of the sample: 3.9.

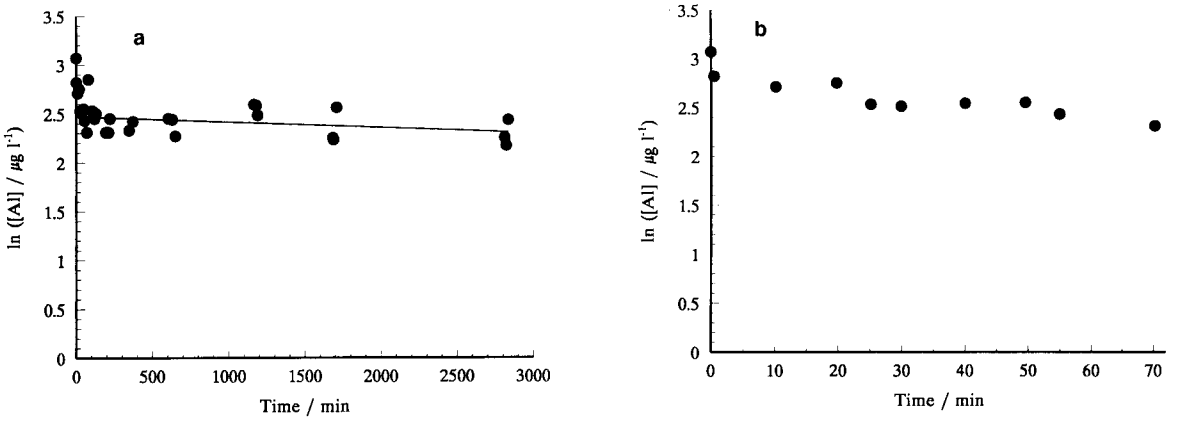

Fig. 3. Aluminium remaining in the sample of Rideau River water as a function of time after uptake by Chelex-100 in the Chelex batch technique. (b) is the expansion of (a) in the specific time range. The concentration of Chelex-100: 1% (w/w). pH of the sample: 8.0.

sample of snow contained relatively low concentrations of organic matter such as humic materials. Therefore, in an acidic medium (pH 3.9) most of these metals were present as free aqua ions, and/or small, inorganic metal complexes. The main factors that affected the distribution of these metal species were the presence of inorganic complexing agents and colloidal materials. In the snow sample, the Fe and the Al might have probably formed polymeric colloids, or the iron and aluminium species might have been adsorbed on or trapped in other colloidal materials, which might also adsorb or trap other metal species. Other ligands or anions existing in the snow sample may also affect the distribution of the metal species, even when the concentrations of these ligands or anions are very low; for example, the solubility product constant of CuS is 6×10^{-36}, and of Cu_2S is 2×10^{-48}. The logarithm of stepwise formation constants, log K, of $Cu(NH_3)_4^{2+}$ are 4.2, 3.7, 3.0 and 2.3. Therefore, traces of S^{2-} or NH_3 may change the distribution of copper species in snow.

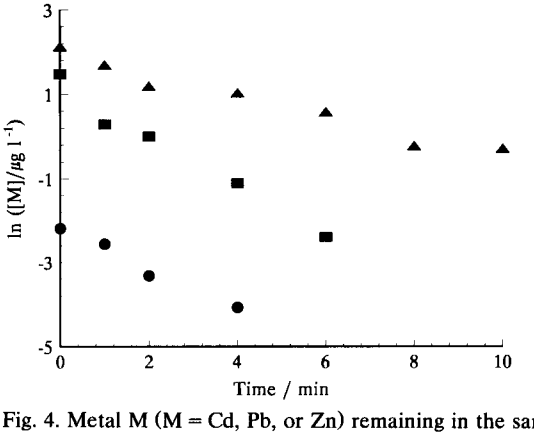

Fig. 4. Metal M (M = Cd, Pb, or Zn) remaining in the sample of snow as a function of time after uptake of the metal by Chelex-100 in the Chelex batch technique. The concentration of Chelex-100: 1% (w/w). pH of the sample: 3.9. ▲, Zn; ■, Pb; ●, Cd.

In summary, the metal species in the rain water (pH < 7) and in the snow (pH < 7) samples were probably present as free aqua ions, hydroxo species, or simple inorganic complexes. On the other hand, Al species in the Rideau River water sample (pH > 7) were probably present as complexes of organic complexing agents such as humic materials, or other macromolecules (e.g., large organic molecules), or as surface-complexes of polymeric hydrous oxides, or as adsorbed or trapped species by colloidal materials [41].

Kinetics of the complex dissociation

Figures 2–4 present kinetic curves for the dissociation of the metal complexes in the Chelex-100 batch technique.

As shown earlier under Kinetic model, the measured rate represented the rate of metal

species dissociation, which was assumed to be first-order or pseudo-first-order. The assumption that the rate is first-order or pseudo-first-order is demonstrated by plotting the data according to the integrated first-order rate equation

$$\ln[M^{n+}] = -kt + C \quad (4)$$

where k was a first-order (or pseudo-first-order) rate constant, t was time and C was a constant of integration. Results of the analysis for the copper and the aluminium species are shown in Figs. 2 and 3, respectively, where the time scales were chosen to illustrate the separation of the total uptake of metal ion into distinct first-order reactions. Each of these separate reactions shows a linear dependence of $\ln[M^{n+}]$ on time over a well-defined period of the reaction. Similar plots of the data for Zn, Cd, and Pb are shown in Fig. 4. For Cd and Pb only one dissociation reaction for each was observed over the range where detection was possible.

The data for all species were fitted by non-linear regression to the following function:

$$C_t = \sum C_{o,i} \exp(-k_i t) \quad (5)$$

where C_t stands for the total concentration of metal species at time t, and $C_{o,i}$ stands for the concentration of metal species i at the initial time ($t = 0$), and k_i stands for the rate constant for the dissociation of the metal species. This function is a sum of exponential functions, each representing a first-order or pseudo-first-order reaction. In the application of the computer program for Non-Linear Regression Analysis it was assumed from the kinetic model presented earlier that the dissociation of the metal species occurred from different sites of a polyfunctional (multi-site) complexant, the sites having different chemical affinities for bonding metal ions. For Cu, the dissociation occurred from the copper bound to four types of such sites, for Al three types, for Zn two types, and for Cd and Pb only one type of such sites were present. For Al, Fig. 3a and b shows only the two faster dissociations because of the short time span of these figures. The values for the rate constants and for $C_{o,i}$ obtained by the non-linear regression analysis for each first-order process are summarized in Table 12. These values of $C_{o,i}$ indicate the initial concentration of the species which dissociate at a rate corresponding to the respective rate constant. The decay of each copper species in the analyte sample plotted according to Eqn. 4 is shown in Fig. 5. The kinetic analysis shows that for the polyfunctional (multi-site) complexant the copper (and also Al and Zn) bound to each type of binding site dissociates independently and simultaneously with its own rate constant.

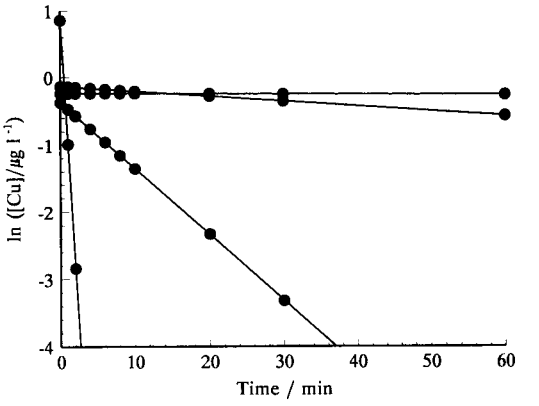

Fig. 5. Separate decay of each copper species obtained by kinetic analysis of the decay curve for the total copper in the sample.

The method of analysis of consecutive first-order rate processes introduced by Olson and Shuman [22,23], called the kinetic spectrum method, was also applied to the data. The application of Laplace transform gave values of k_2 and k_3 for copper identical to the values obtained from the non-linear regression analysis [14,15]. However, the value of k_1 was too close to k_2 and the value of k_4 was too close to k_3 to permit evaluation of these constants by the kinetic spectrum method.

Since in the analysis of Cu, Pb, Cd and Zn in the snow sample only one set of measurements could be made because of limited sample, the uncertainty in the rate constants represents one standard deviation of the data points used for the evaluation of each rate constant. In the analysis of Al in the Rideau River water sample, three parallel sets of measurements could be made on one sample because of the adequacy of the sample volume, and the rate constants, k_1 and k_2,

were evaluated separately for each set of measurements. From three values, average values for k_1 and k_2 were obtained and reported as the values of k_1 and k_2; the uncertainty quoted represents the standard deviation of these three measurements. It should be noted that in the determination of Al, Cu, Cd, Pb and Zn, the random dispersion in the data obtained by graphite platform furnace atomic absorption spectrometry was small compared to the scatter of the data points in Figs. 2–4. Loss of the Al species (at pH 8.0 of the sample) by adsorption on the surface of the containers and gain by contamination from various sources probably caused systematic errors and resulted in the observed scatter in the data for Al. Because of the considerable scatter in the data for Al further statistical analysis of the results of Al was not considered useful.

Interpretation of the kinetics of the Chelex-100 batch process

The four rate constants for the copper species in the snow sample (Fig. 2), the two rate constants for the zinc species in the snow sample and the three rate constants for the aluminium species in the Rideau River water sample (Fig. 3) can be interpreted in terms of polyfunctionality of the complexing agents [7,14,22,23,41]. Some indication of the lability of the complexes in relation to their molecular weight is given by the results in Tables 6 and 9 for the aluminium species, showing the distribution of the molecular weight of the aluminium species which are removed by the Chelex column technique (Chelex-column-labile) and which are not removed by the Chelex column technique (Chelex-column-nonlabile). In these experiments the uptake of the aluminium by the Chelex takes place in a few minutes, during the time it takes for the sample solution to pass through the Chelex column, as illustrated by the results of Table 6. Most of the species which are retained by the Chelex (the Chelex-column-labile species) are in the lower molecular weight range (70% MW cut-off $< 100\,000$). The complexes in this range of molecular weight appear to have the most rapid rate of dissociation. Most of the complexes which are not retained by the Chelex (the column-nonlabile species) have molecular weight $> 100\,000$. Thus, the complexes with high molecular weight appear to have the slowest rate of dissociation. For aluminium species in the Rideau River water sample, 47.8% of the soluble phase was in the size fraction corresponding to the MW cut-off $> 100\,000$. From the rate measurements shown in Fig. 3a and b, and Table 12, the initial concentration of the species with the rate constants for dissociation $\leq 10^{-6}$ was 43.5% of the total soluble aluminium species. Therefore, it is reasonable to conclude that the slower rate is due to complexes with molecular weight $> 100\,000$.

The observation of the four rate constants for the copper species and the two rate constants for the zinc species in the snow sample suggests the presence of different binding sites having different binding energies on the ligand molecule. The variety of polymeric ligands such as humic materials, which are abundant in natural waters, would not be expected in the snow sample. For copper, about 30% of the soluble phase was in the size fraction corresponding to the MW cut-off 5000–500 and the remaining 70% was in the size fraction corresponding to the MW cut-off < 500. The former fraction might well consist of Cu complex of air-borne, polymeric hydrous oxides which are acidic and polyfunctional [14,15,41] and which originate from industrial operations and are abundant in the atmosphere [65]. The snow-melt (water) acts as a favourable medium in which the binding by different functional groups on such polymeric oxides is facilitated.

Conclusions

The scheme of metal speciation presented in this paper has been successfully applied to freshwaters and atmospheric precipitation samples. The present scheme addresses the whole size continuum of metal species and correlates the size of the metal species with their chemical characteristics (dissociation kinetics) and provides a comprehensive scheme for characterization of metal species in the environment. Addressing the whole size continuum of metal species is of particular value in view of the growing recognition that a major proportion of metals in natural waters can be associated with colloidal matter [29].

Kinetic studies of metal speciation described in this paper cover a time scale of measurement of ca. 2 ms for anodic stripping voltammetry and up to 6 days for the Chelex batch technique, a range of 8 orders of magnitude. This scheme provides a means of classifying soluble trace metal species into "very labile", "moderately labile", "slowly labile" and "inert" categories with estimates for rate constants for dissociation of metal complexes for the various size fractions. A decided advantage of this scheme is that the extremely high absolute sensitivity and excellent precision of graphite platform furnace atomic absorption spectrometry allows direct determination of trace metals in natural waters to be done routinely, rapidly and inexpensively with excellent precision.

Application of the kinetic scheme (Fig. 1) to river water and atmospheric precipitation samples has shown that the distribution of metal species in the soluble phase varies from sample to sample. The distribution of the metal species in aqueous media is pH-dependent. In the Rideau River water sample at pH 8, most of the Al species are in the particulate phase, and have large molecular size (> 100000 MW cut-off) in the soluble phase, and are most probably bound by macromolecular complexing agents, e.g., humic materials, and/or adsorbed or occluded by polymeric colloidal materials, e.g., hydrous oxides, whereas most of the Al species in the soluble phase present in the small size-fraction (< 500 MW cut-off) are Chelex-column-nonlabile, and are probably $Al(OH)_4^-$. In the rain water at pH 6.0 and in the snow-melt at pH 3.9, most of the Pb, Cd, Cu and Zn species are both ASV-labile ("very labile") and Chelex-column-labile ("moderately labile"), and some are complexes of polyfunctional complexing agents having bonding sites of different chemical affinity for metal ions, and are present in small size fractions (< 1000 MW cut-off).

The authors are grateful to the Natural Sciences and Engineering Research Council of Canada and Environment Canada Atmospheric Environment Service for financial support for this research project.

REFERENCES

1 W.G. Sunda and R.R. Guillard, J. Mol. Res., 34 (1976) 511.
2 D.M. Anderson and F.M.M. Morel, Limnol. Oceanogr., 23 (1978) 283.
3 M.A. Anderson and F.M.M. Morel, Limnol. Oceanogr., 27 (1982) 789.
4 T.C. Hutchinson and P.M. Stokes, in S. Barabas (Ed.), Water Quality Parameters, ASTM STP 573, ASTM, Philadelphia, PA, 1975, p. 320.
5 M.J. Stiff, Water Res., 5 (1971) 171.
6 R.D. Guy, C.L. Chakrabarti and L.L. Schramm, Can. J. Chem., 53 (1975) 661.
7 R.D. Guy and C.L. Chakrabarti, Can. J. Chem., 54 (1976) 2600.
8 W.C. Li, D.M. Victor and C.L. Chakrabarti, Anal. Chem., 52 (1980) 520.
9 W.E. Baker, Geochim. Cosmochim. Acta, 37 (1973) 269.
10 R.D. Guy and C.L. Chakrabarti, in T.C. Hutchinson (Ed.), Proceedings of International Conference on Heavy Metals in Environment, Toronto, October 27–31, 1975, p. 275.
11 R.D. Guy and C.L. Chakrabarti, Chemistry in Canada, 28 (1976) 26.
12 R.D. Guy and C.L. Chakrabarti, in G.W. Ewing (Ed.), Environmental Analysis, Academic Press, New York 1977, p. 235.
13 R.D. Guy, C.L. Chakrabarti and D.C. McBain, Water Res., 2 (1978) 21.
14 C.H. Langford and D.W. Gutzman, Anal. Chim. Acta, 256 (1992) 183.
15 J.A. Lavigne, C.H. Langford and M.K.S. Mak, Anal Chem., 59 (1987) 2616.
16 C.H. Langford and M.K.S. Mak, Comments Inorg. Chem., 2 (1983) 127.
17 P.G.C. Campbell and A. Tessier, in J.-P. Vernet (Ed.), Heavy Metals in the Environment, Vol. 1, CEP Consultants, Edinburgh, 1989, p. 516.
18 P.G.C. Campbell and A. Tessier, in J. W. Patterson and R. Passino (Eds.), Metals Speciation, Separation, and Recovery, Lewis Publishers, Chelsea MI, 1987, p. 201.
19 P.G.C. Campbell and A. Tessier, Water, Air, and Soil Pollut., 30 (1986) 1023.
20 P. Figura and B. McDuffie, Anal. Chem., 52 (1980) 1433.
21 P. Figura and B. McDuffie, Anal. Chem., 51 (1979) 120.
22 D.L. Olson and M.S. Shuman, Geochim. Cosmochim. Acta, 49 (1985) 1371.
23 D.L. Olson and M.S. Shuman, Anal. Chem., 55 (1983) 1103.
24 A. Tessier, P.G.C. Campbell and M. Bisson, Anal. Chem., 51 (1979) 844.
25 P.G.C. Campbell, M. Bisson, R. Bougle, A. Tessier and J.-P. Villeneuve, Anal. Chem., 55 (1983) 2246.
26 J.R. Kramer, P. Brassard, P.V. Collins, T. Clair, J. Guo and M. LeBeuf, Book of Abstracts XXVII-CSI Post-Symposium: Speciation of Elements in Environmental and Biological Sciences, June 16–18, 1991, Loen, Norway, p. I-1.

27 Y.K. Chau, Analyst, 117 (1992) 551.
28 T.M. Florence, Talanta, 29 (1982) 345.
29 D.P.H. Laxen and R.M. Harrison, Sci. Total Environ., 19 (1981) 59.
30 G.E. Batley (Ed.), Trace Element Speciation: Analytical Methods and Problems, CRC Press, Boca Raton, FL, 1989.
31 D.S. Gamble, in M. Bernhard, F.E. Brinkman and P.J. Sadler (Eds.), The Importance of Chemical "Speciation" in Environmental Processes, Springer-Verlag, Berlin, 1986, p. 217.
32 Y.K. Chau, R. Gachter and K. Lum-Shue-Chan, J. Fish. Res. Board Can., 31 (1974) 1515.
33 B.G. Willis, W.H. Woodruff, J.R. Frysinger, D.W. Margerum and H. L. Pardue, Anal. Chem., 42 (1970) 1350.
34 D.K. Cabbiness and D.W. Margerum, J. Am. Chem. Sco., 92 (1970) 2151.
35 S.E. Cabaniss, Environ. Sci. Technol., 24 (1990) 583.
36 M.K.S. Mak and C.H. Langford, Inorg. Chim. Acta, 70 (1983) 237.
37 M.K. Benjamin and J.O. Leckie, J. Colloid Interface Sci., 79 (1981) 209.
38 M.S. Shuman, B.J. Collins, P.J. Fitzgerald and D.L. Olson, in R.F. Christman and E.T. Gjessing (Eds.), Aquatic and Terrestrial Humic Materials, Ann Arbor Science Publ., Ann Arbor, MI, 1983, p. 349.
39 D.S. Gamble, A.W. Underdown and C.H. Langford, Anal. Chem., 52 (1980) 1901.
40 C.H. Langford, S.M. Wong and A.W. Underdown, Can. J. Chem., 59 (1981) 181.
41 J. Buffle, Complexation Reactions in Aquatic Systems: an Analytical Approach, Ellis Horwood, Chichester, 1988.
42 J.G. Hering and F.M.M. Morel, Environ. Sci. Technol., 24 (1990) 242.
43 J. Vuceta and J.J. Morgan, Environ. Sci. Technol., 12 (1978) 1302.
44 G.E. Batley and T.M. Florence, Talanta, 24 (1977) 151.
45 W. Lund, Fresenius' J. Anal. Chem., 337 (1990) 557.
46 J. Buffle, Trends Anal. Chem., 1 (1981) 90.
47 J.F. Pankow and J.J. Morgan, Environ. Sci. Technol., 15 (1981) 1155.
48 J.F. Pankow and J.J. Morgan, Environ. Sci. Technol., 15 (1981) 1306.
49 T.C. Hutchinson, Proceedings of the International Conference, Heavy Metals in the Environment, Heidelburg, West Germany, September 1983, Vol. 1, CEP Consultants, Edinburgh, 1983, p. 17.
50 A.J. Dobbs, P. French, A.M. Gunn, D.T.E. Hunt and D.A. Winnard, in T.E. Lewis (Ed.), Environmental Chemistry and Toxicology of Aluminum, Lewis Publishers, Chelsea MI, 1989, p. 209.
51 Editorial, Lancet i, 339 (1992) 713.
52 E. Courtyn, C. Vandecasteel and R. Dams, in J.-P. Vernet (Ed.), Proceedings of the International Conference, Heavy Metals in the Environment, Geneva, September 1989, Vol. 1, CEP Consultants, Edinburgh, 1989, p. 391.
53 W. Stumm and J.J. Morgan, Aquatic Chemistry, Wiley-Interscience, New York, 1970, p. 238.
54 W. Lund, in M. Bernhard, F.E. Brinkman and P.J. Sadler (Eds.), The Importance of Chemical "Speciation" in Environmental Processes, Springer-Verlag, Berlin, 1986, p. 533.
55 G. Scarano, E. Morelli, A. Seritti and A. Zirino, Anal. Chem., 62 (1990) 943.
56 W. Davison, J. Electroanal. Chem. Interface Electrochem., 87 (1978) 395.
57 J.A. Buckley, G.A. Yoshida, N.R. Wells and R.T. Aquino, Water Res., 19 (1985) 1549.
58 R.W. Karin, J.A. Buono and J.L. Flashing, Anal. Chem., 47 (1975) 2296.
59 J.E. Gorsky and A.A. Dietz, Clin. Chem., 24 (1978) 1485.
60 D.C. Manning, W. Slavin and G.R. Carnrick, Spectrochim. Acta, 37B (1982) 331.
61 K.S. Subramanian, C.L. Chakrabarti, J.E. Sueiras and I.S. Maines, Anal. Chem., 50 (1978) 445.
62 L.S. Clesceri, A. E. Greenberg and R. R. Trussell (Eds.), Standard Methods for the Examination of Water and Wastewater, Port City Press, Baltimore, MD, 17th edn., 1989.
63 J.R. Wheeler, Limnol. Oceanogr., 21 (1976) 846.
64 Helmut Sigel (Ed.), Metal ions in biological systems, Vol. 24, Marcel Dekker, New York, 1988, p. 65.
65 R.W. Shaw, Scientific American, 257 (1987) 96.

Analytica Chimica Acta, 276 (1993) 65–68
Elsevier Science Publishers B.V., Amsterdam

Photosynthetic activity sensor for microalgae based on an oxygen electrode integrated with optical fibres

Toshifumi Takeuchi, Kenji Yokoyama, Kazuki Kobayashi, Masayasu Suzuki, Eiichi Tamiya and Isao Karube

Research Centre for Advanced Science and Technology, University of Tokyo, Meguro-ku, Tokyo 153 (Japan)

Kazuhiro Utsunomiya

Research Centre for Environmental Conservation, Electric Power Development Co., Ltd., Shinjuku-ku, Tokyo 160 (Japan)

Osamu Imai and Yuzo Masuda

Faculty of Engineering, Science University of Tokyo, Shinjuku-ku, Tokyo 162 (Japan)

(Received 24th August 1992; revised manuscript received 2nd November 1992)

Abstract

A photosynthetic activity sensor which consists of a Clark-type oxygen electrode integrated with optical fibres is described and the usefulness of the sensor is demonstrated for model microalgae of *Scenedesmus* sp., *Chlorella* sp. and *Spirulina* sp. Light is introduced into a sample medium from a halogen lamp through the optical fibres, and oxygen production by photosynthesis is measured as the increase in dissolved oxygen. The sensor responded linearly with the density of the three microalgae under constant light intensity. A light–response curve was also obtained by changing the light intensity.

Keywords: Biosensors; Potentiometry; Fibre-optic sensors; Microalgae; Photosynthesis

It is known that microalgae produce organic compounds from CO_2 and H_2O by photosynthesis using sunlight as an energy source. The initial stage of the photosynthetic process involves the conversion of light energy into chemical energy, which is associated with H_2O reduction followed by O_2 production. The rate of electron transport from water is widely used as an index of photosynthetic activity of microalgae, because fixation of CO_2 followed by metabolic syntheses of organic compounds are dependent on the chemical energy stored during the initial process.

Previously, O_2 generation or CO_2 uptake has been measured in electron transport research by manometry using a Warburg manometer, infrared gas analysis, mass spectrometry using ^{18}O and ^{16}O, photoacoustic spectrometry, ion-selective electrodes, and various spectrophotometric methods [1,2]. Currently, the Clark-type oxygen electrode is the most widely used for the determination of electron transport rates, although the stoichiometry of net O_2 evolution is not clear because of competing O_2 uptake by respiration. For the measurements, a combination of a Clark-type oxygen electrode and a thermostated vessel is

Correspondence to: I. Karube, Research Centre for Advanced Science and Technology, University of Tokyo, Meguro-ku, Tokyo 153 (Japan).

useful because it is simple and easy to use; such systems are commercially available from, e.g., Hansatech (Norfolk, UK) and Rank (Cambridge, UK).

Although these commercial systems are convenient, they still require improvements in handling. Miniaturization may provide a useful system and further applicability, but it is difficult to miniaturize the present systems because the oxygen electrode is fixed with the reaction vessel and the light source is separate from the vessel. In this paper an integrated photosynthetic activity sensor is described that consists of an oxygen electrode and bundled optical fibres. This integration allows the system to be simple and provides easy handling. The usefulness of the integrated sensor is demonstrated on the measurement of oxygen production rates, defined as photosynthetic activity, for model microalgae of *Scenedesmus* sp., *Chlorella* sp. and *Spirulina* sp.

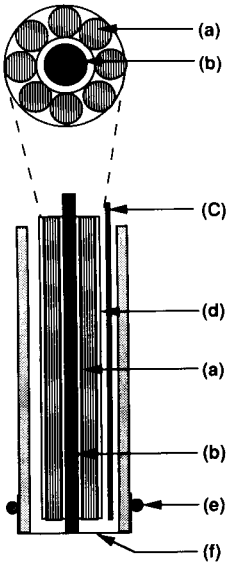

Fig. 1. Schematic diagram of the photosynthetic activity sensor. (a) Optical fibre; (b) Pt electrode; (c) Ag/AgCl electrode; (d) electrolyte solution; (e) O-ring; (f) gas-permeable membrane.

EXPERIMENTAL

Sensor construction

The construction of the integrated sensor is shown in Fig. 1. A platinum (1 mm o.d.) electrode covered with a heat-shrinkable tube was employed as the working electrode and a silver/silver chloride electrode was used as the reference electrode. Eight optical fibres (1 mm o.d.) were placed around the working electrode and fixed with a heat-shrinkable tube. This bundle was placed in the plastic cylinder and the end was covered with a gas-permeable membrane (PTFE, 10 μm thick; Able, Tokyo) Potassium chloride solution (0.1 M) was used as the internal solution. The light source was a 150-W halogen lamp (Nikon, Tokyo). Light intensities were measured with a quantum sensor (LI-190 type, Li-Cor, Lincoln, NE). The potentiostat was made in the laboratory.

Cultivation of the model microalgae

The model microalgae used were *Scenedesmus* sp., *Chlorella* sp. and *Spirulina* sp. *Scenedesmus* sp. and *Chlorella* sp. were cultivated in a modified Fitzgerald medium [3] at pH 7, 25°C and 120 μE m^{-2} s^{-1} (where E = Einsteins). The medium contained $NaNO_3$ (0.496), K_2HPO_4 (0.039), $MgSO_3 \cdot 7H_2O$ (0.075), $CaCl_2 \cdot 2H_2O$ (0.036), Na_2CO_3 (0.020), $Na_2SiO_3 \cdot 9H_2O$ (0.058), iron(III) citrate (0.006), citric acid (0.006), and Na_2EDTA (0.001 g l^{-1}) and Gaffron solution (0.1%). Gaffron solution consists of H_3BO_4 (3.1), $MnSO_2 \cdot 4H_2O$ (2.23), $ZnSO_4 \cdot 7H_2O$ (0.283), $(NH_4)_6MO_7O_{24} \cdot 4H_2O$ (0.088), $Co(NO_3)_2 \cdot 4H_2O$ (0.146), $Na_2WO_2 \cdot 2H_2O$ (0.033), KBr (0.119), KI (0.083), $Cd(NO_3)_2 \cdot 4H_2O$ (0.154), $NiSO_4(NH_4)_2SO_4 \cdot 6H_2O$ (0.198), $VOSO_4 \cdot 2H_2O$ (0.020) and $Al_2(SO_4)_3K_2SO_4 \cdot 24H_2O$ (0.474 g l^{-1}) and 0.05 M H_2SO_4 to 1000 ml. *Spirulina* sp. was grown in a modified Fitzgerald medium (pH 8) containing 1.61 g l^{-1} of $NaHCO_3$ at 25°C and 120 μE m^{-2} s^{-1}. Chlorophyll-*a* (Chl-*a*) in these microalgae was determined spectrophotometrically [4].

Measurement of photosynthetic activity of the model microalgae

Cultivations were performed for the preparation of samples to be tested. Microalgae in the logarithmic phase, where they grew exponentially, were used as samples in the following experi-

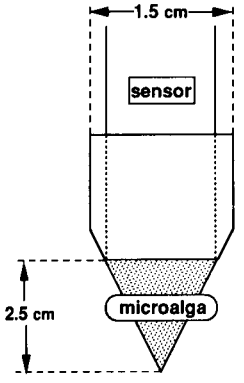

Fig. 2. Sample vessel for the sensor.

ments. A 2-ml volume of culture medium was placed in a laboratory made sample cup (Fig. 2) and the change in dissolved oxygen was measured for the microalgae. In this work gross photosynthesis was calculated by adding net photosynthesis and respiration. Net photosynthetic activity was measured at 200 μE m^{-1} s^{-1} for 15 min. Respiration was measured in the dark for 15 min. The light response of the *Scenedesmus* sp. curve was examined by varying the irradiance from 50 to 250 μE m^{-2} s^{-1}.

RESULTS AND DISCUSSION

Fabrication of oxygen electrode integrated with optical fibres

The integrated sensor was based on a Clark-type oxygen electrode, which consisted of platinum as the cathode and silver as the anode. The electrode response was measured in oxygen-saturated water and nitrogen-saturated water at various electrode potentials, and the maximum current change was observed at −700 mV vs. Ag/AgCl. The concentration of KCl in the internal solution was also examined and 0.1 M KCl gave a better result than KCl-saturated solution. Under these conditions, a linear response was obtained between current change and dissolved oxygen (DO) concentration in the solutions, which were saturated with various ratios of mixing gases of oxygen and nitrogen {$\Delta\mu A = 0.09$[DO(mg l^{-1})] + 10}. The response time of the oxygen electrode was ⩽ 15 s, which was good enough to monitor oxygen production by photosynthesis of microalgae.

The sensor was integrated with optical fibres, i.e., the platinum electrode was surrounded by eight optical fibres of 1 mm o.d. Light was introduced from a 150-W halogen lamp and the intensity was controlled by changing the light intensity of the lamp. The highest irradiance at the electrode surface was 600 μE m^{-2} s^{-1}. During the experiments, no heating problems caused by the introduction of light were observed around the electrode surface. In this study, plastic optical fibres were used because ultraviolet radiation is unnecessary for the growth of microalgae.

Measurement of photosynthetic activities for microalgae

The measurements were performed for three different densities of *Scenedesmus* sp., *Chlorella* sp. and *Spirulina* sp. In the experiments, photosynthetic activity is defined as O_2 production (mg per litre of medium) which is calculated by the summation of the apparent O_2 increase and respiration, where the O_2 decrease by respiration was measured without light.

Dissolved oxygen concentrations increased linearly with time for all of model microalgae. Figure 3A shows typical results for *Scenedesmus* sp. This means that the sensor responded to the photosynthetic activity of microalgae. The rate of DO increase (mg O_2 l^{-1} min^{-1}) was also linear

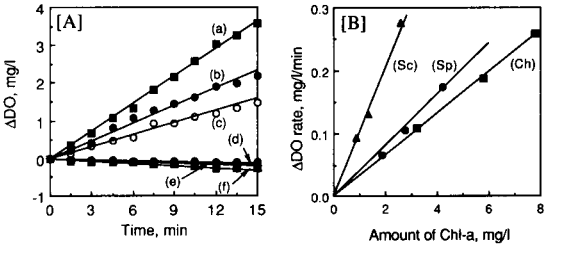

Fig. 3. (A) Gross photosynthesis (a–c) and respiration (d–f) of *Scenedesmus* sp.: (a) and (d) 2.59 mg l^{-1} Chl-*a*; (b) and (e) 1.32 mg l^{-1} Chl-*a*; (c) and (f) 0.89 mg l^{-1} Chl-*a*. In these experiments, Chl-*a* concentrations are considered to be densities of the microalga. (B) Relationship between amount of Chl-*a* and rate of increase of DO in photosynthesis of *Scenedesmus* sp. (Sc), *Spirulina* sp. (Sp) and *Chlorella* sp. (Ch).

with the density of microalgae examined, as shown in Fig. 3B. These results indicate that the sensor is reasonably acceptable for the measurement of microalgal photosynthetic activity.

Compared with conventional sensing systems for photosynthetic activity such as the Rank System, the proposed sensor is significantly simpler and the handling is easier because the sensor can measure DO changes without the use of a special reaction vessel and light can be introduced into the sample cup by optical fibres, i.e., the light source is separated from the sensor and can be placed anywhere, depending on the length of the optical fibres. The sensor showed good reversibility and stability; the photosynthetic activity has been measured at least 50 times over about 3 months without any problems.

Light–response curve of Scenedesmus sp.

Relationships between light intensity and photosynthetic activity of microalgae are commonly examined for the characterization of the light–response properties. A light–response (P–I) curve gives two important factors: the photosynthetic maximum value (P_{max}), where the system becomes light saturated, and the quantum yield from the initial slope [1].

Because it would be useful if such P–I curves could be obtained without a tedious procedure, an attempt was made to obtain a P–I curve using the present photosynthetic activity sensor. In this experiment, *Scenedesmus* sp. was used as a model microalga. Figure 4 shows that the photosynthesis increased with increasing light intensity up to 200 μmol m^{-2} s^{-1}, after which the photosynthetic activity became constant. The P_{max} value was ca. 6.5 mg O_2 (mg Chl-a)$^{-1}$ min^{-1}. These results were consistent with those [5] measured with a Dubinsky-type chamber [6]. Consequently, it has been demonstrated that the proposed sensor could be applied to preliminary experiments on photosynthesis such as light–response studies.

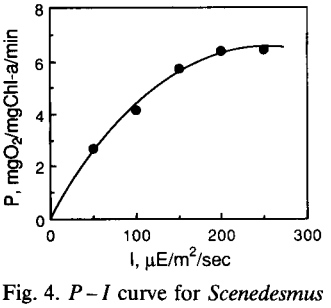

Fig. 4. $P-I$ curve for *Scenedesmus* sp. P = gross photosynthesis rate; I = irradiance.

Currently the biological fixation of carbon dioxide emitted from thermal power plants by using photosynthetic microorganisms is being studied [7]. For this purpose, microalgae that have high photosynthetic activities are suitable, and such microalgae from nature are therefore currently being screened [8,9]. Because this sensor system is simple and rapid measurements can be achieved, it is believed that the sensor will contribute not only to basic photosynthesis research, but also to the screening of microalgae that have high photosynthetic activities.

The authors thank the late Dr. Ooki Nakayama for valuable suggestions and thoughtful help.

REFERENCES

1 T.R. Parsons, M. Takahashi and B. Hargrave, Biological Oceanographic Processes, Pergamon, Oxford, 3rd edn., 1984, Chap. 3.
2 J.F. Allen and N.G. Holmes, in M.F. Hipkins and N.R. Baker (Eds.), Photosynthesis, IRL, Oxford, 1986, Chap. 5.
3 E.O. Hughes, P.R. Gorham and A. Zehnder, Can. J. Microbiol., 4 (1958) 225.
4 S.W. Jeffrey and G.F. Humphrey, Biochem. Physiol. Pflanz., 167 (1975) 191.
5 K. Kobayashi, B.E. Chalker, T. Takeuchi and I. Karube, unpublished results.
6 Z. Dubinsky, P.G. Falkowski, A.F. Post and U.M. van Hes, J. Plankton Res., 9 (1987) 607.
7 N. Hanagata, T. Takeuchi, Y. Fukuju, D.J. Barnes and I. Karube, Phytochemistry, 31 (1992) 3345.
8 T. Takeuchi, K. Utsunomiya, K. Kobayashi, M. Owada and I. Karube, J. Biotechnol., 205 (1992) 117.
9 I. Karube, T. Takeuchi and D.J. Barnes, Adv. Biochem. Eng. Biotechnol., 46 (1992) 63.

Analytica Chimica Acta, 276 (1993) 69–74
Elsevier Science Publishers B.V., Amsterdam

Screen printed glucose electrodes based on platinised carbon particles and glucose oxidase

M.F. Cardosi

Biology Department / Sensors Group, University of Paisley, High Street, Paisley PA1 2BE (UK)

S.W. Birch

Cranfield Biotechnology Limited, 20 Howard Way, Newport Pagnell, Bucks MK16 9QS (UK)

(Received 22nd July 1992; revised manuscript received 5th October 1992)

Abstract

Simple strip type enzyme electrodes prepared from platinised Vulcan XC-72 carbon particles using silk screen printing techniques are described. Such electrodes combine the efficient electrocatalytic activity of metal microparticles with the attractive features of mass produced screen printed sensors. Immobilisation of glucose oxidase to the surface of the particles allows coupling of the biocatalytic reaction with the electrocatalytic oxidation of the liberated peroxide, thus providing a sensor for glucose with a detection limit of 2×10^{-5} M.

Keywords: Catalytic methods; Sensors; Enzyme electrodes; Glucose

Over the past decade a considerable body of literature has accumulated regarding the design of practical amperometric enzyme electrodes for the rapid analysis of clinically important metabolites. Such devices consist of an indicator electrode, which monitors the change in concentration of a reactant or product, and a highly selective enzyme which is immobilised or retained next to the surface of the sensing head [1]. An example of such a device is a commercially available glucose sensor based on a disposable glucose oxidase/ferrocene electrode which is widely used for at-home blood glucose monitoring by diabetic patients [2]. In this configuration, the ferricinium ion acts as an efficient electron transfer mediator shuttling electrons from the active site of the enzyme to the surface of the electrode.

Correspondence to: M.F. Cardosi, Biology Department/ Sensors Group, University of Paisley, High Street, Paisley PA1 2BE (UK).

An alternative method for measuring the activity of glucose oxidase is by monitoring the production of hydrogen peroxide which is formed as a byproduct of the natural catalytic oxidation of glucose to gluconic acid. This approach to sensor design has been particularly successful resulting in various analytical applications including flow-injection analysis [3] off line analysis as part of an artificial pancreas [4] and in vivo monitoring [5].

Although peroxide can be oxidised at platinum electrodes, several workers have been interested in finding alternative electroactive surfaces with a view of decreasing the overpotential required for the reaction. Particularly useful in this respect have been electrodes made from carbon particles modified with platinum and palladium microcrystallites [6,7]. These powders are characterised by a strong adhesion of the metal centre to the substrate and are thus amenable to bulk chemical treatments such as surface oxidation and solvent extractions.

This paper describes the manufacture of disposable strip type electrodes by silk screen printing techniques based on platinised Vulcan XC-72 particles. Immobilisation of glucose oxidase to the carbon particles allows the production of disposable glucose sensors based on the electrocatalytic oxidation of hydrogen peroxide. The electrochemistry of L-ascorbic acid, a potential interferent in blood glucose measurement, at these electrodes is also discussed.

EXPERIMENTAL

All chemicals used in this study were obtained from Fluka (Glossop) and were of the highest available purity. Solutions were routinely prepared in ultrapure water and passed through 0.2-μm thick cellulose acetate membrane filters immediately prior to use. Biochemicals were obtained from Sigma (Poole) and dissolved in appropriate sterile buffers. Prior to use, stock solutions of hydrogen peroxide were standardised by titration against acidified potassium permanganate.

Vulcan XC-72, a carbon black with a volatile content of 2% and a surface area of 254 $m^2\ g^{-1}$ (mean particle size 300 Å), modified with platinum microparticles, mean particle size 15–25 Å (approximate surface area of supported platinum 150–175 $m^2\ g^{-1}$) was obtained from E-Tek (Framingham, MA). Prior to use, the material was extracted (Soxhlet) in petroleum ether (60–80°C fraction) for 24 h. The carbon was collected by filtration and "dried" under vacuum and then stored desiccated over silica gel.

Two surface treatments were examined in this study. The first involved refluxing the material with boiling water for periods of up to 2 h. The second process, a mild oxidation, involved leaving the carbon particles in contact with a 20% (v/v) solution of nitric acid at room temperature for 48 h. During this treatment, the particles were kept in suspension by the use of an orbital shaker. Following these procedures, the persistence of the platinum particles was checked by surface x-ray microanalysis using a Camscan Series III scanning electron microscope equipped with an energy dispersive x-ray analyser (EDX) (Oxford Instruments, High Wycombe). The elemental identity of the platinum modifier was verified by EDX (Ma 1 line 2.051 KeV, La 1 line 9.441 KeV, Lb 1 line 11.069 KeV). Prior to surface analysis, the carbon powders were washed in a stream of doubly distilled water and dried over silica gel.

Enzyme was covalently attached to the surface of the carbon particles following activation of the carbon surface with *N*-hydroxysuccinimide (NHS). NHS in a suitable compound that will react with COOH groups to form activated acyl amino esters. These will then react with primary amine functions to render stable, covalent amide bonds [8]. NHS is commonly used as the coupling agent in solid phase peptide synthesis [8].

For activation, 0.1 g of platinised carbon particles was added to 5 ml of 0.25 M NHS in dimethyl formamide. To this, 3 ml of a 0.5 M solution of *N*-(dimethyl aminopropyl)-*N'*-ethylcarbodiimide · HCl in collidine–HCl pH 5.5 buffer was added and the resultant mixture incubated with shaking overnight at room temperature. After this treatment, the carbon was collected by vacuum filtration through a ceramic filter and washed with copious amounts of doubly distilled water until the washings contained no UV adsorbing material. The carbon was washed with a 25-ml aliquot of acetone and then further washed by refluxing in acetone for 2 h. After cooling, the carbon was collected by filtration, washed with ultrapure water and dried over silica gel.

The NHS reacted carbon particles were examined by Auger spectroscopy (Riber Auger spectrometer with cylindrical mirror analyser). Nitrogen and oxygen spectra were recorded with derivatised carbon particles indicating the presence of the surface activator. With unreacted washed carbon particles only carbon bands were observed suggesting that the observed spectra with the treated samples were not simply due to atmospheric contamination.

Glucose oxidase was covalently attached to the surface of the carbon particles by suspending the activated particles (0.05 g) in 10 ml of 0.1 M phosphate buffer pH 7.6 containing 0.014 g of enzyme per ml for 24 h at room temperature. After this time, the particles were collected by

vacuum filtration and washed with ice cold phosphate buffer containing 0.5 M KCl until no enzyme activity was detected in the washings. The carbon was then washed with 100 ml of ice cold water and dried over silica gel. The modified carbon was stored at −4°C until required. Immobilised activity was detected in the first instance by measuring the decrease in dissolved oxygen tension in the presence of glucose using a Clark-type oxygen electrode. Control experiments using bovine serum albumin were carried out to ensure that any detectable activity was due to immobilised glucose oxidase. Prior to analysis, 10 mg samples of carbon particles were washed with water and then suspended in 1 ml of sodium acetate pH 5.6 buffer. Experiments where inactivated carbon particles were treated with glucose oxidase in an identical manner resulted in no immobilised activity being detected.

The electrode ink for screen printing was formulated as follows. To 5 g of an aqueous solution consisting of 2% (w/v) hydroxyethyl cellulose, 6% (w/v) ethylene glycol and 0.15% (w/v) Triton QS 44 (required to disperse the carbon particles), 0.5 g of enzyme-modified platinised Vulcan XC-72 (or unmodified carbon) was added. The mixture was blended at room temperature by end over end tumbling for at least 16 h an then printed through a polyester screen onto a PVC (0.65 mm thick) substrate using a Model 245 screen printer (DEK, Weymouth). Electrical contact to the sensor was via screen printed silver tracks (Electrodag 477 SS RFU silver ink). (A carbon overlay pad was first positioned over the silver track ensuring that the silver did not make electrical contact with the electrolyte. The working electrode was then printed directly on top of the overlay pad.) Finally, a water insoluble insulating layer with openings allowing external electrical contact at one end of the strip and access of analyte to the working electrode was printed over the entire strip. Calibration graphs for the electrodes were determined under hydrodynamic conditions in 0.02 M potassium phosphate buffer pH 7.4 containing 0.1 M KCl. The printed sensors were immersed in the test solution and the voltage (0.65 V vs. SCE) applied to commence the measurement.

All electrochemical measurements were made in a thermostatted glass cell at 25°C using a conventional 3-electrode format. All potentials are referenced to the KCl/SCE half cell. A platinum wire served as the counter electrode. Electrochemical measurements were made with an Autolab PSTAT 10 computer controlled system (Windsor Scientific, Slough).

RESULTS AND DISCUSSION

Electrocatalytic oxidation of glucose with screen printed enzyme electrodes

A linear sweep voltammogram in the presence of 3.25 mM hydrogen peroxide in pH 7.0 McIlvaine buffer at a platinised carbon electrode is shown in Fig. 1. Under these conditions, the peak oxidation (E_{pa}) occurred at approximately 0.55 V, comparable with that observed on platinum. Background currents with the platinised carbon, however, were much lower. For example, the current density at 0.55 V with this material measured in background electrolyte was calculated as 1.8×10^{-5} A cm^{-1} compared to 7.3×10^{-5} A

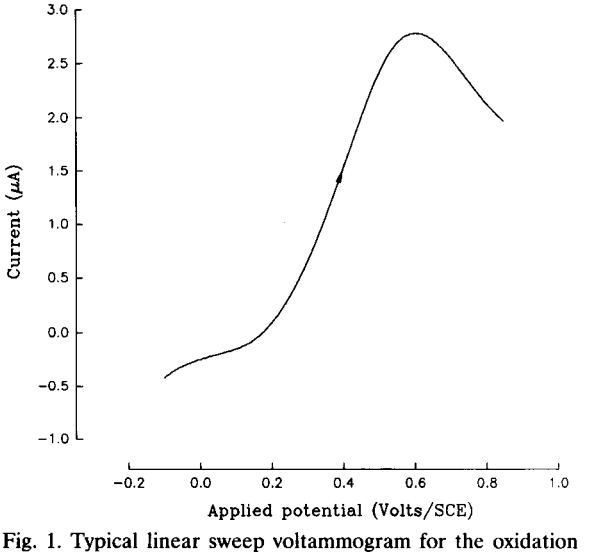

Fig. 1. Typical linear sweep voltammogram for the oxidation of 3.5 mM hydrogen peroxide in McIlvain pH 7.5 buffer at a platinised carbon electrode. In this experiment, the voltage was scanned from −0.2 to 0.9 V at a sweep rate of 25 mV s^{-1} in a quiescent solution.

cm^{-1} for bare platinum. This result has implications for improved signal-to-noise characteristics. In addition, the response from this material was found to be more stable than with platinum. Repetitive scanning with the electrode ($n > 50$) under the above conditions resulted in no loss of sensitivity with respect to hydrogen peroxide determination. The position of E_{pa} was found to be sensitive to pH with a slope of $-0.088\ \Delta V/\Delta pH$ ($r = 0.995$, $n = 5$). Hydrodynamic voltammograms obtained with the screen printed electrodes showed limiting diffusion currents for the oxidation of hydrogen peroxide at potentials greater than 0.55 V with oxidation starting at 0.2 V, in agreement with the voltammetry data (not shown).

A typical calibration graph for a screen printed enzyme sensor is shown in Fig. 2. The response to glucose is linear up to a concentration of 8 mM [$y\ (\mu A) = 17.5x\ (mM) + 0.98$, $r = 0.999$, $n = 14$] indicating over this concentration range, the response is under diffusion control. This is also borne out by the non-linear Hanes plot obtained

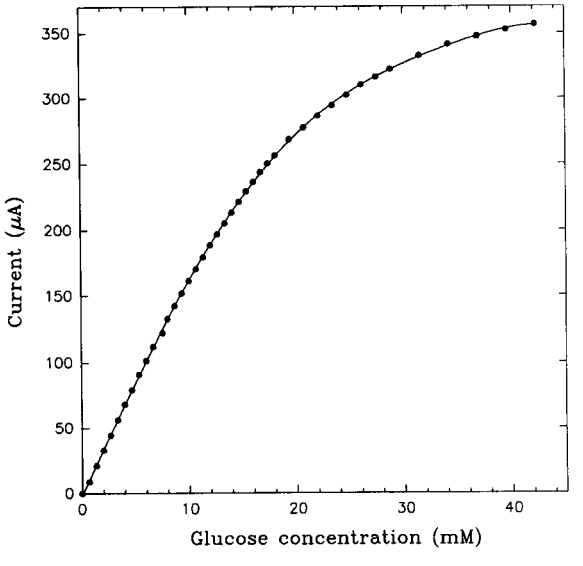

Fig. 2. Typical calibration curve for the electrocatalytic oxidation of glucose at a screen printed enzyme electrode. The curve is linear with respect to glucose concentration up to 8 mM indicating a diffusion limited response. The electrode was tested in 20 mM phosphate buffer containing 0.1 M KCl at an applied voltage of 0.65 V vs. SCE

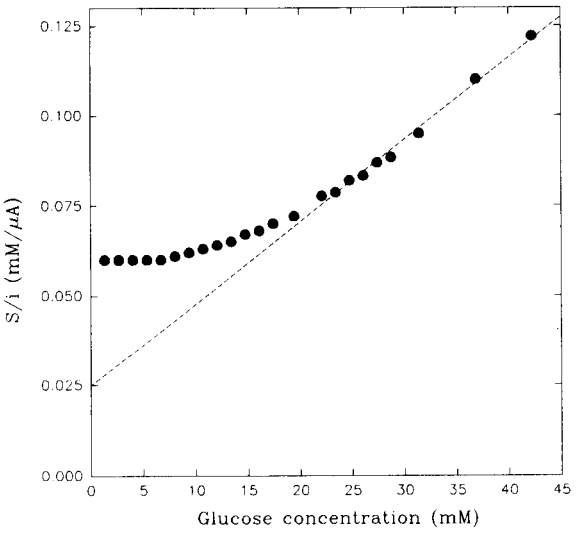

Fig. 3. Hanes plot of the calibration data obtained with the screen printed sensor. The poor linearity at low substrate concentration (i.e., horizontal plot of the data points) is indicative of diffusional limitations. The dashed line represents the linear portion of the graph used to estimate the kinetic constants reported in the text.

for this electrode (Fig. 3) at low substrate concentrations [9]. Analysis of the response in the kinetic regime, i.e., the linear portion of the curve where $s > 14$ mM, gave values for the Michaelis constant ($K_{M(app)}$) and maximum steady state current of 16.1 mM and 498 μA, respectively for the screen printed electrode. A detection limits of 2×10^{-5} M glucose can be estimated on the basis of a signal-to-noise ratio of 3.

Investigations of long-term storage stability revealed that the strip sensors could be stored in the dry state at room temperature for at least one month with no apparent loss of catalytic activity. Since the aim of this study was to produce disposable "one-shot" electrodes no investigation into operational stability was carried out.

Electrochemistry of L-ascorbic acid.

The importance of vitamin C electrochemistry in enzyme electrode research arises from the fact that it is present in serum as a major electroactive interferent [10]. Consequently, it is important to establish the electrochemical behaviour of ascorbate at a proposed transducer surface.

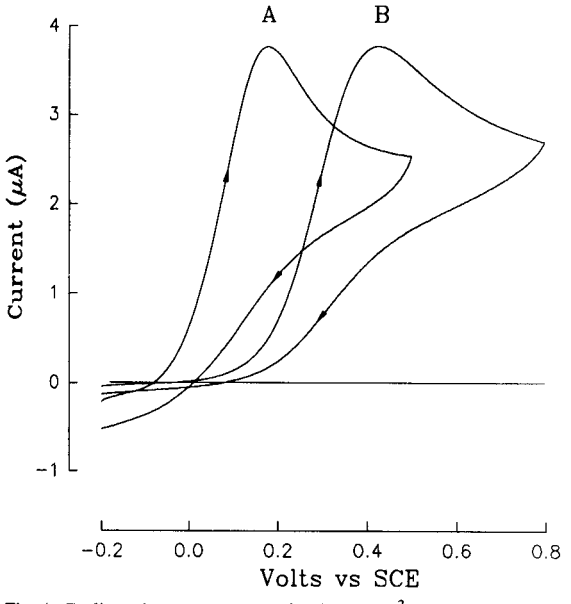

Fig. 4. Cyclic voltammograms of 1.27×10^{-3} M ascorbic acid recorded at (A) untreated and (B) oxidised platinised carbon electrodes. Scan rate, 20 mV s^{-1}; supporting electrolyte citrate–phosphate buffer pH 7.5.

Figure 4a shows a cyclic voltammogram for 1.27×10^{-3} M ascorbic acid in citrate–phosphate pH 7.5 electrolyte obtained with a strip electrode made from petroleum ether extracted platinised carbon. Figure 4b displays a voltammogram recorded under identical conditions except that an electrode made from HNO_3-oxidised carbon was used. Of particular note is the negative shift in potential resulting from this treatment indicative of an enhanced heterogeneous rate constant. Heat treatment of the carbon particles on the other hand results in a more drawn out wave with a peak potential of 0.520 V vs. SCE. The ability to influence the electrocatalytic oxidation of ascorbic acid at these electrodes by simple chemical treatment of the carbon particles has implications for improving the selectivity of the sensors.

Conclusions

This article demonstrates the feasibility of using platinised carbon particles in enzyme electrode construction in a screen printed format. Electrodes made from this material were found to be efficient transducers for the oxidation of hydrogen peroxide, albeit at elevated voltages and in the presence of immobilised glucose oxidase.

The results obtained with vitamin C highlight the importance of understanding the effects of surface treatment on the ensuing voltammetric waves. In this case it is interesting to note that the effects of ascorbic acid interference can be minimised by choosing the "surface chemistry" of the carbon. For example, in sensors based on peroxide detection operating at ca. 0.5 V, the sensitivity of the electrode to vitamin C could be decreased by using carbon particles which had been heat treated. Different chemical treatments coupled with a better understanding of the surface chemical reactions involved may lead to even greater selectivity for peroxide oxidation over vitamin C. In addition, the possibility of screen printing effective perm-selective membranes on the electrode surface is currently being pursued.

Finally, it is worth speculating that carbon particles modified with metals other than platinum, or indeed combinations of metals, may lead to particularly useful catalytic transducers. A glassy carbon electrode sputtered with a palladium–gold mixture for example has been reported on the literature which shows a decrease in the overvoltage for the oxidation of hydrogen peroxide of approximately 0.8 V, i.e., the anodic limiting current was reached at 0.4 V vs. Ag/AgCl [11]. Electroplating metallic particles from solution onto these materials could result in similar or indeed better electrocatalytic surfaces and is currently under investigation. This, coupled with the possibility of influencing the reaction through the modification of the surface properties of the carbon should lead to useful transducers for enzyme electrode research.

The authors are grateful to Dr. Francis Placido and Mrs. Margaret Corrigan (Department of Physics, University of Paisley) for help with the x-ray microanalysis and Auger spectroscopy.

REFERENCES

1 S.P. Hendry, I.J. Higgins and J.V. Bannister, J. Biotechnol., 15 (1990) 227.

2 D.R. Mathews, E. Brown, A. Watson, R.R. Holman, J. Steemson, S. Hughs and D. Scott, Lancet, i (1987) 778.
3 H.J. Wieck, G.H. Heider, Jr. and A.M. Yacynych, Anal. Chim. Acta, 158 (1984) 137.
4 E.F. Pfeiffer, C. Thum and A.H. Clemens Horm. Metab. Res., 6 (1974) 339.
5 L.C. Clarke, Jr., L.K. Noyes, R.B. Spokane, R. Sudan and M.L. Miller, Ann. N.Y. Acad. Sci., 501 (1987) 534.
6 H.P. Bennetto, D.R. DeKeyzer, G.M. Delaney, A. Koshy, J.R. Mason, G. Mourla, L.A. Razack, J.L. Stirling, C.F. Thurston, D.J. Anderton and W.H. Mullen, Int. Ind. Biotechnol., 8 (1988) 5.
7 J. Wang, N. Naser, L. Agnes, H. Wu and L. Chen, Anal. Chem., 64 (1992) 1285.
8 G.W. Anderson, J. Am. Chem. Soc., 86 (1964) 1839.
9 W.J. Albery and D.H. Cranston, in A.P.F. Turner, G.S. Wilson and I. Karube (Eds.), Biosensors: Fundamentals and Applications Oxford University Press, Oxford, 1987, p. 180.
10 G. Palleschi, M.A.A. Rahni, G.L. Lubrano, A.L. Ngwainbi and G.G. Guilbault, Anal. Biochem., 159 (1986) 114.
11 L. Gorton, Anal. Chim. Acta, 178 (1985) 247.

Analytica Chimica Acta, 276 (1993) 75–86
Elsevier Science Publishers B.V., Amsterdam

Robust estimation of selectivity coefficients using multivariate calibration of ion-selective electrode arrays [1]

Dermot Diamond and Robert J. Forster [2]

School of Chemical Sciences, Dublin City University, Glasnevin, Dublin 9 (Ireland)

(Received 18th August 1992)

Abstract

Selectivity coefficients for sodium, calcium and potassium ion-selective electrodes estimated by traditional methods such as the separate solution and mixed solution methods are compared with values obtained by a more rigorous approach based on multivariate calibration using simplex optimisation and non-linear modelling of the array characteristics. The validity of the latter approach is demonstrated by using the models to predict the concentration of sodium, calcium and potassium in blood plasma and mineral water samples using dip and flow-injection analysis (FIA) measurements. For the array FIA data, the possibility of using an enhanced kinetic-based selectivity for analytical measurements is raised. Further improvement in the three electrode array performance by using a fourth "multiple ionophore electrode" (MIE) is discussed. Results obtained are compared with single electrode dip and FIA measurements of sodium in plasma samples.

Keywords: Flow injection; Ion-selective electrodes; Multivariate calibration; Selectivity coefficients; Simplex optimisation

Selectivity is perhaps the single most important characteristic of any chemical sensor. It is this characteristic which defines the nature of the device, and the range of applications to which it may be successfully employed. This in turn will dictate the commercial potential of the sensor and hence whether or not is will survive. For the past thirty years or so, research into ion-selective electrodes has been dominated by the search for more selective ligands. Despite the huge effort, there have been relatively few notable advances. The best electrode is undoubtedly the pH glass electrode, which has been in general use for over sixty years. This followed by the fluoride electrode, which is by far the most successful anion-selective electrode, and then by a range of cation-selective electrodes based on neutral-carriers such as antibiotics (valinomycin, potassium selective) and "designer ligands" such as ETH129 (calcium selective).

Along the way, the literature describes many structures which were synthesised, evaluated and then discarded as not being selective enough. What is more surprising is that the most popular method of assessing the selectivity of these systems has been the separate-solution (SS) method, mainly for convenience. This approach normally involves measuring the potential generated by an ISE/reference electrode cell in a series of separate solutions of the primary ion and the main

Correspondence to: D. Diamond, School of Chemical Sciences, Dublin City University, Glasnevin, Dublin 9 (Ireland).

[1] Presented at the *Fourth European Conference on Electroanalysis, ESEAC'92, Noordwijkerhout, May 31–June 3, 1992*, The majority of papers presented at this symposium has been published in Anal. Chim. Acta, Volume 273.

[2] Present address: School of Chemical Sciences, University of Illinois, 1209 W. California St., Urbana, IL 61801 (USA)

interfering ions at equal activities. Selectivity coefficients can then be quickly estimated using a simple formula (see Eqn. 2 below).

A major criticism of this approach has been that it does not pay any attention to the conditions under which the device will be used, i.e., in practice, the primary ion and interfering ions will co-exist in the sample, and the matrix composition may vary widely from sample to sample. The mixed-solution (MS) or fixed-interference method goes some way to answering this criticism, as it involves measuring the electrode response to a varying activity of the primary ion in the presence of a fixed background of an interfering ion or vice versa. Selectivity coefficients are subsequently obtained by a graphical method [1].

In practical terms, the coefficients obtained by both methods can be regarded as little more than a tentative guide as to the selectivity of an ISE, and are never used in any quantitative manner [2]. Instead, empirical calibration approaches such as standard additions are used. This has the advantage of enabling calibration to be performed in the sample, thus providing a matched sample/calibrant background composition. However, the method does not allow selectivity coefficients to be determined in multicomponent mixtures.

ELECTRODE RESPONSE CHARACTERISTICS

ISEs can be characterised in terms of the response slope (S_j), the cell constant (E_j°) and selectivity coefficients (K_{jkl}) for the primary ion (k) of charge z_k against a range of interfering ions (l) of charge z_l. In mathematical terms, these are related by the well-known Nikolskii–Eisenmann equation;

$$E_{ij} = E_j^\circ + S_j \log\left(a_{ik} + \sum K_{jkl} a_{il}^{z_k/z_l}\right) \qquad (1)$$

where E_{ij} is the potential of an electrode (j) measured in a solution (i) of the primary ion at activity a_k and interfering ions at activity a_l. In the separate solution method, to estimate the selectivity coefficient for particular electrode against an interfering ion of the same charge as the primary ion one makes two potential measurements, one in a pure solution of the primary ion and the second in a pure solution of the interfering ion. If both the ion activities are equal, and the electrode response slope is known, the above equation simplifies to;

$$\frac{\Delta E}{S_j} = \log K_{jkl} \qquad (2)$$

where ΔE is the difference in the two measured potentials.

From the point of view of convenience, this approach is still a very attractive proposition for the screening of new devices as it is conceptually and computationally very simple, and practically very easy. In fact, in the sixties and early seventies, when calculators were still not widely available, this and the mixed solution method were the only feasible ways of "quantifying" selectivity. However, the coefficients obtained could not be used to obtain values for the activity of the primary ion in unknown solutions using the Nikolskii–Eisenmann equation, as sample solutions could have an unknown and varying background ion composition. Hence potentials measured in sample solutions would contain a significant unknown error in the summation factor in Eqn. 1. This explains the preoccupation with the development of very selective electrodes as, with the ideal "specific" electrode, the selectivity coefficients for all interfering ions would be zero and hence the summation factor would entirely disappear from Eqn. 1.

In reality, this is never achieved, although the pH glass electrode and the fluoride electrode come near. Consequently, matrix matching between samples and standards is vital if the analytical error is to be kept within acceptable limits. Standard additions is thus an attractive method which can provide very precise and accurate results, provided the contribution from the interferents in the summation (Eqn. 1) does not dominate that of the primary ion. The matched matrix ensures that the interferent contribution to the overall cell potential and the standard cell potential (E°) are constant for the sample and standards. However, shifts in the reference electrode junction potential can be a problem.

THE MULTIVARIATE APPROACH

The multivariate approach to calibration is the complete opposite in philosophy to that described above [3,4]. In this technique, an array of electrodes is used, and one deliberately makes the contribution from important interferents significantly large in the calibration process. These contributions are then used to calculate selectivity coefficients and other model parameters for each electrode in the array. The modelled array can then be used to determine the primary ions in sample solutions. In this work, we used ISEs for sodium, potassium and calcium. Mathematically, the array response can be described by an extended version of the Nikolskii–Eisenmann equation [5];

$$E_{ij} = E_j^o + S_j \log\left(a_{ik} + K_{jkl} a_{il}^{z_k/z_l} + K_{jkm} a_{im}^{z_k/z_m} + K_{jkLi} a_{Li}^{z_k} + \sum K_{jkn} a_{in}^{z_k/z_n}\right) \quad (3)$$

where the model is arranged in terms of the primary ion (k) and two interfering ions (l and m), and we need to determine a selectivity coefficient for each of the two modelled interferents, i.e., K_{jkl} and K_{jkm} in Eqn. 3 above. As with the Nikolskii–Eisenmann equation, in the ideal situation, all other contributions from unmodelled interferents (given by the summation factor above) will tend to zero, i.e., $K_{jkn} \rightarrow 0$ for all unmodelled interferents n, as this unmodelled contribution to the electrode signal will constitute an error which cannot be deconvoluted. However, as we have included contributions from two important interferents for each ISE, the system will tend much more towards ideallity than in the case of single electrode determinations (Eqn. 1). As lithium chloride is used as an ionic strength adjuster for the sample and calibration solutions, we include a selectivity coefficient K_{jkLi} for lithium implicitly in the model to facilitate correction for any contribution from lithium to the array response (see calibration section). Furthermore, as the calibration procedure involves using mixed solutions of all four ions, the selectivity coefficients will reflect their "real" values in a particular application. Hence, like standard additions, this approach enables electrodes to be calibrated very precisely for a particular application but unlike the former, computes the unknown values via selectivity coefficients determined in the modelling procedure. Finally, the use of the array enables multicomponent analysis to be performed on a single sample in contrast to standard additions with a single electrode.

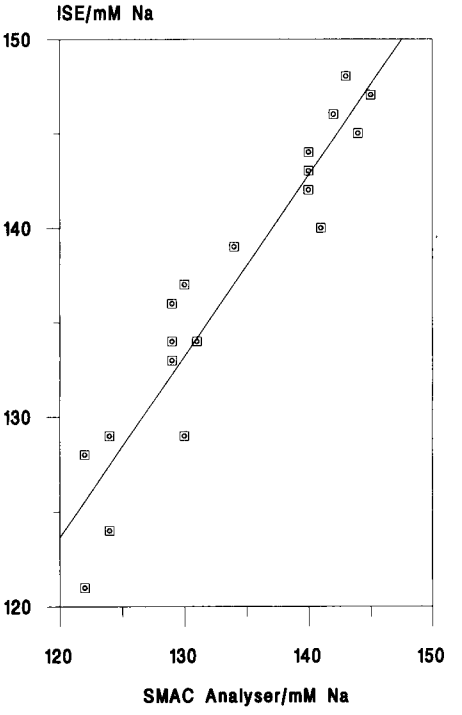

Fig. 1. Comparison of results obtained using mini-ISE static measurements and a SMAC analyser for plasma sodium analysis. Although there is a correlation between the data sets, a systematic bias is also evident [6].

Similar electrode arrays are used routinely in clinical analysers such as the Technicon SMAC used as the reference method in this research for validating array performance in plasma samples (see below for details). Through the use of automated calibration and dignostic tests and regular rigorous inter-hospital comparisons, these machines can produce very precise and accurate analyses of plasma sodium, potassium and calcium. However, manufacturers are reluctant to reveal the exact composition of the calibration solutions used and the software routines and algorithms which enable the instrument to calcu-

late unknowns. These most likely involve vaguely defined "fudge factors" incorporating a mixture of instrumental and chemical parameters and not implicit solution of selectivity coefficients in order to arrive at a result, although with suitable modification to the software and calibration regimes, the approach we describe could be introduced.

CALIBRATION STRATEGY

Figure 1 shows typical results for plasma sodium determinations obtained by dipping the ISE into the plasma samples and referring the potentials obtained to a calibration curve [6]. A linear relationship between these results and those obtained using a Technicon SMAC analyser is apparent with a reasonable correlation coefficient ($r^2 = 0.90$), but a systematic error or bias in the results is clear. This is caused by small amounts of drift in the ISE potential, which makes precise determination of the electrode standard potential (E°) difficult. Removal of this bias is not easy as the measurements are performed under high-impedance conditions, and the potential scale from the upper to lower limits of plasma sodium is around 2 mV or less, with most values being clustered within a 1 mV range. Hence small errors in determinations of unusually high or low sodium can have a very large bearing on the equation of the best-fit line. Given the well-documented concentration dependence of ISE errors, one can expect the lower than average sodium determinations to have a particularly significant effect.

Single electrode measurements using FIA [7] lead to some improvement in this situation. Calibration and analysis of samples can be performed much more quickly and sample presentation is very reproducible. Perhaps most importantly, measurements are made relative to a continuous baseline which tends to minimise drift, as this occurs on both the FIA peak and the baseline. This improvement is apparent in the results presented in Fig. 2, where the bias is greatly reduced.

However, both the above approaches involve an imperial calibration procedure with no determination of the ISE characteristics. A much more robust approach to ISE calibration based on a three-electrode array (sodium, potassium and calcium) has been described recently for both dip [8] and FIA [5] measurements. Calibration involves the following steps:

(1) design of a factorial set of calibration solutions which contain the primary ion (e.g., sodium) and large and varying amounts of the other two ions (e.g., potassium and calcium). The approach requires 2^n calibrant solutions, where n is the number of electrodes in the array;

(2) presentation of the three-electrode array to

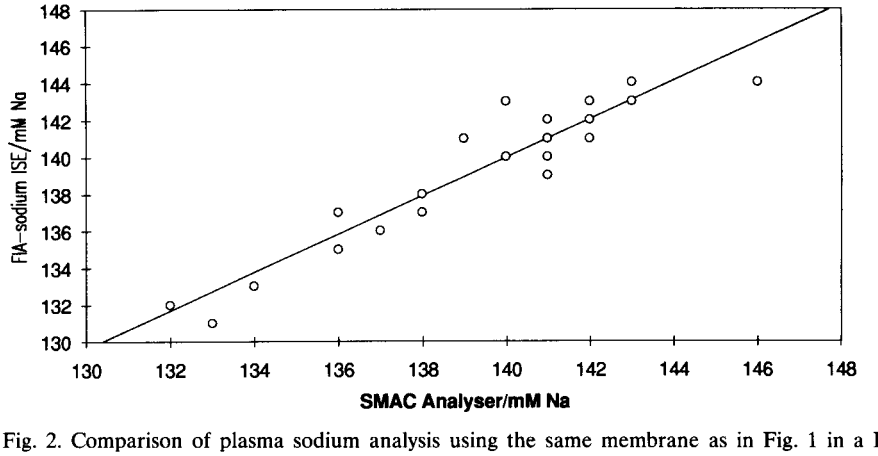

Fig. 2. Comparison of plasma sodium analysis using the same membrane as in Fig. 1 in a FIA system, with a SMAC analyser. Again, a good correlation is clear, but the bias is not totally removed [7].

TABLE 1

Example of array electrode characteristics determined using FIA approach [5]
(Standard deviation obtained using five separate calibration sets on a single array)

Electrode	E_j^o (mV)	S_j (mV/decade)	$K_{k,Na^+} \times 10^3$	$K_{k,K^+} \times 10^3$	$K_{k,Ca^{2+}} \times 10^3$	$K_{k,Li^+} \times 10^3$
ISE						
j,k = Na^+	348.2(1.1)	55.9(0.51)	1000	21.3(0.8)	8.0(1.0)	0.1(0.01)
j,k = K^+	154.2(1.1)	55.2(0.40)	5.5(0.18)	1000	6.2(0.11)	1.8(0.12)
j,k = Ca^{2+}	326.8(0.9)	27.8(0.23)	4.3(0.31)	5.1(0.32)	1000	2.8(0.19)
MIE						
j,k = Na^+	99.5(1.0)	57.4(0.61)	1000	995(65)	900(51)	5.7(0.35)
j,k = K^+	99.4(0.8)	57.4(0.55)	1005 (43)	1000	818(45)	5.7(0.21)
j,k = Ca^{2+}	96.9(0.9)	57.4(0.60)	1054 (52)	1051(63)	1000	79.5(3.51)

the 24 calibration solutions and storing the 3 × 24 matrix of potentials obtained;

(3) modelling of the 3-electrode array characteristics E, S and selectivity coefficients for each electrode) is achieved by setting approximate initial values and calculating a 3 × 24 array of potentials based on the activities of the three ions in each of the calibrant solutions;

(4) the least-squares error between these predicted potentials and the experimental potentials is calculated;

(5) iteration about steps 3 and 4 is performed until the error is minimised below a preset threshold using simplex optimisation.

EXPERIMENTAL

Instrumentation

Detailed descriptions of the experimental procedures have been presented elsewhere [5,8]. Array measurements were made by either dipping miniaturised ISEs (tip ca. 1 mm o.d.) into the sample solutions or alternatively, by means of a multi-sensor flow cell attached to a FIA system. In both cases, data capture was by means of a multi-channel data acquisition (I/O) card fitted into a 286-PC expansion slot following impedance conversion with voltage followers. Data acquisition and post-run processing was performed using in-house developed software written in Microsoft QuickBasic. The FIA system was completely automated, with facilities such as pump on/off, direction and speed, and sample injection controlled from the PC via the I/O card.

RESULTS AND DISCUSSION

Electrode parameters

Typical model characteristics obtained using this approach are shown in Table 1. These characteristics can be inserted into a three-equation matrix which describes the array response surface. Presentation of the array to unknown samples gives three potentials which can also be passed into the three-equation matrix to obtain the three unknown ion activities. Results for determinations of sodium in plasma and mineral water samples obtained using the modelled FIA-Array are shown in Figs. 3 and 4, respectively. In both cases, the bias is totally removed and good accuracy and precision is obtained. An important

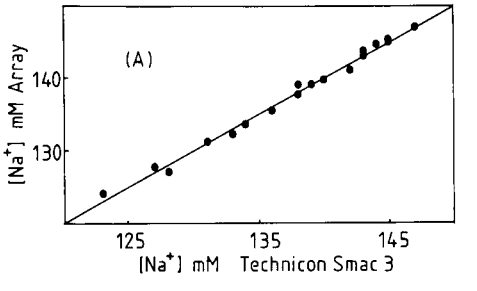

Fig. 3. Comparison of plasma sodium analysis using the array-FIA approach with a SMAC analyser. Good correlation without bias is obtained [5].

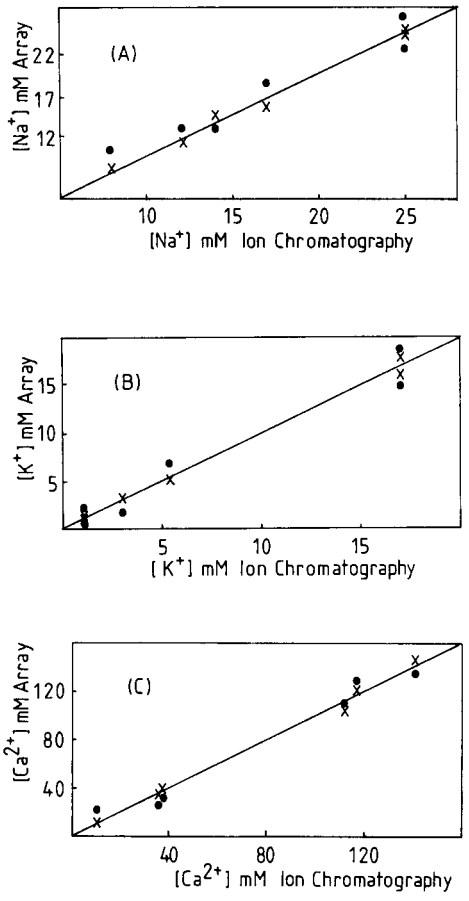

Fig. 4. Analysis of mineral water samples for Na, K and Ca by (×) the mean of four combinations of three electrodes generated by switching the MIE into the modelling procedure and (○) the single prediction obtained from the ISE array using ion chromatography for the reference method [5].

advantage of the array/non-linear calibration approach is that the concentration dependence of the error in potentiometric determinations is eliminated, which greatly reduces the influence of high and low points on the overall results as described above.

Multiple-ionophore electrodes

Overdetermined systems offer many attractive features including prediction polling and improved precision and accuracy arising from averaging of results. However, this normally involves increasing the number of sensors in the array compared to the number of determinants, which leads to more complex calibration procedures and the possibility of introducing unmodelled errors into the results. In earlier work, we investigated the possibility of using a sparingly selective electrode (SSE) in addition to the three selective electrodes for Na, K and Ca [8]. The SSE responded to varying degrees to all three ions, and a broad range of other ions as well. Consequently, the SSE could be modelled as a reasonable Na, K or Ca ISE, and the selectivity coefficients obtained in each case. The SSE could then be switched in place of one of the selective electrodes in the array in turn to give an additional three semi-independent determinations of the three unknowns in addition to the selective electrode array results (i.e., Na K Ca; Na K SSE; Na SSE Ca; SSE K Ca). Hence by polling the results, the SSE could be used to validate the performance of the ISEs (and vice versa). Furthermore, the four data sets could be averaged to improve the precision and accuracy of the final result. Figure 4 shows the scatter in results obtained by the three selective electrode array with the averaged values from the 4×3 determinations obtained with the permutations outlined above. A clear improvement in precision is evident in for all three ions, and the accuracy improved in the case of calcium. However, it should be emphasised that these results were obtained using samples containing the three ions only. When the approach was extended to real samples (plasma), the accuracy and precision of the results were much better for the three selective electrode array than for the averaged 4×3 determinations, reflecting most likely the effect of unmodelled interferents on the response of the SSE [8]. Nevertheless, this research suggested that it was possible to use this approach to realise the benefits of an overdetermined system without significantly increasing the number of sensors in the array.

In an effort to overcome the problem of unmodelled interferences on the results, the concept of using multiple ionophore electrodes (MIEs) was introduced recently as a simple method for tuning the selectivity of a PVC electrode [5]. The idea is to use several very selective ionophores in a single PVC membrane so as to

TABLE 2

Composition of multiple ionophore electrode membrane

Component	% (m/m)
Valinomycin	00.33
ETH129	00.33
Calix[4]arene	00.33
Exchanger	00.25
Plasticiser	32.75
PVC	66.00

produce an electrode which responds only to a restricted band of ions (i.e., those of analytical interest), unlike the SSE. In this research, all four electrodes were characterised, i.e., selective electrodes for Na, K and Ca, and the MIE based on the membrane composition given in Table 2. The resulting membrane was characterised as a sodium, potassium or calcium electrode which gave a significant response only to these three ions (interestingly, this type of characterisation could produce data on competitive complexation of the metal ions from the sample by the ligand mixture in the membrane). Results were generated by processing the potentials obtained in the samples with the 3 × selective electrode array, and then switching the MIE into the array in place of each one of the selective electrodes as described above for the SSE to give 4 semi-independent determinations of the unknown sample (Na K Ca; Na K MIE; Na MIE Ca; and MIE K Ca). Figure 5 shows that the averaged data from the four data sets gives a more precise result than the 3 × selective electrode array alone in the analysis of mineral water samples [5]. These results illustrate that the switching technique outlined above can be successfully applied to real samples provided the overall array response is overwhelmingly dominated by a restricted band of ions as is the case with the MIE, in contrast to the use of sparingly selective electrodes [4,8].

Do real selectivity coefficients exist?

Data collated in Table 3 illustrates how the value of selectivity coefficients are strongly dependent on the method used for estimation. Values obtained using the array approach are approximately 10–50 times larger than those obtained with the MS and SS methods. However, we obtained reasonable agreement between our coefficients for the potassium ISE and those published by other workers using the same technique (equal concentrations of primary and interfering

TABLE 3

Comparison of selectivity coefficients ($\times 10^4$) obtained by different methods

K ISE								
Method	MS [9]	SS [9] [a]	SS [9] [b]	MPM [9]	Array dip [8]	Array FIA [5] [d]	Array FIA [5] [e]	SS [c]
$K_{K,Na}$	2.9	70	6.8	0.83	40.6	55	55	4.1
$K_{K,Ca}$	N/A	1.8	2.1	3.7	50.9	98	62	1.6

Ca ISE						
Method	MS [10]	SS [10] [f]	Array dip [8]	Array FIA [5] [d]	Array FIA [5] [e]	SS [c]
$K_{Ca,Na}$	3.98×10^{-4}	1.99	0.1	40	43	0.2
$K_{Ca,K}$	1.00×10^{-4}	1	0.16	63	51	0.28

Na ISE					
Method	SS [11] [f]	Array dip [8]	Array FIA [5] [d]	Array FIA [5] [e]	SS [c]
$K_{Na,K}$	31.6	204	339	213	125
$K_{Na,Ca}$	0.525	173	122	80	31.6

[a] Separate solution method, equal concentrations of primary and interfering ions [9]. [b] Separate solution method, unequal concentrations of primary and interfering ions [9]. [c] Separate solution method, using 0.1 M solutions of primary and interfering ion chlorides (this research). [d] Using calibrants for mineral water analysis, ionic strength buffered at 40 mM [5]. [e] Using calibrants for diluted (×5) blood samples, ionic strength buffered at 250 mM [5]. [f] Using 0.1 M chloride solutions of primary and interfering ions [10].

ions). While it is clear that the coefficients obtained are method dependent, we do not believe that the SS or MS methods are accurate indicators of electrode selectivity, except for the very restricted conditions under which they are generated (i.e. separate pure solutions of ions for the SS method, and normally binary mixtures of the primary and one interfering ion for the MS method, with the interfering ion activity usually being held constant), and are thus of limited value in the more complex matrices generally encountered in real samples. In contrast to values obtained with our array approach, these methods do not produce numbers which can be used in the Nikolskii–Eisenmann equation to determine unknown ion activities. For this reason, we regard the array results as being a better estimation of the true selectivity coefficients for these electrodes. However, selectivity is a complex function of the membrane composition, the instrumentation used, the experimental design, and the type of sample and its matrix. Hence our selectivity coefficients are valid only for the particular set of conditions employed in their determination, and cannot be extended to other experimental designs or analytical conditions. Some examples from Table 3 illustrate the point. Values for $K_{K,Na}$ obtained by the same workers but with different approaches to the SS method gave results which were different by an order of magnitude (7.0×10^{-3} and 6.8×10^{-4}), while values obtained for the calcium ISE varied over many orders of magnitude with no agreement between any of the methods being apparent. This latter case perhaps reflects the greater difficulty in calculating selectivity coefficients for ions of differing charge, as the charge difference has an exponential effect on values calculated. Within the array approach, the spread obtained is relatively small between the dip and FIA array results and for the FIA array using different calibration ranges. Differences between the dip and FIA array are not unexpected, as the membrane geometry, sampling regime and measurement techniques are different.

The array results clearly show that values of selectivity coefficients can be regarded as "real" only for the particular conditions under which they were obtained. This emphasises the need for careful calibration and experimental design when using ISEs in any application.

Kinetic-based selectivity

In flow-injection analysis (FIA), the peak height (at peak maximum), or less commonly, peak area, is the parameter which is used for

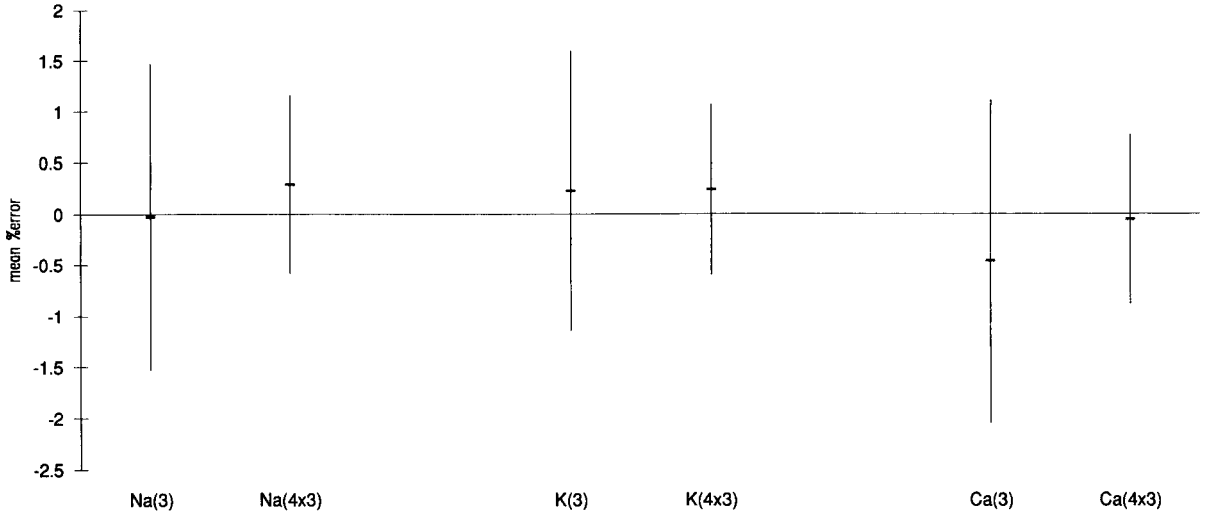

Fig. 5. Comparison of results obtained in tertiary mixtures of Na, K and Ca with the $3 \times$ ISE array (3) and the averaged data sets obtained with the four combinations of three electrodes (4×3) generated by switching the SSE into the modelling procedure [8].

analytical purposes. However, with our system, as the array response is available in digital form over the entire FIA time scale, it is possible to select data at any equivalent time for each sensor as the sample plug passes through the array block. These data can then be processed via the modelling procedure and the model parameters compared to those obtained under stopped-flow (steady-state) conditions. Hence it is possible to test whether the individual sensors produce an equilibrium response to the sample plug during the time scale for which it is in contact with the sensor membrane, and if so, at what stage equilibrium is achieved.

Typical results for the variation in the potassium selectivity of the sodium electrode ($K_{Na,K}$) as the sample plug passes by the ISE membrane in the flow cell are shown in Fig. 6. The same form is evident for the selectivity coefficients for lithium and calcium for this electrode [5]. It can be divided into three distinct regions:

(i) An initial stage (0.0 to 0.5 s) during which the selectivity coefficients broadly follow the values of the ionic mobility of each ion (stage 1, Fig. 7). This suggests that potentials recording over this time scale are dominated by the ability of the ion to move to the membrane diffusion layer and

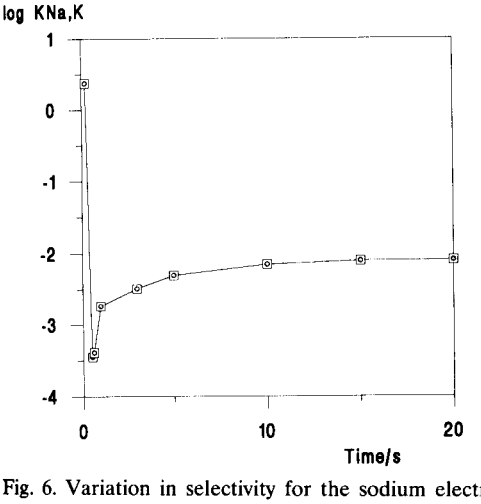

Fig. 6. Variation in selectivity for the sodium electrode with respect to potassium ions ($K_{Na,K}$) as a function of time as the sample plug passes the ISE membrane in the FIA detector block.

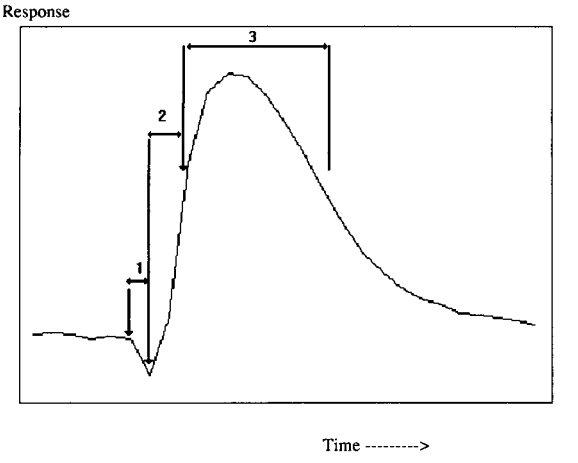

Fig. 7. Schematic illustration of the three selectivity regions within an FIA peak profile (time axis not to scale).

participate in partition. This stage is equivalent to the transient artefacts often noticed at the beginning of an FIA peak.

(ii) This is followed by a stage (0.5 to 5.0 s) coinciding with the rising portion of the peak, during which the selectivity for the primary ion is enhanced (stage 2, Fig. 7). This can be explained in terms of the kinetics of ion uptake and complexation with the ionophore in the membrane. Uptake of interferents is slower and so over this period, the interfering ions are below their final equilibrium concentrations in the membrane. Later in this paper, we discuss the possibility of using this kinetic enhanced selectivity for analytical purposes.

(iii) During the third stage, all ions reach their final equilibrium concentrations and the selectivity coefficients become relatively invariant and in close agreement with their steady-state values as measured under stopped-flow conditions (stage 3, Fig. 7). This implies that there is no net change in the ion populations in the membrane over this time scale, i.e., the rates of uptake and release of each ion are equal. This coincides with upper part of the rising portion of the peak, the peak maximum, and the upper part of the falling portion of the peak.

Similar results have been obtained for sodium, potassium and calcium electrodes using a different algorithm [12]. The problem of time depen-

dency of selectivity coefficients is of growing interest [13], and explanations based on the diffusion-layer model have been proposed [14]. Competitive processes involving primary and interfering ions have also been discussed in detail for solid-state ion-selective electrodes and the suitability of various models compared [15]. The availability of digitised experimental data at short time intervals across FIA-array peak profiles provides a useful practical method for examining these processes in relatively complex matrices, as the variability in selectivity coefficient at short

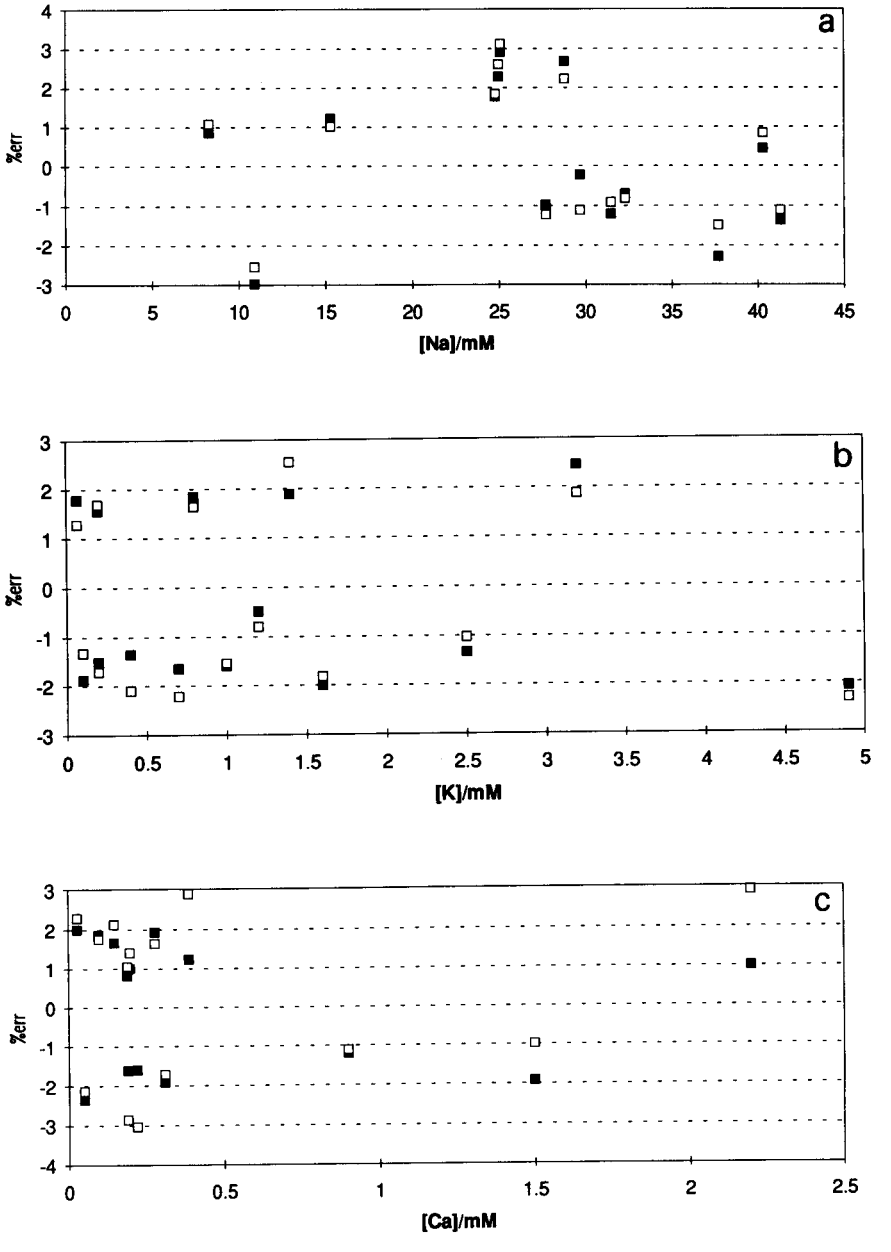

Fig. 8. Comparison of the error vs. analyte concentration for (a) Na, (b) K, (c) Ca using kinetic [%err(kin)] (□) and steady-state [%err(ss)] (■) models. Samples are tertiary mixtures of the three ions [5] (Na, K and Ca).

time intervals following arrival of the sample plug provides us with some insight into competitive ion-exchange. A greater understanding of the importance of various transient processes to the overall shape of the dynamic response profile will enable better sensor membranes to be developed from which more dependable results can be obtained. Furthermore, the use of a well-characterised sensor array will greatly enhance the quantity and quality of information available to the user, and hopefully lead to broader commercialisation.

In order to investigate whether this kinetic enhanced selectivity could be used for analytical purposes, the kinetic parameters were used to process potentials obtained by passing the calibration solutions through the array. Figure 8 shows the %error obtained with the kinetic parameters [%err(kin)] and steady-state parameters [%err(ss)] for sodium, potassium and calcium determinations as a function of the analyte concentration. Surprisingly, there is no difference between both approaches, and the error in both cases is independent of the concentration of the analyte ion. Figure 9 compares the precision and accuracy of both approaches, and again there is little difference, except perhaps in the case of the calcium determinations where the equilibrium measurements are slightly better. This is surprising as the kinetic results are obtained by processing potentials on the rising portion of the FIA peak, which is difficult to reproduce exactly. It seems that this uncertainty counteracts the improvements which would be expected from enhanced selectivity. Nevertheless, these results suggest that one can successfully employ data taken prior to the development of the peak maximum for analytical measurements, with increased sample throughput as a result, provided the sampling regime employed is very reproducible.

It is anticipated that the use of rigorous calibration and optimisation procedures will become more widespread in sensor research and electrochemistry. Although there are several papers published describing the use of simplex optimisation for modelling electrochemical parameters in

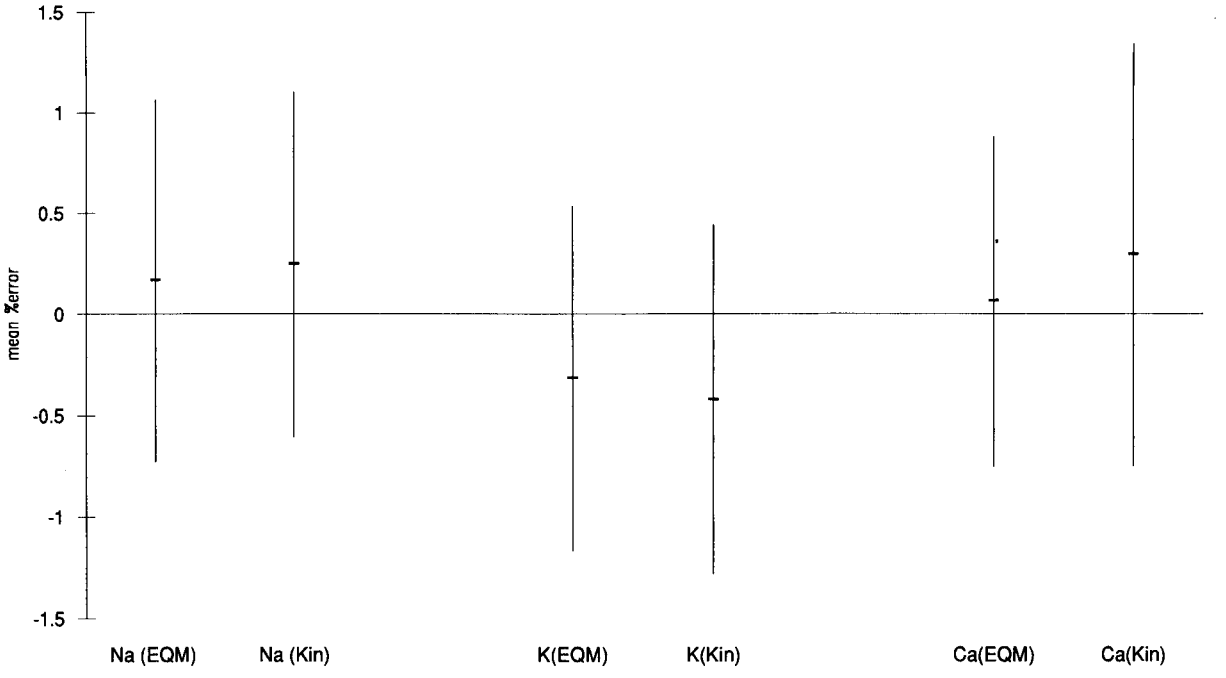

Fig. 9. Overall comparison of the precision and accuracy obtained using the equilibrium (EQM) and kinetic (Kin) models for Na, K and Ca determinations [5].

applications as diverse as the characterisation of an enzyme electrode [16], voltametric curves [17], and the chronoamperometry of microelectrodes [18], little work has been done on modeling sensor arrays.

This work demonstrates that there are important advantages to be realised from this approach, both from the point of view of producing sensors which are more precise and accurate through better modelling and calibration, and to generate data which can help us to gain a clearer understanding of the processes involved in generating the signals on a molecular scale in complex matrices.

Conclusions

A four-sensor array has been fabricated and successfully applied to the analysis of blood using both simple dip and FIA measurements. Characterisation of the arrays using simplex optimisation gave precise values for the electrode parameters in tertiary mixtures of sodium, potassium and calcium. These parameters, and particularly the selectivity coefficients have much more realistic values than those obtained with the separate solution and mixed solution techniques.

A multiple ionophore electrode with tuneable selectivity was constructed and used to generate four semi-independent data sets of results which could then be averaged to give more accurate results in real samples than the three-selective electrode array alone, unlike a sparingly-selective electrode used in previous studies.

Results generated by using potentials obtained in the kinetic controlled region of the FIA response peaks were very similar to those obtained under equilibrium conditions and could possibly be used for analytical purposes, providing the response profiles did not change significantly from sample to sample.

Selectivity towards the primary ion was found to be enhanced in the kinetic-controlled region of the response peak, and to gradually assume the equilibrium value. In addition, selectivity coefficients determined using the array-simplex method were found to be precise, and could be used for calculating unknown activities of the primary ions in real samples. However, these values were very different from results obtained using the separate and mixed solution techniques.

REFERENCES

1 G.J. Moody and J.D.R. Thomas, Selective Ion-Sensitive Electrodes, Merrow, Watford, 1971.
2 A.K. Covington, in A.K. Covington (Ed.), Ion-Selective Electrode Methodology, CRC Press, Boca Raton, FL, 1979, p. 18.
3 R.J. Forster and D. Diamond, Anal. Proc., 29 (1991) 117.
4 K.R. Beebe, D. Uerz, J. Sandifer and B.R. Kowalski, Anal. Chem., 60 (1988) 66.
5 R.J. Forster and D. Diamond, Anal. Chem., 64 (1992) 1721.
6 M. Telting Diaz, M.R. Smyth, D. Diamond, E.M. Seward, G. Svehla and A.M. McKervey, Anal. Proc., 26 (1989) 29.
7 M. Telting Diaz, D. Diamond and M.R. Smyth, Anal. Chim. Acta, 251 (1991) 149.
8 R.J. Forster, F. Regan and D. Diamond, Anal. Chem., 63 (1991) 876.
9 V.P.Y. Gadzekpo and G.D. Christian, Anal. Chim. Acta, 164 (1984) 279.
10 U. Schefer, D. Ammann, E. Pretsch, U. Oesch and W. Simon, Anal. Chem., 58 (1986) 2282.
11 D. Diamond, G. Svehla, E.M. Seward and A.M. McKervey, Anal. Chim. Acta, 204 (1988) 223.
12 M. Hartnett and D. Diamond, presented at the Royal Society of Chemistry R&D Topics Meeting, University of Birmingham, July 1992.
13 A. Lewenstam and A. Hulanicki, Selective Electrode Rev., 12 (1990) 161.
14 A. Hulanicki and A. Lewenstam, Talanta, 24 (1977) 171.
15 A. Lewenstam, A. Hulanicki and T. Sokalski, Anal. Chem., 59 (1987) 1539.
16 S.K. Beh, G.J. Moody and J.D.R. Thomas, Anal. Proc., 27 (1990) 82.
17 I. Lavagnini, P. Pastore and F. Magno, Anal. Chim. Acta, 223 (1988) 193.
18 Z. Liu, Z. Jia and G. Gu, J. Electroanal. Chem. Interfacial Electrochem., 259 (1989) 39.

Analytica Chimica Acta, 276 (1993) 87–97
Elsevier Science Publishers B.V., Amsterdam

Behaviour of a series piezoelectric sensor in electrolyte solution

Part I. Theory

D.Z. Shen, W.H. Zhu, L.H. Nie and S.Z. Yao

New Materials Research Institute, Hunan University, Changsha 410082 (China)

(Received 19th May 1992; revised manuscript received 16th September 1992)

Abstract

The theory, methodology and behaviour of a piezoelectric and conductivity sensor in electrolyte solution are reported. The sensor was constructed by connecting an AT-cut piezoelectric quartz crystal and a conductivity electrode in series. It has a sensitive and selective frequency response to the change in solution conductivity and permittivity. The relationship between frequency and solution conductivity was derived according to the oscillating theory and supported by the experiments. The effects of the solution conductivity, permittivity, temperature, density and viscosity, cell constant of the conductivity electrode, foreign electrolytes and the operating voltage of the integrated circuit–TTL oscillator on the behaviour of the series piezoelectric sensor were investigated. The sensor possesses high sensitivity to the solution conductivity and a low frequency–temperature coefficent, and its frequency depends very little on the operating voltage and density and viscosity of the solution. Its sensitivity and accuracy were improved in the presence of foreign electrolytes.

Keywords: Conductimetry and oscillometry; Piezoelectric sensors

Conductivity methods are widely applied in analytical chemistry [1], e.g., for end-point detection in conductimetry and high-frequency titrimetry [2–5]. However, the sensitivity of such methods is limited and the accuracy is poor in solution systems when foreign electrolytes are present. "Frequencymetric" titrimetry based on the fact that the frequency of a piezoelectric quartz crystal is an almost linear function of the solution conductivity has been proposed and found applied in chemical analysis [6–11]. This method offers the advantage of higher sensitivity over classical conductimetry, especially in the solution systems where large amounts of foreign electrolytes are present. However, its frequency is affected by the density and viscosity of the solution and by adsorption, contamination and corrosion of the crystal. The series piezoelectric quartz crystal (SPQC) sensor reported in this paper possesses the same sensitivity as a normal piezoelectric quartz crystal sensor (PQC), but a better frequency stability, lower frequency–temperature coefficient and low frequency dependence on the density and viscosity of the solution.

Correspondence to: S.Z. Yao, New Materials Research Institute, Hunan University, Changsha 410082 (China).

THEORY

When a conductivity electrode is immersed in a solution, the equivalent circuit of an SPQC can be obtained by combining the electrical equiva-

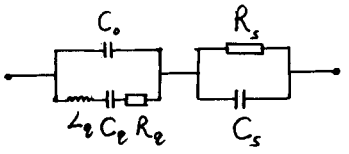

Fig. 1. Equivalent circuit of the SPQC. C_0 = static capacitance; L_q = motional inductance; R_q = motional resistance; C_q = motional capacitance of the piezoelectric quartz crystal; C_s = solution capacitance; R_q = solution resistance.

lent circuit of a piezoelectric quartz crystal with that of a conductivity electrode in series, as illustrated in Fig. 1. The motional capacitance, C_q, represents the mechanical elasticity of the vibrating system. The motional inductance, L_q, is a measure of the vibrating mass. The motional resistance, R_q, corresponds to the loss of mechanical energy dissipated to the surrounding medium and the supporting structures. The parallel capacitance, C_0, originates from the electrodes and the stray capacitance of the supporting structures. The solution resistance, R_s, is the reciprocal of the solution conductivity. The solution capacitance, C_s, depends on the dielectric constant of the solution and the stray capacitance of the leading wires.

The impedance, Z, of an SPQC is complex: $Z = R + jX$, where R is the real part of Z, the resistive part, X is the imaginary part of Z, the reactance and $j = \sqrt{-1}$. For the circuit shown in Fig. 1, the motional resistance, R_q, is ignored for simplification as its value is very small (4.5 Ω for the crystal used in the experiments). The real and imaginary parts of the impedance of SPQC are

$$R = \frac{G}{G^2 + \omega^2 C_s^2} \tag{1}$$

$$X = \frac{-\omega C_s}{G^2 + \omega^2 C_s^2} + \frac{\omega L_q - 1/\omega C_q}{1 + C_0/C_q - \omega^2 L_q C_0} \tag{2}$$

where $\omega = 2\pi F$ and F is the oscillating frequency. $G = 1/R_s$ is the conductivity of the solution. The values of G and C_s can be calculated as follows:

$$G = k\chi \tag{3}$$

$$C_s = k\epsilon + C' \tag{4}$$

where χ is the specific conductivity of the solution, ϵ is the dielectric constant of the solution, k is the cell constant of the conductivity electrode and C' is the parasitic capacitance of the circuit.

There are two conditions that must be satisfied for oscillation to occur: the phase shift around the loop should be zero and the loop gain should be unity, the loop being the closed path from the input of the amplifier through the amplifier to its output, and back to the input through the feedback circuit element. If the amplifier used in the oscillator has a phase shift of θ then the feedback circuit must have a phase shift of $-\theta$ in order to satisfy the first oscillation condition. Because the SPQC is the feedback network of an integrated circuit (IC)–TTL oscillator, its real and imaginary parts of the impedance should satisfy the phase shift condition

$$-\theta = \tan^{-1}(X/R) \tag{5}$$

From Eqns. 1, 2 and 5,

$$\frac{\omega L_q - 1/\omega C_q}{1 + C_0/C_q - \omega^2 L_q C_0} + \frac{GA - \omega C_s}{G^2 + \omega^2 C_s^2} = 0 \tag{6}$$

where $A = \tan\theta$.

The relationship between frequency and conductivity can be established by solving Eqn. 6. With the help of a Taylor series, the relationship can be approximated as follows:

$$\omega = \omega_0 \left[1 + \frac{0.5\omega_0 C_q(\omega_0 C_s - AG)}{G^2 - \omega_0 C_0 GA + \omega_0^2 C_s(C_0 + C_s)} \right] \tag{7}$$

where $\omega_0 = 2\pi F_0$ and $F_0 = 1/2\pi\sqrt{L_q C_q}$ is the resonant frequency of the crystal. Equation 7 is the general response function for the SPQC.

The sensitivity of the method, that is, the slope of the plot of ω vs. G, can be calculated by differentiating with respect to G as follows:

$$\frac{\partial\omega}{\partial G} = \frac{0.5\omega_0^2 C_q(G^2 A - 2G\omega_0 C_s - A\omega_0^2 C_s^2)}{\left[G^2 + \omega_0^2 C_s(C_0 + C_s) - \omega_0 C_0 GA\right]^2} \tag{8}$$

It can be seen that the sensitivity of the SPQC depends on the parameters of the circuit, the crystal and the solution. The higher the fundamental frequency of the crystal, the higher is the sensitivity. When the parameters of the circuit and crystal are fixed, the slope of the frequency

shift versus conductivity plot is affected by the solution capacitance and conductivity. As the dielectric constant of a solution varies little in dilute electrolyte solution, the solution capacitance can be considered to be constant. Hence the slope of the response curve is affected mainly by the specific conductivity of the solution and the cell constant of the conductivity electrodes. In solutions of low conductivity, assuming that $G \ll \omega_0 C_s$, the slope can be simply calculated from the equation

$$\frac{\partial \omega}{\partial G} = \frac{-AC_q}{2(C_0 + C_s)^2} \tag{9}$$

It is clear that the slope is constant, and as a result the relationship between the frequency shift and the conductivity or the concentration of electrolyte is linear in the low concentration range.

If the solution conductivity is much greater than its reactance, that is, $G \gg \omega_0 C_s$, as in a high-conductivity solution, the slope may be evaluated approximately by the equation

$$\partial\omega/\partial G = A\omega_0^2 C_q / 2G^2 \tag{10}$$

This equation shows that the slope of the frequency shift vs. conductivity plot decreases as G^2 approaches zero. Therefore, the sensitivity of the SPQC is poor for a high-conductivity solution system. The cases between the two extreme conditions are complex. The slope of the plot increases with increase in conductivity at first, then decreases as the conductivity continues to increase. The maximum slope can be found by differentiating Eqn. 8 with respect to G. Assuming that the differential equals zero, the expression is

$$AG^3 - 3\omega_0 C_s G^2 - 3A\omega_0^2 C_s^2 G + \omega_0^3 C_s^2 (A^2 C_0 + C_0 + C_s) = 0 \tag{11}$$

The numerical solution of Eqn. 11 for a potassium chloride solution system with a cell constant of 1.04 cm is $G = 0.261$ mS, which corresponds to a concentration of 2.0 mmol l^{-1}. The slope at this point is 169 kHz m S^{-1}, which is about 2.35 times of that in a low-concentration solution (72 kHz m S^{-1} in a 0.02 mmol l^{-1} solution). Because the slope increases only 1.35 times with increasing concentration from 0.01 to 2 mmol l^{-1}, the frequency shift vs. conductivity plot is nearly linear and can be treated as linear in a narrow conductivity range.

Usually, the frequency shift measured is the frequency difference between the sample and a reference solution. If pure solvent with a very low conductivity is used as the reference solution, the frequency shift can be calculated from the equation

$$\Delta F = \left[-0.5F_0 C_q G(G + \omega_0 C_s A)\right] / \left\{(C_0 + C_s) \times \left[G^2 - \omega_0 C_0 GA + \omega_0^2 C_s (C_0 + C_s)\right]\right\} \tag{12}$$

If a solution with conductivity G_0 is chosen instead of pure solvent as the reference solution, and the change in conductivity between sample and reference solutions (ΔG) is much less than G_0, the relationship between frequency shift and the conductivity change, ΔG, can be expressed as

$$\Delta F = \left[\Delta G \pi F_0^2 C_q (2G_0\omega_0 C_s + A\omega_0^2 C_s^2 - AG_0^2) / \left[G_0^2 - \omega_0 C_0 G_0 A + \omega_0^2 C_s (C_0 + C_s)\right]^2\right. \tag{13}$$

It is obvious that the ΔF vs. ΔG relationship is linear. The slope of the plot may be greater than the value obtained with pure solvent as the reference solution with the same conductivity change provided that the conductivity of the reference solution does not exceed the value at which the sensitivity begins to drop with increasing conductivity. Therefore, the SPQC offers an advantage over the classical conductimetric method in a solution system in the presence of foreign electrolytes. If the conductivity of the foreign electrolytes is much greater than that of analyte, the sensitivity and accuracy of the classical conductimetric method become worse, whereas those of the SPQC improve.

EXPERIMENTAL

Apparatus and reagents

The experimental set-up employed is illustrated in Fig. 2. The IC–TTL crystal oscillator

and frequency counter were described in a previous paper [6]. The series piezoelectric sensor was constructed by connecting an AT-cut 9-MHz piezoelectric quartz crystal and a conductivity electrode in series to make up the feedback circuit of the oscillator. One of the crystal lead wires was connected to the input terminal of the oscillator, another crystal lead was connected with one of the lead wires of the conductivity electrode and a third lead wire was connected to the output terminal of the oscillator. The lead wires should be as short as possible and separated physically to decrease the parasitic capacitance. A conductivity electrode with a cell constant of 1.04 cm was used is all experiments except in that on the influence of the cell constant. An HP-9153C computer was used for data analysis. A HP-4192A LF impedance analyser (Hewlett-Packard) was employed to measure the parameters of the crystal and the conductivity and capacitance of the electrode. The solution temperature was controlled by a thermostated water jacket at 20.0 ± 0.1°C in all experiments except the temperature experiment.

Analytical-reagent grade chemicals and redistilled water were used throughout. Tetrabutylammonium tetraphenylborate (TBATPB) was prepared as follows: equal volumes of 0.01 mol l^{-1} tetrabutylammonium iodide and sodium tetraphenylborate solutions were mixed with stirring and the precipitate was washed three times with water, dried under vacuum, recrystallized twice from acetone, then dried under vacuum.

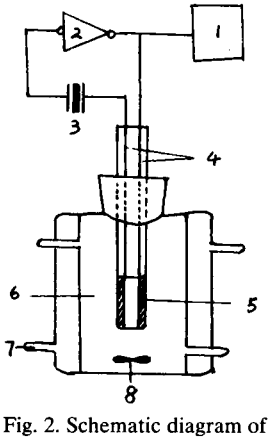

Fig. 2. Schematic diagram of the SPQC system. 1 = Frequency counter; 2 = IC–TTL oscillator; 3 = piezoelectric quartz crystal; 4 = lead wire; 5 = conductivity electrodes; 6 = detection cell; 7 = thermostated water-jacket; 8 = magnetic stirrer.

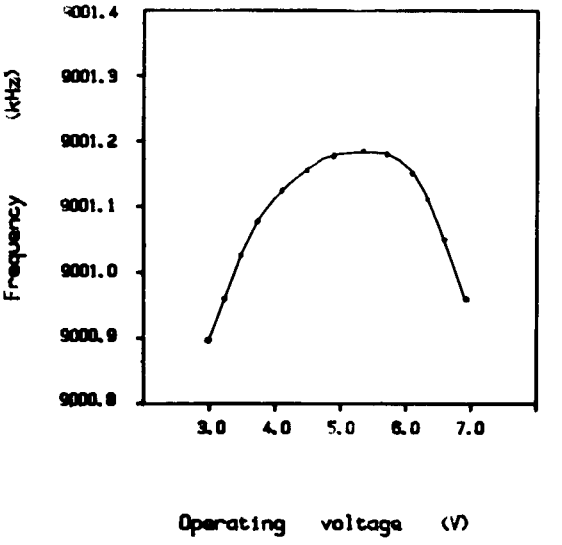

Fig. 3. Dependence of the frequency on the operating voltage.

Procedure

A 20-ml volume of reference solution was placed in the detection cell, the conductivity electrode was immersed in the solution and the stable frequency (F_0) was recorded as the reference frequency. The reference solution was then replaced with the solution to be measured and the stable frequency (F_1) was recorded. The frequency shift was calculated as $\Delta F = F_1 - F_0$.

RESULTS AND DISCUSSION

Influence of operating voltage on frequency

In the suitable operating voltage range 3–7 V, the influence of the operating voltage of the IC–TTL oscillator on the frequency of the SPQC in water is as shown in Fig. 3. It can be seen that the influence of voltage on the frequency is slight. The change in frequency is less than 25 Hz in the voltage range 4.0–6.0 V. The change in frequency is slightly greater outside this range as the voltage is less suitable for the oscillator.

Dependence of frequency shift on specific conductivity of solution

Equation 7 gives the theoretical relationship between frequency and solution conductivity, and if it is possible to fit this equation to a curve of F versus G for electrolyte solutions determined experimentally, this may be taken as evidence of the correctness of the equation.

To demonstrate this, the response curves were measured in aqueous potassium chloride solutions and TBATPB in nitrobenzene (NB) and 1,2-dichloroethane (DCE) solutions of known concentrations. The experimental points are shown in Fig. 4. The smooth curve was drawn according to Eqn. 12 with the following parameters of the crystal and circuit: $F_0 = 9 \times 10^6$ Hz, $C_q = 3.10 \times 10^{-14}$ F, $C_0 = 6.48 \times 10^{-12}$ F, $C' = 1.23 \times 10^{-12}$ F and $A = 0.624$. It can be seen that the agreement between the calculated and experimental values is very good, which indicates that the SPQC can be approximately represented by the circuit in Fig. 1.

The sensitivity of the method, that is, the slopes of the frequency shift versus conductivity curves, are shown in Fig. 5 (the smooth curve was drawn according to Eqn. 8). It can be seen that the theoretical model agrees well with the experimental results. The slopes are nearly constant at low conductivity and increase slightly with increase in specific conductivity until a maximum is reached, then decrease as the specific conductivity increases further. The maximum slopes are reached at 0.026, 0.021 and 0.013 S m^{-1} with values of -169, -408 and -1380 kHz m S^{-1} in aqueous, NB and DCE solutions, respectively. Because the maximum sensitivities are only 2.3, 3.1 and 5.1 times the values at low conductivity for aqueous, NB and DCE solution systems, respectively, when the conductivity increases about 100-fold, the plots of frequency shift vs. specific conductivity can be treated as straight lines in a narrow conductivity range, especially at low conductivities. This result is obvious in Fig. 4.

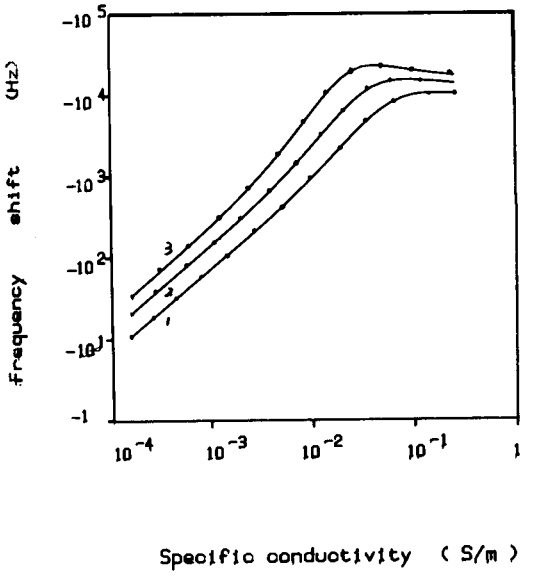

Fig. 4. Dependence of the frequency on the solution conductivity. Solvents: 1 = water; 2 = NB; 3 = DCE.

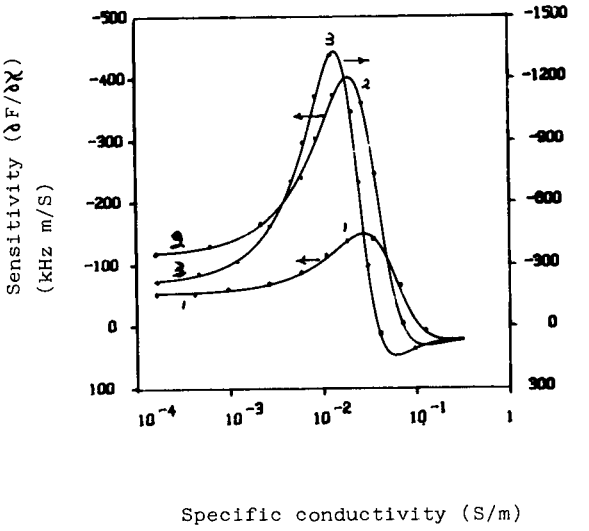

Fig. 5. Dependence of the sensitivity on the solution conductivity. Solvents: 1 = water; 2 = NB; 3 = DCE.

From Fig. 5 it can be seen that the sensitivity is related to the permittivity of the solutions. The dielectric constants of water, NB and DCE are 80.1, 35.74 and 10.65 at 20°C [12], respectively. As the dielectric constant of the solution increases, the sensitivity decreases and the maximum sensitivity is obtained at higher conductivity.

Dependence of the frequency of SPQC on the density and viscosity of solution

The influence of density and viscosity on the behaviour of the SPQC was investigated in 0–50%

aqueous sucrose solutions containing 1.0 mmol l^{-1} potassium chloride. The changes in solution density, viscosity, capacitance and conductivity and the frequency of the SPQC with variation in the concentration of sucrose are shown in Table 1. It can be seen that the density, viscosity, conductivity and frequency increase and the capacitance decreases with increasing concentration of sucrose. It is more important that the frequency shifts calculated according to Eqn. 7 due to the varying capacitance and conductivity are close to the frequency shifts experimentally measured. That is, the density and viscosity of the solution have little effect on the frequency of the SPQC, but do on the capacitance and conductivity. This result is expected because the crystal in SPQC is not in contact with the solution and its frequency should depend only on those solution parameters relating to the conductivity factors such as specific conductivity and dielectric constant. However, it is well known that the frequency shift is proportional to the square root of the product of the solution density and viscosity in both normal and electrode-separated PQCs [13–15]. It is clear that the frequency stability of the PQC depends greatly on the loss of oscillating energy due to acoustic impedance: the smaller the loss, the better is the frequency stability. The acoustic impedance of the crystal increases with increase in the density and viscosity of the medium in which it oscillates. Therefore, the SPQC possesses excellent frequency stability because its crystal oscillates in vacuum and the acoustic impedance and the loss of oscillating energy are much less than those in normal and electrode-separated PQCs in which the crystal oscillates in a liquid environment.

Dependence of the behaviour of SPQC on the cell constant

Because the sensitivity of the SPQC is related to the solution conductivity and capcitance, according to Eqns. 3 and 4, both the solution conductivity and capacitance are proportional to the cell constant of the conductivity electrode, so the cell constant is an important parameter for the SPQC. The dependence of the behaviour of the SPQC on the cell constant was investigated by measuring the response curves with conductivity electrodes with different cell constants. Potassium chloride was used in aqueous solutions and TBATPB in DCE and NB solutions as the electrolytes.

The frequency changes of the SPQC in pure solvents due to the varying cell constant are shown in Fig. 6. It is obvious that the frequency declines as the cell constant increases. On the other hand, the maximum frequency shift in electrolyte solutions with pure solvent as the reference becomes smaller with increasing cell constant, as shown in

TABLE 1

Frequency shift and solution parameters in sucrose solutions containing 1.0 mmol l^{-1} KCl [a]

$C_{sucrose}$ (%)	ρ (g cm^{-3})	η (cP)	G (mS)	C_s (pF)	$\Delta F_{calc.}$ (Hz)	$\Delta F_{meas.}$ (Hz)
0	0.9982	1.005	0.1244	8.472	0	0
6.0	1.0281	1.177	0.1143	8.437	122	128
12.0	1.0465	1.426	0.0982	8.298	356	362
17.0	1.0478	1.716	0.0870	8.184	526	531
22.0	1.0899	2.120	0.0755	8.063	703	716
28.0	1.1175	2.849	0.0615	7.908	920	927
32.0	1.1366	3.754	0.0529	7.797	1066	1044
37.0	1.1613	4.958	0.0424	7.651	1248	1293
42.0	1.1868	7.220	0.0341	7.523	1402	1382
50.0	1.2295	15.40	0.0197	7.228	1717	1705

[a] $C_{sucrose}$ is the concentration of sucrose in water (w/w), ρ is the density, η is the viscosity; all the data are from [12]. $\Delta F_{calc.}$ is the frequency shift calculated according to Eqn. 7 with 1.0 mmol l^{-1} KCl solution as the reference; $\Delta F_{meas.}$ is the frequency shift determined experimentally with the same reference.

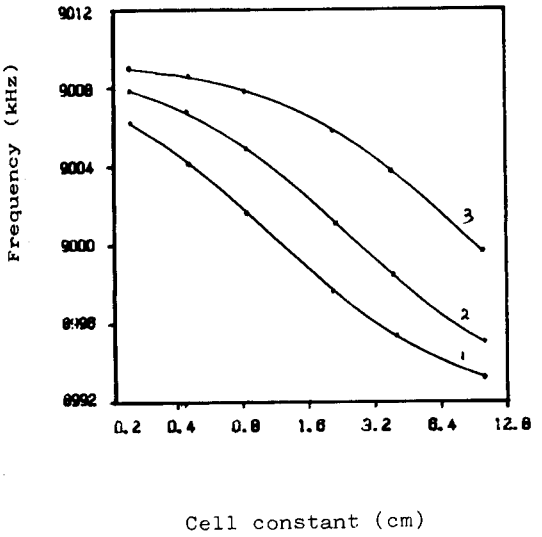

Fig. 6. Dependence of frequency on the cell constant. Solvents: 1 = water; 2 = NB; 3 = DCE.

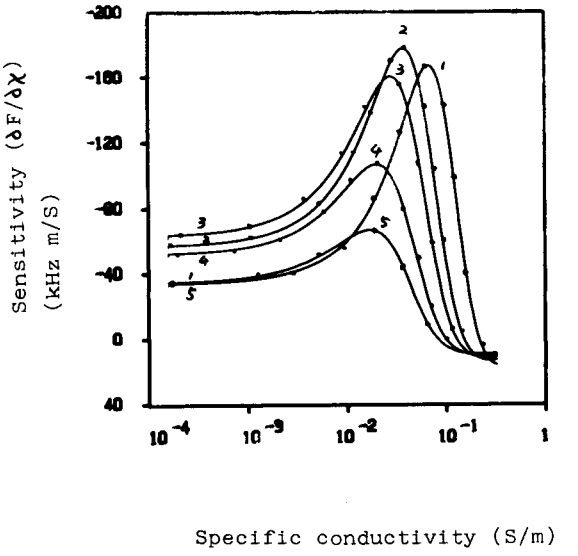

Fig. 8. Dependence of sensitivity on specific conductivity and the cell constant in aqueous KCl solution. Cell constants: 1 = 0.24; 2 = 0.59; 3 = 1.04; 4 = 2.56; 5 = 4.87 cm.

Fig. 7, i.e., the variable frequency shift range is narrowed when an electrode with greater cell constant is employed.

Figures 8, 9 and 10 illustrate the dependence of the sensitivity on both the specific conductivity and the cell constant in aqueous, NB and DCE solutions, respectively. It can be seen that the sensitivity increases with increasing cell constant at first, then it begins to decrease. The maximum sensitivity is obtained when C_0 and C_s are approximately equal. The optimum cell constant

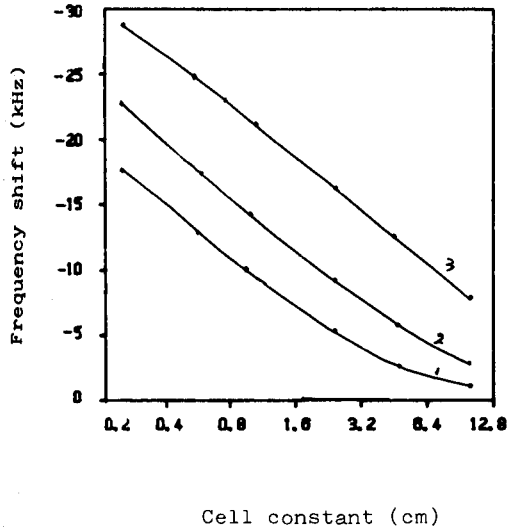

Fig. 7. Dependence of maximum frequency shift on the cell constant. Solvents: 1 = water; 2 = NB; 3 = DCE.

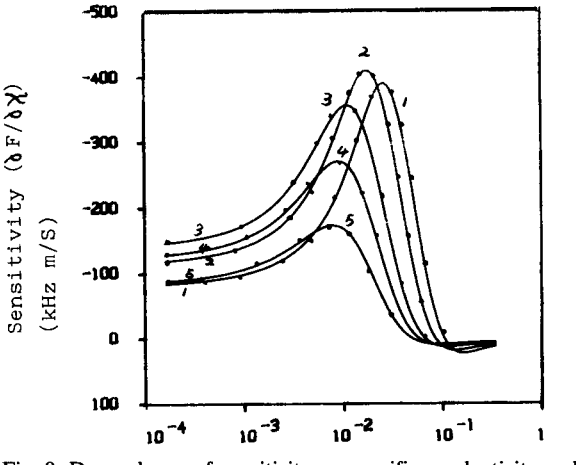

Fig. 9. Dependence of sensitivity on specific conductivity and the cell constant in TBATPB solution in nitrobenzene. Cell constants: 1 = 0.59; 2 = 1.04; 3 = 2.56; 4 = 4.87; 5 = 9.6 cm.

depends on the dielectric constant of the solvent and the stray capacitance of the electrode and also the range of the conductivity to determined. On the other hand, the conductivity corresponding to the maximum sensitivity decreases as the cell constant increases.

Effect of temperature on frequency of SPQC

The influence of temperature on the SPQC was investigated in aqueous potassium chloride solutions in the range 10–50°C. With the frequency in solutions of each concentration at 10°C as the reference frequency, the frequency shifts due to the increase in temperature are as shown in Fig. 11. The frequency–temperature behaviour of the SPQC depends on the concentration of KCl and the temperature. When the solution temperature increases, the frequency increases in solutions of low concentration (10^{-5}–10^{-4} mol l^{-1}), varies very little at certain concentrations (e.g., 5×10^{-4} mol l^{-1}), then decreases in solutions of high concentration. The frequency–temperature coefficient at 20°C is 21, 19.5, 4.2, −6.3 and −132 Hz °C^{-1} in KCl solutions of 1×10^{-5}, 1×10^{-4}, 5×10^{-4}, 1×10^{-3} and 3×10^{-3} mol l^{-1}, respectively.

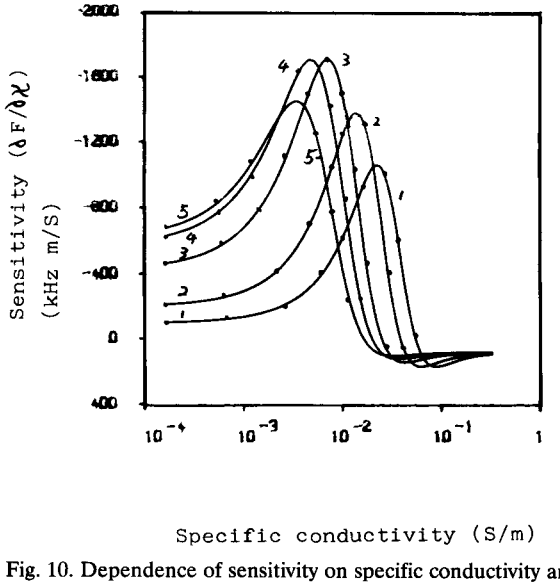

Fig. 10. Dependence of sensitivity on specific conductivity and the cell constant in TBATPB in 1,2-dichloroethane. Cell constants: 1 = 0.59; 2 = 1.05; 3 = 2.56; 4 = 4.87; 5 = 9.6 cm.

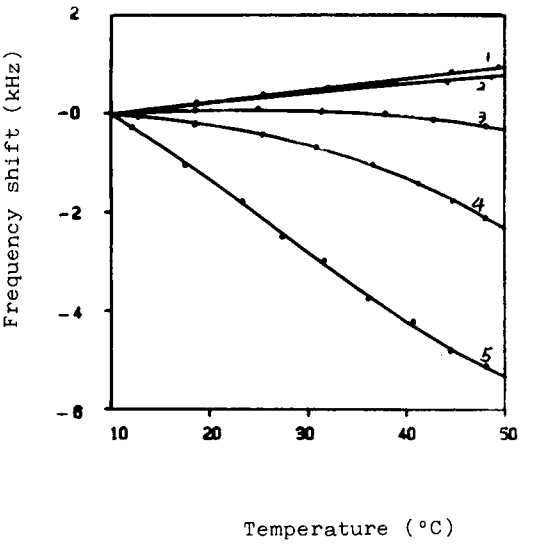

Fig. 11. Dependence of frequency on temperature in aqueous KCl solutions. Concentration of KCl: 1 = 0.01; 2 = 0.1; 3 = 0.5; 4 = 1.0; 5 = 3.0 mmol l^{-1}.

Usually, the dielectric constant of a liquid decreases and the specific conductivity increases as the liquid temperature increases; as a result, the former makes the solution capacitance decrease and the frequency of the SPQC increase, and the latter causes the specific conductivity of the liquid to increase and the frequency of the SPQC to decrease. In electrolyte solutions of low concentration, the influence of solution capacitance is dominant and the frequency increases with increasing solution temperature. In electrolyte solutions of high concentration, the influence of solution conductivity is dominant and the frequency decreases as the solution temperature increases. In order to explain quantitatively the dependence of the frequency–temperature coefficient on the concentration of electrolyte, the solution capacitance, C_s, and conductivity, G, were measured at different temperatures in the range 10–50°C. Two regressed relationships are obtained:

$$C_s = C_s'(0.9945)^{(t-10)} + C_1 \quad (14)$$

$$G = G'(1.0205)^{(t-10)} + G_1 \quad (15)$$

where t is the temperature in °C, C_s' is the solution capacitance and G' is the solution con-

ductivity at 10°C and C_1 and G_1 are constants for each solution. Consequently, the frequency–temperature coefficients can be evaluted according to Eqns. 9, 14 and 15 as follows:

$$\frac{dF}{dt} = \frac{\partial F}{\partial C_s} \cdot \frac{\partial C_s}{\partial t} + \frac{\partial F}{\partial G} \cdot \frac{\partial G}{\partial t} \quad (16)$$

From Eqns. 7, 14 and 15,

$$\frac{\partial F}{\partial C_s} \cdot \frac{\partial C_s}{\partial t} = \frac{M\omega_0^2 C_q C_s'\left(G^2 + 2AG\omega_0 C_s - \omega_0^2 C_s^2\right)}{\left[G^2 - AG\omega_0 C_0 + \omega_0^2 C_s(C_0 + C_s)\right]^2} \quad (17)$$

$$M = -3.95 \times 10^3 (0.9945)^{(t-10)} \quad (18)$$

$$\frac{\partial F}{\partial G} \cdot \frac{\partial G}{\partial t} = \frac{NG'\omega_0 C_q\left(AG^2 - 2G\omega_0 C_s - A\omega_0^2 C_s^2\right)}{\left[G^2 - AG\omega_0 C_0 + \omega_0^2 C_s(C_0 + C_s)\right]} \quad (19)$$

$$N = 1.44 \times 10^4 (1.0205)^{(t-10)} \quad (20)$$

The frequency–temperature coefficients due to C_s are shown in Fig. 12 according to Eqn. 17. It is obvious that the values depend both on the the concentration of the electrolyte or the conductivity G and temperature. When the solution

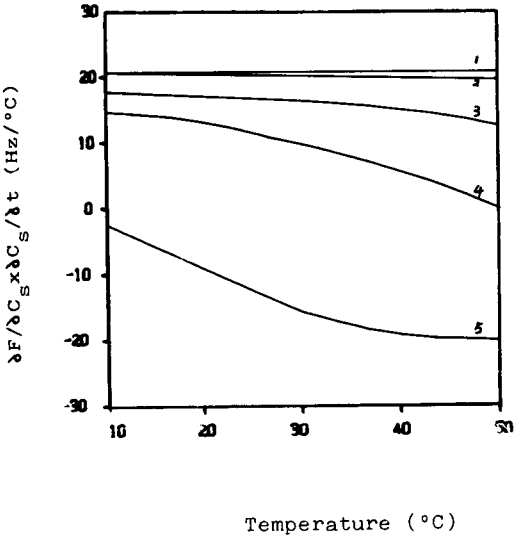

Fig. 12. Contribution of capacitance term to the frequency–temperature coefficient. Concentration of KCl: 1 = 0.01; 2 = 0.1; 3 = 0.5; 4 = 1.0; 5 = 3.0 mmol l^{-1}.

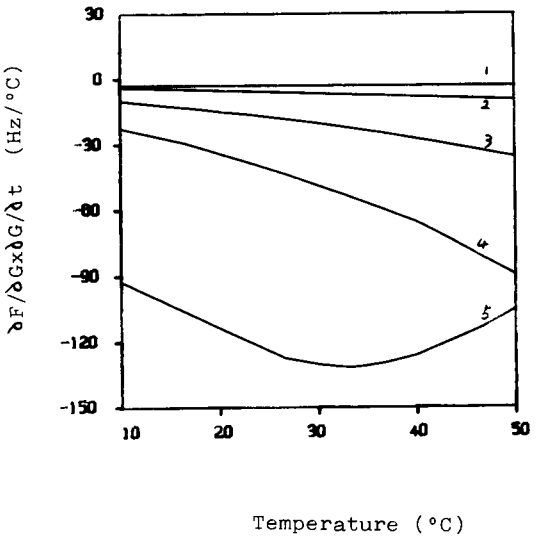

Fig. 13. Contribution of conductivity term to the frequency–temperature coefficient. Concentration of KCl: 1 = 0.01; 2 = 0.1; 3 = 0.5; 4 = 1.0; 5 = 3.0 mmol l^{-1}.

temperature rises from 10 to 50°C, the coefficient can be considered to be constant in KCl solutions of low concentration; the values are 20.4 Hz $°C^{-1}$ in 1×10^{-5} mol l^{-1} and 20.1 Hz $°C^{-1}$ in 1×10^{-4} mol l^{-1} KCl. When the concentration of electrolyte continues to increase, the coefficient declines slightly with increase in both concentration and temperature. The values at 50°C are smaller than those at 10°C by 5.2, 14.2 and 14.6 Hz $°C^{-1}$ in 5×10^{-4}, 1×10^{-3} and 3×10^{-3} mol l^{-1} KCl solutions, respectively.

Figure 13 shows that the contribution of the G term to the frequency–temperature coefficient also depends on the concentration of electrolyte and temperature. The values of the G term are close to zero in low-concentration KCl solutions. However, they become more negative and vary with temperature in higher concentration KCl solutions. When the solution temperature rises from 10 to 50°C, the values increase in the negative direction from −9.4 to −26.1 Hz $°C^{-1}$ in 5×10^{-4} mol l^{-1} solution and from −24.7 to −89.0 Hz $°C^{-1}$ in 1×10^{-3} mol l^{-1} solution. The situation is slightly different in 3×10^{-3} mol l^{-1} solution: the coefficient increases from −93.5 to −139.6 Hz $°C^{-1}$ when the temperature rises

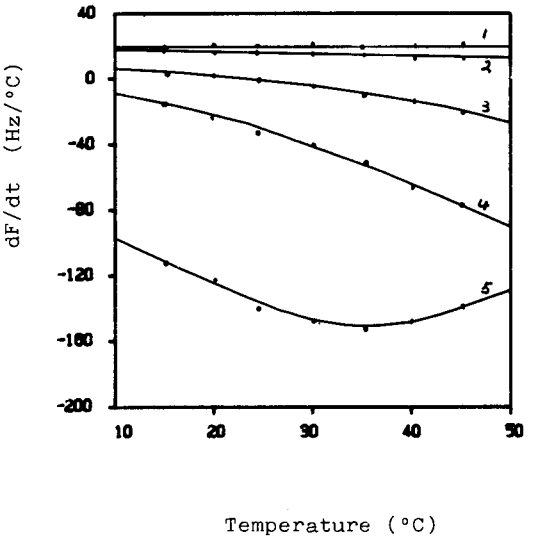

Fig. 14. Total frequency–temperature coefficient in aqueous KCl solutions. Concentration of KCl: 1 = 0.01; 2 = 0.1; 3 = 0.5; 4 = 1.0; 5 = 3.0 mmol l^{-1}.

from 10 to 32.5°C then decreases from −139.6 to 110.8 Hz $°C^{-1}$ when the temperature increases from 32.5 to 50°C.

The total frequency–temperature coefficients of SPQC in KCl solutions are shown in Fig. 14. The smooth curves were obtained according to Eqn. 16 and the points are the values of $\Delta F/\Delta t$ measured in a narrow temperature range. It can be seen that the agreement between the calculated and experimentally measured frequency–temperature coefficients is good. The different frequency–temperature behaviour of the SPQC in KCl solutions can be explained quantitatively from Eqns. 16–19. In KCl solutions of low concentration (10^{-5}–10^{-4} mol l^{-1}), the contribution of the G term is much smaller than that of the C_s term, so the coefficients are positive and vary slightly with temperature; as a result, the frequency increases linearly with increasing temperature. In 5×10^{-4} mol l^{-1} solution, the positive values due to the C_s term and the negative values due to the G term are approximately equal and offset, hence the total frequency–temperature coefficient is small and a zero value is obtained at 27.5°C. Consequently, the SPQC possesses good temperature stability. In 1×10^{-3} mol l^{-1} solution, the negative value of the G term is greater than the positive value of the C_s term, hence, the total coefficient is negative and the frequency decreases with increasing temperature. As both the C_s and G terms are negative in 3×10^{-3} mol l^{-1} solution, the total coefficients are large and the frequency declines abruptly with increasing solution temperature.

It is worth mentioning that the crystal temperature is independent of the solution temperature and the changes in density and viscosity of solution due to temperature changes do not affect the frequency in the SPQC. Therefore, the SPQC offers better temperature stability than a normal PQC. That the frequency–temperature coefficients are near to zero in 5×10^{-4} mol l^{-1} KCl solution at room temperature indicates that the most suitable concentration range for the SPQC is between 1×10^{-4} and 1×10^{-3} mol l^{-1} when both sensitivity and reproducibility are taken into consideration. This range can be easily obtained either by dilution or by adding a foreign electrolyte.

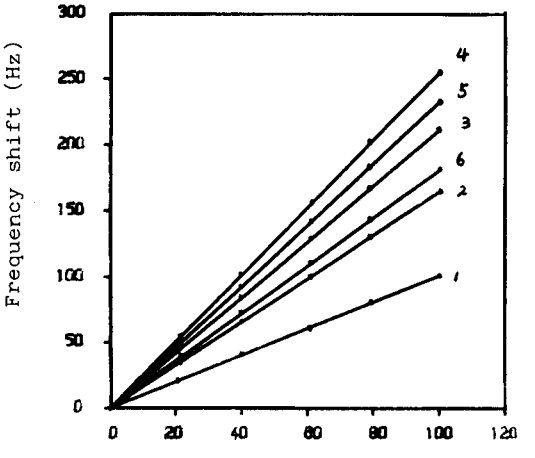

Fig. 15. Response curves in the presence of a foreign electrolyte. Concentration of NaCl as foreign electrolyte: 1 = 0; 2 = 0.5; 3 = 1.0; 4 = 2.0; 5 = 3.0; 6 = 4.0 mmol l^{-1}.

Behaviour of SPQC in the presence of a foreign electrolyte

The frequency response curves of the SPQC to the concentration of potassium chloride in the presence of sodium chloride as the foreign electrolyte are illustrated in Fig. 15. It is apparent that the slopes of the curves in solutions in the presence of NaCl are greater than those in its absence. In addition, the increase in the slope depends on the concentration of NaCl. As the concentration of NaCl increases, the slope of the curves becomes greater and reaches a maximum at 2.0 mmol l^{-1}, which is about 1.5 times greater than that without NaCl. The slopes of the curves then decrease as the concentration of NaCl increases further. This is concordant with the fact that the sensitivity of the SPQC to conductivity is related to the conductivity, as discussed previously. As a result, the sensitivity and accuracy of the SPQC are improved in the presence of a foreign electrolyte within certain concentration limits, whereas the sensitivity and accuracy in classical conductimetry become worse in such a case.

Conclusions

The SPQC method presented in this paper has a highly sensitive and selective frequency response to changes in the solution permittivity and conductivity. Compared with a normal PQC oscillating in the liquid phase, the frequency stability, frequency–temperature coefficent and lifetime of the crystal in the SPQC are greatly improved. One of the advantages of this method is that it can detect a slight change in solution conductivity in the presence of an excess of a foreign electrolyte.

The application of the SPQC to end-point determination in titrimetry will be discussed in Part II.

This work was supported by the Natural Science Foundation and the Education Commission Foundation of China.

REFERENCES

1 I.M. Kolthoff and P.J. Elving, Treatise on Analytical Chemistry, Part I, Vol. 4, Interscience, New York, 1963, Chap. 51.
2 C.N. Reilley, in P. Delahay (Ed.), New Instrumental Methods in Electrochemistry, Interscience, New York, 1954, pp. 319–345.
3 E. Pungor, Oscillometry and Conductometry, Pergamon, Oxford, 1965.
4 J.J. Lingane, Electroanalytical Chemistry, Interscience, New York, 1953.
5 G.G. Blake, Conductometric Analysis at Radio Frequency, Chemical Publishing, New York, 1953.
6 S.Z. Yao, Z.H. Mo and L.H. Nie, Anal. Chim. Acta, 193 (1987) 205.
7 S.Z. Yao and Z.H. Mo, Anal. Chim. Acta, 193 (1987) 97.
8 Z.H. Mo and S.Z. Yao, Anal. Chim. Acta, 229 (1990) 205.
9 Z.H. Mo and S.Z. Yao, Anal. Chim. Acta, 230 (1990) 51.
10 Z.H. Mo and S.Z. Yao, Anal. Chim. Acta, 246 (1991) 421.
11 Z.H. Mo, L.H. Nie and S.Z. Yao, Sci. China (Ser. B), 35 (1992) 1.
12 R.C. Weast, M.J. Astle and W.H. Beyer (Eds.), CRC Handbook of Chemistry and Physics, CRC, Boca Raton, FL, 65th ed., 1984.
13 K.K. Kanazawa and J.G. Gordon, Anal. Chim. Acta, 177 (1985) 99.
14 H. Muramatsu, E. Tamiya and I. Karube, Anal. Chem., 60 (1988) 2142.
15 T. Nomura and T. Yanagihara, Anal. Chim. Acta, 248 (1991) 329.

Analytica Chimica Acta, 276 (1993) 99–108
Elsevier Science Publishers B.V., Amsterdam

Determination of trace aluminium by differential pulse adsorptive stripping voltammetry of aluminium(III)–8-hydroxyquinoline complex

Qiantao Cai and Soo Beng Khoo

Department of Chemistry, National University of Singapore, Kent Ridge, Singapore 0511 (Singapore)

(Received 10th August 1992; revised manuscript received 6th November 1992)

Abstract

A rapid and sensitive differential-pulse adsorptive stripping voltammetric method, based on the formation of an electroactive complex between aluminium(III) and 8-hydroxyquinoline (HOx), is presented for the determination of trace levels of aluminium. The complex showed an oxidative peak potential at +0.876 V vs. Ag/AgCl (saturated KCl) at a glassy carbon (GC) electrode in aqueous ammonium acetate (0.024 M, pH 6.8). A good linear relationship between the peak current and Al(III) concentration in the ranges 4.00×10^{-8}–5.00×10^{-6} and 8.00×10^{-6}–4.00×10^{-5} M were observed. In the lower Al(III) concentration region, the anodic peak was the result of the stripping of the adsorbed Al(III)–HOx complex, whereas in the higher concentration range, the diffusional oxidation current of the solution species predominated. A surface saturation region was observed from 5.00×10^{-6} to 8.00×10^{-6} M Al(III). Relatively few interferences were found and these were easily masked. The detection limit for Al(III) for this method is 1.00×10^{-8} M and ten determinations of Al(III) at 1.00×10^{-7} M gave a relative standard deviation of 6.2%. The method was employed in the analysis of Al(III) in a US Environmental Protection Agency water pollution quality control sample (WP 386) and excellent agreement with the certified value was obtained.

Keywords: Stripping voltammetry; Aluminium; Waters

Aluminium is determined in studies of natural and industrial products, in production quality control, in the analysis of environmental and biological samples, etc. The analytical problems involved are becoming increasingly difficult as the levels of aluminium that must be determined in pure metals and other materials are continually decreasing, so that reliable and highly sensitive methods must be employed. At the same time, rapid methods with few and easily masked and/or eliminated interferences are sought, especially in continuous process monitoring and with difficult samples.

Methods based on spectrophotometry [1], spectrofluorimetry [2] and atomic absorption and emission spectrometry [3–6] are commonly employed for the determination of aluminium. Analysis by direct electrolysis is difficult because of the high reduction potential of Al(III) [7]. However, electroanalysis exploiting the complexation of Al(III) with electroactive ligands has been reported [8,9]. More recently, several sensitive stripping methods have been developed. Wang et al. [10] described a method involving the adsorptive stripping of the Al(III)–Solochrome Violet RS (SVRS) complex at a hanging mercury drop electrode (HMDE). Although a good detection

Correspondence to: S.B. Khoo, Department of Chemistry, National University of Singapore, Kent Ridge, Singapore 0511 (Singapore).

limit was obtained (5.5×10^{-9} M for 10-min adsorptive accumulation), heating of the sample solution for 10 min at 90°C was necessary to ensure quantitative complexation. An adsorptive stripping procedure at an HMDE was also reported for Al(III)–1,2-dihydroxyanthraquinone-2-sulphonic acid (DASA) [11]. The detection limit using this complex was 1.00×10^{-9} M Al(III) for an adsorption time of 45 s. Another cathodic stripping method based on the adsorption of Al(III)–Pyrocatechol Violet on the HMDE was developed by Vukomanovic et al. [12]. For a 10-s adsorption, this method yielded a detection limit of 3.7×10^{-9} M Al(III). Although the sensitivities of these cathodic stripping voltammetric methods at the HMDE are high, for continuous monitoring or in other applications where flowing streams are employed (e.g., in flow-injection analysis and liquid chromatography), the mercury electrode is inconvenient.

A carbon paste electrode has been employed for the adsorption of the Al(III)–SVRS complex followed by oxidative stripping. However, this method showed poor detectability, at 3.7×10^{-6} M Al(III) [13]. In another approach, a graphite electrode modified with 1,2-dihydroxyanthraquinone was used to accumulate Al(III) as the Al(III)–1,2-dihydroxyanthraquinone complex at open circuit, which was then stripped oxidatively. The detection limit was 1.5×10^{-7} M for an accumulation time of 1 min, using differential-pulse voltammetry [14]. Recently, a method for the determination of Al(III) in a flow-injection system involving the formation of the Al(III)–DASA complex and amperometric measurement of excess of DASA at a gold electrode was reported, in which the DASA oxidation current decreased linearly with increasing Al(III) concentration. The detection limit for Al(III) was 2.5×10^{-7} M when using 2.0×10^{-5} M DASA [15].

In this paper, a procedure for determining aluminium by differential-pulse adsorptive stripping voltammetry [DP(Ad)SV] of its complex with 8-hydroxyquinoline at a glassy carbon electrode is reported. The advantages of this new procedure are the fast complexation kinetics which obviate the need to heat the solution after addition of reagent, a detection limit of 1.00×10^{-8} M (0.27 $\mu g\ l^{-1}$) Al(III) for a solid electrode and relatively few interferences, which are easily masked or eliminated.

EXPERIMENTAL

Apparatus

All electrochemical experiments were performed with a microprocessor-controlled Princeton Applied Research Model 384B polarographic analyser (EG&G, PARC, Princeton, NJ) coupled to a Houston DMP-40 Series digital plotter. A locally fabricated three-electrode glass cell with a total capacity of about 5 ml was used for all electrochemical experiments. The working electrode was 3 mm diameter glassy carbon (GC) (Tokai) in the shape of a circular disc and the counter electrode was a platinum coil. The reference electrode was Ag/AgCl (saturated KCl), placed in a compartment containing the background solution and separated from the working electrode compartment by a 4 mm diameter Vycor frit. pH measurements were made with a Model HI 8417 microprocessor-controlled pH meter (Hanna Instruments).

Chemicals and reagents

Analytical-reagent grade chemicals were used unless noted otherwise. All stock solutions were stored in nitric acid-washed polyethylene bottles. Water obtained from a Millipore Alpha-Q water purification system was used for all solutions and dilutions.

Al(III) stock solution (1.00×10^{-2} M) was prepared by dissolving $Al(NO_3)_3 \cdot 9H_2O$ (99.999%) (Aldrich) in 0.010 M nitric acid. Stock solutions of 8-hydroxyquinoline (5.00×10^{-3} M) and 1,10-phenanthroline (1.00×10^{-2} M) were prepared by first dissolving the respective solids in warm water. The solutions were then cooled, transferred to volumetric flasks and diluted to volume. The stock solution of the background electrolyte, ammonium acetate (NH_4OAc) (0.60 M), was prepared by dissolving the solid in water. All other stock solutions were similarly prepared.

In all instances, background and sample solutions, whether individual or mixed, were pre-

pared by placing appropriate aliquot(s) of the corresponding stock solution(s) in 25-ml volumetric flasks and diluting to volume to give the required analytical concentration of the substance or of each of the substances (for mixtures). In the pH variation studies, solutions of different pH were prepared by using the stock solutions of NH_4OAc (0.60 M) and acetic acid (0.60 M) for acidic pH or NH_4OAc (0.60 M) and ammonia solution (0.60 M) for basic pH. By using appropriate volumes of these stock solutions, the pH of these solutions can be varied in such a way that the total analytical concentration of acetate (acidic solutions) or ammonium (basic solutions) was kept constant at 0.024 M.

A US Environmental Protection Agency (USEPA) water sample (WP 386) was received in a sealed glass ampoule. After breaking open the ampoule, the test solution was prepared by pipetting 0.50 ml of the solution into a 25-ml volumetric flask, then adding aliquots of the stock solutions of HOx and NH_4OAc so that the analytical concentrations were 4.00×10^{-5} and 0.024 M, respectively. The resulting solution represented a 50-fold dilution of the original Al(III) sample.

Procedure

In all voltammetric experiments, the working electrode compartment was filled with ca. 3 ml of the solution to be studied and deaerated for 2 min with high-purity nitrogen. Earlier experiments indicated that the adsorptive stripping peak for the Al(III)–HOx complex was sensitive to the presence of oxygen, shifting to less positive potentials if oxygen was present. For the typical volume of solution used, it was determined that deaeration for 2 min at a controlled nitrogen pressure was sufficient for complete deaeration.

For cyclic voltammetric experiments, the initial and final potentials were +0.40 and +1.10 V, respectively, and a scan rate of 100 mV s^{-1} was used. The voltammograms obtained were stored in software before being output to the plotter. Peak potentials were also located by the software and printed out together with the voltammograms.

The standard procedure for performing DP(Ad)SV experiments is as follows: The cell was thoroughly rinsed with water and then with the test solution. Approximately 3 ml of the test solution were poured into the working electrode compartment, then pure nitrogen was bubbled through for 2 min, this interval being timed manually. Simultaneously, the polarographic analyser was set to operate in the differential-pulse stripping model. In this mode, a sequence of steps, namely deaeration, deposition, equilibration and stripping, have been preprogrammed. For the present purpose, as the deaeration was performed manually, the time for the programmed deaeration step was set to zero. After setting the desired parameters of deposition potential (+0.50 V), deposition time (10 s), equilibration time (10 s), scan rate (10 mV s^{-1}), final potential (+1.10 V) and pulse height (50 mV), the instrument was ready to run (the values in parentheses are the optimized values used for analysis). As soon as the deaeration time of 2 min had elapsed, the differential-pulse stripping sequence was started with nitrogen still passing through the solution so that deposition occurred in the stirred solution. At the end of deposition step the nitrogen was turned off manually so that the equilibration step and subsequently the stripping step were carried out in quiet solution. The data for each run were collected and stored in software. The above procedure was performed for both sample and blank solutions. The blank-subtracted voltammogram was then output to the plotter, together with values of peak potentials and peak currents that were calculated by the software package. All experiments were carried out at ambient temperature (25 ± 1°C).

Pretreatment of the glassy carbon electrode

Prior to use every morning, the glassy carbon electrode was polished with a 0.3-μm alumina–water slurry on a microcloth. It was then conditioned electrochemically by scanning from +0.50 to +1.10 V several times using the blank solution in the differential-pulse stripping model until a reproducible background curve was obtained. One such pretreatment daily was usually sufficient unless reproducibility problems were encountered. In subsequent experiments, between runs, the electrode was wiped with acetone-wetted filter-

paper followed by water-wetted filter-paper, rinsed with water and dried.

RESULTS AND DISCUSSION

Choice of medium

HOx gave an oxidation peak $E_p(1)$ of ca. +0.528 V in weakly acidic and basic media under DP(Ad)SV conditions. In the presence of Al(III), a new oxidation peak appeared at $E_p(2) = +0.876$ V due to the Al(III)–HOx complex, while the peak height at +0.528 V decreased. The suitability of NH_4OAc (pH 6.8), NH_4Cl–NH_3 (pH 8.0), NaOAc (pH 7.1), NaOAc–HOAc (pH 5.4), NaH_2PO_4–NaOH (pH 7.0) and KH_2PO_4–$Na_2B_4O_7$ (pH 7.0) (all at a total analytical concentration of 0.024 M) as supporting electrolytes was investigated. The oxidation peak for the complex was found to be different in each electrolyte and NH_4OAc was finally chosen as the supporting electrolyte for all subsequent studies because of the superior peak sensitivity and shape. The

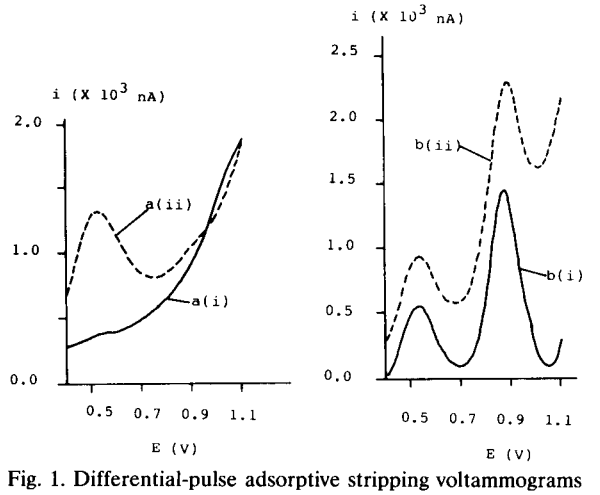

Fig. 1. Differential-pulse adsorptive stripping voltammograms at glassy carbon electrode. [a(i)] Blank solution, 0.024 M NH_4OAc (pH 6.8); [a(ii)] 0.024 M $NH_4OAc + 1.00\times10^{-4}$ M HOx, $E_p = +0.528$ V, no background subtraction; [b(i)] 0.024 M $NH_4OAc + 1.00\times10^{-4}$ M HOx $+ 2.00\times10^{-5}$ M Al(III), $E_p(1) = +0.532$ V, $E_p(2) = +0.876$ V, with background subtraction; [b(ii)] same as [b(i)], $E_p(1) = +0.536$ V, $E_p(2) = +0.884$ V, without background subtraction. In all instances, pulse height = 50 mV, scan rate = 10 mV s^{-1} and deposition time = 10 s.

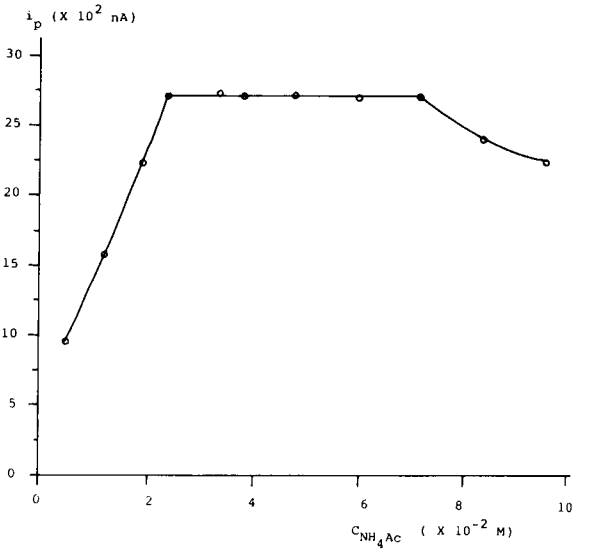

Fig. 2. Differential-pulse adsorptive stripping voltammetric peak current for Al(III)–HOx complex vs. concentration of ammonium acetate. $C_{Al(III)} = 4.00\times10^{-5}$ M; $C_{HOx} = 2.00\times10^{-4}$ M. pH = 6.8 ± 0.1 for all concentrations of ammonium acetate.

DP(Ad)SV peaks, with and without background subtraction, for HOx and Al(III)–HOx in aqueous ammonium acetate are shown in Fig. 1. Figure 2 shows the peak height of the complex as a function of NH_4OAc concentration. From 0.024 to 0.072 M, the peak height was constant; below and above this region, the peak height decreased. The decrease at lower concentrations was due to the increase in solution resistance, whereas at the higher concentrations hydrolysis of Al(III) to insoluble basic acetates [16] was probably the cause. The optimum NH_4OAc concentration for aluminium analysis was therefore 0.024 M, as this leads to minimum contamination from the supporting electrolyte.

Electrode processes from cyclic voltammetry and DP(Ad)SV: influence of pH

A knowledge of the electrochemical behaviour of the species present in solution under the experimental conditions and the effect of pH on this behaviour is important for method development. Figure 3 shows the cyclic voltammograms for 1.00×10^{-4} M HOx in the absence and pres-

ence of 2.00×10^{-5} M Al(III) at the GC electrode. An oxidation wave can be seen for HOx at $E_p(1) = +0.612$ V [Figure 3b(i)] with no reduction wave on scan reversal. The peak height decreased and disappeared on repeated scans (not shown). These observations are presumably due to the decay of the primary product of HOx oxidation. Further polymerization reactions could give rise to the formation of polymerized oxidation products which led to deactivation of the GC electrode surface [15,17,18]. With addition of 2.00×10^{-5} M Al(III), a new oxidation wave appeared [Figure 3b(ii)] due to the Al(III)–HOx complex at $E_p(2) = +0.905$ V with an accompanying decrease in the height of the first peak [as noted earlier for DP(Ad)SV]. Again, no reversal wave was observed for this oxidation and the wave height decreased and finally disappeared on repeated scanning, for the same reasons as before.

The effect of the solution pH on the DP(Ad)SV peak potentials and current for free HOx and the Al(III)–HOx complex was investigated. The results showed that $E_p(1)$ (for free HOx) varied linearly with pH from 6.0 to 9.0 but became curved and nearly constant in the pH range 4.3–6.0 and at pH > 9.0 [at pH 4.3–6.0, $E_p(1) = +0.620$ V; at pH > 9.0, $E_p(1) = +0.434$ V]. Linear regression analysis of this linear portion of

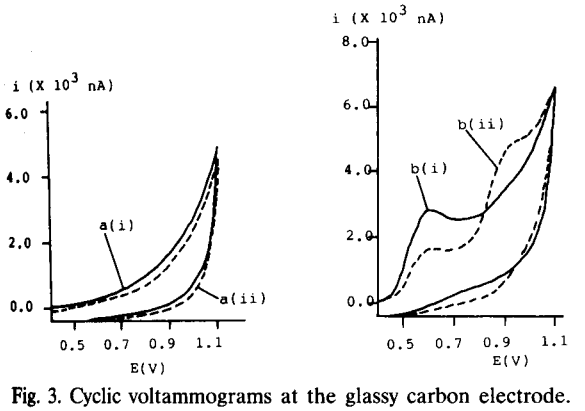

Fig. 3. Cyclic voltammograms at the glassy carbon electrode. [a(i)] Blank solution, 0.024 M NH_4OAc (pH 6.8); [a(ii)] 0.024 M $NH_4OAc + 4.00 \times 10^{-5}$ M Al(III); [b(i)] 0.024 M $NH_4OAc + 1.00 \times 10^{-4}$ M HOx, peak potential = +0.612 V; [b(ii)] 0.024 M $NH_4OAc + 2.00 \times 10^{-5}$ M Al(III) + 1.00×10^{-4} M HOx, peak potentials = +0.620 and +0.905 V.

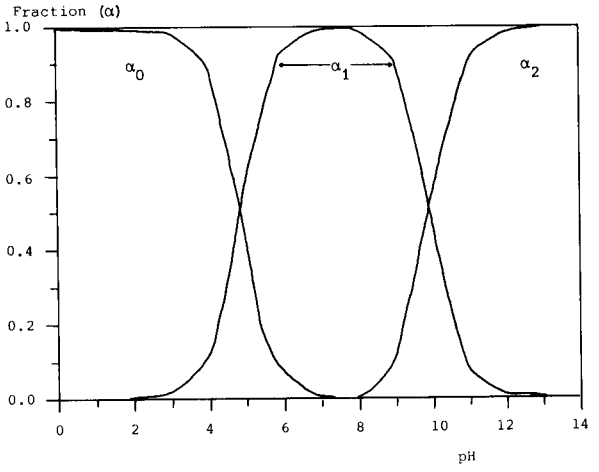

Fig. 4. Distribution of various forms of 8-hydroxyquinoline as a function of pH. $\alpha_1 = [H_2Ox^+]/C_{HOx}$; $\alpha_2 = [HOx]/C_{HOx}$; $\alpha_3 = [Ox^-]/C_{HOx}$, where C_{HOx} = analytical concentration of 8-hydroxyquinoline.

the $E_p(1)$–pH curve (not shown) gave the regression equation $E_p(1) = 0.968 - 0.0588$ pH (for 8.00×10^{-5} M free HOx, calculated from twelve points) and a correlation coefficient of −0.994. As $E_p(1)$ shifted to less positive values with increasing pH, this indicates that hydrogen ions take part in the electrooxidation of free HOx as a reaction product [17,18]. In the pH range 6.0–9.0, HOx exists mainly as the neutral form (Fig. 4), C_9H_6NOH. At pH > 9.0 and in the pH range 4.3–6.0, HOx is converted to the phenolate $C_9H_6NO^-$ and the cation $C_9H_6N^+OH$, respectively, leading to a loss of linearity of $E_p(1)$ vs pH.

$E_p(2)$ was found to be independent of pH [for 4.00×10^{-5} M Al(III) + 2.00×10^{-4} M HOx, $E_p(2) = +0.880$ V, R.S.D. = 0.91% for $n = 16$] from pH 5.1 to 9.6. For the concentrations used here, complexation of Al(III) by HOx to form a sparingly soluble chelate compound of composition $Al(C_9H_6NO)_3$ [16,19] in the pH range 6.0–9.0 was essentially complete. The oxidation of this complex is probably due to the oxidation of the phenolate complexed to Al(III), producting species such as $Al(H_2O)(C_9H_6NO)_2^+$ [16] and polymerized oxidation products of the phenolate ion [15,17,18]. Is is reasonable to assume that no

free Al(III) was produced, otherwise hydrogen ions resulting from the hydrolysis of free Al^{3+} produced in the electrooxidation of $Al(C_9H_6NO)_3$ should lead to a pH dependence of $E_p(2)$.

The DP(Ad)SV peak height of the complex was constant in the pH range 6.0–9.0, whereas at lower or higher pH values it diminished (Fig. 5). The solution pH affects the distribution of both Al(III) species [20] and HOx species (Fig. 4) and through these the extent of complexation, and also the electrode process of HOx [17,18], but does not affect the electrooxidation of $Al(C_9H_6NO)_3$. Therefore, the data in Fig. 5 indicate that the peak height of the complex was controlled solely by the extent of complexation. In the pH range 6.0–9.0, the complete reaction of Al(III) with HOx gave a constant DP(Ad)SV peak height, whereas outside this pH range incomplete complexation led to a decrease in $Al(C_9H_6NO)_3$ and therefore peak height.

Although the DP(Ad)SV peak height for the complex remained constant in the pH range 6.0–9.0, for the purpose of analytical application it was found that a neutral or slightly acidic solution gave the lowest background current and the most reproducible baseline. This reinforced the choice

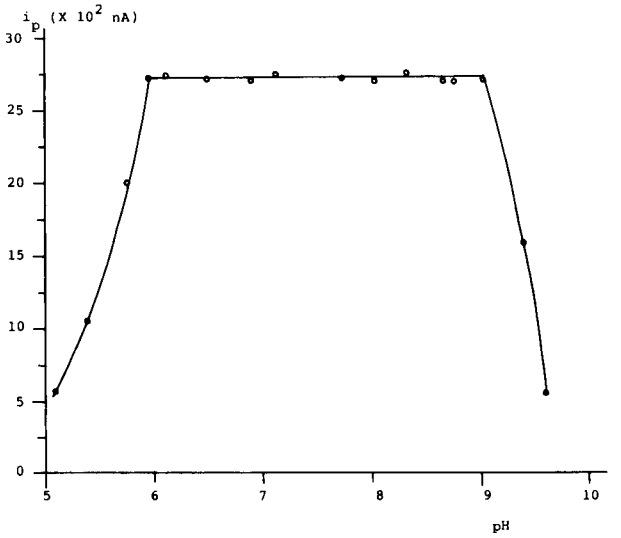

Fig. 5. Differential-pulse adsorptive stripping voltammetric peak current for Al(III)–HOx complex vs. pH. $C_{Al(III)} = 4.00 \times 10^{-5}$ M; $C_{HOx} = 2.00 \times 10^{-4}$ M.

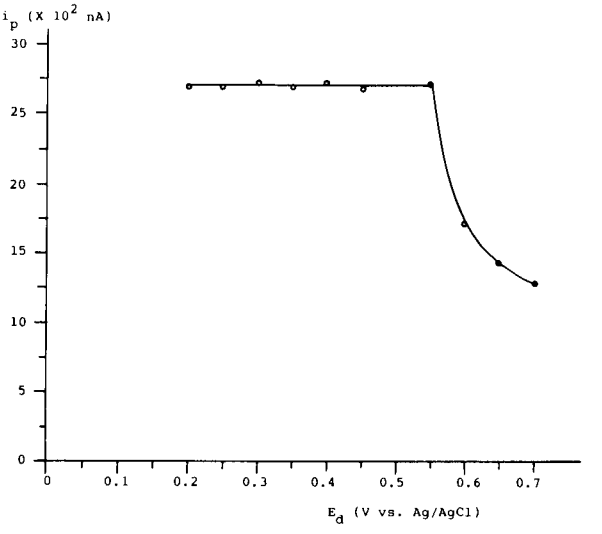

Fig. 6. Differential-pulse adsorptive stripping voltammetric peak current for Al(III)–HOx complex vs. deposition potential. $C_{Al(III)} = 4.00 \times 10^{-5}$ M; $C_{HOx} = 2.00 \times 10^{-4}$ M; $C_{NH_4OAc} = 0.024$ M (pH = 6.8).

of 0.024 M NH_4OAc of pH 6.8 as the background electrolyte.

Effect of deposition potential

The potential applied to the electrode during the period of deposition affects the complex peak height as shown in Fig. 6. The peak height was diminished when the deposition potentials near to or more positive than the oxidation peak potential for free HOx were selected; in these instances, the relatively large anodic currents from excess of HOx led to deactivation of the GC electrode by adsorption of polymerized oxidation products as discussed earlier. Also, deposition potentials too near to the complex peak were unfavourable for the adsorption of the Al(III)–HOx complex. A maximum and constant peak height was obtained at deposition potentials less positive than +0.550 V and accordingly a potential of +0.500 V was selected for further studies.

Effect of HOx concentration

The peak height of the Al(III)–HOx complex was measured by DP(Ad)SV as a function of HOx concentration for different concentrations of Al(III). It was found (Fig. 7) that for a given

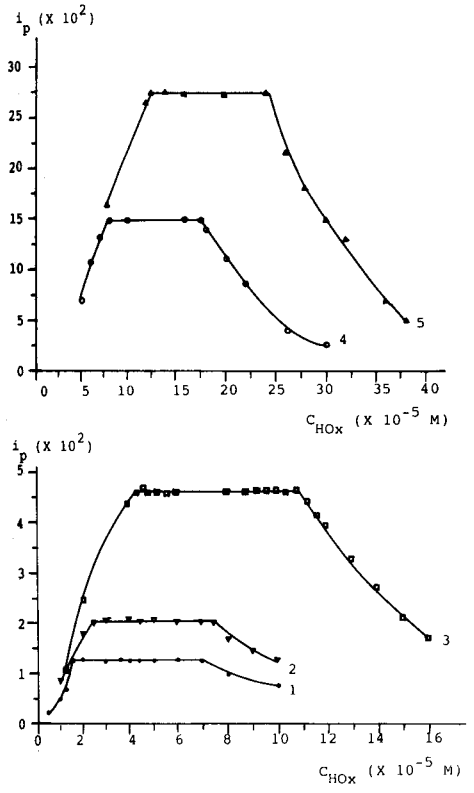

Fig. 7. Differential-pulse adsorptive stripping voltammetric peak current for Al(III)–HOx complex vs. concentration of 8-hydroxyquinoline. $C_{Al(III)}$ = (1) 1.00×10^{-7}, (2) 1.00×10^{-6}, (3) 4.00×10^{-6}, (4) 2.00×10^{-5} and (5) 4.00×10^{-5} M. C_{NH_4OAc} = 0.024 M (pH = 6.8).

concentration of Al(III), the peak height increased with increase in HOx concentration up to a certain value $C_{HOx}(1)$, then remained constant until a concentration $C_{HOx}(2)$ before decreasing at HOx concentrations higher than $C_{HOx}(2)$. The initial increase reflects the increased formation of Al(III)–HOx at higher HOx concentrations. In the interval between $C_{HOx}(1)$ and $C_{HOx}(2)$, complete complexation of Al(III) occurred. At HOx concentrations greater than $C_{HOx}(2)$, the increased adsorption of free HOx and its polymerized oxidation products caused decreased adsorption of the Al(III)–HOx complex. As can be expected (Fig. 7), the interval $C_{HOx}(1)$–$C_{HOx}(2)$ shifted towards higher HOx concentrations as the Al(III) concentration increased. For the determination of Al(III) in the concentration range 1.00×10^{-8}–4.00×10^{-6} M, an HOx concentration range of 2.00×10^{-5}–4.4×10^{-5} M is recommended. For Al(III) concentrations > 1.00×10^{-5} M but $\leqslant 4.00\times10^{-5}$ M, an HOx concentration of ca. 12.5×10^{-5} M is optimum.

Effect of deposition time

With increasing deposition time, the complex peak height increased because the adsorption of the Al(III)–HOx complex on the GC electrode was enhanced (Fig. 8). The increased adsorption was nearly a linear function of deposition time. At adsorption times longer than 10 s [for 3.60×10^{-5} M HOx + 4.00×10^{-7} M Al(III)] or 6 s [for 4.00×10^{-5} M HOx + 4.00×10^{-6} M Al(III)], the peak height decreased very slightly. It was probable that the adsorption of the complex and also HOx reached rapid saturation on the GC electrode as the peak height reached a maximum (for 10 or 6 s). At longer times, the slight decrease was due to the comparatively slower deactivation of the GC electrode by a small extent of adsorption of polymerized products of the oxidation of free HOx at +0.500 V.

DP(Ad)SV calibration graph

Figure 9 shows the variation of DP(Ad)SV peak height with Al(III) concentration in the

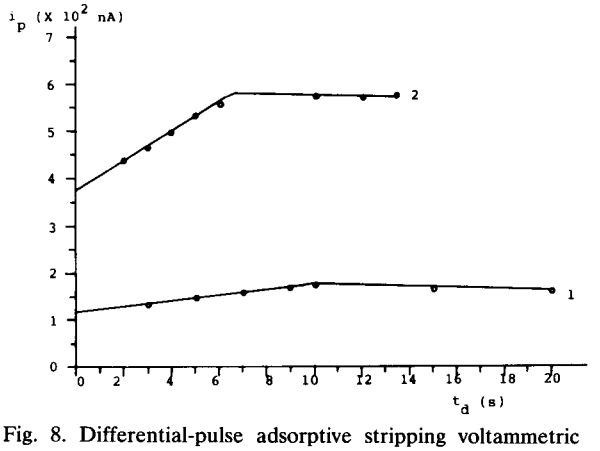

Fig. 8. Differential-pulse adsorptive stripping voltammetric peak current for Al(III)–HOx complex vs. deposition time. (1) $C_{Al(III)} = 4.00\times10^{-7}$ M, $C_{HOx} = 3.60\times10^{-5}$ M; (2) $C_{Al(III)} = 4.00\times10^{-6}$ M, $C_{HOx} = 4.00\times10^{-5}$ M. $C_{NH_4OAc} = 0.024$ M (pH = 6.8).

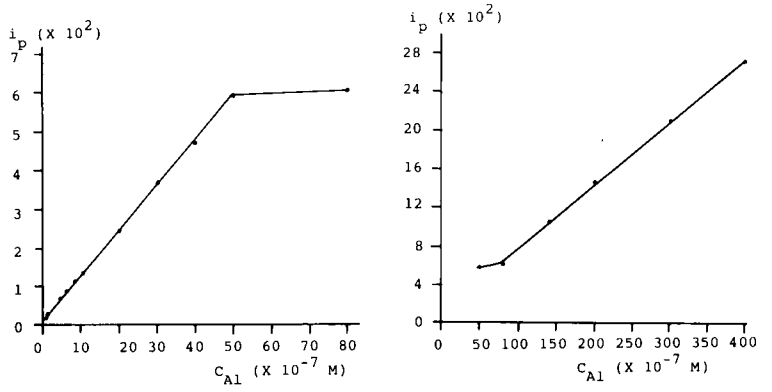

Fig. 9. Differential-pulse adsorptive stripping voltammetric calibration graphs for Al(III).

range 4.00×10^{-8}–4.00×10^{-5} M. Two portions of good linearity can be observed, in the concentration ranges 4.00×10^{-8}–5.00×10^{-6} and 8.00×10^{-6}–4.00×10^{-5} M, when a stirred deposition time of 10 s was used. For the region of lower Al(III) concentration, linear regression analysis gave the equation $I_p = (0.192 \times 10^2) + 0.111 \times 10^2 C_{Al(III)}/10^{-7}$ (correlation coefficient 0.9996). The peak current at this lower concentration region resulted mainly from the oxidative stripping of adsorbed complex. In the concentration range 5.00×10^{-6}–8.00×10^{-6} M Al(III), there appears to be saturation of the electrode surface by the adsorbed complex as manifested by the nearly horizontal region in the calibration graph in Fig. 9. For the higher Al(III) concentration region, the linear regression equation is $I_p = (1.048 \times 10^2) + 0.0643 \times 10^2 C_{Al(III)}/10^{-7}$ (correlation coefficient 0.991). The peak current for this region is predominantly the result of oxidation of the Al(III)–HOx complex in solution. Note that the slope of the adsorbed portion is higher than the solution-based portion because of the preconcentration effect in adsorptive stripping. Table 1 gives the precision for two points on the lower linear portion of the calibration graph. The detection limit was estimated to be 1.00×10^{-8} M based on twice the standard deviation of the blank.

Interferences and their elimination

Trace metals can interfere if, under the conditions used, they form complexes with HOx which give oxidation peaks not completely resolved from that of Al(III)–HOx. When the recommended procedure was applied in the determination of 1.00×10^{-6} M Al(III), no interference was observed from additions of 2.00×10^{-6} M Pb(II), Cd(II), Zn(II), Hg(II), Cr(III), Ag(I), Sb(III), Bi(III), Mg^{2+}, Ba^{2+} and 1.00×10^{-3} M K^+ and Na^+. However, concentrations greater than 0.500×10^{-6} M Co(II) [E_p for Co(II)–HOx = +0.796 V], 0.800×10^{-6} M Mn(II) [E_p for Mn(II)–HOx = +0.952 V], 0.800×10^{-6} M Fe(III) [E_p for Fe(III)–HOx = +0.824 V], 2.00×10^{-6} M Ni(II) [E_p for Ni(II)–HOx = +0.772 V] and 2.00×10^{-6} M Cu(II) [E_p for Cu(II)–HOx = +0.780 V] gave interferences arising from incompletely resolved peaks from that of Al(III)–HOx. Organic and other inorganic materials can also interfere by competitive complexation and masking of Al(III), by surface-active effects which can reduce the surface area of the GC electrode for Al(III)–HOx complex adsorption or by their oxidation close to that of the Al(III)–HOx complex.

TABLE 1

Precision of peak currents of Al(III)–HOx complex for Al(III) standard solutions

Parameter	C_{HOx}	
	2.00×10^{-5}	4.00×10^{-5}
$C_{Al(III)}$ (M)	1.00×10^{-7}	1.00×10^{-6}
Mean current (nA) ($n = 10$) [a]	45.3	161
Standard deviation (nA)	2.8	3.4
Relative standard deviation (%)	6.2	2.1

[a] n = Number of replicate determinations.

In the determination of 1.00×10^{-6} M Al(III), no interference was found after additions of 1.00×10^{-3} M ClO_4^-, CO_3^{2-}, BrO_3^-, NO_3^-, IO_4^-, SO_4^{2-}, F^-, Cl^-, $(NH_2)_2CO$ and ammonium tartrate, 2.00×10^{-4} M 1,10-phenanthroline and 1.00×10^{-4} M 2,2′-bipyridyl.

The possible interfering effects of strong chelating agents were tested by adding ethylenediaminetetraacetic acid (EDTA) and sodium citrate in the determination of 1.00×10^{-6} M Al(III). The complex peak height was suppressed by 50% by 2.00×10^{-5} M EDTA and 1.40×10^{-4} M sodium citrate. Possible interferences by reducing agents were tested by adding SCN^-, I^-, $C_2O_4^{2-}$ and Br^- to a solution containing 1.00×10^{-6} M Al(III). The Al(III)–HOx complex peak was not adversely affected by up to 1.60×10^{-4} M $C_2O_4^{2-}$ or Br^- although large background currents were observed for these ions. However, the oxidative current of 1.60×10^{-4} M SCN^- or I^- completely swamped the Al(III)–HOx complex peak.

Interferences from these reducing materials can be overcome by digesting samples containing Al(III) with concentrated nitric acid–perchloric acid or concentrated sulphuric acid–perchloric acid. Interferences from the HOx complexes of Mn(II), Co(II), Ni(II), Fe(III) and Cu(II) can be eliminated by masking with ammonium tartrate or 1,10-phenanthroline. For example, in the determination of 1.00×10^{-6} M Al(III), the interferences caused by 2.00×10^{-6} M Cu(II), Mn(II) and Fe(III) were masked by adding 1.00×10^{-3} M ammonium tartrate. It was also found that addition of 1.20×10^{-5} M 1,10-phenanthroline to the solution containing 1.00×10^{-6} M Al(III) masked 2.00×10^{-6} M Mn(II), Co(II) and Ni(II) without affecting the response of the Al(III)–HOx complex.

TABLE 2

Comparison of experimentally observed and certified value of Al content for USEPA water quality control sample WP 386 [a]

Certified values [b]		Experimentally observed values by DP(Ad)SV [b,c]		
X ($\mu g\,l^{-1}$)	s ($\mu g\,l^{-1}$)	X ($\mu g\,l^{-1}$) ($n = 4$)	s ($\mu g\,l^{-1}$)	R.S.D. (%)
522.6	50.0	528.0	40.5	7.7

[a] This water sample contains Al and the following other elements: As (100), Be (100), Cd (25), Co (100), Cr (100), Cu (100), Fe (100), Hg (5.0), Mn (100), Ni (100), Pb (100), Se (25), V (250) and Zn (100 $\mu g\,l^{-1}$). [b] X = Mean Al concentration; s = standard deviation; R.S.D. = relative standard deviation. [c] $C_{HOx} = 4.00 \times 10^{-5}$ M.

Medium exchange and electrode reactivation

Medium exchange experiments were carried out to provide evidence for the adsorption of Al(III)–HOx complex on the electrode surface. In these experiments, the deposition procedure was carried as usual but at the end of deposition the analyte solution was replaced with a blank solution of 0.024 M NH_4OAc and stripping of the adsorbed Al(III)–HOx complex was completed in this blank solution. For the determination of 1.00×10^{-6} M Al(III), an oxidation peak with the same shape and peak potential as for the recommended DP(Ad)SV was observed but the peak height was reduced by 32%. This indicated that the peak was the result of oxidation of adsorbed Al(III)–HOx complex and supported the arguments expounded earlier. The 32% reduction in height may be due to loss from the exposure of the electrode to the atmosphere and breaking of electrical contact while changing the solution [21]. Also, some loss of adsorbed Al(III)–HOx into the blank solution (re-establishment of adsorptive equilibrium) could have occurred.

Investigations showed that for the recommended method, for replicate experiments in the determination of 1.00×10^{-6} M Al(III), the peak current decreased by 54% in the second run if the electrode was not reactivated between runs, and almost disappeared in the third run. The reason for this deactivation has been discussed earlier. In this work, simple physical cleaning of the electrode (wiping with acetone-wetted filter-paper followed by water-wetted filter-paper, rinsing and drying) between runs proved effective in retaining the electrode activity and the reproducibility of peak current measurement.

Determination of aluminium in standard water sample

Aluminium in a water pollution quality control sample (USEPA WP 386) was determined in

replicate from the linear regression equation of a calibration graph by using the recommended DP(Ad)SV procedure. The values obtained were compared with the certified value and excellent agreement was observed (Table 2).

This work was supported by a grant from the National University of Singapore.

REFERENCES

1 N.L. Banerjee and B.C. Sinha, Talanta, 37 (1990) 1017.
2 P. Fernandez, C. Perez Conde, A. Gutierrez and C. Camara, Talanta, 38 (1991) 1387.
3 A.D. Woolfson and G.M. Gracey, Analyst, 112 (1987) 1387.
4 M. Bettinelli, U. Baroni, F. Fontana and P. Poisetti, Analyst, 110 (1985) 19.
5 M.R. Pereiro, A. Lopez, M.E. Diaz and A. Sanz Medel, J. Anal. At. Spectrom., 5 (1990) 15.
6 S. Hirata, K. Honda and J. Kumamaru, Anal. Chim. Acta, 221 (1989) 65.
7 A.J. Downard, H. Kipton, J. Powell and S. Xu, Anal. Chim. Acta, 251 (1991) 157.
8 H.H. Willard and J.A. Dean, Anal. Chem., 22 (1950) 1264.
9 M. Kapel and D.W. Selby, Talanta, 16 (1969) 915.
10 J. Wang, P.A.M. Farias and J.S. Mahmoud, Anal. Chim. Acta, 172 (1982) 57.
11 C.M.G. Van Den Berg, K. Murphy and J.P. Riley, Anal. Chim. Acta, 188 (1986) 177.
12 D.V. Vukomanovic, J.A. Page and G.W. Vanloon, Can. J. Chem., 69 (1991) 1418.
13 H. Specker, H. Monien and B. Lendermann, Chem. Anal. (Warsaw), 17 (1971) 1003.
14 A.J. Downard, H. Kipton, J. Powell and S. Xu, Anal. Chim. Acta, 251 (1991) 157.
15 A.J. Downard, H. Kipton, J. Powell and S. Xu, Anal. Chim. Acta, 256 (1992) 117.
16 V.N. Tikhonov, Analytical Chemistry of Aluminium, Wiley, New York, 1973, pp. 12, 27, 29.
17 Ole Hammerich, in M.M. Baizer and H. Lund (Eds.), Organic Electrochemistry, Dekker, New York, 2nd edn., 1983, p. 485.
18 Ralph N. Adams, Electrochemistry at Solid Electrodes, Dekker, New York, 1969, p. 363.
19 K.L. Cheng, K. Ueno and T. Imamura, Handbook of Organic Analytical Reagents, CRC, Boca Raton, FL, 1982, p. 253.
20 C.F. Baes and R.E. Mesmer, Hydrolysis of Cations, Wiley, New York, 1976, p. 122.
21 J. Wang, Stripping Analysis—Principles, Instrumentation, and Applications, VCH, Deerfield Beach, FL, 1985, p. 50.

Analytica Chimica Acta, 276 (1993) 109–113
Elsevier Science Publishers B.V., Amsterdam

Electrostatic effect of chelation with metal ions on streaming potentials in chelating resins containing formazan derivatives

Tsutomu Watanabe, Kuniko Terajima, Masaaki Kubota and Akira Uchiumi

National Institute of Materials and Chemical Research, Higashi, Tsukuba-shi, Ibaraki 305 (Japan)

(Received 26th May 1992; revised manuscript received 20th October 1992)

Abstract

Electrostatic phenomena in chelating resins containing formazan derivatives were studied by measuring streaming potentials. It was found that the adsorption of metal ions can be related to the chelation due to proton replacement in the low pH region whereas it will be changed to adsorption due to electronegativity in the neutral pH region. The electrostatic potentials in the resin phase vary with metal chelation of the formazan groups. Metal chelation lowers the electrostatic energy, enhancing the stability of the resins.

Keywords: Ion chromatography; Ion exchange; Chelating resins; Cobalt; Copper; Electrostatic effects; Formazans; Streaming potentials

In recent years, with the proliferation of ion chromatography (IC) and flow-injection analysis, IC columns with high ion-selectivity have been developed [1,2]. Novel stationary phases with functional groups on the resins that can chelate with specific ions have been developed. The behaviour in such columns is complex, and the properties of the functional groups in the resins not always reflect the properties of the column.

The mutual interaction between ion exchangers and exchanging ions is controlled by various factors, e.g., the properties of the functional groups on the resin surface, the electrostatic interaction between fixed charges of the resins and free ions in the inner phase of the resins and steric and hydrohobic effects. Ion-exchange phenomena occur under such complicated conditions, and the properties of the column are governed by interactions related to all the factors mentioned above [3].

Formazan derivatives are known to chelate selectively with metal ions by replacing the cyclized proton of the imino group. The selectivity varies with the location and kind of substituent groups of formazan [4,5]. This effect is caused by the charge and dimensions of the ions, the electron affinity and the steric effects of the ligands. It is important to understand the mechanism of metal chelation of the formazan derivatives, especially under specific circumstances, such as in the inner phase of the resins.

The electrostatic effect of the streaming potential on ion exchange phenomena in conventional resins for IC have been reported previously [6]. In this work, the behaviour of functional groups in chelating resins containing formazan derivatives was investigated by measuring streaming potentials.

Correspondence to: T. Watanabe, National Institute of Materials and Chemical Research, Higashi, Tsukuba-shi, Ibaraki (Japan).

EXPERIMENTAL

Materials

Experiments were done using chelating resins containing formazan derivatives prepared by mixing a resin (Amberlite IRA, 70 μm, R–Ph–$NH_4^+Cl^-$ type; Orugano, Tokyo) with three kinds of synthetic formazan derivatives: sodium 1-(2-carboxylphenyl)-3-phenyl-5-(3-sulphophenyl)formazan (CPSFNa), sodium 1,3-diphenyl-5-(3-sulphophenyl)formazan (PPSFNa) and sodium 1-phenyl-3-(3,5-disulphophenyl)-5-phenylformazan (PdSPFNa). A 5.0-g amount of purified formazan derivative was dissolved in 1 l of deionized water, 10 g of the resin were added to the solution and the mixture was stirred for 5 h at 50–60°C. After reaction, the resins were filtered and washed with water–ethanol–dioxane (1:1:1, v/v/v) at 50–60°C and dried under reduced pressure for 10 h at 80°C.

The structures of the resins (R) that had reacted with formazan derivatives (CPSF-R, PPSF-R and PdSPF-R) are shown in Fig. 1. These resins were found to be stable in the pH range 1–14. Nitrogen analyses were done to determine the amount of formazan derivatives that had reacted with 1 g of the resin, and were found to be 0.0232, 0.0365 and 0.1480 g for CPSF-R, PPSF-R and PdSPF-R, respectively, per gram of IRA.

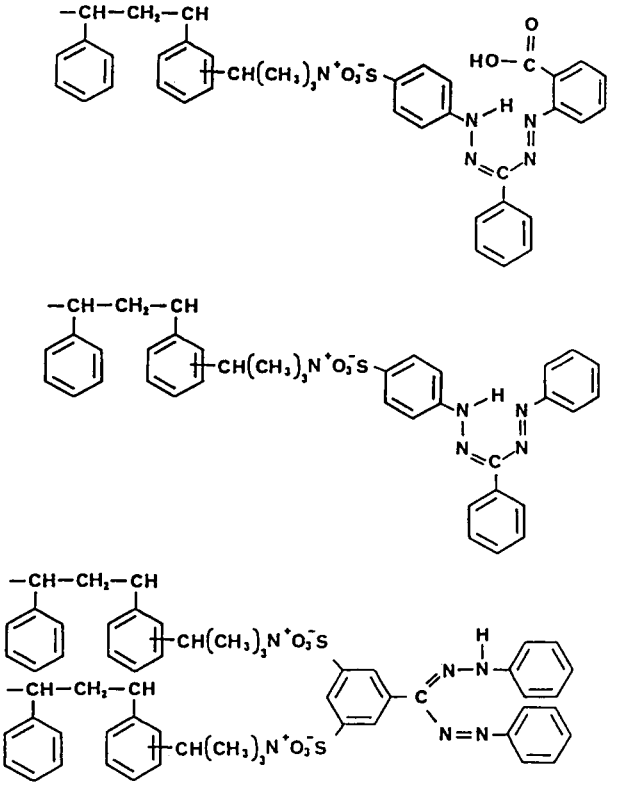

Fig. 1. Structures of three kinds of chelating resins containing formazan derivatives. From top to bottom: 1-(2-carboxylphenyl)-3-phenyl-5-(3-sulphophenyl)formazan resin (CPSF-R), 1,3-diphenyl-5-(3-sulphophenyl)formazan resin (PPSF-R) and 1-phenyl-3-(3,5-disulphophenyl)-5-phenylformazan resin (PdSPF-R).

Streaming potential measurements

Streaming potentials were measured by using the apparatus described previously [6]. It permits the accurate monitoring of the streaming potential, E, and the pressure drop, P, across the plug holder. The P–E plots are linear at P values $< 10^{-2}$ kg cm^{-2}. All measurements were conducted in this region. The ζ-potential and the Donnan potential were evaluated by using the Helmholtz–Smoluchowski equation and the approximate equation for a system with a permeable surface charge layer, respectively [6].

The ionic strength in the solution was kept constant (1×10^{-3} M). For buffer solutions, sodium carbonate–carbonic acid (pH < 7) and sodium carbonate–sodium hydroxide (pH > 7) mixtures were employed.

From to the measurement of current–potential plots [7], a linear relationship between the conductivity of the plug and the conductivity of the solution was observed under the experimental conditions. Therefore, the plug conductivity was taken as the conductivity of the solution.

Measurements of adsorption of metal ions

The amount of metal ions adsorbed on the resins was measured by a batch method. A 20-mg amount of prepared resin was accurately weighed into a stoppered test-tube and 0.5 ml of 0.001 M metal ion solution and 4.5 ml of buffer solution adjusted to pH 3.0–7.0 and containing an inert salt to adjust the ionic strength to 1×10^{-3} M were added. After shaking for 24 h at 25°C, the

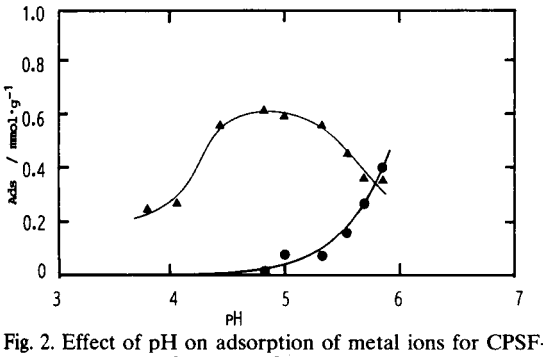

Fig. 2. Effect of pH on adsorption of metal ions for CPSF-R. Metal ion: ▲ = Co^{2+}; ● = Cu^{2+}.

concentration of the metal ions remaining in the solution phase was determined by atomic absorption spectrometry.

RESULTS AND DISCUSSION

Figures 2, 3 and 4 show the amount of adsorbed metal ions versus pH for the CPSF-R PPSF-R and PdSPF-R resins, respectively. The behaviours of the curve differ for Co^{2+} and Cu^{2+} ions and for the three resins. These phenomena can be related to the mechanism of chelation of formazan derivatives. In the neutral pH region, the imino group in the formazan derivatives will dissociate, producing a proton, and the cyclic state will be broken up. In this situation ions having high electronegativity can chelate. In the low pH region chelation by proton replacement will prevail. With the CPSF-R resin, Co^{2+} ions

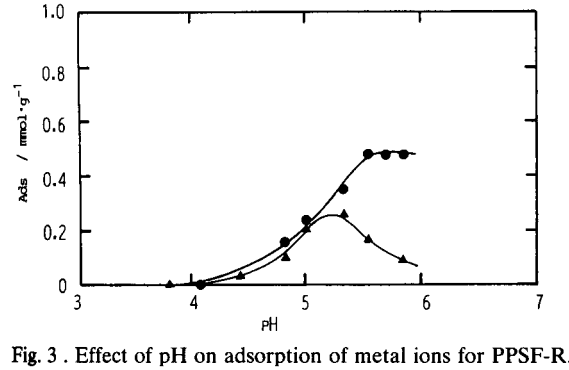

Fig. 3 . Effect of pH on adsorption of metal ions for PPSF-R. Metal ion: ▲ = Co^{2+}; ● = Cu^{2+}.

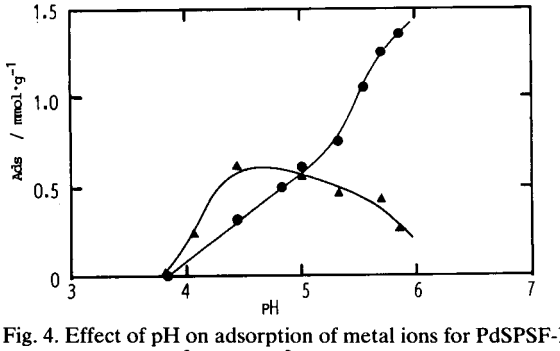

Fig. 4. Effect of pH on adsorption of metal ions for PdSPSF-R. Metal ion: ▲ = Co^{2+}; ● = Cu^{2+}.

are very strongly adsorbed in this region of low pH, but Cu^{2+} ions are not. In the neutral region, this tendency is reversed. It is well known that Co^{2+} and Cu^{2+} ions can be complexed by quadridentate ligands, Co^{2+} in the form of a regular polyhedron (sp^3) and Cu^{2+} in a plane configuration (dsp^2) [8]. It is suggested that the regular polyhedron form is preferred for the cyclic state and the plane form for the broken-up state. Similar phenomena were also observed for PPSF-R and PdSPF-R, with this distinction that adsorption of Cu^{2+} ions is stronger for these resins than for CPSF-R.

Figure 5 shows the effect of pH on ζ-values evaluated from streaming potential measurements for the various resins. The IRA resin shows a constant positive ζ-value in the pH range 5–9. This is due to the fixed charges of the NH_4^+ functional group. The ζ-value varies in the other pH regions, where anions and cations will be adsorbed on the resin interface. The ζ-potentials

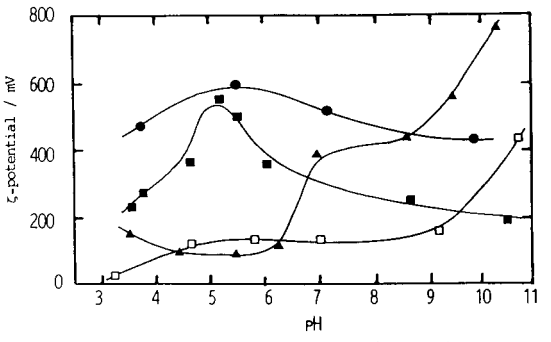

Fig. 5. Effect of pH on ζ-potential for various resins: □ = IRA; ▲ = CPSF-R; ■ = PPSF-R; ● = PdSPF-R.

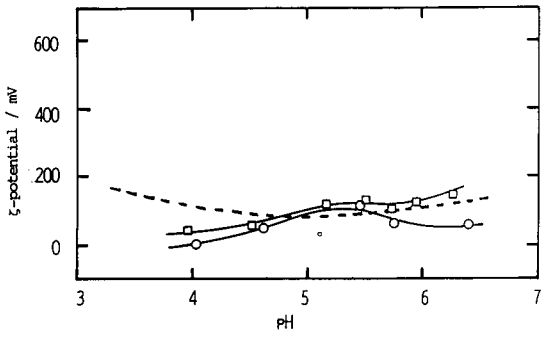

Fig. 6. Effect of metal chelation on ζ-potential for CPSF-R. Metal ion: ○ = Co^{2+}; □ = Cu^{2+}. The dashed line indicates the ζ-potential under metal-free conditions.

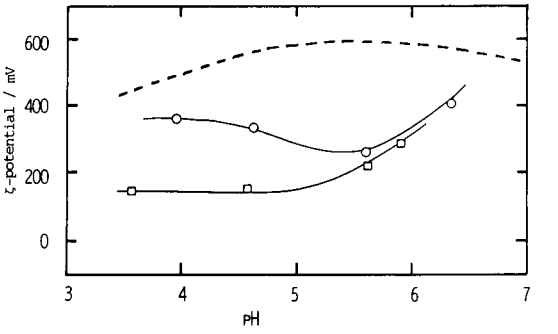

Fig. 8. Effect of metal chelation on ζ-potential for PdSPF-R. Metal ion: ○ = Co^{2+}; □ = Cu^{2+}. The dashed line indicates the ζ-potential under metal-free conditions.

for the PPSF-R and PdSPF-R resins are more positive than those for the IRA resin. The CPSF-R resin shows low ζ-potentials in the pH range 3–7, but high values at pH > 7. This increase in ζ-value may contribute to the adsorption of cations to the formazan functional groups. It is assumed that the instability of the ring of the formazan functional group will accelerate the adsorption of cations to the group, i.e., the electronegativity of the ring accelerates the adsorption. The rings for PPSF-R and PdSPF-R seems to be unstable under metal-free conditions. The carboxyl group in CPSF-R may play a role in the stabilization of the ring at pH < 7. At pH > 7, the lack of stability may cause a progressive adsorption of cations.

Figures 6, 7 and 8 show the effect of metal chelation on ζ-potentials for the CPSF-R, PPSF-R and PdSPF-R resins, respectively. The ζ-pH curve for each system behaves in a different way, and the ζ-value in the metal-chelating state is lower than that in the metal-free state for PPSF-R and PdSPF-R and is as small as in the metal-free state for CPSF-R. The pH values of the inflection points in the ζ–pH curves almost coincide with those from the adsorption experiment (at pH ≈ 5.5). These phenomena mean that the electrostatic conditions change with the state of metal chelation. The metal chelation lowers the electrostatic energy and enhances the stability of the resins. The influence of the configuration of the formazan functional group bound to the IRA resin may be small, because the behaviour of PPSF-R is similar to that of PdSPF-R (although the density of the functional group may be more effective than its configuration, i.e., the overlap of the ion atmosphere and steric effects occur at high density).

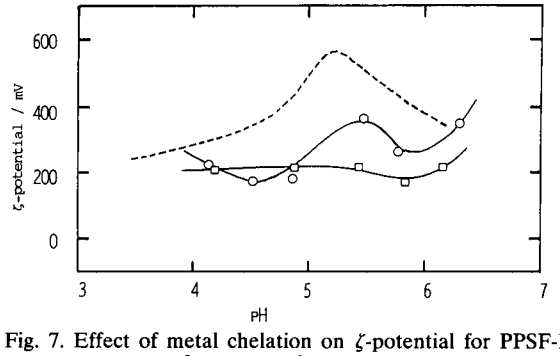

Fig. 7. Effect of metal chelation on ζ-potential for PPSF-R. Metal ion: ○ = Co^{2+}; □ = Cu^{2+}. The dashed line indicates the ζ-potential under metal-free conditions.

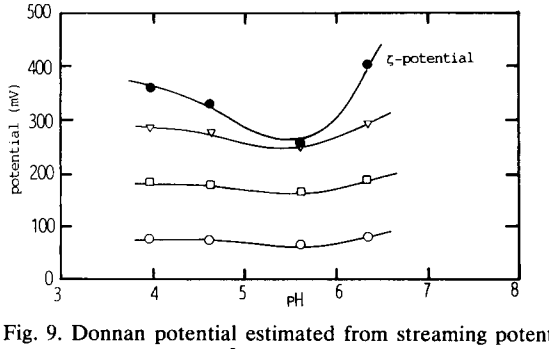

Fig. 9. Donnan potential estimated from streaming potential data in the system of Co^{2+} ions for PdSPF-R. Length of $1/\lambda$: ▽ = 0.1 nm; □ = 1 nm; ○ = 10 nm. ● = ζ-Potential.

Figure 9 shows the plots of the Donnan potential in the system of Co^{2+} ions for PdSPF-R. The parameter $1/\lambda$ has the dimension of length and corresponds to the depth of streaming in the inner phase, determined by frictional force [6]. It is found that the Donnan potential is lower than the ζ-potential, and becomes low when $1/\lambda$ becomes large. If it is assumed that the potential is very high and $1/\lambda$ is very small, because the capacity of the resin is very large in this system, the surface of the resin may be considered as being solid, making it difficult for the solution to stream into the inner phase of the resin.

REFERENCES

1 C.A. Pohl and E.L. Johnson, J. Chromatogr. Sci., 18 (1980) 442.
2 D.T. Gjerde, G. Schmuckler and J.S. Fritz, J. Chromatogr., 187 (1980) 35.
3 H. Shimizu, Ion Exchange Resins, Kyoritsu, Tokyo, 1953.
4 A. Uchiumi and H. Tanaka, Anal. Sci., 5 (1989) 425.
5 A. Uchiumi and H. Tanaka, Chromatographia, 27 (1989) 622.
6 T. Watanabe and M. Kubota, Anal. Chim. Acta, 228 (1990) 61.
7 Th.J.J. van den Hoven and B.H. Bijsterbosch, Colloids Surf., 22 (1987) 187.
8 N. Tanaka and H. Sugi, Complex Formation Reactions, Sangyo Tosho, Tokyo, 1965.

Analytica Chimica Acta, 276 (1993) 115–119
Elsevier Science Publishers B.V., Amsterdam

Determination of urease activity by flow-injection analysis using an ammonium-selective optrode as the detector

Hong Li and Otto S. Wolfbeis

Analytical Division, Institute of Organic Chemistry, Karl-Franzens University, A-8010 Graz (Austria)

(Received 25th August 1992; revised manuscript received 13th November 1992)

Abstract

Urease activity is determined by a combination of flow-injection analysis with optical sensor detection. Enzymatic hydrolysis of urea at pH 7.14 yields ammonium ions, which are determined using a fully reversible optical fibre ammonia sensor. Urea is contained in a buffered carrier stream into which urease samples of various activities are injected. The ammonium ions are measured fluorimetrically using a sensor membrane based on an ion-exchange sensing scheme using nonactin as the ion carrier. The amount of ammonium ion formed is a direct indication of the enzyme activity. The system linearly correlates with urease activity in the range 1–30 U ml^{-1}, the dynamic range being between 0.3 and 30 U ml^{-1}. The method provides an easy and rapid assay for urease activity.

Keywords: Biosensors; Enzymatic methods; Flow injection; Fluorimetry; Ammonia sensor; Fibre-optic sensors; Urease

The most frequent use of enzymes in analytical science is in the assay of enzyme substrates such as glucose. However, the determination of enzyme activity is another important application of bioassays. Typical examples include the measurement of enzyme activity during fermentation control [1], in immunoassay [2], in clinical chemistry [3] and in quality control during enzyme preparation.

The activity of urease is frequently assayed in routine biochemical studies [4,5], in agriculture [6,7] and in medicine [8,9], and rapid and reliable assays are sought. Thus, frequent urease activity assays are required in DNA sequencing and gene studies [4] and in the determination of urea-dependent cell populations in cell cultures [5]. Also, there is a relationship between urease activity and the number and activity of bacteria in soil [6] which, in turn, is important in wheat management [7]. Also, urease activity seems to be related to the bacterial capability of self-destruction [8].

Several flow-injection (FI) methods for the determination of urease activity have been presented and are described in textbooks [9,10]. FI assays are considered to be more practical than discontinuous (cuvette) assays because of the number of samples that can be analysed within a reasonable time, the relative ease of maintaining a controlled environment (in terms of temperature, pH, ionic strength, etc.) and the capability of being automated.

Recently, assays based on a combination of chromatographic techniques and flow-injection analysis (FIA) have been reported [11–13]. Obviously, FIA is the preferred method for the reasons given above. This paper describes a method for the determination of urease activity with the combination of FIA and an optical sensor tech-

Correspondence to: O.S. Wolfbeis, Analytical Division, Institute of Organic Chemistry, Karl-Franzens University, A-8010 Graz (Austria).

nique which may be advantageous in certain situations in view of the specific advantages of optrode sensors [14] over other sensor types.

EXPERIMENTAL

Sensor membrane materials and reagents

The lipophilic pH indicator *N,N'*-dioctadecylrhodamine (DODR) was synthesized according to [15]. Poly(vinyl chloride) (PVC, high molecular weight), potassium tetrakis(4-chlorophenyl)borate (PTCPB), tris(2-ethylhexyl) phosphate (TOP), tris(hydroxymethyl)aminomethane (Tris), nonactin (the ammonium carrier) and tetrahydrofuran (THF) were obtained from Fluka (Buchs, Switzerland), urease (E.C. 3.5.1.5., from jack beans, type IX) with a specific activity of 54 U mg^{-1} solid from Sigma (Deisenhofen, Germany) and Mylar polyester film, type GA 10, from DuPont (Bad Homburg, Germany). A 50 mM Tris–HCl buffer was used for the preparation of solutions and as the carrier stream.

Preparation of the ammonium sensor membrane

This type of ammonium sensor has been described before [16]. It was modified in order to obtain a fluorosensor. In essence, a batch of 2.7 mg of PVC, 0.4 mg of PTCPB, 0.75 mg of DODR, 1.1 mg of nonactin and 6.4 mg of TOP were dissolved in 1.5 ml of freshly distilled THF and 100 μl of the solution were pipetted on to a $0.175 \times 12 \times 50$ mm dust-free Mylar membrane, located in a THF-saturated desiccator. After about 15 min the membranes (with a ca. 2-μm coating) were exposed to air for 15 min for further drying. Before measurement, the membranes were activated in 1 mM hydrochloric acid for 10 min and another 10 min in 0.1 M ammonium chloride solution. The sensor responds fully reversibly to ammonium ion over the 0.03–10 mM concentration range at near neutral pH. The response times are between 1 and 3 min.

Instrumentation

An Aminco SPF 500 spectrofluorimeter was used to study the effect of pH on the ammonium optrode. FI experiments were performed with the flow-injection manifold shown in Fig. 1. It is composed of an autosampler (Besta, Heidelberg, Germany), a peristaltic pump (Minipuls 3, from Gilson Medical Electronics, Villiers-le-Bel, France), an injection valve (Berger, Heidelberg) with a 200-μl sample loop and a flow cell containing the ammonium-sensitive membrane placed at the end of the optical fibre. The components of the manifold were connected with silicone-rubber tubing (Fig. 1). Optical measurements were performed with an Oriel 3090 fibre-optic photometer (Chelsea Instruments, London) equipped with a xenon lamp pulsed at 9 Hz. A 515-nm interference filter was used to isolate the excitation light,

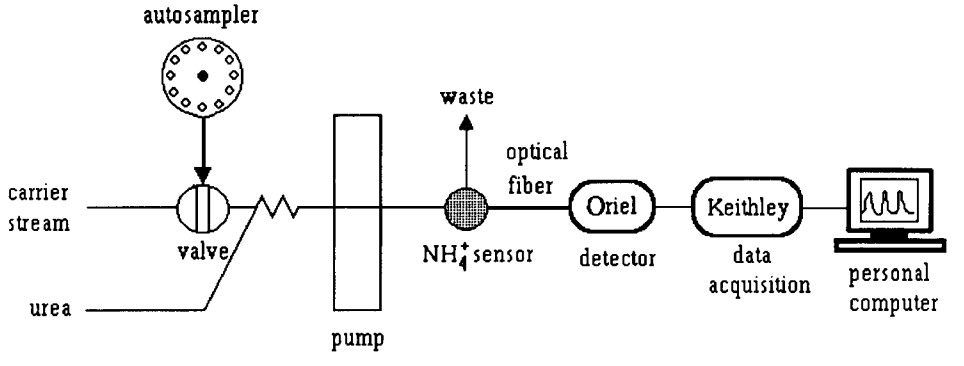

Fig. 1. Schematic diagram of the FIA manifold. The sample is injected into the pH 7.14 buffer carrier stream in the injection valve, mixed with the urea solution and passes to the ammonium optrode detector, whose fluorescence is monitored by the fibre-optic fluorimeter. The whole flow-injection system is controlled by a PC; the signal from the Oriel photomultiplier is processed first with the Keithley data acquisition unit before being fed into the PC.

and a 550-nm cut-off glass filter was placed in the emission beam so to minimize stray light. Fluorescence intensity data were transferred into a data acquisition unit (Keithley 575, Keithley, Taunton, MA) controlled by an AT-PC.

Preparation of urease solution

Urease (10.71 mg) was dissolved in ca. 2 ml of Tris–HCl buffer (0.05 M, pH 7.14) and the solution was diluted to 20.0 ml with buffer. This urease solution has an activity of 30 U ml^{-1}. The solution was diluted to an activity of 10, 3, 1 or 0.3 U ml^{-1}.

Procedures

Volumes of 2-μl of urease solutions of various activities (0.3, 1.0, 3.0, 10.0 and 30.0 U ml^{-1}) were injected into the carrier stream (Tris–HCl buffer, 50 mM, pH 7.14), and mixed with a 10 mM urea solution before the stream reached the ammonium sensor in the flow-through cell. The product of the enzymatic reaction passed through the flow cell and changed the fluorescence intensity of the ammonium sensor. The optical signal was collected by the fibre-optic photometer, converted into another data format in the Keithley acquisition unit and fed into the PC. All experiments were performed at 24°C.

RESULTS

Sensing scheme

The sensing scheme is based on the measurement of ammonium ions formed as a result of the enzymatic hydrolysis of urea according to

$$H_2NCONH_2 + 2H_2O + H^+ \longrightarrow 2NH_4^+ + HCO_3^- \quad (1)$$

The ammonium ions formed are extracted into the PVC membrane by the ammonium carrier nonactin. In order to maintain electroneutrality, a proton is released from the dye (DODR) in the PVC membrane and transported into the (aqueous) sample phase. This causes the fluorescence intensity of DODR to change. Because the binding process is coupled to proton transport, the work function and the sensitivity of the sensor membrane are highly pH dependent. The response of such sensor membranes is fully reversible and specific for ammonium ions, alkylamines and potassium ion being the major interferents [16].

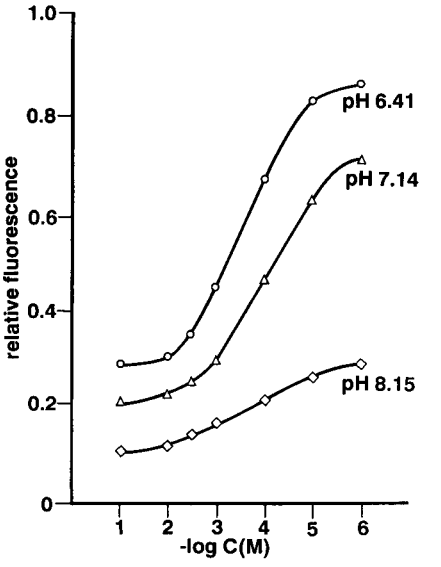

Fig. 2. Calibration graphs for the ammonium optrode at various pH values.

Optimization of flow-injection system

The following experimental conditions were found to be most appropriate: injected sample volume, 200 μl; flow-rate, 0.8 ml min^{-1} for both the carrier and the urea solution; loading time, 10 s; total signal acquisition time 4 min; and sampling frequency, 15 h^{-1}.

Flow-injection analysis of urease activity

Figure 2 shows the calibration graph for the ammonium sensor at various pH values. The response times are in the order of 1 min for the full signal change of 2-μm sensor layers to occur in the forward direction, and up to 2 min for the reverse response. The response times depend strongly on the membrane thickness, and also on the amounts of plasticizer, PCTB and nonactin in the membrane. The peak height is the parameter used for establishing the calibration graph. For

higher sample frequencies, kinetic methods may be favoured.

The pH-dependent work functions shown in Fig. 2 can be approximately described by the general equation

$$F_{norm} = A + S \log[NH_4^+] \quad (2)$$

where $[NH_4^+]$ is the concentration of ammonium ion, A and S are constants determined in the calibration process and F_{norm} is the normalized relative fluorescence intensity, defined as

$$F_{norm} = [(F_x - F_{min})/(F_{max} - F_{min})] \quad (3)$$

where F_{max} and F_{min} are the relative fluorescence intensities of the completely deprotonated and protonated dye, respectively and F_x is the measured intensity in the presence of urease. A more comprehensive description of the work function has been presented by Morf et al. [17].

The limit of detection (three times the standard deviation) for ammonium ion is ca. 6 μM at pH 6.41. The detection limits shift to lower concentrations with increasing pH. At the same time, the intensity of the fluorescence at zero ammonium concentration becomes higher and the sensitivity (slope of the graph) becomes smaller. Because urea has a broad activity maximum near pH 7, pH 7.14 was chosen as a reasonable compromise where both the relative signal change of the sensor and the activity of the enzyme are reasonably high. Figure 3 shows a typical recorder output as obtained in the analysis of urease activity with the FI system, and Fig. 4 the respective calibration graph. An almost linear range is observed over the range 1–30 U ml^{-1}.

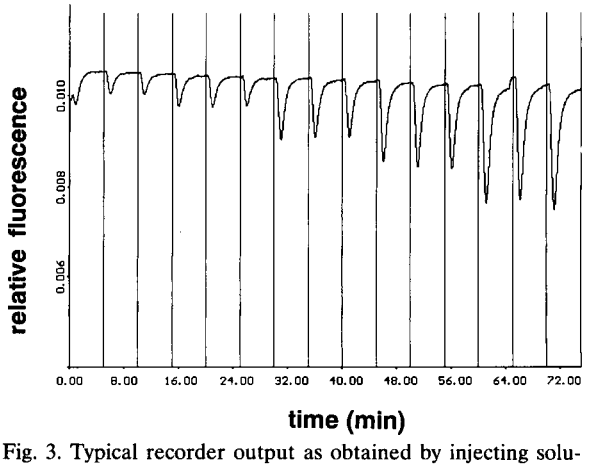

Fig. 3. Typical recorder output as obtained by injecting solutions of various activities of urease. All injections were done in triplicate. From left to right: 0.3, 1.0, 3.0, 10.0 and 30.0 U ml^{-1} urease.

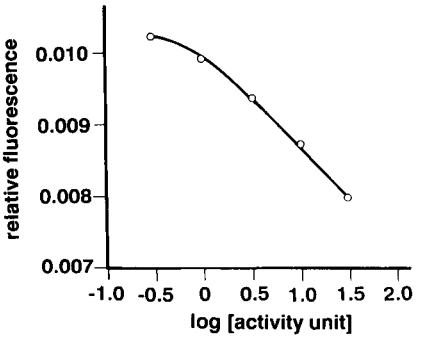

Fig. 4. Calibration graph for determination of urease activity using the FIA–optrode combination.

Precision

Analysis of the data obtained with twelve repetitive injections of urease standard solutions of 3.0 U ml^{-1} showed the relative standard deviation to be 3.7%. However, the system requires frequent re-calibration in view of a slight drift in the baseline (see Fig. 3). It is assumed that some leaching of membrane components (including dye, nonactin, PCTB and plasticizer) is responsible for the slow decrease in the maximum signal intensity.

DISCUSSION

Urease activity has been determined by measurement of the ammonium ions formed (Eqn. 1) by spectrophotometry [18], calorimetry [19] and conductimetry [20], for example. The method reported here is the first that makes use of an optical sensor as the detector. The use of ion-selective optrodes as detectors in FIA has a number of interesting aspects. In classical optical detection in FIA, a chromogenic or fluorogenic reagent is usually injected into the carrier stream.

In the FIA–optrode combination, in contrast, the sensor specifically recognizes the analyte that has been formed in the reaction coil. In other words, the optical properties of the sensor are being detected, not those of the analyte or those of any product of a chemical reaction with an injected reagent. No chromogenic or fluorogenic reagents need to be added. In addition, the effect of optically interfering species, potentially contained in the analyte solution and adversely affecting the accuracy of the optical measurement, can be minimized if they do not enter the sensor membrane, which usually is the case.

Notwithstanding these advantages, there are certain drawbacks, e.g., good FIA instrumentation is still comparatively expensive and rather sophisticated; unlike the use of injected reagents, the indicators used in optrodes are the same during the whole lifetime of a sensor, which can cause problems with respect to dye leaching, leaching of other sensor components, photobleaching and membrane swelling, and hence may require frequent re-calibration of the sensor; and some optrodes have a response time that is too long to be useful in FIA.

Ureases exhibit absolute specificity [21]. Of a large number of compounds tested by various workers, including substituted ureas, only urea was metabolized. The enzyme is competitively inhibited by thiourea, ammonia and large concentrations of Na^+ and K^+. Inorganic phosphate is an activator [21]. As these species can be present in samples were enzyme activities are to be determined, they are potential interferents. In addition, urease is sensitive to inhibition traces of heavy metals [22]. Silver(I), mercury(II), copper(II), cadmium(II), cobalt(II), nickel(II), manganese(II) and lead(II) have all been determined using data from the inhibition of the urea–urease reaction by the metal. The urease inhibition is relatively selective for mercury(II), with a selectivity of 100 (or greater) over the other metals. Conceivably, this offers a method for the FIA assay of mercury in environmental samples, using the above system. Experiments in that direction are in progress.

Financial support by the Austrian Science Foundation within project S5701-PHY is gratefully acknowledged.

REFERENCES

1 G. Blankenstein and M.-R. Kula, in R.D. Schmid (Ed.), Flow Injection Analysis (FIA) Based on Enzymes or Antibodies (GBF Monographs, Vol. 14), VCH, Weinheim, 1991, p. 85.
2 C.J. McNeil, J.V. Bannister and I.J. Higgins, Biosensors, 3 (1987) 199.
3 E.H. Ho and E.H. Cantor, Clin. Chem., 33 (1987) 893.
4 A. Labigne, V. Cussac and P. Courcoux, J. Bacteriol., 173 (1991) 1920.
5 H.E. Spinnler, C. Beal, A. Rozzi and G. Corrieu, Process Biochem., 24 (1989) 187.
6 S.M. Allison and J.I. Prosser, Soil Biol. Biochem., 23 (1991) 45.
7 H.J. Barreto and R.L. Westerman, Soil Sci. Soc. Am. J., 53 (1989) 1455.
8 M.A. Greig, W.D. Neithercut, M. Hossack and K.E.L. McColl, J. Clin. Pathol., 44 (1991) 157.
9 J. Ruzicka and E.H. Hansen, Flow Injection Analysis, Wiley, New York, 2nd edn., 1989.
10 M. Valcarcel and M.D. Luque de Castro, Flow Injection Analysis: Principles and Applications, Horwood, Chichester, 1990.
11 M.D. Luque de Castro and J.M. Fernandez-Romero, in R.D. Schmid (Ed.), Flow Injection Analysis (FIA) Based on Enzymes or Antibodies (GBF Monogr., Vol. 14), VCH, Weinheim, 1991, p. 123.
12 W. Künnecke, H.M. Kalisz and R.D. Schmid, Anal. Lett., 22 (1989) 1471.
13 M.D. Luque de Castro and J.M. Fernandez-Romero, Anal. Chim. Acta, 263 (1992) 43.
14 O.S. Wolfbeis (Ed.), Fiber Optic Chemical Sensors and Biosensors, Vols. 1 and 2, CRC, Boca Raton, FL, 1991.
15 T. Werner, H. He, M. Kessler and O.S. Wolfbeis, J. Fluoresc., in press.
16 K. Seiler, W.E. More, B. Rusterholz and W. Simon, Anal. Sci., 5 (1989) 557.
17 W.E. Morf, K. Seiler, B. Rusterholz and W. Simon, Anal. Chem., 62 (1990) 738.
18 E. Kandeler and H. Gerber, Biol. Fertil. Soils, 6 (1988) 68.
19 M.L. Antonelli, V. Carunchio, M. Luciani and G. Vinci, Thermochim. Acta, 122 (1987) 95.
20 U. Gosewinkel and F.E. Broadbent, Commun. Soil Sci. Plant Anal., 15 (1984) 1377.
21 Th. E. Barman, Enzyme Handbook, Vol. II, Springer, New York, 1969, p. 648.
22 L. Ögren and G. Johansson, Anal. Chim. Acta, 96 (1978) 1.

Analytica Chimica Acta, 276 (1993) 121–125
Elsevier Science Publishers B.V., Amsterdam

Multi-site detection in flow analysis

Part 2. Monosegmented systems with relocating detectors for the spectrophotometric determination of boron in plants

Ana Rita A. Nogueira

Empresa Brasileira de Pesquisa Agropecuária, S. Carlos SP (Brazil)

Sandra M.B. Brienza and Elias A.G. Zagatto

Centro de Energia Nuclear na Agricultura, Universidade S. Paulo, P.O. Box 96, 13400 Piracicaba SP (Brazil)

José Luis F. Costa Lima and Alberto N. Araújo

Faculdade de Farmácia, Universidade do Porto, Porto (Portugal)

(Received 4th August 1992)

Abstract

Monosegmented systems with detector relocation are proposed. The sample is injected with an air plug positioned at its tailing portion in order to minimize dispersion. After the peak maximum, the detector is displaced from its original position, allowing the air phase to be discarded without flowing through it. The sample portion inside the detector is either trapped or pushed towards waste. The advantages and limitations of the approach are described, and the need for an optional washing stream is discussed. As an application, an improved system for the spectrophotometric determination of boron in plants is proposed. Four samples are simultaneously processed at a sampling frequency of 120 h^{-1}. With a low reagent consumption (0.52 mg of Azomethine-H per determination), the system yields precise results (R.S.D. $< 3\%$), in agreement with those given by inductively coupled plasma atomic emission spectrometry.

Keywords: Flow analysis; UV–Visible spectrophotometry; Boron; Plants

Multi-site detection with a single relocating detector in flow analysis was recently proposed [1]. The detector was associated with different manifold sites in such a way that its relocation among them allowed either parallel or serial monitoring. When applied to the simultaneous determination of aluminium and iron in plant digests and to iron speciation in natural waters, the approach proved to be worthwhile for large-scale analysis. The sampling rate was increased because the detector was removed after the peak maximum, so that the washing time was no longer a limiting factor.

Detector relocation can also be exploited to avoid the cumbersome step of air removal in monosegmented continuous-flow systems [2]. Monosegmentation can be regarded as an improvement of the "rapid-flow" approach [3], and was conceived as means of reducing tailing effects, thus permitting long sample residence times

Correspondence to: E.A.G. Zagatto, Centro de Energia Nuclear na Agricultura, Universidade S. Paulo, P.O. Box 96, 13400 Piracicaba SP (Brazil).

to be achieved without pronounced sample dispersion. It combines the favourable characteristics of both segmented and unsegmented flow analysis.

In the original system [2], the sample was injected between two air plugs which were removed immediately before reaching the spectrophotometric flow cell. For this task, several devices have been used [2–7]. When applied to continuous-flow atomic absorption spectrometry [8], monosegmentation was accomplished by placing a single air plug in the trailing edge of the sample zone. As the air phase reached the detector after the analytical signal was recorded, and did not affect the flame stability, its removal was not necessary. The system could then be simplified.

This strategy can be extended to spectrophotometry providing that air passage through the flow cell can be avoided by relocating the detector from its original site after top peak measurement. In this way, bubble gating devices are not needed.

This paper demonstrates the feasibility of combining a relocating flow cell with a monosegmented continuous-flow system (Fig. 1), and discusses advantages and limitations. Different assemblies are critically examined by using model systems, and the feasibility of the approach for routine analysis is demonstrated. The spectrophotometric determination of boron in plants with Azomethine-H [5,9,10] was selected by taking into account the requirements of sample residence time, sample volume, sensitivity and reagent costs [9].

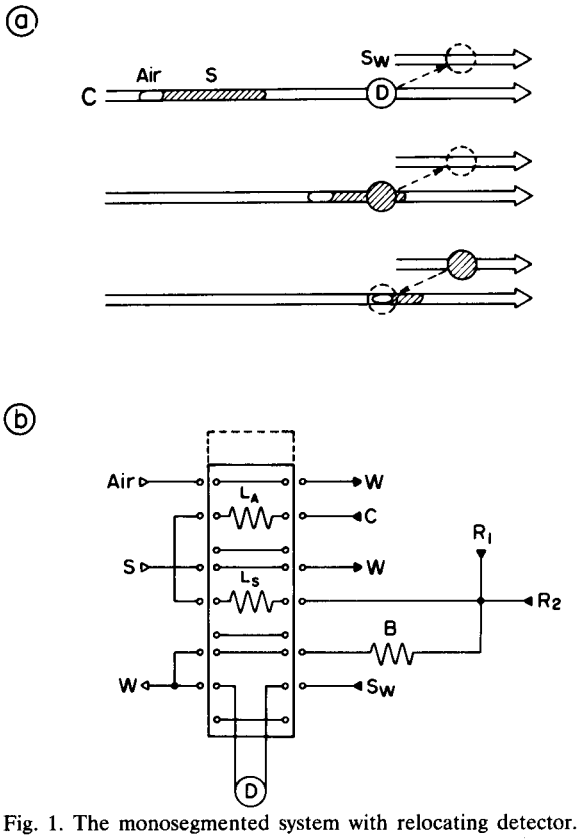

Fig. 1. The monosegmented system with relocating detector. (a) Schematic representation. Sample (S, hatched) introduced into carrier stream (C) with an air plug (Air) which does not flow through the detector (D) because of its relocation (interrupted lines). Optional washing stream specified by S_w. (b) Flow diagram. S = sample aspirated at 4.0 ml min^{-1}; L_s = sample loop (40 cm, 200 μl); Air = air flow (4.0 ml min^{-1}); L_A = air loop (10 cm, 25 μl); C = carrier stream (2.0 ml min^{-1}); R_1 and R_2 = colour and buffer/masking reagents (0.4 ml min^{-1}); B = 500-cm reactor; D = detector (420 nm); S_w = optional washing stream [C–R_2 (5:1, v/v), 4.0 ml min^{-1}]; W = waste. Boxed components are linked to the central sliding portion of the commutator, its displacement being indicated by interrupted lines.

CONSIDERATIONS FOR SYSTEM DESIGN

Introduction of a sample plug followed by air into an unsegmented carrier stream is efficiently carried out by using loop-based injectors with two external loops, as shown in Fig. 2a and b. In the loading position, the loops are filled with sample and air, which are simultaneously introduced into the main channel by switching the injector. Immediately after injection with the rotary valve, the air and sample plugs are in close contact, whereas with sliding bar commutators, a small volume of carrier solution remains between the newly established plugs. In situations where this effect should be avoided, the system can be designed as in earlier work [8].

Regarding detector relocation, it was originally accomplished [1] by replacing the sampling loop of a commutator with the flow cell with its inlet and outlet tubing (Fig. 2c). After switching the commutator, the detector was displaced to an-

other manifold site, located either in the same or in a different channel, depending on whether serial or parallel monitoring was involved. This approach can be implemented by using any loop-based injector; with a six-port rotary valve, the system could be designed as in Fig. 2d. In the present procedure, the detector is trapped or intercalated into a washing stream, the former situation resulting in a system analogous to the stopped-flow analyser.

In monosegmented systems with detector relocation, the partial diagrams of Fig. 2 are simply implemented. If simultaneous movement is required, the system can be designed with a single moving element, e.g., as in Fig. 1b. Alternatively, commercial rotary valves either mounted in the same axis or with electronically synchronized movement can be used.

EXPERIMENTAL

The components of the systems were described in Part 1 [1]. In addition, a Jenway Model 6050 colorimeter with a 420-nm filter and equipped with a Hellma 178.713 flow cell (8 μl) was used. For sample injection together with the air plug, a three-section commutator (Fig. 2a) or a ten-port rotary valve similar to the VICI model 10 UWT (Fig. 2b) was used. The flow cell was removed from the main channel by switching the commutator or a six-port Reodyne Model 5020 rotary valve.

All solutions were prepared with analytical-reagent grade chemicals and distilled, deionized water and stored in polyethylene flasks. Samples were mineralized by ashing 1.5 g of dried ground leaves at 550°C for 2–4 h, adding 10 ml of 0.5 M HCl, filtering and diluting to 50 ml with water. Working standard solutions, 0.1 M in HCl and covering the range 0.00–5.00 mg B l^{-1}, were prepared by dilutions of a 100.0 mg l^{-1} stock standard solution of boron (as boric acid). The sample carrier stream was also 0.1 M HCl, reagent R_1 was a freshly prepared 0.25% (w/v) Azomethine-H plus 2.0% (w/v) ascorbic acid solution and R_2 was a 2.0 M $(NH_4)_2HPO_4$ plus 5.0% (w/v) Na_2EDTA [2] solution. Preliminary tests indicated that no improvement was achieved with a modified reagent composition [11].

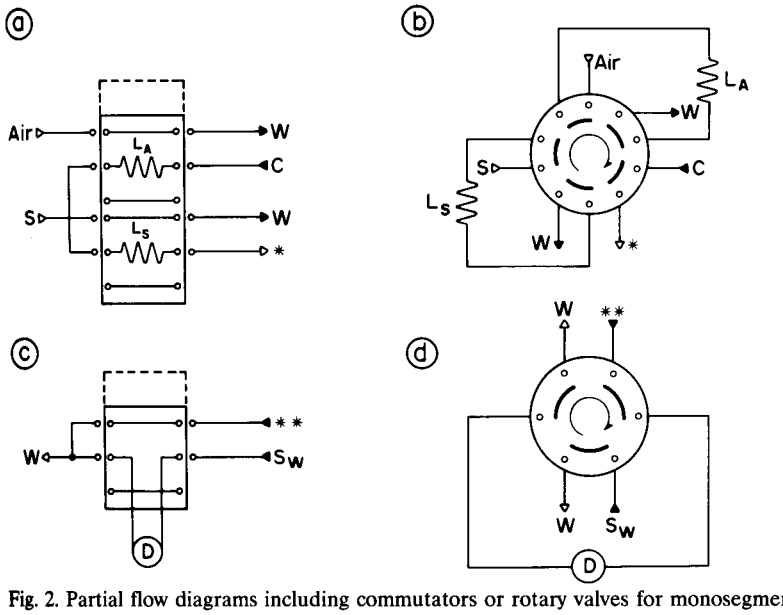

Fig. 2. Partial flow diagrams including commutators or rotary valves for monosegmented sample injection and detector relocation. * = To relocating detector; * * = from injection port. Other symbols as in Fig. 1.

The influence of the main parameters related to boron determination was investigated with the system shown in Fig. 1b. The chemical reactions involved have been discussed previously [9,10].

RESULTS AND DISCUSSION

Pronounced dispersion inside the detector plus accessories (420 μl) [1] was observed when the sample volume injected was only about 50 μl (length of $L_s = 10$ cm), the sample volumetric fraction being determined as 0.31. When 50-cm transmission lines attached to the flow cell were used, the dispersion increased because the inner volume of the detector plus accessories increased and the sample passed through them without being protected against dispersion by the air phase. With these longer transmission lines, no relevant changes were found when a low-volume flow cell (8 μl) was employed, emphasizing the relevance of the length of the transmission lines. Here, they were fixed as 12 cm. As sensitivity was critical, the length of the sample loop L_s was selected as 40 cm (200 μl). The peak height corresponded to 95% of the absorbance plateau relative to the situation of infinite sample volume [9].

The need for monosegmentation was checked by using a 0.1 M HCl stream instead of air, resulting in a flow-injection system equivalent to that proposed (Fig. 1b) but without monosegmentation. The recorded peak height underwent a 35% decrease and the carryover increased to about 10% confirming the beneficial influence of air in avoiding band broadening.

The system in Fig. 1b is remarkably stable regardless of the utilization of the washing solution. No measurable changes in the baseline were observed when the flow cell was displaced. As devices for air removal were not present in the analytical path, reproducible measurements were attained in all experiments. For a typical sample (97.2 mg B kg^{-1}, dry basis) the relative standard deviation of the results was estimated to be 0.74% after ten successive measurements.

The sampling rate was limited mainly by the dead volume of the detection unit, the number of samples in the analytical path and the sample processing time. Although monosegmentation was involved, the number of samples inside the analytical path could not be increased at will, being limited by the inner volume of the flow cell plus accessories. A minimum distance between successive samples should be maintained in order to avoid carryover effects due to sample interpenetration inside the detection unit. With the system in Fig. 1b, four sample zones were always present in the analytical path and the sample mean residence time was 105 s. The commutator was then switched every 15th second, which determined a sampling frequency of 120 h^{-1} at the 2% carryover level. This corresponds to 0.52 mg of Azomethine-H consumed per determination. Those figures compare favourably with than those reported for the original procedure [9].

With an 8-μl flow cell and the use of rotary valves attached to short (5-cm) transmission lines, the sampling rate increased by about 60% without impairing other analytical characteristics.

Without the optional washing stream, multi-site detection permits the measurement of processed samples under flow conditions before detector relocation, and provides information about trends of the chemistry involved when the sample is trapped. For boron determination using the system in Fig. 1b without S_w, an increase in the slope of the calibration graph was observed (Fig. 3a) because the absorbance at the end of the stop

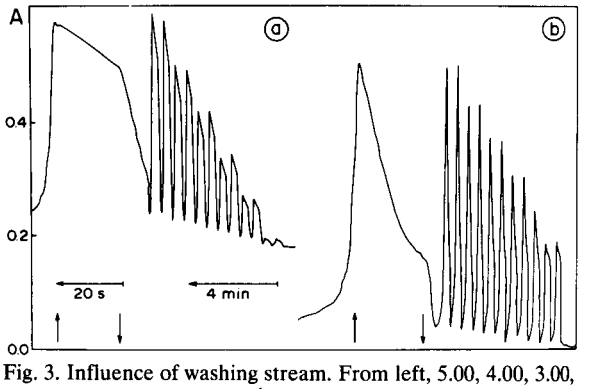

Fig. 3. Influence of washing stream. From left, 5.00, 4.00, 3.00, 2.00, 1.00 and 0.00 mg B l^{-1} solutions injected into the system in Fig. 1b, (a) without and (b) with S_w addition. Arrows indicate instants of commutator switching.

period was higher than that associated with the flow conditions. As Azomethine-H condensation proceeds also in the absence of boron [10], a blank absorbance value of 0.04 was observed after a 15-s stop period, emphasizing the uncatalysed reaction. However, without S_w, the reproducibility was not as good, probably because of the tendency of the condensate Azomethine-H to settle. Also, in this situation the carryover was dependent on the boron content of previous sample.

These drawbacks were circumvented by adding the S_w washing stream, which resulted, however, in a slight decrease in the analytical signal and the presence of non-linear baseline (Fig. 3b). The residual absorbance was not dependent on the boron content in previous sample but a constant value determined by the characteristics of the solutions and washing time. Establishment of a non-linear baseline could be avoided by using an S_w stream similar to the solution flowing through the main channel [12]. In order to avoid excessive consumption of Azomethine-H, S_w was a 5:1 (v/v) combination of C and R_1 solutions. In this situation, Schlieren noise was not observed.

After a 4-h working period, only slight variations in the calibration equations ($< 5\%$) were found and baseline drift was not observed. Although the sample processing time relative to the original flow-injection procedure [9] was longer, selectivity was comparable, emphasizing that the proposed system can be applied to plant analysis without restrictions. In addition, the accuracy can be assessed from Table 1, which reveals no statistical differences between the methods at the 99% confidence level.

Finally, it should be stressed that the proposed approach without the S_w stream can be also accomplished with a three-way valve placed immediately before the detector. After measurement of the sample central portion, the valve is switched, directing the air phase towards waste and stopping the stream at the flow cell. Studies on this aspect are in progress.

TABLE 1

Boron contents in plant leaves as determined by the proposed procedure and by inductively coupled plasma atomic emission spectrometry (ICP-AES) [13] [a]

Sample No.	Boron concentration (mg kg^{-1}, dry basis)	
	Proposed procedure	ICP-AES
1	70.0 (0.0)	72.1 (1.4)
2	56.7 (1.6)	60.3 (1.2)
3	48.3 (1.9)	50.6 (1.0)
4	58.3 (1.2)	56.9 (1.1)
5	51.6 (2.1)	50.6 (1.5)
6	56.6 (0.2)	57.3 (1.1)
7	28.3 (0.1)	25.6 (0.7)
8	144.8 (1.7)	142.7 (2.8)

[a] Numbers in parentheses are estimated relative standard deviations (%) determined after three repetitions.

Partial support from CNPq (Conselho Nacional de Desenvolvimento Científico e Tecnológico) and JNICT (Junta Nacional de Investigação Científica e Tecnológica), constructive comments from M.A.Z. Arruda and assistance in the laboratory by B. Pereira are greatly appreciated.

REFERENCES

1 E.A.G. Zagatto, H. Bergamin F°., S.M.B. Brienza, M.A.Z. Arruda, A.R.A. Nogueira and J.L.F.C. Lima, Anal. Chim. Acta, 261 (1992) 59.
2 C. Pasquini and W.A. Oliveira, Anal. Chem., 57 (1985) 2575.
3 P.W. Alexander and A. Thalib, Anal. Chem., 55 (1983) 497.
4 C. Pasquini, Anal. Chem., 58 (1986) 2346.
5 J.C. Andrade, M. Ferreira, N. Baccan and O.C. Bataglia, Analyst, 113 (1988) 289.
6 J.C. Andrade, S.P. Eiras and R.E. Bruns, Anal. Chim. Acta, 255 (1991) 149.
7 L.C. Tiam, X.P. Sun, Y.Y. Xu and Z.L. Zhi, Anal. Chim. Acta, 238 (1990) 183.
8 B.F. Reis, M.A.Z. Arruda, E.A.G. Zagatto and J.R. Ferreira, Anal. Chim. Acta, 206 (1988) 259.
9 F.J. Krug, J. Mortatti, L.C.R. Pessenda, E.A.G. Zagatto and H. Bergamin F°., Anal. Chim. Acta, 125 (1981) 29.
10 M.A.Z. Arruda and E.A.G. Zagatto, Anal. Chim. Acta, 199 (1987) 137.
11 J. Ferran, Agrochim. 32 (1988) 171.
12 E.A.G. Zagatto, B.F. Reis, M. Martinelli, F.J. Krug, H. Bergamin F°. and M.F. Giné, Anal. Chim. Acta, 198 (1987) 153.
13 M.F. Giné, MSc Thesis, ESALQ/USP, Piracicaba, 1986.

Analytica Chimica Acta, 276 (1993) 127–131
Elsevier Science Publishers B.V., Amsterdam

Double-membrane phase separator for liquid–liquid extraction in flow-injection analysis

Tadao Sakai, Yong Soon Chung [1] and Noriko Ohno

Department of Chemistry, Asahi University, 1851 Hozumi, Hozumi-cho, Gifu 501-02 (Japan)

Shoji Motomizu

Department of Chemistry, Faculty of Science, Okayama University, Tsushimanaka, Okayama-shi 700 (Japan)

(Received 11th September 1992)

Abstract

A double-membrane phase separator for liquid–liquid extraction in flow-injection analysis was designed and its usefulness was examined in order to achieve smooth, long-term and efficient phase separation with good reproducibility. The construction and performance of the flow-injection system using the phase separator were illustrated by the extraction of berberine–perchlorate ion associates.

Keywords: Flow injection; Fluorimetry; Berberine; Extraction; Membrane separator; Phase separator

Liquid–liquid extraction techniques have often been used for sample pretreatment in order to remove interfering substances, to preconcentrate analytes and to enhance sensitivity. In 1978, the first extraction system coupled with a flow-injection technique was reported by Karlberg and Thelander [1]. A chloroform stream was mixed with an aqueous stream containing a sample (caffeine) at a mixing point, which with a specially constructed fitting made it possible to obtain a regular pattern of aqueous and organic segments. The phase-separating device consisted of a T-connector with PTFE fibres twisted together to a thread and inserted in the bend from the inlet down into the outlet directed toward the flow cell. The aqueous phase was forced upwards in the fitting to waste and only organic phase was sucked into the flow cell. Moreover, the adaptation of the system to more complicated extraction procedures has been made for the determination of codeine as the picrate ion pair [2]. However, it has proved difficult to achieve successful phase separation with the device described above in a complicated extraction system such as water–methanol–chloroform.

A phase-separating system was designed with a PTFE porous membrane which is permeable to an organic phase but impermeable to an aqueous solution for extraction of anionic surfactants [3]. The inner volume of the separator was 500 μl. A stirring bar was inserted into the cavity to decrease the inner volume. A sharper and higher peak was obtained when the stirring bar was rotated, compared with the unrotated condition. A simpler and more practically useful separator with a PTFE porous membrane sheet (7 mm diameter) and an inner volume of 12.5 μl was constructed for extraction of cationic surfactants [4]. Later, a detailed study of the effect of the

Correspondence to: T. Sakai, Department of Chemistry, Asahi University, 1851 Hozumi, Hozumi-cho, Gifu 501-02 (Japan).
[1] On leave from the Department of Chemistry, Chungbuk National University, Cheongju 360-763 (Korea).

dimensions of the cylindrical cavity-type phase separator (4.2 mm diameter, 2.3 mm deep) was reported by Motomizu and Korechika [5]. Also, a membrane phase separator that caused only a small dispersion was proposed [6]. The phase separator with a PTFE membrane is more versatile than that developed by Karlberg and Thelander.

Motomizu and Oshima [7] designed phase separators whose membrane chambers have as small a volume as possible, to give efficient and stable phase separation. Of these, a separator with a sloped groove (membrane chamber depth 2 mm, width 2 mm) with a PTFE membrane (0.8 μm pore size) gave good results and the organic phase was completely recovered through the membrane filter by using two needle valves. On the other hand, double-tube systems with an inner tube of microporous PTFE (i.d. 1 mm; thickness 0.5 mm; porosity 60%; length 2.0–2.5 cm) were designed by Mise [8], Miyaji et al. [9] and Sakai [10] individually. The recovery of the organic phase by these separators was adequate. However, the peak shapes became broader and the heights were lower compared with others. In addition, the retention time was long because long tubing was used to obtain good extraction.

Many liquid–liquid extraction systems have been reported and various kinds of phase separators have been designed and their efficiencies investigated. However, there are some problems with long-term continuous runs and permeation of a small amount of water. In general, it is difficult to maintain the hydrophobicity of membrane and/or porous PTFE tube surfaces for a long time and to prevent leakage of the aqueous phase.

This paper describes an approach involving a newly designed device for a practically useful phase-separating system that can be used in long-term applications.

EXPERIMENTAL

Reagents and solutions

A standard berberine solution (1×10^{-3} mol dm^{-3}) was prepared by dissolving 0.0407 g of berberine chloride dihydrate (Nakalai Tesque, Kyoto) in hot water and diluting to 100 ml with distilled water. The stock solution was standardized by an official method [11]. Working solutions were prepared by accurate dilution. A borate–phosphate buffer solution (pH 5.5) containing 1×10^{-3} mol dm^{-3} perchlorate was prepared by dissolving 0.14 g of sodium perchlorate monohydrate and adjusting the pH with 1 mol dm^{-3} sodium hydroxide or 1 mol dm^{-3} sulphuric acid. 1,2-Dichloroethane was used as an extracting solvent without further purification. In the ion-pair extraction system using the dyestuff tetrabromophenolphthalein ethyl ester (TBPE · H) (Tokyo

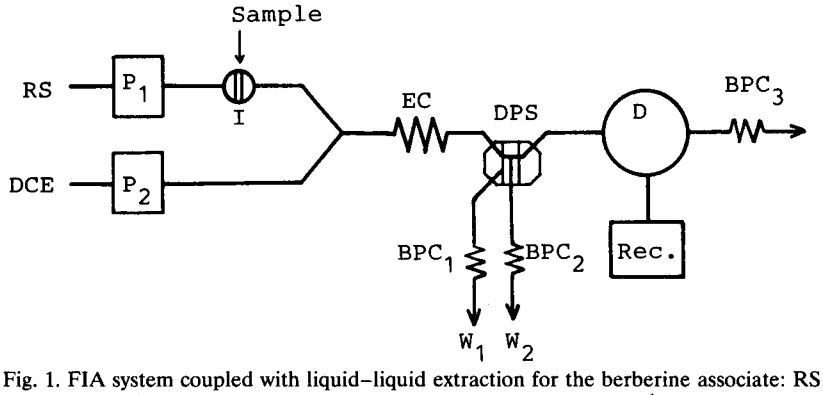

Fig. 1. FIA system coupled with liquid–liquid extraction for the berberine associate: RS = 1×10^{-3} mol dm^{-3} sodium perchlorate buffered at pH 5.5; P_1,P_2 = pumps (flow-rates, P_1 1.24 ml min^{-1}, P_2 0.62 ml min^{-1}); EC = extraction coil (0.5 m long); BPC = back-pressure coils (BPC_1 1 m, BPC_2 3.5 m, BPC_3 2 m, all 0.25 mm i.d.); DPS = double-membrane phase separator; D = spectrofluorimetric detector [λ(ex) 355.2 nm, λ(em) 516.8 nm]; Rec. = recorder.

Kasei, Tokyo), the dichloroethane solution and the buffer solution (pH 8.0) were prepared as described in a previous paper [10].

Apparatus

The fluorescence intensity was monitored by a spectrofluorimetric detector (Model S-3350, Soma Optics, Tokyo) with a micro-flow cell (15 μl) and a spectrophotometer (Model S-3250, Soma Optics) with a micro-flow cell (8 μl) was used for absorbance measurements.

A double-plunger micro-plump (Model DM2U-1026, Sanuki Kogyo, Tokyo) was used to propel the carrier solution and extracting solvent. The samples (140 μl) were injected via a six-way injection valve to which a volume control loop was attached. A Toa Electronics Model FBR-251A recorder was used.

Flow-injection system

The manifold of the flow-injection system used is shown in Fig. 1. A 1×10^{-3} mol dm^{-3} sodium perchlorate solution buffered at pH 5.5 (RS) was delivered at a rate of 1.24 ml min^{-1}, and 1,2-dichloroethane (DCE) at 0.62 ml min^{-1}. A T-segmenter (Sanuki Kogyo, Tokyo) in which the aqueous phase flows straight through and organic phase at right-angles was used for mixing organic and aqueous phases. The extraction coil (EC) was 0.5 m long and the back-pressure coils were BPC_1 1 m, BPC_2 3.5 m and BPC_3 2 m long. The PTFE tubing was of 0.5 mm i.d. except for the back-pressure coils, which were of 0.25 mm i.d. The excitation wavelength was set at 355.2 nm and the emission intensity was measured at 516.8 nm, as described previously [12].

RESULTS AND DISCUSSION

Design of the phase separator

In previous work, although Motomizu and Oshima [7] and Sakai [10] could obtain good and efficient separations of the organic phase with the phase separator mentioned above, it was very difficult to use the porous membrane for long-term operations without its exchange because the membrane function decreased and trace water passed through the membrane with the organic phase. When a fraction of the aqueous phase penetrates the membrane and/or passes through, it has to be exchanged and in addition the contaminated tube and flow cell must be washed using acetone or ethanol. Then 1,2-dichloroethane has again to penetrate the membrane. This is a difficult problem with the extraction–flow-injection system. It is especially troublesome in spectrophotometry using adsorptive dyestuffs. Manzoori and Miyazaki [13] used two phase separators to remove the remaining traces of aqueous phase in the organic phase separated with the first separator and only pure organic phase was obtained with the second separator. We also tried to use two phase separators in joined with a very short tube (2 cm) (Fig. 2) in an extraction–spectrophotometry–flow-injection system using the dyestuff TBPE · H. Although good results were obtained, the flow system was slightly compli-

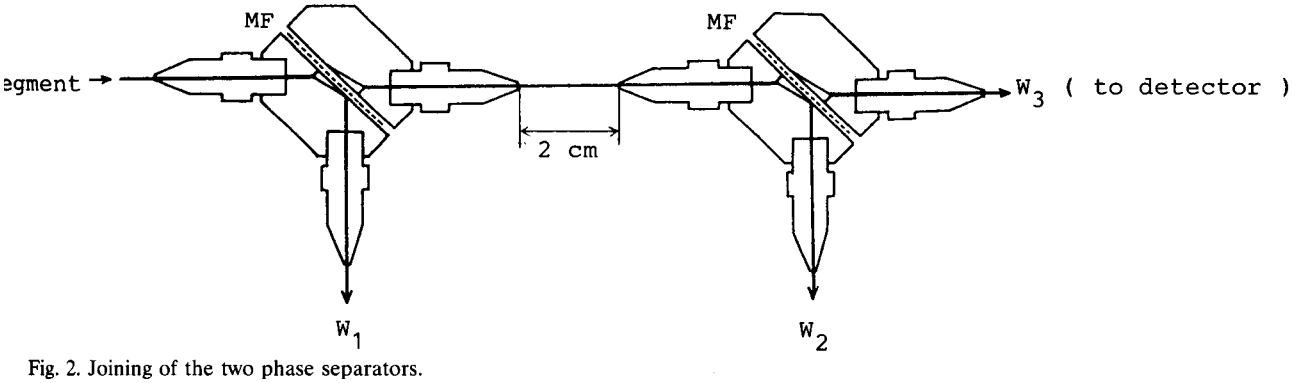

Fig. 2. Joining of the two phase separators.

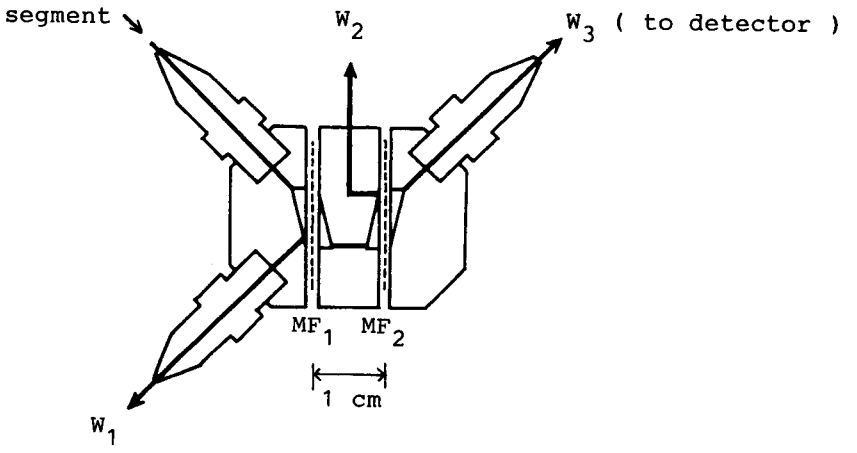

Fig. 3. Construction of the double-membrane phase separator.

cated. As a result, the phase separator designed by Motomizu and Oshima [7] was simply modified. A double-phase separator was designed as shown in Fig. 3. The fraction of the organic phase penetrating the first membrane (MF_1) and the remaining organic phase and large amounts of aqueous phase were conducted to the waste tube (W_1 in Fig. 1). However, when the first membrane became weak from long-term and frequent usage and/or when high recoveries of the organic phase

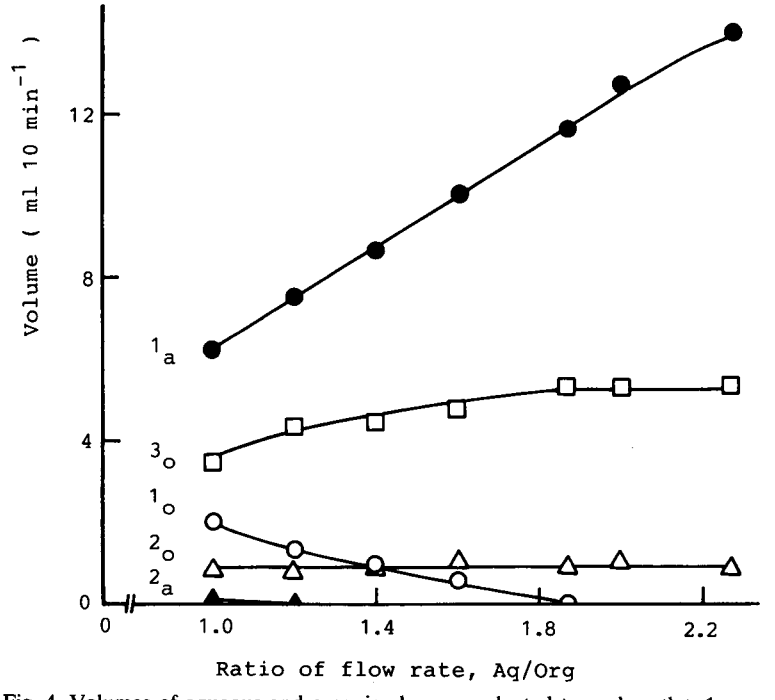

Fig. 4. Volumes of aqueous and organic phases conducted to each outlet: 1_a, aqueous phase exhausted to W_1; 1_o, organic phase exhausted to W_1; 2_a, aqueous phase exhausted to W_2; 2_o, organic phase exhausted to W_2; 3_a, aqueous phase exhausted to W_3; 3_o, organic phase exhausted to W_3; flow-rate of organic phase, 0.62 ml min^{-1}.

via needle valves are needed so that the pressure in the lines increases, permeation of the aqueous phase sometimes occurred. However, in the newly designed separating system, the permeating aqueous phase with the organic phase was completely separated by a second membrane (MF_2 in Fig. 3). As a result, only organic phase can be transferred to the flow cell in the detector.

Separation efficiency with the phase separator

The volumes of aqueous and organic phases which were conducted to W_1, W_2 and W_3 in Fig. 1 were compared at different flow-rates. The results are shown in Fig. 4. Lines 1_a and 1_o refer to the aqueous and organic phases exhausted to W_1. The flow-rate of the organic stream was 0.62 ml min^{-1}. The aqueous flow rate was varied in the range of 0.62–1.40 ml min^{-1}. When the ratio was small, the permeation volume of the organic phase to the first membrane was small and a small amount of water passed through the first membrane. On the other hand, the volume (2_a) of the aqueous phase which was guided away to W_2 decreased with increasing ratio and aqueous phase was conducted to W_1. The volume of the organic phase exhausted to W_1 decreased with increasing ratio. It is assumed that the pressure of the aqueous stream pushes out a moderately small amount of organic phase to the hydrophobic membrane surface. With increasing ratio, the volume (3_o) of the organic phase in W_3 gradually increased. When the ratio was over 1.9, the volume (3_o) was constant because all organic phase passed through the membrane (MF_1). In this system, although the final recovery of the organic phase was 85% because a small volume (2_o) of organic phase was drained to W_2, pure organic phase could be transferred to the flow cell by using the new phase separator. Also, this separator could be used for about 1 week without exchanging the membrane in the berberine–perchlorate extraction system. On the other hand, in the extraction system using dyestuffs as counter ions, when the long-term runs were done, noisy baselines and drift occurred because of adsorption of dyestuffs on the membrane, although the passage of water was not be observed.

TABLE 1

Concentration effect of berberine associate by extraction in flow-injection system [a]

Ratio of flow-rates, aqueous/organic	Peak height (cm)		
	1.0×10^{-8} [b]	2.5×10^{-8} [b]	5.0×10^{-8} [b]
1	1.89	4.60	9.26
1.4	2.20	5.33	10.72
2	3.00	7.22	14.41

[a] Flow-rate of organic phase = 0.62 ml min^{-1}. [b] Concentration of berberine (mol dm^{-3}).

Concentration effect by liquid–liquid extraction

The concentration effect of berberine ion associates was investigated by varying the flow-rate of the reagent solution stream (pH 5.5) at a constant flow-rate of the extracting solvent of 0.62 ml min^{-1}. The results are shown in Table 1. When the ratio of the organic to the aqueous phase was 1 : 2, the fluoresence intensity was enhanced about 1.6 times compared with that at a 1 : 1 ratio.

This research was partially supported by a Grant-in-Aid for General Scientific Research from the Ministry of Education, Science and Culture (Japan).

REFERENCES

1 B. Karlberg and S. Thelander, Anal. Chim. Acta, 98 (1978) 1.
2 B. Karlberg, P.A. Johansson and S. Thelander, Anal. Chim. Acta, 104 (1979) 21.
3 J. Kawase, A. Nakae and M. Yamanaka, Anal. Chem., 51 (1979) 1640.
4 J. Kawase, Anal. Chem., 52 (1980) 2124.
5 S. Motomizu and K. Korechika, Anal. Chim. Acta, 220 (1989) 275.
6 K. Ogata, K. Taguchi and T. Imanari, Anal. Chem., 54 (1982) 2127.
7 S. Motomizu and M. Oshima, Analyst, 112 (1987) 295.
8 T. Mise, J. Flow Injection Anal., 5 (1988) 87.
9 T. Miyaji, K. Hibi and T. Sakai, Bunseki Kagaku, 39 (1990) 73.
10 T. Sakai, Analyst, 117 (1992) 211.
11 The Japanese Pharmacopoeia, XI, Hirokawa Publishing, Tokyo, 1986, p. C-315.
12 T. Sakai, Y.S. Chung and N. Ohno, Anal. Sci., 8 (1992) 377.
13 J.L. Manzoori and A. Miyazaki, Anal. Chem., 62 (1990) 2457.

Analytica Chimica Acta, 276 (1993) 133–139
Elsevier Science Publishers B.V., Amsterdam

Characteristics of potassium ion-doped glass slab optical waveguide as an absorption cell and its application to the spectrophotometric detection of Methylene Blue

Kin-ichi Tsunoda, Hiromitsu Itabashi and Hideo Akaiwa

Department of Chemistry, Gunma University, Tenjin-cho, Kiryu, Gunma 376 (Japan)

(Received 11th September 1992; revised manuscript received 16th November 1992)

Abstract

The characteristics of a K^+-doped glass slab optical waveguide (SOWG) as an absorption cell are discussed in terms of effective path length (L_{eff}) and relative sensitivity (S/cm). The longest L_{eff} value of 11 μm was observed with TM_0 mode of the SOWG with a 30-min ion-exchange process in molten KNO_3, which was in good agreement with the calculated value of 9.7 μm. The K^+-doped SOWG provides higher sensitivity by one to two orders of magnitude than conventional absorption measurements of an analyte on a glass surface to which perpendicular irradiation of source light on the surface is applied. Octadecylsilane modification of the SOWG surface was effective for the sensitive detection of Methylene Blue by flow analysis where an ion pair of Methylene Blue and lauryl sulphate was formed.

Keywords: UV–Visible spectrophotometry; Absorption cell; Methylene Blue; Optical waveguide

A slab optical waveguide (SOWG), which is one of the most important devices in opto-electronics, has also been recognized by spectroscopists as a useful tool for the highly sensitive spectroscopic measurement of a thin film and its surface [1–3]. Moreover, the SOWG has recently been applied to opto-chemical sensors [4–6] and opto-biosensors. [7,8].

In a previous paper [9] a K^+-doped glass SOWG coated with octadecylsilane (ODS) to concentrate analytes on the SOWG by hydrophobic interaction between the analytes and the ODS was described. The blue dye Coomassie Brilliant Blue G-250, which is strongly adsorbed on the ODS–SOWG, could be detected with the ODS–SOWG detector in a flow analysis system with sensitivity for a sample of 200 μl comparable to that of a conventional spectrophotometer (1-cm cell). On the other hand, the SOWG detector was almost insensitive to another blue dye, Bromothymol Blue, which is not adsorbed on the glass surface at all.

In this paper, the characteristics of the K^+-doped glass SOWG as an absorption cell are discussed in terms of effective path length (L_{eff}) and relative sensitivity (S/cm) (see Appendix). The ODS–SOWG detector was applied to the spectrophotometric detection of Methylene Blue by flow analysis.

Correspondence to: K.-i. Tsunoda, Department of Chemistry, Gunma University, Tenjin-cho, Kiryu, Gunma 376 (Japan).

EXPERIMENTAL

K^+-doped glass slab optical waveguide

SOWGs were fabricated by an ion-exchange process using commercial soda-lime slide glasses in molten potassium nitrate at 673 K for times ranging from 30 min to 4 h [3]. The SOWG propagates only light at discrete incident angles owing to the boundary conditions [1]. The SOWGs in this experiment supported between one and four propagation modes. Octadecylsilane was then introduced on to the surface of the SOWG by the procedure of Kingston and Gerhart [10] with minor modifications.

Measurement system

Although the measurement system used in this study was the same as that in the previous paper [9], a brief description of this system is also given here. A helium–neon laser (632.8 nm, 2 mW, random polarization) was used as a light source. The SOWG was mounted on a 360° rotational stage with X–Y–Z translation to determine the angle of incident light for each propagation mode. The laser light was coupled into the SOWG with a prism coupler [1]. The refractive index of the coupler prisms (CL-01 from Kogaku Giken) was 1.8785 at 632.8 nm. A polarizer was placed between the coupler and the laser to select the polarization of propagating light. The out-coupled beam was collected with optical fibres and the light intensity was measured with a photodiode. The photocurrent was monitored with a digital electrometer and the signal was fed into a personal computer through a GP-IB cable.

The flow cell was made on the SOWG with a polytetrafluoroethylene (PTFE) block and poly(tetrafluoroethylene–co-hexafluoropropylene) (FEP) film and PTFE (0.05 mm and 0.50 mm thick) spacers. The physical cell length was 1.5 cm, the cell volume being 25 μl. Distilled water was sent with an HPLC pump and the sample solution was introduced through a silicone-rubber septum with a syringe.

Theoretical calculation of L_{eff}

The effective refractive index (RI) (N_{eff}) of propagated light of each mode was obtained by experimentally measuring the incident angle (see Fig. 5 in Appendix). An inverse Wentzel–Kramers–Brillouin (WKB) method was applied to a set of N_{eff} for each K^+-doped SOWG to estimate the effective depth (D_{eff}) of each propa-

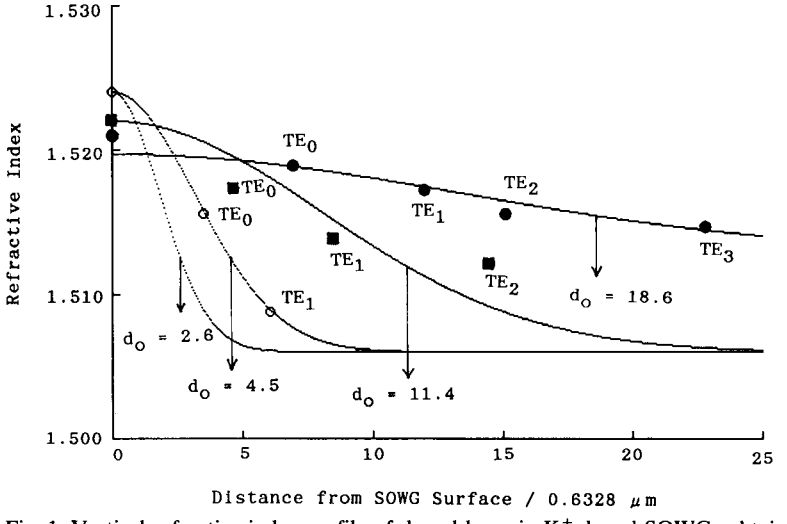

Fig. 1. Vertical refractive index profile of doped layer in K^+-doped SOWGs obtained by inverse WKB method. SOWGs with the following ion-exchange processes: ● = 4 h; ■ = 2 h; ○ = 1 h; ——— = 30 min. Each point (n_2 or a set of D_{eff} and N_{eff} for each propagating mode) in the figure was obtained by the inverse WKB method. The Gaussian curve of $n(z) = n_1 + \Delta n \exp(-z^2/d_0^2)$ ($\Delta n = n_2 - n_1$; d_0 = thickness of doped layer) was used for curve fitting (see Fig. 5 for n_1 and n_2).

gation mode and also n_2 (see Fig. 5) [11]. Moreover, the vertical RI profile of the K^+-doped SOWG was approximated by a Gaussian curve which was obtained by method of least squares with the n_2 value and the set of N_{eff} and D_{eff} values, because K^+-doped SOWGs have a Gaussian-like vertical RI profile [12]. Then, the reflection number per unit length (N_{refl}) of propagating light at the liquid/SOWG interface was calculated by the ray approximation method adapted to the vertical RI profile [13]. In addition, the effective path length per reflection (l_0) was calculated according to Harrick [14] to obtain the L_{eff} ($= l_0 N_{refl}$) of the SOWG (see Appendix).

Theoretical calculation of relative sensitivity (S / cm)

The relative sensitivity per reflection (s_0) was calculated according to Swalen et al. [1], then the S value ($= s_0 N_{refl}$) was obtained (see Appendix). All the calculations were done with a personal computer.

Experimental measurement of L_{eff}

A solution of the blue dye Bromothymol Blue (BTB) (Wako) was used as an absorbance standard to measure the L_{eff} of the SOWG, because BTB molecules are not adsorbed on a glass surface [5]. BTB dye was dissolved in 0.05 M phosphate buffer (pH 8.02). BTB solutions used in the SOWG measurements were 0.63–2.5 mmol/l, which gave absorbances of 8.2–32.8 with an ordinary 1-cm cell at 632.8 nm. BTB solution (0.5 cm^3) was injected into the flow system (1.0 cm^3/min) to obtain the maximum possible absorbance.

RESULTS AND DISCUSSION

Estimation of vertical refractive index profile in SOWGs

Figure 1 shows the vertical RI profiles in the K^+-doped SOWGs obtained by the inverse WKB method and the Gaussian curve fitting. As the SOWG with a 30-min ion exchange was single mode, the inverse WKB method could not be applied to obtain its n_2 and D_{eff} values [11]. In other words, no points for the 30-min SOWG could be fitted (Fig. 1). Hence, the vertical RI profile of the 30-min SOWG was estimated by extrapolating those of the SOWGs with 1–4 h of ion exchange. That is, as the d_0 value of the SOWG (for the thickness of doped layer, see Fig.1) increased almost proportionally with increase in the ion-exchange period as shown in Fig. 1, the d_0 value of the 30-min SOWG was calculated by extrapolating a least-squares line for pairs of d_0 and ion-exchange period of the other SOWGs. Moreover, the n_1 and n_2 values of the 30-min SOWG were postulated to be the same as those of the 1-h SOWG for the following reason: the error in the measurement of the N_{eff} value increased for the SOWG with a longer ion-exchange period because the propagating light became more diffuse. For evaluating the vertical RI profiles in the figure, the following should be taken into account. First, the inverse WKB method should be considered as a rough approximation method [3,11]. As the method can provide information on only a few points, it is not sufficient for the precise determination of the vertical RI profile. Second, the vertical RI profile may not be uniform in the SOWG. Nevertheless, the present results were consistent with those in the literature. Nishihara et al. [15] and Itoh and Fujishima [3] also applied the inverse WKB method to obtain the vertical RI profile of K^+-doped SOWGs. Although their ion-exchange conditions and slide glasses used were slightly different from ours, the present results were consistent with theirs, i.e., the RI difference between guiding layer and substrate $\Delta n = 0.01$–0.014 ($\Delta n = n_2 - n_1$ in Fig. 5) and d_0 (3.5 and 8.0 μm for SOWGs with 2- and 4-h ion exchange at 673 K, respectively) [3,15].

Characteristics of SOWG as an absorption cell

The values of L_{eff} and S/cm and also N_{refl} obtained in this study are summarized in Table 1. The calculated L_{eff}s were in good agreement with the experimental values, considering that the inverse WKB method is a rough approximation, as mentioned above. Among the K^+-doped SOWGs tested, the SOWG with a 30-min ion-exchange process supported only one mode, and its

TABLE 1

Observed and calculated effective path lengths (L_{eff}), relative sensitivities (S/cm) and reflection numbers (N_{refl}/cm) of K^+-doped SOWGs

Ion-exchange process	Mode	L_{eff} (μm)		S/cm [a]	N_{refl}/cm [a]
		Calc.	Obs.		
30 min	TE_0	13.6	6.5	214	166
1 h	TE_0	7.9	4.1	114	93
	TE_1	6.9	6.3	98	60
2 h	TE_0	2.1	2.8	30	43
	TE_1	2.9	3.1	42	35
	TE_2	2.9	3.4	41	29
30 min	TM_0	9.7	11	151	202
1 h	TM_0	9.5	5.1	135	97
	TM_1	9.4	5.3	138	69
2 h	TM_0	3.5	4.2	28	45
	TM_1	3.7	6.0	52	38
	TM_2	2.4	4.2	51	29

[a] Calculated values.

TM_0 (transverse magnetic) mode provided the longest L_{eff} of 11 μm in the experiment. However, the L_{eff} of the TE_0 (transverse electric) mode of the 30-min SOWG gave the longest L_{eff} in calculation. This discrepancy may also arise from an error in estimating the vertical RI of the 30-min SOWG, because the inverse WKB method could not be directly applied to the 30-min SOWG, as mentioned above. Nevertheless, the results in Table 1 demonstrate the usefulness of the present method to estimate roughly the L_{eff}. Moreover, Itoh and Fujishima [3] experimentally gave 45/cm as the S value for their K^+-doped SOWG with 2 h of ion exchange at 673 K, which is in good agreement with our calculated S value (52/cm for TM_1 mode) of the SOWG with a 2-h ion-exchange process. As shown in Table 1, the SOWG with the shorter ion-exchange process gave the longer L_{eff}. As the thickness of doped layer d_0 (guiding layer) was almost proportional to the ion-exchange time (see Fig. 1), the SOWG with the shorter ion exchange time had the greater N_{refl} value, as shown in Table 1, resulting in a longer L_{eff}.

As mentioned in the Appendix, the S/cm value shows the relative sensitivity of the SOWG method with respect to conventional absorption spectrometry in which perpendicular irradiation with source light is applied to the glass surface. Thus, the SOWGs in this study can provide one to two orders of magnitude higher sensitivity than conventional absorption spectrometry, although they are still less sensitive than Ta_2O_5 and $FePO_4$ SOWGs, which have a greater Δn (RI difference between guiding layer and substrate) than the K^+-doped SOWG [4,16]. The K^+-doped SOWG has various analytical advantages, e.g., ease and cheapness of preparation and high transmissivity of propagating light. Nevertheless, another type of SOWG is required for further improvements in the sensitivity. The dependence of S/cm on RI and the thickness of the guiding layer was calculated according to Swalen et al. [1] for a step index SOWG whose RI changes stepwise between the guiding layer and the substrate. As is shown in Fig. 2, an amplification of up to ca. 3×10^4 in sensitivity could be achieved if the

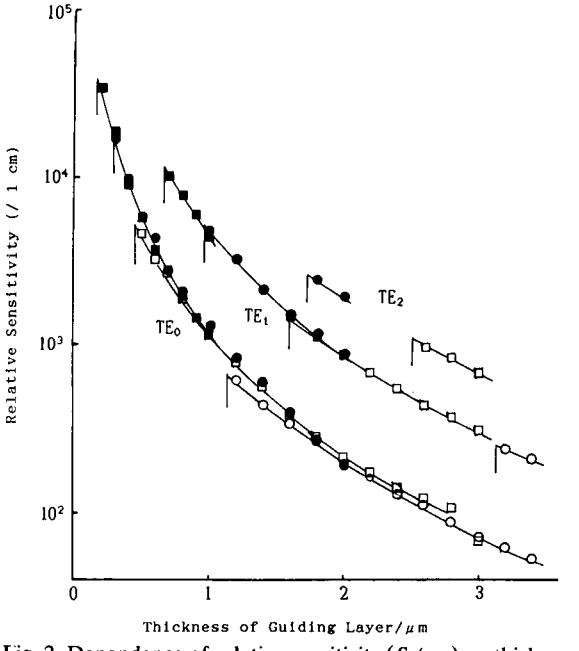

Fig. 2. Dependence of relative sensitivity (S/cm) on thickness and refractive index of guiding layer in step index SOWG. The S values were calculated according to Swalen et al. [1] under the following conditions: n_1 (RI of substrate) = 1.512 (soda-lime glass); n_3 (RI of sample solution) = 1.333 (water); λ = 632.8 nm; n_2 (RI of guiding layer) = (○) 1.520, (□) 1.540, (●) 1.580 and (■) 1.640.

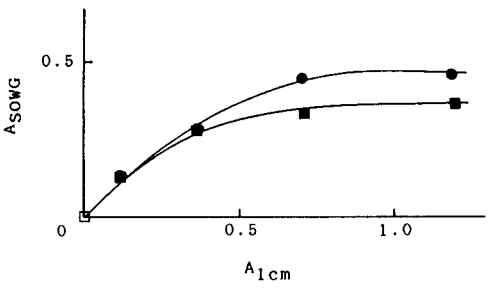

Fig. 3. Absorbance response of SOWG with and without ODS to Methylene Blue solutions. ■ = Non-ODS–SOWG; ● = ODS–SOWG. A_{SOWG} = absorbance obtained with the SOWG detector; $A_{1\text{-cm}}$ = absorbance obtained with a conventional spectrophotometer (1-cm cell). Sample volume, 0.5 cm^3; flow-rate, 1.0 cm^3 min^{-1}. The propagated light of TM_0 of the K^+-doped SOWG with a 30 min ion-exchange process was used for the absorption measurements.

guiding layer of the SOWG were thinner and had a higher RI.

Detection of methylene blue

In a previous paper [9], the blue dye Coomassie Brilliant Blue G-250, which is strongly adsorbed on the ODS–SOWG, could be detected with the ODS–SOWG detector with a sensitivity for a sample of 200 μl comparable to that of a conventional spectrophotometer (1-cm cell). In this work, this approach was extended to the detection of trace amounts of Methylene Blue. Although Itoh and Fujishima [3] used Methylene Blue as an oxidation–reduction indicator in their application of SOWG to spectroelectrochemistry, the potential of the ODS–SOWG for the determination of Methylene Blue has not been evaluated. Thus, Methylene Blue was measured by flow analysis with the SOWG detector.

Figure 3 shows the absorbance response of the SOWG detectors with and without ODS to 0.5 cm^3 of Methylene Blue standard solutions whose absorbances are in the range 0.1–1.2 at 632.8 nm with a conventional spectrophotometer (path length = 1 cm). Although 0.5 cm^3 of the Methylene Blue solutions gave sensitivities with non-ODS- and ODS–SOWG detectors comparable to that with a 1-cm cell, the calibration graphs were non-linear in both instances. The ODS modification did not improve the situation. The adsorption of Methylene Blue to the non-ODS–SOWG may be caused by the cation-exchange properties of the glass surface owing to silanol groups. On the other hand, the sensitivity for Methylene Blue was considerably improved with the addition of sodium lauryl sulphate in the ODS–SOWG detector, whereas no improvement was observed with the non-ODS–SOWG detector, as shown in Fig. 4. An ion pair of Methylene Blue and lauryl sulphate might be partitioned to the ODS phase of the SOWG as in ion-pair reversed-phase HPLC. The absolute sensitivity of the SOWG detector (defined as 1% absorption) was estimated to be 1.8×10^{-13} mol for methylene blue from Eqn. 7 in the Appendix, to which $\epsilon = 3.3 \times 10^4$ dm^3 mol^{-1} cm^{-1}, $a_s = 4.5 \times 10^{-4}$ dm^3 cm^{-1} and $S/1.5$ cm = 340 were applied.

Conclusion

The longest L_{eff} value of 11 μm was observed with the TM_0 mode of the SOWG with a 30-min ion-exchange process, which was in good agreement with the calculated value of 9.7 μm. The K^+-doped SOWGs provides by one to two orders of magnitude higher sensitivity than conventional absorption spectrometry. Moreover, the ODS

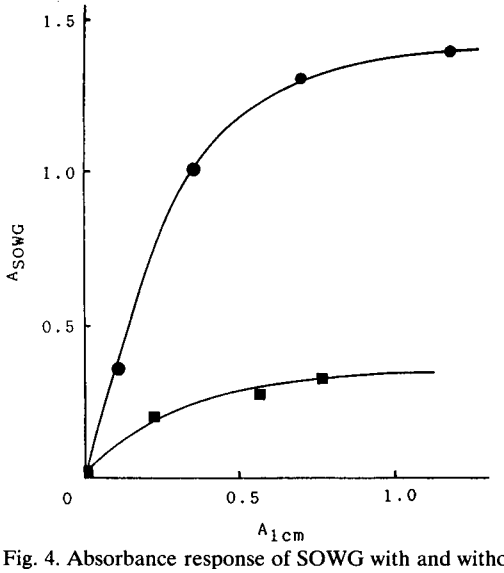

Fig. 4. Absorbance response of SOWG with and without ODS to Methylene Blue solutions with the addition of sodium lauryl sulphate. ■ = non-ODS–SOWG; ● = ODS–SOWG. Measurement conditions in Fig. 3.

modification of the SOWG surface was effective for the sensitive detection of Methylene Blue, when an ion pair of Methylene Blue and lauryl sulphate was formed. As the ODS–SOWG detector show almost no sensitivity to the sample matrix in solution [9], it can introduce high selectivity to the spectrophotometric detection of Methylene Blue. Although the present method has not yet been applied to practical samples, the ODS–SOWG may provide a highly sensitive and selective technique for the spectrophotometric determination of Methylene Blue.

APPENDIX

Effective path length (L_{eff})

When the SOWG detector is used for absorption measurements of liquid samples, L_{eff} is defined according to the Lambert–Beer law as

$$A_{\mathrm{SOWG}} = \epsilon c L_{\mathrm{eff}} \tag{1}$$

where A_{SOWG} = absorbance obtained with the SOWG detector, ϵ = molar absorptivity of the analyte ($\mathrm{dm^3\ mol^{-1}\ cm^{-1}}$) and c = concentration of analyte ($\mathrm{mol\ dm^{-3}}$).

In the SOWG, only the evanescent wave of propagating light is absorbed by liquid samples. Hence the L_{eff} of the SOWG is much shorter than its physical cell length. When the physical cell length is 1 cm, L_{eff} is expressed as

$$L_{\mathrm{eff}} = l_{\mathrm{o}} N_{\mathrm{refl}} \tag{2}$$

where l_{o} is the effective path length per reflection of the propagating light at the liquid/SOWG interface.

For the TE mode,

$$l_{\mathrm{o}} = \frac{\lambda n_1^2 \sqrt{n_2^2 - N_{\mathrm{eff}}^2}}{\pi (n_2^2 - n_1^2) \sqrt{N_{\mathrm{eff}}^2 - n_1^2}} \tag{3}$$

where N_{refl} is the reflection number per 1 cm of propagating light at the liquid/SOWG interface and λ is the wavelength of the source light. The meaning of other notations is given in Fig. 5.

Relative sensitivity (S / cm)

The ratio of the sensitivity of the SOWG technique (unit length of the physical cell) to that of the light absorption with perpendicular irradiation for adsorbed analytes on to the SOWG surface is defined as S/cm. Thus, the following equation is satisfied;

$$A_{\mathrm{SOWG}} = \epsilon n S / a_{\mathrm{s}} \tag{4}$$

where n = total amount of analyte (mol) and a_{s} = area of the SOWG surface ($\mathrm{dm^3\ cm^{-1}}$).

According to Swalen et al. [1], S/cm is expressed as

$$S = s_{\mathrm{o}} N_{\mathrm{refl}} \tag{5}$$

where s_{o} = relative sensitivity per reflection of the propagated light at the liquid/SOWG interface.

For the TE mode,

$$s_{\mathrm{o}} = \frac{4 n_1 \sqrt{n_2^2 - N_{\mathrm{eff}}^2}}{n_2^2 - n_1^2} \tag{6}$$

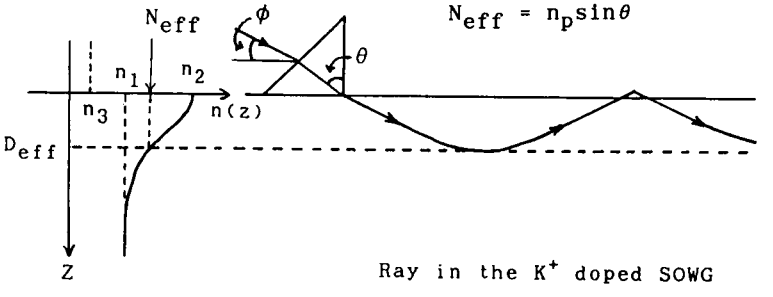

Fig. 5. Diagrams of vertical refractive index profile and ray of K^+-doped SOWG. n_1 = RI of substrate; n_2 = RI of SOWG surface; n_3 = RI of sample; n_{p} = RI of coupler prism; N_{eff} = effective RI; D_{eff} = effective depth.

From Eqns 2, 3, 5 and 6, the following equation is satisfied:

$$L_{\text{eff}} = d_p S \quad (7)$$

where,

$$d_p = \lambda / 4\pi\sqrt{N_{\text{eff}}^2 - n_1^2} \quad (8)$$

and d_p is the depth of penetration of the evanescent wave into the sample solution [14]. In this work, the thickness of the analyte layer on the SOWG surface is considered to be negligible.

REFERENCES

1 J.D. Swalen, M. Tacke, R. Santo, K.E. Rieckhoff and J.F. Fischer, Helv. Chim. Acta, 61 (1978) 960.
2 P.W. Bohn, Prog. Anal. Spectrosc., 12 (1989) 41.
3 K. Itoh and A. Fujishima, J. Phys. Chem., 92 (1988) 7043.
4 M.D. Degrandpre, L.W. Burgess, P.L. White and D.S. Goldman, Anal. Chem., 62 (1990) 2012.
5 S.S. Saavedra and W.M. Reichert, Anal. Chem., 62 (1990) 2251.
6 C. Piraud, E. Mwarania, G. Wylangowski, J. Wilkinson, K. O'Dwyer and D.J. Schiffrin, Anal. Chem., 64 (1990) 651.
7 T. Hara, K. Hashimoto, K. Itoh, M. Murabayashi and A. Fujishima, Abstracts of the 61st Annual Meeting of the Chemical Society of Japan, Yokohama, 1991, p. 3.
8 S.J. Choquette, L. Locascio-Brown and R.A. Durst, Anal. Chem., 64 (1992) 55.
9 K. Tsunoda, H. Itabashi and H. Akaiwa, Bull. Chem. Soc. Jpn., 65 (1992) 1581.
10 D.G.I. Kingston and B.B. Gerhart, J. Chromatogr., 116 (1992) 82.
11 J.M. White and P.F. Heidrich, Appl. Opt., 15 (1976) 151.
12 K. Itoh, H. Niikura, O. Odawara and M. Murabayashi, Jpn. J. Appl. Phys. I, 30 (1991) 3416.
13 H. Nishihara, M. Haruna and T. Suhara, Optical Waveguides, Ohm-sha, Tokyo, 1985, p. 25.
14 N. J. Harrick, Internal Reflection Spectroscopy, Harrick, New York, 1987.
15 H. Nishihara, M. Haruna and T. Suhara, Optical Waveguides, Ohm-sha, Tokyo, 1985, p. 153.
16 K. Itoh and M. Madou, J. Appl. Phys., 69 (1991) 7425.

Analytica Chimica Acta, 276 (1993) 141–149
Elsevier Science Publishers B.V., Amsterdam

Simultaneous determination of 2-furfuraldehyde, 5-hydroxymethylfurfuraldehyde and malonaldehyde in mixtures by derivative spectrophotometry and partial least-squares analysis

A. Espinosa-Mansilla, A. Muñoz de la Peña and F. Salinas

Department of Analytical Chemistry, University of Extremadura, 06071 Badajoz (Spain)

M. Martínez-Galera

Department of Analytical Chemistry, Experimental Sciences Faculty of Almeria, University of Granada, 04071 Almeria (Spain)

(Received 27th March 1992; revised manuscript received 3rd September 1992)

Abstract

2-Furfuraldehyde, 5-hydroxymethylfurfuraldehyde and malonaldehyde are known to react with 2-thiobarbituric acid when heated in an acidic medium. A study of the influence of several chemical and physico-chemical variables on the reaction was undertaken. The products of reaction show high absorption in the visible spectral region with several degrees of overlapping. The resolution of ternary mixtures of these compounds was accomplished by several chemometric approaches. A comparative study of the results obtained for simultaneous determinations in mixtures by using derivative spectrophotometry and partial least-squares analysis is presented. The multi-wavelength factor analysis-based method is demonstrated to be the method of choice for the multi-component analysis of ternary mixtures of these compounds.

Keywords: UV–Visible spectrophotometry; Aldehydes; Derivative spectroscopy; Furfuraldehyde; Hydroxymethylfurfuraldehyde; Malonaldehyde; Partial least squares

Malonaldehyde (MLD) or substances with properties very similar to it ("malonaldehyde-like" substances) occur in many biological samples such as peroxidized tissues, cells and cell fractions [1]. Several compounds other than MLD are produced in peroxidized biological samples, such as several carbonyl compounds (2-furfuraldehyde, 5-hydroxymethylfurfuraldehyde, 4-hydroxy-*trans*-non-2,3-enal, etc.) [2]. The aldehydes appear to be involved in the formation of age pigments, and there have been reports that they have mutagenic properties and may be chemical carcinogens [3].

MLD measurements serve as an indicator of free radical damage in lipid peroxidation reactions [4]. An increase in the lipid peroxidation susceptibility of the erythrocyte membrane has been described in hematological disorders and in abetalipoproteinaemia and tocopherol deficiency [5].

Non-enzymatic degeneration is considered to be one of the major causes of the production of

Correspondence to: F. Salinas, Department of Analytical Chemistry, University of Extremadura, 06071 Badajoz (Spain).

several aldehydes. 5-Hydroxymethyl-2-furfuraldehyde (HMF) is the principal decomposition product of the acid-catalysed hydrolysis of hexoses and 2-furfuraldehyde (FUR) is the principal product of the hydrolysis of ascorbic acid by means of the Strecker mechanism [6]. Several techniques have been proposed for the determination of these compounds. The spectrophotometric methods proposed have in common that they do not differentiate between these compounds and need a previous separation step.

The most generally used procedure for determining MLD is the 2-thiobarbituric acid (TBA) method [7,8]. Stocks and Dormandy [9] adapted the MLD–TBA reaction for the measurement of human red cell lipid autoxidation induced by hydrogen peroxide and their assay has become standard for the determination of the susceptibility of red blood cells to lipid peroxidation.

TBA has been also employed as a photometric reagent for the determination of FUR and HMF [10] and for the simultaneous determination of both compounds [11].

Several compounds present in diverse biological materials, such as sucrose–acetaldehyde-degraded products, HMF, FUR, biliverdin and glyoxal, react on heating with TBA to give absorbing compounds [2]. For this reason, a distillation step has commonly been used in the analysis of food samples [12].

The need for analyses of substances such as body fluids, foods, and enviromental samples is continuously increasing. Chemical separation of the various components of complex samples prior to analysis is usually time consuming and often unsuccesful. An analysis that requires little or no separation is far more appealing.

In order to avoid time-consuming clean-up procedures, attempts to resolve complex spectra by using instrumental approaches or various chemometric methods have been made. Derivative techniques and multivariate statistical analysis, such as partial least squares (PLS), have been successfully applied to the multi-component analysis of mixtures by spectroscopy [13,14]. Both approaches are useful for the reduction of band overlapping errors in quantitative analysis. Both derivative and PLS methods presume that there is a linear relationship between absorbance and component concentrations. Each method has a calibration step in which the relationship between the spectra and the component concentrations is elucidated from a set of reference samples. This step is followed by a prediction step in which the results of the calibration are used to calculate the component concentrations from an "unknown" sample spectrum [15].

In this work, both derivative and PLS methods were applied to the simultaneous determination of the components of ternary mixtures of MLD, FUR and HMF by using the TBA reaction, and the quantitative prediction abilities of these two approaches were compared.

EXPERIMENTAL

Apparatus

A Beckman DU-50 spectrophotometer connected via an RS-232 to an Olivetti PC 286 microcomputer was used for all absorption measurements. Beckman Data Leader Software, Version 3.0 [16], was used for spectral acquisition, storage, manipulation and analysis of the spectrophotometric data. Differentiation was performed by the simplified least-squares procedure of Savitzky and Golay [17]. The Lab Calc software package, Version A 1.01, and the PLSplus Version 2.0 Application software [18] were used for the statistical treatment of the data and the application of the PLS-2 method. A Selecta Unitronic 320 OR thermostated bath was used for temperature control.

Reagents

All experiments were performed with analytical-reagent grade chemicals. Doubly distilled and demineralized water was used. Solutions of 0.01% (w/v) HMF, FUR and Standard 1,1,3,3-tetraethoxypropane (TET) were prepared by dissolving 0.01 g of the reagent (Sigma) in 100 ml of water. Malonaldehyde was prepared by generation in situ from TET in acidic medium. A 0.03 M standard solution of TBA was prepared by dissolving 0.4503 g of reagent (Sigma) in 100 ml of water and sonicating for 20 min.

Malonaldehyde generation

Malonaldehyde was obtained from TET in acidic medium. A study of the influence of reaction time and hydrochloric acid concentration on the MLD generation reaction at room temperature was undertaken. The rate of MLD generation depends on the acid concentration in the medium. The product of reaction shows a maximum at 244 nm and constant absorption for reaction times longer than 5 min when [HCl] = 1 M. A reaction time of 7 min and [HCl] = 1 M are sufficient for proper development of the reaction. A calibration graph was obtained from absorbance measurements for MLD from standards containing up to 7.0 μg ml^{-1} of TET to test that the MLD generation is quantitative in this concentration range.

Derivative method

In a 25-ml volumetric flask, introduce an aliquot of the sample solution containing between 12.5 and 100 μg of HMF, between 12.5 and 100 μg of FUR and between 7.5 and 130 μg of MLD. Add 8.5 ml of concentrated hydrochloric acid and 7 ml of 0.03 M TBA solution, heat at 40°C for 60 min and dilute to the mark with water. Record the absorption spectra between 300 and 600 nm against a solution containing the same amount of TBA and hydrochloric acid as the blank. Obtain the first-derivative spectra with a band width of 15 nm. For FUR determination take the analytical signal as the vertical distance from the first-derivative absorption spectrum at 436 nm ($^1D_{436}$) to the baseline. For MLD determination, take the amplitude between the maximum at 523 nm to the minimum at 545 nm ($^1D_{523,545}$). The vertical distance from the first-derivative absorption spectrum at 414 nm ($^1D_{414}$) to the baseline is the sum of HMF (positive contribution) plus MLD (negative contribution). HMF is calculated by difference.

PLS method

In a 25-ml volumetric flask, introduce an aliquot of the sample solution containing between 25 and 125 μg of HMF, between 25 and 125 μg of FUR and between 25 and 125 μg of MLD. Add 8.5 ml of concentrated hydrochloric acid, 7 ml of 0.03 M TBA solution, heat at 40°C for 60 min and dilute to the mark with water. Record the absorption spectra between 300 and 600 nm against a solution containing the same amount of TBA and hydrochloric acid as the blank. Prepare a calibration matrix with mixtures of the three components, according to the ratios shown in Fig. 4. Apply the optimized calibration matrix, calculated by the application of the PLS-2 method, to analyse the spectra obtained and to calculate the concentrations of the three components of the mixture.

RESULTS AND DISCUSSION

Optimization of chemical variables

In a previous study [11], the influence of several chemical variables on the reaction of TBA with FUR and HMF was investigated. A method was proposed for their simultaneous determination in binary mixtures by derivative spectrophotometry. The use of this approach allowed the resolution of the spectral overlapping shown by the TBA derivatives of FUR and HMF. The method was sucessfully applied to the determination of FUR and HMF in food and pharmaceutical preparations. For the determination of these compounds, the optimum conditions established were [HCl] = 4 M, [TBA] = 8.4×10^{-3} M, heating time = 30 min and heating temperature = 40°C.

With the aim of investigating the possibility of determining FUR, HMF and MLD in ternary mixtures, the derivatization reaction of MLD was studied under the conditions previously established for FUR and HMF derivatives. Concentrations of hydrochloric acid higher than 4 M are not recommended because the product of reaction of FUR with TBA is unstable.

Effect of temperature and heating time on the MLD–TBA reaction

At [HCl] = 4 M, the MLD–TBA product of reaction shows two maxima located at 394 and 532 nm (Fig. 1). The absorbance at 394 nm increases with increase in temperature up to 35°C; increases in temperature above 35°C do not fur-

ther affect the absorbance of that maximum. The absorbance at 532 nm increases dramatically as the temperature increases, fitting an exponential curve. Although increasing the temperature notably favours the derivatization reaction of MLD, a temperature of 40°C was selected because of the instability of the product of reaction of FUR with TBA above 50°C [11]. The absorbance at 394 nm increases as the reaction time increases, reaching a constant value for periods of heating longer than 60 min, whereas the absorbace at 532 nm increases as the heating time increases following an exponential curve. A heating time of 60 min was chosen as the optimum for the development of the reaction, to increase the sensitivity of the reaction of MLD with TBA, taking into account that the products of reaction of FUR and HMF are not affected by longer periods of heating [11]. As the effects of temperature and heating time are critical, careful control of these two variables is necessary.

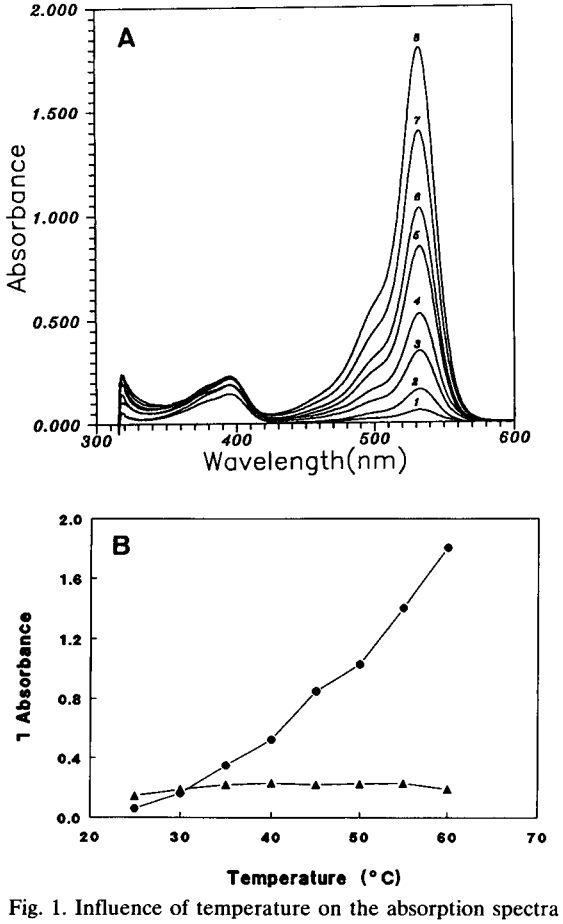

Fig. 1. Influence of temperature on the absorption spectra of the product of reaction of TBA with MLD. [HCl] = 4 M; heating time = 30 min. (A) 1 = 25; 2 = 30; 3 = 35; 4 = 40; 5 = 45; 6 = 50; 7 = 55; 8 = 60°C. (B) λ = (▲) 394 and (●) 532 nm.

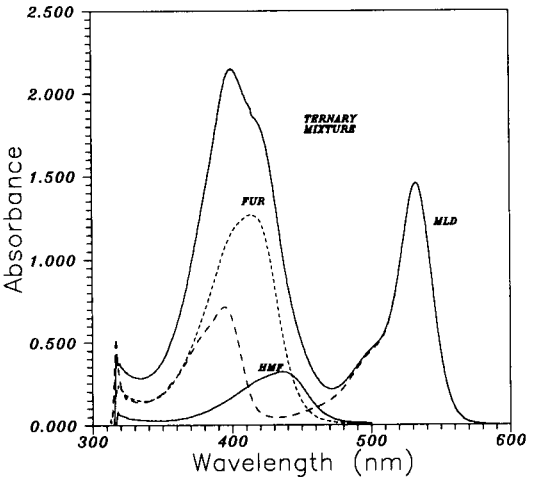

Fig. 2. Absorption spectra of TBA reaction products with FUR (4 μg ml^{-1}), HMF (3 μg ml^{-1}) and MLD (4 μg ml^{-1}), and of a mixture of the three components.

Absorption spectral characteristics and first-derivative spectra

Under the optimum conditions selected, the MLD derivative shows two absorption maxima at 394 and 532 nm. On the other hand, the FUR derivative shows an absorption maximum at 414 nm and the HMF derivative one at 436 nm. The spectral bands are broad and considerably overlapped, which precludes the possibility of the simultaneous determination of these compounds by conventional spectrophotometry. In Fig. 2, the absorption spectra of FUR, HMF and MLD in the presence of TBA and of a mixture of the three compounds are shown.

Figure 3 shows the first derivatives of the absorption spectra of the products formed by FUR, HMF and MLD with TBA. Because of the closeness of the three overlaping spectra, they are not sufficiently well resolved to generate three

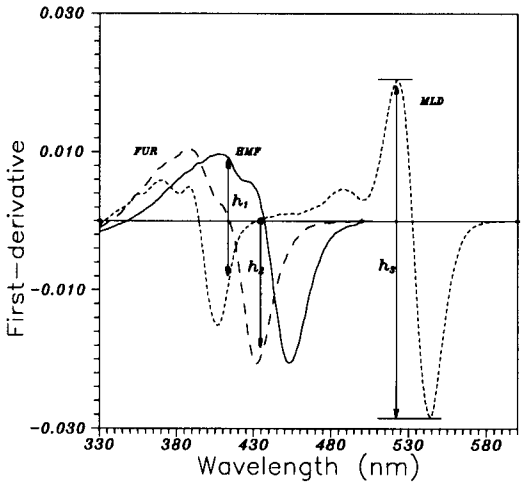

Fig. 3. First-derivative spectra of TBA reaction products with FUR (4 μg ml^{-1}), HMF (3 μg ml^{-1}) and MLD (4 μg ml^{-1}). Selection of the analytical signals used in the derivative method for resolution of the mixture.

distinct peaks in the first-derivative spectra of the mixture.

In general, derivative techniques are sucessfully applied to the resolution of binary mixtures of compounds. More complicated mixtures usually cannot be resolved by differentiation. In this particular instance, it can be observed that in the reaction with TBA, MLD presents an absorption maximum at 532 nm, where FUR and HMF do not absorb. As a consequence, at this wavelength the amplitude of the derivative signal between the maximum at 523 nm and the minimum at 545 nm ($^1D_{523,545}$) must depend only on the MLD concentration (h_3). On the other hand, at 436 nm ($^1D_{436}$), the derivative signals from MLD and HMF are zero, whereas FUR presents a minimum in its derivative profile, which can be used to determine the contribution of FUR to the ternary mixture (h_2).

Although in the first-derivative spectrum of the mixture no wavelength at which the signal is due only to HMF–TBA is observed, HMF could be determined as follows. At 414 nm, the first-derivative signal from the FUR contribution is zero and, as a consequence, the amplitude (h_1) of the derivative signal of a mixture of these compounds is proportional to the contributions from HMF plus MLD. The contribution of HMF is positive (h_1'), the contribution from MLD is negative (h_1'') and the total signal is $h_1 = h_1' + h_1''$. As the MLD concentration can be independently calculated from h_3, HMF can be calculated at 414 nm by difference.

Determination of FUR, HMF and MLD in mixtures by derivative spectrophotometry

Calibration graphs were obtained from height (h) measurements for standards containing between 0.5 and 4.0 μg ml^{-1} of FUR, between 0.5 and 4.0 μg ml^{-1} of HMF and between 0.3 and 5.2 μg ml^{-1} of MLD. The calibration graphs were obtained by taking the amplitudes $^1D_{436}$ for FUR, $^1D_{523,545}$ and $^1D_{414}$ for MLD and $^1D_{414}$ for HMF. In Table 1, the statistical data for the calibration lines obtained are summarized. The correlation coefficients indicate the good linearity of all the calibration graphs of the first-derivative measurements. In Table 2, the results of the analysis of mixtures of these compounds in different proportions are summarized. It can be seen that the results obtained by applying this approach were not satisfactory.

Partial least-squares method

The PLS method is a full-spectrum method with the advantages of signal averaging as in other full-spectrum methods such as principal components regression (PCR) and classical least squares (CLS) [19]. Multivariate calibrations are more powerful than methods based on measurement at only one wavelength, such as spectral differentiation, because the simultaneous inclu-

TABLE 1

Statistical parameters in the determination of FUR, HMF and MLD by the derivative method

Analytical signal	Component	Equation [a]	Linear regression coefficient
$^1D_{523,545}$	MLD	$h_3 = +0.0132$[MLD] $- 0.004$	0.9973
$^1D_{414}$	MLD	$h_1'' = -0.0022$[MLD] $- 0.000$	0.9996
$^1D_{436}$	FUR	$h_2 = -0.0061$[FUR] $- 0.000$	0.9985
$^1D_{414}$	HMF	$h_1' = +0.0024$[HMF] $+ 0.000$	0.9950

[a] Concentration units are μg ml^{-1}.

TABLE 2

Results obtained for the analysis of ternary mixtures by the derivative method

Ternary mixture	[FUR] (μg ml^{-1})		Relative error (%)	[HMF] (μg ml^{-1})		Relative error (%)	[MLD] (μg ml^{-1})		Relative error (%)
	Actual	Found		Actual	Found		Actual	Found	
M1	1.00	0.44	56	5.00	3.90	22	5.00	3.71	26
M2	2.00	1.44	28	4.00	3.97	1	5.00	4.78	44
M3	3.00	2.46	18	3.00	2.77	8	5.00	4.75	5
M4	4.00	3.54	12	2.00	1.74	13	5.00	4.86	3
M5	5.00	4.51	10	1.00	1.08	8	5.00	5.27	5
M6	5.00	4.26	15	2.00	1.90	5	4.00	4.63	16
M7	5.00	4.05	19	3.00	2.17	28	3.00	3.69	23
M8	5.00	3.84	23	4.00	1.57	60	2.00	2.53	26
M9	5.00	3.56	29	5.00	3.44	31	1.00	1.57	57
M10	4.00	2.77	31	5.00	3.43	31	2.00	2.83	41
M11	3.00	1.90	37	5.00	5.04	1	3.00	3.95	32
M12	2.00	1.02	49	5.00	5.83	17	4.00	5.05	26
M13	4.00	2.82	30	4.00	4.12	3	3.00	4.32	44
M14	3.00	1.93	35	4.00	5.36	34	4.00	5.62	41
M15	4.00	2.90	28	3.00	4.29	43	4.00	5.59	40
M16	3.75	2.51	33	3.75	5.15	37	3.50	5.30	51
M17	4.50	3.05	32	4.50	3.77	16	2.00	3.25	63
M18	4.50	3.20	29	3.50	4.25	21	3.00	4.60	53
M19	3.50	2.33	33	3.50	5.48	56	4.00	6.16	54
M20	3.50	2.15	39	4.50	3.06	32	3.00	4.79	68

sion of multiple spectral intensities can greatly improve the precision and applicability of quantitative spectral analysis of mixtures. The PLS-2 method was applied to the determination of FUR, HMF and MLD in ternary mixtures on the basis of the TBA reaction.

Experimental design of the calibration matrix

A training set of fifteen samples was taken from a mixture design [20] to maximize statistically the information content in the spectra, and the absorption spectra were recorded under the chemical conditions selected as optima. The samples in the calibration set were labelled M1–M15. Figure 4 illustrates the mixture calibration design in the concentration range examined. Each component concentration was constrained to be between 1 and 5 μg ml^{-1}. Properly designed calibration sets should, in general, yield more precise results. The spectral region between 338 and 513 nm, which implies working with 475 experimental points per spectrum, was selected for analysis, because this is the zone with the maximum spectral information from the components of the mixtures.

Selection of the optimum number of factors for the partial least-squares method

To select the number of factors in the PLS algorithm, to model the system without overfit-

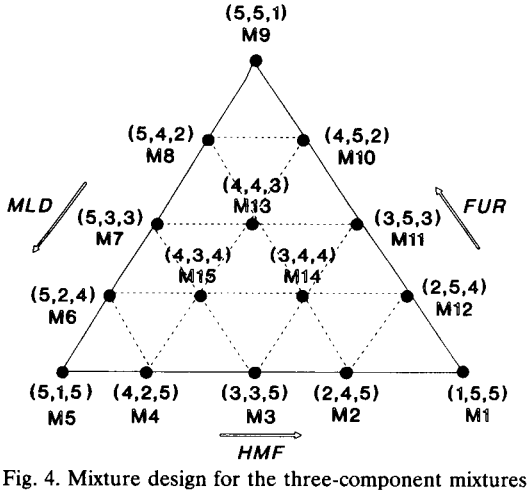

Fig. 4. Mixture design for the three-component mixtures used in the data set for the PLS-2 method. Numbers in parentheses correspond to the concentrations of FUR, HMF and MLD (μg ml^{-1}) in the mixtures.

TABLE 3

Statistical PRESS and F parameters

Factor	PRESS	$F_{calc.}$	Probability ($F \leqslant F_{calc.}$)
0	70.0000	502.256	1.00
1	51.2952	368.047	1.00
2	0.4164	2.987	0.98
3	0.3714	2.665	0.96
4	0.3005	2.156	0.92
5	0.1410	1.012	0.51
6	0.1394	1.000	0.50
7	0.2010	0.000	0.00
8	0.2738	0.000	0.00

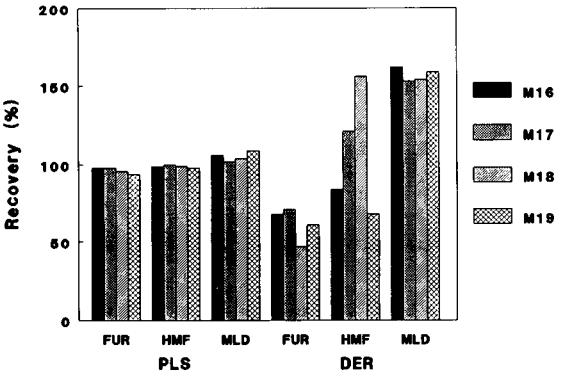

Fig. 5. Comparison of the predicted concentrations of FUR, HMF and MLD concentrations in four "unknown" samples (M16–M19) by derivative spectrophotometry and PLS-2 methods.

ting the concentration data, the cross-validation method leaving out one sample at a time was used [21]. Given the set of fifteen calibration spectra, the PLS-2 calibration on fourteen calibration spectra was performed and, using this calibration, the concentration of the sample left out during calibration was predicted. This process was repeated a total of fifteen times until each sample had been left out once. The concentration of each sample was then predicted and compared with the known concentration of this reference sample.

The prediction error sum of squares (PRESS) is a measure of how well a particular PLS model fits the concentration data. PRESS was calculated in the same manner each time a new factor was added to the PLS model. One reasonable

TABLE 4

Results obtained for the analysis of ternary mixtures by the PLS method

Ternary mixture	[FUR] (μg ml^{-1})		R.S.D. (%)	[HMF] (μg ml^{-1})		R.S.D. (%)	[MLD] (μg ml^{-1})		R.S.D. (%)
	Actual	Predicted [a]		Actual	Predicted [a]		Actual	Predicted [a]	
M1	1.00	1.04	3.4	5.00	4.97	0.8	5.00	4.99	0.7
M2	2.00	1.96	4.4	4.00	4.00	0.7	5.00	5.01	1.2
M3	3.00	2.96	1.3	3.00	3.06	1.5	5.00	4.98	1.5
M4	4.00	3.98	0.5	2.00	1.99	1.8	5.00	5.02	0.7
M5	5.00	5.11	0.2	1.00	0.96	4.0	5.00	4.93	0.8
M6	5.00	4.97	0.6	2.00	1.98	1.9	4.00	4.05	1.2
M7	5.00	5.03	0.2	3.00	3.00	0.1	3.00	2.98	0.7
M8	5.00	4.93	1.4	4.00	4.01	1.1	2.00	2.06	5.3
M9	5.00	4.85	4.0	5.00	4.95	1.2	1.00	1.62	3.0
M10	4.00	4.05	1.0	5.00	4.99	0.2	2.00	1.96	1.5
M11	3.00	3.07	0.7	5.00	4.98	0.3	3.00	2.95	1.0
M12	2.00	2.03	1.7	5.00	4.98	0.5	4.00	3.99	0.9
M13	4.00	3.95	0.3	4.00	4.02	0.6	3.00	3.02	1.1
M14	3.00	3.00	0.8	4.00	3.98	0.5	4.00	4.01	1.2
M15	4.00	3.97	1.1	3.00	3.04	1.5	4.00	4.01	1.5
M16 [b]	4.50	4.46	1.6	4.50	4.52	1.2	2.00	2.02	5.9
M17 [b]	4.50	4.63	6.9	3.50	3.42	5.2	3.00	2.98	3.0
M18 [b]	3.50	3.43	2.5	3.50	3.68	8.2	4.00	3.89	7.7
M19 [b]	3.50	3.40	3.1	4.50	4.48	1.6	3.00	3.12	7.0

[a] Average of three determinations. [b] Unknown samples.

choice for the optimum number of factors would be that number which yielded the minimum PRESS. However, PRESS calculation is based on a finite number of samples, and therefore it is subject to error. Hence, using the number of factors (h^*) that yields a minimum PRESS usually leads to some overfitting. A better criterion for selecting the optimum number of factors involves the comparison of PRESS from models with fewer than h^* factors. The model selected is that with the smallest number of factors such that PRESS for that model is not significantly greater than PRESS from the model with h^* factors. The F-statistic was used to make the significance determination. As the difference between the minimum PRESS and other PRESS values becomes smaller, the probability that each additional factor is significant becomes smaller. Haaland and Thomas [15] empirically determined that an F-ratio probability of 0.75 is a good choice. The number of factors for the first PRESS value whose F-ratio probability drops below 0.75 was selected as the optimum.

The maximum number of factors used to calculate the optimum PRESS was selected as 8 (half the number of standards + 1). In Table 3, the statistical results obtained for PRESS and F probability are summarized. A number of factors of 5 was selected as the optimum.

In Table 4, the results predicted by the PLS model for the training set model are summarized. Also, a set of four unknown problems were predicted by applying the PLS model calculated with five factors. As can be seen from the results, the PLS method gives very satisfactory results. In Fig. 5, the results are compared with those obtained by applying the derivative method.

Conclusions

A comparative study of the utilization of derivative and PLS approaches for the resolution of ternary mixtures of HMF, FUR and MLD has been accomplished. In a previous paper [22], a comparative study of the application of derivative and PLS approaches to the resolution of mixtures of carbaryl and chlorpyrifos was reported. It was demonstrated that derivative spectrophotometry can be applied to the resolution of simple binary mixtures, showing the same resolution capacity as more complex multi-component methods such as PLS. However, on dealing with more complicated mixtures, the higher resolution power of the multivariate method, compared to spectral differentiation, is evident.

Despite of the potential of the new methods of multi-component analysis, the development of new analytical methodologies is still slow because the application of these techniques requires a chemical knowledge about the samples to be analysed and the constituents to be determined, mathematical and statistical knowledge of data analysis and computer knowledge in order to implement new methods in an efficient form. The PLS approach used in this work is simple to perform, with adequate software support, and provides a clear example of the high resolving power of this technique.

This work was supported by the DGICYT of the Ministry of Education and Science of Spain (Project PB91-0856).

REFERENCES

1 W.A. Pryor, Free Rad. Biol., 1 (1982) 1977.
2 B. Halliwell and J.M. Gutteridge, Free Radicals in Biology and Medicine, Oxford University Press, Oxford, 1985.
3 H. Esterbauer, J. Lang, S. Zadranec and T.F. Slater, Methods Enzymol., 105 (1984) 320.
4 R.P. Bird, S.S. Hung, M. Hadley and H.H. Draper, Anal. Biochem., 128 (1983) 240.
5 J. Stocks, M. Kemp and T.L. Dormandy, Lancet, i (1971) 266.
6 G. Bonn and O. Bobletez, J. Radioanal. Chem., 79 (1983) 171.
7 R.O. Sinnhuber, I.C. Yu and T.C. Yu, Food Res., 23 (1958) 620.
8 J. Bartos and M. Pesez, Practique de l'Analyse Organique Colorimètrique et Fluorimètrique, Mason, Paris, 2nd edn., 1984.
9 J. Stocks and T.L. Dormandy, Br. J. Haematol., 20 (1971) 95.
10 S. Meydav and Z. Berck, J. Agric. Food Chem., 26 (1978) 282.
11 D. Tu, S. Xue, C. Meng, A. Espinosa-Mansilla, A. Muñoz de la Peña and F. Salinas, J. Agric. Food Chem., 40 (1992) 1022.
12 B.G. Tarladgis, B.M. Watts, M.T. Younathan and L.R. Dugan, Jr., J. Am. Oil Chem. Soc., 37 (1960) 44.

13 T.C. O'Haver, Anal. Chem., 51 (1979) 91A.
14 P. Geladi and B. R. Kowalski, Anal. Chim. Acta, 185 (1986) 1.
15 D.M. Haaland and E.V. Thomas, Anal. Chem., 60 (1988) 1193.
16 Data Leader Software Package, Beckman, Fullerton, CA, 1987.
17 A. Savitzky and M. J. E. Golay, Anal. Chem., 36 (1964) 1627.
18 Lab Calc Software Packcage, Galactic Industries, Salem, NH, 1989.
19 D.M. Haaland and R.G. Easterling, Appl. Spectrosc., 34 (1980) 539.
20 J.A. Cornell, Experiments with Mixtures, Wiley, New York, 1981.
21 M. Stone, J. R. Stat. Soc., B, 36 (1974) 111.
22 A. Espinosa-Mansilla, A. Muñoz de la Peña, F. Salinas and A. Zamoro, Anal. Chim. Acta, 258 (1992) 47.

Analytica Chimica Acta, 276 (1993) 151–160
Elsevier Science Publishers B.V., Amsterdam

Determination of thiamine (vitamin B_1) by in situ sensitized photochemical spectrofluorimetry

Xiang-Qun Guo, Jin-Gou Xu, Yu-Zhou Wu, Yi-Bing Zhao, Xian-Zhi Huang and Guo-Zhen Chen

Department of Chemistry, Xiamen University, Xiamen 361005 (China)

(Received 17th July 1992; revised manuscript received 21st October 1992)

Abstract

An in situ photochemical spectrofluorimetric flow-injection method for the determination of thiamine (vitamin B_1) is proposed. It is based on the conversion of thiamine in alkaline medium into an intensively fluorescent compound. The photochemical reaction is sensitized by acetone. The determination can be carried out by measuring the fluorescence intensity when the fluorescent signal reaches its maximum or at a fixed time. The calibration graph was linear up to 10.0 μg ml^{-1} thiamine ($r = 0.9996$), the limit of detection was 0.46 ng ml^{-1} thiamine and the relative standard deviation was 1.5% for 50.0 ng ml^{-1} thiamine ($n = 6$). The kinetic behaviour of the reaction and the effects of some experimental conditions were investigated and are discussed in detail. The mechanism of the sensitization of acetone was examined. Its application to vitamin B_1 tablets and injections was found to be satisfactory. By use of a selection valve and combination with a synchronous fluorescence technique, vitamin B_1, B_2 and B_6 in pharmaceuticals were simultaneously determined.

Keywords: Flow injection; Fluorimetry; Pharmaceuticals; Photochemical derivatization; Thiamine; Vitamin B_1

Thiamine (vitamin B_1), which occurs naturally in the bran coat of grains, in yeast and in meat, is essential in humans. It is necessary for carbohydrate metabolism, maintenance of normal neural activity and prevention of beri-beri. Since its discovery and isolation, numerous reports have appeared on the determination of thiamine by microbiological methods [1,2], spectrophotometry [3–6], chemiluminescence [7], selective membrane electrodes [8,9], micro-band electrodes [10], molecular emission cavity analysis [11], spectrofluorimetry [12], potentiometry [13,14] and thin-layer chromatography [15,16].

The most widely used method for the assay of thiamine is the so-called thiochrome method, which was first used by Jansen [12] in 1936 and which involves the reaction between thiamine and hexacyanoferrate(III) in alkaline solution and extraction of the thiochrome formed from the aqueous phase into an organic phase. This method, however, suffers from several disadvantages [17]. The amount of hexacyanoferrate(III) must be sufficient to oxidize thiamine, but a large excess is undesirable as it may result in the decomposition of thiochrome. The presence of other oxidizable materials in the sample complicates the choice of the proper amount of oxidant. The yield of the reaction is about 67%. Extraction of thiochrome with butan-2-ol is necessary to separate thiochrome from hexacyanoferrate(III), which quenches the fluorescence of thiamine. The addition of the oxidizing reagent, the mixing and extraction must be performed quickly and must be carefully standardized in order to be reproducible. Many papers have been published to improve the thiochrome method. Hg(II) [17–19] and BrCN [20–22] have been used as oxidants to

Correspondence to: X.-Q. Guo, Department of Chemistry, Xiamen University, Xiamen 361005 (China).

replace $K_3[Fe(CN)_6]$. In order to obtain reproducible results, flow-injection analysis (FIA) [18] and extraction based on the flow-injection principle [23] have been suggested. A procedure based on continuous addition of reagent was used to overcome the quenching problem caused by excess of $K_3[Fe(CN)_6]$ [24]. The thiochrome method has been applied to the determination of thiamine in many samples [15–18,24–29].

This paper presents a flow-injection method based on in situ photochemical spectrofluorimetry for the determination of thiamine. It is based on the photochemical reaction sensitized by acetone. Thiamine, a non-fluorescent compound, is converted in alkaline medium by the sensitized photochemical reaction into an intensively fluorescent compound, which has the same characteristic maxima of fluorescence excitation and emission spectra as those of thiochrome. The use of photons as the "reagent" has the advantage of being easily "added"to and "removed" from the reaction system, and therefore there are no problems caused by undesirable or dangerous reagents, such as the quenching problem caused by an excess of hexacyanoferrate(III) and environmental problems caused by the use of Hg(II) and BrCN. The use of the flow-injection method, has a beneficial effect on the reproducibility. The sensitized photochemical reaction takes place in situ (in an 18-μl flow cell) with irradiation by UV radiation from the light source of the spectrofluorimeter, so this method can be easily carried out with a commercial spectrofluorimeter and there is no need for a complicated photochemical reac-

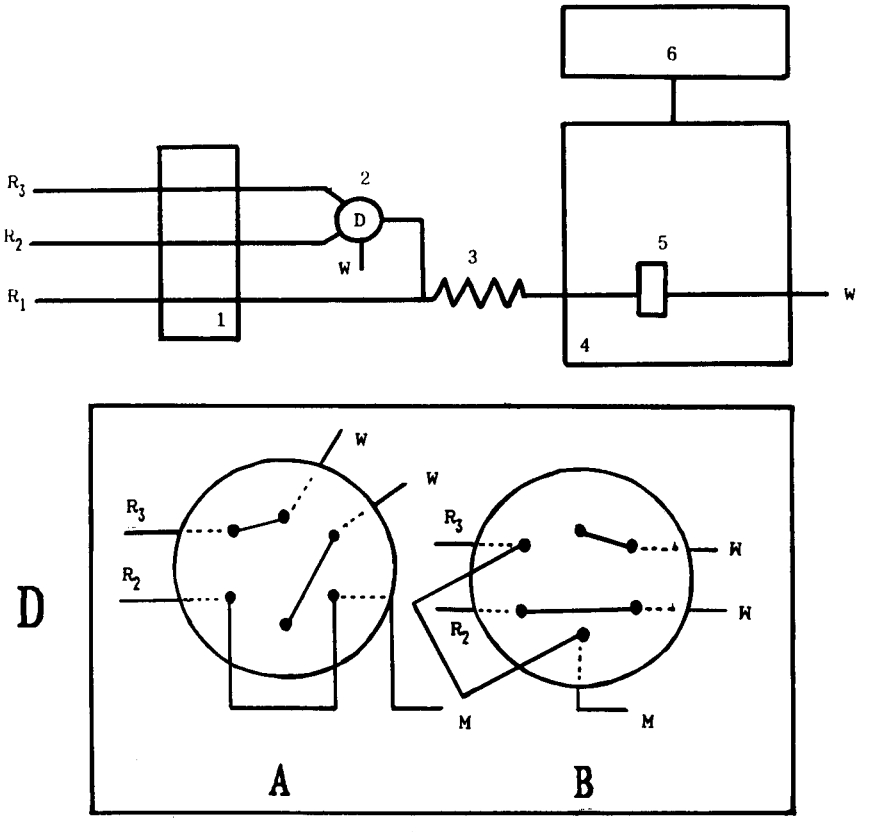

Fig. 1. Schematic diagram for the flow-injection method with in situ photochemical reaction and fluorescence measurement. R_1 = mixture of thiamine and acetone; R_2 = mixture of NaOH and Na_2SO_3; R_3 = pH 7.0 buffer solution; 1 = peristaltic pump; 2 (D) = diverging valve [in (A) R_1 merges with R_2; in (B) R_1 merges with R_3; W = waste; M = PTFE mixing tubing]; 3 = PTFE mixing tubing; 4 = spectrofluorimeter; 5 = 18-μl flow cell; 6 = recorder; W = waste solution.

tor [30] and an extra light source [31] as reported in other papers.

Chen et al. [32] reported a stopped-flow injection method for the photochemical–spectrofluorimetric determination of phenothiazine. In their method, the injected sample plug was propelled along a 50-cm reactor at a flow-rate of 2.0 ml min^{-1}, then halted in the flow cell and irradiated directly by excitation radiation, the irradiation and detection process taking place simultaneously. Because the wavelength of the most effective radiation for inducing a photochemical reaction is usually different from the wavelength of the most effective excitation, the use of radiation with the same wavelength for two purposes might cause a lower detection sensitivity. In the present experiments two light bands with different wavelengths were used, one as the radiation (λ_p) to induce a photochemical reaction and the other as the excitation radiation (λ_F) for fluorescence measurement. That is, radiation of λ_p was first used to irradiate the flow cell, and the photochemical reaction occurred right away. When the reaction reached equilibrium, the radiation wavelength was changed from λ_p to λ_F to measure the fluorescence intensity of the photochemical reaction product. In this way, good use is made of the source.

EXPERIMENTAL

Apparatus

All fluorescence measurements were made with a Hitachi 650-10S spectrofluorimeter equipped with a 125-W xenon lamp, an 18-μl flow cell and a peristaltic pump (made by ZHAOFA Automatic Analysis Research Institute, China). Absorption spectra were measured on a Beckman DU-8B spectrophotometer. The photochemical reaction was carried out in the flow cell after the peristaltic pump had been stopped. A schematic diagram of the set-up is shown in Fig. 1. D is a selection valve that allows mixing of R_1 with either R_2 or R_3. In position A R_1 merges with R_2, whereas in position B R_3 merges with R_1.

Reagents

Thiamine hydrochloride (vitamin B_1), riboflavin (vitamin B_2) and pyridoxine (vitamin B_6) were biochemical-grade reagents. All other reagents were of analytical-reagent grade and doubly deionized water was used. Stock solutions of B_1 (0.50 mg ml^{-1} in 0.01 mol l^{-1} hydrochloric acid), B_2 (0.010 mg ml^{-1} in 0.02 mol l^{-1} acetic acid) and B_6 (0.25 mg ml^{-1} in water) were stored in the dark.

A buffer solution of pH 7.0 was prepared by mixing citric acid (0.1 mol l^{-1}) and sodium dihydrogen phosphate (0.2 mol l^{-1}) in a volume ratio of 1:6 and adjusting the mixed solution to pH 7.0.

Sodium sulphite solution (2%) was prepared daily.

Procedure for determination of thiamine

A 2.00-ml volume of acetone (10%) and a portion of sample solution or standard solution were placed in a 10-ml flask and diluted to volume with water. This solution was used as solution R_1 (see Fig. 1).

A 7.50-ml volume of 2% Na_2SO_3 solution and 10.00 ml of 2 mol l^{-1} NaOH solution were placed in a 25-ml flask and diluted to volume with water. This solution was used as solution R_2 (see Fig. 1).

Set the selection valve (D) in position A (Fig. 1). Solutions R_1 and R_2 are pumped into a 40-cm mixing tubing (0.5 mm i.d.) at a rate of 5 ml min^{-1} and halted in the flow cell. Open the light shutter for 60 s to irradiate the solution [with the following settings of the spectrofluorimeter: excitation wavelength, λ(ex), 280 nm; excitation slit, EX, 5 nm; emission wavelength, λ(em), 440 nm; emission slit, EM, 5 nm]. Then change the λ(ex) to 370 nm and measure the fluorescence intensity of the photochemical reaction product.

Procedure for simultaneous determination of B_1, B_2 and B_6 in a mixture

Prepare solutions R_1 and R_2 described above. Use pH 7.0 buffer solution as R_3.

Set the selection valve in position B. Solutions R_1 and R_3 are pumped into the mixing tubing and halted in the flow cell. Measure the fluorescence intensities at 393 nm (excitation at 333 nm)

for B_6 and at 522 nm (excitation at 473 nm) for B_2 with both excitation and emission slits at 5 nm. Then set the selection valve in position A and follow the above procedure for the determination of thiamine in order to determine thiamine in the mixture.

When the effect of temperature on photochemical reaction was investigated, the flow cell was replaced with a normal cell and the cell holder was surrounded by tubing with circulating water connected to a thermostat.

RESULTS AND DISCUSSION

Sensitized photochemical reaction of thiamine

Thiamine can be easily oxidized in alkaline medium to fluorescent thiochrome. It was found that thiamine could be converted into a highly fluorescent compound on irradiation with UV radiation in alkaline medium in the absence of an oxidant. The uncorrected excitation and emission spectra showed an excitation maximum at 370 nm and an emission maximum at 440 nm. This photochemical reaction was significantly accelerated on addition of acetone. The reaction rate increased with increasing concentration of acetone (Fig. 2); however, the maximum fluorescence intensity, when the reaction reached equilibrium, did not depend on the concentration of acetone but on that of thiamine (Fig. 3), and the excitation and emission maxima remained unchanged. These results show that acetone acts as a sensitizer in the photochemical reaction.

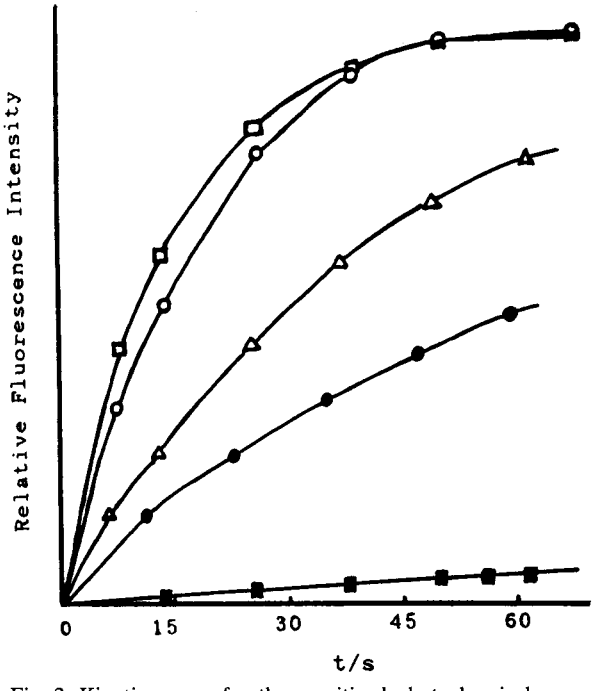

Fig. 2. Kinetic curves for the sensitized photochemical reaction of thiamine (4.0 μg ml^{-1}). Na_2SO_3 at 0.016 mol ml^{-1}, acetone at ■ = 0, ● = 0.2, △ = 0.4, ○ = 1.6 and □ = 2.8% (v/v).

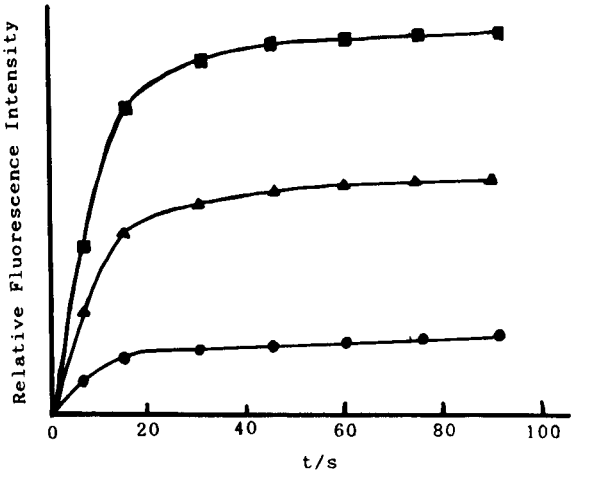

Fig. 3. Kinetic curves for the sensitized photochemical reaction of thiamine. Na_2SO_3 at 0.016 mol l^{-1}, acetone at 2% (v/v), thiamine at ● = 0.1, ▲ = 0.3 and ■ = 0.5 μg ml^{-1}.

Acetone has long been known as an excellent triplet-state sensitizer in photochemistry [33]. There might be two ways in which acetone sensitizes the photochemical reaction of thiamine. The excited triplet state of acetone may be quenched by the dissolved oxygen, forming the excited singlet state of oxygen, which subsequently oxidizes thiamine to fluorescent thiochrome. The other possibility is that oxygen is not involved but acetone acts as an energy donor; the excited triplet state of acetone transfers its energy to thiamine, which acts as an energy acceptor, and the latter is subsequently converted photochemically into the fluorescent product.

To establish which mechanism occurs, nitrogen was pumped into the reaction system just before irradiation (in a normal cell), but an unsatisfac-

tory signal was obtained. As thiamine is unstable in alkaline medium, it cannot be decided whether the lower signal was due to the absence of oxygen or the decomposition of thiamine during the process of deoxygenation. Then Na_2SO_3 was added to the NaOH solution before mixing with R_1 (Fig. 1). The result showed that the reaction rates of both sensitized (with acetone) and non-sensitized (without acetone) photochemical reactions were increased on addition of Na_2SO_3 (Fig. 4), but the excitation and emission maxima remained at 370 and 440 nm, respectively. Based on these results, it is considered that the sensitized photochemical reaction takes place through the triplet state of thiamine which is directly sensitized by acetone. Oxygen, as a triplet-state quencher, is unfavourable to the sensitized photochemical reaction of thiamine.

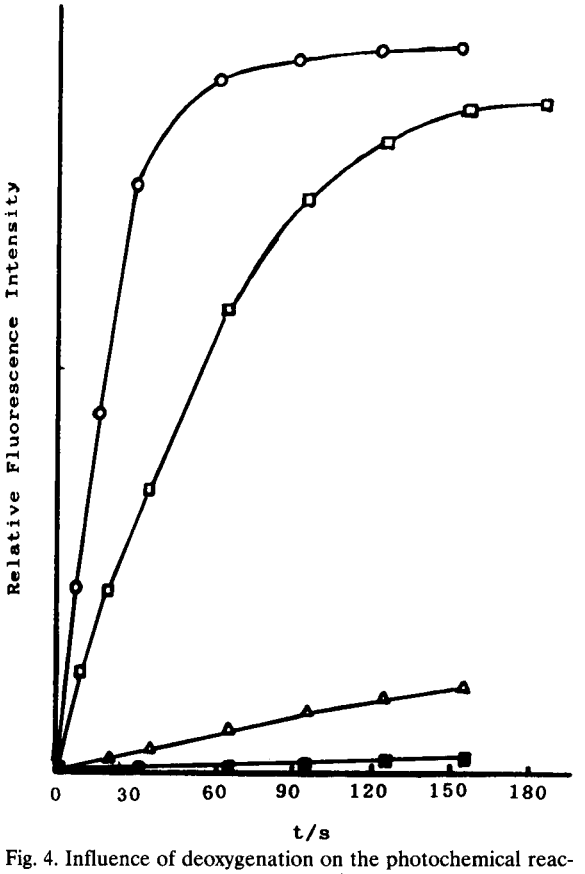

Fig. 4. Influence of deoxygenation on the photochemical reaction rate of thiamine (4.0 μg ml^{-1}). ■ = Thiamine alone; △ = thiamine with 0.016 mol l^{-1} Na_2SO_3; □ = thiamine with 2% acetone; ○ = thiamine with 0.016 mol l^{-1} Na_2SO_3 and 2% (v/v) acetone.

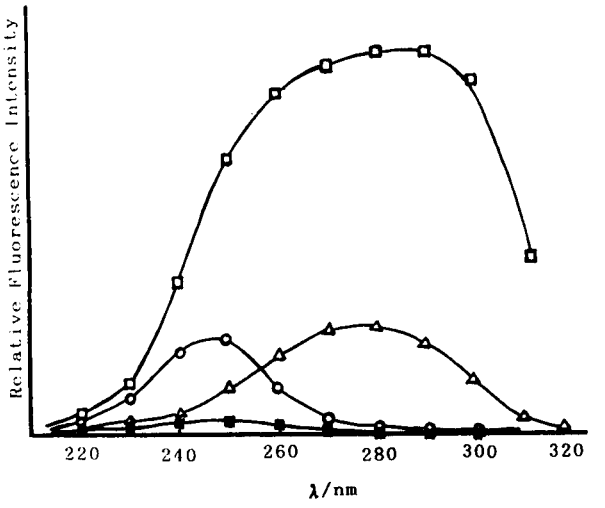

Fig. 5. Influence of the wavelength of irradiation on the fluorescence intensity. Irradiation time, 60 s; thiamine at 4.36 μg ml^{-1}. ■ = Thiamine alone; ○ = thiamine with 0.016 mol l^{-1} Na_2SO_3; △ = thiamine with 2% (v/v) acetone; □ = thiamine with both Na_2SO_3 and acetone.

Effect of radiation wavelength

To investigate the effect of the radiation wavelength, light bands of different wavelengths were used as the source for initiating the photochemical reaction. After irradiating the solution for 60 s, fluorescence measurements were made at 440 nm (excitation at 370 nm). The results are shown in Fig. 5 (not corrected for the effect of the energy distribution of the xenon lamp). The light band of 250 nm favoured the non-sensitized photochemical reaction, whereas the light band of 280 nm favoured the sensitized photochemical reaction. On addition of Na_2SO_3 the most effective radiation for the non-sensitized photochemical reaction was still that with a wavelength of 250 nm. From comparison with the absorption spectra (Fig. 6), it can be seen that the radiation absorbed by acetone is more effective for the sensitized photochemical reaction, so it is concluded that the sensitized photochemical reaction begins with the absorption of acetone. This conclusion is consistent with the mechanism of triplet–triplet energy transfer suggested above.

Effect of temperature

To study the effect of temperature on the reaction system, the cell in which the photochemical reaction took place was surrounded by tubing through which water from a thermostat was circulated and the temperature was varied from 20 to 60°C. The solution was irradiated with ultraviolet radiation of 280 nm (EX = 5 nm) for 60 s and the fluorescence intensity of the product was measured at 440 nm (excitation at 370 nm). The effect of temperature on the sensitized and non-sensitized reaction system is shown in Fig. 7. The effect of temperature can be basically divided into three parts. The first is the effect of temperature on the lifetime of the triplet state of acetone, the second is the effect on the rate of the photochemical reaction and the third is the effect on the fluorescence quantum yield of the product. The result shown here is the effect of temperature on the reaction system as a whole. The experiments were carried out at 22 ± 0.5°C with a fan cooling the reaction chamber.

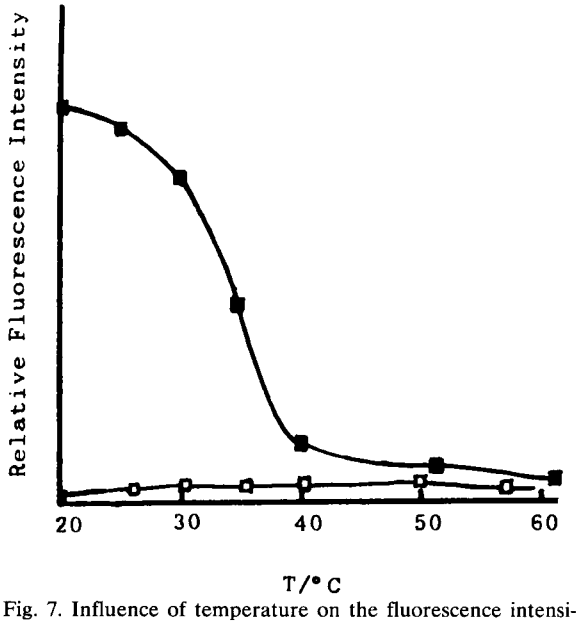

Fig. 7. Influence of temperature on the fluorescence intensities of the (□) non-sensitized and (■) sensitized photochemical reaction systems of thiamine. Irradiation time: 60 s.

Effect of medium and length of mixing tubing

The photochemical reaction of thiamine takes place in alkaline medium. As thiamine decomposed rapidly in alkaline medium, the fluorescence intensity obtained decreased rapidly when the time in alkaline medium before thiamine was irradiated increased. By use of the flow-injection technique, the mixing time can be controlled exactly. The effect of the length of the mixing tubing was also investigated. If the tubing was too short, the solution might not be mixed efficiently. On the other hand, longer tubing might result in decomposition of thiamine. The tubing length was varied from 30 to 140 cm, and the results showed that it affected the fluorescence intensity of the product significantly when the solution did not contain Na_2SO_3, but had hardly any influence when the reaction system contained Na_2SO_3.

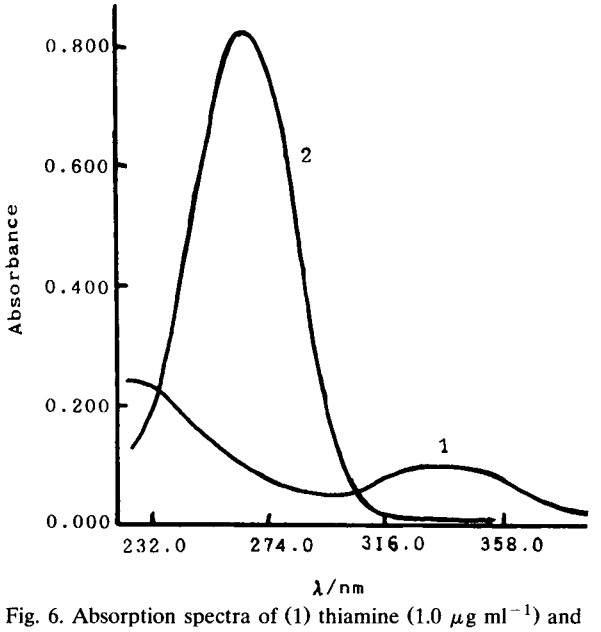

Fig. 6. Absorption spectra of (1) thiamine (1.0 μg ml^{-1}) and (2) acetone (1%, v/v) in NaOH.

Effect of irradiation intensity

To investigate the effect of the irradiation intensity, two experiments were done. In the first experiment, the solution was irradiated for 30 s (signal a in Fig. 8) with parameters λ(ex) = 280 nm, λ(em) = 440 nm and EX = EM = 5 nm. Immediately thereafter λ(ex) was switched to 370 nm and the fluorescence intensity of the photochemical reaction product was measured (b).

Then the light shutter was closed and kept unopened for 30 s (c). Subsequently the light shutter was opened again and the fluorescence intensity measured (b′). Finally, λ(ex) was changed from 370 to 280 nm for irradiating the solution again. By repeating these five steps, the results shown in Fig. 8 were obtained.

The second experiment was done by measuring the fluorescence intensities at 440 nm (excitation at 370 nm) with both slits at 5 nm after irradiating the solution for 60 s with different bandpasses of UV radiation [λ(ex) = 280 nm, EX changed from 2 to 8 nm].

The results showed that on irradiating the solution with UV radiation, the photochemical reaction took place and the reaction stopped when the radiation was shut off. It also showed that the larger the slit width, the faster the reaction proceeds. In view of the photochemical reaction, a larger slit width should be used to speed up the reaction. However, the light source was also used, as the excitation light, and a larger slit width might lead to poorer resolution of spectra. Therefore, an excitation slit width of 5 nm was adopted.

The reaction occurred in the central region of the cell which was irradiated. During shutting off the light the reaction was stopped and the concentration of the product in the central part was decreased because of diffusion. Hence signal b′ was smaller than b.

Effect of irradiation time

From the kinetic curves (Fig. 4) for this photochemical reaction it can be seen that it took about 60 s to reach the maximum fluorescence intensity. The fluorescence intensities were measured at both 60 and 90 s, and the difference

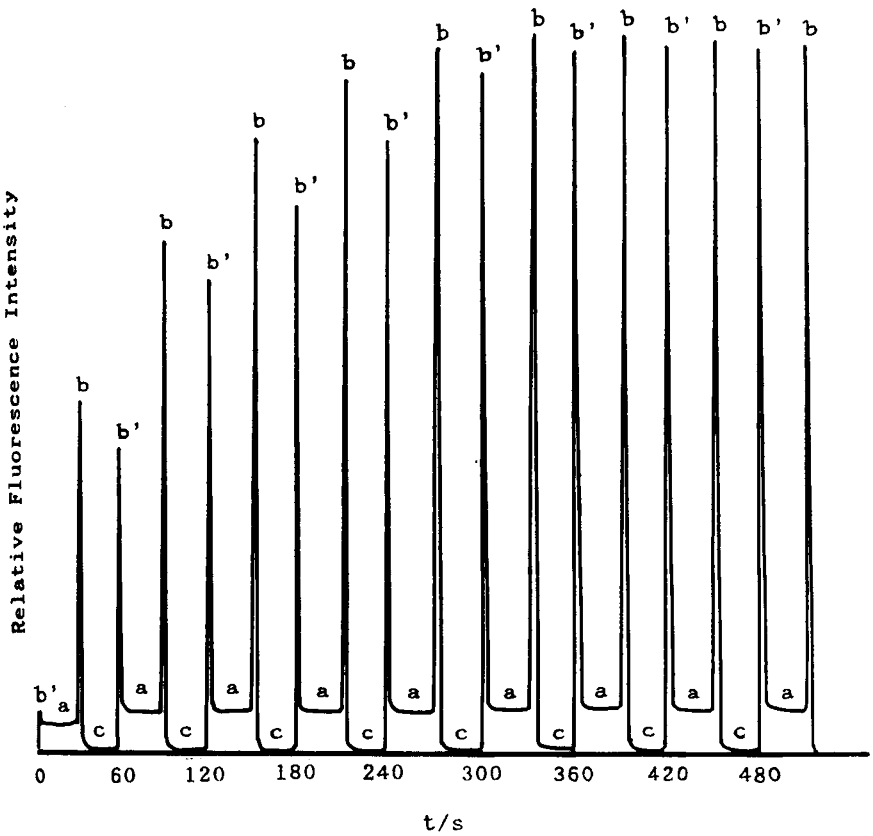

Fig. 8. Influence of radiation on inducing the photochemical reaction of thiamine. (a) Recorded at 440 nm [λ(ex) = 280 nm]; (b and b′) measured at 440 nm (excitation at 370 nm); (c) with light shutter closed.

between the two signal magnitudes was found to be less than 0.5% when the concentration of thiamine was less than 5.0 μg ml^{-1}. For higher concentrations, an irradiation time of 90 s would be better, and the difference between the fluorescence intensities measured at 90 and 120 s was also less than 0.5%.

Limit of detection and linear concentration range

The fluorescence intensity showed a linear relationship with the concentration of thiamine over a wide range, up to 10.0 μg ml^{-1} thiamine (r = 0.9996). The limit of detection (LOD) was given by the equation LOD = KS_0/S, where K is a numerical factor chosen according to the confidence level desired, S_0 is the standard deviation of the blank measurements (n = 11) and S is the sensitivity of the calibration graph. A value of 3 for K was used. The LOD was 0.46 ng ml^{-1} thiamine, and the relative standard deviation was 1.5% for 50.0 ng ml^{-1} thiamine (n = 6).

Effect of foreign substances

Interferences from foreign substances were tested by analysing a standard solution of thiamine (50.0 ng ml^{-1}) to which increasing amounts of interfering species were added. The tolerable concentrations of some interfering species are reported in Table 1.

APPLICATION

The application of the method to commerical tablets, vitamin B_1 injection and vitamin B complex was tested, and a standard addition recovery test was also carried out in a serum matrix.

TABLE 1

Tolerable concentration ratios with respect to thiamine for some interfering species (< 5% error)

Substance	Tolerable concentration ratio
Pyridoxine	> 800
Ascorbic acid	> 1000
Nicotinamide	> 100
Menadione sodium hydrogen sulphite	1
Riboflavin	> 100

TABLE 2

Determination of thiamine hydrochloride in vitamin B_1 tablets labelled to contain 10 mg

Sample	Amount found (mg)	Error (%)
I [a]	9.50 [c]	5.0
I [b]	9.50	5.0
II [a]	9.25 [c]	7.5
II [b]	9.28	7.2

[a] Analysed by calibration graph method. [b] Analysed by standard addition method. [c] Means for three measurements.

Analysis of vitamin B_1 tablets

Fifteen commercial vitamin B_1 pills, each containing a nominal amount of 10 mg of B_1, were weighed and ground to powder and a portion of the powder was weighed and dissolved in 0.01 mol l^{-1} HCl, filtered and diluted to 100 ml. Aliquots of this solution were diluted by a factor of 10 for the analysis, giving an approximate B_1 concentration of 0.4 μg ml^{-1}. The results of the analyses are given in Table 2. The values obtained for the commercial preparations agreed reasonably well with the nominal values. In the commercial tablets, age and tablet variations could cause the amount of thiamine present to be different from the amount claimed by the manufacturer.

Analysis of vitamin B_1 injection

Injection samples, each with a nominal content of 100 mg of vitamin B_1 in 2 ml, were diluted to 100 ml with 0.01 mol l^{-1} HCl. Aliquots of this solution were diluted by a factor of 1000 for the analysis, giving an approximate B_1 concentration of 1 μg ml^{-1}. The results of the analyses are given in Table 3. Again, the values obtained for the commercial preparations agreed reasonably well with the nominal values.

Determination of thiamine in serum

A 1.00-ml volume of serum was diluted to 100 ml with water. Aliquots of this solution were diluted by a factor of 10 for the analysis, and different amounts of standard solution of thiamine were added. The results are given in Table

TABLE 3

Determination of thiamine hydrochloride in vitamin B_1 injections labelled to contain 50 mg ml^{-1}

Sample	Amount found [a] (mg ml^{-1})	Error (%)
I	46.5	7.0
II	48.1	3.8

[a] Means for four measurements, determined by calibration graph method.

4. The results show that this method might be suitable for the determination of thiamine in biological materials.

Simultaneous determination of thiamine, riboflavin and pyridoxine in vitamin B complex

The applicability of the method to multivitamin B mixtures was tested on two kinds of samples: a sample prepared artificially by mixing standard solution of B_1, B_2 and B_6, and commercial tablets. Both riboflavin and pyridoxine are naturally fluorescent compounds. By use of a synchronous fluorescence technique [34], the two compounds can be simultaneously determined in pH 7.0 medium without interference from thiamine, which is a non-fluorescent compound.

TABLE 4

Determination of thiamine in serum

Sample	Amount in sample [a] (μg ml^{-1})	Amount added (μg ml^{-1})	Amount found (μg ml^{-1})	Recovery (%)
I:	0.010 [b]			
1		0.20	0.21	100.0
2		0.40	0.42	102.5
3		0.60	0.61	100.0
4		0.80	0.83	102.5
5		1.00	1.05	104.0
II:	0 [b]			
1		0.20	0.21	105.0
2		0.40	0.42	105.0
3		0.60	0.61	101.7
4		0.80	0.83	103.8
5		1.00	1.03	103.0

[a] Concentration of the solution for measurement (serum diluted by a factor of 1000 with water. [b] Means of four measurements.

With the present procedure, the calibration graphs were linear up to 6.3 μg ml^{-1} riboflavin ($r = 0.9996$) and 10.0 μg ml^{-1} pyridoxine ($r = 0.9991$). The limits of detection were 0.83 ng ml^{-1} for riboflavin and 0.81 ng ml^{-1} for pyridoxine. The relative standard deviations were 3.3% for 88.0 ng ml^{-1} riboflavin ($n = 6$) and 1.2% for 50.9

TABLE 5

Simultaneous determination of thiamine, riboflavin and pyridoxine in an artificial mixture

Sample	Amount added (μg ml^{-1})			Amount found (μg ml^{-1})			Recovery (%)		
	B_1	B_2	B_6	B_1	B_2	B_3	B_1	B_2	B_6
1	0.20	0.60	1.00	0.18	0.59	1.04	90.0	98.3	104.0
2	0.40	0.20	0.80	0.38	0.21	0.85	95.0	105.0	106.0
3	0.60	1.00	0.60	0.60	0.99	0.61	100.0	99.0	101.7
4	0.80	0.40	0.40	0.80	0.40	0.41	100.0	100.0	102.5
5	1.00	0.80	0.20	0.96	0.77	0.20	96.0	96.2	100.0

TABLE 6

Simultaneous determination of thiamine hydrochloride, riboflavin and pyridoxine in vitamin B complex

Sample	Amount in sample (mg)			Amount found (mg)			Error (%)		
	B_1	B_2	B_6	B_1	B_2	B_6	B_1	B_2	B_6
I	3	1.5	0.2	2.46	1.45	0.24	18.0	3.3	20.0
II	3	1.5	0.2	2.46	1.45	0.24	18.0	3.3	20.0
III	3	1.5	0.2	2.48	1.50	0.23	17.3	0	15.0
IV	3	1.5	0.2	2.46	1.50	0.23	18.0	0	15.0

ng ml^{-1} pyridoxine ($n = 6$). The results of the analyses of artificial mixture are given in Table 5.

For the analysis of vitamin B complex, ten commercial vitamin B complex pills were weighed and ground to powder. A portion of the powder was weighed and dissolved in 0.01 mol l^{-1} HCl, filtered and diluted to 100 ml. Aliquots of this solution were diluted by a factor of 10 for the analysis. The results are given in Table 6. The values obtained for the commercial preparations agreed reasonably well with the nominal values.

This study was supported by the National Natural Science Foundation of China and the National Education Commission Foundation of China.

REFERENCES

1 R.F.M. Macias, Appl. Microbiol., 5 (1957) 249.
2 R.H. Diebel, J.B. Evans and C.F. Niven, Jr., J. Bacteriol., 74 (1957) 818.
3 E.C. Nicolas and K.A. Pfender, J. Assoc. Off. Anal. Chem., 73 (1990) 792.
4 J. Xu, B. Xiang and D. An, Zhongquo Yaoxue Zazhi, 24 (1989) 853.
5 J. Xu, B. Xiang and D. An, Zhongquo Yaoxue Zazhi, 25 (1990) 77.
6 G.W. Chase and A.M. Soliman, J. Micronutr. Anal., 7 (1990) 15.
7 N. Grekas and A.C. Calokerinos, Talanta, 37 (1990) 1043.
8 Z. Zhang, Y. Li, D. Mao and V.V. Cosofret, J. Pharm. Biomed. Anal., 8 (1990) 385.
9 G.H. Zhang, T. Imato, Y. Asano, T. Sonoda, H. Kobayashi and N. Ishibashi, Anal. Chem., 62 (1990) 1644.
10 D.H. Craston, C.P. Jones, D.E. Williams and N.E. Murr, Talanta, 38 (1991) 17.
11 N. Crekas, A.C. Calokerinos and T.P. Hadjiioannou, Analyst, 114 (1989) 1283.
12 B.C.P. Jansen, Rec. Trav. Chim., 55 (1936) 1046.
13 S.A. Halvatzis and M. Timotheous-Potamia, Anal. Chim. Acta, 227 (1989) 405.
14 S.S.M. Hassan and E. Elnemma, Talanta, 36 (1989) 1011.
15 H. Wei and Y. Cheng, Yaowu Fenxi Zazhi, 10 (1990) 371.
16 Y. Zang and Z. Mo, Sepu, 7 (1989) 243.
17 M.A. Ryan and J.D. Ingle, Jr., Anal. Chem., 52 (1980) 2177.
18 C. Martinez-Lozano, J. Perez-Ruiz, V. Tomas and C. Abellan, Analyst, 115 (1990) 217.
19 E.E. Edwin, Methods Enzymol., 62 (1979) 51.
20 T. Kawasaki, Methods Enzymol., 122 (1986) 15.
21 A.E. Teeri, J. Biol. Chem., 196 (1952) 547.
22 Y. Shiobara, J. Biochem., 59 (1966) 76.
23 B. Karlberg and S. Thelander, Anal. Chim. Acta, 114 (1980) 129.
24 M. Marquez, M. Silva and D. Perez-Bendito, Anal. Lett., 22 (1989) 2485.
25 K. Higashi, Bunseki Kagaku, 40 (1991) 115.
26 A.L. Bailey and D.M. Finglus, J. Micronutr. Anal., 7 (1990) 147.
27 J.W.I. Brunnekreeft, H. Eidhof and J. Gerrits, J. Chromatogr., 491 (1989) 89.
28 S.M. Fernando and P.A. Murphy, J. Agric. Food. Chem., 38 (1990) 163.
29 C. Hasselmann, D. Franck, P. Crimm, P.A. Diop and C. Soules, J. Micronutr. Anal., 5 (1989) 269.
30 M. Tsuehiya, E.L. Torres, J.J. Aaron and J.D. Winefordner, Anal. Lett., 17 (1984) 1831.
31 J.M. Calatayud and C.G. Benido, Anal. Chim. Acta, 245 (1991) 101.
32 D. Chen, A. Rios, M.D. Luque de Castro and M. Valcarcel, Analyst, 116 (1991) 171.
33 N.J. Turro, in Modern Molecular Photochemistry, Benjamin/Cummings, CA, 1978, pp. 296–361.
34 Y.Q. Li, X.Z. Huang, J.G. Xu and G.Z. Chen, Fenxi Huaxue, 19 (1991) 538.

Analytica Chimica Acta, 276 (1993) 161–166
Elsevier Science Publishers B.V., Amsterdam

Determination of major and minor elements in sintered fine ceramics by inductively coupled plasma emission spectrometry utilizing a sputtering technique [1]

Hiroshi Uchida

Industrial Research Institute of Kanagawa Prefecture, 3173, Showa-machi, Kanazawa-ku, Yokohama 236 (Japan)

(Received 10th August 1992; revised manuscript received 17th November 1992)

Abstract

A sputtering technique was applied to the decomposition of sintered fine ceramics for contamination-free analysis. Alumina-, zirconia- and lanthanum-doped lead zirconate titanates (PLZT) prepared as sputtering target were converted into thin films on a quartz plate by r.f. sputtering. The sample films were dissolved in hydrochloric or sulphuric acid as easily as the powdered samples. Major, minor and trace elements were determined by inductively coupled plasma atomic emission spectrometry (ICP-AES). The analytical results for alumina and zirconia agreed well with the original target composition under wide sputtering conditions, but it was necessary to optimize the r.f. power used in the sputtering process and the sputtering gas pressure for PLZT analysis. The relative standard deviations were approximately 1% for major, 1–3% for minor and 3–8% for trace components.

Keywords: Atomic emission spectrometry; Ceramics; Plasma

Sintered fine ceramics have been used in a variety of fields because of their excellent characteristics such as high solidity and high resistance to chemical substances. There are many kinds of constitution in sintered ceramics; some of them are complex oxides and some are non-oxides. The exact determination of major, minor and trace elements is necessary in order to maintain the excellent characteristics, but the high resistance to chemicals of these materials sometimes hampers their chemical analysis. There are significant matrix effects in the analysis of solids, and the detection power without chemical separation is not always sufficient for ultra-trace determinations. Dissolution of samples is appropriate for the simple and exact determination of major and minor elements, and chemical separation is necessary for the determination of trace elements. Acid dissolution in a PTFE-lined bomb is simple to apply and suitable for the subsequent atomic absorption (AAS) and inductively coupled plasma atomic emission spectrometric (ICP-AES) determination of major and minor elements in silicates [2,3]. The decomposition of powdered alumina [4], zirconia [5] and silicon nitride [6] has been investigated by using such sealed bombs. Powdered alumina [7], zirconia [8] and silicon carbide [9] are decomposed by fusion with alkali metal carbonate, but many kinds of sintered fine ceramics cannot be easily decomposed by acid dissolution or alkali fusion. Further, crushing of solid ceramics causes contamination from the tools used.

In this work, a radiofrequency (r.f.) magnetron

Correspondence to: H. Uchida, Industrial Research Institute of Kanagawa Prefecture, 3173, Showa-machi, Kanazawa-ku, Yokohama 236 (Japan).

[1] Part of this work was presented the International Congress on Analytical Sciences (Chiba, Japan, 1991) [1].

sputtering technique was applied to the decomposition of sintered fine ceramics without contamination. The sputtered sample was collected on the quartz plate, followed by dissolution in acids. Major and minor elements were determined by ICP-AES, and the results obtained were compared with reported values and values obtained by other decomposition methods. Optimization of the sputtering conditions is discussed.

EXPERIMENTAL

Fine ceramic and other chemical samples

Sintered samples of pure alumina ($\geqslant 99\%$), mixed alumina containing about 3% of calcium and magnesium oxides, stabilized zirconia containing about 6% of yttrium oxide (Kojundo Chemical Laboratory) and lanthanum-doped lead zirconate titanate (PLZT) (Kyodo International) were prepared as sputtering targets (10 cm diameter, 5 mm thick). A Siemens D500 x-ray diffractometer was used for studying the crystallization.

Ultra-pure hydrochloric acid (36%) (Kanto Kagaku Kogyo) and sulphuric acid (96%) (Kanto Kagaku Kogyo) were used to dissolve the sample, and 1000 mg l^{-1} standard solutions for atomic absorption spectrometry (Kanto Kagaku Kogyo) were used to prepare the solutions for calibration.

Sputtering method

An Anelva SPF-210 sputtering device was used for r.f. sputtering. The r.f. power was 200–800 W, where the plate voltage was 2.0–4.5 kV and the current was 50–200 mA. Pure argon and argon mixed with 30% of oxygen were used as sputtering gases at pressures of 0.4–11.0 Pa. The sputtered sample was collected on a quartz plate ($\geqslant 99.99\%$) ($25 \times 25 \times 2$ mm). The sputtering time was 0.5–3.0 h to collect several mg of the thin-film sample on the plate. Details of the sputtering conditions are discussed later.

Thin-film dissolution and ICP analysis

The mixed alumina and PLZT samples converted into thin-films were dissolved in hydrochloric acid (1 + 1) in a PTFE beaker on a hotplate. The pure alumina and stabilized zirconia were decomposed with sulphuric acid (1 + 3) in a PTFE-lined bomb (San-ai Kagaku) at 230°C for 16 h [4,5].

The ICP spectrometer used and the operating conditions including analytical lines are given in Table 1. For the zirconia and PLZT analyses, the Al I 394.40 nm and Ca I 422.67 nm lines were employed to avoid overlap of emission caused by co-existing zirconium, titanium and yttrium. Analytical results were calculated as a typical oxide (indicated as M_xO_y below).

RESULTS AND DISCUSSION

Thin-film decomposition and limit of detection

The sintered mixed alumina sample after crushing with an agate mortar and pestle was decomposed with sulphuric acid (1 + 3) in a sealed

TABLE 1

ICP spectrometer and operating conditions

ICP spectrometer	Seiko SPS1200VR
Mounting	Czerny–Turner (1.0 m)
Grating	3600 lines mm^{-1}
Slit width	20–40 μm
R.f. power	1.3 kW
Argon flow-rate	16.0, 0.8, 0.6 l min^{-1}
Observation height	15 mm above the induction coil
Signal integration	3 times 3 s
Analytical lines (nm)	Al I 396.15 (I 394.40 [a]), Ca II 393.37 (I 422.67 [a]), Mg II 279.53, Si I 251.61, Fe II 259.94, Na I 590.54, Pb II 217.00, La II 408.67, Zr II 343.82, Ti II 334.90, Y II 371.03, Hf II 264.14

[a] Used for determinations in zirconia and PLZT.

TABLE 2

Limits of detection [a] (%) for the sputtering method using ICP-AES

Analyte	HCl dissolution	H_2SO_4 decomposition
Al_2O_3	0.02	0.03
CaO	0.01	0.005
MgO	0.005	0.002
SiO_2	0.02 [b]	–
Fe_2O_3	0.01	0.01
Na_2O	0.01	0.02
PbO	0.008	
La_2O_3	0.002	
ZrO_2	0.001	0.002
TiO_2	0.006	0.001
Y_2O_3		0.0003
HfO_2	0.003	0.004

[a] Limit of detection was calculated as the concentration which gave a net signal equal to three times the standard deviation of five blank determinations, and converted to the content in 8 mg of collected sample. [b] The blank value of 0.093% was subtracted in each determination.

bomb, but could not dissolved in hydrochloric acid (1 + 1) in a beaker on the hot plate. However, the converted mixed alumina on the quartz plate was easily dissolved in hydrochloric acid (1 + 1). This might be due to a change in the chemical structure or an increase in the specific surface area of the sintered mixed alumina in the sputtering process. The crystal structures of α-Al_2O_3, $MgAl_2O_4$ and $CaAl_4O_7$ were observed in the original target by x-ray diffractometry, but no crystallization was found in the converted thin film. The converted PLZT was also dissolved in hydrochloric acid (1 + 1), but converted pure alumina and stabilized zirconia samples were only decomposed in sulphuric acid (1 + 3) in a sealed bomb.

The limit of detection was obtained from five blank samples using only acid without ceramic sample and treated in the same decomposition process. Results calculated as the typical oxide assuming that 8 mg of sample were collected on the plate (5–10 mg collected under the investigated sputtering conditions) are given in Table 2. The values obtained with hydrochloric acid dissolution were almost identical with those for sealed bomb decomposition with sulphuric acid, except for SiO_2. A trace amount of silicate in the quartz

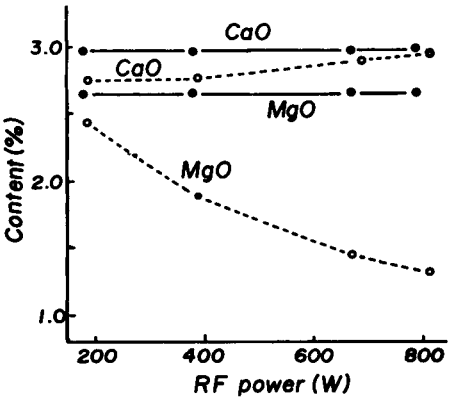

Fig. 1. Effect of r.f. power on the composition of mixed alumina. Mixed argon–oxygen gas pressure, 0.8 Pa (solid line); pure argon gas pressure, 0.8 Pa (dashed line).

plate is dissolved in hydrochloric acid, which might make the SiO_2 detection limit poorer then those for other elements. Further, the detection limit of SiO_2 could not be obtained in the sealed vessel decomposition with sulphuric acid, because approximately 1 mg of silicate was dissolved from the quartz plate. The limits of detection in Table 2 indicate that major and minor components except silicate are determined when several mg of the sputtered sample are collected on the quartz plate.

Effect of sputtering r.f. power and gas

The amount of sample collected on the plate increased with increase in the r.f. power. The

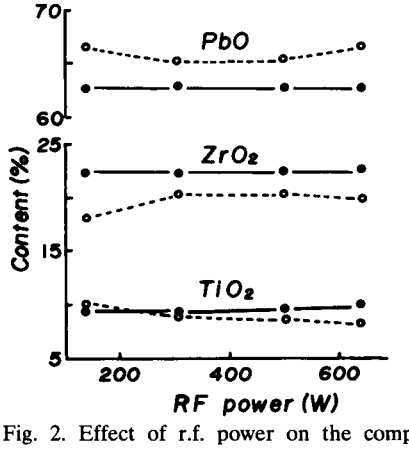

Fig. 2. Effect of r.f. power on the composition of PLZT. Mixed argon–oxygen gas pressure, 0.8 Pa (solid line); 11.0 Pa (dashed line).

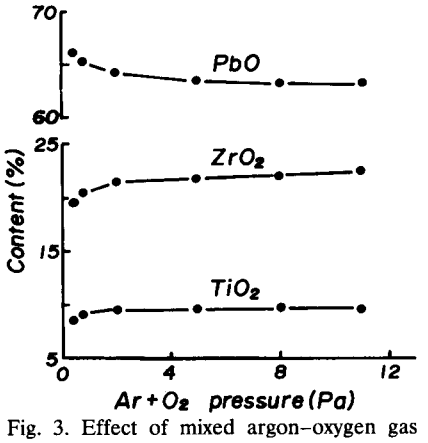

Fig. 3. Effect of mixed argon–oxygen gas pressure on the composition of PLZT. R.f. power, 300 W.

amount with pure argon sputtering was greater than that with mixed argon–oxygen, which means that pure argon is better suited for the determination of minor elements. However, the content of MgO significantly decreased and that of CaO slightly increased on increasing the r.f. power in pure argon sputtering, as shown in Fig. 1. On the other hand, the contents of CaO and MgO were constant for r.f. powers varying from 200 to 800 W when mixed argon–oxygen sputtering was ap-

TABLE 3

Optimized sputtering conditions

Parameter	Alumina	Zirconia	PLZT
Incident r.f. power (W)	670	580	510
Gas composition	$Ar–O_2$	$Ar–O_2$	$Ar–O_2$
Gas pressure (Pa)	0.8	2.0	3.0
Sputtering time (h)	3.0	1.0	0.5
Amount collected (mg)	8.46 [b]; 8.75 [c]	6.78	7.14
R.S.D. (%) [a]	1.4 [b]; 5.3 [c]	2.5	0.9

[a] Obtained from five samples. [b] Mixed $Ar–O_2$. [c] Pure Ar.

TABLE 4

Analytical results (%)

Oxide	Mixed alumina				Pure alumina			
	Proposed method	R.S.D. [a]	Crushed tablet [b]	Report [c]	Proposed method	R.S.D. [a]	Report [c]	
Al_2O_2	94.3	0.9	93.0	–	99.8	1.0	–	
CaO	2.95	1.5	2.92	3.1	0.03	5.2		
MgO	2.67	1.3	2.71	3.0	0.01	4.3		
SiO_2	0.08	18	0.98		–	–	0.14	
Fe_2O_3	0.02	4.7	0.03		0.03	6.3	0.10	
Na_2O	0.03	5.6	0.03		0.08	8.4	0.14	
	Stabilized zirconia				PL			
	Proposed method	R.S.D. [a]	Powder [a]	Report [c]	Proposed method	R.S.D. [a]	Scraping [e]	Report [c]
PbO					64.7	0.2	64.2	63.0
La_2O_3					3.99	0.8	3.90	3.91
ZrO_2	92.8	0.3	93.0	–	21.2	1.3	22.4	24.4
TiO_2	0.16	2.5	0.022	0.02	9.16	0.3	8.66	8.64
HfO_2	0.61	1.1	0.65	1.2	0.40	2.0	0.49	
Y_2O_3	6.21	1.7	6.05	5.5				
Al_2O_3	0.021	21	0.023	0.01	0.16	4.0	0.13	
CaO	0.24	3.6	0.18	0.1	0.058	9.6	0.074	
MgO	0.046	9.1	0.040	0.03	0.013	7.5	0.013	
SiO_2	–	–	0.091		0.15	20	0.089	
Fe_2O_3	0.021	22	0.012	0.01	0.011	24	0.013	
Na_2O	0.064	4.8	0.038		0.047	7.2	0.034	

[a] Obtained from five independent determinations. [b] Analytical value for tablet with composition and structure the same as those of the target, crushed with an agate mortar and pestle. [c] Value reported by the target manufacturer. [d] Analytical value for the powder sample before sintering. [e] Analytical value for a scraping taken from the target.

plied. This result indicates that the species in the target are selectively sputtered under different sputtering conditions. Mixed argon–oxygen was subsequently used as the sputtering gas to avoid selective sputtering. In this work, selective sputtering between metals and oxygen is not considered. Excess and lack of oxygen were observed in collected samples obtained using mixed argon–oxygen and pure argon, respectively. The amount of the sample collected was defined as the total of the obtained typical oxides.

Variation of the r.f. power did not affect the contents of ZrO_2 and Y_2O_3; they were constant, as with alumina sputtering with mixed argon.

In the case of PLZT sputtering at 0.8 Pa, the contents of the three major oxides were slightly shifted when the r.f. power increased, but they fluctuated at 11.0 Pa, as shown in Fig. 2. Further, the measured content of PbO increased by more than 2% and that of ZrO_2 decreased oppositely when the pressure of mixed argon–oxygen was increased from 0.8 to 11.0 Pa. The r.f. power and the sputtering gas pressure should be optimized to make a thin film with a composition the same as that of the original target.

Hardly any effect of mixed argon–oxygen pressure on the composition of mixed alumina and stabilized zirconia was observed. The contents of major oxides were almost constant in the range 1.0–11.0 Pa.

However, in the PLZT sputtering shown in Fig. 3, the measured contents of three major oxides were changes significantly below 2.0 Pa. The content of TiO_2 was constant above 2.0 Pa, but that of PbO decreased and that of ZrO_2 increased. The pressure of mixed argon–oxygen as a sputtering gas should also be optimized in the case of PLZT.

Analytical results and reproducibility

The final sputtering conditions used and the sample amounts collected are summarized in Table 3. In the PLZT optimization, the r.f. power for sputtering was higher and the gas pressure was lower than in the previous work [1]. A sputtering time was chosen such that about 6–8 mg of the sample were collected. The actual sputtering time for alumina, zirconia and PLZT was 3.0, 1.0 and 0.5 h, respectively. The amount of alumina collected per hour was less than those for the other two ceramics. The relative standard deviations (R.S.D.s) from five samples were in the range 1–5%.

Analytical results obtained by the proposed method are summarized in Table 4, with R.S.D. values obtained from five independent determinations. The analytical value for SiO_2 in crushed mixed alumina was higher than by the proposed method because of contamination from the agate mortar and pestle used. The R.S.D.s of the determination of SiO_2 with hydrochloric acid dissolution were ca. 20%, which was caused by the trace dissolution of SiO_2 from the quartz plate. Further, SiO_2 could not be determined by sealed bomb decomposition with sulphuric acid, where the blank level was ca. 100 times larger than the amount to be determined. The final results agreed well with values reported by the target manufacturer and values obtained by other methods. The R.S.D.s were approximately 1% for major, 1–3% for minor and 3–8% for trace components.

Conclusion

The proposed sputtering technique is effective for the determination of major and minor elements in sintered fine ceramics with low contamination. The collected samples are dissolved in acids just as easily as the powdered samples. Thin films with the same content are prepared from the original target under widely varying sputtering conditions in the case of alumina and zirconia. Optimization on the r.f. power and the gas pressure are required for PLZT to avoid selective sputtering.

REFERENCES

1 H. Uchida, Anal. Sci., 7 (1991) 1237.
2 H. Uchida, T. Uchida and C. Iida, Anal. Chim. Acta, 108 (1979) 87.
3 H. Uchida, T. Uchida and C. Iida, Anal. Chim. Acta, 116 (1980) 433.
4 H. Morikawa, Y. Iida, T. Ishizuka and F. Yokota, Bunseki Kagaku, 35 (1986) 636.

5 T. Ishizuka, Y. Uwamino and A. Tsuge, Bunseki Kagaku, 34 (1985) 487.
6 T. Ishizuka, Y. Uwamino and A. Tsuge, Bunseki Kagaku, 33 (1984) 486.
7 T. Ishizuka, Y. Uwamino, A. Tsuge and T. Kamiyanagi, Anal. Chim. Acta, 161 (1984) 285.
8 A. Izquierdo, L.G. Puignou and J. Rovira, Mikrochim. Acta, II (1984) 331.
9 M. Namiki and E. Hirokawa, Bunseki Kagaku, 33 (1984) T34.

Analytica Chimica Acta, 276 (1993) 167–171
Elsevier Science Publishers B.V., Amsterdam

Azeotropic distillation as an enrichment strategy for determination of aromatic hydrocarbons

Woodfin V. Ligon, Jr.

General Electric Company, Corporate Research and Development, Schenectady, NY (USA)

(Received 12th October 1992; revised manuscript received 26th October 1992)

Abstract

A wide variety of environmentally significant aromatic hydrocarbons have been found to undergo azeotropic distillation with glycerol and related hydroxylic azeotroping agents. This classical but previously neglected separation method is often quicker and more efficient than Soxhlet extraction for many sample types. In addition, many interfering substances typically encountered in environmental analyses such as large triglycerides do not form azeotropes and therefore are cleanly excluded from the analysis. Azeotropic distillation is much faster and often more complete than solvent extraction. Additionally, this approach significantly minimizes the use of organic solvents in the environmental laboratory while introducing only relatively benign materials such as glycerol.

Keywords: Gas chromatography–mass spectrometry; Azeotropic distillation; PAHs; Polychlorinated biphenyls; Polychlorinated diphenyl ethers; Polychlorinated terphenyls

Azeotropic distillation is a classical separation method [1]. It involves the addition of an azeotroping agent which can serve as one component of a low boiling azeotrope. A distillation is then performed and the low boiling azeotrope distills as the first fraction. Generally the azeotroping agent is added in excess so that all of the desired material will be carried overhead followed by later fractions consisting of pure azeotroping agent which serves to purge the apparatus. Separations can be obtained because azeotrope formation is sensitive to molecular structure.

It has long been recognized that many aromatic hydrocarbons form azeotropes with hydroxylic materials such as glycerol. When the aromatic substance has a boiling point near that of glycerol, the boiling point depression may be quite large and the azeotrope may have a composition which incorporates comparable amounts of both components. For example, glycerol has an (atmospheric pressure) boiling point of about 292°C. Biphenyl has a boiling point of 254.9°C. The azeotrope formed between these materials has a boiling point of 243.8°C and consists of 55% glycerol [2].

Azeotrope formation is quite sensitive to molecular structure. For example, biphenyl and chlorobiphenyl form azeotropes with glycerol whereas hydroxybiphenyl does not. This effect has been used to separate certain chlorobiphenyls from hydroxybiphenyls as part of an organic synthesis effort [3]. Reference 2 has an extensive list of materials which do and do not form glycerol azeotropes. In this paper, experiments designed to evaluate azeotropic distillation as an enrichment strategy for aromatic hydrocarbons are described.

Correspondence to: W.V. Ligon, Jr., General Electric Co., Corporate Research and Development, Schenectady, NY 12309 (USA).

EXPERIMENTAL

Materials

Aroclor™ 1260 [a] was obtained from Accustandards, New Haven, CO Pentachlorodiphenyl ether and trichloroterphenyl isomers were obtained from Ultra Scientific (N. Kingston, RI).

Spectrophotometric grade (99.5%) glycerol was obtained from Aldrich (Milwaukee, WI). A solution in methanol of the aromatic hydrocarbons acenaphthene, fluoranthene, naphthalene, benz[*a*]anthracene, benzo[*a*]pyrene, benzo[*b*]fluoranthene, benzo[*k*]fluoranthene, chrysene, acenaphthylene, anthracene, benzo[*ghi*]perylene, fluorene, phenanthrene, dibenz[*a*,*h*]anthracene, indenopyrene, and pyrene was obtained from Chem Service (West Chester, PA). "Chicken fat" was obtained by manually separating fatty tissue from "grocery store chicken" available locally.

Procedures

In a typical experiment, approximately 100 g of glycerol was placed in a 200-ml round bottom flask equipped with a magnetic stirrer and a heating mantle. This flask was further equipped with a distillation head leading to a air cooled condenser. The entire apparatus was blanketed with dry nitrogen gas at atmospheric pressure. The pure glycerol specimen was brought to the boiling point and approximately 10 ml collected. This procedure served to remove low boiling materials such as water from the glycerol. The glycerol remaining in the distillation flask was cooled to about 100°C and approximately 30 mg of the aromatic hydrocarbon was added. The mixture was then raised to the boiling point and distillation fractions collected.

Raw chicken fat was prepared for analysis by spiking with a commercial mixture of polynuclear aromatic hydrocarbons (see *Materials*) at about 3 $\mu g\ g^{-1}$ per component and then thoroughly homogenizing this combination with an equal volume of glycerol in a commercial blender. The distillation of this mixture was carried out as described above except that no attempt was made to remove water first. Distillation was simply carried out until 1 ml had been collected with a vapor temperature of about 290°C.

[a] Aroclor™ 1260 is a Monsanto trademark for a chlorinated biphenyl fluid with approximately 60% by weight chlorine.

Analysis

Analysis of glycerol distillation fractions consisted of dilution with about five-fold their volume of water followed by extraction with methylene chloride. The methylene chloride was concentrated to a small volume using a stream of dry nitrogen. When quantitative data were required, each distillate fraction was spiked with a known quantity of trichlorobiphenyl ether as an internal standard before dilution and extraction with methylene chloride. A 2-μl aliquot of the respective concentrated methylene chloride extract was injected into a GC–MS system.

The GC–MS system was equipped with a J&W Scientific Model DB-1 fused-silica capillary having the dimensions 30 m × 0.32 mm i.d. and a film thickness of 1.0 μm. The GC oven was programmed linearly from 100°C to 290°C at 12°C per minute while mass spectra were acquired using a high resolution magnetic sector mass spectrometer operating at 1000 resolution in electron ionization mode. For PCB samples, reconstructed ion chromatograms (RICs) were generated for the parent masses corresponding to the respective chlorination levels of the chlorinated biphenyls present. The areas under these RICs were evaluated relative to the internal standard areas to give the data presented in Figs. 1 and 2.

RESULTS AND DISCUSSION

As the difference in boiling point between an azeotroping agent and the species of interest becomes larger, the fraction of the higher boiling material in the azeotrope generally becomes progressively smaller. In addition, boiling point depression of the lower boiling component also becomes progressively smaller. Consequently, attempts to form an azeotrope between environmentally important aromatic species such as Aroclor™ 1260 (boiling range 385–420°C) [4] and glycerol would be expected to produce azeotropes which consist predominantly of glycerol and have

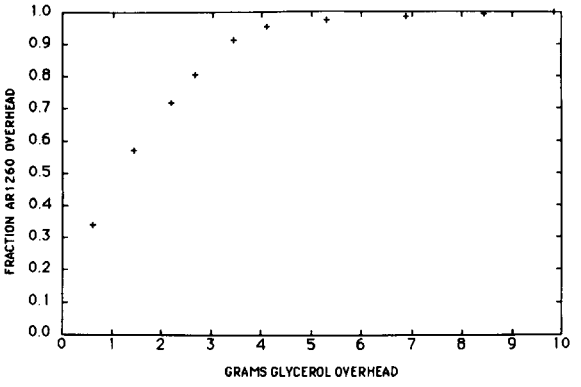

Fig. 1. Azeotropic distillation of Aroclor™ 1260 at atmospheric pressure using excess glycerol. The distillation flask was charged with 0.030 g PCB and 100 g glycerol. Numerous small fractions were collected and analyzed for PCB content using GC–MS. The data are presented as the fraction of the total PCB which distilled as a function of the grams of distillate (largely glycerol) collected.

boiling ranges near that of glycerol. Such azeotropes do form, consist largely of glycerol, and boil slightly below glycerol.

Figure 1 presents the results of an experiment in which 30 mg of Aroclor™ 1260 were added to 100 g of glycerol and the mixture distilled with the collection and analysis of small fractions of distillate. Since Aroclor™ 1260 is a mixture, these data represent the formation of many independent azeotropes. An analysis of the glycerol remaining in the "pot" after collection of the distillation fractions shown in Fig. 1, revealed that an undetectable quantity (< 50 ng g^{-1}) of polychlorinated biphenyl (PCB) remained in the large volume of undistilled glycerol. This process is not analogous to steam distillation. The amount of glycerol distilled is much smaller than the amount of steam which would be needed to transfer the same amount of PCB.

Figure 2 partially deconvolutes the curve shown in Fig. 1. In this case, the composition of the distillation fractions is presented as a function of the number of chlorines on the biphenyl nucleus. These curves must be interpreted in light of the fact that these data are a function of the relative amounts of each congener which were present in the original PCB composition. For example, the very rapid removal of lightly chlorinated biphenyls reflects both the fact that they form an azeotrope richer in PCB and the fact that there is very little of them present in the original mixture. Nevertheless, it is clear that as the number of chlorines increases, the ratio of glycerol to PCB congener in the azeotrope rises, and consequently, more glycerol is needed to completely remove higher chlorinated species.

In Figs. 1 and 2, the quantity of glycerol needed to completely remove all PCB congeners was about 10 g. Since the original amount of PCB was about 30 mg, the ratio of glycerol to PCB in the azeotrope was (on average) about 333 to 1. (Note that part of this glycerol undoubtedly reflects inefficiencies in purging the distillation apparatus itself and therefore the quantity of glycerol is most likely overstated.) This gives an estimate of the minimum amount of glycerol which must be added to a sample in order to ensure complete removal of this amount of a PCB composition similar to Aroclor™ 1260.

This quantity of glycerol (about 300:1) may seem large, but because materials such as PCBs are generally present in environmental samples at quite low levels, the addition of modest amounts of glycerol as an azeotroping agent are still adequate to cause all of the PCBs to distill as a first fraction when the sample is heated. Consider, for example, that the amount of PCBs used in the above experiment would represent 300 $\mu g\ g^{-1}$ in 100 g of soil or 30 $\mu g\ g^{-1}$ in 1000 g of soil.

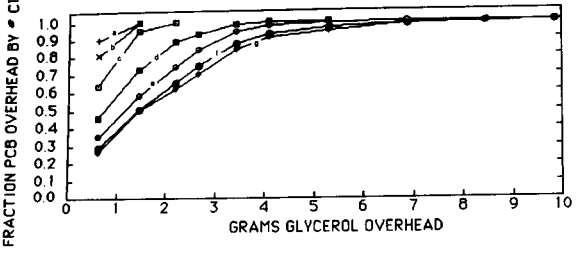

Fig. 2. An alternative presentation of the data discussed in Fig. 1, where the ordinate now represents the fraction of each individual PCB chlorination level which distilled as a function of the number of grams of distillate (largely glycerol) collected. (a) dichlorobiphenyl; (b) trichlorobiphenyl; (c) tetrachlorobiphenyl; (d) pentachlorobiphenyl; (e) hexachlorobiphenyl; (f) heptachlorbiphenyl; (g) octachlorobiphenyl.

In some cases it is not practical to carry out a distillation at or near the atmospheric pressure boiling point of glycerol. Many environmental samples contain materials which begin to thermally decompose before reaching this temperature. In addition, certain matrices may catalyze the decomposition of glycerol itself. Such thermal decomposition products can, in principal, constitute analytical interferences in the distillate. Very rapid heating has been found to minimize these decomposition processes. Alternatively, distillation at reduced pressure may be employed. Preliminary experiments have demonstrated that the azeotrope between Aroclor™ 1260 and glycerol is preserved at pressures of about 1 mmHg which yields a glycerol boiling point of about 125°C. However, the composition of azeotropes may change significantly at reduced pressure and this variable must be evaluated for each system studied.

Azeotropic distillation is not limited to PCB determinations. It is also useful for a broad range of polynuclear aromatic species (PNAs). Figure 3 provides two reconstructed ion chromatograms (RICs) generated from an experiment in which raw chicken fat was spiked with a PNA mixture which included naphthalene, acenaphthene, anthracene, fluorene, phenanthrene, pyrene, chrysene, and 1,2 benzanthracene (each about 3 $\mu g\ g^{-1}$) and then subjected to azeotropic distillation. The first gram of distillate was collected. Dilution of the distillate with water followed by methylene chloride extraction and concentration provided a sample ready for GC–MS. All of the above mentioned PNAs were readily detected in the distillate by GC–MS. Figure 3 provides RICs (1000 resolution, electron ionization) corresponding to the molecular ion signal for several of the spiked materials. These data clearly indicate the presence of a number of materials in addition to the desired PNAs. However, the quantities of these other species are such that they do not significantly interfere with either chromatography or mass spectrometry. The largest PNAs which formed an azeotrope were 1,2-benzanthracene and chrysene. Benzo[*b*]fluoranthene, 3,4-benzpyrene and 1,2:5,6-dibenzanthracene are examples of PNAs which did not form azeotropes with glycerol. PCBs have also been recovered at low $\mu g\ g^{-1}$ levels from chicken fat using azeotropic

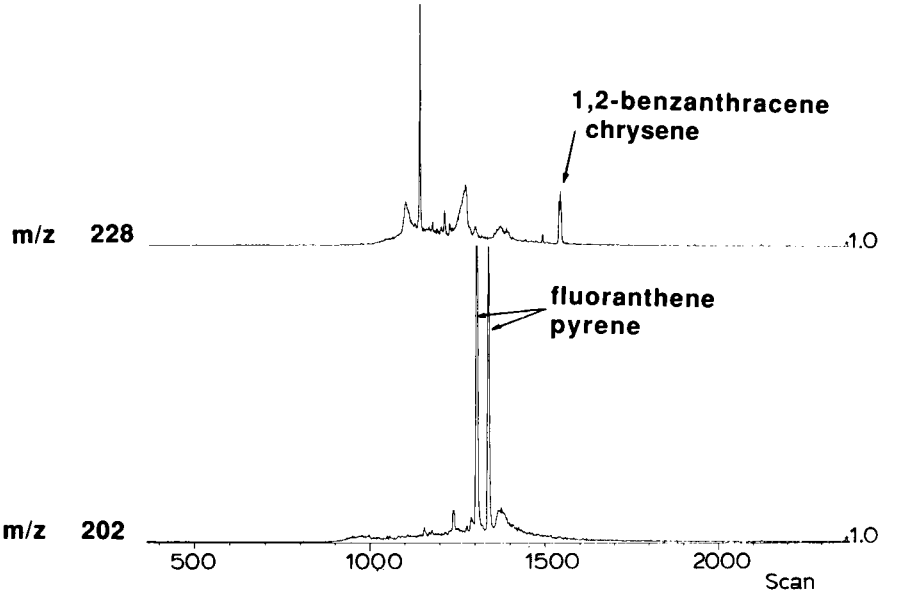

Fig. 3. Reconstructed ion chromatograms obtained from the GC–MS analysis of a sample obtained by glycerol azeotopic distillation of raw chicken fat which had been spiked with a variety of polynuclear aromatic hydrocarbons at the 3 $\mu g\ g^{-1}$ level.

distillation and analyzed by GC–MS without further purification.

In separate experiments, both chlorinated diphenyl ethers and chlorinated terphenyls have been found to form azeotropes with glycerol. Although not yet tested, these data suggest the likelihood that both chlorinated dioxins and chlorinated dibenzofurans will also form azeotropes with glycerol.

The sensitivity of azeotropic distillation to molecular structure can be particularly advantageous when attempts are made to use azeotropic distillation as an enrichment procedure for enviromental samples. When azeotropic distillation with glycerol is performed on materials as inherently complex as soil and animal fat, only a very limited group of materials form azeotropes and appear in the distillate. The first fractions obtained by glycerol azeotropic distillation from such materials (soil, fat), include all of those materials which boil *lower* than glycerol plus a small selection of materials which would normally boil higher than glycerol, but because of azeotrope formation actually boil slightly lower than glycerol. Of particular importance is the observation that many of the materials which have classically caused the greatest difficulty in the enrichment process for environmental samples do not form glycerol azeotropes. For example, large triglycerides appear not to form glycerol azeotropes.

Azeotropic distillation with glycerol has a number of significant advantages relative to other methods of enrichment. For example, in experiments with soils, the azeotropic method is much faster than Soxhlet extraction. In addition, because azeotropic distillation occurs at an elevated temperature and azeotrope formation is energetically favorable, PCBs are fully removed from all soil types examined to date. A "resistant fraction" often described for other methods has not been observed with azeotropic distillation. (Note: data describing the use of azeotropic distillation for soil remediation will be described elsewhere).

It should also be noted that the total amounts of organic solvents required in this procedure are drastically minimized relative to the quantities used in more conventional enrichment schemes which, in addition to Soxhlet extraction, often involve liquid chromatography. Solvents used in these alternative procedures ultimately become a hazardous waste stream from the environmental laboratory itself and their minimization is not insignificant. As a waste product, glycerol itself is unusually benign. It is certified as a foodstuff and occurs in hand lotions and infant medicinal formulations.

From the standpoint of GC–MS analysis, azeotropic distillation has the advantage that it produces enriched specimens which are entirely free of nonvolatile residues. In alternative enrichment schemes, non-volatile residues often shorten the useful life of gas chromatography columns.

It should be pointed out that the azeotropic distillation technique is very general and is not limited to the use of glycerol as an azeotroping agent. PCBs also form an azeotrope with 2,2-dihydroxymethyl-1-propanol. In principle, higher boiling azeotropic agents can extend the temperature range of substances amenable to azeotropic distillation beyond the 400°C level already demonstrated in this work for chlorinated biphenyls.

REFERENCES

1 Kirk-Othmer Encyclopedia of Chemical Technology, 3rd edn., Wiley, New York, Vol. 3, 1978, p. 352.
2 C.S. Minor and N.N. Dalton (Eds.), Glycerol, American Chemical Society, Monograph Series, Reinhold, New York, 1953, p. 262.
3 H.O. Seeburger and L.H. Horsley, Method for Separating a 2- and 4-Chlorobiphenyl from the Corresponding Hydroxybiphenyl Compounds, U.S. Pat., 3,655,523 iss. April 1972.
4 O. Hutzinger, S. Safe and V. Zitko, The Chemistry of PCBs, CRC Press, Cleveland, OH, 1974, p. 10.

Analytica Chimica Acta, 276 (1993) 173–179
Elsevier Science Publishers B.V., Amsterdam

Preconcentration of aluminium by micellar-enhanced ultrafiltration

Miguel de la Guardia, Empar Peris-Cardells and Angel Morales-Rubio

Department of Analytical Chemistry, University of Valencia, 50 Dr. Moliner Street, 46100 Burjassot, Valencia (Spain)

Alessandra Bianco-Prevot and Edmondo Pramauro

Dipartimento di Chimica Analitica, Università di Torino, 10125 Turin (Italy)

(Received 24th July 1992; revised manuscript received 23rd October 1992)

Abstract

Traces of aluminium were preconcentrated in water samples by forming a complex with lumogallion, and successfully accumulated in the micellar phase obtained from cationic or non-ionic surfactants and filtered through 10000 molecular weight cut-off ultrafiltration membranes. Studies indicated that, at pH 5.9, with 1×10^{-3} M lumogallion and 2×10^{-2} M cetyltrimethylamonium bromide, quantitative retention of aluminium present at μg ml^{-1} concentration levels was achieved. A micellar-enhanced fluorimetric procedure was employed to analyse the permeate solutions, whereas nitrous oxide–acetylene flame atomic emission spectrometry was used to determine aluminium in the retentate. The experimental parameters that influence the micellar-enhanced ultrafiltration (MEUF) efficiency were investigated and the analytical procedures were optimized. The MEUF of trace levels of aluminium allows for either preconcentration of the analyte or enhancement of the emission signals.

Keywords: Atomic emission spectrometry; Fluorimetry; Aluminium; Micellar-enhanced ultrafiltration; Preconcentration; Ultrafiltration; Waters

Micellar-enhanced ultrafiltration (MEUF) is a separation technique based on the principles of ultrafiltration membranes but improved by the use of micellar assemblies, which permit the removal of dissolved molecular species [1–8]. In MEUF, a surfactant at concentrations greater than the critical micelle concentration (c.m.c.) is added to the samples. The interactions between micelles and dissolved species results in the binding of organic molecules or ions within or at the surface of the surfactant aggregates. These bound species are retained together with their host aggregates, as most micelles do not pass through membranes having a molecular weight cut-off (MWCO) of ca. 10000.

This basic idea has been applied to the removal of organic molecules from water, such as phenols, benzene, chlorinated hydrocarbons, 1,1,1-trichloro-2,2-bis(*p*-chorophenyl)ethane (DDT), aliphatic alcohols, chloroaromatic herbicides and aniline derivatives [8–11]. Inorganic ions, such as iron, copper, calcium, zinc, cadmium and chromate [12,13], have been also removed from aqueous solutions using surfactants possessing an opposite charge to the species considered (anionic surfactants have been employed for cations and cationic surfactants for the removal of anions). A new approach to metal ion concentration by MEUF is based on the use of functional chelating micelles, which can increase the

Correspondence to: M. de la Guardia, Department of Analytical Chemistry, University of Valencia, 50 Dr. Moliner Street, 46100 Burjassot, Valencia (Spain).

rejection percentage and/or improve the selectivity of the separations [14–16].

Based on published reports, it can be concluded that MEUF is an interesting means with which to decontaminate waste waters and to remove inorganic species from liquid baths employed in industrial areas. However, little attention has been paid to the analytical applications of MEUF as a preconcentration technique for analytes to be determined in dilute samples or to improve the selectivity of the analytical methods.

The aim of this work was to study the separation of trace amounts of aluminium from aqueous solution by the formation of a complex with lumogallion (LG), concentrated in the retentate by MEUF in the presence of cetyltrimethylammonium bromide (CTAB). This separation system was succesfully employed to preconcentrate the analyte and to improve the sensitivity of its determination by flame atomic emission spectrometry.

EXPERIMENTAL

Apparatus and reagents

An S-43-70 ultrafiltration stirred cell with a volume of 70 ml (Spectrum) was used to carry out the ultrafiltration experiments. Spectra Por-C10 disc ultrafiltration membranes (43 mm diameter) with an MWCO of 10 000 were employed. These membranes are composed of solubilized and cast cellulose material (mainly cellulose acetate and hydrolysed cellulose acetate) and have pore sizes of about 25 Å. In all the experiments, a constant nitrogen pressure of 3 atm was applied.

A preliminary washing treatment of the membranes with 30 ml of water is necessary to eliminate the wetting agents incorporated in the cellulose filter.

A Perkin-Elmer LS 50 single-beam, luminescence spectrometer, equipped with 1-cm pathlength quartz cells, was employed for the fluorescence measurements of the permeate solutions. The experimental conditions are summarized in Table 1. The spectrometer is equipped with a 1% attenuator of the emission light, which permits the emission signals to be reduced in order to avoid saturation of the detector in the study of highly fluorescent systems. In this work in all instances the fluorescence of the aluminium–lumogallion complex was using this attenuator.

TABLE 1

Experimental conditions employed in fluorescence measurements

Parameter	Experimental value
λ(exc.)	498 nm
λ(em.)	552 nm
Slit(exc.)	7 nm
Slit(em.)	7 nm
Lumogallion concentration	1.5×10^{-5} M
Brij-35 concentration	1.26×10^{-2} M
pH	5 (acetic acid–acetate buffer)

A Varian SpectrAA-10 flame atomic absorption spectrometer, equipped with a laminar burner for nitrous oxide–acetylene, was employed to carry out emission measurements of the retentate solutions under the experimental conditions indicated in Table 2. A Gilson P-2 Minipuls peristaltic pump was used for experiments carried out at a fixed carrier flow-rate.

The reagents employed, provided by Panreac and Probus (Spain), unless indicated otherwise, were of analytical-reagent grade.

An aluminium stock standard solution was prepared by dissolving 1.0000 g of Al metal (Merck) in a minimum amount of HCl (1 + 1) and diluting to 1 l with 1% (v/v) HCl.

Lumogallion (LG) (ICN Pharmaceuticals) was employed to complex aluminium. A 3.9×10^{-3} M

TABLE 2

Experimental conditions used to measure the atomic emission of aluminium

Parameter	Experimental value
Wavelength	391.1 nm
C_2H_2 flow-rate	5.5 l min^{-1}
N_2O flow-rate	9.7 l min^{-1}
Burner height [a]	10 mm
Slit width	0.5 nm
Aspiration flow-rate	7 ml min^{-1}
Pump flow-rate	7 ml min^{-1}

[a] The burner height is the distance below the focal point of the optical system.

stock solution was prepared in distilled, deionized water.

A 0.05 M stock standard solution of *N*-acetyl-*N*,*N*,*N*-trimethylammonium bromide (CTAB) (Merck) was prepared in distilled, deionized water. A 0.05 M stock standard solution of Brij-35 (Aldrich) was prepared. Both surfactants were used as received.

Ultrafiltration experiments

To samples containing Al at concentrations ≤ 6 mg l^{-1}, were added appropriate amounts of LG, CTAB and acetic acid–acetate buffer, in order to obtain final concentrations of 0.02 M CTAB and 1×10^{-3} M LG and a pH ≥ 5. This solution was heated at 75°C for 60 minutes, cooled, 30 ml were placed in the ultrafiltration cell, and ultrafiltration was carried out at a constant nitrogen pressure (3 atm) until 25 ml of permeate had been collected. The retentate was analysed directly by flame atomic emission spectrometry and the rejection factor was evaluated.

The mass balance of the analyte was also checked by analysing the permeate solution by micellar-enhanced fluorescence, after addition of appropriate amounts of LG and the non-ionic surfactant Brij-35.

Micellar-enhanced fluorimetric analysis

To determine the concentration of Al in the permeate solutions, LG and Brij-35 were added to filtered samples to give final concentrations of 1.5×10^{-5} M LG and 1.26×10^{-2} M surfactant. The samples were then heated at 75°C for 1 h and cooled. The fluorescence of these solutions was measured against a calibration graph obtained from aluminium standards (in the concentration range 8–40 μg l^{-1}) prepared under similar conditions.

Flame atomic emission analysis

The retentate solutions were introduced directly into a nitrous oxide–acetylene flame by means of a peristaltic pump working at the same carrier flow-rate as used for the direct aspiration of aqueous solutions. The Al emission of these solutions was measured at 396.1 nm. Standard solutions containing 3–12 mg l^{-1} Al and the same LG and surfactant concentrations as previously mentioned were employed.

RESULTS AND DISCUSSION

Fluorescence of the aluminium–lumogallion complex

Ishibashi and Kina [17] reported that LG forms a complex with Al that can be used for the spectrophotometric and fluorimetric determination of traces of this metal. Previously, it was reported that the Al–LG complex interacts with micelles and that a fluorescence enhancement of 200% can be obtained in the presence of micelles composed of ethylene oxide condensates with fatty alcohol-type surfactants [18]. Based on that work, two surfactants, CTAB and Brij-35, were selected to obtain an appropriate micellar medium to conduct the ultrafiltration of water solutions containing Al in the presence of LG.

The ultrafiltration of the Al solution results in concentration of analyte in the retentate. The permeate is of little analytical interest. However, in order to determine accurately the rejection coefficient of the analyte (R), the aluminium concentration in the permeate (C_p) and in the initial solution (C_0) must be known. The rejection factor is calculated from the equation

$$R = 1 - (C_p/C_0)$$

C_p can be determined fluorimetricaly.

During the ultrafiltration in the presence of CTAB it was found that LG is quantitatively retained, whereas in the presence of Brij-35 1% of initial LG passes through the membranes. Hence it is necessary to add LG to the permeate solutions in order to ensure the complexation of the unretained Al, prior to the analysis of the permeate solutions. On the other hand, if the retentate concentration is not very high, only surfactant monomers pass through the ultrafiltration membrane. Therefore, a concentration of Brij-35 higher than the c.m.c. must be added to the permeate solutions in order to reconstitute the micellar medium.

A typical calibration line obtained for the analysis of the permeate solutions provides the

equation $I_r = 3.77 + 0.77C$ (μg l^{-1}) with a regression coefficient of 0.9998 (see Fig. 1). The detection limit of the micellar-enhanced fluorescence determination of Al with LG, in the presence of Brij 35, corresponds to 0.46 μg l^{-1} (established for a confidence level of 95%). The relative standard deviation, determined for ten independent measurements of a solution containing 32 μg l^{-1} Al, is 1%.

It was confirmed (results not shown) that the presence of CTAB concentrations from 8×10^{-5} to 1.2×10^{-4} M does not affect the fluorescence of the complex. Hence it is not necessary to compensate for the presence of CTAB monomers in the permeate solutions.

The concentration of LG (between 1×10^{-5} and 1.6×10^{-5} M) does not affect the fluorescence measurements of the complex in the presence of Brij-35 micelles. Hence the analysis of permeate solutions obtained in the presence of this non-ionic surfactant (in which a small amount of LG passes through the membrane) can be performed without modifying the LG concentration added.

Micellar-enhanced ultrafiltration of aluminium

Using the described procedure, aqueous solutions containing 6 mg l^{-1} Al were filtered in both CTAB and Brij-35 micellar media. Different ultrafiltration parameters, such as surfactant concentration, LG concentration and pH, were varied in order to attempt to obtain quantitative retention of the analyte.

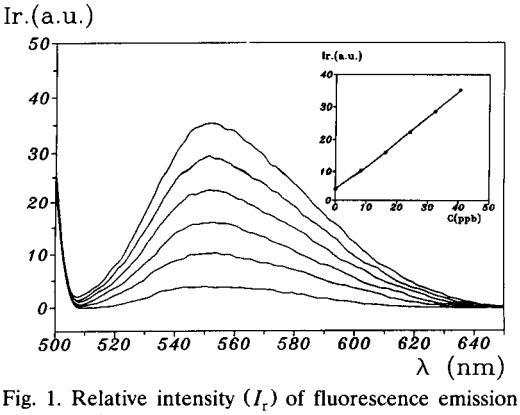

Fig. 1. Relative intensity (I_r) of fluorescence emission (arbitrary units) obtained for several standard solutions of Al in the presence of LG in a Brij-35 micellar medium. Inset: calibration graph obtained using the experimental conditions reported in Table 1.

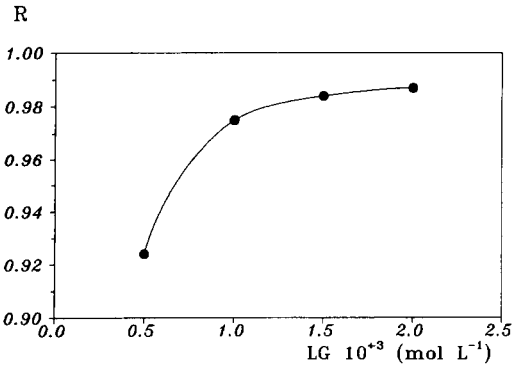

Fig. 2. Effect of the lumogallion concentration on the MEUF of Al. pH = 5; [Al] = 6 mg l^{-1}; [CTAB] = 0.02 M; R = rejection factor.

MEUF of aluminium in the presence of CTAB. Figure 2 indicates that, working at pH 5 in the presence of 0.02 M CTAB, the rejection factor (R) tends to 1 when the LG concentration is $\geq 1 \times 10^{-3}$ M. It is convenient to use this concentration in order to avoid the consumption of an excess of ligand.

The influence of the ligand on the preconcentration performances is very important. A rejection factor of 0.33 was found in the absence of ligand. This effect, which probably implies an electrostatic repulsion due to the surfactant absorbed in the membrane, has also been observed previously [14].

It appears evident that in order to achieve quantitative preconcentration of Al in the retentate, it is necessary to ensure complex formation. This step is favoured by heating the solution. In fact, a rejection factor of only 0.84 was found in the presence of 1×10^{-3} M LG in unheated solutions, indicating that complexation is not complete without heating.

Previous studies on MEUF separations of cations indicated that an increase in pH enhances the retention of these species. However, a high pH values also favours the hydrolysis of matrix components and the precipitation of hydroxides

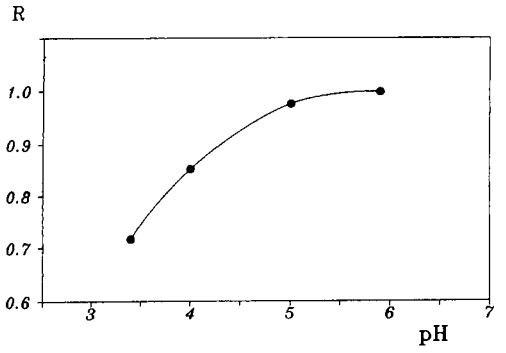

Fig. 3. Effect of pH on the MEUF of Al. [CTAB] = 0.02 M; [Al] = 6 mg l^{-1}; [LG] = 1×10^{-3} M; R = rejection factor.

can occur, which reduces the filtration rate and the selectivity of the process.

Figure 3 indicates that, at pH 5, the rejection factor for Al is > 0.97 and at pH 5.9 the retention of this analyte become quantitative.

At pH 5.9 in the presence of 1×10^{-3} M LG, the retention of Al was quantitative for CTAB concentrations $\geq 7.5 \times 10^{-3}$ (see Fig. 4). In an experiment carried out with 5×10^{-3} M CTAB, Al was quantitatively recovered in the retentate but, during the filtration step, the formation of a precipitate was noted. This could be due to the limited amount of micellized CTAB which is not able to solubilize the Al–LG complex. Therefore, a surfactant concentration of about 10^{-2} M is recommended in order to obtain a good Al separation with low reagent consumption.

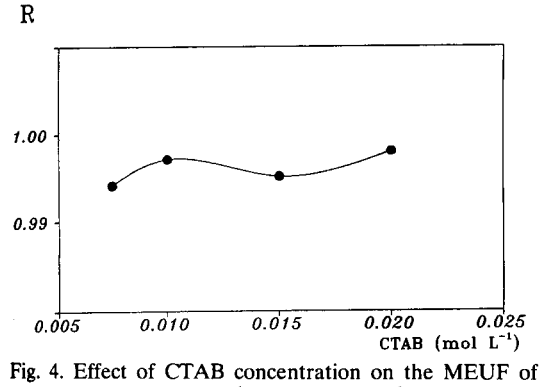

Fig. 4. Effect of CTAB concentration on the MEUF of Al. pH = 5.9; [Al] = 6 mg l^{-1}; [LG] = 1×10^{-3} M; R = rejection factor.

MEUF of aluminium in the presence of Brij-35. Previous studies, carried out in 1×10^{-2} M solutions of Brij-35 demonstrated that, starting from a 1×10^{-3} M concentration of LG, a concentration of 1.58×10^{-5} M of this ligand passes through the membrane. The viscosity of the retentate solution is higher than that obtain in CTAB. These two unfavourable aspects dictated the use of CTAB. However, when working under the same experimental conditions as established previously for CTAB (pH 5.9, 1×10^{-3} M LG and 1×10^{-2} M surfactant) the rejection factor obtained using Brij-35 was 0.98, which indicates that a good recovery of the analyte also resulted in this instance.

Flame atomic emission of aluminium in the presence of surfactant

As the aim of this study was to develop a sensitive procedure for the determination of trace amounts of Al after preconcentration by MEUF, the final step was the measurement of the flame emission of Al in the retentate.

Previous work showed that flame atomic emission in a nitrone oxide–acetylene flame provides a higher sensitivity that atomic absorption measurements and can be applied to the determination of trace levels of Al both in aqueous solutions [19] and in oil-in-water emulsions [20].

The effects of the flame parameters, such as the burner height and the acetylene flow-rate, on the emission of Al solutions, were studied. Figure 5 shows the slope of the calibration lines obtained for an aqueous solution of Al and micellar solutions in the presence of LG. Both exhibit similar variations of the signal as a function of the burner height. Only for solutions containing 2×10^{-3} M LG and 7×10^{-2} M Brij-35 was a strong reduction of the sensitivity (of the Al determination) observed. This could be due to the high viscosity of these solutions, which reduces the aspiration flow. Alternatively, a 5.5 l min^{-1} acetylene flow-rate and a 9.7 l min^{-1} nitrous oxide flow-rate provided the best emissions values for all the standards assayed.

The effect of surfactant concentration on the aspiration flow-rate of the retentate solutions into the flame emission spectrometer was studied. As

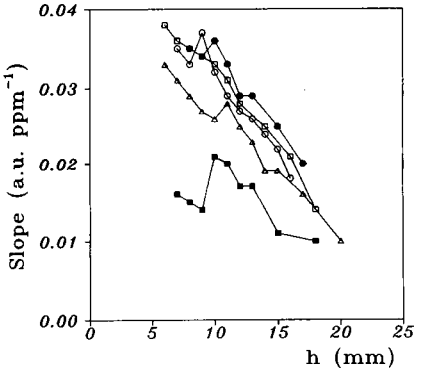

Fig. 5. Effect of the burner height on the sensitivity obtained by flame atomic emission spectrometry for different types of Al solutions. △ = Aqueous standard; □ = standards containing 1×10^{-3} M LG and 2×10^{-2} M Brij-35; ■ = standards containing 2×10^{-3} M LG and 7×10^{-2} M Brij-35; ○ = standards containing 1×10^{-3} M LG and 2×10^{-2} M CTAB; ● = standards containing 2×10^{-3} M LG and 7×10^{-2} M CTAB.

shown in Fig. 6, the aspiration flow-rate of 6 mg l^{-1} Al in the presence of increasing concentrations of CTAB or Brij-35 tends to decrease as the surfactant concentration increases.

The effect of surfactant concentration on the emission signal obtained for Al solutions is shown in Fig. 7. CTAB increases the sensitivity slightly. On the other hand, a strong reduction in the aspiration flow-rate in the Brij-35 system, as discussed previously, negatively affects the sensitivity. In order to correct for this effect, it is necessary to use a peristaltic pump, which imposes a carrier transport flow, independently of the rheological features of the solutions. The results of this approach can be seen in the inset in Fig. 7.

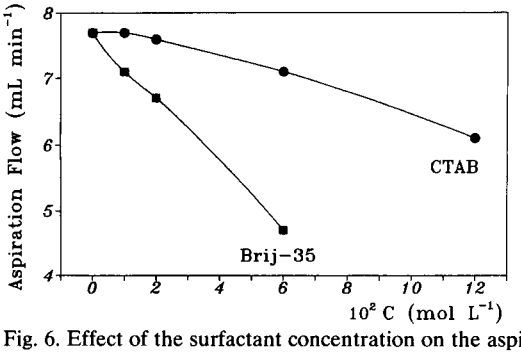

Fig. 6. Effect of the surfactant concentration on the aspiration flow-rate of Al solutions into the flame.

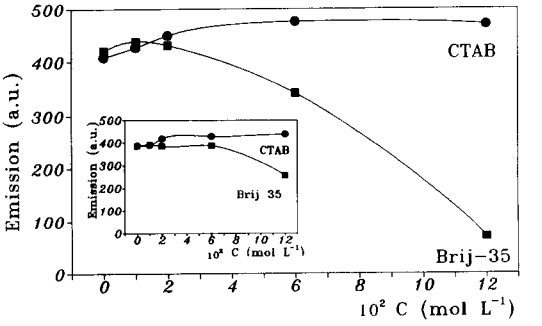

Fig. 7. Effect of the surfactant concentration on the emission intensity (arbitrary units) obtained for the determination of Al by flame atomic emission spectrometry. Inset: same effects studied with an imposed carrier flow-rate of 7 ml min^{-1}. [Al] = 6 mg l^{-1}.

Analytical performance of the developed procedure

CTAB was selected for the MEUF preconcentration of Al solutions, which provides advantages in the flame atomic emission of Al. An LG concentration of the order of 6×10^{-3} M and a CTAB concentration of 0.12 M in the Al standards are recommended for the determination of Al in samples previously concentrated by MEUF.

A typical calibration graph obtained for these standards (in the range 3–12 mg l^{-1}) corresponds to the equation $E = 0.161 + 0.037C$ (mg l^{-1}) with $r = 0.9996$. The high value of the intercept is due to the influence of both LG and the surfactant on the emission background; it can be corrected by adjusting the zero instrument for a blank solution containing LG and CTAB in the absence of aluminium.

Using the experimental conditions previously established, a detection limit of 0.5 mg l^{-1} of Al (for a confidence level of 95%) with a relative standard deviation of 0.3% for ten independent measurements of a 6 mg l^{-1} Al solution was achieved.

Analytical application of the MEUF–flame emission method

Aqueous solutions containing 1 mg l^{-1} of Al were treated as indicated under Experimental. The MEUF of 30 ml of sample was performed until a retentate volume of 5 ml had been ob-

tained, thus providing a sixfold preconcentration factor. The analysis by flame atomic emission of these retentates provided concentration values of 6.3 ± 0.3 mg l^{-1}, which are comparable to the expected result (6 mg l^{-1}).

A 16-fold preconcentration factor was obtained by ultrafiltering 80 ml of the aqueous solution until to obtain 5 ml of retentate. In this instance the analysis of a water sample (containing 0.2 mg l^{-1} Al) after MEUF gave a concentration of 3.9 ± 0.2 mg l^{-1}, of the same order as the 3.2 mg l^{-1} value expected for a 16-fold preconcentration.

From the above results, and taking into account the detection limit of the flame atomic emission of Al for CTAB solutions, samples containing Al concentrations of the order of 30 μg l^{-1} could still be analysed.

Conclusions

MEUF of aqueous Al solutions, in the presence of LG and CTAB at pH 5–5.9, provides a quantitative preconcentration of Al. This surfactant-rich matrix can be exploited to improve the analytical detection limit of the flame atomic emission spectrometric determination of Al.

When cationic surfactants are used, the accumulation of uncomplexed metal ions in the retentate is possible, as some electrostatic repulsion from the membrane surfactant system occurs. However, taking into account that the atomic spectrometric analysis is less sensitive to the presence of interferences, the determination of Al in the CTAB surfactant-rich retentate can be performed without problems.

MEUF of metal complexes provides an alternative means of preconcentrating trace elements, comparable to that obtained by liquid–liquid extraction but avoiding the problems related to the handling of large volumes of organic solvents.

Studies are in progress in order to develop a multi-elemental preconcentration method based on the use of non-specific ligands and MEUF, which could be employed as a preliminary step for analyses by atomic spectrometry.

A. Morales-Rubio acknowledges an FPI grant from the Ministerio de Educación y Ciencia.

REFERENCES

1 H. Strathmann, J. Membr. Sci., 9 (1981) 121.
2 J.H. Ephraim and J.A. Marinsky, Anal. Chim. Acta, 232 (1990) 171.
3 S.T. Hwang and K. Kammermeyer, in P.J. Elving, E. Grushka and I.M. Kolthoff (Eds.), Treatise on Analytical Chemistry, Vol. 5, Wiley, New York, 2nd edn., 1982, p. 185.
4 P.S. Leung, in A.R. Cooper (Ed.), Membranes and Applications, Plenum, New York, 1979, p. 415.
5 R.O. Dunn, Jr., J.F. Scamehorn and S.D. Christian, Sep. Sci. Technol., 20 (1985) 257.
6 G. Jonsson, Desalination, 53 (1985) 3.
7 J.F. Scamerhon and J.H. Harwell, in D.T. Wasan, D.O. Shah and M.E. Ginn (Eds.), Surfactants and Chemical Engineering, Dekker, New York, 1988.
8 E. Pramauro, Ann. Chim. (Rome), 80 (1990) 101.
9 G.A. Smith, S.D. Christian, E.E. Tucker and J.F. Scamehorn, in W.L. Hinze and D.W. Armstrong (Eds.), Ordered Media in Chemical Separations (ACS Symposium Series, No. 342), American Chemical Society, Washington, DC, 1987, p. 1894.
10 L.L. Gibbs, J.F. Scamehorn and D.S. Christian, J. Membr. Sci., 30 (1987) 67.
11 E. Pramauro, A. Bianco-Prevot, P. Savarino, G. Viscardi, M. de la Guardia and E. Peris-Cardells, unpublished results.
12 J.F. Scamehorn, R.T. Ellington, S.D. Christian, B.W. Penney, R.O. Dunn and S.N. Bhat, AIChE Symp. Ser., 82 (1986) 48.
13 K.J. Sasaki, S.L. Burnett, S.D. Christian, E.E. Tucker and J.F. Scamehorn, Langmuir, 5 (1989) 363.
14 E. Pramauro, A. Bianco, E. Barni, G. Viscardi and W.L. Hinze, Colloids Surf., 63 (1992) 291.
15 E. Pramauro, A. Bianco-Prevot, E. Pelizzeti, R. Marchelli, A. Dossena and A. Biancardi, Anal. Chim. Acta, in press.
16 U.R. Dharmawardana, S.D. Christian, R.W. Taylor and J.F. Scamerhorn, Langmuir, 8 (1992) 414.
17 N. Ishibashi and K. Kina, Anal. Lett., 5 (1972) 637.
18 J.L. Carrión and M. de la Guardia, Anal. Chim. Acta, 198 (1987) 53.
19 J. Quiñonero, C. Mongay and M. de la Guardia, Microchem. J., 43 (1991) 213.
20 M. de la Guardia, V. Berenguer and J.L. Carrión, Analusis, 8 (1980) 166.

Analytica Chimica Acta, 276 (1993) 181–187
Elsevier Science Publishers B.V., Amsterdam

Liquid–liquid extraction of palladium(II) from nitric acid by bis(2-ethylhexyl) sulphoxide

J.P. Shukla

Radiochemistry Division, Bhabha Atomic Research Centre, Trombay, Bombay 400085 (India)

R.K. Singh, S.R. Sawant and N. Varadarajan

Power Reactor Fuel Reprocessing Plant, Bhabha Atomic Research Centre, Trombay, Bombay 400085 (India)

(Received 28th May 1992; Revised manuscript received 12th August 1992)

Abstract

The extraction of palladium(II) nitrate by bis(2-ethylhexyl) sulphoxide (BESO) was evaluated over a wide range of acidity, and BESO was shown to have a strong extraction ability toward this thiophilic "soft" metal. Essentially quantitative extraction of trace and macro amounts of palladium is easily accomplished from about 8 M HNO_3 down to pH 2 solutions by 0.2 M BESO into toluene. Optimum conditions such as aqueous phase acidity, solvent, period of equilibration, aqueous to organic phase ratios, reagent concentration and strippant were established for the selective and reversible extraction and separation of palladium. Slope analyses applied to Pd(II) distribution experiments from nitrate solutions showed a predominant formation of the solvated organic phase complex $Pd(NO_3)_2 \cdot 2BESO$. Recovery of the extractant from loaded palladium is easily accomplished by using sodium thiosulphate or a mixture of 2 M sodium carbonate + 0.5 M ammonia solution. The extracted complex was characterized by elemental analysis and IR and UV–visible spectrometry, and its composition was confirmed to be $Pd(NO_3)_2 \cdot 2BESO$.

Keywords: Extraction; Nitric acid; Palladium

Liquid–liquid extraction has been developed as one of the most important methods for the separation and purification of precious metals [1,2], of which palladium is one of the most important. Although extraction of palladium has been studied with numerous commercial extractants, most of them contain oxygen or nitrogen as donor atoms, such as hydroxy oximes, carboxylic acids and organophosphorus compounds, e.g., dithizone [3], diethylammonium dithiocarbamate [4], 2-nitroso-1-naphthol-4-sulphonic acid [5] and a synergistic mixture of quinolin-8-ol and tributyl phosphite [6]. Some thia cyclic and acyclic crown compounds (sulphide podands) have also recently been explored as potential extractants for palladium [7,8].

Relatively few data are available on extractants possessing sulphur as the donor atom. Numerous studies have unambiguously established that sulphur-containing extractants are highly effective and selective for Pd(II), classified as a "soft" Lewis acid [9–12]. Among such extractants, long-chain dialkyl sulphoxides have been gaining importance as extractants for many radioactive, non-ferrous, transition and post-transition metals [13–15]. Their extraction capacity for metals is comparable to or even greater than that

Correspondence to: J.P. Shukla, Radiochemistry Division, Bhabha Atomic Research Centre, Trombay, Bombay 400085 (India).

of tributyl phosphate. Little attention seems to have been focused on investigating their extraction characteristics particularly for thiophilic heavy metals such as the platinum group metals. Although bis(2-ethylhexyl) sulphoxide (BESO), a sterically hindered branched-chain solvating extractant, has proved to be a powerful extractant for U, Pu, Am, etc. [16–19], no effort has been made to study its complexation behaviour with palladium. Recently, dioctyl sulphoxide (DOSO) in xylene was used to extract Pd(II) over a narrow acid range restricted to 0.5–1.5 mol dm^{-3} HNO_3 [20].

Owing to its importance, studies have been initiated recently particularly to recover palladium from acidic high-level radioactive wastes (HLAW) generated from nuclear fuel reprocessing operations containing palladium and other useful fission products [21]. The recovery of noble metals such as Ru, Rh and Pd offers an alternative potential source of supply to meet part of the ever-increasing demand for platinium metals. As a part of a continuing programme to explore the usefulness of sulphoxides as extractants for rare metals as nitrates, in this work the liquid–liquid extraction of palladium(II) into toluene by BESO was studied under a wide range of experimental conditions, mainly from moderately acidic nitrate solutions as encountered in decontaminating HLAW. BESO was chosen as radiolytic breakdown products are expected to cause minimum process difficulties and also because its branched structure confers improved solubility in common organic diluents. As palladium and other platinum group metals are usually maintained as their chloro complexes, separation based on selective extraction of the chloro complexes was also attempted. The effects of aqueous phase acidity, time of equilibration, aqueous to organic phase ratios, reagent concentration, strippant and nature of the diluent on metal extraction were studied in order to optimize the conditions. Attempts were also made to understand the nature of the metal ion and the nitric acid species extracted into the diluted sulphoxide phase. Pd–S bond formation in the extraction of palladium(II) was confirmed by the IR spectra of the solid complex.

EXPERIMENTAL

Apparatus

A Shimadzu UV-160 UV–visible spectrophotometer with 10-mm matched quartz cells was used for recording the absorption spectra of organic extracts. IR spectra of samples in Nujol mulls between CsI discs were recorded using a Pye Unicam Model 9512 spectrophotometer in the range 4000–200 cm^{-1}.

Reagents

All the chemicals were of analytical- or general-reagent grade unless specified otherwise.

Benzene, chloroform, *o*-dichlorobenzene, 1,2-dichloroethane, carbon tetrachloride, xylene and toluene solvents were used as received. The organic phase and aqueous acidic phase were saturated with each other prior to their use in order to prevent any volume change that may occur during extraction.

BESO (Fairfield Chemical, Blythewood, SC) was used after treating it with an excess of 11 M HNO_3 in order to oxidize any sulphide present as an impurity. The mixture obtained was treated with NaOH and then washed with distilled water until free from alkali. The product obtained was then distilled at reduced pressure (0.4 mmHg) and the middle fraction distilling at around 140°C was collected and used for the experiments. The BESO product obtained as above was found to be more than 99.6% pure as determined by non-aqueous titration in acetic anhydride using standard perchloric acid in dioxane [22].

Tracer

Radiopalladium tracer (Pd-103), obtained in the Pd(II) state from the Isotope Division, BARC, was used throughout. Its radiochemical purity was ascertained by γ-ray spectrometry using the low-energy photon scintillation (LEPS) method. Pd-103 was assayed using a well-type NaI(Tl) scintillation detector coupled to a single-channel analyser.

Distribution ratio (D_{Pd}) measurements

Equal volumes (1 ml) of aqueous Pd-103 tracer in nitric acid of the desired molarity and BESO

dissolved in an organic solvent were pipetted into a 15-ml glass-stoppered equilibration tube and shaken mechanically for ca. 40 min. Extractions were done at room temperature (23–25°C). Preliminary experiments revealed that a 20–30-min shaking time was adequate to ensure the attainment of equilibrium. After settling for 30 min and centrifuging if necessary, suitable aliquots from both phases were withdrawn and radioassayed. The distribution ratio (D_{Pd}), defined as the total concentration of Pd in the organic phase per millilitre divided by the total concentration of Pd in the aqueous phase per millilitre, was calculated. From a knowledge of D_{Pd}, the volume of the aqueous phase (V_a) and the volume of the organic phase (V_o), the percentage extraction of Pd (E) was calculated: $E = 100D_{Pd}/D_{Pd} + (V_a/V_o)$. All the measurements were done at least in duplicate and the agreement of the D_{Pd} values obtained was within $\pm 2\%$ with a good material balance ($> 95\%$).

For studying the back-extraction, a suitable aliquot from the loaded organic phase was withdrawn into an equilibration tube and back-extracted for about 20 min with same volume of the strippant.

The uptake of nitric acid by various concentrations of BESO (0.05–0.4 M) after contacting with either 0.5 or 2 M HNO_3 was determined alkalimetrically using phenol red as indicator.

The palladium complex was prepared by liquid–liquid extraction of 5 mM aqueous palladium nitrate solution (10 ml) at pH 2 with dodecane (10 ml) containing 10 mM BESO. The organic layer was dried with anhydrous sodium sulphate, evaporated to dryness and the crude product recrystallized from hexane.

RESULTS AND DISCUSSION

Kinetic experiments showed that equilibrium was attained after phase contact for 10–15 min and was dependent to some extent on the solvent used. The equilibration time required for quantitative extraction depended on the metal concentration, the aqueous to organic phase volume ratio, etc. A shaking time of 30–35 min was

TABLE 1

Extraction of palladium(II) into toluene by BESO as a function of acid concentration [a]

HNO_3 (M)	[BESO] (M)						HCl (M)	0.20	
	0.01		0.05		0.20				
	D_{Pd}	E [b] (%)	D_{Pd}	E (%)	D_{Pd}	E (%)		D_{Pd}	E (%)
0.01	0.89	47.1	4.49	81.8	17.62	94.6	0.01	16.42	94.3
					12.46 [c]	92.6		11.66 [d]	92.1
0.5	0.85	46.0	4.43	81.6	16.90	94.4	0.5	6.48	86.3
					12.35 [c]	92.5		5.73 [d]	85.1
1.0	0.83	45.4	4.40	80.5	16.53	94.3	1.0	0.44	30.6
2.0	0.77	43.5	4.02	80.1	13.44	93.1	2.0	0.42	29.6
3.0	0.61	37.9	3.55	78.0	13.02	92.9	3.0	0.40	28.6
4.0	0.51	33.8	3.25	76.4	12.84	92.8	4.0	0.39	28.1
5.0	0.42	29.6	3.11	75.7	11.13	91.8	5.0	0.38	27.5
6.0	0.33	24.8	3.02	75.1	11.02	91.7	6.0	ND [e]	ND
7.0	0.25	20.0	2.72	73.1	10.81	91.5	7.0	ND	ND
8.0	0.19	15.9	2.55	71.8	10.60	91.4	8.0	ND	ND

[a] Initial Pd concentration $\approx 10^{-4}$ M Pd-103 tracer; aqueous to organic volume ratio, 1; temperature = 23–25°C (room temperature). [b] E = extraction. [c] Values correspond to those obtained with ca. 1 mg ml^{-1} Pd dissolved in HNO_3 and spiked with tracer Pd-103. [d] Values correspond to those obtained with ca. 1 mg ml^{-1} Pd dissolved in HCl and spiked with tracer Pd-103. ND = not determined.

adequate for almost quantitative recovery of palladium from aqueous nitrate–chloride solutions.

Extraction of HNO_3 by BESO

Extraction of nitric acid by BESO can be represented by the reaction

$$H^+_{(a)} + NO^-_{3(a)} + n\text{BESO}_{(o)} \overset{K_H}{\rightleftharpoons} HNO_3 \cdot n\text{BESO}_{(o)}$$

where the subscripts a and o refer to the aqueous and organic phases, respectively. The equilibrium constant , K_H, is given by

$$K_H = [HNO_3 \cdot n\text{BESO}]_{(o)} / [H^+]_{(a)}[NO^-_3]_{(a)}[\text{BESO}]^n_{(o)}$$

assuming that the activity coefficients of the various species do not change significantly in the concentration ranges used. Taking logarithms on both sides of above equation and rearranging, it can be shown that

$$\log[H^+]_{(o)} - 2\log[H^+]_{(a)} = \log K_H + n \log[\text{BESO}]_{(o)}$$

where $[H^+]_{(o)} = [HNO_3 \cdot n\text{BESO}]_{(o)}$ and $[H^+]_{(a)} = [NO^-_3]_{(a)}$.

$[H^+]_{(a)}$ was evaluated from the value of $[H^+]_{(o)}$ and the known dissociation constant (23.5) of nitric acid [23]. $[\text{BESO}]_{(o)}$ was calculated from the initial total BESO concentration and the value of $[H^+]_{(o)}$. A plot of $\log[H^+] - 2\log[H^+]_{(a)}$ versus $\log[\text{BESO}]_{(o)}$ should be a straight line with a slope of unity if the species extracted is $HNO_3 \cdot$ BESO. BESO extracts nitric acid considerably from aqueous solutions. Nitric acid formed a 1:1 solvated complex composition in the toluene phase where one molecule of the acid is required for one molecule of the sulphoxide. This is in accord with previous observations with several other dialkyl sulphoxides [14,15]. The value of K_H was found to be 0.41.

Variation of D_{Pd} values with HNO_3–HCl concentration

To assess the dependence of the extraction capacity on the aqueous phase acidity, the extractability of palladium from 8 M HNO_3 down to pH 2 solutions into toluene by BESO from unbuffered aqueous nitrate solutions was systematically studied (Table 1). It can be seen that lowering the acidity from 8 to 0.01 M HNO_3 caused an increase in extraction from 72 to 82% by 0.05 M BESO. With an increased extractant concentration of 0.2 M, maximum extraction was accomplished at a lower acidity of about 0.01 M (pH ≈ 2) to 0.5 M HNO_3. Therefore, a good extraction efficiency can be achieved at low acidity.

The extraction efficiency was unchanged whether nitrate or chloride was used as the anion and the high efficiency of extraction was not affected by the presence of relatively high concentrations (ca. 2 M) of nitric acid. The degree of extraction of palladium(II) with 0.2 M BESO in toluene was independent of the HNO_3 or HCl concentrations in the range 0.5–5 M, although an increase in acidity from 0.01 M (pH 2) to 1.0 M HCl drastically reduced the extraction from 94 to 31%. The shaking time necessary for extraction of Pd from 5 M HNO_3 was not greater than that needed with 0.5 M HNO_3. The values of D_{Pd} were virtually independent of the initial palladium concentration investigated in the range (ca. 10^{-4} M), indicating that only mononuclear species were involved in the extraction systems. Also these D_{Pd} values between aqueous acidic solutions and various BESO–diluent phases were generally high, which was as expected from the strong "soft–soft" interaction of sulphur with palladium(II).

Variation of D_{Pd} values with sulphoxide concentration

The extractability of Pd(II) from 2 M HNO_3 into toluene by BESO (0.05–0.5 M) increased with increasing extractant concentration. A 0.2 M BESO solution extracted more than 95% of 1 mg ml^{-1} Pd(II) in a single step.

Extraction of Pd(II) by BESO from nitrate solution can be represented by the reaction

$$Pd^{2+}_{(a)} + 2NO^-_{3(a)} + n\text{BESO}_{(o)} \rightleftharpoons Pd(NO_3)_2 \cdot n\text{BESO}_{(o)}$$

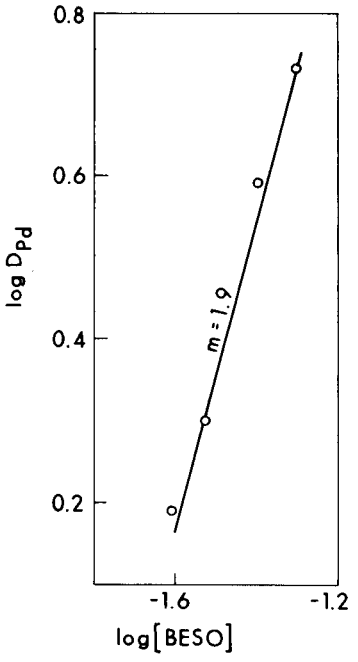

Fig. 1. Plot of extraction of Pd(II) into toluene by BESO from 2 M HNO_3 as a function of initial extractant concentration.

for which the equilibrium constant, K_{ex}, is given by

$$K_{ex} = [Pd(NO_3)_2 \cdot n\text{BESO}]_{(o)} / [Pd^{2+}]_{(a)}[NO_3^-]^2_{(a)}[\text{BESO}]^n_{(o)} \quad (1)$$

where the distribution ratio, D_{Pd}, of palladium is $D_{Pd} = [Pd(NO_3)_2 \cdot n\text{BESO}]_{(o)}/[Pd^{2+}]_{(a)}$. Assuming $[NO_3^-]$ is constant and taking logarithms on both sides of the Eqn. 1 and rearranging gives

$$\log D_{Pd} = \log K_{ex} + n \log[\text{BESO}] + 2 \log[NO_3^-] \quad (2)$$

A plot of log D_{Pd} versus $\log[\text{BESO}]_{free}$ in the organic phase is shown in Fig. 1. The line drawn through the experimental points gave a slope of $n = 2$ by maintaining the extractant at low concentrations in the range 0.05–0.2 M. This slope obtained for Pd(II) indicates that the extracted species in the sulphoxide diluent phase is predominantly of the type $Pd(NO_3)_2 \cdot 2\text{BESO}$. This is in accord with the results obtained for extraction of palladium by DOSO from aqueous HCl or HNO_3 media [24]. As BESO is a neutral extractant, it follows that its role in the extraction is solely solvation of the palladium complex extracted, which itself must therefore be neutral.

Influence of diluents

The extractability and selectivity for the extraction of metals by organic extractants are greatly affected by the nature of the solvent. To study the influence of several typical commonly available aliphatic and aromatic organic solvents on the efficiency of palladium extraction by BESO, the extractability of palladium from 2 M HNO_3 was investigated with 0.2 M BESO dissolved in various solvents (diluents).

Table 2 summarizes the results for the effect of diluents on the extraction of palladium. Nonpolar diluents such as xylene yielded less extraction than polar diluents, but polarizable solvents such as benzene, and toluene gave high metal extraction. Among halogenated hydrocarbon solvents, 1,2-dichloroethane and *o*-dichlorobenzene gave a higher metal extraction than chloroform. A high D_{Pd} may be associated with the low dielectric constants of aliphatic hydrocarbons, which favour the formation of a solvated neutral Pd(II)–BESO complex. The straight lines with slopes of ca. 2 obtained for the plots of log D_{Pd}

TABLE 2

Influence of organic diluents on the extraction of Pd(II) from aqueous nitric acid medium by BESO [a]

Diluent	Dielectric constant [25,26]	D_{Pd}	Extraction (%)
Benzene	2.28	7.44	88.2
Dodecane	2.02	12.00	92.3
Chloroform	4.81	1.96	66.2
Carbon tetrachloride	2.24	9.22	90.2
Cyclohexane	2.10	8.00	88.8
o-Dichlorobenzene	9.93	7.32	88.0
1,2-Dichloroethane	10.36	4.98	83.3
Solvesso-100	–	10.00	90.9
Toluene	2.38	13.41	93.1
Xylene	2.27	3.74	78.9

[a] Extractant: 0.2 M BESO, dissolved in organic diluents. Aqueous phase acidity: 2 M HNO_3.

versus $\log[BESO]_{free}$ for benzene, dodecane and toluene confirm that Pd(II) is extracted essentially as a 1:2 ion pair irrespective of the organic medium. Toluene was selected as the diluent throughout this study, however, owing to its relatively lower aqueous solubility and ready availability.

Volume ratio studies

A study was made to assess whether large aqueous to organic ratios could be tolerated for the successful extraction of palladium by BESO under the optimum conditions. The results show that for aqueous to organic volume ratios up to 10:1, Pd(II) could be extracted with > 90% efficiency in a single step into toluene by 0.2 M BESO; ca. 80% of this cation was extracted at a high volume ratio of 20:1 under similar conditions.

Back-extraction of palladium

In any extraction process it becomes almost imperative to back-extract the metal from the loaded organic phase. As the values of D_{Pd} were high from low to high concentrations of nitric acid its stripping became almost impractical with nitric acid solutions alone (Table 3). Among many strippants tried, a mixture of sodium carbonate and 0.5 M ammonia solution was found to be effective (> 95%) for stripping palladium with a single equal-volume contact. The stripping of palladium was ca. 30–50% even with three equal-volume contacts with solutions of 2 M each of sodium carbonate and ammonia solution applied separately. Stripping was almost complete (> 95%) within 10–15 min (aqueous to organic volume ratio = 1) with 0.2 M or higher concentrations of sodium thiosulphate.

TABLE 3

Back-extraction of palladium(II) from loaded BESO phase [a]

Strippant	D_{Pd}	Palladium back-extracted (%)
HNO_3 (10 M)	16.50	5.7
HCl (10 M)	16.30	5.8
Sodium carbonate (2 M)	2.35	29.9
Ammonia solution (2 M)	1.00	50.0
Mixture of sodium carbonate (1 M) + ammonia (0.5 M)	0.43	69.9
Mixture of sodium carbonate (2 M) + ammonia (0.05 M)	0.25	80.0
Mixture of sodium carbonate (2 M) + ammonia (0.5 M)	0.05	95.2
Sodium thiosulphate (0.2 M)	0.01	> 99.0

[a] Extractant: 0.2 M BESO–toluene.

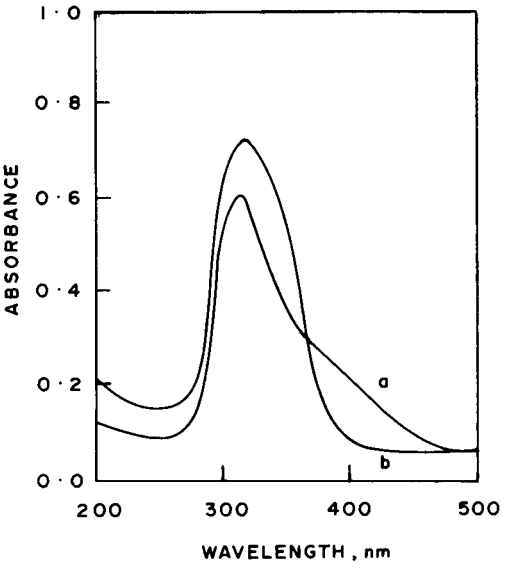

Fig. 2. Absorption spectra of palladium(II) nitrate extracted from 0.5 M HNO_3 aqueous medium by (a) 0.2 M BESO–toluene and (b) 30% TBP–toluene.

Characterization of the extracted complex

The extracted complex is dark brown, stable in air and not deliquescent. It is readily soluble in common aliphatic and aromatic solvents such hexane, benzene, toluene, dodecane and halogenated hydrocarbons, e.g., CH_2Cl_2, $CHCl_3$ and CCl_4, and the solutions are also generally stable, but it is only slightly soluble in methanol. The complex is negligibly soluble in water and readily decomposes, depositing palladium.

Figure 2 shows the absorption spectra of the Pd(II) complex extracted with BESO–toluene and with TBP–toluene. The similarity of the spectra confirms that the species involved are also similar.

Elemental analysis of the extracted complex gave C 49.5, H 8.6, N 3.7, Pd 13.8%, which compared with calculated values for $Pd(NO_3)_2 \cdot$

2BESO of C 49.3, H 8.8, N 3.6, Pd 13.7%. Hence the extracted complex in the organic phase is confirmed to be $Pd(NO_3)_2 \cdot 2BESO$. The IR spectra (Nujol mulls) indicate coordination of the BESO molecule to palladium through sulphur. A frequency shift (δ) of 190 cm^{-1} of the S=O stretch towards higher frequency was observed in the palladium(II) nitrate complex with BESO, which definitely suggests a strong coordination through sulphur.

Recovery of palladium from synthetic waste solution

Experiments were performed to recover palladium from a synthetic mixed fission product acidic waste solution spiked with Pd-103. More than 95% of Pd ($D_{Pd} = 18.77$) could be recovered in a single contact (aqueous to organic volume ratio = 1) from 0.5 M HNO_3 or HCl into toluene by 0.5 M BESO. Finally, Pd could be readily back-extracted almost completely (> 98%) from the loaded sulphoxide phase with aqueous sodium thiosulphate solution (ca. 0.2 M). Hence palladium Pd can be efficiently and reversibly extracted from HLAW solutions.

Conclusions

A rapid, simple and efficient method for the recovery of palladium by BESO–toluene from aqueous acidic nitrate and chloride solutions was developed. The high extraction efficiencies for palladium recovery from aqueous matrices suggest potential application of the sulphoxides in hydrometallurgy. Application of this method to the removal of palladium from high-level radioactive waste is also indicated.

The authors thank Dr. P.R. Natarajan, Head Radiochemistry Division, and Shri M.K.T. Nair, Head, PREFRE, BARC, for their keen interest in this work.

REFERENCES

1 G.M. Ritcey and A.W. Ashbrook, Solvent Extraction, Part II, Elsevier, Amsterdam, 1979, p. 372.
2 R.I. Edwards and W.A.M. te Riele in T.C. Lo, M.H.I. Baird and C. Hanson (Eds.), Handbook of Solvent Extraction, Wiley, New York, 1983, p. 725.
3 T. Ashizawa, K. Haruyama, K. Nagasawa and Y. Morimoto, Bunseki Kagaku, 13 (1964) 11.
4 H. Bode and F. Neumann, Fresenius' Z. Anal. Chem., 172 (1960) 1.
5 S. Komatsu and S. Kamiyama (1960) J. Chem. Soc. Jpn., Pure Chem. Sect., 81 (1960) 1940.
6 G. Lee and K. Chung, Analyst, 115 (1990) 965.
7 J.P. Shukla and R.A. Bartsch, in preparation.
8 E. Lachowicz and M. Czapiuk, Talanta, 37 (1990) 1011.
9 F.E. Beamish, The Analytical Chemistry of the Noble Metals, Pergamon Oxford, 1966.
10 R.I. Edwards, in B.H. Lucas, G.M. Ritcey and H.W. Smith (Eds.), Proceedings of ISEC-77, Canadian Institute of Mining and Metallurgy, Montreal, 1979, p. 24.
11 J.M. Barnes and J.D. Edwards, Chem. Ind. (London), (1982) 151.
12 Y. Baba, T. Eguehi and K. Inoue, J. Chem. Eng. Jpn., 19 (1986) 361.
13 Y.E. Nikitin, Y.I. Murinov and A.M. Rozen, Russ. Chem. Rev., 45 (1976) 1155.
14 S.A. Pai, J.P. Shukla, P.K. Khopkar and M.S. Subramanian, J. Radioanal. Chem., 42 (1978) 323.
15 J.P. Shukla, M.S. Nagar and M.S. Subramanian, in R.B. Akell and C.J. King (Eds.), Proceedings of International Solvent Extraction Conference Denver, American Inst. of Chemical Engineers, New York, 1983, p. 460.
16 B. Moyer, W.J. McDowell and G.N. Case, in R.B. Akell and C.J. King (Eds.), Proceedings of International Solvent Extraction Conference, Denver 1983, American Inst. of Chemical Engineers, New York, p. 144.
17 B.A. Moyer, C.F. Baes, Jr., W.J. McDowell, C.E. Coley and G.N. Case, paper presented at International Conference on Separation Science and Technology, Hamilton, 1989.
18 J.P. Shukla and C.S. Kedari, Radiochim. Acta, 56 (1992) 21.
19 G.R. Mahajan, D.R. Prabhu, J.P. Shukla and G.M. Nair, Thermochim. Acta, 196 (1992) 357.
20 G.H. Rizvi and P.R. Natarajan, Fresenius' J. Anal. Chem., 336 (1990) 498.
21 R.G. Shuler, C.B. Bowers, Jr., J.E. Smith, Jr., V. Van Brunt and M.W. Davis, Jr., Polyhedron, 6 (1987) 1125.
22 D.C. Wimer, Anal. Chem., 30 (1958) 2060.
23 J. Bjerrum, G. Schwarzenbach and L.G. Sillén (Eds.), Stability Constants of Metal Complexes, II. Inorganic Ligands, Chemical Society, London, 1958.
24 V.A. Mikhailov, V.G. Torgov, E.N. Gilbert, L.N. Mazalov and A.V. Nikolaev, in J.G. Gregory, B. Evans and P.C. Weston (Eds.), Proceedings of ISEC-71, 1971, Society of Chemical Industry, London, Volume II, p. 1112.
25 T. Sekine and Y. Hasegawa, Solvent Extraction: Fundamentals and Application, Dekker, New York, 1977, pp. 48–50.
26 C. Reichardt, Solvent Effects in Organic Chemistry, Verlag Chemie, New York, 1979, pp. 270–272.

Analytica Chimica Acta, 276 (1993) 189–195
Elsevier Science Publishers B.V., Amsterdam

Three-level screening designs for the optimisation or the ruggedness testing of analytical procedures

Y. Vander Heyden, M.S. Khots and D.L. Massart

Vrije Universiteit Brussel, Farmaceutisch Instituut, Laarbeeklaan 103, B-1090 Brussels (Belgium)

(Received 2nd October 1992)

Abstract

Several Plackett–Burman designs have been proposed as screening designs for the optimisation or the ruggedness testing of a test procedure. One of these, a three-level design, described in the literature can lead to wrong conclusions about the influence of the different factors due to the construction of the design. When three levels of the variables that may have an influence on the test procedure require examination, one should use a reflected two-level design or a well balanced three-level design. A proposal for the latter is given.

Keywords: Ruggedness testing; Optimisation

Screening designs such as Plackett–Burman designs [1] are used for optimisation or ruggedness testing of an analytical procedure to determine the influence of experimental factors on measured responses [2–5]. In optimisation studies they are used for selecting from many variables those that have the more meaningful effects. In ruggedness testing one investigates the effect of relatively small changes of the value of the factors given in the analytical procedure. For instance, if a colorimetric procedure is carried out at pH 10.0 and $T^0 = 20°C$, one might wonder whether small departures from the stated value, e.g., pH 9.8–10.2 or $T^0 = 18–22°C$ cause variations in the measured absorption.

Classically a two-level design is used for this purpose [2,4,5]. One calls the values of the procedure the nominal values (pH 10.0, $T^0 = 20°C$) and the changed values the extreme values. A two-level design is then a design which compares the nominal value to one of the extreme values.

When one would like to obtain information about three levels of a factor (e.g., level 0, the nominal level, and levels 1 and -1, the extreme levels, e.g., pH 10.2 and 9.8) an attractive possibility at first sight appeared to be the three-level design as proposed by Plackett and Burman [1]. However in the literature there are few practical examples in which a three-level Plackett–Burman design is used. An exception is the paper by Jones [3]. Mostly two-level Plackett–Burman designs are used for this purpose. To obtain information about three levels of a factor one can apply two-level designs as follows. One performs a reflected two-level design, i.e., a two-level design executed twice, namely once with the levels 0 and 1 for the factors and once with the levels 0 and -1. Another possibility is the use of fractional factorial designs, as well for two levels as for three levels of the factors to be considered [6,7]. In the course of our work on ruggedness testing we decided to study the application of the three-level Plackett–Burman design.

Correspondence to: D.L. Massart, Vrije Universiteit Brussel, Farmaceutisch Instituut, Laarbeeklaan 103, B-1090 Brussels (Belgium).

DISCUSSION AND THEORY

Let us first consider a two-level Plackett–Burman design (Table 1). After performing the design one or more responses have been measured for each experiment. Here we shall suppose that only one, namely y, was measured. A (main) effect for each factor is calculated with these responses.

$$E_J = \frac{\sum y(1)}{n} - \frac{\sum y(0)}{n} \quad (1)$$

where E_J is the effect for factor J; $\sum y(1)$ is the sum of the responses where factor J is at level 1; $\sum y(0)$ is the sum of the responses where factor J is at level 0 and n is the number of times factor J is at each level ($n = 4$ for an eight-experiment matrix). Because of the very reduced number of experiments (N) with which a large number of factors ($N - 1$) are investigated in a Plackett–Burman design each main effect is confounded with a number of two-factor, three-factor and higher multiple-factor interactions. The Plackett–Burman designs for which N is a power of 2 are in fact saturated fractional factorials. For instance, the $N = 8$ Plackett–Burman design, as shown in Table 1, is a 2^{7-4} fractional factorial or a 1/16 fractional factorial design. This means that each main effect is confounded with 15 multiple-factor interactions [8]. However the main effects of different factors are not confounded with each other. For the Plackett–Burman designs that are fractional factorials the multiple-factor interactions that are confounded with a main effect can be identified by constructing a confounding matrix or columns of contrast coefficients [8,9].

TABLE 1

Two-level, eight-experiment ($N = 8$), Plackett–Burman design

(In the design 0 and 1 represent the two levels for the factors)

Exp.	Factors							Measured response
	A	*B*	*C*	*D*	*E*	*F*	*G*	
1	1	1	1	0	1	0	0	y_1
2	0	1	1	1	0	1	0	y_2
3	0	0	1	1	1	0	1	y_3
4	1	0	0	1	1	1	0	y_4
5	0	1	0	0	1	1	1	y_5
6	1	0	1	0	0	1	1	y_6
7	1	1	0	1	0	0	1	y_7
8	0	0	0	0	0	0	0	y_8

TABLE 2

Three-level, nine-experiment ($N = 9$) matrix derived by linear transformation from the design as proposed by Plackett and Burman ($0 \rightarrow -1$, $1 \rightarrow 0$, $2 \rightarrow 1$)

(In the design 0, −1, 1 represent the different levels of the factors)

Exp.	Factor								Measured response
	A	*B*	*C*	*D*	*E*	*F*	*G*	*H*	
1	−1	0	1	1	−1	1	0	0	y_1
2	0	−1	0	1	1	−1	1	0	y_2
3	0	0	−1	0	1	1	−1	1	y_3
4	1	0	0	−1	0	1	1	−1	y_4
5	−1	1	0	0	−1	0	1	1	y_5
6	1	−1	1	0	0	−1	0	1	y_6
7	1	1	−1	1	0	0	−1	0	y_7
8	0	1	1	−1	1	0	0	−1	y_8
9	−1	−1	−1	−1	−1	−1	−1	−1	y_9

The fact that main effects are not confounded with each other is due to a well balanced design. This means that e.g., in an $N = 8$ design (Table 1) each factor (e.g., factor A) is 4 times at level 0 (exp. 2, 3, 5, 8) and 4 times at level 1 (exp. 1, 4, 6, 7). Furthermore the four times that factor A is at level 0, each other factor (e.g., factor E) is twice at level 0 (exp. 2, 8) and twice at level 1 (exp. 3, 5). This is also the case when this factor A is at level 1 (then factor E is at level 0 in exp. 6 and 7; and at level 1 in exp. 1 and 4). Now when E_A is calculated the influences of the factors except for factor A cancel and an effect is obtained that is not confounded with another main effect.

The three-level Plackett–Burman design should have the same properties to be useful. An $N = 9$ design is shown in Table 2. In Ref. 3, three effects are calculated for each factor:

$$E_{J,0} = \frac{\sum y(0)}{n} - \frac{1}{2}\left(\frac{\sum y(-1)}{n} + \frac{\sum y(1)}{n}\right) \quad (2)$$

$$E_{J,(-1)} = \frac{\sum y(-1)}{n} - \frac{1}{2}\left(\frac{\sum y(0)}{n} + \frac{\sum y(1)}{n}\right) \quad (3)$$

$$E_{J,1} = \frac{\sum y(1)}{n} - \frac{1}{2}\left(\frac{\sum y(-1)}{n} + \frac{\sum y(0)}{n}\right) \quad (4)$$

where $E_{J,i}$ ($i = 0, -1, 1$) is the effect of variable J at level i on the determined parameter; $\sum y(0)$ is the sum of the n ($n = 3$ for $N = 9$) experimental values associated with level 0; $\sum y(-1)$ with level -1 and $\sum y(1)$ with level 1.

To determine whether a factor has a significant influence or not on the considered response the authors performed a t-test:

$$t_{J,i} = \frac{|E_{J,i}|}{s_m} \quad (5)$$

In this formula $t_{J,i}$ is the calculated t value; $|E_{J,i}|$ is the absolute value of the effect $E_{J,i}$ and s_m is the standard measurement error. This standard error represents the experimental error and is obtained by entering a number of dummy variables [3,9] in the design. The s_m is calculated with the effects of these dummy variables

$$(s_m)^2 = \frac{1}{d}\left[\sum_1^d \left(\frac{\sum (E_{Z,0})^2 + \sum (E_{Z,-1})^2 + \sum (E_{Z,1})^2}{2}\right)\right] \quad (6)$$

where $E_{Z,i}$ is the effect of a dummy variable and d the number of dummies.

Unfortunately, as we will proceed to show, this design is not well balanced. In the design there are 9 experiments and each factor is three times at each level. When factor A is at level 0, the other factors of the design should be respectively once at level 0, -1 and 1. The same is the case when factor A is at another level so that, when $E_{A,0}$ is calculated, the influences of the other factors cancel. This should be the case for all factors at each level. However from the design it can be seen that this is not so. When factor A is at level 0 then factor E is three times at level 1; when it is at level -1 then E is three times at level -1 and when it is at level 1 then E is three times at level 0. The same can be observed between the factors B and F; C and G; D and H.

When for example $E_{A,(-1)}$ and $E_{E,(-1)}$ are calculated:

$$E_{A,(-1)} = \frac{y_1 + y_5 + y_9}{3} - \frac{1}{2}\left(\frac{y_2 + y_3 + y_8}{3} + \frac{y_4 + y_6 + y_7}{3}\right) \quad (7)$$

$$E_{E,(-1)} = \frac{y_1 + y_5 + y_9}{3} - \frac{1}{2}\left(\frac{y_4 + y_6 + y_7}{3} + \frac{y_2 + y_3 + y_8}{3}\right) \quad (8)$$

it can be seen that $E_{A,(-1)} = E_{E,(-1)}$. It can also be calculated that $E_{A,1} = E_{E,0}$ and $E_{A,0} = E_{E,1}$. In other words, A is confounded with E. The same confounding of effects can be seen between the factors B and F; C and G; D and H.

A similar confounding of effects as in the $N = 9$, $L = 3$ design can also be observed between the effects of factors F_i and F_{i+13} (for $i = 1, 2, \ldots, 13$) in the $N = 27$, $L = 3$ Plackett–Burman design which is described in Ref. 1.

Mathematically a confounding of main effects of factors can be discovered by calculating $\mathbf{X}^T \cdot \mathbf{X}$ or its inverse $(\mathbf{X}^T \cdot \mathbf{X})^{-1}$, the variance–covariance matrix. The symbol $\mathbf{X}$ represents the matrix of independent variables and $\mathbf{X}^T$ is the transpose of $\mathbf{X}$. For the design as proposed by Plackett–Burman (Table 2) $\mathbf{X}$ is given by

$$\mathbf{X} = \begin{array}{c} \begin{array}{ccccccccc} b_0 & A & B & C & D & E & F & G & H \end{array} \\ \left|\begin{array}{ccccccccc} 1 & -1 & 0 & 1 & 1 & -1 & 1 & 0 & 0 \\ 1 & 0 & -1 & 0 & 1 & 1 & -1 & 1 & 0 \\ 1 & 0 & 0 & -1 & 0 & 1 & 1 & -1 & 1 \\ 1 & 1 & 0 & 0 & -1 & 0 & 1 & 1 & -1 \\ 1 & -1 & 1 & 0 & 0 & -1 & 0 & 1 & 1 \\ 1 & 1 & -1 & 1 & 0 & 0 & -1 & 0 & 1 \\ 1 & 1 & 1 & -1 & 1 & 0 & 0 & -1 & 0 \\ 1 & 0 & 1 & 1 & -1 & 1 & 0 & 0 & -1 \\ 1 & -1 & -1 & -1 & -1 & -1 & -1 & -1 & -1 \end{array}\right| \end{array} \quad (9)$$

and $\mathbf{X}^T \cdot \mathbf{X}$ by

$$(\mathbf{X}^T \cdot \mathbf{X}) = \begin{array}{c|ccccccccc|c} & b_0 & A & B & C & D & E & F & G & H & \\ \hline b_0 & 9 & 0 & 0 & 0 & 0 & 0 & 0 & 0 & 0 & b_0 \\ A & 0 & 6 & 0 & 0 & 0 & 3 & 0 & 0 & 0 & A \\ B & 0 & 0 & 6 & 0 & 0 & 0 & 3 & 0 & 0 & B \\ C & 0 & 0 & 0 & 6 & 0 & 0 & 0 & 3 & 0 & C \\ D & 0 & 0 & 0 & 0 & 6 & 0 & 0 & 0 & 3 & D \\ E & 0 & 3 & 0 & 0 & 0 & 6 & 0 & 0 & 0 & E \\ F & 0 & 0 & 3 & 0 & 0 & 0 & 6 & 0 & 0 & F \\ G & 0 & 0 & 0 & 3 & 0 & 0 & 0 & 6 & 0 & G \\ H & 0 & 0 & 0 & 0 & 3 & 0 & 0 & 0 & 6 & H \end{array} \quad (10)$$

One can see that some coefficients are correlated. Otherwise values different from zero would be obtained only on the diagonal. Each coefficient of the regression equation is determined by two factors and there is a confounding of (main) effects (A with E, B with F, C with G and D with H as already described above).

The three-level Plackett–Burman designs cannot therefore be used for examining the number of factors they intend to, without a confounding of main effects. It is impossible to draw conclusions about the influence of each factor separately, which was the aim in the first place of applying the design.

TABLE 3

Example of a well balanced $N = 9$, $L = 3$ design for four factors

Exp.	Factors			
	A	B	C	D
1	−1	−1	1	0
2	−1	1	0	−1
3	−1	0	−1	1
4	1	−1	0	1
5	1	1	−1	0
6	1	0	1	−1
7	0	−1	−1	−1
8	0	1	1	1
9	0	0	0	0

TABLE 4

One of the well balanced $N = 9$, $L = 3$ designs for four factors which can be derived from the original $N = 9$, $L = 3$ Plackett–Burman design

Exp.	Factors			
	A	B	C	D
1	−1	0	1	1
2	0	−1	0	1
3	0	0	−1	0
4	1	0	0	−1
5	−1	1	0	0
6	1	−1	1	0
7	1	1	−1	1
8	0	1	1	−1
9	−1	−1	−1	−1

We determined how many factors at the most can be investigated in a well balanced $N = 9$, $L = 3$ and an $N = 27$, $L = 3$ design. There are 4 factors for the $N = 9$, $L = 3$ design and 13 factors for the $N = 27$, $L = 3$ design. Four is also the number of factors that can be investigated in the 3^{4-2} fractional factorial three-level design described in Ref. 6. An example of a well balanced $N = 9$, $L = 3$ design is given in Table 3.

There are different possibilities of constructing a well balanced design. An easy way to construct a well balanced three-level design is to construct the Plackett–Burman design as described in Ref. 1 and then omit the first half or the second half of the factors. Up to 4 factors can be investigated in the reduced $N = 9$, $L = 3$ Plackett–Burman design (see Table 4) and up to 13 factors in the reduced $N = 27$, $L = 3$ Plackett–Burman design (see Table 5). Both the designs obtained in this way from the $N = 9$, $L = 3$ Plackett–Burman design can be rearranged to be equal to the design proposed by Hunter [6], which was constructed as an extension of a Graeco–Latin square design. This is not the case for the design proposed in Table 3.

An additional advantage of a well balanced three-level design compared to a two-level design is that second order effects can be estimated. These second order effects are biased by the constant term of the regression equation. However, they are not confounded, neither with each

other nor with first order effects (see below). On the other hand they are confounded with a number of two-factor interactions [6]. Second order effects are smaller than main effects. Because two-factor interactions can have the same order of magnitude as the second order effects it will not always be clear what in fact is determined.

The use of multiple regression is not recommended for ruggedness tests because in these tests the levels for the factors are chosen too close to each other to use regression in a proper way.

If second order effects are estimated the considered model is:

$$y = \beta_0 + \sum_{i=1}^{4} \beta_i \cdot x_i + \sum_{i=1}^{4} \beta_{ii} \cdot x_i^2 + e$$

This yields the following matrix of independent variables **X** for the design of Table 4:

$$\mathbf{X} = \begin{array}{c} b_0 \quad A \quad B \quad C \quad D \quad AA \quad BB \quad CC \quad DD \\ \left|\begin{array}{rrrrrrrrr} 1 & -1 & 0 & 1 & 1 & 1 & 0 & 1 & 1 \\ 1 & 0 & -1 & 0 & 1 & 0 & 1 & 0 & 1 \\ 1 & 0 & 0 & -1 & 0 & 0 & 0 & 1 & 0 \\ 1 & 1 & 0 & 0 & -1 & 1 & 0 & 0 & 1 \\ 1 & -1 & 1 & 0 & 0 & 1 & 1 & 0 & 0 \\ 1 & 1 & -1 & 1 & 0 & 1 & 1 & 1 & 0 \\ 1 & 1 & 1 & -1 & 1 & 1 & 1 & 1 & 1 \\ 1 & 0 & 1 & 1 & -1 & 0 & 1 & 1 & 1 \\ 1 & -1 & -1 & -1 & -1 & 1 & 1 & 1 & 1 \end{array}\right| \end{array} \quad (11)$$

The variance–covariance matrix for **X** is then:

TABLE 5

One of the well balanced $N = 27$, $L = 3$ designs for 13 factors derived from the original $N = 27$, $L = 3$ Plackett–Burman design

Exp.	Factors												
	A	*B*	*C*	*D*	*E*	*F*	*G*	*H*	*I*	*J*	*K*	*L*	*M*
1	−1	−1	0	−1	0	1	0	0	1	−1	0	0	0
2	1	−1	−1	0	−1	0	1	0	0	1	−1	0	0
3	1	1	−1	−1	0	−1	0	1	0	0	1	−1	0
4	1	1	1	−1	−1	0	−1	0	1	0	0	1	−1
5	−1	1	1	1	−1	−1	0	−1	0	1	0	0	1
6	0	−1	1	1	1	−1	−1	0	−1	0	1	0	0
7	1	0	−1	1	1	1	−1	−1	0	−1	0	1	0
8	1	1	0	−1	1	1	1	−1	−1	0	−1	0	1
9	0	1	1	0	−1	1	1	1	−1	−1	0	−1	0
10	1	0	1	1	0	−1	1	1	1	−1	−1	0	−1
11	−1	1	0	1	1	0	−1	1	1	1	−1	−1	0
12	1	−1	1	0	1	1	0	−1	1	1	1	−1	−1
13	−1	1	−1	1	0	1	1	0	−1	1	1	1	−1
14	−1	−1	1	−1	1	0	1	1	0	−1	1	1	1
15	0	−1	−1	1	−1	1	0	1	1	0	−1	1	1
16	0	0	−1	−1	1	−1	1	0	1	1	0	−1	1
17	0	0	0	−1	−1	1	−1	1	0	1	1	0	−1
18	−1	0	0	0	−1	−1	1	−1	1	0	1	1	0
19	1	−1	0	0	0	−1	−1	1	−1	1	0	1	1
20	0	1	−1	0	0	0	−1	−1	1	−1	1	0	1
21	0	0	1	−1	0	0	0	−1	−1	1	−1	1	0
22	1	0	0	1	−1	0	0	0	−1	−1	1	−1	1
23	0	1	0	0	1	−1	0	0	0	−1	−1	1	−1
24	−1	0	1	0	0	1	−1	0	0	0	−1	−1	1
25	0	−1	0	1	0	0	1	−1	0	0	0	−1	−1
26	−1	0	−1	0	1	0	0	1	−1	0	0	0	−1
27	−1	−1	−1	−1	−1	−1	−1	−1	−1	−1	−1	−1	−1

$$(\mathbf{X}^{T}\cdot\mathbf{X})^{-1}=$$

	A	B	C	D	AA	BB	CC	DD	
1	0	0	0	0	−0.333	−0.333	−0.333	−0.333	
0	0.167	0	0	0	0	0	0	0	A
0	0	0.167	0	0	0	0	0	0	B
0	0	0	0.167	0	0	0	0	0	C
0	0	0	0	0.167	0	0	0	0	D
−0.333	0	0	0	0	0.5	0	0	0	AA
−0.333	0	0	0	0	0	0.5	0	0	BB
−0.333	0	0	0	0	0	0	0.5	0	CC
−0.333	0	0	0	0	0	0	0	0.5	DD

(12)

If one is interested only in first order effects of the factors and a three-level design is performed one can calculate effects which are analogous to those calculated in two-level designs, instead of the main effects (2, 3, 4) defined in Ref. 3. Only 2/3 of the experiments will be used then for calculating each main effect. For example the following effects could be calculated:

$$E_{J,-10}=\frac{\sum y(0)}{N/3}-\frac{\sum y(-1)}{N/3} \tag{13}$$

$$E_{J,01}=\frac{\sum y(1)}{N/3}-\frac{\sum y(0)}{N/3} \tag{14}$$

$$E_{J,-11}=\frac{\sum y(1)}{N/3}-\frac{\sum y(-1)}{N/3} \tag{15}$$

We recommend this manner of interpreting the results because it might be easier to understand the physical meaning of these E_J values (13, 14, 15) for the examination of the influence of factors on responses than it is by calculating the E_J values as proposed in Ref. 3 (2, 3, 4). The last proposed E_J values (13, 14, 15) show the magnitude of the influence of the change of a factor from one level to another on a measured response while this is less obvious for the former ones (2, 3, 4). Because they (13, 14, 15) are analogous to the main effects defined for two-level designs they can be compared with results obtained with such designs. Furthermore the calculation of these three E_J values can give an indication whether second order effects are present or not. If for a factor J the levels −1, 0, 1 are in increasing order and have values which are at an equal distance from each other, then $E_{J,-10}$, $E_{J,01}$ and $\frac{1}{2}E_{J,-11}$ should not be significantly different from each other when there is no second order effect for J.

Conclusion

A three-level design as described by Plackett and Burman cannot properly be used to determine the influence of factors on measured responses for ruggedness testing or for optimisation of test procedures. A useful design instead of the three-level design as proposed by Plackett–Burman is the half of this design (Table 4), the well balanced design of Table 3 or three-level fractional factorials designs. Furthermore, reflected two-level Plackett–Burman designs can also be used. The former designs should be preferred to the reflected two-level designs if one wants to estimate also the second order effects of the factors.

The authors thank the National Fund for Scientific Research (NFWO) for financial support.

REFERENCES

1 L. Plackett and J.P. Burman, Biometrika, 33 (1946) 305.
2 K. Jones, J. Chromatogr., 392 (1987) 1.

3 K. Jones, J. Chromatogr., 392 (1987) 11.
4 J.A. Van Leeuwen, L.M.C. Buydens, B.G.M. Vandeginste, G. Kateman, P.J. Schoenmakers and M. Mulholland, Chemom. Intell. Lab. Syst., 10 (1991) 337.
5 J. Vindevogel and P. Sandra, Anal. Chem., 63 (1991) 1530.
6 J.S. Hunter, J. Quality Technol., 17 (1985) 210.
7 J.A. Van Leeuwen, L.M.C. Buydens, B.G.M. Vandeginste, G. Kateman, P.J. Schoenmakers and M. Mulholland, Chemom. Intell. Lab. Syst., 11 (1991) 37.
8 E. Morgan, in E. Chadwick (Ed.), Chemometrics: Experimental Design, Analytical Chemistry by Open Learning, Wiley, Chichester, 1991, p. 110.
9 K. Jones, Int. Lab., November (1986) 32.

Analytica Chimica Acta, 276 (1993) 197–204
Elsevier Science Publishers B.V., Amsterdam

Application of multivariate chemometric techniques to the study of Roman pottery (terra sigillata)

Roberto Aruga and Piero Mirti

Dipartimento di Chimica Analitica, Università di Torino, via Giuria 5, I-10125 Turin (Italy)

Antonella Casoli

Istituto di Chimica Generale e Inorganica, Università di Parma, viale delle Scienze 78, I-43100 Parma (Italy)

(Received 22nd May 1992; revised manuscript received 28th October 1992)

Abstract

Supervised and unsupervised pattern recognition techniques were used to classify 48 sherds of Roman pottery (terra sigillata), analysed by inductively coupled plasma atomic emission spectrometry and atomic absorption spectrometry for seven major and minor elements (Al, Fe, Ca, Mg, K, Ti and Mn). Hierarchical agglomerative clustering and principal component analysis were used to classify the studied material into compositional groups which could account for different centres of production; soft independent modelling of class analogy (SIMCA) was used to solve questions regarding doubtful assignments. The results indicate that, in the case study, a throughout statistical treatment can allow one to discriminate wares produced in different geographical areas on the basis of the seven elements accounted for.

Keywords: Atomic absorption spectrometry; Atomic emission spectrometry; Inductively coupled plasma spectrometry; Pattern recognition; Ceramics; Pottery; Principal component analysis

Roman terra sigillata was produced in central Italy since the first century BC and then traded and produced throughout the Roman world. The ware was characterized by a red to orange glossy slip and was sometimes stamped with the "sigillum" of the producing workshop. Specimens of terra sigillata found in excavation campaigns carried out in the territory of the Roman town of Augusta Praetoria (today Aosta, north-western Italy) have been analysed on several occasions by atomic spectrometric techniques as part of an archaeometric project for the characterization of the archaeological materials excavated in the site. Analyses were carried out on a first set of 21 samples by atomic absorption spectrometry with electrothermal atomization in a graphite furnace (GFAAS), allowing one to characterize compositionally an orange ware (sigillata chiara B) of north-western Italian production and to differentiate it from the imported wares from either Gaulish or Italic workshops [1,2]. Further analyses were subsequently performed on new samples, either by GFAAS or by inductively coupled plasma atomic emission spectrometry (ICP-AES) to determine major and minor elements, while trace elements were determined by neutron activation analysis (NAA). Trace elements are usually considered most suitable for characterization and provenance studies on ceramic materials, because they contribute a peculiar signature on a geochemical basis, which major and minor ele-

Correspondence to: R. Aruga, Dipartimento di Chimica Analitica, Università di Torino, via Giuria 5, I-10125 Turin (Italy).

ments alone can often fail to give. In a few instances, however, major and minor elements may contribute fairly good information when the pottery production is the result of an accurate selection and/or treatment of clays. This applies to the production of terra sigillata, which was normally worked out of selected and refined clays to produce a fine ware.

Analytical data obtained for seven major and minor elements by GFAAS and ICP-AES on 48 samples of terra sigillata were statistically treated by supervised and unsupervised techniques of pattern recognition. Hierarchical agglomerative clustering and principal component analysis (PCA) were used to classify the excavated material on the basis of the considered elements, viz., Al, Fe, Ca, Mg, K, Ti and Mn. Soft independent modelling of class analogy (SIMCA) was then performed to solve questions arising from the doubtful attribution of a few objects. Finally, a comparison was performed between the obtained classification and the information provided by a visual inspection of the sherds.

ANALYTICAL PROCEDURE

Forty-eight sherds of terra sigillata were analysed for the seven major and minor elements by ICP-AES and AAS with either flame or electrothermal atomization. As the analyses were performed in several stages on the various samples, some of the data were obtained by ICP-AES alone or GFAAS alone, and a few of them were obtained by both techniques. A comparison of the data obtained on the same samples by both techniques showed that the data obtained by either technique were consistent and could all be used for the characterization of the 48 samples.

All the analyses were performed on dissolved samples. Sample dissolution was achieved by fusion with lithium metaborate in graphite crucibles at 950°C [1,2]. ICP-AES analyses were performed by using a Philips PU7450 spectrometer in either the sequential single- or sequential multi-element mode of operation. Flame AAS (FAAS) determinations were carried out with a Perkin-Elmer 303 spectrometer to determine potassium in those samples which had been analysed by ICP-AES; in fact, potassium could not be determined by ICP-AES because of argon interference from the gas making up the plasma. GFAAS analyses were carried out with a Hitachi Z-9000 spectrometer, which could perform the determination of up to four elements at a time. However, only the single-element mode of operation was selected for the analysis of the samples studied.

Eighteen samples out of the total 48 were analysed by both ICP-AES and GFAAS, 25 were analysed by ICP-AES alone (and FAAS for determining potassium) and 5 by GFAAS alone.

STATISTICAL TREATMENT OF ANALYTICAL DATA

Multivariate analysis was performed on the analytical data by the use of computer programs included in the package PARVUS [3]. Cluster analysis and visual displays were used to classify the 48 sherds into compositional groups, and doubtful assignments were checked by supervised pattern recognition techniques.

The data were first normalized by the autoscaling procedure [4–8]. Autoscaling (NORMAL program) was performed by scaling each concentration to zero mean value and unit variance:

$$z_{ki} = (x_{ki} - x_{.i})/s_i$$

where z_{ki} is the scaled value of variable i for object k, x_{ki} its unscaled value, $x_{.i}$ the mean of the values of variable i for the whole set of objects and s_i the corresponding standard deviation.

Hierarchical agglomerative clustering was performed on the scaled data by means of the programs SIMIL and HIER of the package. Euclidean distances were used to calculate dissimilarities between objects and dendrograms for displaying the results of clustering operations. The latter were performed by three different methods: average linkage (weighed pair group), average linkage (unweighed) and complete linkage [4].

Principal component analysis (PCA) (EIGEN program) was used as a display method. It displays objects in a reduced space by finding a

TABLE 1

Composition of the studied fragments of terra sigillata (wt.%)

Sample	K_2O	MgO	CaO	TiO_2	MnO	Fe_2O_3	Al_2O_3
02A	2.08	3.55	8.63	0.77	0.08	6.16	17.40
02B	1.88	3.33	9.52	0.93	0.13	7.07	18.20
02C	2.08	3.40	8.31	0.91	0.14	7.03	19.80
02D	1.94	3.17	9.99	0.95	0.15	7.32	18.80
03	2.54	1.37	11.50	0.82	0.11	5.18	23.10
05A	3.15	8.00	1.85	0.92	0.14	8.88	19.10
05B	3.13	8.45	1.81	0.91	0.14	9.12	20.00
05C	2.77	7.67	1.71	0.89	0.11	8.84	19.10
05E	2.96	7.80	1.69	0.88	0.12	9.24	19.60
05H	1.72	1.45	1.02	1.40	0.01	6.58	18.60
05I	3.04	1.84	3.34	1.02	0.09	7.14	20.80
06A	3.06	4.79	1.48	0.84	0.18	9.32	21.90
06B	3.03	2.00	11.60	1.18	0.06	5.90	23.30
06C	1.98	3.51	8.98	0.91	0.16	7.30	18.40
08	2.61	3.08	6.14	1.01	0.10	7.92	18.80
09A	1.96	3.57	10.10	0.89	0.17	7.48	18.30
09B	3.61	4.63	3.94	0.84	0.11	8.60	19.80
09C	2.24	4.09	8.70	0.86	0.09	6.81	17.40
10A	1.93	1.38	0.75	1.70	0.02	8.32	25.50
10B	1.88	1.41	0.76	1.72	0.02	8.21	25.10
11A	2.75	1.34	8.23	0.84	0.07	5.67	20.80
11B	2.86	2.10	10.90	1.28	0.06	6.05	23.30
12A	2.26	1.27	10.60	0.93	0.03	4.97	19.20
12B	2.88	2.02	11.50	1.10	0.07	6.33	22.20
13A	3.60	5.32	1.78	0.96	0.15	8.93	19.80
13B	1.76	3.26	12.30	0.86	0.14	6.01	17.30
13C	2.18	3.40	9.73	0.81	0.08	6.19	16.00
13D	2.10	3.37	9.00	0.94	0.16	7.39	17.40
13E	1.92	3.22	12.50	0.93	0.15	7.76	17.00
13F	2.02	3.24	11.10	0.93	0.14	7.18	17.30
14C	2.92	1.19	12.60	0.85	0.07	5.37	21.80
14E	3.20	1.94	9.71	1.21	0.05	5.76	22.30
15A	3.19	2.01	12.30	1.32	0.07	6.30	21.70
15B	3.06	1.78	9.53	1.20	0.05	6.62	20.90
16A	3.18	8.08	1.73	0.89	0.12	9.22	19.20
16B	2.97	8.59	1.78	0.86	0.11	8.90	18.90
16C	3.08	3.97	1.40	0.90	0.09	6.86	19.50
16D	3.09	6.20	1.81	0.93	0.15	9.39	20.30
16E	2.68	5.78	2.25	1.03	0.12	8.60	19.00
16F	2.49	8.12	2.18	0.88	0.09	8.32	18.00
16G	2.85	8.00	2.15	0.88	0.14	8.91	19.10
16H	3.25	7.43	1.65	0.89	0.11	9.05	19.80
16I	3.19	5.95	1.86	0.93	0.13	8.47	20.10
22	3.33	4.39	1.42	0.88	0.17	10.50	23.60
25	3.10	3.01	0.99	0.93	0.14	8.30	22.00
27	2.04	1.37	0.81	1.66	0.02	8.80	24.40
28	2.95	6.63	1.82	0.96	0.14	9.90	21.50
32	3.19	6.93	1.61	1.03	0.10	8.70	21.50

direction (first principal component) that best preserves the scatter of the observations in the original multi-dimensional space. This corresponds to calculating a new variable as a weighed linear combination of the original ones. A second principal component is then chosen among all directions orthogonal to the first, so that maximum preservation of the residual variance can be obtained, and so on. In some instances, just two (or three) principal components are sufficient for a projection of the original hyperspace on to two (or three) dimensions, without excessive loss of information [4]. The program EIGEN obtains new variables from the matrix of covariances and calculates eigenvectors by the method of Malinowski and Howery [9].

R-mode PCA gives both the coordinates (or scores) of objects and the loadings of variables on principal components. The latter allow a clustering of variables on the basis of mutual correlations. Q-mode PCA, in contrast, allows a clustering of objects on the basis of mutual correlations. It is carried out on the transpose of the original data matrix [10].

Supervised pattern recognition was used for verifying class assignments and solving doubtful attributions. Soft independent modelling of class analogy (SIMCA) was used for this purpose. This is a modelling technique that performs a principal component analysis independently for each class. This allows one to compare objects of a given group in a reduced space, the dimensions of which depend on the minimum number of components required for good preservation of the original variance [11]. Depending on the dimensionality of this space, each class is modelled as a line, a plane and a hyperplane and a critical distance is calculated for objects with a given probability, say 95%, of belonging to the class. Objects whose distance is greater than the critical distance for each of the considered classes are classified as outliers, at the chosen confidence level.

Class separation by pattern recognition methods can be improved by a selection of variables. In addition, variable reduction is required by the use of some computer programs. Feature selection was performed by the program SELECT,

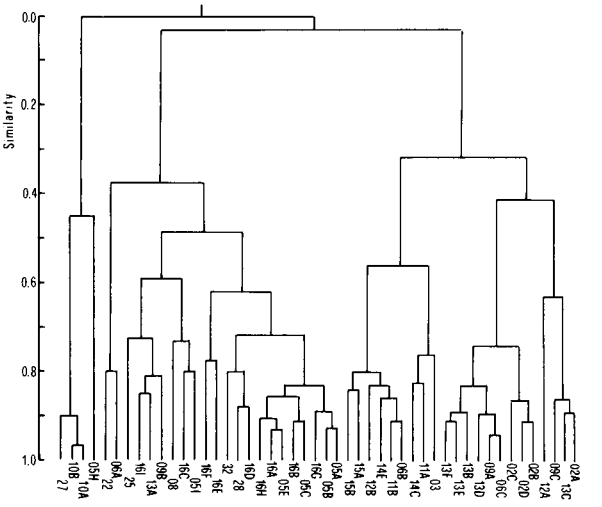

Fig. 1. Example of dendrogram based on agglomerative hierarchical clustering ("complete linkage" method) for 48 pottery sherds.

which decorrelates variables on the basis of Fisher weights and correlation coefficients [7].

RESULTS AND DISCUSSION

Table 1 reports the data obtained from the analysis of the 48 pottery sherds for the seven elements accounted for. The results obtained from the initial matrix of data (dimensions: 48 × 7) after autoscaling, hierarchical clustering and principal component analysis are shown in Figs. 1 and 2. The average linkage dendrograms and the PC(1,3) diagram are not reported here, for the sake of brevity. The two first principal components [PC(1,2), Fig. 2] account for 73.8% of the total variance.

Three clusters can be identified in the first place, which appear well defined in all the representations. They are indicated as A, B and C in Fig. 2 and are made up of the following objects: 10A, 10B, 27 (cluster A); 11B, 14E, 06B, 15A, 15B, 12B (cluster B); and 14C, 11A, 03 (cluster C). It should be noted that 05H and 12A are separated from clusters B and C, respectively, in both PC(1,3) and the dendrograms.

One further group (cluster D), made up of twelve objects, appears well defined in the lower

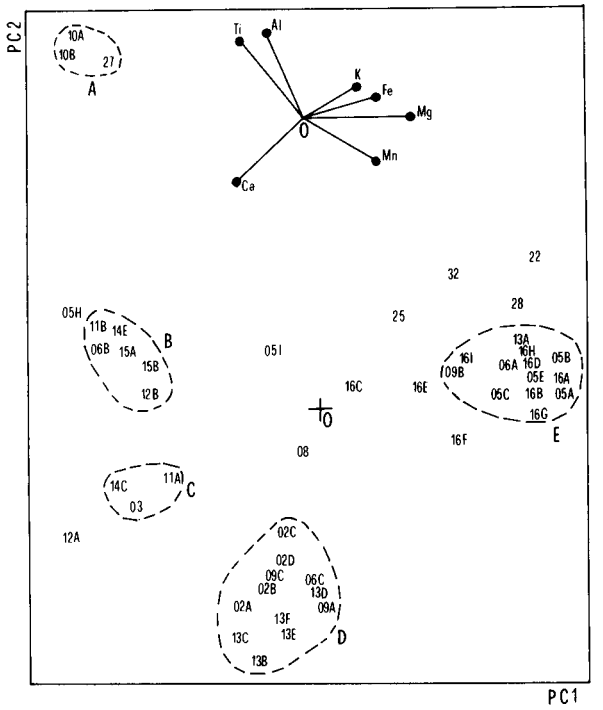

Fig. 2. Scores of 48 pottery sherds and loadings of seven variables on the first two principal components. The origin of the two systems, indicated by 0, must be imagined as coincident.

part of Fig. 2 (object 02C only appears slightly distant from the others). Objects 09C, 13C and 02A of cluster D, on the other hand, appear fairly distant from the others in the dendrograms.

A group can be finally recognized (cluster E), made up of eight objects tightly grouped in all the dendrograms and in the PC(1,2) diagram (i.e., 05A, 05B, 05C, 05E, 16A, 16B, 16G and 16H). Three more objects (16D, 06A and 13A) appear very close to those of cluster E in the PCA diagrams [on both PC(1,2) of Fig. 2 and PC(1,3)], whereas they appear more scattered from cluster E in the dendrograms.

All the other objects, not mentioned in the preceding discussion, are displayed in more isolated positions in all the representations.

Questionable assignments regarding clusters D and E were checked by SIMCA at the 95% confidence level. By placing 02C, 09C, 13C, 02A, 16D, 06A, 13A, 16I and 09B as test objects (see above), the program assigned the first four objects to cluster D and the other five to cluster E.

In conclusion, the whole of the above treatment leads to the recognition of five compositional groups, as indicated in Fig. 2.

Relationships between variables

The loadings of the variables are also reported in Fig. 2 (together with the scores of the objects) on PC(1,2). They can be useful in order to recognize clusters of variables on the basis of mutual correlations and, moreover, in the present instance, to point out elements more responsible for variability among different clusters of objects. It can be inferred from Fig. 2 that Ti and Al (correlation coefficient 0.64) are the best discriminating elements between cluster A and the other groups (D and E, in particular). The group made up of K, Fe and Mg and, in the opposite direction, Ca, discriminates cluster E from clusters B, C and D on the whole. The direction of the loadings of Mn on PC(1,2), on the other hand, seems to indicate a fairly limited discriminating ability for this element in this particular instance.

Temper additions

The problem of possible additions of temper to a clay matrix is often of importance in the categorization of ceramic wares [12]. The temper may be another clay, but it is more often a non-plastic material. When the added temper is a relatively pure material, such as quartz, or when it contains some of the elements considered in the statistical treatment, but in considerably lower concentrations than those in the original clay, the addition causes a general dilution of the elements considered, at constant mutual proportions. With reference to the scores of objects on principal components, such a dilution causes a radial shifting (i.e., towards the origin of the diagram) of the objects to which temper has been added. Consequently, different provenances can be assigned with certainty to objects which are distant in a tangential direction whereas, on the other hand, cautious conclusions should be drawn for objects that are radially scattered [12]. Such a dilution process could concern cluster E in the present instance, as at least two objects (16C and 16E, see

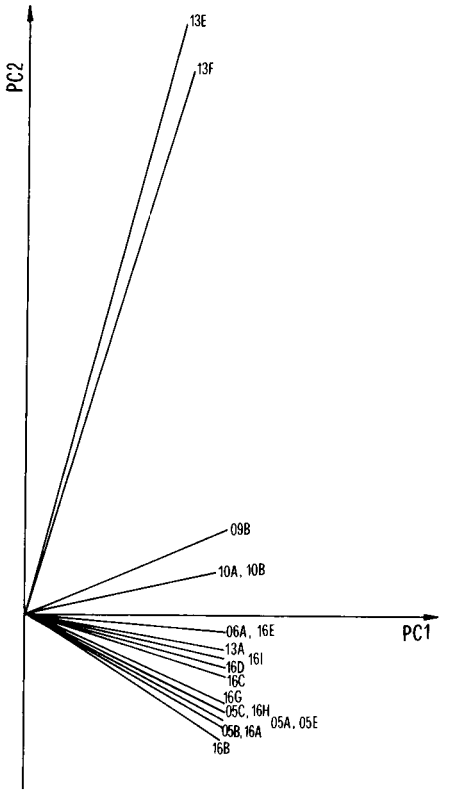

Fig. 3. Loadings of 19 pottery sherds obtained by Q-mode PCA on the first two principal components.

Fig. 2) appear radially scattered from this group. As radial shifting maintains unaltered the correlations between objects, a categorization of objects based on Q-mode PCA could clarify this point. A maximum set of twenty objects could be submitted to Q-mode PCA, for reasons of capacity of the computer program used. The following objects were chosen: the eight sherds which all representations assign to cluster E (see above); the five objects in doubtful positions, which were tested by SIMCA (i.e., 09B, 16I, 06A, 13A, 16D); the two objects under investigation, radially scattered from cluster E (i.e., 16C and 16E); and four objects belonging to two clusters tangentially distant from cluster E (namely 10A and 10B of cluster A and 13E and 13F of cluster D). The results of the treatment, expressed as the loadings of the above objects on PC(1,2), are shown in Fig. 3. Apart from the two expected clusters made up of 10A and 10B and of 13E and 13F, and from sample 09B, only one wide cluster can be recognized in Fig. 3, made up of mutually correlated objects; 16C and 16E belong to this cluster. A common origin could not be excluded, on this basis, for 16C, 16E and the other objects of this group. As for 09B, its scattered position in Fig. 3 is worth mentioning, because on the basis of Q-mode PCA this sherd should not be assigned to cluster E. In fact, visual examination suggests a different origin for 09B with respect to the other objects of cluster E (see below).

Redundancy of variables

At this stage, the redundancy content of the set of the seven variables considered here was evaluated. The discriminating ability of each variable was determined first. This was done on the basis of the five classes identified in the previous step, and after the elimination of the objects that were classified as outliers in the preceding treatment. A multivariate decorrelation of variables, on the basis of both discriminating ability and mutual correlations, give the following sequence (in order of decreasing information content): Ti, Mg, K, Ca, Fe, Al, Mn. The univariate criterion, based only on discriminating ability (which was measured as the Fisher weight) gave the order Ti, Fe, Mg, Ca, K, Al, Mn. It can be observed that a good categorizing ability of Ti is shown by both methods, and the relatively poor utility of Mn, already shown in the treatment of Fig. 2, is confirmed.

Second, a series of consecutive R-mode PCAs were carried out, each accompanied by a representation of the scores of the objects on the first two principal components. One variable was eliminated for each step, beginning with the variables that resulted in being less discriminating on the basis of the multivariate decorrelation. It was found that the elimination of Mn does not affect considerably the subdivision into classes obtained previously with all seven variables. In contrast, the elimination of Mn and Al makes the representation of the classes on PCA(1,2) worse, in the sense that the clusters previously indicated as B, C and D are heavily overlapped in this instance.

It can be concluded that the set of seven variables used in this study on the one hand

allows a reliable classification of the samples under investigation (see below) and, on the other it shows a minimal redundancy content, attributable to Mn only.

Comparison with previous classifications

Subsequently, a comparison was made among the possible provenances of the 48 sherds of terra sigillata in this study and 14 other samples of terra sigillata excavated on the site of Augusta Praetoria and investigated in the course of a previous work by AAS [1]. Eight samples of the latter set of 14 gathered in a well defined cluster, which, on the basis of archaeological evidence, had been considered representative of a peculiar orange ware ("sigillata chiara B") originating from north-western Italy. The other six samples, belonging to two different clusters, had been attributed to imported (Gaulish) productions. A representation of the scores of the whole of the 62 objects on the first two principal components (Fig. 4) shows an exact overlapping of the objects of cluster E in this study on the group of "sigillata chiara B" previously studied (these two overlapping clusters are indicated by E in Fig. 4). The other two groups of terra sigillata previously classified as imported wares (which are indicated as F and G in Fig. 4) are not distant from clusters C and D, respectively, in this study. Their closeness, in any case, does not seem such that an identical provenance can be inferred for the corresponding sherds. It must be noted, in particular, that clusters C and F in Fig. 4 appear fairly distant from each other along the axis of the third principal component.

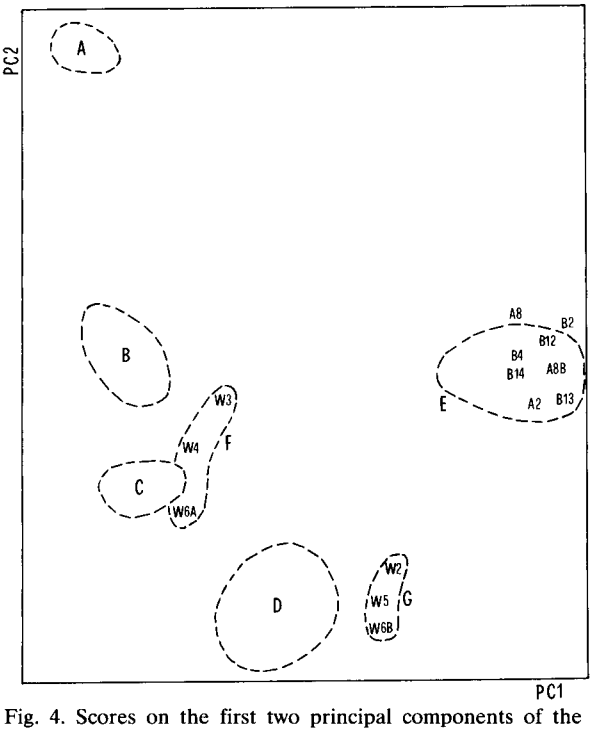

Fig. 4. Scores on the first two principal components of the present sherds (clusters A–E, see also Fig. 2) and of 14 sherds from a previous study. The sherds of the latter group are indicated with their individual symbols.

Comparison with visual examination

A comparison of the classification discussed above with the results of a visual examination of the pottery sherds could be made. This indicated that the seven elements accounted for may adequately discriminate wares produced in different geographical areas. However, a differentiation among wares produced in the same area but in different localities is not always possible on this basis, and calls for the determination of a suitable number of trace elements. In fact, visual inspection assigned all the sherds of cluster A to northern African workshops, all the sherds of clusters B and C to Gaulish workshops and all the sherds of cluster D to Italic centres of production. As for the sherds in cluster E, the archaeological examination assigned most of them as specimens of "sigillata chiara B", covering a span of time from the end of the first to the third century AD. Thus, at this stage, major and minor elements suffice for characterizing wares produced in one of the above major areas and also separate two groups of Gaulish wares. However, visual inspection suggests that each of the above clusters is made up of wares produced in more than one locality and/or at a different age. It follows that major and minor elements alone do not allow one to assign these sherds to more definite centres of production within a given broad area. It is remarkable, however, that just a few elements may be used to discriminate easily among northern African, Gaulish and Italic productions, at least in the case under study. As discussed above,

titanium and aluminium are the best discriminating elements between northern-African and Gaulish and Italic productions, while potassium, iron, magnesium and calcium discriminate the "sigillata chiara B" from the Gaulish and the other Italic wares. It should be noted, however, that two sherds falling in cluster E are actually misclassified, namely 09B and 06A. In fact, visual inspection alone would assign them to central or southern Italic centres of production, instead of north-western centres; the lower magnesium content in these sherds would actually point to a different provenance with respect to the other sherds of cluster E, excluding the possibility of north-western imitations of a more southern typology. It is a fact, as mentioned above, that sample 09B is actually separated from the others in cluster E when Q-mode PCA is carried out.

Conclusions

An inexpensive determination of major and minor elements by atomic spectrometric techniques, followed by a throughout treatment of the analytical data on a statistical basis, may lead to a first classification of terra sigillata wares in broad groups, corresponding to different geographical areas of production. This may be particularly useful, for example, in the case of Gaulish and Italic productions, taking into account that Italian potters often set up branch workshops in Gaulish regions, and that wares stamped by the same potter have been found in both areas.

REFERENCES

1 P. Mirti, R. Aruga, V. Zelano, L. Appolonia and M. Aceto, Fresenius' J. Anal. Chem., 336 (1990) 215.
2 P. Mirti, V. Zelano, R. Aruga, E. Ferrara and L. Appolonia, Archaeometry, 32 (1990) 163.
3 M. Forina, Trends Anal. Chem., 3 (1984) 38.
4 D.L. Massart and L. Kaufman, The Interpretation of Analytical Chemical Data by the Use of Cluster Analysis, Wiley, New York, 1983.
5 M.P. Derde and D.L. Massart, Fresenius' Z. Anal. Chem., 313 (1982) 484.
6 M. Forina, C. Armanino, S. Lanteri, C. Calcagno and E. Tiscornia, Riv. Ital. Sostanze Grasse, 60 (1983) 607.
7 M. Forina, S. Lanteri and C. Armanino, Top. Curr. Chem., 141 (1987) 91.
8 R. Aruga, P. Mirti and V. Zelano, Analusis, 18 (1990) 597.
9 E.R. Malinowski and D.G. Howery, Factor Analysis in Chemistry, Wiley, New York, 1980.
10 J.C. Davis, Statistics and Data Analysis in Geology, Wiley, New York, 1986.
11 S. Wold, C. Albano, W.J. Dunn, III, U. Edlund, K. Esbensen, P. Geladi, S. Hellberg, E. Johansson, W. Lindberg and M. Sjostrom, in B.R. Kowalski (Ed.), Chemometrics. Mathematics and Statistics in Chemistry, Reidel, Dordrecht, 1984, pp. 17–95.
12 R.L. Bishop and N. Heff, in R.O. Allen (Ed.), Archaeological Chemistry IV, American Chemical Society, Washington, DC, 1989, pp. 57–86.

Analytica Chimica Acta, 276 (1993) 205–210
Elsevier Science Publishers B.V., Amsterdam

Liquid scintillation applied to alpha counting of plutonium

Joseph Bubernak

Los Alamos National Laboratory, Los Alamos, NM (USA)

(Received 4th August 1992; revised manuscript received 9th September 1992)

Abstract

A liquid scintillation counter has been modified with fast electronic modules to extend its range for α-counting rate measurements. The practical upper limit for accurate counting is about 30×10^6 cpm, at which 5% dead-time loss corrections are applied. Solutions of ^{239}Pu up to 200 g l^{-1} can be aliquoted directly with capillary pipets, thereby obviating the need for dilutions. The aliquots are mixed with 250 μl of cocktail in 400-μl plastic centrifuge tubes for counting so that waste generation is minimized. Although the counting set-up includes no coincidence circuitry, blanks show less than 10 cpm. Therefore, low-activity samples can also be measured accurately.

Keywords: Alpha counting; Liquid scintillation counting; Plutonium

The principal method for accurate measurement of α-activity in our laboratory and others is 2-π proportional counting of dried deposits. A less popular method is liquid scintillation (LS) counting. Although many automated LS counting instruments are commercially available, they are applied mainly to measurement of β-activity, such as from ^3H or ^{14}C. Objections to their use in α-counting include problems associated with quenching and with the generation of waste in the form of a radioactive LS cocktail. Because of the high dilution rate employed, 1 part or less of sample per 50 parts LS cocktail, quenching has not caused loss of counts in any sample. Waste generation can be minimized as the sample size is decreased. LS counting offers some advantages over 2-π plate counting; for example, LS count rates are much less affected by salts.

A significant feature in LS counting is the short pulse duration, permitting the measurement of count rates accompanied by low dead-time losses. Commercial LS counting instruments are generally designed for work with low activities and strive for low background. Even so, relatively high count rates, up to 2×10^6 cpm, have been measured accurately [1]. To extend this capability in the present work, fast electronics in the form of a constant-fraction discriminator (CFD) and a fast counter were used.

One goal of this work was to extend the LS counting method to concentrated solutions (up to 200 g l^{-1} of ^{239}Pu) without the necessity for dilutions. Toward this end, capillary pipets ("microcaps" made by Drummond, Broomall, PA) provided sufficient accuracy, down to a 1-μl aliquot.

Correspondence to: J. Bubernak, Los Alamos National Laboratory, Los Alamos, NM 87545 (USA).

EXPERIMENTAL

Instrumentation

A diagram of the equipment is shown in Fig. 1. A Packard (Meriden, CT) Model 3255 LS counter

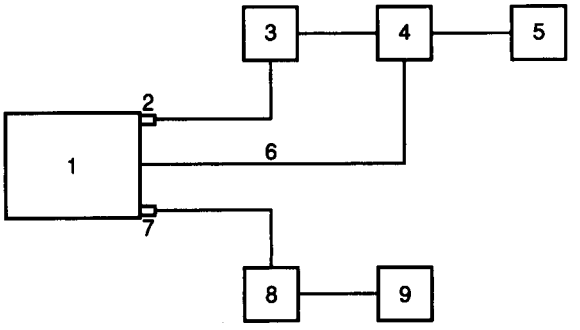

Fig. 1. Configuration of counting equipment: (1) liquid scintillation counter; (2) negative (coincidence) pulses; (3) constant-fraction discriminator; (4) counter; (5) PC; (6) sample-changer control line; (7) positive (signal) pulses; (8) amplifier; (9) multichannel analyzer.

was used in the present investigation. Although it has a useful upper limit of only about two million total counts in its original form, many extra connections in the rear of the instrument permit easy manipulation of signals and modification of counting conditions. Negative pulses from the anodes of both photomultiplier tubes (PMTs) were T'd off with a 50-Ω cable and served as input to an Ortec (Oak Ridge, TN) Model 473A CFD. The CFD served two purposes. First, it allowed processing of pulses having an amplitude below the minimum 250-mV threshold setting of our Ortec Model 997 counter (that is, timer/scaler). Second, circuitry in the CFD limited pulse pair resolution to a 65-ns minimum and thus prevented multiple triggering. The negative output logic pulses of the CFD, operated with the mode switch set to Ge, was input to the Model 997, which is a 100-MHz, 8-decade counter.

Altering the basic operation of the LS counter made it necessary to control the operation of the sample changer in the instrument. This task required a logic 5-V pulse. Ortec modified the Model 997 so that the pulse was generated by the STOP signal. Also, software supplied by Ortec enabled an IBM PC to control the operation of the counter and to output data.

Independent of the above operation, the positive output pulses from both PMTs were T'd together and amplified, then the pulse-height spectrum was displayed on a Canberra (Meriden, CT) Model 35 Plus multichannel analyzer (MCA). Amplification was carried out with an Ortec Model 450 amplifier at 0.1 μs differential and 1.5 μs integral pulse shaping. The spectra obtained were useful for interpreting the extent of quenching and other phenomena.

Preparation of samples for counting

Microcaps having capacities of 1–5 μl were used for aliquoting liquid samples. Operation is simple: touch the lower end of the microcap to the surface of the liquid and the microcap fills by capillary action.

The rate of filling for individual microcaps varies. It was necessary not only to allow sufficient time for filling but also to examine the upper meniscus with a 10× magnifier. If the meniscus did not appear flat, the microcap was reintroduced into the sample. A curved meniscus can indicate an underfilling of less than 1%. The microcaps cannot overfill. Drummond offers microcaps with specified 1% and 0.25% accuracies.

The filled microcap was tilted at an angle of about 45° and the outside lower end rinsed with a few drops of 7 M nitric acid. The rinsings were discarded to waste. The filled microcap was dropped into a 400-μl polyethylene centrifuge tube and cocktail was added. The cocktail consisted of 250–300 μl of Packard Optifluor containing 10 mg ml^{-1} of trioctylphosphine oxide (TOPO). The TOPO was used to prevent adsorption of plutonium onto the vial walls if too little acid was present in the sample [2]. The centrifuge tube was capped and placed in a 4-ml plastic LS vial, which was marked on the top of the lid for identification. This reusable vial thus serves both for handling and for identification of the centrifuge tube. The capped vial was inverted and shaken on a Vortex-Genie mixer (VWR, Denver, CO) for 1 min. The contents of the centrifuge tube were mixed best when the tube was inverted. The assembly of centrifuge tube and vial was then centrifuged in the upright position for 1 min at 1500 rpm (249 *g*). For counting, the vial was placed in a suitable holder in the Model 3255 LS counter.

The counting tube arrangement is drawn to scale in Fig. 2. A series of microcaps having capacities ranging from 1 to 5 μl are all 32 mm

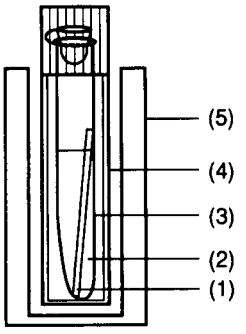

Fig. 2. Counting tube arrangement (actual size): (1) microcap; (2) liquid scintillation cocktail; (3) micro centrifuge tube; (4) plastic vial; (5) plastic sleeve.

long and vary only in their diameters. The 250 μl of cocktail fill about two-thirds of the 400-μl centrifuge tube. The microcap protrudes slightly above the surface of the cocktail. This protrusion causes no problem in counting and serves as a visual indication that a tube contains a sample. Some LS counting instruments can handle the 4-ml vials directly, but because the Model 3255 LS counter was designed to accept standard 20-ml vials, a plastic sleeve having outer dimensions similar to a 20-ml vial was needed to accommodate the 4-ml vial.

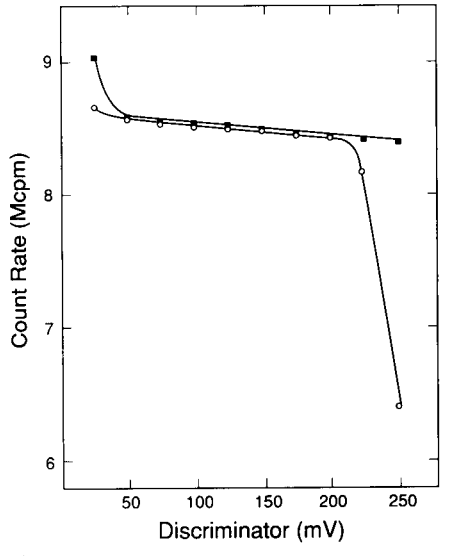

Fig. 3. Count rate variation with discriminator setting. (■) Low quench; (○) high quench.

Discriminator setting

A 3-μl aliquot of plutonium in 1 M nitric acid and 3 μl of 1 M nitric acid were mixed with 250 μl of cocktail to produce a source having very little quenching. A similar source containing 16 M rather than 1 M nitric acid represented much greater quenching. Each source was counted at varying discriminator settings on the Model 473A CFD. Figure 3 shows that a relatively flat plateau was obtained when the count rate was plotted against discriminator setting. A setting of 125 mV is seen to be optimum for counting in this wide range of quenching conditions. This discriminator voltage was used in all measurements to be described.

RESULTS AND DISCUSSION

Dead-time corrections

A stock solution was made up containing about 40 g l^{-1} of plutonium in 1 M nitric acid. Three 1-ml portions of the solution were taken with glass micropipets and made up to 10 ml with 1 M nitric acid in volumetric flasks, effectively diluting the original portions 10-fold. Three other portions were diluted 100-fold in the same manner except that 100-μl micropipets were used. Different pipets were used for each dilution. All pipets and flasks were calibrated with water; for three runs of each calibration, the average volumes measured were within 0.4% of the nominal values.

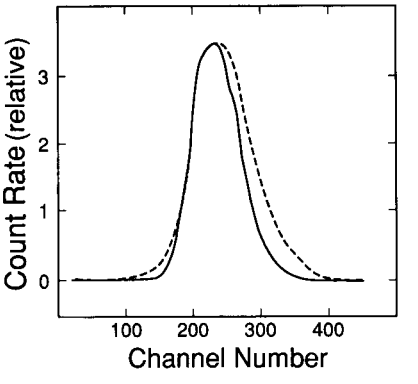

Fig. 4. Pulse-height spectra for two runs. (———) 0.060×10^6 cpm; (— — —) 28×10^6 cpm.

TABLE 1

Specific activities

Aliquot [a] (μl)	Nominal [b] (10^6 cpm)	Specific activity (cpm μl^{-1})	Average R.S.D. (%)
1	0.060	59841	0.44
2	0.120	59751	0.24
3	0.180	59646	0.44
4	0.240	59725	0.37
5	0.300	59647	0.49
10	0.600	59440	1.02
20	1.20	59637	0.65
30	1.80	59250	0.46
40	2.40	59340	0.68
50	3.00	59100	0.50
100	6.00	59390	1.00
200	12.0	58656	0.70
300	18.0	57670	0.35
400	24.0	57266	1.06
500	30.0	56673	0.22

[a] Relative to 1 μl of 1:100 dilution. [b] One μl of the 1:100 dilution measured 0.0598×10^6 cpm, as seen in column 3.

From each of the dilutions and original stock solution, the Drummond microcaps having 0.25% accuracy were used to take duplicate aliquots of 1–5 μl for counting. The range of aliquot size was thus a factor of 500 and included α-activities from about 0.060×10^6 to 30×10^6 cpm. Spectra taken with the MCA showed smooth peaks in all cases. Those for the lowest and highest α-activities, normalized to the same peak channel counts, are shown in Fig. 4.

Results for the mean of six runs at each concentration are given in Table 1. One microliter of the weakest solution is denoted as 1 μl on a relative scale, whereas 5 μl of the strongest solution is represented as an equivalent 500 μl of the weakest solution. The specific activities, counts per minute per microliter of the weakest solution, are shown in column 3. Little change (less than 1%) is seen up to an α-count rate of more than 2×10^6 cpm. Average standard deviations are 1% or less.

Values of specific activities as a function of nominal count rate are plotted in Fig. 5. Also shown is a fit of the data done by linear regression. Individual values fall within $\pm 0.5\%$ of this line. The equation of the line is $y = 59677 - 101.5x$, where x is in millions cpm. Thus, the dead-time correction $[(y_0 - y)/y_0 \times 100]$ amounts to 0.170% per million cpm. At 30×10^6 cpm, the

TABLE 2

Comparison of α-activities

LS counting				2-π counting		Difference (LS − 2-π) (%)
Aliquot (μl)	Counts (10^6 cpm μl^{-1})	Average R.S.D. (%)	Average (10^6 cpm μl^{-1})	Counts (10^6 cpm μl^{-1})	Average R.S.D. (%)	
1	5.709	0.01				
3	5.737	0.13	5.708	5.724	0.78	−0.27
5	5.679	0.00				
1	5.801	0.25				
3	5.863	0.15	5.828	5.820	0.32	+0.14
5	5.819	0.29				
1	2.864	0.17				
3	2.884	0.18	2.872	2.902	1.00	−1.03
5	2.869	0.09				
1	5.715	0.12				
3	5.770	0.05	5.747	5.755	0.36	−0.13
5	5.757	0.30				
1	2.807	0.54				
3	2.817	0.23	2.813	2.830	0.64	−0.62
5	2.814	0.13				

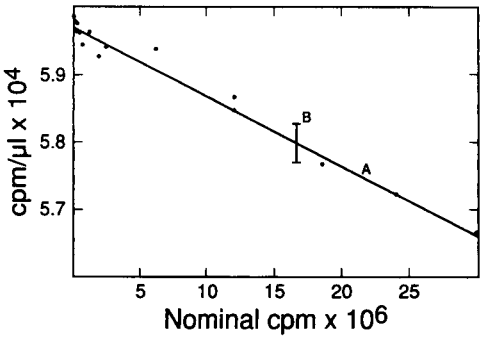

Fig. 5. Variation of measured specific activity with count rate: (A) curve fit by linear regression; (B) ±0.5% error bar.

dead-time correction is 5.1%. This count rate is probably an upper limit for providing accurate counting with corrections applied.

α-Activity measurements

The LS counting method was used to analyze for total α-activity in five typical samples containing either about 20 or 40 g l^{-1} of ^{239}Pu. The samples were aliquoted with 1-, 3-, and 5-µl microcaps and appropriate dead-time corrections made. Results were compared with α-activity measurements obtained by 2-π proportional counting. For these latter measurements, the samples were aliquoted by diluting 25 µl to 25 ml and evaporating 25 µl of the dilution onto a glass plate. The glass micropipets had been calibrated to 0.5% accuracy by weighing dispensed mercury and the flasks with similar accuracy by filling with water. Dead-time corrections in 2-π counting amounted to about 1.5% at the highest rate of 75 000 cpm in these runs.

Comparison of LS counting and 2-π counting results requires a conversion factor relating their counting efficiencies. When similar aliquots of a solution were used, this geometry factor, $eff_{2\text{-}\pi}/eff_{LS}$, was 0.509. This ratio arises from the fact that 2-π counting detects about 50% of the total α-particles, whereas LS counting detects about 100%.

Results of the comparison between the two types of counting are shown in Table 2. Column 2 lists the average count rate obtained for duplicate runs by LS counting and column 3 lists the average standard deviation. Similar values for 2-π counting are given in columns 5 and 6, respectively. For LS counting, specific activities, counts per minute per microliter, agree well for 1- to 5-µl aliquots when the proper dead-time correction is applied. The overall average of these activities (column 4) agree to within 1% of 2-π counting values after the geometry factor is applied. LS counting probably involves fewer errors than 2-π counting. The former method involves only one pipeting; the latter requires two pipetings plus a measurement of flask volume.

The LS counting method requires little operator time because only one pipeting is needed per analysis. Waste generation includes mainly a 400-µl centrifuge tube containing 250 µl of cocktail and a glass microcap. This amount of waste is less than that generated in the 2-π counting method when dilution is required. Waste and analysis time can be further reduced when α-counting is combined with γ-counting for determination of both plutonium and americium in samples [3]. The 2-π method requires a separate aliquot of solution in a plastic tube for measurement of the gamma activity. In the LS counting method, the same 4-ml vial plus 400-µl centrifuge tube combination used in α-counting can be used directly for γ-counting in an automatic counter such as the Packard Model 500.

In the present counting arrangement for the LS counting method with the modified Packard Model 3255, coincidence pulses are used for counting rather than for reducing background at the signal output. The background associated with these negative coincidence pulses fall below 10 cpm, comparable to other LS counting instruments.

Conclusions

LS counting offers a feasible method for measuring α-activity in plutonium samples. This paper illustrates one way to modify an existing instrument to extend its range up to 30×10^6 cpm. Solutions of ^{239}Pu up to 200 g l^{-1} (that is, 1 µl, equivalent to 5 µl of 40 g l^{-1} solution examined in this report) can be aliquoted directly with microcaps for analysis to be carried out.

The author wishes to thank Thomas Sampson of the Los Alamos National Laboratory for suggesting some electronic modules used in the counting. Also, Jim Hare and Tom Gerber of Packard Instruments advised on alternative operation of the sample changer.

REFERENCES

1 D.L. Bokowski, Am. Ind. Hyg. Assoc. J., 35 (1974) 333.
2 H.R. Ihle, A.P. Murrenhoff and M. Karayannis in D. Nastasia-Scotti (Ed.), Standardization of Radionuclides, IAEA Symposium, Vienna, 1966, International Atomic Energy Agency, Vienna, 1967, p. 69.
3 J. Bubernak, M.S. Lew and G.M. Matlack, Anal. Chem., 30 (1958) 1759.

Analytica Chimica Acta, 276 (1993) 211–221
Elsevier Science Publishers B.V., Amsterdam

Ionic equilibria in non-aqueous solvents

Part 1. General equations for calculation of pH, dissociation constants and reference potentials from potentiometric data

Martí Rosés

Departament de Química Analítica, Universitat de Barcelona, Diagonal 647, 08028 Barcelona (Spain)

(Received 1st July 1992; revised manuscript received 20th October 1992)

Abstract

Equations for the calculation of pH, reference potentials and dissociation constants of acids, bases and salts in non-aqueous solvents are derived and tested. They are of general application to many non-aqueous solvents of diverse nature, and their simplification leads to common equations used for particular solvents. A method is also proposed for computation of pH, dissociation constants and reference potentials in pure solvents through titration with titrants which can introduce significant changes in the properties of the titration medium. Application of the method and equations to the determination of the pK values of phenols and β-blocking bases in different non-aqueous solvents is presented.

Keywords: Potentiometry; Titrimetry; Blocking agents; Dissociation constants; Ionic equilibria; pH; Phenols; Reference potentials

Non-aqueous and mixed solvents are widely used in various analytical techniques, e.g., titrimetry, liquid–liquid extraction and liquid chromatography. Following the pioneering work of Kolthoff [1,2], the ionic equilibria in many solvents have been elucidated [1–4]. However, each of the equations applies only for a single solvent, or at most for a small group of solvents with similar characteristics. Equations of general application to solvents of low or high dielectric constant, protic or aprotic, have not been completely developed.

In previous work, equations of general application to solvents of low dielectric constant were proposed [5]. They were applied to the computation of pH, buffer capacity, dissociation constants, reference potentials and titration curves in solvents such as *tert*-butyl [5–7] and 2-propyl [8] alcohol, anhydrous acetic acid [9–11] or tetrahydrofuran [12,13]. In this work these equations are modified and extended to solvents of high dielectric constant which have salts, and sometimes acids and bases, that are completely dissociated. The equations take into account the possible modification of the solvent during titration of acids or bases by formation of water in the neutralization reaction or addition of another solvent with the titrant.

Application of the proposed equations is illustrated by the determination of the pK values of phenols in 2-propyl and *tert*-butyl alcohols and of β-adrenoacceptor blocking bases in anhydrous acetic acid and acetonitrile solvents. Further examples in nitrobenzene and in tetrahydrofuran

Correspondence to: M. Rosés, Departament de Química Analítica, Universitat de Barcelona, Diagonal 647, 08028 Barcelona, Catalonia (Spain).

are presented in Part 2. In current work, satisfactory results are being obtained in the application of the proposed method to titrations in 2-propyl alcohol–water mixtures [14].

IONIC EQUILIBRIA IN NON-AQUEOUS SOLVENTS

Autoprotolysis and solvent equilibria

It is commonly accepted that the autoprotolysis of a solvent governs the pH scale of this solvent:

$$2HS \rightleftharpoons H_2S^+ + S^- \quad K_{ap} = [H_2S^+][S^-]y^2 \quad (1)$$

where K_{ap} is the autoprotolysis constant and y the mean ionic molar activity coefficient. For simplicity, the activity coefficients of all the ions involved in the studied equilibria will be considered equal, despite the differences in size of the ions.

The practical solvent used can contain small amounts of substances capable of competing with the main solvent, solvating H^+ ions or giving other basic ions different from S^-. The most important of these substances is water, which cannot be completely eliminated from many non-aqueous solvents. Water can give H_3O^+ and OH^- ions which have a similar behaviour to the H_2S^+ or S^- ions of the pure main solvent. In order to take into account these ions, a solvent constant ($K_{solvent}$) different from the autoprotolysis constant has been defined [5]:

$$K_{solvent} = ([H_2S^+] + [H_3O^+])([S^-] + [OH^-])y^2 \quad (2)$$

$[H_3O^+]$ and $[OH^-]$ can be computed from the acidity ($K_{a(H_2O)}$) and basicity ($K_{b(H_2O)}$) constants and concentration of water in the solvent:

$$H_2O + HS \rightleftharpoons H_2S^+ + OH^-$$

$$K_{a(H_2O)} = [H_2S^+][OH^-]y^2/[H_2O] \quad (3)$$

$$H_2O + HS \rightleftharpoons H_3O^+ + S^-$$

$$K_{b(H_2O)} = [H_3O^+][S^-]y^2/[H_2O] \quad (4)$$

Substituting Eqns. 3 and 4 in Eqn. 2:

$$K_{solvent} = K_{ap} + (K_{a(H_2O)} + K_{b(H_2O)})[H_2O] + K_{a(H_2O)}K_{b(H_2O)}[H_2O]^2/K_{ap} \quad (5)$$

Equation 5 indicates that if the water concentration is constant, $K_{solvent}$ is also constant, but higher than K_{ap}. If the water concentration is low enough, $K_{solvent}$ value approaches K_{ap}, but if the water concentration is high and/or K_{ap} is very low, $K_{a(H_2O)}$, $K_{b(H_2O)}$ and $[H_2O]$ determine the value of $K_{solvent}$ and therefore it is the water present in the medium which in fact manifests the acid–base behaviour of the solvent.

A more complex equation is obtained if more substances with acid and/or base properties are present in the non-aqueous solvent. Nevertheless, $K_{solvent}$ remains constant if the concentration of these substances is constant. $K_{solvent}$ is the apparent autoprotolysis constant of the solvent, usually determined by potentiometric methods, because these measure the overall proton concentration. For simplicity, this overall proton concentration will be indicated as $\Sigma[H^+]$, i.e., $\Sigma[H^+] = [H_2S^+] + [H_3O^+] + \ldots$ In the same way, $\Sigma[S^-]$ will indicate the overall lyate concentration coming from all the "solvents" present in the medium, i.e., $\Sigma[S^-] = [S^-] + [OH^-] + \ldots$

The solvent equilibria of water and other acid/base impurities present in the medium explains the pH scale observed in aprotic solvents, which in fact is the $pK_{solvent}$ value. Therefore, it is $pK_{solvent}$ that represents the pH scale of the solvent, and it will be used instead of pK_{ap} in this work.

Acid and base equilibria

The dissociation of an acid in a non-aqueous solvent is usually described in two steps:

$$HA \rightleftharpoons H^+A^- \rightleftharpoons H^+ + A^-$$

$$K_a = \sum [H^+][A^-]y^2/([HA] + [H^+A^-]) \quad (6)$$

where K_a is the acidity constant of the acid and H^+ can be solvated by any of the solvents present in the medium.

The equilibria of a base depends on the original basic species. The most common are neutral (B) and solvent ion pair (B^+S^-) bases. However, the latter includes tetralkylammonium hydroxides (B^+OH^-), widely used as titrants in non-aqueous and mixed solvents. As indicated above, OH^-

ions can act as the S^- ions of the main solvent. The most important equilibria for tetralkylammonium hydroxides are

$$B^+OH^- \rightleftharpoons B^+ + OH^-$$

$$K_{d(BOH)} = [B^+][OH^-]y^2/[B^+OH^-] \quad (7)$$

$$OH^- + HS \rightleftharpoons S^- + H_2O$$

$$K_{ap}/K_{a(H_2O)} = [S^-][H_2O]/[OH^-] \quad (8)$$

$$B^+ + S^- \rightleftharpoons B^+S^-$$

$$K_{d(BS)} = [B^+][S^-]y^2/[B^+S^-] \quad (9)$$

An overall basicity constant can be written:

$$K_b = \frac{[B^+](\sum[S^-])y^2}{\sum[B^+S^-]}$$

$$= \frac{[B^+]([S^-] + [OH^-])y^2}{[B^+S^-] + [B^+OH^-]} \quad (10)$$

From Eqns. 7–9:

$$K_b = \frac{\{K_{ap} + K_{a(H_2O)}[H_2O]\}K_{d(BOH)}K_{d(BS)}}{K_{a(H_2O)}[H_2O]K_{d(BS)} + K_{ap}K_{d(BOH)}} \quad (11)$$

As in the solvent equilibria, the presence of water affects the basicity of the base. If the water concentration is low enough, K_b becomes $K_{d(BS)}$, but if the water concentration is very high, K_b becomes $K_{d(BOH)}$. It should be noted that in the titration of an acid with a tetralkylammonium hydroxide, water is formed in the neutralization reaction and therefore K_b cannot be considered constant. The formation of water also affects the other constants, because it changes the dielectric constant of the medium. This effect will be discussed later.

The same equation (Eqn. 11) is obtained if the original base is B^+S^-, because the S^- ions reacts with the water present giving OH^- ions, which form B^+OH^-. With a neutral base B, a similar equation, with $\Sigma[B^+S^-] = [B] + [BH^+S^-] + [BH^+OH^-]$ and replacing $[B^+]$ by $[BH^+]$, is also obtained.

In poor solvating solvents, the acids and, to a minor extent, some bases, can exhibit homoconjugation and heteroconjugation reactions. However, systems with these equilibria have little practical application in analytical chemistry. Analytical chemists tend to avoid these systems, using substances with negligible conjugation reactions. A typical example is acetonitrile, which is used for differential titration of bases [2,15,16], but not for acids because of the conjugation reactions. When accurate measurements in acidic medium are needed, e.g., to standardize a potentiometric system, the acid chosen is usually picric acid because the high charge dispersion through the aromatic ring into the three nitro groups overcomes conjugation [4,15,17].

Therefore, for most general applications, which is the scope of this paper, conjugation reactions can be neglected. In spite of that, extension of the equations developed here to homoconjugation is interesting in order to study the influence of these equilibria in pH and pK computations, and it will be discussed in a further paper.

Salt equilibria

In a solvent of low dielectric constant, partial dissociation of the salt must be considered:

$$B^+A^- \rightleftharpoons B^+ + A^-$$

$$K_{salt} = [B^+][A^-]y^2/[B^+A^-] \quad (12)$$

If the dielectric constant is very low and the salt concentration is high enough, formation of ternary ions by electrostatic interaction between one anion or cation and one ionic pair should also be considered. The two kinds of ternary ions ($A^-B^+A^-$ and $B^+A^-B^+$) cannot be differentiated and a common formation constant [$K_{f(tern)}$] is considered:

$$B^+A^- + A^- \rightleftharpoons A^-B^+A^-$$

$$B^+A^- + B^+ \rightleftharpoons B^+A^-B^+$$

$$K_{f(tern)} = ([A^-B^+A^-] + [B^+A^-B^+])$$
$$/([A^-] + [B^+])[B^+A^-] \quad (13)$$

However, the formation of one ternary ion implies the disappearance of one ion but also of one ion pair, and therefore it has little influence on the dissociation of the salt. Also, as will be shown later, the methods proposed in this paper imply extrapolation to zero salt concentration, where ternary ions of the salt cannot be formed. Ternary ions of acids and bases are usually less important than those of the salt because acids

and bases are usually less dissociated than salts. For all these reasons ternary ion formation will not be considered in the equations developed here.

COMPUTATION OF pH IN NON-AQUEOUS SOLVENTS OF FIXED COMPOSITION

From the above equilibria, the pH during the titration of an acid or a base in any non-aqueous solvent can be computed. Two main types of solutions will be considered: mixtures of acid and salt, and mixtures of base and salt. Solutions of acids and bases alone are particular cases of the mixtures, and the same equation can be used. Equations for the computation of the pH value of salt solutions were derived previously [5]. These solutions are the end-point of titrations, but they do not have practical interest for pK computation because of their low buffer capacity and they will not be considered in this paper.

Mixtures of acid and salt

The mass and charge balances in these mixtures are

$$c_a = \left(\sum[H^+] - \sum[S^-]\right) + [H^+A^-] + [HA] \quad (14)$$

$$c_{salt} = [B^+] + [B^+A^-] \quad (15)$$

$$\sum[H^+] + [B^+] = \sum[S^-] + [A^-] \quad (16)$$

where c_a and c_{salt} are the analytical concentrations of acid and salt, respectively. $\Sigma[S^-]$ can be neglected when $\Sigma[H^+] \gg \Sigma[S^-]$. As many non-aqueous solvents have low K_{ap} values, $\Sigma[H^+]$ is larger than $\Sigma[S^-]$ even for solutions of low acidity and

$$[B^+] = [A^-] - \sum[H^+] \quad (17)$$

$$[B^+A^-] = c_{salt} - [B^+] = c_{salt} - [A^-] + \sum[H^+] \quad (18)$$

Substituting these two equations in Eqn. 12,

$$K_{salt} = \left([A^-] - \sum[H^+]\right)[A^-]y^2 \Big/ \left(c_{salt} - [A^-] + \sum[H^+]\right) \quad (19)$$

From Eqn. 6 and the mass balance in Eqn. 14, neglecting $\Sigma[S^-]$,

$$\sum[H^+] = c_a/\left(1 + K_a^{-1}[A^-]y^2\right) \quad (20)$$

Substituting Eqn. 20 in Eqn. 19 and rearranging terms, the following equation is obtained:

$$\left(K_{salt}^{-1}K_a^{-1}y^4\right)[A^-]^3 + \left(K_{salt}^{-1}y^2 + K_a^{-1}y^2\right)[A^-]^2 + \left(1 - K_a^{-1}c_{salt}y^2 - K_{salt}^{-1}c_a y^2\right)[A^-] - (c_{salt} + c_a) = 0 \quad (21)$$

In the computation of pH, Eqn. 21 is solved by an iterative procedure, i.e., the Newton–Raphson method. Starting values of $[A^-]$ and y can be the salt concentration and unity, respectively. In each iteration the y value is directly computed from the calculated $[A^-]$ value (which is the ionic strength of the solution) and the Debye–Hückel equation. The procedure converges quickly to a constant $[A^-]$ value. $\Sigma[H^+]$ is computed from Eqn. 20, and the pH from

$$pH = -\log\left(\sum[H^+]y\right) \quad (22)$$

The pH of a solution of an acid alone can also be computed from Eqn. 21 taking $c_{salt} = 0$.

Equation 21 is equivalent to the cubic equation in $\Sigma[H^+]$ developed in previous work [5], but the use of $[A^-]$ instead of $\Sigma[H^+]$ leads to a simpler equation which can be solved faster. The use of the inverse of the constants allows the application of Eqns. 20 and 21 to electrolytes that are completely dissociated ($K^{-1} = 0$).

Application of Eqn. 21 to solvents of high dielectric constant, where salts are completely dissociated, can be done considering $K_{salt}^{-1} = 0$. In this instance Eqns. 20–22 become equal to the equations usually employed in water [14].

On the other hand, application of Eqns. 20 and 21 to solvents of low dielectric constant can also lead to some simplified equations. If the dielectric constant is low enough, $K_a^{-1} \approx K_{salt}^{-1} \gg c_a^{-1} \approx c_{salt}^{-1}$, $[A^-] \ll c_a \approx c_{salt}$, and combination of Eqns. 20–22 gives the equation derived by Kolthoff for acid–salt mixtures in anhydrous acetic acid (Eqn. 82 in [1]).

If the acid is much weaker than the salt, $K_a^{-1} \gg K_{salt}^{-1}$ or $K_a \ll K_{salt}$, and Eqns. 20–22 can be

simplified to the equation derived for tetrahydrofuran (Eqn. 5 in [12]).

As can be observed from these simplifications, Eqn. 21 is of general application to any solvent of low or high dielectric constant if the formation of conjugated species and ionic aggregates higher than ion pairs can be neglected.

Mixtures of base and salt

The development of a general equation for base–salt mixtures is parallel to that for acid–salt mixtures and equations parallel to Eqns. 20 and 21 are obtained:

$$\sum[S^-] = c_b/(1 + K_b^{-1}[B^+]y^2) \quad (23)$$

$$(K_{salt}^{-1}K_b^{-1}y^4)[B^+]^3 + (K_{salt}^{-1}y^2 + K_b^{-1}y^2)[B^+]^2 + (1 - K_b^{-1}c_{salt}y^2 - K_{salt}^{-1}c_b y^2)[B^+] - (c_{salt} + c_b) = 0 \quad (24)$$

Equation 24 can be solved in the same way as Eqn. 21 and the pH can be calculated from

$$pS = -\log\left(\sum[S^-]y\right) \quad (25)$$

$$pH = pK_{solvent} - pS \quad (26)$$

Equations 23 and 24 can be also simplified in the same way as Eqns. 20 and 21 for solvents of high or very low dielectric constant.

COMPUTATION OF REFERENCE POTENTIALS AND ACID, BASE AND SALT DISSOCIATION CONSTANTS IN NON-AQUEOUS SOLVENTS OF FIXED COMPOSITION

Standardization of potentiometric systems in an acidic medium can easily be done from the measurement of the potential (E) of mixtures of acid and salt of known dissociation constants. The pH of these solutions can be easily computed from Eqns. 20 and 21 and related to the measured potential through the Nernst equation:

$$E = (E_a^0 - E_j) - g\ pH \quad (27)$$

where E_a^0 is the standard potential and E_j is the junction potential, which is assumed to be constant. In the standardization of a potentiometric system the standard and junction potentials cannot be determined separately, but this is not necessary because pH values are related to the $(E^0 + E_j)$ term. In order to avoid confusion with the true standard potential, the term $(E^0 + E_j)$ will be called reference potential in this work.

Standardization in a basic medium can be done in the same way from mixtures of base and salt. The equations used are Eqns. 23 and 24, and the Nernst equation becomes

$$E = (E_b^0 + E_j) + g\ pS \quad (28)$$

where

$$E_b^0 = E_a^0 - g\ pK_{solvent} \quad (29)$$

This last equation allows the computation of $K_{solvent}$ from the acidic and basic reference potentials.

K_a can be computed from potential measurements of acid–salt mixtures (with a previously standardized potentiometric system), if the pK_{salt} value is known. $\Sigma[H^+]$ is calculated from the measured potential by using Eqn. 27. $[A^-]$ can be computed from $\Sigma[H^+]$ and the K_{salt} value by rearranging and solving Eqn. 19:

$$[A^-] = \left(\sum[H^+]y^2K_{salt}^{-1} - 1\right)/2y^2K_{salt}^{-1} + \left\{\left(1 - \sum[H^+]y^2K_{salt}^{-1}\right)^2 + 4y^2K_{salt}^{-1} \times \left(c_{salt} + \sum[H^+]\right)\right\}^{1/2}/2y^2K_{salt}^{-1} \quad (30)$$

However, if the salt is completely dissociated, $K_{salt}^{-1} = 0$ and Eqn. 30 is indeterminate. In this case, $[A^-]$ is computed from

$$[A^-] = c_{salt} + \sum[H^+] \quad (31)$$

Once $\Sigma[H^+]$ and $[A^-]$ have been calculated, K_a can be easily computed from Eqns. 6 and 14.

Computation of K_b is done from base–salt mixtures. $\Sigma[S^-]$ is computed from Eqn. 28 and $[B^+]$ from an equation similar to Eqn. 30:

$$[B^+] = \left(\sum[S^-]y^2K_{salt}^{-1} - 1\right)/2y^2K_{salt}^{-1} + \left\{\left(1 - \sum[S^-]y^2K_{salt}^{-1}\right)^2 + 4y^2K_{salt}^{-1} \times \left(c_{salt} + \sum[S^-]\right)\right\}^{1/2}/2y^2K_{salt}^{-1} \quad (32)$$

or similar to Eqn. 31 if the salt is completely dissociated:

$$[B^+] = c_{salt} + \sum[S^-] \quad (33)$$

Subsequently K_b is easily computed from Eqn. 10.

K_{salt} can be computed in acid–salt mixtures from the $\Sigma[H^+]$ value obtained from the measured potential and Eqn. 27, and the $[A^-]$ value can be computed from Eqn. 20 if K_a is known. K_{salt} is then calculated from Eqn. 19. If the acid is completely dissociated, $K_a^{-1} = 0$ and $[A^-]$ cannot be computed from Eqn. 20. In this case K_{salt} is undetermined because the salt association cannot have any influence in the acid equilibria, which is always completely dissociated.

In base–salt mixtures a similar procedure is used. $\Sigma[S^-]$ is computed from Eqn. 28 and $[B^+]$ from Eqn. 23. K_{salt} is computed from an equation similar to Eqn. 19:

$$K_{salt} = \left([B^+] - \sum[S^-]\right)[B^+]y^2 / \left(c_{salt} - [B^+] + \sum[S^-]\right) \quad (34)$$

Also if the base is completely dissociated, K_{salt} cannot be determined from pS measurements.

COMPUTATION OF pH, REFERENCE POTENTIALS AND ACID, BASE AND SALT DISSOCIATION CONSTANTS IN NON-AQUEOUS SOLVENTS WITH COMPOSITION CHANGING THROUGH TITRATION

The equations developed in the previous section apply when the composition of the solvent remains unchanged during titration. However, that is not the general case. In the titration of acids with tetralkylammonium hydroxides, water is formed in the neutralization reaction. Moreover, strong acid or base titrants are not stable in every solvent, and often they are used dissolved in a solvent different from the titration medium. From a practical point of view, commercial titrants are available only in a few solvents. Therefore, it is evident that in general the titration medium cannot be considered as a solvent of fixed composition. For example, the commercial tetrabutylammonium hydroxide solution used in titrations in *tert*-butyl alcohol is solved in 2-propyl alcohol containing 8% of methyl alcohol. Thus, titration of an acid will change the medium adding three new solvents (water and 2-propyl and methyl alcohol).

It has been shown that $K_{solvent}$ and K_b depend on the concentration of water and other solvents present in the medium, and the same could have been demonstrated for K_a. Moreover, the addition of other solvents changes the dielectric constant of the medium, changing the dissociation of electrolytes and reference potentials. It has been demonstrated [18,19] that for small additions of a co-solvent, the change in pK_a, pK_b and pK_{salt} values can be considered proportional to the volume fraction (v) of co-solvent added, the proportionality coefficients being s_a, s_b and s_{salt}, respectively. Assuming that the reference potential of the system also changes linearly with v (according to the proportionality coefficient gs_{Ea} and gs_{Eb}, where g is the Nernst constant), a method for the computation of reference potentials and dissociation constants in pure solvents from titration with a titrant dissolved in a different solvent has been developed [12]. According to this method the plot of the computed reference potentials or pK values through a potentiometric acid–base titration (indicated by the subscript "comp") against the volume fraction of titrant added should give a straight line with the intercept being the reference potential or pK value in the pure main solvent [indicated by the subscript "(S)"]. That is, from acid–salt mixtures,

$$\left(E_a^0 + E_j\right)_{comp} = \left(E_a^0 + E_j\right)_{(S)} + gs_{am}v \quad (35)$$

$$(pK_a)_{comp} = pK_{a(S)} - s_{am}v \quad (36)$$

$$(pK_{salt})_{comp} = pK_{salt(S)} - s_{am}v \quad (37)$$

where

$$s_{am} = s_{Ea} - s_a + s_{salt}/2 \quad (38)$$

and from base–salt mixtures,

$$\left(E_b^0 + E_j\right)_{comp} = \left(E_b^0 + E_j\right)_{(S)} + gs_{bm}v \quad (39)$$

$$(pK_b)_{comp} = pK_{b(S)} - s_{bm}v \quad (40)$$

$$(pK_{salt})_{comp} = pK_{salt(S)} - s_{bm}v \quad (41)$$

where

$$s_{bm} = s_{Eb} - s_b + s_{salt}/2$$
$$= s_{solvent} - s_{Ea} - s_b + s_{salt}/2 \quad (42)$$

In these equations $s_{solvent}$ is the proportionality coefficient for variation of the $pK_{solvent}$ value with the medium change, and s_{am} and s_{bm} indicate the overall coefficients in acidic and basic media.

Equations 35–42 are valid if there is a linear relationship between the pH value and the pK values of the acid, base and salt, but if the pH value is not linearly related with the pK values then s_{am} and s_{bm} are not rigorously constant. However, if the variation in solvent composition is small, averaged coefficients can be assumed, and the extrapolation to $v = 0$ can be used to compute pK or reference potentials in the pure main solvent. Therefore, this procedure is proposed as a general method to compute pK or reference potential values in non-aqueous media.

EXPERIMENTAL

Apparatus

A Crison Digilab 517 pH meter, equipped with Radiometer G202B glass electrodes and appropriate reference electrodes and salt bridges as described previously [19–22], was used. The potentiometric cells and salt bridges were externally thermostated by water-jackets at 25.0 ± 0.1°C, except for *tert*-butyl alcohol solvent, which was at 30.0 ± 0.1°C (the melting point of *tert*-butyl alcohol is 25.5°C).

Reagents

The solvents used and the substances titrated have been described previously [5–11,18–24]. The titrant for phenols was 0.1 M tetrabutylammonium hydroxide solution in 2-propyl alcohol containing 8% (v/v) of methyl alcohol [5–8]. For titrations in *tert*-butyl alcohol the stock titrant solution was diluted fivefold in pure *tert*-butyl alcohol [5–7] in order to minimize the effects of medium changes. The titrant of β-blocking bases was 0.1 M perchloric acid. For titrations in acetonitrile, perchloric acid was dissolved in nitromethane because the solutions are unstable in acetonitrile [24]. For titrations in anhydrous acetic acid, perchloric acid was prepared in this solvent [9,23] according to the usual procedure [3] with acetic anhydride.

Procedure

The potentiometric systems in 2-propyl and *tert*-butyl alcohol and in acetonitrile were standardized by titration of picric acid with tetrabutylammonium hydroxide as described in Part 2 [25]. In acetic acid, standardization was performed by titration of sodium acetate with 0.1 M perchloric acid as described elsewhere [23]. The method proposed in this paper was used for determination of reference potentials in the studied solvents.

The procedure for the titration of phenols and β-blockers has been described elsewhere [7,8,23, 24].

RESULTS AND DISCUSSION

The proposed method was applied to determination of pK_a values of 4-nitrophenol and 2,4,6-trichlorophenol in *tert*-butyl and 2-propyl alcohol. pH values were determined from the potentiometric data obtained during titration of the acid with tetrabutylammonium hydroxide [7,8]. $[A^-]$ was calculated from the pH obtained and the previously conductimetrically determined pK_{salt} values [7,8] through Eqn. 30. From $[A^-]$ and $\Sigma[H^+]$ a pK_a value was computed for each point of the titration, and the series of $(pK_a)_{comp}$ values were plotted against the volume fraction of titrant added. Figures 1 and 2 show the results obtained. Straight lines are obtained for the points in the middle part of the titration, where the solution is well buffered. Extrapolation of the lines leads to the pK_a values of the phenols in pure *tert*-butyl and 2-propyl alcohol ($pK_{a(S)}$). The slope of the lines ($-s_{am}$) indicates the degree of influence on the pK_a values of the change in medium caused by the addition of titrant. It can be observed that 2,4,6-trichlorophenol is virtually unaffected by the medium change (s_{am} values of −0.12 and −0.03

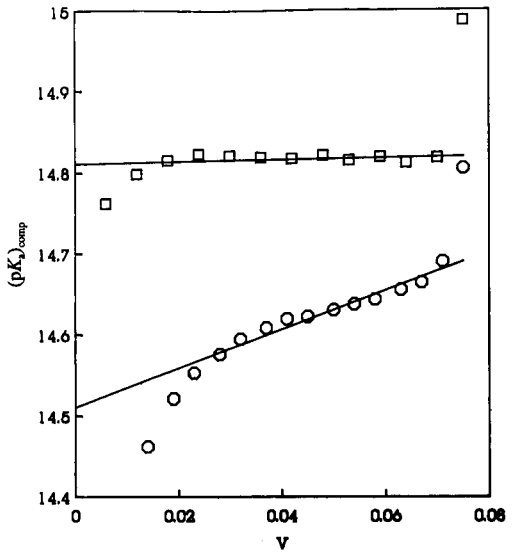

Fig. 1. Determination of pK_a values of phenols in *tert*-butyl alcohol. ○ = 4-Nitrophenol; □ = 2,4,6-trichlorophenol.

in *tert*-butyl and 2-propyl alcohol, respectively), whereas 4-nitrophenol is more affected (s_{am} values of −2.41 and 1.76 for *tert*-butyl and 2-propyl alcohol, respectively).

The effect on the observed s_{am} values caused by the addition of other solvents with the titrant has been explained previously for substituted benzoic acids in tetrahydrofuran [12,13]. The same explanation can be applied to phenols. The addition of a co-solvent (HS) which is a stronger hydrogen bond donor than the main solvent to a solution of phenol and tetrabutylammonium phenolate stabilizes the phenoxide anion by hydrogen bond donation from the co-solvent to the anion, $RPhO^- \leftarrow HS$, and therefore favours dissociations of the phenol and tetrabutylammonium phenolate. However, if the co-solvent added is a stronger hydrogen bond acceptor than the main solvent it also stabilizes the phenol by hydrogen bond donation from the phenol to the co-solvent, $RPhOH \rightarrow SH$, and therefore it disfavours dissociation of the phenol, but does not affect dissociation of the salt. However, in contrast with benzoic acids, in phenols *ortho* substituents are very close to the reaction centre (–OH or $-O^-$ group) and make solvation of this group difficult, so addition of stronger hydrogen bond donors or acceptors has little influence on the $(pK_a)_{comp}$ values.

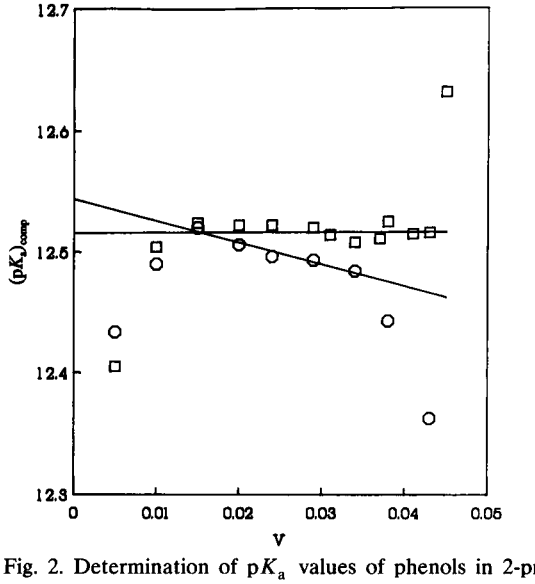

Fig. 2. Determination of pK_a values of phenols in 2-propyl alcohol. ○ = 4-Nitrophenol; □ = 2,4,6-trichlorophenol.

4-Nitrophenol shows different behaviours in *tert*-butyl and 2-propyl alcohol. Whereas in *tert*-butyl alcohol s_{am} is negative, in 2-propyl alcohol it is positive. The s_{am} value depends on the s_a, s_{salt} and s_{Ea} values according to Eqn. 38. In solvents of low dielectric constant s_{Ea} usually has a small influence compared with s_a or s_{salt}, which should have negative values if the addition of titrant increases the dielectric constant of the medium, and positive in the contrary case. The variation in hydrogen bond capabilities of the medium also affects the s_a and s_{salt} values. As indicated above, an increase in these capabilities should decrease s_{salt} (favouring salt dissociation), whereas s_a will decrease if the phenoxide anion is more stabilized by an increase in hydrogen bond donation from the solvent than the phenol is stabilized by an increase in solvent hydrogen bond accepting capability. If the opposite is true s_a will increase. The titrant solvent used contains 2-propyl and methyl alcohol, and in the neutralization reaction water is formed, which increase the dielectric constant and hydrogen bond capabilities of the medium, and therefore s_{salt} should be negative for both media; s_a should also be nega-

tive, but higher than s_{salt}. If s_a and s_{salt} have the same sign, they partially compensate according to Eqn. 38. Assuming that s_{Ea} can be neglected, if $s_{salt}/2 < s_a$ then s_{am} is negative, but if $s_{salt}/2 > s_a$ then s_{am} is positive. In *tert*-butyl alcohol, addition of 2-propyl and methyl alcohol with the titrant, and formation of water in the neutralization reaction, lead to an s_{salt} value much more negative than s_a, and therefore s_{am} is also negative. However, in 2-propyl alcohol the medium is less changed because the added co-solvent is only methyl alcohol, a solvent more similar to 2-propyl alcohol than to *tert*-butyl alcohol. Also, the variation in pK_{salt} values should be less important because tetrabutylammonium nitrophenolate is more dissociated in 2-propyl than in *tert*-butyl alcohol (pK_{salt} values of 2.79 and 3.85, respectively). Hence, $s_{salt}/2$ is less negative than s_a, and s_{am} is positive.

The pK_a values obtained for 2,4,6-trichlorophenol (14.81 and 12.52 for *tert*-butyl and 2-propyl alcohol, respectively) agree very well with those previously determined (14.82 and 12.55 [7,8]). However, the pK_a value of 14.51 obtained for 4-nitrophenol in *tert*-butyl alcohol is lower than that of 14.60 determined previously [7]. In contrast, the pK_a value of 12.54 obtained for 4-nitrophenol in 2-propyl alcohol is higher than that of 12.45 determined previously [8]. The reason for these small discrepancies is that the pK_a values previously reported were computed by averaging, instead of extrapolation to the pure main solvent.

The proposed method has also been applied to the determination of basicity constants of β-adrenoacceptor blocking agents in acetonitrile. These drugs are widely used in the treatment of cardiac arrhythmias, hypertension, angina and thyrotoxicosis. They are also used as doping agents in sport, and for this reason they have been forbidden by the International Olympic Committee. The importance of these drugs and the increasing use of acetonitrile as a solvent for basic drugs titration suggested the determination of the pK_a values of the conjugated acids of a series of β-adrenergic blocking agents [24]. In order to test the equations proposed in this paper for the determination of pK_b values, they were

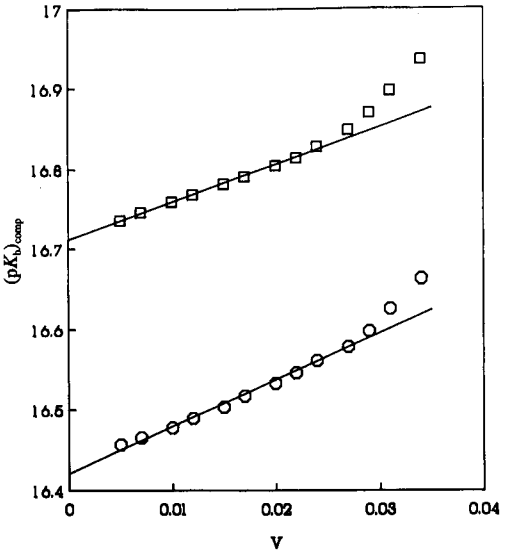

Fig. 3. Determination of pK_b values of β-adrenergic blocking agents in acetonitrile. ○ = oxprenolol; □ = penbutolol.

applied to a pair of these drugs, oxprenolol and penbutolol. The $(pK_b)_{comp}$ values obtained are plotted against the volume fraction of titrant added (perchloric acid in nitromethane) in Fig. 3. Straight lines are obtained in the buffered region, which allow the computation of the pK_b values of 16.42 and 16.71 in pure acetonitrile for oxprenolol and penbutolol, respectively. The slope of the lines (s_{bm} values of −5.83 and −4.69 for oxprenolol and penbutolol, respectively) shows that the addition of nitromethane causes an appreciable medium change. As salts are completely dissociated in acetonitrile, the only parameters that influence the s_{bm} values according to Eqn. 42 are $s_{solvent}$, s_{Ea} and s_b. The most important of these parameters is $s_{solvent}$, whereas s_{Ea} and s_b tend to zero because nitromethane is a solvent similar to acetonitrile. However, addition of nitromethane decreases the $pK_{solvent}$, as explained at the beginning of the theoretical section, and therefore $s_{solvent}$ and s_{bm} have negative values. From the determined pK_b values and the $pK_{solvent}$ value of 34.36 for pure acetonitrile [25], pK_{HB^+} values of 17.94 and 17.65 are obtained for oxprenolol and penbutolol, respectively. These values are slightly higher than those reported previously [24], which were computed by averag-

ing. However, as with phenols, the difference is less than 0.1 pK unit.

The same series of β-blocking agents were studied in anhydrous acetic acid [23], which is the classical solvent used for the titration of basic drugs. Anhydrous acetic acid is a solvent of low dielectric constant, and therefore electrolytes are sparingly dissociated in it. The low dissociation of electrolytes precludes the determination of the dissociation constants of salts by conductimetry. The usual method consists in the determination of the pK_b value of the base from potentiometric measurements of solutions of pure base, and determination of the pK_{salt} value from potentiometric measurements of base–salt mixtures. A titration of the base with perchloric acid is usually employed, and pK_b is determined from the first point of the titration and pK_{salt} from the others. This method can be applied because the solution is usually well buffered at the beginning of the titration, as demonstrated previously [10]. For example, Fig. 4 displays the buffer capacity during the titration of oxprenolol and penbutolol.

From the potentiometric data obtained during titrations of oxprenolol and penbutolol [23], pK_b was computed from the first point of the titration (pK_b values of 6.12 and 6.36 for oxprenolol and

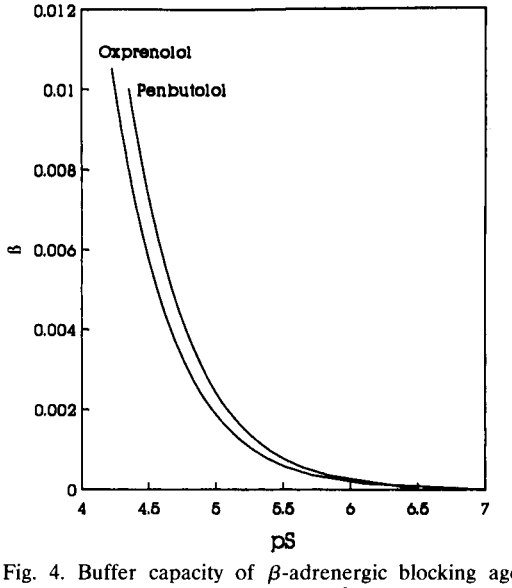

Fig. 4. Buffer capacity of β-adrenergic blocking agents in anhydrous acetic acid at $c = 5 \times 10^{-3}$ M.

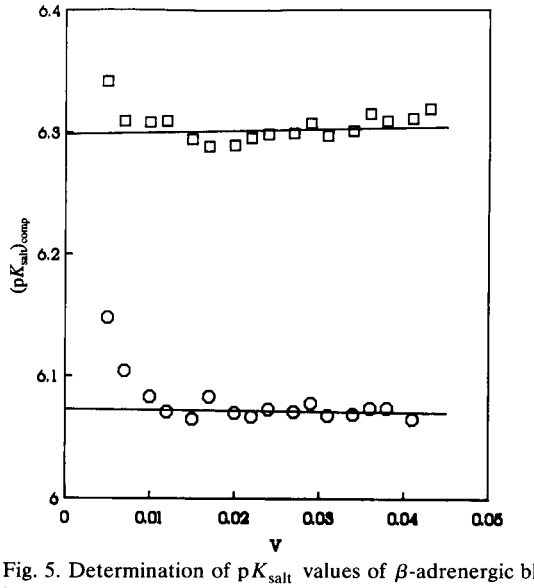

Fig. 5. Determination of pK_{salt} values of β-adrenergic blocking agents in anhydrous acetic acid. ○ = Oxprenolol; □ = penbutolol.

penbutolol, respectively) and pK_{salt} values from the other points. pK_{salt} values were plotted against the volume fraction of titrant added (perchloric acid in anhydrous acetic acid), according to the method proposed in this paper. As Fig. 5 shows, a flat, straight line is obtained for each drug, as expected as the titrant is dissolved in the same solvent as the titrated drug and no water is formed during titration. Although the solution is well buffered, the points at the beginning of the titration deviate from the straight line because of the low salt concentration. The pK_{salt} values obtained by extrapolation (6.07 and 6.30 for oxprenolol and penbutolol, respectively) agree very well with those obtained previously by averaging [23].

From these examples, it can be concluded that the equations derived in this paper and the proposed method of extrapolation of the results to zero volume of titrant added allow the accurate determination of the dissociation constants of acids, bases and salts in non-aqueous solvents of low and high dielectric constant. The classical method of averaging the results obtained in the buffered part of the titration produces the same results as the proposed method when the titrant

added does not change the titration medium significantly, an event that is not very frequent in non-aqueous titrations.

The author thanks J. Barbosa, E. Bosch, C. Ràfols and M.E. Torrero for kindly providing the experimental data for the examples presented and making helpful comments. Financial support from the DGICYT (project PB88-0194) is also gratefully acknowledged.

REFERENCES

1 I.M. Kolthoff, in I.M. Kolthoff and P.J. Elving (Eds.), Treatise on Analytical Chemistry, Part I, Vol. 1, Wiley, New York, 1959, Chap. 13.
2 I.M. Kolthoff and P.J. Elving (Eds.), Treatise on Analytical Chemistry, Part I, Vol. 2, Wiley, New York, 2nd edn., 1979.
3 L. Safarik and Z. Stransky, Titrimetric Analysis in Organic Solvents (Wilson and Wilson's Comprehensive Analytical Chemistry, Vol. XXII), Elsevier, Amsterdam, 1986.
4 E.P. Serjeant, Potentiometry and Potentiometric Titrations, Wiley, New York, 1984.
5 E. Bosch and M. Rosés, Talanta, 36 (1989) 615.
6 E. Bosch and M. Rosés, Talanta, 36 (1989) 623.
7 E. Bosch and M. Rosés, Talanta, 36 (1989) 627.
8 E. Bosch, C. Ràfols and M. Rosés, Talanta, 36 (1989) 1227.
9 J. Barbosa, E. Bosch, J.L. Cortina and M. Rosés, Anal. Chim. Acta, 256 (1991) 203.
10 J. Barbosa, E. Bosch, J.L. Cortina and M. Rosés, Anal. Chim. Acta, 256 (1991) 211.
11 J. Barbosa, E. Bosch, J.L. Cortina and M. Rosés, Anal. Chim. Acta, 256 (1991) 177.
12 J. Barbosa, D. Barrón, E. Bosch and M. Rosés, Anal. Chim. Acta, 264 (1992) 229.
13 J. Barbosa, D. Barrón, E. Bosch and M. Rosés, Anal. Chim. Acta, 265 (1992) 157.
14 C. Ràfols, M. Rosés and E. Bosch, in preparation.
15 I.M. Kolthoff, Anal. Chem., 46 (1974) 1992.
16 J.F. Coetzee and G.R. Padmanabhan, J. Am. Chem. Soc., 87 (1965) 5005.
17 I.M. Kolthoff, M.K. Chantooni, Jr., and H. Smagowski, Anal. Chem., 42 (1970) 1622.
18 E. Bosch and M. Rosés, Anal. Chem., 60 (1988) 2008.
19 E. Bosch, C. Ràfols and M. Rosés, Anal. Chem., 62 (1990) 102.
20 J. Barbosa, E. Bosch and M. Rosés, Analyst, 112 (1987) 179.
21 J. Barbosa, J. Sánchez and E. Bosch, Talanta, 31 (1984) 279.
22 J. Barbosa, M. Rosés and V. Sanz-Nebot, Talanta, 35 (1988) 1013.
23 J. Barbosa and M.E. Torrero, Mikrochim. Acta, I (1991) 79.
24 J. Barbosa, V. Sanz-Nebot and E. Torrero, Talanta, 38 (1991) 425.
25 M. Rosés, Anal. Chim. Acta, 276 (1993) 223.

Analytica Chimica Acta, 276 (1993) 223–234
Elsevier Science Publishers B.V., Amsterdam

Ionic equilibria in non-aqueous solvents

Part 2. Computer programs for calculation of pH, dissociation constants and reference potentials from potentiometric data

Martí Rosés

Departament de Química Analítica, Universitat de Barcelona, Diagonal 647, 08028 Barcelona, Catalonia (Spain)

(Received 1st July 1992; revised manuscript received 20th October 1992)

Abstract

Computer programs to perform automatic potentiometric titrations, to compute reference potentials and dissociation constants and to plot titration curves and buffer capacities in non-aqueous solvents are presented. The computer programs were tested with experimental potentiometric data obtained in titrations of picric acid with tetrabutylammonium hydroxide in acetonitrile, nitrobenzene, tetrahydrofuran and *tert*-butyl and isopropyl alcohol solvents with satisfactory results.

Keywords: Potentiometry; Titrimetry; Computer programs; Dissociation constants; Ionic equilibria; Non-aqueous solvents; pH; Reference potentials

The general computation of dissociation constants in non-aqueous solvents is usually difficult because of the lack of adequate computer programs. Programs used in water, such as SCOGS [1], MINIQUAD [1], PKAS [2], TITFIT [3] and MINIGLASS [4], have been developed for metal–ligand complex systems and they assume the ionic strength to be constant. Therefore, they cannot be applied to non-aqueous solvents of low dielectric constant where the formation of salt ionic pairs changes the ionic strength during titration. Even the program NABTIT [5], developed specially for the computation of acid–base constants in non-aqueous solvents, assumes that there is no formation of salt ionic pairs. An interesting exception is EQUIL [6], which allows activity coefficient corrections in systems of variable ionic strength. However, it computes activity coefficients only for aqueous media. Moreover, this program was written before the development of microcomputers and therefore a large computer is needed. Also, all these programs do not consider the common case of addition of other solvents together with the titrant, which changes the constants of the titration medium [7].

In Part 1 [7], general equations for application to any solvent were developed and proposed for calculating dissociation constants from potentiometric titrations. In this paper, computer programs to determine reference potentials, acid, base and salt dissociation constants, pH, buffer capacity and titration curves using the proposed equations are presented. They are complemented with computer programs to control automatic titrations, collect the data and facilitate their management.

The equations and programs were tested with a set of potentiometric titrations of picric acid

Correspondence to: M. Rosés, Departament de Química Analítica, Universitat de Barcelona, Diagonal 647, 08028 Barcelona, Catalonia (Spain).

with tetrabutylammonium hydroxide in diverse solvents such as tetrahydrofuran, *tert*-butyl and isopropyl alcohol, nitrobenzene and acetonitrile with satisfactory results. Table 1 presents the properties of the solvents studied [8–10], together with the dissociation constants of picric acid, tetrabutylammonium picrate and tetrabutylammonium hydroxide [11–18]. According to Kolthoff's classification of solvents [19], tetrahydrofuran is an aprotic dipolar protophilic solvent of low dielectric constant, *tert*-butyl and isopropyl alcohol are neutral amphiprotic solvents of low dielectric constant and nitrobenzene and acetonitrile are aprotic dipolar protophobic solvents of high dielectric constant. As expected, tetrabutylammonium hydroxide and picrate are completely dissociated in the solvents of high dielectric constant. Application to the titration of bases in a protogenic amphiprotic solvent of low dielectric constant such as acetic acid has also been successfully achieved [7].

The following programs were developed: VALORA, which performs automatic titrations through serial ports; PREPOT, which manages and prepares the potentiometric data to be used by the other programs; POTENCI, which computes reference potentials; PK and PKSIMULT, which compute dissociation constants of acids, bases, and salts; and CORVAL, which computes pH values and simulates and displays titration curves and buffer capacities. All the programs work in interpreted Microsoft GW-BASIC and in compiled Borland TURBO BASIC. Copies of the programs on floppy disk (or listings) are available on request.

EXPERIMENTAL

Apparatus

A Crison Digilab 517 pH meter and a manual burette were used for titrations in most solvents. For the titration in tetrahydrofuran a Crison 2002 pH meter and a Crison 2031 autoburette, controlled by the VALORA program, were used. The potentiometers were equipped with Radiometer G202B glass electrodes and appropriate reference electrodes and salt bridges previously described for most solvents [12,20–22]. For titrations in nitrobenzene the reference electrode was Ag/AgCl in saturated tetramethylammonium chloride in nitrobenzene, with a double salt bridge of 0.1 M tetraethylammonium perchlorate in nitrobenzene. The potentiometric cells and salt bridges were externally thermostated by water-jackets at 25.0 ± 0.1°C, except for *tert*-butyl alcohol solvent at 30.0 ± 0.1°C (the melting point of *tert*-butyl alcohol is 25.5°).

Reagents

Picric acid from Doesder (analytical-reagent grade, > 99.8%, ACS vacuum-dried) was titrated with the commercial 0.1 M tetrabutylammonium hydroxide solution in isopropyl alcohol containing 8% (v/v) methanol [7]. Nitrobenzene and tetrahydrofuran were obtained from Fluka [analytical-

TABLE 1

Properties of solvents and dissociation constants of picric acid (pK_a), tetrabutylammonium picrate (pK_{salt}) and tetrabutylammonium hydroxide (pK_b) at 25°C [a]

Solvent	ϵ	A	α	β	π^*	pK_{ap}	pK_a	pK_{salt}	pK_b
Tetrahydrofuran	7.6	16.54	0.00	0.55	0.58		11.84	5.21	6.47
tert-Butyl alcohol [b]	10.7	8.51	0.68	1.01	0.41	28.5	5.35	4.36	4.91
Isopropyl alcohol	18.3	4.59	0.76	0.95	0.48	20.8	4.02	2.80	2.58
Methanol	32.6	1.69	0.93	0.62	0.60	16.7			
Nitrobenzene	34.8	1.89	0.00	0.39	1.01		7.46	d [c]	d
Acetonitrile	35.9	1.64	0.19	0.31	0.75	~ 33	11.00	d	d
Water	78.4	0.51	1.17	0.47	1.09	14.0	0.33	d	d

[a] ϵ = Dielectric constant; A = Debye–Hückel constant; α = Kamlet–Taft parameter of hydrogen bond acidity; β = Kamlet–Taft parameter of hydrogen bond basicity; π^* = Kamlet–Taft parameter of dipolarity; $pK_{ap} = pK$ of autoprotolysis. Data from [8–18]. [b] Data at 30°C. [c] d = Electrolyte completely dissociated.

reagent grade (> 99.5%) and for HPLC, respectively]. Acetonitrile and *tert*-butyl and isopropyl alcohol were the same as used previously [7].

Procedure

Volumes of 10–25 ml of 4×10^{-3}–8×10^{-3} M solutions of picric acid in each pure solvent were titrated with 0.1 M tetrabutylammonium hydroxide solution and the potential measurements were recorded during titration.

AUTOMATIC CONTROL OF TITRATIONS: THE VALORA PROGRAM

The VALORA program is specially designed to perform automatic titrations in non-aqueous solvents. The main difference between automatic titrations in aqueous and non-aqueous solvents is the determination of the equivalence point. In aqueous solution the equivalence point can usually be computed from Gran functions. However, the complexity of the equilibria in non-aqueous solvents precludes linearization of the titration curves, and methods based on the first or second derivative of the potential curve must be used. In these methods the accuracy of the equivalence volume depends on the frequency of the titrant additions. However, a high frequency during the whole titration curve increases the titration time, specially because in non-aqueous solvents stabilization of potential can require a considerable time.

In order to optimize the accuracy of the equivalence point and the time of titration, the latter is divided into three parts: before, near and after the equivalence point. For each of these parts the operator can choose different volume additions of titrant, time between measurements, maximum number of measurements and maximum allowable potential variation adopted as the criterion for considering the potential to be stable. Before the equivalence point very stable measurements are usually needed to compute accurate constants, but the use of small volume increments would increase the titration time. However, near the equivalence point a small volume increase is convenient in order to compute an accurate equivalence volume, but as potential measurements are not stable because of the low buffer capacity, the time between measurements and the maximum number of measurements can be reduced to a minimum.

To determine the closeness to the equivalence point, the ratio between the buffer capacity of the last measurement (β) and the maximum buffer capacity (β_{max}) is used. When this ratio comes below a fixed value, VALORA turns to the parameters near to the equivalence point. The fixed value is recommended to be set to 0.1–0.35 depending on the strength of the protolyte being titrated. For a strong acid or base the β/β_{max} ratio decreases to 0.1 at 90% of the equivalence point, whereas for a very weak acid or base the decrease at 90% is only to 0.35. In non-aqueous solvents a strong acid or base means an acid or base dissociated equally to or more than the salt, and a weak acid or base means an acid or base less dissociated than the salt [7].

In fact, the buffer capacity cannot be directly computed. What is computed is the variation of potential with the volume of titrant added (dE/dV), which is proportional to the variation of pH with the concentration of titrant added ($dpH/dc_{titrant}$), that is, to the inverse of the buffer capacity ($\beta = dc_b/dpH$). Therefore, the ratio $(dE/dV)_{max}/(dE/dV)$ is equal to the ratio β/β_{max}. dE/dV is computed by cubic smoothing of the last five measured potentials by the Savitzky and Golay method [23].

The titration automatically stops when an overall prefixed volume of titrant added is exceeded. VALORA outputs two ASCII files. The main file (which is used by the PREPOT program) contains only volume and potential measurements. The auxiliary file (which has the same name as the main file but with the extension DAD) contains all the potential readings (including those which are not stable) and the titration part changes. This last file is used in order to trace the development of the titration if unexpected results are obtained.

Control of burette and reading of potentiometers are done through RS-232 serial ports. As each peripheral device has its own communica-

tions protocol, appropriate subroutines are needed for each particular burette or potentiometer implementation.

PRETREATMENT OF POTENTIOMETRIC DATA: THE PREPOT PROGRAM

The potentiometric data obtained by the VALORA program cannot be used directly to determine reference potentials or dissociation constants. Parameters such as initial volume of solution, titrant concentration, the parameter A in the Debye–Hückel equation and the Nernst constant (g) are also needed. If the data are to be used for the determination of reference potentials, the dissociation constants of the acid, base and salt used in the titrations are also needed. If the aim of the titration is to determine dissociation constants, the potential values must be converted into pH or pS (see Part 1 [7]) values by means of the reference potentials. The PREPOT program allows the introduction of the supplementary data and conversion of potential to pH or pS.

The equivalence volume of the titration is also needed to compute acid, base and salt concentrations for each titration point, PREPOT computes the equivalence volume from the second derivative of the smoothed cubic spline of the potentiometric data [23]. A plot of potential and second derivative of potential against volume of titrant is presented by the program, and the possible equivalence points are computed by local interpolation as the zero-crossing points of second derivative.

Input of the volume–potential data can be done through the keyboard or from the VALORA output file or any equivalent ASCII file. The output of PREPOT is an ASCII file containing an identifier of the use of the file (determination of reference potentials, dissociation constants of acids and/or bases or dissociation constants of salts) and all the data needed by the program to be used (POTENCI, PK or PKSIMULT).

COMPUTATION OF REFERENCE POTENTIALS: THE POTENCI PROGRAM

The first step in the determination of dissociation constants from potentiometric data is the standardization of the potentiometric system used. In this process standards of known pH or pS are used to relate the measured potentials (E) with the pH or pS values of the standards, usually through the Nernst equation. The method described in Part 1 [7] can be used for this purpose [7]. In this method the pH or pS of the standard is computed from a general cubic equation which can be written as

$$\left(K_{\text{salt}}^{-1}K_n^{-}y^4\right)[\text{X}]^3 + \left(K_{\text{salt}}^{-2}y^2 + K_n^{-1}y^2\right)[\text{X}]^2 + \left(1 - K_n^{-1}c_{\text{salt}}y^2 - K_{\text{salt}}^{-1}c_n y^2\right)[\text{X}] - (c_{\text{salt}} + c_n) = 0 \quad (1)$$

where K_n, c_n and [X] indicate K_a, c_a and $[A^-]$ for an acid–salt mixture or K_b, c_b and $[B^+]$ for a base–salt mixture and y is the mean ionic molar activity coefficient (see Part 1 [7]). The POTENCI program solves Eqn. 1 by a Newton–Raphson approach and computes [X] for all the points of an acid–base potentiometric titration of known K_a, K_b and K_{salt} values. From the [X] value, pH or pS (which will be indicated as pN) values are computed from the expression

$$\text{pN} = -\log\left\{c_n/\left(1 + K_n^{-1}[\text{X}]y^2\right)\right\} \quad (2)$$

Once pH or pS has been computed, it can be related to the potential measurements (E) through the Nernst equation:

$$E + g\,\text{pH} = \left(E_a^0 + E_j\right) \quad (3)$$

$$E - g\,\text{pS} = \left(E_b^0 + E_j\right) \quad (4)$$

where $(E_a^0 + E_j)$ and $(E_a^0 + E_j)$ are the reference potentials in acidic and basic media, respectively. The terms $E + g\,\text{pH}$ for an acid–salt mixture and $E - g\,\text{pS}$ for a base–salt mixture should be constant for all the titration points if the junction potential (E_j) is constant. However, as explained in Part 1 [7], the addition of other solvents together with the titrant can change the reference potentials and dissociation constants of the standards. The plot of the computed reference poten-

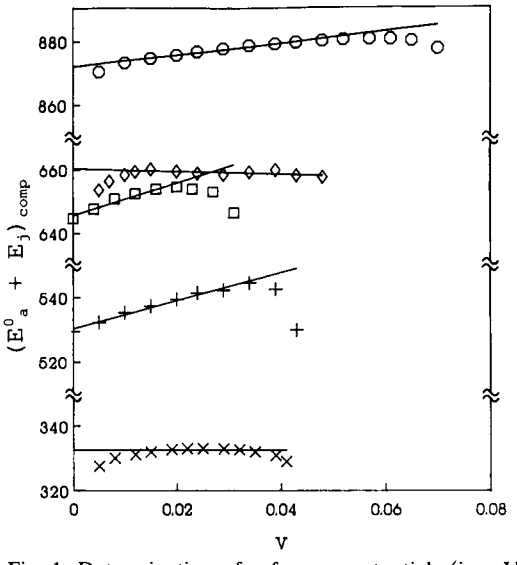

Fig. 1. Determination of reference potentials (in mV) from picric acid–tetrabutylammonium picrate mixtures in pure non-aqueous solvents. × = Tetrahydrofuran; + = isopropyl alcohol; □ = *tert*-butyl alcohol; ◇ = acetonitrile; ○ = nitrobenzene.

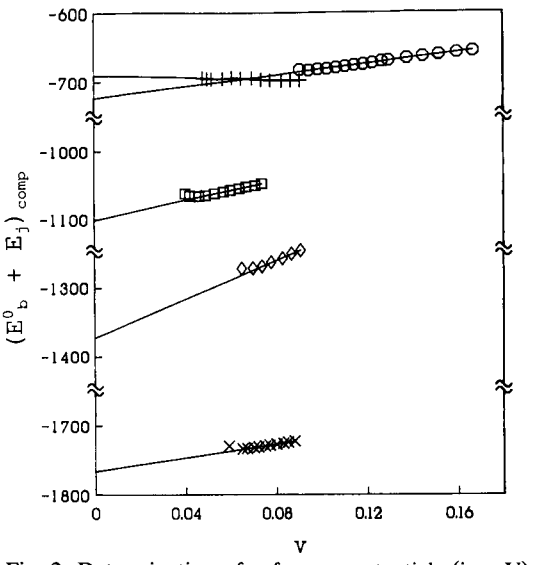

Fig. 2. Determination of reference potentials (in mV) from tetrabutylammonium picrate–tetrabutylammonium hydroxide mixtures in pure non-aqueous solvents. Symbols as in Fig. 1.

tials $[(E^0_a + E_j)_{comp}$ or $(E^0_b + E_j)_{comp}]$ against the volume fraction of titrant added (v) should give a straight line with the intercept being the reference potentials in the pure solvent:

$$E + g\,\mathrm{pH} = \left(E^0_a + E_j\right)_{comp} = \left(E^0_a + E_j\right)_{(S)} + gs_{am}v \quad (5)$$

$$E - g\,\mathrm{pS} = \left(E^0_b + E_j\right)_{comp} = \left(E^0_b + E_j\right)_{(S)} + gs_{bm}v \quad (6)$$

where s_{am} and s_{bm} are the coefficients for medium charge in acidic and basic media (see Part 1, Eqns. 35–42 [7]).

The POTENCI program computes $E + g\,\mathrm{pH}$ or $E - g\,\mathrm{pS}$ for each titration point, plots it against v and computes the reference potentials.

The results obtained for the data sets studied are presented in Figs. 1 and 2 and Table 2. In picric acid–tetrabutylammonium picrate mixtures (Fig. 1), straight lines are obtained in the buffered part of the titration. In tetrahydrofuran, acetonitrile and nitrobenzene, picric acid is very weak and well buffered solutions are obtained only in the middle part of the titration. However, in isopropyl and *tert*-butyl alcohol, picric acid is fairly strong and well buffered solutions are obtained from the first points of the titration.

The intercept $[(E^0_a + E_j)_{(S)}]$ and the slope (s_{am}) of the straight lines in Fig. 1 are represented in

TABLE 2

Reference potentials and $pK_{solvent}$ values in pure solvents computed by the POTENCI program

Solvent	$(E^0_a + E_j)_{(S)}$ (mV)	s_{am}	N	$(E^0_b + E_j)_{(S)}$ (mV)	s_{bm}	N	$pK_{solvent}$
Tetrahydrofuran	332.5 ± 0.7	0.0	7	−1766.5 ± 1.3	−8.3	10	35.5
tert-Butyl alcohol	645.7 ± 0.7	8.4	7	−1001.7 ± 0.5	−11.8	8	27.4
Isopropyl alcohol	530.5 ± 1.5	7.2	9	−690.8 ± 1.5	1.6	12	20.5
Nitrobenzene	922.1 ± 0.4	3.1	9	−723.8 ± 0.8	−6.9	15	27.8
Acetonitrile	660.3 ± 0.6	−0.8	9	−1372.4 ± 3.0	−23.4	5	34.4

Table 2. The reference potentials depend on the main solvent and on the potentiometric assembly used, and the slopes on the co-solvents added with the titrant and on the variation of pK values of the acid titrated and salt formed with this addition of co-solvents, according to the equation

$$s_{am} = s_{Ea} - s_a + s_{salt}/2 \quad (7)$$

In all the titrations the co-solvent added with the titrant is mainly isopropyl alcohol, but also some methanol (contained in the commerical titrant used) and water (which is formed in the neutralization reaction). The variation in electrode potentials (s_{Ea}) is usually negligible as compared with s_a and s_{salt}. s_a and s_{salt} should be negative if the co-solvent added favours dissociation of the electrolyte or positive in the opposite case. In solvents of low dielectric constant the dielectric constant values of the main solvent and co-solvent added determine the sign of s_a and s_{salt}, but specific hydrogen bond interactions between the co-solvent added and the solutes are also important.

In solvents of high dielectric constant, where ionic pairs are not formed, the specific interactions play a key role. In these solvents salt is completely dissociated, $s_{salt} = 0$, and $s_{am} = s_{Ea} - s_a$. In acetonitrile, s_{am} is close to zero, which means that the addition of isopropyl alcohol, methanol and water (all strong hydrogen bond donors, unlike acetonitrile; see Table 1) does not affect the dissociation of picric acid in this medium, as has been described previously [8,19,24]. The extensive delocalization of the negative charge in the picrate anion prevents the hydrogen bond donation from the co-solvent to the phenoxide anion that would stabilize the picrate anion and favour picric acid dissociation. However, in nitrobenzene, s_{am} has a significant positive value, that is, s_a should be negative, and therefore addition of hydrogen bond donors stabilizes the negative charge of the anion in the phenoxide group and favours picric acid dissociation. The high dipolarity of nitrobenzene (see Table 1) prevents complete delocalization of the negative charge into the nitro substituents and partially localizes it in the phenoxide group allowing co-solvent–picrate ion hydrogen bonding. The higher solvation ability due to the dipolarity of nitrobenzene explains the lower pK value of picric acid in nitrobenzene compared with acetonitrile (Table 1).

In solvents of low dielectric constant, s_a and s_{salt} can be balanced according to Eqn. 7, as occurs in tetrahydrofuran, which has an s_{am} value close to zero. The large charge delocalization of the picrate anion in this non-hydrogen bond donor solvent implies weak hydrogen bond interactions and the s_a and $s_{salt}/2$ terms cancel mutually. In anions with no charge delocalization, such as perchlorate and trifluoromethanesulphonate, high s_{am} values have been observed in tetrahydrofuran [12].

As *tert*-butyl alcohol is a hydrogen bond donor solvent, the charge of picrate anion is localized at the phenoxide group and addition of stronger hydrogen bond donor and dipolar solvents (isopropyl alcohol, and especially methanol and water) favours solute dissociation, and thus high negative values of s_a and s_{salt} are obtained. However, *tert*-butyl alcohol is a stronger hydrogen bond acceptor than the co-solvents added, and addition of these co-solvents weakens the hydrogen bond donation from the picric acid to the solvent, and favours acid dissociation but not salt dissociation. Therefore, s_a is more negative than s_{salt}, which results in a high positive value of s_{am}.

The behaviour of isopropyl alcohol medium is very similar to that of *tert*-butyl alcohol, but the only co-solvents that affect the s values are methanol and water. This implies that they must have a strong effect on picric acid dissociation, as has been demonstrated previously [13], because these co-solvents are added or formed in small amounts.

The variation of reference potentials in basic medium (Fig. 2) from tetrabutylammonium hydroxide–tetrabutylammonium picrate mixtures was obtained from the points after the equivalence point of the picric acid titrations. The slope s_{bm} follows the equation [7]

$$s_{bm} = s_{solvent} - s_{Ea} - s_b + s_{salt}/2 \quad (8)$$

In basic medium variation of the $pK_{solvent}$ values ($s_{solvent}$) is essential. $s_{solvent}$ should be negative for addition of co-solvents with $pK_{solvent}$ lower

than that of the medium or positive in the opposite case. All the solvents studied, except isopropyl alcohol, have $pK_{solvent}$ values higher than those of the co-solvents added (isopropyl alcohol, and to a minor extent methanol and water), as Tables 1 and 2 show. Therefore, acetonitrile, nitrobenzene, tetrahydrofuran and *tert*-butyl alcohol have large negative $s_{solvent}$ values which result in large negative s_{bm} values. For isopropyl alcohol, $s_{solvent}$ and s_{Ea} are negligible in comparison with s_b and s_{salt}, and the latter determine the sign of s_{bm}. As addition of methanol and water favours dissociation of tetrabutylammonium hydroxide and picrate, s_b and s_{salt} are both negative and s_{bm} is close to zero.

The extrapolation of the straight lines in Fig. 2 allows the computation of the reference potentials in basic media. However, the computed reference potentials in basic media (Table 2) are less accurate than in acidic media because the extrapolation is performed from further experimental points. The high absolute value of the slope in most media also contributes to the higher inaccuracy. However, although not completely accurate, the reference potentials in basic media allow a good estimation of the $pK_{solvent}$ of the medium by means of the equation

$$pK_{solvent} = (E_a^0 - E_b^0)/g \qquad (9)$$

The $pK_{solvent}$ values obtained are also presented in Table 2 and are in good agreement with the known autoprotolysis constants (pK_{ap}) of the solvents (Table 1), although neither pK values correspond exactly to the same equilibria. pK_{ap} measures the autoionization of the pure main solvent, whereas $pK_{solvent}$ measures the ionization of all the solvents present in the titration medium. As demonstrated in Part 1 [7], $pK_{solvent}$ should be $\leqslant pK_{ap}$.

COMPUTATION OF DISSOCIATION CONSTANTS: THE PK AND PKSIMULT PROGRAMS

The PK program computes dissociation constants of acids, bases and salts following the procedure described in Part 1 [7]. pK_a can be computed from potential values of acid–salt mixtures if pK_{salt} and the reference potential in acidic medium are known. From the potential and reference potential values pH is computed by the PREPOT program. The volume–pH points are input in the PK program and $[A^-]$ is computed using Eqn. 30 in Part 1 [7], then K_a is computed from the well known equation

$$K_a = \Sigma[H^+][A^-]y^2/(c_a - \Sigma[H^+]) \qquad (10)$$

This procedure should give constant K_a values for all the points of the titration (neglecting random errors). If there is a medium change caused by the addition of titrant (s_{am}), the extrapolation of the plot of the computed pK_a values against the volume fraction of co-solvent added (v) can allow the determination of pK_a in the pure main solvent [7]. However, if the acid is strong and the medium change is important, the potential values can lead to $\Sigma[H^+]$ values higher than c_a, which will result in negative K_a values. To avoid this problem an initial s_{am} value is introduced. PK suggests new s_{am} values to try until the best value (which minimizes the slope of pK_a vs. v) is found. PK presents on the screen the plot of pK_a vs. v and s_{am} and extrapolated pK_a values. These

TABLE 3

Dissociation constants of picric acid (pK_a) and tetrabutylammonium hydroxide (pK_b) in pure solvents computed by the PK program

Solvent	pK_a	s_{am}	N	pK_b	s_{bm}	N
Tetrahydrofuran	11.84 ± 0.01	0.0	7	6.47 ± 0.02	−8.3	10
tert-Butyl alcohol	5.36 ± 0.02	8.9	6	4.91 ± 0.01	−11.8	8
Isopropyl alcohol	4.03 ± 0.01	7.4	8	2.58 ± 0.09	1.6	12
Nitrobenzene	7.46 ± 0.01	3.1	9	1.13 ± 0.31	−6.7	10
Acetonitrile	11.00 ± 0.01	−0.8	9	0.93 ± 1.41	−23.2	5

TABLE 4

Dissociation constants of tetrabutylammonium picrate (pK_{salt}) in pure solvents computed by the PK program

Solvent	From acid–salt mixtures			From base–salt mixtures		
	pK_{salt}	s_{am}	N	pK_{salt}	s_{bm}	N
Tetrahydrofuran	5.21 ± 0.02	0.0	7	5.21 ± 0.05	−8.3	10
tert-Butyl alcohol	4.39 ± 0.05	8.3	4	4.36 ± 0.02	−11.8	8
Isopropyl alcohol	2.91 ± 0.07	6.4	7	2.75 ± 0.27	1.6	12
Nitrobenzene	1.19 ± 0.28	2.7	8			
Acetonitrile	1.24 ± 0.42	−1.3	8			

results are also output in an ASCII file together with the results computed for each titration point.

For base–salt mixtures a similar procedure is followed to determine pK_b from pS values (computing $[B^+]$ instead of $[A^-]$). pK_a and pK_b are determined simultaneously if the input file contains data from before and after the equivalence point of the titration.

PK computes pK_{salt} from acid–salt and/or base–salt potentiometric data if pK_a and/or pK_b is known. From acid–salt mixtures $\Sigma[H^+]$ is computed as described above, but $[A^-]$ is calculated from Eqn. 10 and K_{salt} from

$$K_{salt} = ([A^-] - \Sigma[H^+])[A^-]y^2/(c_{salt} - [A^-] + \Sigma[H^+]) \quad (11)$$

In a similar way, K_{salt} can be computed from pS values in base–salt mixtures.

The results obtained for the studied titrations are presented in Tables 3 (pK_a and pK_b) and 4 (pK_{salt}). The reference potentials in Table 2 were used to compute pH and pS. As expected, the pK values agree with those presented in Table 1 (used to compute reference potentials) and the s coefficients with those in Table 2. The high standard deviation of pK_{salt} of isopropyl alcohol in basic medium is explained by both the salt and the base being strongly dissociated. The K_b and K_{salt} values computed in acetonitrile and nitrobenzene (ca. 0.1) are much higher than the working electrolyte concentration (ca. 5×10^{-3} M) and therefore they mean that tetrabutylammonium hydroxide and picrate are completely dissociated at the working concentration. pK_{salt} values in base–salt mixtures for acetonitrile and nitrobenzene cannot be computed because the

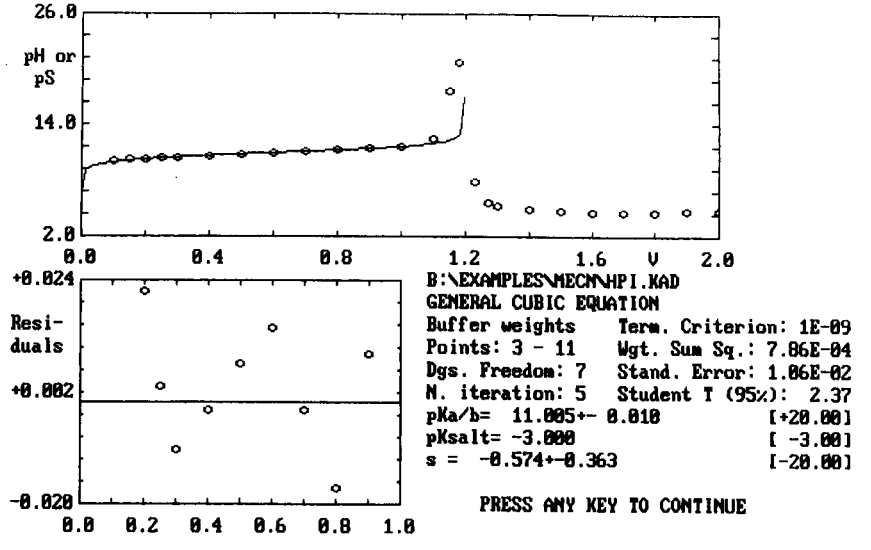

Fig. 3. Determination of pK_a and s_{am} for picric acid in acetonitrile by means of the PKSIMULT program.

TABLE 5

Dissociation constants of picric acid (pK_a) in pure solvents of high dielectric constant computed by the PKSIMULT program

Solvent	pK_a	s_{am}	N	Standard error	s_{bm}	N	Standard error
Nitrobenzene	7.39 ± 0.01	1.3 ± 0.2	10	0.01	−6.9 ± 0.1	9	0.002
	7.40 ± 0.02	1.3 ± 0.3	16	0.02	−6.9 ± 0.1	16	0.003
Acetonitrile	11.00 ± 0.01	−0.6 ± 0.4	9	0.01	−23.4 ± 0.1	6	0.006
	11.02 ± 0.01	−0.1 ± 0.4	12	0.02	−23.4 ± 0.1	9	0.03

base is completely dissociated and therefore the possible salt association cannot have any influence on pS values.

The PKSIMULT program was developed for the simultaneous determination of pK_a and pK_{salt} from acid–salt mixtures of pK_b and pK_{salt} from base–salt mixtures. Non-linear least-squares regression using the Gauss–Newton–Marquadt algorithm [23] is used to determine the pK values which minimizes squared pH or pS residuals. The pH or pS value is computed by solving Eqns. 1 and 2. If the titrant addition changes the medium, s_{am} or s_{bm} is also computed. Therefore, a maximum of three parameters (pK_a, pK_{salt} and s_{am} for acid–salt mixtures or pK_b, pK_{salt} and s_{bm} for base–salt mixtures) can be calculated by iteration from supplied starting values. However, the simultaneous calculation of the three parameters is difficult and not always needed. For example, Fig. 3 shows the results obtained for picric acid in acetonitrile. As acetonitrile has a high dielectric constant, salts are completely dissociated and pK_{salt} should not be iterated. The method converges quickly to the correct values of pK_a and s_{am} even if the starting values (in square brackets in Fig. 3) are far from them.

Two weighing options are offered. In simple weighing the error is assumed to be constant for all the titration points. In "buffer weighing" the error is assumed to be proportional to the reverse of the buffer capacity. Buffer weights are more robust than simple weights because the final result is less dependent of the titration points chosen. They have been used in all the examples presented here. Table 5 presents the results obtained for the solvents of high dielectric constant acetonitrile and nitrobenzene taking different titration points. It can be observed that the computed pK_a value is virtually independent of the considered points if the buffer option is chosen. In base–salt mixtures only s_{bm} is iterated because the salt and the base are both completely dissociated.

In solvents of low dielectric constants pK_a (or pK_b), pK_{salt} and often s_{am} (or s_{bm}) must be computed. Simultaneous computation of the three parameters is difficult for two reasons. On the one hand s is the coefficient of the volume fraction of titrant added, which is colinear with the salt concentration. Therefore, part of the variance of the results can be indistinctly attributed to s or pK_{salt} parameter. On the other hand, it

TABLE 6

$pK_n - pK_{salt}/2$ and s in solvents of low dielectric constant computed by the PKSIMULT program

Solvent	$pK_a - pK_{salt}/2$		s_{am} (computed)	N	$pK_b - pK_{salt}/2$		s_{bm} (computed)	N
	Expected	Computed			Expected	Computed		
Tetrahydrofuran	9.24	9.24 ± 0.01	0.0 ± 0.1	12	3.86	3.73 ± 0.02	−9.8 ± 0.3	9
		9.22 ± 0.01	0.0 ± 0.2	9		3.86 ± 0.04	−9.0 ± 0.5	13
tert-Butyl alcohol	3.17	3.13 ± 0.03	4.7 ± 1.6	7	2.73	2.62 ± 0.03	−13.9 ± 0.5	8
		3.10 ± 0.03	3.4 ± 1.5	6		2.62 ± 0.03	−13.9 ± 0.4	11
Isopropyl alcohol	2.62	2.48 ± 0.03	7.5 ± 1.0	8	1.18	1.50 ± 0.03	0.0 ± 0.3	9
		2.48 ± 0.02	7.6 ± 0.6	6		1.50 ± 0.02	0.0 ± 0.2	12

has been demonstrated [12] that in solvents of low dielectric constant Eqns. 1 and 2 tend to the following:

$$pN = pK_n - pK_{salt}/2 - \log c_n + (\log c_{salt})/2 \quad (12)$$

where pN, K_n and c_n mean the same as in Eqns. 1 and 2.

In Eqn. 12, it is obvious that pK_{salt} and pK_a (or pK_b) cannot be determined simultaneously from pH (or pS) measurements. Only the $pK_a - pK_{salt}/2$ (or $pK_b - pK_{salt}/2$) term can be determined. For this reason Eqn. 12 has also been introduced in the PKSIMULT program. The use of Eqns. 1 and 2 or 12 to compute pH or pS must be chosen according to the features of the solvent and substances. Table 6 presents the results obtained for the solvents of low dielectric constant tetrahydrofuran and *tert*-butyl and isopropyl alcohol by using Eqn. 12. The results agree very well with the expected values for the $pK_a - pK_{salt}/2$ term in tetrahydrofuran, for which Eqn. 12 is accurate, because pK_a is much higher than pK_{salt}. The results are also in good agreement for the $pK_b - pK_{salt}/2$ terms in tetrahydrofuran and *tert*-butyl alcohol and the $pK_a - pK_{salt}/2$ term in *tert*-butyl alcohol, for which Eqn. 12 is only an approximation, because pK_a or pK_b is only slightly higher than pK_{salt}. In isopropyl alcohol the salt is dissociated to an appreciable extent and the accuracy of Eqn. 12 is limited, hence only approximate results are obtained.

The use of Eqn. 12 instead Eqn. 1 allows the pitfalls of the latter for solvents of low dielectric constant to be avoided. The variance in pK_{salt} cannot be distinguished from the variance in pK_n and both are included in the term $pK_n - pK_{salt}/2$; s is the second variance source and it can be accurately determined because the pK_{salt} variance is included in the $pK_n - pK_{salt}/2$ term.

The previous determination of s from Eqn. 12 allows in some instances the simultaneous determination of pK_a (or pK_b) and pK_{salt} by means of the general Eqn. 1. Table 7 shows the results obtained for the three solvents of low dielectric constant. The s values in Table 6 were used. According to Table 7, accurate pK_a and pK_{salt} values are obtained for *tert*-butyl and isopropyl alcohol if the first point of the titration (solution of acid alone) is considered. Equation 12 applies for acid–salt mixtures, but not for solutions with acid alone. If the acid solution is well buffered as for picric acid in the two alcohols studied (see Fig. 4 and the next section for buffer capacities), the pH of this solution allows a good estimate of pK_a and then pK_{salt} can be well estimated from the other titration points. It can be seen in Table 7 that if the first point of the titration is excluded, pK_a and especially pK_{salt} are less accurate for *tert*-butyl and isopropyl alcohol. In contrast, estimation of pK_a and pK_{salt} in tetrahydrofuran is very difficult because the acid is much less dissociated than the salt, and solutions with acid alone are almost not buffered.

The estimation of pK_b and pK_{salt} from base–salt solutions is more difficult than the estimation of pK_a and pK_{salt} because they are estimated from the titration points after the equivalence point. The large negative s_{bm} values, the constancy of salt concentration and the impossibility of obtaining solutions with base alone after the equivalence point determine the high standard

TABLE 7

Dissociation constants of picric acid (pK_a), tetrabutylammonium picrate (pK_{salt}) and tetrabutylammonium hydroxide (pK_b) in pure solvents of low dielectric constant computed by the PKSIMULT program

Solvent	pK_a	pK_{salt}	s_{am}	N	pK_b	pK_{salt}	s_{bm}	N
Tetrahydrofuran	11.42 ± 0.04	4.15 ± 0.13	0.0	9	6.13 ± 0.79	4.73 ± 1.90	−9.8	6
tert-Butyl alcohol	5.24 ± 0.09	4.20 ± 0.23	4.7	8 [a]	4.87 ± 0.27	4.69 ± 0.72	−13.9	8
	5.13 ± 0.13	3.91 ± 0.38	4.7	7				
Isopropyl alcohol	4.00 ± 0.02	2.66 ± 0.12	7.6	8 [a]				
	3.96 ± 0.02	2.33 ± 0.16	7.6	7				

[a] Solution of acid alone included.

deviations of the pK_b and pK_{salt} values obtained. Accurate and reproducible pK_b and pK_{salt} values in isopropyl alcohol could not be obtained because of the high degree of dissociation of the base at the working concentrations.

TITRATION CURVES AND BUFFER CAPACITIES: THE CORVAL PROGRAM

The CORVAL program computes pH values from Eqns. 1 and 2 and plots the titration curve against the titrated fraction and buffer capacity before the equivalence point against pH (or pS). The buffer capacity after the equivalence point is not plotted because the plot is always exponential. After the equivalence point the salt concentration is constant (neglecting dilution), but the base concentration increases linearly with the titrant addition. Hence the buffer capacity always increases.

Different titration curves can be superimposed by changing the appropriate parameters: initial volume (V_i), equivalence volume (V_{eq}), titrant concentration (C_{tit}), pK values of the acid (pK_a), base (pK_b) and salt (pK_{salt}), Debye–Hückel parameter (A), and pK value of the solvent ($pK_{solvent}$). The most recent version of CORVAL uses a modified equation which considers homoconjugation equilibria (log K_{ha} and log K_{hb}, which means the logarithm of the homoconjugation constants of the acid and the base, respectively). This equation will be discussed in a future paper.

Figure 4 shows the graphical output of the CORVAL program for the titrations of picric acid with tetrabutylammonium hydroxide in the five solvents studied. An optional ASCII file with the computed titrant fraction, pH and β values can be also output by CORVAL. The titration curves of picric acid in the different solvents follow the order expected from the pK_a, pK_b and $pK_{solvent}$ values with the exception of tetrahydrofuran. The pK value of picric acid in tetrahydrofuran is slightly higher than that in acetonitrile, but the titration curve in tetrahydrofuran shows lower pH values than in acetonitrile because the formation of tetrabutylammonium picrate ion pairs favours picric acid dissociation. The enhancement of acid acidity by salt association is described in detail elsewhere [11,25,26].

Symmetrical bell-shaped buffer capacity curves centred at $pH = pK_a$ are obtained for picric acid–tetrabutylammonium picrate mixtures in the

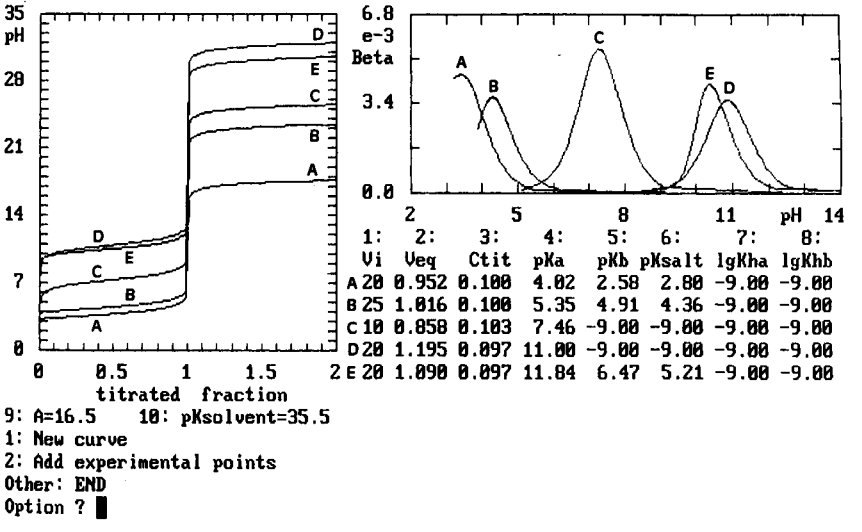

Fig. 4. Titration curves of picric acid with tetrabutylammonium hydroxide and buffer capacities of picric acid–tetrabutylammonium picrate solutions in pure non-aqueous solvents computed by the CORVAL program. (A) Isopropyl alcohol; (B) *tert*-butyl alcohol; (C) nitrobenzene; (D) acetonitrile; (E) tetrahydrofuran.

solvents of high dielectric constant acetonitrile and nitrobenzene because picric acid is a weak acid in these solvents and no salt ion pairs are formed. However, in the solvents of low dielectric constant tetrahydrofuran and *tert*-butyl and isopropyl alcohol the formation of ion pairs of tetrabutylammonium picrate (determined by the pK_{salt} values) shifts the maximum buffer capacity to pH values lower than pK_a, and makes the curve asymmetric. As with the titration curves, the pH value of the maximum buffer capacity in tetrahydrofuran is lower than that in acetonitrile although the pK_a value is higher. The displacement of the maximum of the buffer capacity curves in *tert*-butyl alcohol and especially isopropyl alcohol is to the first titration points and therefore these solutions are well buffered from the beginning of the titration even though the pK_a values are 5.35 and 4.02, respectively.

The set of programs presented is a powerful tool for the acquisition and treatment of potentiometric data in non-aqueous solvents. The VALORA program allows automatic acquisition of the data, which can be managed with the PREPOT program. From titration of standards of known pK values the reference potentials in the studied medium can be computed by the POTENCI program. Once the potentiometric system has been standardized, the programs PK and PKSIMULT allow the determination of dissociation constants of acids, bases and salts from the potentiometric data obtained in titration of the studied substances. CORVAL complements the other programs and helps to explain the observed behaviour. The fit of the computed constants to the experimental data can be tested by superimposing the experimental points on the computed titration curve, and the influence of each parameter in the titration curve or buffer capacity can be studied by giving different values to this parameter and observing the titration curve and buffer capacity obtained.

The titration data sets used in this paper were obtained by J. Barbosa, D. Barrón, E. Bosch, S. Butí, C. Ràfols and V. Sanz-Nebot, all of whom are thanked for kindly providing the data, testing the programs and making helpful comments. Financial support from the DGICYT (project PB88-0194) is gratefully acknowledged.

REFERENCES

1 D.J. Legget (Ed.), Computational Methods for the Determination of Formation Constants, Plenum, New York, 1985.
2 R.J. Motekaitis and A.E. Martell, Can. J. Chem., 60 (1982) 168.
3 A.D. Zuberbühler and T.A. Kaden, Talanta, 29 (1982) 201.
4 A. Izquierdo and J.L. Beltrán, Anal. Chim. Acta, 181 (1986) 87.
5 O. Budevsky, T. Zikolova and J. Tencheva, Talanta, 35 (1988) 899.
6 Ting-Po I and G.H. Nancollas, Anal. Chem., 44 (1972) 1940.
7 M. Rosés, Anal. Chim. Acta, 276 (1993) 211.
8 E.P. Serjeant, Potentiometry and Potentiometric Titrations, Wiley, New York, 1984.
9 C. Reichardt, Solvents and Solvent Effects in Organic Chemistry, VCH, Weinheim, 2nd edn., 1988.
10 Y. Marcus, Ion Solvation, Wiley, New York, 1985.
11 E. Bosch and M. Rosés, Talanta, 36 (1989) 615.
12 J. Barbosa, D. Barrón, E. Bosch and M. Rosés, Anal. Chim. Acta, 264 (1992) 229.
13 E. Bosch and M. Rosés, Anal. Chem., 60 (1988) 2008.
14 I.M. Kolthoff, D. Stocesocá and T.S. Lee, J. Am. Chem. Soc., 75 (1953) 1834.
15 E.G. Taylor and C.A. Kraus, J. Am. Chem. Soc., 69 (1947) 1731.
16 I.M. Kolthoff and M.K. Chantooni, Jr., J. Am. Chem. Soc., 87 (1965) 4428.
17 J.F. Coetzee, G.R. Padmanabhan and G.P. Cunnigham, Talanta, 11 (1964) 93.
18 D. Barrón, PhD Thesis, University of Barcelona, Barcelona, 1992.
19 I.M. Kolthoff, Anal. Chem., 46 (1974) 1992.
20 J. Barbosa, E. Bosch and M. Rosés, Analyst, 112 (1987) 179.
21 J. Barbosa, J. Sánchez and E. Bosch, Talanta, 31 (1984) 279.
22 J. Barbosa, M. Rosés and V. Sanz-Nebot, Talanta, 35 (1988) 1013.
23 P. Valkó and S. Vajda, Advanced Scientific Computing in BASIC with Applications in Chemistry, Biology and Pharmacology, Elsevier, Amsterdam, 1989.
24 I.M. Kolthoff, M.K. Chantooni, Jr., and H. Smagowski, Anal. Chem., 42 (1970) 1622.
25 E. Bosch and M. Rosés, Talanta, 36 (1989) 623.
26 E. Bosch and M. Rosés, Talanta, 36 (1989) 627.

ADVANCES IN MASS SPECTROMETRY, Volume 12

Proceedings of the 12th International Mass Spectrometry Conference, Amsterdam, 26-30 August 1991

edited by **P.J. Kistemaker,** FOM-Institute for Atomic and Molecular Physics, Amsterdam, The Netherlands and **N.M.M. Nibbering,** University of Amsterdam, Amsterdam, The Netherlands

These proceedings, containing the texts of the invited lectures, cover all aspects of mass spectrometry including theory, fundamental studies, applications and instrumentation. Emphasis is placed on recent developments. A complete listing of the posters is included.

Contents:

1992 xxii + 952 pages
Price: US $ 281.50 / Dfl. 450.00
ISBN 0-444-88871-3

ELSEVIER
SCIENCE PUBLISHERS

ORDER INFORMATION

For USA and Canada
ELSEVIER SCIENCE PUBLISHERS
Judy Weislogel
P.O. Box 945
Madison Square Station,
New York, NY 10160-0757
Tel: (212) 989 5800
Fax: (212) 633 3880

In all other countries
ELSEVIER SCIENCE PUBLISHERS
P.O. Box 211
1000 AE Amsterdam
The Netherlands
Tel: (+31-20) 5803 753
Fax: (+31-20) 5803 705

US$ prices are valid only for the USA & Canada and are subject to exchange rate fluctuations; in all other countries the Dutch guilder price (Dfl.) is definitive. Books are sent postfree if prepaid.

711/414\140\0001-00

Methods for Experimental Design

Principles and Applications for Physicists and Chemists

by **J. Goupy**

Data Handling in Science and Technology Volume 12

The choice of ideal experiments is based on mathematical concepts, but the author adopts a practical approach and uses theory only when necessary. Written for experimenters by an experimenter, it is an introduction to the philosophy of scientific investigation. A method for organizing and conducting scientific experiments is described in this volume which enables experimenters to reduce the number of trials run, while retaining all the parameters that may influence the result.

Researchers with limited time and resources at their disposal will find this text a valuable guide for solving specific problems efficiently. The presentation makes extensive use of examples, and the approach and methods are graphical rather than numerical. All calculations can be performed on a personal computer; readers are assumed to have no previous knowledge of the subject. The presentation is such that the beginner may acquire a thorough understanding of the basic concepts. However, there is also sufficient material to challenge the advanced student. The book is, therefore, suitable for both first and advanced courses. The many examples can also be used in detail for self-study or as a reference.

Contents:

1993 xvi + 450 pages
Price: US $ 185.75 / Dfl. 325.00
ISBN 0-444-89529-9

ELSEVIER
SCIENCE PUBLISHERS

ORDER INFORMATION

For USA and Canada
ELSEVIER SCIENCE PUBLISHERS
Judy Weislogel
P.O. Box 945
Madison Square Station,
New York, NY 10160-0757
Tel: (212) 989 5800
Fax: (212) 633 3880

In all other countries
ELSEVIER SCIENCE PUBLISHERS
P.O. Box 211
1000 AE Amsterdam
The Netherlands
Tel: (+31-20) 5803 753
Fax: (+31-20) 5803 705

US$ prices are valid only for the USA & Canada and are subject to exchange rate fluctuations; in all other countries the Dutch guilder price (Dfl.) is definitive. Customers in the European Community should add the appropriate VAT rate applicable in their country to the price(s). Books are sent post-free if prepaid.

PUBLICATION SCHEDULE FOR 1993

	S'92	O'92	N'92	D'92	J	F	M	A	M	J	J	A
Analytica Chimica Acta	267/1 267/2	268/1 268/2	269/1 269/2	270/1 270/2	271/1 271/2	272/1 272/2 273/1–2	274/1 274/2	275/1–2 276/1 276/2	277/1 277/2	278/1 278/2	279/1 279/2	280/1 280/2
Vibrational Spectroscopy		4/1			4/2		4/3	5/1		5/2		5/3

INFORMATION FOR AUTHORS

Manuscripts. The language of the journal is English. English linguistic improvement is provided as part of the normal editorial processing. Authors should submit three copies of the manuscript in clear double-spaced typing on one side of the paper only. *Vibrational Spectroscopy* also accepts papers in English only.

Abstract. All papers and reviews begin with an Abstract (50–250 words) which should comprise a factual account of the contents of the paper, with emphasis on new information.

Figures. Figures should be prepared in black waterproof drawing ink on drawing or tracing paper of the same size as that on which the manuscript is typed. One original (or sharp glossy print) and two photostat (or other) copies are required. Attention should be given to line thickness, lettering (which should be kept to a minimum) and spacing on axes of graphs, to ensure suitability for reduction in size on printing. Axes of a graph should be clearly labelled, along the axes, outside the graph itself. All figures should be numbered with Arabic numerals, and require descriptive legends which should be typed on a separate sheet of paper. Simple straight-line graphs are not acceptable, because they can readily be described in the text by means of an equation or a sentence. Claims of linearity should be supported by regression data that include slope, intercept, standard deviations of the slope and intercept, standard error and the number of data points; correlation coefficients are optional.

Photographs should be glossy prints and be as rich in contrast as possible; colour photographs cannot be accepted. Line diagrams are generally preferred to photographs of equipment.

Computer outputs for reproduction as figures must be good quality on blank paper, and should preferably be submitted as glossy prints.

Nomenclature, abbreviations and symbols. In general, the recommendations of the International Union of Pure and Applied Chemistry (IUPAC) should be followed, and attention should be given to the recommendations of the Analytical Chemistry Division in the journal *Pure and Applied Chemistry* (see also *IUPAC Compendium of Analytical Nomenclature, Definitive Rules*, 1987).

References. The references should be collected at the end of the paper, numbered in the order of their appearance in the text (*not* alphabetically) and typed on a separate sheet.

Reprints. Fifty reprints will be supplied free of charge. Additional reprints (minimum 100) can be ordered. An order form containing price quotations will be sent to the authors together with the proofs of their article.

Papers dealing with vibrational spectroscopy should be sent to: Dr J.G. Grasselli, 150 Greentree Road, Chagrin Falls, OH 44022, U.S.A. Telefax: (+1-216) 2473360 (Americas, Canada, Australia and New Zealand) or Dr J.H. van der Maas, Department of Analytical Molecule Spectrometry, Faculty of Chemistry, University of Utrecht, P.O. Box 80083, 3508 TB Utrecht, The Netherlands. Telefax: (+31-30) 518219 (all other countries).

0003-2670/93/$06.00

This issue is printed on acid-free paper.

PRINTED IN THE NETHERLANDS

Wilson and Wilson's Comprehensive Analytical Chemistry Volume XXVII

Analytical Voltammetry

edited by **M.R. Smyth** and **J.G. Vos,** School of Chemical Sciences, Dublin City University, Dublin, Ireland

Series editor: **G. Svehla,** University College, Cork, Ireland

The aim of this volume is to review the state-of-the-art in analytical voltammetry with regard to theory and instrumentation, and show how these relate to the analysis of inorganic, organometallic, organic and biological molecules. Modern voltammetric techniques have practical applications in biological, pharmaceutical and environmental chemistry. The growing importance of voltammetry in the development of modified electrodes and biological electrodes and chemical and biological sensors is also highlighted.

Contents:

1992 xxvi + 578 pages
Price: US $ 254.00 / Dfl. 495.00
Subscription price: US $ 228.00 / Dfl. 445.00
ISBN 0-444-88938-8

Elsevier Science Publishers

P.O. Box 211, 1000 AE Amsterdam, The Netherlands
P.O. Box 882, Madison Square Station, New York, NY 10159, USA

0003-2670(19930415)276:1;1-C